

370 p

PKT 402

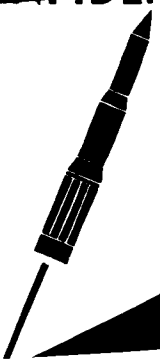
X63-10/35  
Code 2 D

**UNCLASSIFIED**

MSFC  
MPR-SAT-WF-62-5  
June 5, 1962

G3

~~CONFIDENTIAL~~



(MPR-SA-WF-62-5) SATURN SA-2 FLIGHT  
EVALUATION (NASA) 370 p

N73-74554

Unclas  
00/99 19501

**MARSHALL SPACE  
FLIGHT  
CENTER**

**HUNTSVILLE, ALABAMA**

SATURN SA-2 FLIGHT EVALUATION



PROPERTY OF  
TECHNICAL LIBRARY  
M-MS-IPL

~~GROUP (4)  
DOWNGRADED 1 YEAR  
INTERVAL DECLASSIFIED  
ABOUT 12 YEARS.~~

AVAILABLE TO U.S. GOVERNMENT AGENCIES  
AND U.S. GOVERNMENT CONTRACTS ONLY

CLASSIFICATION CHANGE  
TO UNCLASSIFIED  
By authority of E.O. 11652  
Changed by L. Shirley Date 5-16-73

**NATIONAL AERONAUTICS AND SPACE ADMINISTRATION**



~~CONFIDENTIAL~~

GEORGE C. MARSHALL SPACE FLIGHT CENTER

---

MPR-SAT-WF-62-5

---

SATURN SA-2 FLIGHT EVALUATION

By Saturn Flight Evaluation Working Group

(U) ABSTRACT

10135

This report presents the results of the Early Engineering Evaluation of the Saturn SA-2 test flight. The performance of each major vehicle system is discussed with special emphasis on malfunctions and deviations.

The SA-2 flight test was a complete success with all missions of the test being accomplished. No major malfunctions or deviations which could be considered a serious system failure or design deficiency occurred during the test.

Any questions or comments pertaining to the information contained in this report are invited and should be directed to

Director, George C. Marshall Space Flight Center  
Huntsville, Alabama  
Attention: Chairman, Flight Evaluation Working Group,  
M-AERO-F (Phone 876-2701)

~~CONFIDENTIAL~~

GEORGE C. MARSHALL SPACE FLIGHT CENTER

---

MPR-SAT-WF-62-5

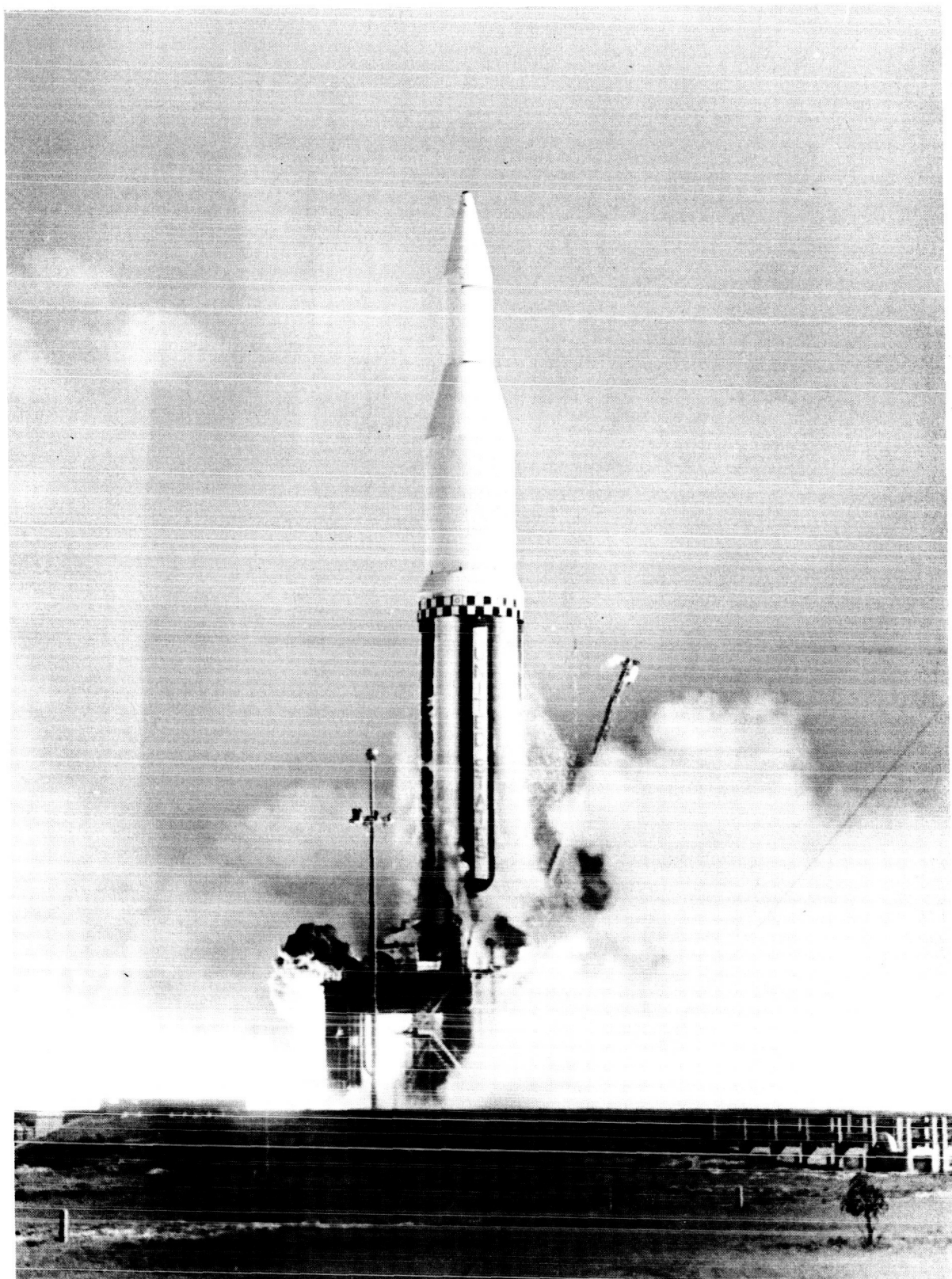
---

June 5, 1962

SATURN SA-2 FLIGHT EVALUATION (U)

SATURN FLIGHT EVALUATION  
WORKING GROUP

~~CONFIDENTIAL~~



Section	Section Title	Locator
1	Flight Test Summary	1
2	Introduction	2
3	Prelaunch Operations	3
4	Trajectory	4
5	Propulsion	5
6	Control	6
7	Guidance	7
8	Vehicle Electrical System	8
9	Structures and Vibration	9
10	Environmental Temperatures and Pressures	10
11	Aerodynamics	11
12	Instrumentation	12
13	Summary of Malfunctions and Deviations	13
14	Appendices A through I	14

(U) TABLE OF CONTENTS

	Page
1.0 Flight Test Summary	1
1.1 Flight Test Results	1
1.2 Test Objectives	2
1.3 Times of Flight Events	5
2.0 Introduction	7
3.0 Prelaunch Operations	8
3.1 Summary	8
3.2 Prelaunch Events	8
3.2.1 Preparations	8
3.2.2 Countdown	12
3.2.3 Holddown	14
4.0 Trajectory	22
4.1 Summary	22
4.2 Tracking Analysis	22
4.2.1 Data Sources	22
4.2.2 Data Utilization	22
4.2.3 Error Analysis of Actual Trajectory	27
4.3 Actual and Predicted Trajectory Comparison	27
4.3.1 Powered Flight	27
4.3.2 Cutoff	35
5.0 Propulsion	39
5.1 Summary	39
5.2 Individual Engine Performance	39
5.3 Vehicle Propulsion System Performance	53
5.4 Pressurization Systems	56
5.4.1 Fuel Tank Pressurization	56
5.4.2 LOX Tanks Pressurization System	59
5.4.3 Control Pressure System	62
5.4.4 Air Bearing Supply	62
5.5 Vehicle Propellant Utilization	66
5.5.1 Propellant Utilization System	68
5.5.2 Liquid Level Discrete Probe Performance	68
5.5.3 Conclusions	68
5.6 Hydraulic System	79
5.7 Mass Characteristics	79
6.0 Control	82
6.1 Summary	82

(U) TABLE OF CONTENTS (CONT')

6.2	S-I Control Analysis	83
6.2.1	Pitch Plane	83
6.2.2	Yaw Plane	94
6.2.3	Roll Plane	98
6.2.4	Attitude After Cutoff	101
6.3	Functional Analysis	104
6.3.1	Control Sensors	104
6.3.1.1	Control Accelerometers	104
6.3.1.2	Rate Gyros	104
6.3.1.3	Angle of Attack Meters	106
6.3.2	Tilt Programmer	109
6.3.3	Control Computer	112
6.3.4	Actuators	113
6.4	Propellant Sloshing	116
7.0	Guidance	127
7.1	Summary	127
7.2	Description of Guidance System	127
7.3	Operational Analysis	128
7.3.1	Guidance Intelligence Errors	128
7.3.2	Accelerometer Outputs	128
7.3.3	Functional Analysis	132
8.0	Vehicle Electrical System	139
8.1	Summary	139
8.2	Power Supply Description	139
8.3	Flight Results	144
9.0	Structures and Vibration	145
9.1	Summary	145
9.2	Bending Moments and Normal Load Factors	146
9.2.1	Instrumentation	146
9.2.2	Results	146
9.3	Longitudinal Loads	155
9.4	Bending Oscillations	155
9.5	Torsional Oscillations	163
9.6	Vibration	163
9.6.1	Introduction	163
9.6.2	Structural Vibrations	178
9.6.3	Propulsion System Vibration	179
9.6.4	Component Vibration	185
9.6.5	Discussion of Vibration Data	187
9.7	Vehicle Acoustic Measurement	215

(U) TABLE OF CONTENTS (CONT')

9.8	Analysis of Ground Acoustic Measurements	217
9.8.1	Summary	217
9.8.2	Near-field Data	217
9.8.3	Mid-field Data	218
9.8.4	Far-field Data	219
10.0	Environmental Temperature and Pressure	223
10.1	Summary	223
10.2	Tail Section	223
10.2.1	Engine Compartment	223
10.2.2	Base Environment	226
10.3	Skin	252
10.4	Instrument Canisters	252
10.4.1	Canister Pressure	252
10.4.2	Canister Temperature	263
11.0	Aerodynamics	264
11.1	Summary	264
11.2	Ratio of Gradients of Angular Acceleration (Stability Ratio)	264
11.3	Gradient of Normal Force Coefficient and Center of Pressure Location	266
11.4	Surface Pressures	268
11.4.1	Station 205 Measurements	268
11.4.2	Measurements at Stations 860 and 863	268
12.0	Instrumentation	272
12.1	Summary	272
12.2	Measuring Analysis	272
12.3	Telemetry Systems Analysis	274
12.4	R. F. Systems Analysis	277
12.5	Photographic Coverage	280
12.6	SA-2 Data Acquisition at Green Mountain Tracking Station	282
13.0	Summary of Malfunctions and Deviations	286
Appendix A	System Description	288
A.1.0	Launch Characteristics	288
A.2.0	Vehicle Description	288
A.2.1	S-I Stage	288
A.2.2	S-IV Dummy Stage	294
A.2.3	S-V Dummy Stage	294
A.2.4	Dummy Payload	294

(U) TABLE OF CONTENTS (CONT')

A.3.0	Ground Support Equipment	299
A.3.1	Short Cable Mast Assembly	299
A.3.2	Long Cable Mast Assembly	299
A.3.3	Support Arms	299
A.3.4	Holddown Arms	302
A.3.5	Fuel and LOX Filling Mast Assemblies	302
A.3.6	Boattail Conditioning System	302
A.3.7	High Pressure Battery	302
A.3.8	LOX Replenishing System	302
A.3.9	Liftoff Switch Installation	303
A.3.10	Water Quench System	303
A.4.0	Ground Instrumentation	303
A.4.1	Telemetry Receivers	303
A.4.2	Optical Systems	304
A.4.3	Tracking	304
Appendix B	Redline Values	306
Appendix C	Ground Sequence Events	310
Appendix D	Mass Characteristics	312
Appendix E	Atmospheric Summary for SA-2	317
E.1	Introduction	317
E.2	General Synoptic Situation at Launch Time	317
E.3	Surface Observations at Launch Time	317
E.4	Time and Space Variations Between Missile Flight Path and Upper Air Measurements by Rawinsonde and Rocketsonde	318
E.5	Wind Data	320
E.6	Thermodynamic Data	326
Appendix F	Data Reduction	329
F.1	Telemetry Data	329
F.2	UDOP Data	331
F.3	Meteorological Data	333
F.4	Optical Tracking Data	333
Appendix G	Flight Simulation of Cluster Performance	334
Appendix H	Bias Adjustment of Flight Mechanical Data	337
Appendix I	Project Highwater	341

(U) LIST OF TABLES

Table		Page
3-I	Prelaunch Milestones	21
4-I	Data Sources for Precision Trajectory	23
4-II	Significant Events	36
4-III	Cutoff Conditions	37
5-I	Engine Operation Times	51
5-II	Cutoff Impulse	52
7-I	Guidance Comparisons	135
9-I	SA-2 Flight Vibration Measurements	174
9-II	SA-2 Flight Vibrations	175
9-III	Compilation of Discrete Frequencies Noted in Turbo Pump Measurements Normalized to a Pump Speed of 6000 RPM	181
12-I	Saturn SA-2 Telemetry Systems	275
B-I	Redline Values	307
D-I	Mass Characteristics Comparison	312
D-II	SA-2 Vehicle Weights	313
H-I	Flight Mechanical Data Bias Calculations SA-2	339
H-II	Comparison of 8 and 16 Equation Bias Determination	340

(U) LIST OF ILLUSTRATIONS

Figure		Page
3-1	RP-1 Specific Weight vs Temperature	11
3-2	Hold Time vs Count Time	13
3-3	View of Long Cable Mast	17
3-4	View of Holddown Arm Showing Water Quench Mast and LOX Replenish Mast	18
3-5	View of Flame Deflector Showing Areas of Jet Impingement	20
4-1	Tracking Comparisons (Tracking-Reference)	26
4-2	Separation Anvil vs Vehicle Support Block	28
4-3	Trajectory	29
4-4	Earth-fixed Velocity	30
4-5	Altitude and Displacement After Liftoff	31
4-6	Dynamic Pressure and Mach Number	32
4-7	Longitudinal Acceleration	33
4-8	Longitudinal Acceleration (Cutoff and Decay Profile)	34
4-9	Outboard Engine Longitudinal Acceleration	38
5-1	H-1 Engine Schematic	40
5-2	Thrust Build-up	42
5-3	Total Flow, Specific Impulse, and Total Thrust Engine Position 1	43
5-4	Total Flow, Specific Impulse, and Total Thrust Engine Position 2	44
5-5	Total Flow, Specific Impulse, and Total Thrust Engine Position 3	45
5-6	Total Flow, Specific Impulse, and Total Thrust Engine Position 4	46
5-7	Total Flow, Specific Impulse, and Total Thrust Engine Position 5	47
5-8	Total Flow, Specific Impulse, and Total Thrust Engine Position 6	48
5-9	Total Flow, Specific Impulse, and Total Thrust Engine Position 7	49
5-10	Total Flow, Specific Impulse, and Total Thrust Engine Position 8	50
5-11	Vehicle Total Propellant Flow and Longitudinal Thrust	54
5-12	Vehicle Specific Impulse and Mixture Ratio	55
5-13	SA-2 Fuel System	57
5-14	Pressure in High Pressure Sphere and Pressure Gas in Fuel Tank	58
5-15	SA-2 LOX System	60
5-16	Pressure and Temperature in LOX Tanks	61
5-17	Control Pressure Schematic	63

(U) LIST OF ILLUSTRATIONS (CONT')

5-18	Pressure Control Equipment, Regulated and Pressure Control Equipment Supply	64
5-19	Air Bearing Supply System Schematic	65
5-20	Pressure Air Bearing Supply Sphere and Air Bearing Supply	69
5-21	Propellant Utilization System	70
5-22	Propellant Height Above Bottom of Center LOX Tank	71
5-23	Liquid Height Above Tank Bottom - Fuel Tank F <sub>2</sub> (0 - 120 sec)	72
5-24	Liquid Height Above Tank Bottom - Fuel Tank F <sub>2</sub> (105 - 116 sec)	73
5-25	Liquid Height Above Tank Bottom - LOX Tank O <sub>4</sub> (105 - 118 sec)	74
5-26	△ Pressure PU Computer, LOX, Fine	75
5-27	△ Pressure PU Computer, Fuel, Fine	76
5-28	Propellant Utilization Computer Output, Fine, (A18-11)	77
5-29	Vehicle Total Propellant Consumption	78
5-30	Hydraulic Source Pressure and Hydraulic Oil Level	80
6-1	Pitch Attitude, Angular Velocity and Actuator Position	84
6-2	Tilt Program and Pitch Velocity Vector Angle	86
6-3	Pitch Plane Wind Components and Local Angle of Attack	87
6-4	Pitch Attitude Minus Program, Free-stream Angle of Attack (Pitch) and Average Pitch Actuator Position	88
6-5	Pitch Normal Acceleration	91
6-6	Pitch Angle Design Criteria	93
6-7	Yaw Attitude, Angular Velocity and Actuator Position	95
6-8	Yaw Plane Wind Components and Local Angle of Attack	96
6-9	Yaw Attitude, Free-stream Angle of Attack (Yaw) and Average Yaw Actuator Position	97
6-10	Yaw Normal Acceleration	99
6-11	Roll Attitude, Angular Velocity and Actuator Position	100
6-12	Angular Velocities During Cutoff	102
6-13	Attitude Angles After Cutoff	103
6-14	Oscillations in Rate Gyro Measurements	105
6-15	Free-stream Angles of Attack	107
6-16	Schematic of Tilt Programmer, SA-2	110
6-17	Tilt Rate and Peak Control Signals	111
6-18	Representative Actuator Loads	114
6-19	Non-control Actuator Loads	115

(U) LIST OF ILLUSTRATIONS (CONT')

6-20	Baffle Configurations	117
6-21	Outer LOX Tank 04 Telemetered Sloshing Amplitudes	120
6-22	Fuel Tank F <sub>2</sub> Telemetered Sloshing Amplitudes	121
6-23	Center LOX Tank Telemetered Sloshing Amplitudes	122
6-24	Sloshing Frequencies	123
6-25	Spatial Plots of Sloshing Motion (Comparison with SA-1)	124
6-26	Spatial Plots of Sloshing Motion (Comparison with SA-1)	125
7-1	Guidance Velocity Comparison (Telemetered Minus Calculated)	130
7-2	Cross Range Guidance Velocity (Telemetered)	131
7-3	Guidance Velocity Comparison Cross Range (Telemetered Minus Calculated)	132
7-4	Slant Altitude Guidance Velocity (Telemetered)	134
7-5	Telemetered Velocity Indications at Ignition	137
8-1	28 Volt DC Power System	140
8-2	Propulsion and Control Distributor Network System	141
8-3	Unit Locations	142
9-1	Strain Gauge Locations	147
9-2	Bending Moment Comparison and Normal Load Factors (63.5 sec)	148
9-3	Bending Moment Comparison and Normal Load Factors (65.3 sec)	149
9-4	Pitch and Yaw Bending Moments at Station 979 and Pitch Bending Moment at Station 869	153
9-5	Moment Loads at Station 979 and Moment Reacted by 70" LOX Tanks	154
9-6	Longitudinal Load at Stations 979 and 869	156
9-7	Maximum Dynamic Response	157
9-8	Bending Mode Accelerometer Locations	158
9-9	SA-2 System Frequency Trend	160
9-10	SA-2 System Frequency Trend	161
9-11	SA-2 Bending Mode - First Mode, Pitch	164
9-12	SA-2 Bending Mode - First Mode, Pitch	165
9-13	SA-2 Bending Mode - First Mode, Yaw	166
9-14	SA-2 Bending Mode - First Mode, Yaw	167
9-15	SA-2 Bending Mode - First and Second Mode, Yaw	168
9-16	SA-2 Bending Mode - Second and Third Mode, Yaw	169
9-17	SA-2 Nose Acceleration Envelope	170
9-18	SA-2 Outer Tank Frequencies - Fuel Tank, Pitch	171
9-19	SA-2 Outer Tank Frequencies - LOX Tank, Pitch	172
9-20	Explanation of Data in Vibration Summary Curves	188
9-21	SA-2 Flight Vibration Data	189
9-22	SA-2 Flight Vibration Data	190

(U) LIST OF ILLUSTRATIONS (CONT')

9-23	SA-2 Flight Vibration Data	191
9-24	SA-2 Flight Vibration Data	192
9-25	SA-2 Flight Vibration Data	193
9-26	SA-2 Flight Vibration Data	194
9-27	SA-2 Flight Vibration Data	195
9-28	SA-2 Flight Vibration Data	196
9-29	SA-2 Flight Vibration Data	197
9-30	SA-2 Flight Vibration Data	198
9-31	SA-2 Flight Vibration Data	199
9-32	SA-2 Flight Vibration Data	200
9-33	SA-2 Flight Vibration Data	201
9-34	SA-2 Flight Vibration Data	202
9-35	SA-2 Flight Vibration Data	203
9-36	SA-2 Flight Vibration Data	204
9-37	SA-2 Flight Vibration Data	205
9-38	Typical Transients in Actuator Data	206
9-39	Hydraulic Actuator Data	207
9-40	SA-2 Flight Vibration Data	208
9-41	SA-2 Flight Vibration Data	209
9-42	SA-2 Composite Vibration Traces	210
9-43	SA-2 Composite Vibration Traces	211
9-44	SA-2 Composite Vibration Traces	212
9-45	SA-2 Composite Vibration Traces	213
9-46	SA-2 Composite Vibration Traces	214
9-47	SA-2 Over-all Sound Pressure Level	216
9-48	Far-field Acoustic Measuring Points	221
9-49	Over-all RMS Sound Pressure Level	222
10-1	Range of Ambient Air Temperature in Engine Compartment	224
10-2	Bulk Temperature of Structural Members in Engine Compartment	225
10-3	S-I Stage Flight Measurements	227
10-4	Heat Shield Instrumentation Location for Saturn SA-2 Flight Test	228
10-5	Gas Temperature Probes for SA-1 and SA-2	229
10-6	S-I Stage Flight Measurements	231
10-7	Base Pressure Minus Ambient Pressure Versus Time	232
10-8	Ratios of Base Pressure to Ambient Pressure Versus Mach Number	234
10-9	Base Pressure Coefficient Versus Time	235
10-10	Star and Base Pressure Minus Lower Compartment Pressure	236
10-11	Compartment Pressure Differences	237
10-12	Gas Temperature Measured 3 Inches Below Heat Shield	239

(U) LIST OF ILLUSTRATIONS (CONT')

10-13	Gas Temperature Measured 3 Inches Below Heat Shield	240
10-14	Heat Shield Gas Temperature	241
10-15	Gas Recovery Temperature Measured 3 Inches Below Flame Shield	242
10-16	Total Heating Rate of the Heat Shield	244
10-17	Measured Flame Shield Heating Rate, $q_t$ , and Total Calorimeter Temperature, T	245
10-18	Temperature Aft of Flame Shield, Conduction Thermocouple	247
10-19	Forward Side Flame Shield Temperature	248
10-20	Forward Side Flame Shield Temperature	249
10-21	Outboard Engine Shroud Stringer Temperature	250
10-22	Outboard Engine Shroud Skin Temperature	251
10-23	S-I Stage Flight Measurements	253
10-24	Outboard LOX Tank Skin Temperature	254
10-25	Center LOX Tank Skin Temperature	255
10-26	LOX Tank Shroud Temperature	256
10-27	Center LOX Tank Skin Temperature	257
10-28	Outboard LOX Tank Skin Temperature	258
10-29	Outboard LOX Tank Skin Temperature	259
10-30	Fuel Tank Skin Temperature	260
10-31	Instrument Canister Cooling System	261
10-32	Pressure Instrument Compartment	262
11-1	Ratio of Gradients of Angular Accelerations vs Range Time	265
11-2	Center of Pressure Location and Gradient of Normal Force Coefficient vs Mach Number	267
11-3	Ratios of Surface Pressure to Ambient Pressure vs Mach Number	269
11-4	Ratios of Surface Pressure to Ambient Pressure vs Mach Number	271
12-1	Telemetry Signal Strength; Cape Telemetry 2 and GBI	279
12-2	System Block Diagram	283
12-3	Telemetry and UDOP Signal Strength Plot	285
A-1	Saturn Configuration	289
A-2	Dummy Second Stage, Saturn SA-2	295
A-3	Dummy Third Stage, Saturn SA-2	296
A-4	Dummy Payload, Saturn SA-2	297
A-5	Engine Compartment Layout	298
A-6	Ground Support Equipment	300
A-7	Saturn Launch Complex 34	301
D-1	Vehicle Weight vs Range Time	314
D-2	Longitudinal Center of Gravity vs Range Time	315

(U) LIST OF ILLUSTRATIONS (CONT')

D-3	Roll and Pitch Moment of Inertia vs Range Time	316
E-1	Launch Site Wind Measurements (Anemometer) for Saturn (SA-2) Launch	319
E-2	SA-2 Wind Speed by Rawinsonde, Angle of Attack and Rocketsonde	321
E-3	Wind Components by Rawinsonde Measurement, Angle of Attack and Rocketsonde	322
E-4	Pitch and Yaw Component Wind Shear (1000 m)	323
E-5	Pitch Component Wind Shear by Rawinsonde and Angle of Attack Measurement ( $W_x$ ) (250 meters)	324
E-6	Yaw Component Wind Shear by Rawinsonde and Angle of Attack Measurement ( $W_z$ ) (250 meters)	325
E-7	SA-2 Absolute Deviation of Optical Refractive Index and Relative Deviation of Pressure from PAFB Reference Atmosphere	327
E-8	SA-2 Relative Deviation of Temperature and Density from PAFB Reference Atmosphere	328
G-1	Flight Simulation Results	335
G-2	Earth-fixed Velocity and Slant Distance (Tracking - Flight Simulation)	336
I-1	Picture Sequence of Project Highwater Experiment	342

~~CONFIDENTIAL~~

GEORGE C. MARSHALL SPACE FLIGHT CENTER

---

MPR-SAT-WF-62-5

---

SATURN SA-2 FLIGHT EVALUATION

By Saturn Flight Evaluation Working Group

1.0 (C) FLIGHT TEST SUMMARY

1.1 FLIGHT TEST RESULTS

Saturn space vehicle SA-2 was launched at 0900:34 EST on April 2, 1962. The flight test was a complete success, as was the SA-1 flight test. The flight test did not reveal any malfunctions or deviations which could be considered a serious system failure or design deficiency.

SA-2 was launched approximately 8 weeks after arrival of the S-I stage at Cape Canaveral. The scheduled ten-hour countdown began at 2230 EST April 24, 1962. No technical difficulties requiring holds were experienced during countdown, but one hold for range clearance was called because of a ship in the launch area. Automatic fueling and sequencing processes were satisfactorily conducted. Compatibility of the ground support equipment and the flight vehicle was again demonstrated. The general condition of the pad and ground support equipment after launch was much the same as after the SA-1 launch.

The actual flight path of SA-2 was slightly lower than predicted due to lower acceleration. Trajectory parameters after inboard engine cutoff were higher due to the later actual cutoff time. Destruction of SA-2 for Project High Water occurred at 162.56 seconds range time at an altitude of 105.3 km.

Operation of the control system was satisfactory. The sloshing instability noted in the SA-1 flight was successfully suppressed by the addition of the baffles in the outer propellant tanks. Engine deflections in the order of 2 degrees resulted from an unexpected binding of the tilt device cam. The deflections were transients and appeared at intervals of approximately 13 seconds.

No active path guidance was flown on SA-2. However, passanger guidance hardware was onboard to establish the operational capabilities

~~CONFIDENTIAL~~

~~CONFIDENTIAL~~

of the equipment in the Saturn flight environment. All telemetered information and trajectory data comparisons indicate satisfactory performance of the equipment.

The over-all performance of the propulsion system was satisfactory. The total cluster performance was within 1.1 percent of predicted. Engine No. 2 operated at a thrust level some 3.6 percent lower than predicted due to an eroded turbine. Performance of other individual engines was satisfactory. The propellant tank pressurization system functioned as expected. All hydraulic systems operated well within the expected limits throughout the powered flight phase.

Vibration instrumentation showed values comparable to those of the SA-1 flight. The instrumentation on SA-2 was telemetered from a Single Side Band system which gives a frequency response (3 kc) much higher than the SA-1 measurements. When this increase in bandwidth is taken into consideration the vibration environments of the two vehicles are much the same.

Vehicle first mode body bending was detected by 10 bending accelerometers located at three stations along the vehicle. The first mode can be readily detected from the instrumentation, and second mode shows up at intervals of very short duration. The maximum bending amplitude recorded was 0.10 inches.

The thermal environment of SA-2 was not detrimental to vehicle performance. Total heat flux to both the flame and heat shields was much the same as in the SA-1 flight test. Thermal radiation to the heat shield was also close to that recorded on SA-1. No indication of fire or other abnormal heat sources was noted during the flight.

Base pressure of the vehicle as telemetered from four measurements was as expected and shows close agreement with wind tunnel results and the SA-1 flight test.

A total of 526 inflight measurements were flown on SA-2. Of this total, only 6 measurements failed, and 1 measurement partially failed. All RF systems performed satisfactorily.

## 1.2 TEST OBJECTIVES

The objectives of the Saturn SA-2 flight test were as follows:

### First Objective - Booster

Prove booster propulsion system, structural design, and control system - achieved.

~~CONFIDENTIAL~~

~~CONFIDENTIAL~~

3

Second Objective - Ground Support Equipment

Prove the operational concept of the supporting launch facilities for Saturn class vehicles, which include propellant systems, GSE, automatic checkout equipment, launch pedestal with holddown arms and other necessary handling and launching equipment - achieved.

Third Objective - Vehicle in Flight

(a) Aeroballistics

Confirm values of aerodynamic characteristics, correlating predicted stability and performance with that encountered in flight - achieved.

(b) Propulsion

Prove booster stage capable of providing the proper thrust to propel the Block I vehicle through the desired trajectory at the required velocity. Determine the in-flight performance of all eight engines, the controlling movements of the four outboard gimballed engines, engines cutoff, and propellant utilization - achieved.

(c) Structural and Mechanical

Verify the structural integrity of the Block I air frame, by correlating theoretical calculations and specification requirements with conditions encountered during flight - specifically, to determine the in-flight stress, vibration levels, and associated frequency content at various locations throughout the vehicle structure and component vibration environment. Measure the over-all structural response to define critical dynamic occurrences. Evaluate the presence of any excessive strain, body bending effects, and accumulate data to be used to determine the mode shape of the bending curve during flight - achieved.

(d) Guidance and Control

Demonstrate the capability of the G&C system, a modified ST-90 stabilized platform, to perform the required control, guidance, and operational sequence for the Block I flight tests. Specifically, to prove the system will establish an accurate space-fixed coordinate reference for determining vehicle altitude and providing an accurate coordinate velocity signal - achieved.

~~CONFIDENTIAL~~

Fourth Objective

A water cloud experiment accomplished by injecting the upper stages' water ballast (22,900 gallons) into the upper atmosphere at an altitude of 105 km by rupturing the upper stages with primacord - achieved.

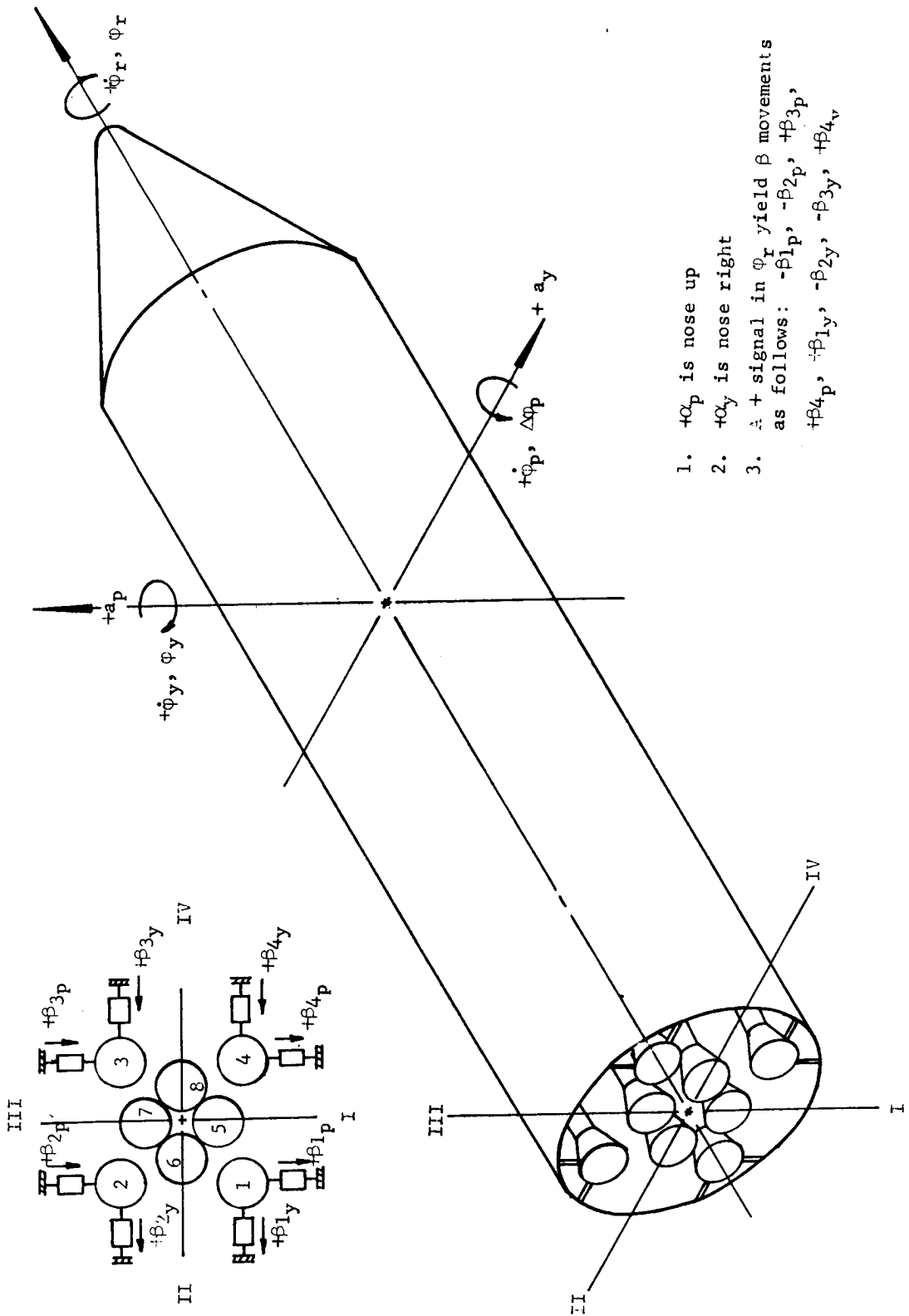
~~CONFIDENTIAL~~

5

## 1.3 TIMES OF FLIGHT EVENTS

Event	Actual Range Time (sec)	Predicted (sec)	Act - Pred (sec)
Ignition Command	-3.61	-3.36	-0.25
Thrust Commit	-0.24	-.05	-0.19
Launch Commit	0.13	.31	-0.18
First Motion	0.22	-	-
Liftoff Signal (Start Program Device)	0.41	0.41	0
Begin Tilt	10.41	10.41	0
Mach One Reached	48.68	48.35	0.33
Maximum Dynamic Pressure Occurred	59.0	61.13	-2.13
End Tilt	99.5	100.15	-0.65
Inboard Engine Cutoff	111.29	109.68	+1.61
Outboard Engine Cutoff	117.29	115.68	+1.61
End of Second Thrust Decay	119.84	119.28	+0.56
End of Test (Destruct)	162.56	160.56	+2.00

~~CONFIDENTIAL~~



SATURN BOOSTER POLARITY CHART

## 2.0 (U) INTRODUCTION

Saturn space vehicle SA-2 was launched at 0900:34 EST on April 25, 1962, from Saturn Launch Complex 34, Atlantic Missile Range, Cape Canaveral, Florida. SA-2 was the second vehicle to be flight tested in the Saturn C-1 R&D program. The major objective of this test was to evaluate the designs of the propulsion system, control system, and structure of the 1.3 million pound thrust booster.

This report presents the results of the Early Engineering Evaluation of the SA-2 test flight. The performance of each major vehicle system is discussed with special emphasis on malfunctions and deviations. The report is organized in ten major sections covering all vehicle systems and ground support equipment. Malfunctions and deviations are briefly summarized in the last section. Important supporting data such as mass characteristics are assembled in several appendices.

This report is published by the Saturn Flight Evaluation Working Group whose members are representatives from all Marshall Space Flight Center Divisions. Therefore the report represents the official MSFC position at this time. This report will not be followed by a similarly integrated report unless continued analysis and/or new evidence should prove the conclusions presented here partly or wholly wrong. Final evaluation reports will, however, be published by the MSFC Divisions covering some of the major systems and/or special subjects.

Special acknowledgement is made to the many individuals of the various MSFC Divisions and the Launch Operations Directorate who contributed to and helped establish this report.

### 3.0 (U) PRELAUNCH OPERATIONS

#### 3.1 SUMMARY

Saturn vehicle SA-2 was successfully launched from Complex 34 at 0900:34.41 EST on April 25, 1962.

The scheduled 10-hour countdown began at 2230 EST, April 24, 1962. No technical difficulties requiring holds were experienced during the countdown, but one hold was called by the Range when a ship entered the range area. All automatic propellant loading and sequencing processes were within expected tolerances. Launch preparations, execution of the countdown, and launch were as expected and successfully demonstrated the compatibility between the Ground Support Equipment and the flight configuration. Overall performance of the boosted flight was highly satisfactory. A destruct command for Project High Water was given by the Range Safety Officer when real time trajectory plots indicated an altitude of 105 km (162.15 seconds of flight).

#### 3.2 PRELAUNCH EVENTS

##### 3.2.1 PREPARATIONS

##### Emplacement, Assembly, and Checkout

Saturn vehicle SA-2 (consisting of the S-I first stage booster, second and third dummy stages S-IV and S-V, and payload body) arrived by the barge "Promise" at Cape Canaveral on February 27, 1962. The S-I booster was transferred to complex 34 the same day. On March 1, 1962 the S-I booster was erected on Pad 34 and stages S-IV, S-V, and payload body were transported to complex 34.

The following is a chronological summary of the work and milestones accomplished during the Saturn vehicle SA-2 erection and checkout.

March 2, 1962 thru March 9, 1962 - Fuel loading simulation tests, electrical continuity checks, positioning of retract arms under vehicle, and connection of long and short umbilical masts completed. Vehicle measuring calibrations and mechanical systems tests in process. Milestone - second and third dummy stages S-IV and S-V and payload body erected and mated to the S-I booster.

March 10, 1962 thru March 16, 1962 - Electro - mechanical components tests completed. Stabilized platform ST-90 laboratory checks in process. Milestone - LOX loading simulation test completed.

March 17, 1962 thru March 23, 1962 - Engine purge systems functional test, network malfunction sequence tests, C-band radar checks with range, overall test simulators installation, RF radiation shield installation, and stabilized platform ST-90 installation completed. Navigation ground support equipment calibration and functional cooling test in process. Milestone - Fuel and LOX systems - full tank pressure tests completed.

March 24, 1962 thru March 30, 1962 - Vertical and azimuth alignment, destruct command receivers functional tests, fire detection systems tests, hydraulic power swivel - check of outboard curtain on engine position number 2, and gas generator installation completed. Milestone - RF checks with range completed with service structure in both the launch position and around the vehicle.

March 31, 1962 thru April 6, 1962 - Long cable mast eject tests, overall test number 1, overall test number 2, overall test number 3, stabilized platform ST-90 alignment, verification of rate gyro alignment, heat shield installation, inboard curtain installation, holddown arms preload, retract arms preload, fuel density lines modification, and fuel sensing lines modification completed.

April 7, 1962 thru April 13, 1962 - Twist measurements, ground facilities measurements, vehicle measuring calibrations, telemeter measuring program change, simulated LOX loading test, water loading of stages S-IV and S-V, acoustical drag cable installation, and outboard curtain installation completed. LOX loading test, and telemeter packages 7 and 8 modification in process. Milestone - Fueling test including drain sequence completed.

April 14, 1962 thru April 20, 1962 - Overall test number 4, canister pressure check, telemeter packages 7 and 8 installation and check, fuel loading computer repair and check, primacord installation and pad safety acceptance, vehicle inverter replacement, change to permit integrator cutout with ignition command, redundant retract indicating switches installation completed. Modified hydraulic pressure differential indicators installation in process. Milestone - Simulated flight test and evaluation performed satisfactorily.

April 21, 1962 thru April 24, 1962 - Modified hydraulic pressure differential indicator installation, final launch detailed systems inspections, and fuel loading completed. Milestone - Countdown started.

April 25, 1962 - Launch

### Propellant Loading

The Saturn propellant loading system is designed to tank propellants to a given total weight at a ratio to give simultaneous depletion at cutoff. By design it is easier to drain fuel and tank LOX for final adjustments. At T-20 minutes in the countdown, a final fuel density check is made. Based on this density, fuel is drained and LOX tanked to the proportions necessary to give the designed total propellant load. This system is designed to load propellants to an accuracy of 0.25 percent total weight load.

The following is a summary of the fuel (RP-1) and liquid oxygen (LO<sub>2</sub>) loading operations performed for Saturn vehicle SA-2. Also included is a comparison of the propellant loading computer system readings to those of the backup systems.

1. Fuel (RP-1). RP-1 fuel was loaded on L-2 days. The vehicle was loaded to 15.7 percent fuel level to allow a fuel system leak check. This loading was accomplished by manually operating component switches at a flow rate of approximately 200 gallons per minute.

Upon completion of the leak check, the remainder of the fuel was loaded by the automatic computer circuit to 98 percent at a rate of approximately 2000 gallons per minute. At 98 percent the automatic circuitry entered into "slow fill" (approximately 200 gallons per minute) and the level settled to 92.7 percent due to the uneven filling of the tanks. The 98 percent signal was maintained by the circuitry and "slow fill" was continued until fuel tanking was complete at 100 percent.

A course adjust level was made on L-1 day by adding 1.5 percent to the density digital readout and adjusting per propellant loading tables, dated April 16, 1962. Flight propellant weights were based on a fuel density of 50.22 lb/ft<sup>3</sup> (Figure 3-1).

2. Liquid Oxygen (LO<sub>2</sub>). Liquid oxygen (LO<sub>2</sub>) was loaded on launch day. The vehicle was filled to approximately 14 percent for an LO<sub>2</sub> system leak check by using storage tank pressure in the precool sequence. This level was maintained by the replenish system after jumpering 75 percent and 98 percent signals into the system. The system remained in this condition for approximately 290 minutes.

The vehicle was filled to 100 percent at T-60 minutes by the automatic sequence of the LO<sub>2</sub> loading computer at an approximate rate of 3800 gallons per minute.

At the final adjust level (99.52 percent), a correction was made to the computer set pressure by inserting the corrected fuel density

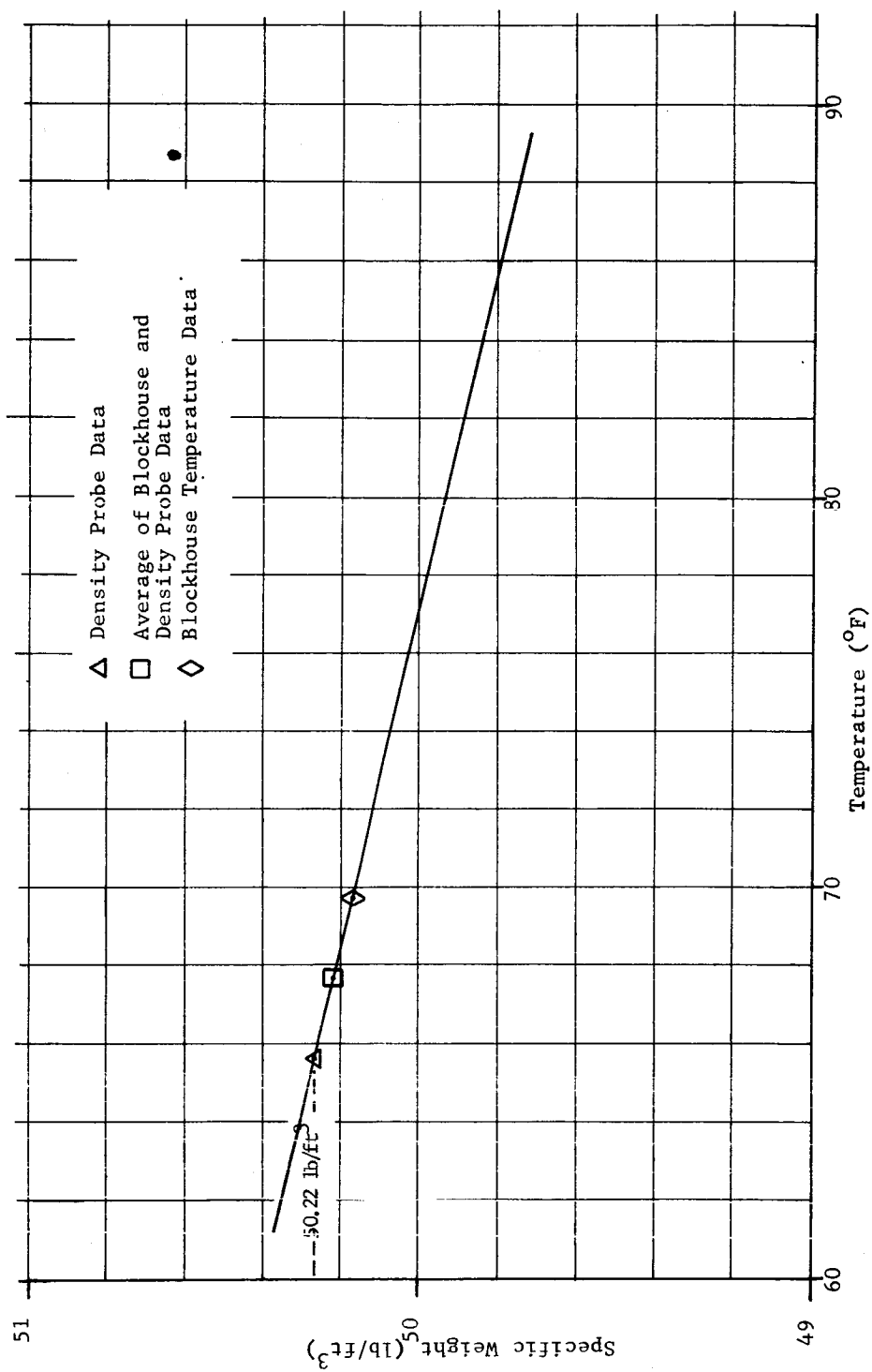


Fig. 3-1 RP-1 SPECIFIC WEIGHT VS TEMPERATURE

value into the computer. The correct fuel density value for the computer was obtained from the propellant loading tables, dated April 16, 1962.

3. Propellant Loading Computer System. The propellant loading computer system was backed up by a manometer system and cross checked with the on-board fuel temperature. At T-9 minutes the percent error between the computer readings and those of the Back up systems were as follows:

RP-1 Density computer vs. Density manometer = 0.431 percent

RP-1 Loading computer vs. Loading manometer = 0.206 percent

RP-1 Density computer vs. Temperature (Density) = 0.156 percent

LO<sub>2</sub> Loading computer vs. LO<sub>2</sub> manometer = 0.0364 percent (At T-25)

The computer system reading was used for the final adjustments to the propellant load.

### 3.2.2 COUNTDOWN

#### Weather

General weather conditions around Cape Canaveral at the time of launch were exceptionally good. There was no precipitation. Visibility was limited to 8 miles (12.87 km) by smoke and haze. Barometric pressure was 30.138 inches (1020.6 mbs), relative humidity 58 percent, and temperature 76° F. Surface winds were from 180 degrees (southerly) at 3.6 m/sec. For detailed and more complete atmospheric data, refer to Appendix E.

#### Holds

Launch countdown began at T-600 minutes at 2230 EST on April 24, 1962 and was continuous except for one 30-minute hold called by the Range at T-10 minutes (Figure 3-2). The events of the hold were as follows:

At approximately T-15 minutes the Range notified the test conductor of a ship in the downrange area. At T-12 minutes the Range Safety Officer declared the range foul with no estimate as to how long this condition would exist. The count was held at T-10 minutes; all RF equipment was secured, and the Range dispatched an aircraft to investigate. The ship was located approximately 60 miles downrange within the flight safety azimuth boundaries. Approximately 20 minutes later, the Range determined the exact position, direction, and speed of the ship and forecast a clear area at liftoff time. Approximately eight minutes was

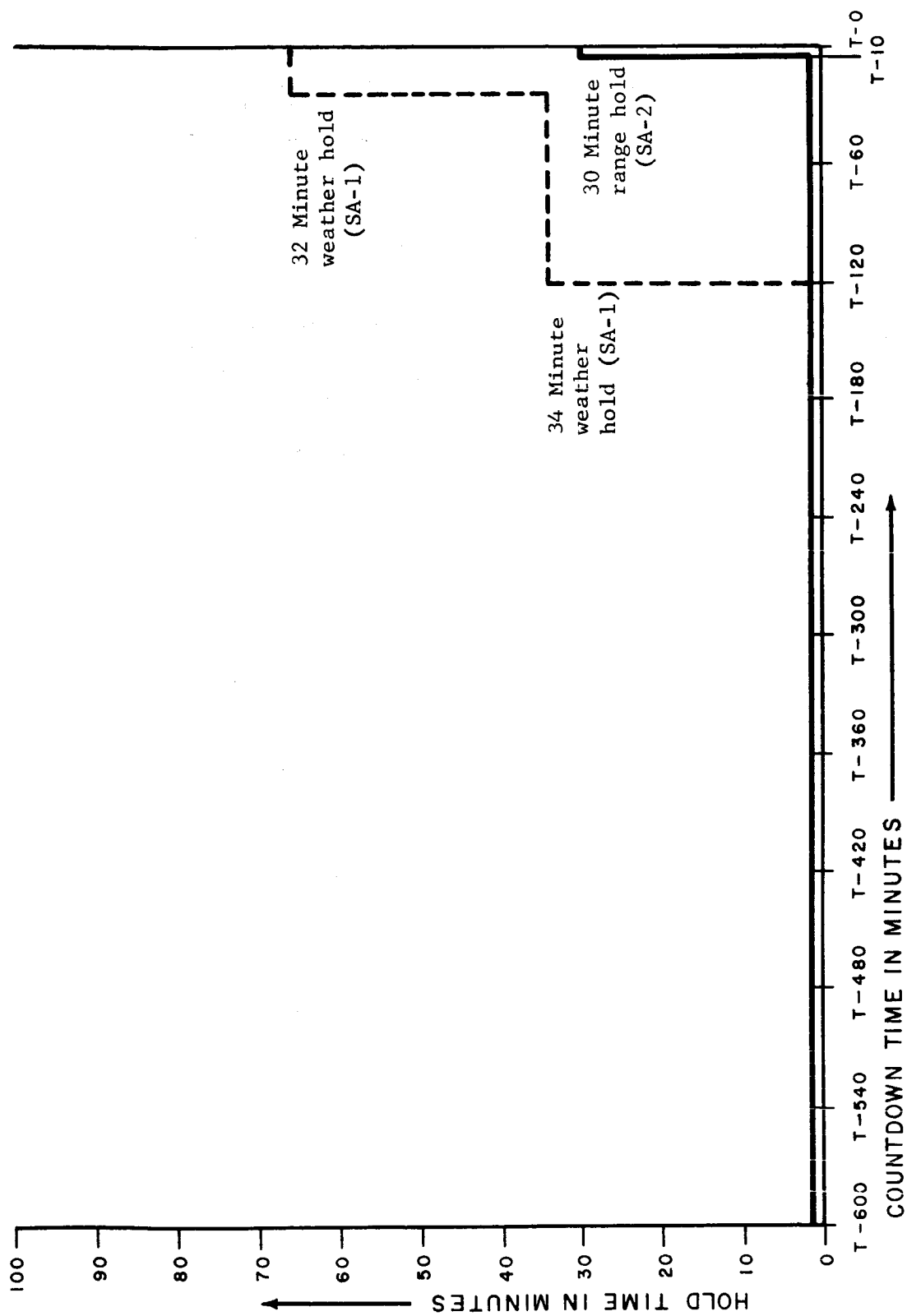


Fig. 3-2 HOLD TIME VS COUNT TIME

then required to reactivate and verify proper operation of the vehicle RF equipment in addition to repeating the command checks at the request of the Range Safety Officer. At 0850 EST the count was resumed.

#### Automatic Countdown

The automatic countdown sequence was initiated by the firing command 374 seconds prior to ignition command (T-0).

The automatic countdown operation was normal. Comparisons of predicted and actual times for ground sequence events are listed in Appendix C. The "actual time" readings were read from the sequence records. Starting with SA-2, the countdown sequence times were also printed out by a computer output. The comparison of the sequence record results with the computer outputs (digital output for events) showed that excellent results were obtained from ignition command to liftoff. During this period the computer was in the fast scan mode which has an accuracy of  $\pm 4$  ms. The events before ignition command (slow scan mode) were uncertain by as much as 1 second. The system is to be improved for SA-3 so that the maximum slow scan error will be 0.1 second.

#### 3.2.3 HOLDDOWN

##### Vehicle

Engine start and transition were smooth with all engines receiving a positive ignition from a LOX lead in the gas generator ignition sequence. Engine #2 turbine was possibly eroded from a too advanced LOX lead (.069 sec) causing low performance during flight for this engine. All critical blockhouse measurements were within the established redline values or were sufficiently close to specified values to proceed with the launch. Maximum and minimum values observed during the countdown are included in Appendix B.

A rippling in the tail shroud and considerable vibrations were observed in the areas around the retractable support arms and holddown arms during ignition and transition.

The following vibration levels were recorded during the period from ignition to launch commit:

<u>Meas.</u>	<u>Engine Nr.</u>	<u>Max. (peak-to-peak)</u>	<u>Average (peak-to-peak)</u>
XE57-1	1	23g	18g
XE57-2	2	20g	15g
XE57-3	3	25g	18g
XE57-4	4	25g	18g
XE57-5	5	35g	15g
XE57-6	6	20g	12g
XE57-7	7	25g	15g
XE57-8	8	30g	18g

Since shroud undulation was observed during SA-1 ignition, a checkered pattern was painted on the shroud of SA-2 to facilitate a detailed analysis of the skin undulation.

Fire detection measurements XC114 and XC115 gave no indication of a temperature rise during the period between ignition and launch commit. Measurements XC116 and XC117 showed slight increases (approx. .6 millivolt) between T + 2 and T + 3.3 sec. These slight increases were not sufficient to cause a cutoff signal to be given. A 2.5 millivolts/sec increase is required to give cutoff.

#### Ground Support Equipment

In general, the SA-2 postlaunch damage is considered equivalent to that observed after SA-1; however, in some areas the damage was more severe and in other areas less severe. Evaluation of the overall resultant damage indicates that it is roughly equivalent to that of SA-1. The following contains prelaunch malfunctions and an assessment of the damage inflicted on the ground support equipment.

The short cable mast fuel injector manifold GN<sub>2</sub> purge line at Fin IV disconnected from the vehicle prematurely (approximately two seconds before liftoff). The function of this line was to purge the thrust chamber fuel injector manifold with 500 psi GN<sub>2</sub> before ignition (beginning at T-36 seconds). There were no consequences caused by this early disconnect.

The long cable mast basic structure was destroyed. There are some components of the complete installation which will be reusable in their present condition (i.e. the base assembly, guy cable tie-downs, and preflight cooler package). The long cable mast remained erect a few seconds after launch and then it collapsed, presumably due to a combination of blast pressure and heat. The resultant damage is shown in Figure 3-3.

The short cable masts and tail cable masts suffered damage ranging from mild to moderately severe. The electrical cables and some minor components will have to be replaced, but the major portions of the basic installation will be reusable after appropriate refurbishment.

The propellant loading installation suffered damage ranging from mild to severe. The fuel loading mast received very minor damage. The LOX loading mast received severe damage in that the upper portion failed structurally, presumably due to blast pressure. Postlaunch inspection revealed that some of the welds in the upper mast support framework had what may have been marginal fillets. This could have contributed directly to the structural failure. The flexible coupling assemblies and light gauge components of the LOX transfer piping and LOX replenishing installation were burned away (Figure 3-4). The heavier piping remained and will be reused after appropriate cleaning and reworking.

The holddown arms and valve panels received only superficial to minor damage. The general condition of the holddown arms is shown in Figure 3-4.

The retractable support arms received only superficial to minor damage (Figure 3-4). The vehicle support point opening door supports which were mounted on the retractable support arms were completely destroyed. Some of the mounting brackets were damaged or burned away.

The torus ring suffered minor damage in that approximately four water spray nozzles were burned off or severely damaged at four locations, corresponding to outboard engine jet impingement. There was also some minor burning away of various retaining bands.

The boattail conditioner unit and water quench installation received minor to moderate damage. This damage will result in extensive minor refurbishment of a relatively insignificant nature.

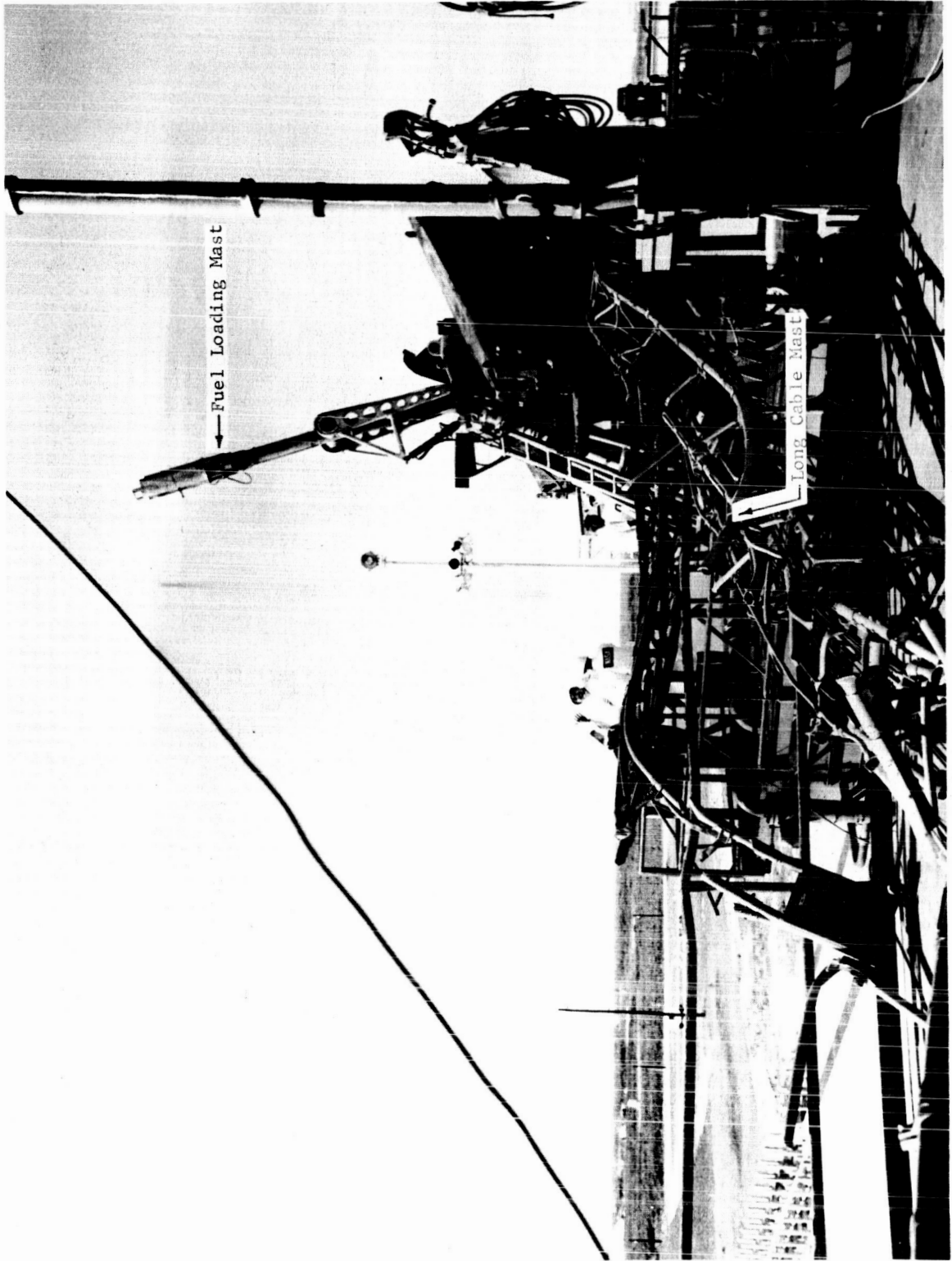


FIGURE 3-3 VIEW OF LONG CABLE MAST

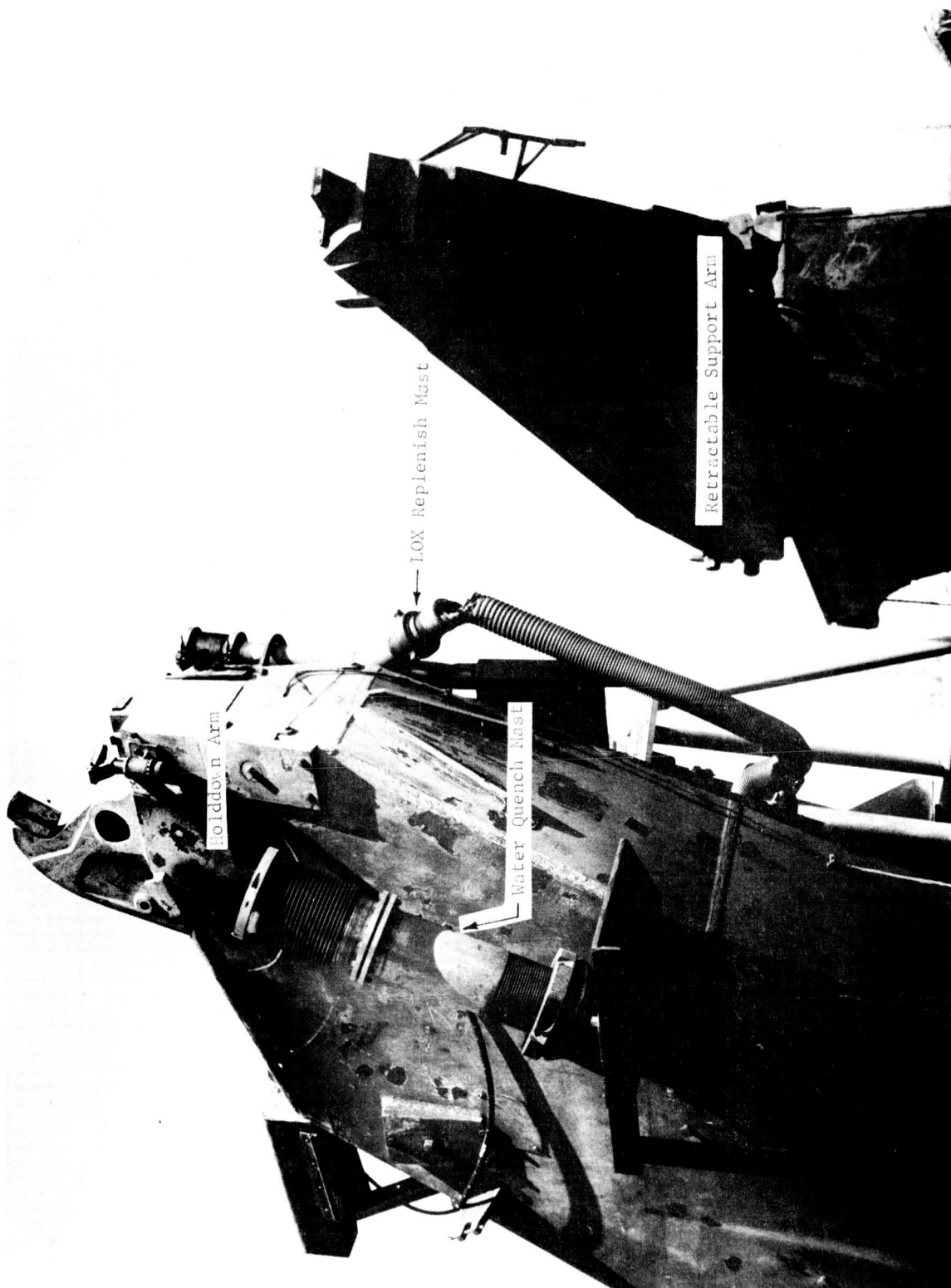


FIGURE 3-4 VIEW OF HOLDDOWN ARM SHOWING WATER QUENCH MAST AND LOX REPLENISH MAST

The turbine exhaust ducts received minor to severe damage. This damage will require cutting and rewelding some components but no replacement.

The launcher pneumatic installation received moderate damage. One 3000 psig GN<sub>2</sub> line ruptured due to heat and the internal pressure. This was the retractable support arm supply inter-connect. The other exposed portions of the pneumatic installation received scorching and burning and will necessitate replacement. The portion within the confines of the torus ring was protected by the steel plates and insulation added after launch of SA-1.

The flame deflector suffered minor damage. There was a small amount of metal erosion at the points of engine jet impingement, and some slight warping as evidenced by observation of support shims; however, the deflector will be usable after minor rework. The conditions described are shown in Figure 3-5.

The retractable support arms returned to the support position after vehicle liftoff. This was caused by last minute changes of timer sequences at the Cape. Normal operation of the retractable support arms consists of the following:

- 1.) At ignition command the retract support arms are given a hold signal to maintain the support arms in the hold position to protect them from pulling out due to vibrations.
- 2.) At Thrust Commit the hold signal is disconnected and a retract signal is initiated.
- 3.) The support arms are retracted and remain unless difficulties occur causing cutoff signal to be given.

Prior to launch of SA-2 it was decided to include a check to determine whether all plugs disconnected. This is used only for emergency measures if the manual cutoff is not given and could save the vehicle only in case the holddowns failed to release. In establishing this circuit for SA-2, the relay (K73) was not completely cleared, and when the check was made some 8 seconds after ignition command, the signal was given for support arms to move to the support position. This will be corrected before the next launch.

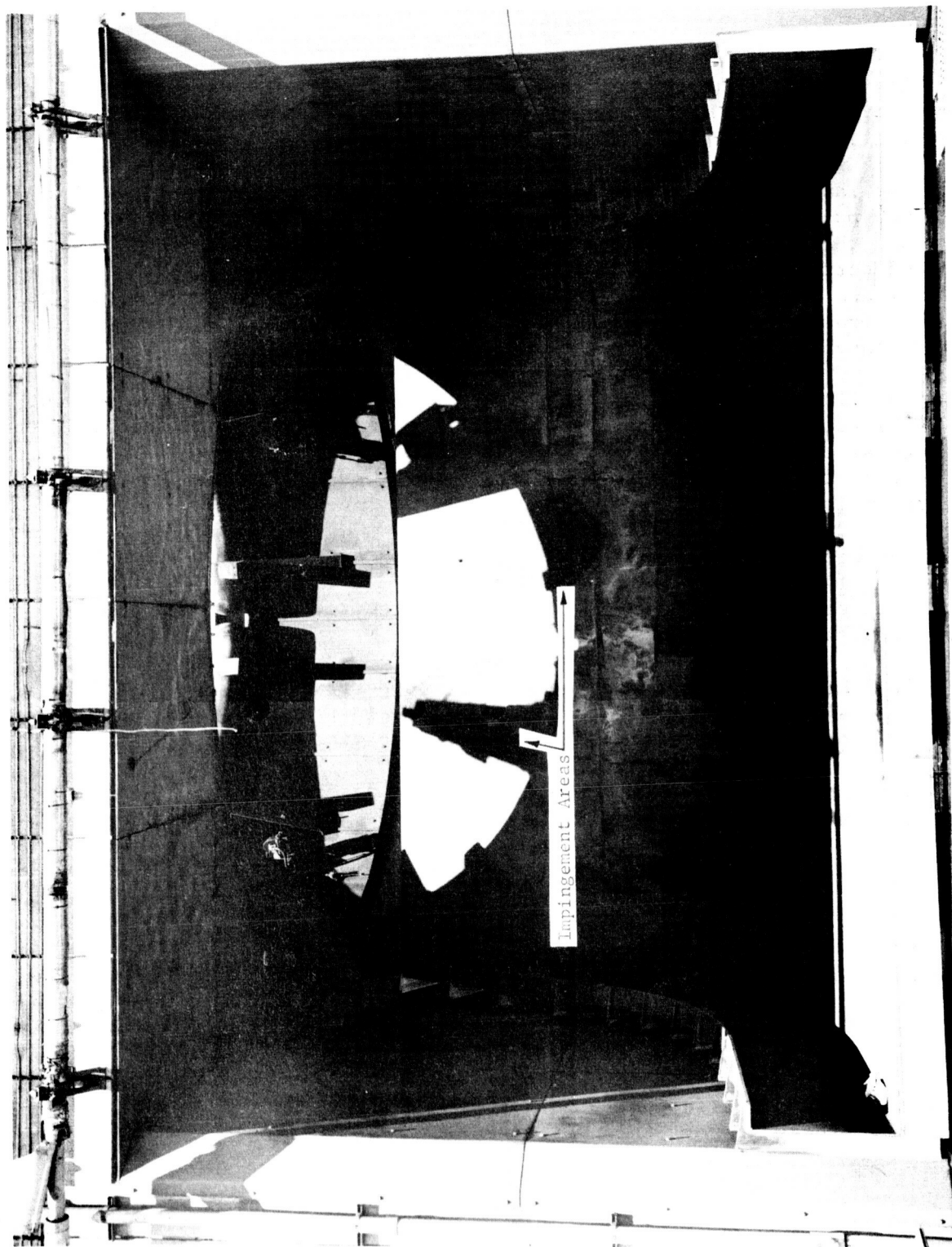


FIGURE 3-5 VIEW OF FLAME DEFLECTOR SHOWING AREAS OF JET IMPINGEMENT

TABLE 3-I  
PRE-LAUNCH MILESTONES

Date	Event
February 27, 1962	S-I booster, second and third dummy stages S-IV and S-V, and payload arrived Cape Canaveral on barge "Promise"
March 1, 1962	S-I booster erected on launch pedestal at pad 34
March 2, 1962	Dummy stages S-IV, S-V and payload assembled to the S-I booster
March 27, 1962	Service structure removed for RF checks
April 9, 1962	Fuel test completed
April 12, 1962	LOX loading test completed
April 16, 1962	Overall test No. 4 completed
April 19, 1962	Simulated flight test performed
April 21, 1962	Engine swivel checks completed
April 23, 1962	RP-1 fuel loaded
April 25, 1962	Launch

#### 4.0 (C) TRAJECTORY

##### 4.1 SUMMARY

The actual flight path of SA-2 was close to the predicted. The actual trajectory during powered flight, however, was slightly lower than predicted due to lower accelerations. The earth-fixed velocity after outboard engine cutoff was proportionally higher due to the later cutoff time of the actual flight. Destruct of SA-2 for Project High Water occurred at 162.56 sec range time at an altitude of 105.3 km.

The flow rates for the SA-2 flight were lower than nominal causing both the cutoff to occur later and the accelerations to be lower than expected. This caused small differences between actual and nominal trajectory parameters. The range was 1.33 km more at OEEO than expected, and the altitude was 1.33 km higher. The largest deviation was 2.9 m/s less earth-fixed velocity at OEEO than expected.

The postflight precision trajectory is extensively used in analyzing the guidance and propulsion systems (Sections 5.0 and 7.0).

##### 4.2 TRACKING ANALYSIS

Comprehensive tracking coverage was obtained for the entire flight. The launch phase coverage was very good.

###### 4.2.1 DATA SOURCES

###### External

The preliminary UDOP data was received from the Tracking Reduction Section, Computation Division, within one day after the firing; however, no downrange UDOP data was obtained on SA-2. The final Radar, Azusa, and Fixed Camera data was received six days after the firing. There was redundant coverage from the time of liftoff to destruct at 162.56 sec. All available tracking data is shown in Table 4-I.

###### Onboard

The onboard measurements used to establish the trajectory are shown in Table 4-I.

###### 4.2.2 DATA UTILIZATION

The postflight trajectory was established principally from external data, but the telemetered accelerations were also used in establishing both the Mach 1 interval, and the cutoff and thrust decay profile.

TABLE 4-I DATA SOURCES FOR PRECISION TRAJECTORY

Data Source	Interval
External	
Fixed Camera (light)	.451 - 7.988 sec
Fixed Camera (target track)	.451 - 7.988 sec (intermittent)
Fixed Camera (nose)	.451 - 20.662 sec
Theodolite	4.50 - 127.25 sec 130.00 - 162.00 sec
UDOP	0.0 - 162.50 sec
Mark II Azusa	15.0 - 162.00 sec
FPS-16 Radar 1.16 (Cape)	0.0 - 162.80 sec
FPS-16 Radar 1P.16 (PAFB)	24.0 - 111.20 sec
FPS-16 Radar 3A.16 (Carter Cay)	64.5 - 162.80 sec
Supporting Flight Data	
Tilt Program	Powered Flight
Guidance Outputs (Meas: I1-15, I2-15, and I3-15)	0.0 - 162.56 sec
Longitudinal Acceleration Meas: F5-13 Sweeper F6-13 Coarse F7-13 $\pm 1$ g	0.0 - 111.29 sec 0.0 - 162.56 sec Decay - 162.56 sec
Cutoff Signals	-
Observed Meteorological	0.0 - 93.00 sec
Chamber Pressure Meas: D1-1, D1-2, D1-3, D1-4, D1-5, D1-6, D1-7, D1-8	0.0 - End outboard decay
$\Delta\phi_p$ , Meas: H1-15	0.0 - 162.56 sec
$\phi_y$ , Meas: H2-15	0.0 - 162.56 sec
*Separation, Anvil vs Vehicle Support Block YL1, YL2	-4.0 - 1.0 sec

\* Pad measurement

External

The tracking data used to establish the trajectory is given below:

<u>Data Source</u>	<u>Interval</u>	<u>*Estimated Accuracy of Position Data</u>
Fixed Camera (light)	0.0 - 7.50 sec	.05 m
Fixed Camera (nose)	7.50 - 20.00 sec	.55 m
Azusa	20.00 - 162.56 sec	3.2 m

\* Estimated accuracies are the worst which occurred during the specified time interval.

There were three sources of Fixed Camera data on SA-2. These were:

- 1) "Close-in" data obtained from track of the west CZR light located over Fin position III at Station #889.
- 2) "Close-in" data obtained from track of the Northwest paint pattern located between Fin positions II and III at Station #889.
- 3) "Regular" data obtained from track of the nose of the vehicle.

Data of an exceptionally high quality is a necessity for accurately determining the accelerations during the first few seconds of flight. The standard deviations of the acceleration components from the three sources of Fixed Camera data are given below:

	$\sigma \ddot{X}$ (m/s <sup>2</sup> )	$\sigma \ddot{Y}$ (m/s <sup>2</sup> )	$\sigma \ddot{Z}$ (m/s <sup>2</sup> )
Light	$\pm .012$	$\pm .009$	$\pm .009$
Target Track	$\pm .011$	$\pm .010$	$\pm .014$
Nose	$\pm .054$	$\pm .086$	$\pm .058$

Practically all acceleration during the first few seconds of flight is in the vertical direction. The Fixed Cameras tracking either the light source or the paint pattern (target track) are about 8-10 times more accurate in this direction than the Fixed Camera tracking the nose. The Fixed Camera reduction using the target track provided data equivalent in accuracy to that of the light source. However, two seconds of the target track data was lost because this target was obscured by smoke.

There was some degradation in the quality of the Radar and Azusa data during the first 20-35 seconds of flight because of multipath effects.

There was also a quite significant bias in the UDOP data after inboard engine cutoff (see Figure 4-2); however, this may have been attributable to poor tracking geometry because of lack of downrange data.

The relative motion between the vehicle and support arms was determined from pad measurements YL-1 and YL-2 which were mounted on support arms R-2 and R-4, respectively. These measurements were of a plunger type with a range of 0-1.3 inches. These measurements are shown from ignition command to liftoff signal in Figure 4-1. The vehicle moved from the support arm to the holddown arms (about 0.5 inches) about 1.3 sec after ignition command. The vehicle was released by the holddown arms 3.82 sec after ignition command or at 0.21 sec range time. First motion of the vehicle was considered to occur 10 ms later or at 0.22 sec range time which was 0.19 sec earlier than the telemetered liftoff signal.

#### Onboard

Telemetered accelerations in conjunction with tracking data were used to determine the acceleration profile during the Mach 1 interval (43.0 - 54.0 sec).

The cutoff signals, time of decay of the chamber pressures, and the telemetered accelerations were used to establish the shape of the acceleration profile during the time period of cutoff transients (105.0 - 119.0 sec).

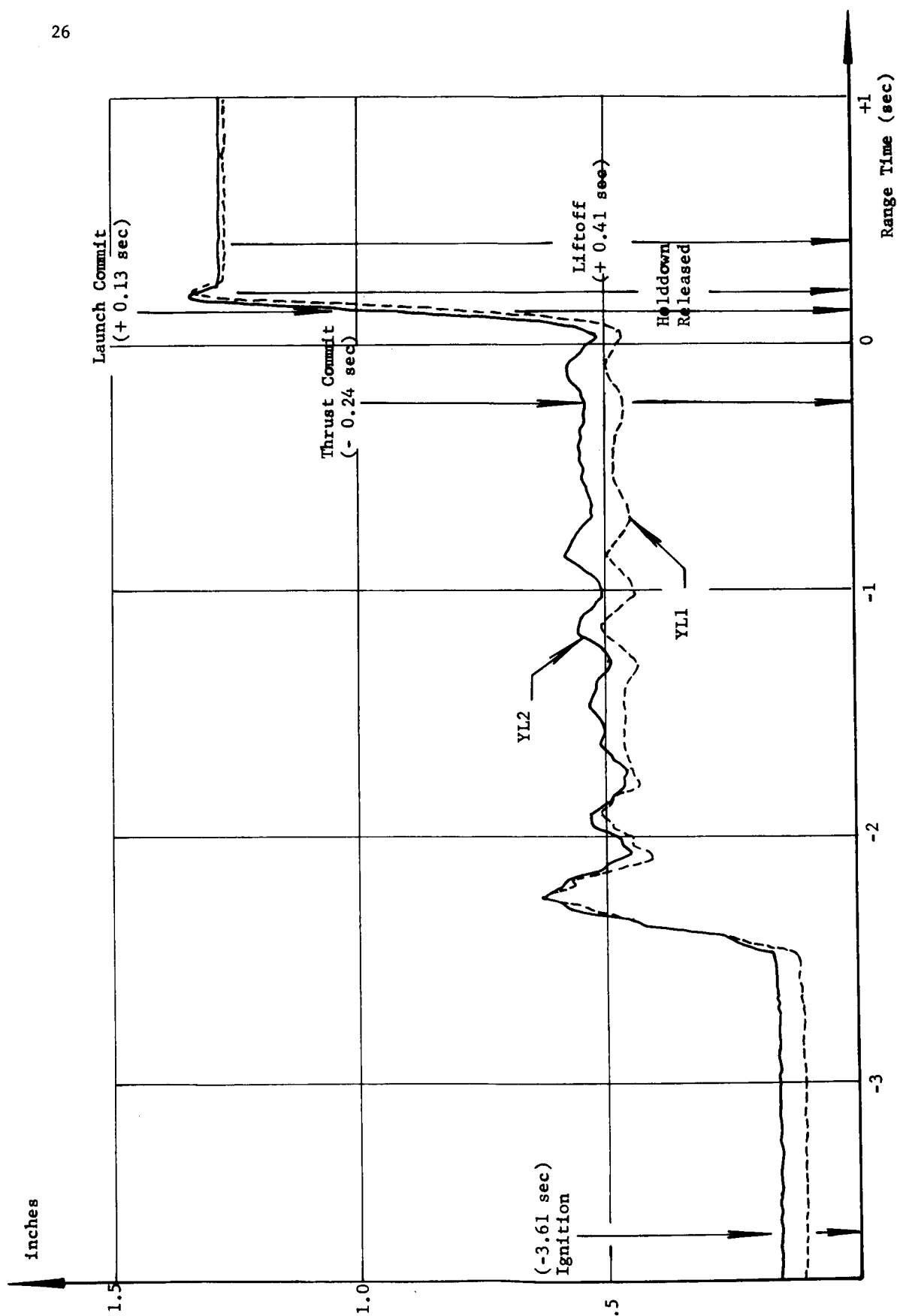


Fig. 4-1 SEPARATION, ANVIL VS VEHICLE SUPPORT BLOCK

74

#### 4.2.3 ERROR ANALYSIS OF ACTUAL TRAJECTORY

Comparisons of the tracking data with the post-flight trajectory are given below (also see Figure 4-2).

	Inboard Engine Cutoff			160 sec		
	$\Delta X$ (m)	$\Delta Y$ (m)	$\Delta Z$ (m)	$\Delta X$ (m)	$\Delta Y$ (m)	$\Delta Z$ (m)
Theodolite-Postflight	-15	6	4	N/A	N/A	N/A
Radar-Postflight	-5	-5	12	-5	7	16
*UDOP-Postflight	-2	5	6	-45	30	37

\* The differences between UDOP and the postflight trajectory at outboard cutoff were:

$$\Delta X = -24 \text{ m}, \Delta Y = 23 \text{ m}, \Delta Z = 20 \text{ m}$$

This bias in the UDOP data occurred at the time of inboard engine cutoff.

#### 4.3 ACTUAL AND PREDICTED TRAJECTORY COMPARISON

Mach number and dynamic pressure are based on measured Cape Canaveral meteorological data to 31.6 km altitude in the ascent and adjusted to the 1959 ARDC atmosphere at 47.0 km. The 1959 ARDC atmosphere was used above 47.0 km.

##### 4.3.1 POWERED FLIGHT

Actual and nominal altitude, range and cross range ( $Z_e$ ) are shown in Figure 4-3. Earth-fixed velocity is shown in Figure 4-4 (Ref. 4).

Vehicle displacement versus time and altitude during early flight is shown in Figure 4-5 (see paragraph 6.2.1). The vehicle's lateral displacement was 0.9 m at the time the vehicle exceeded the height of the proposed umbilical tower for use on Block II vehicles.

Mach number and dynamic pressure (both actual and nominal) are shown in Figure 4-6.

Longitudinal acceleration for the powered flight is shown in Figure 4-7 and for the cutoff and decay interval in Figure 4-8.

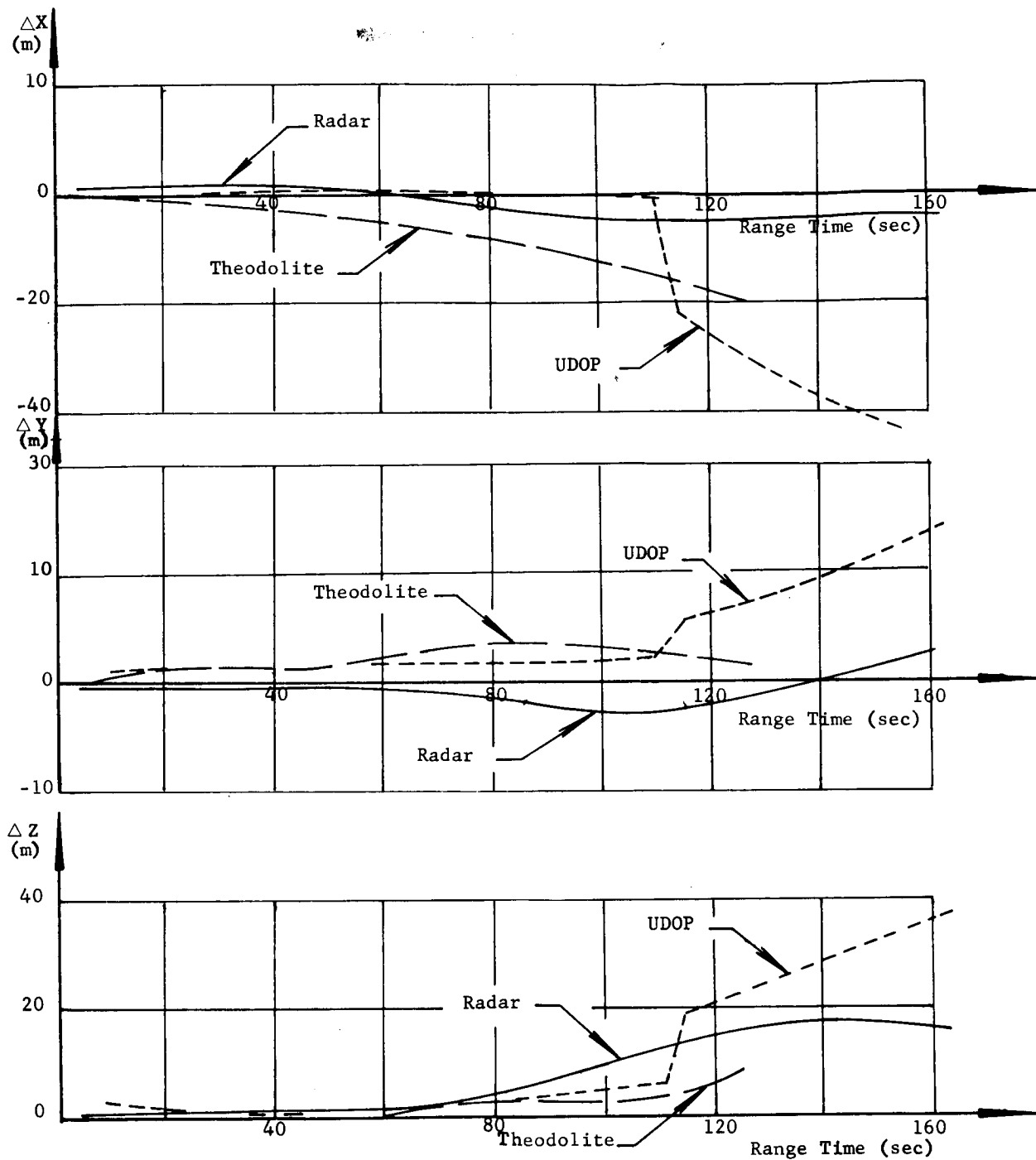


Fig. 4-2 TRACKING COMPARISONS  
(TRACKING-REFERENCE)

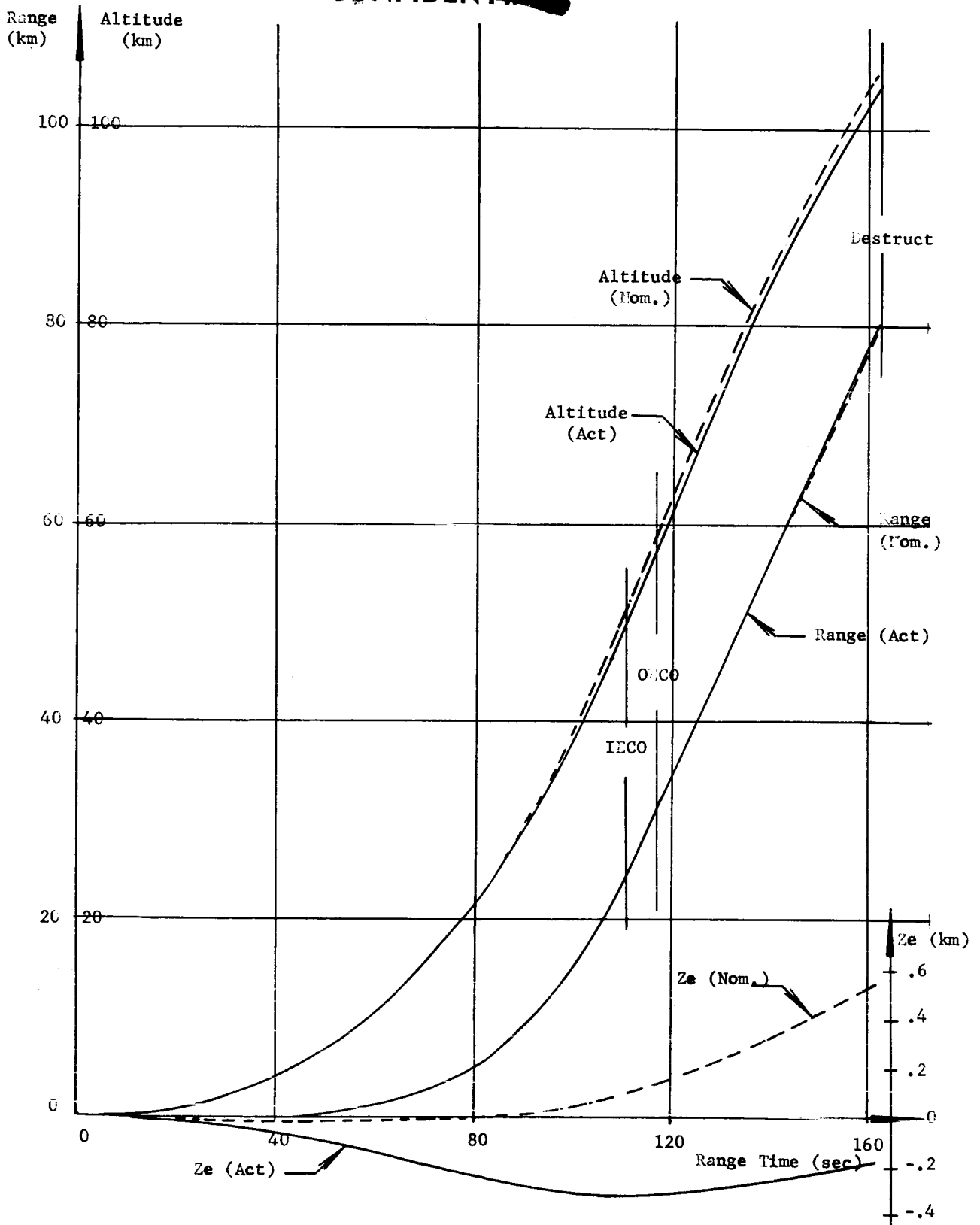


Fig. 4-3 TRAJECTORY

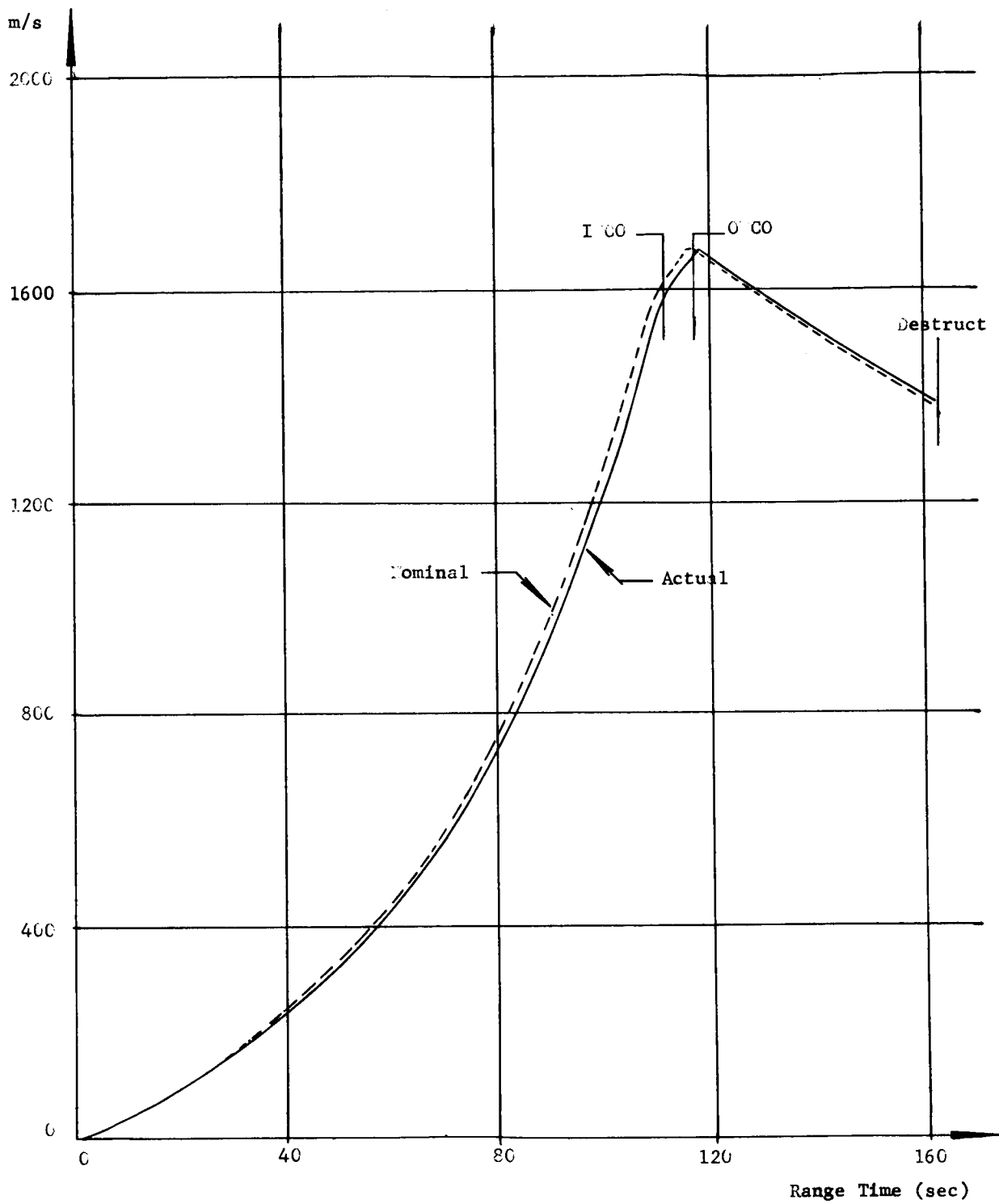


Fig. 4-4 EARTH-FIXED VELOCITY

~~CONFIDENTIAL~~

MPR-SAT-WF-62-5

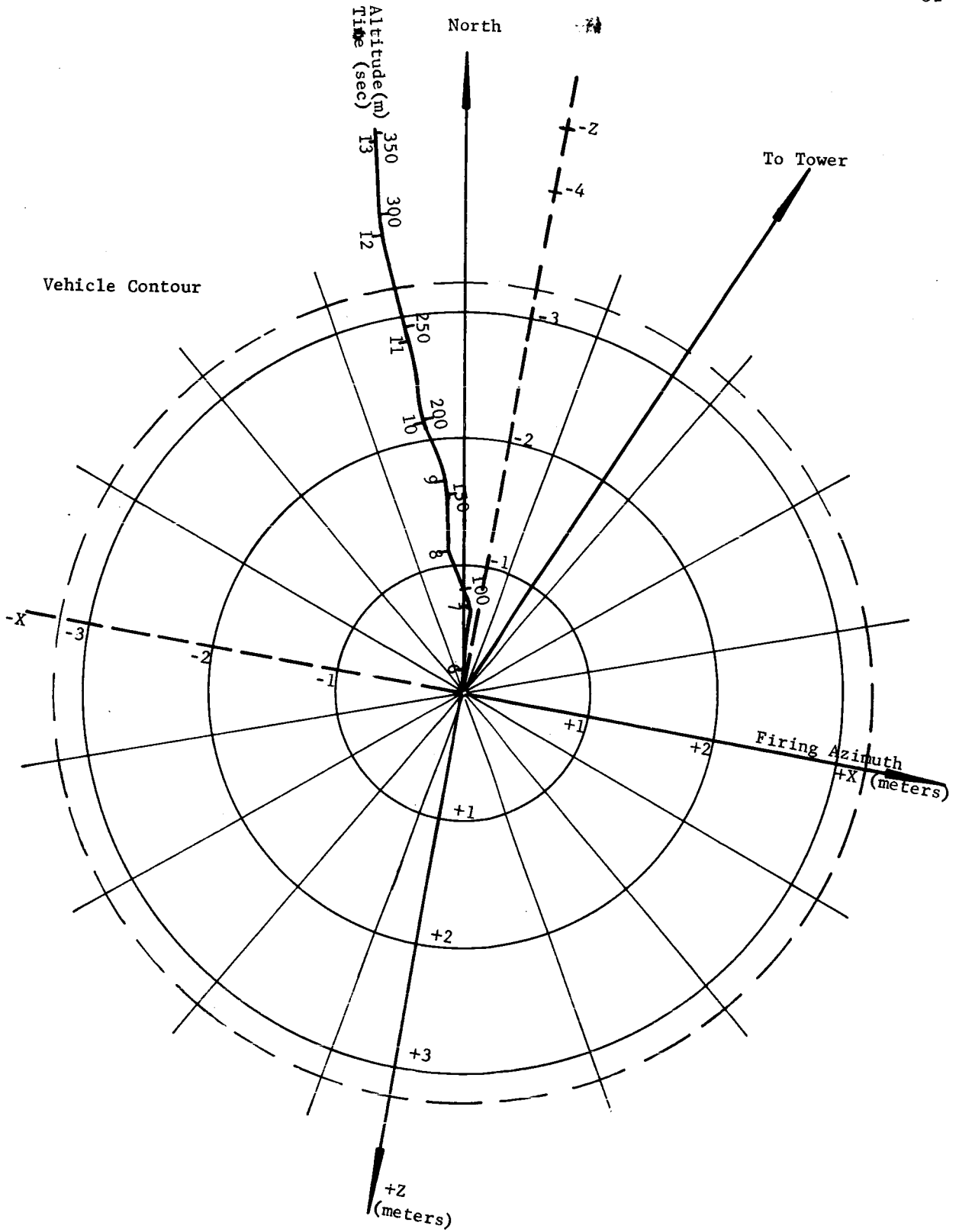


Fig. 4-5 ALTITUDE AND DISPLACEMENT IMMEDIATELY AFTER LIFTOFF

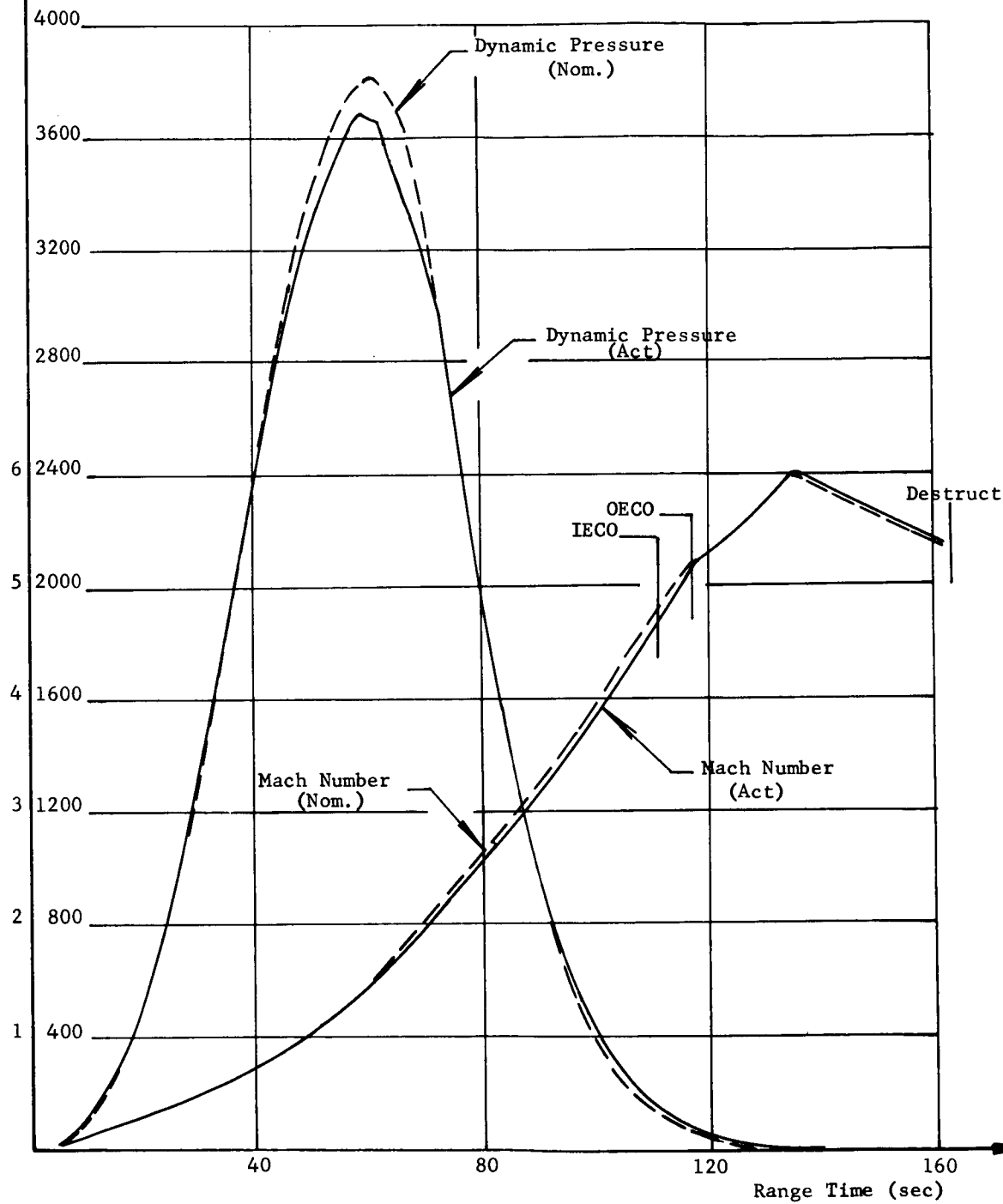
Mach Dynamic Pressure  
kp/m<sup>2</sup>

Fig. 4-6 DYNAMIC PRESSURE AND MACH NUMBER

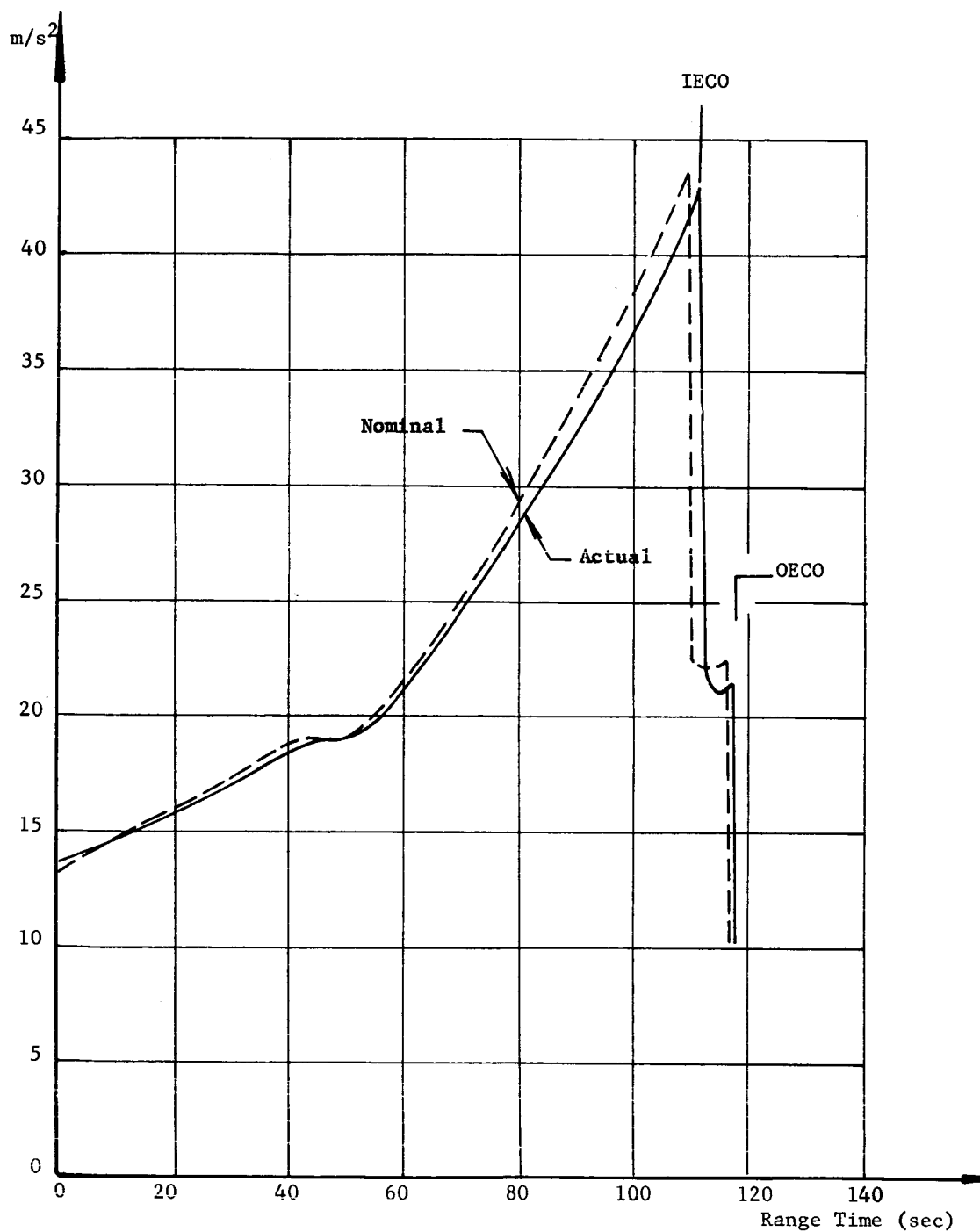


Fig. 4-7 LONGITUDINAL ACCELERATION

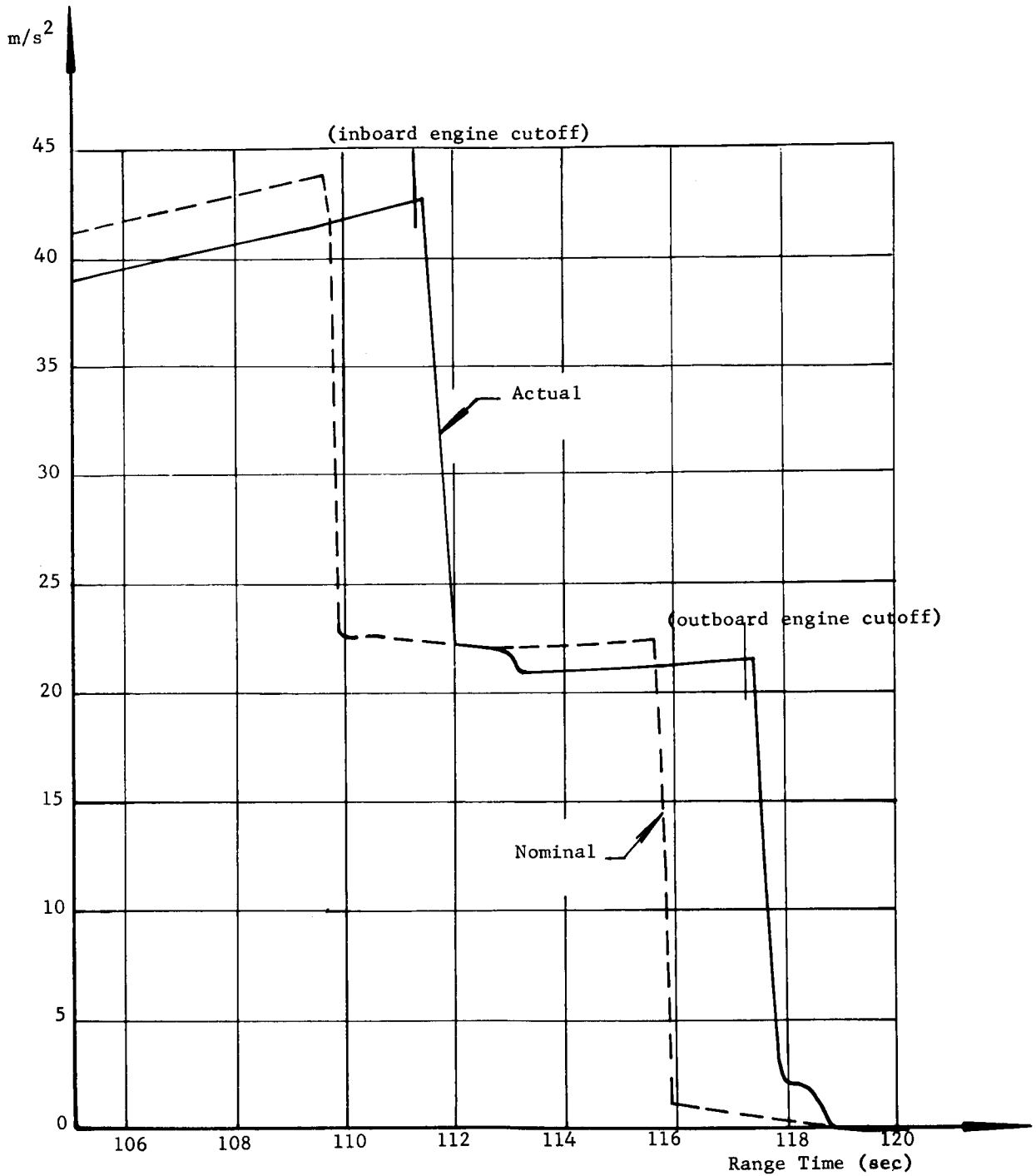


Fig. 4-8 LONGITUDINAL ACCELERATION (CUTOFF AND DECAY PROFILE)

~~CONFIDENTIAL~~

A number of significant events, such as first motion, Mach 1, and destruct are given in Table 4-II. Maximum values for dynamic pressure, longitudinal acceleration, and earth-fixed velocity are also shown. Both actual and nominal values and their differences are given.

#### 4.3.2 CUTOFF

A comparison of the actual parameters with the nominal at both inboard and outboard cutoff is shown in Table 4-III. The significant differences are due to the lower than nominal accelerations which resulted in a late cutoff time.

##### Thrust Decay

The velocity gain during thrust decay of both inboard and outboard engines is compared with the nominal below:

	Inboard	Outboard
Actual (m/s)	8.3	7.0
Nominal (m/s)	8.2	8.6
Act-Nom (m/s)	0.1	-1.6

Table 4-III indicates that the difference between actual and nominal earth-fixed velocity at IECO is +2.5 m/s and at OECO is -2.9 m/s or a relative velocity deficit between the points of 5.4 m/s. Since the velocity gain from inboard engine thrust decay is the same for actual and nominal, this velocity deficit must have occurred during the six additional seconds of outboard engine operation and is probably due to a combination of higher mass and lower thrust. The velocity comparison at IECO and OECO for SA-1 indicates essentially the same deficit.

Actual and nominal longitudinal acceleration for SA-1 and SA-2 during the six additional seconds of operation of the outboard engines is shown in Figure 4-9 with time referenced to IECO in each case. The nominal longitudinal acceleration is about  $1 \text{ m/s}^2$  higher in each case.

~~CONFIDENTIAL~~

TABLE 4-II SIGNIFICANT EVENTS

Event	Parameter	Actual	Nominal	Act-Nom
First Motion	Range Time (sec)	0.22	0.22	0
	Long't. Acceleration ( $\text{m/s}^2$ )	13.56	13.20	0.36
Mach 1	Range Time (sec)	48.68	48.35	0.33
	Altitude (km)	6.63	6.52	0.11
Maximum Dynamic Pressure	Range Time (sec)	59.00	61.13	-2.13*
	Dynamic Pressure ( $\text{kp/m}^2$ )	3676	3810	-134
	Altitude (km)	10.39	11.36	-0.97
Maximum Longitudinal Acceleration	Range Time (sec)	111.42	109.78	1.64
	Long't. Acceleration ( $\text{m/s}^2$ )	42.82	43.58	-0.76
Maximum Earth-fixed Velocity	Range Time (sec)	117.60	116.01	1.59
	Earth-fixed Velocity ( $\text{m/s}$ )	1676.3	1680.3	-4.0
Destruct	Range Time (sec)	162.56	160.56	2.00
	Altitude (km)	105.27	105.00	0.27
	Range (km)	80.93	78.59	2.34
	Elevation Angle from Pad (deg)	51.85	52.59	-0.74

\* Maximum dynamic pressure for actual and nominal are not directly comparable since the density-altitude curves are not identical.

~~CONFIDENTIAL~~

CONFIDENTIAL

TABLE 4-III CUTOFF CONDITIONS

Parameter	IECO			OEEO		
	Actual	Nominal	Act-Nom	Actual	Nominal	Act-Nom
Range Time (sec)	111.29	109.68	1.61	117.29	115.68	1.61
Range (km)	25.11	23.87	1.24	31.46	30.13	1.33
Altitude (km)	50.50	49.62	0.78	57.80	57.11	0.69
Cross Range (Ze) (km)	-0.33	0.09	-0.42	-0.33	0.13	-0.46
Earth-fixed Velocity (m/s)	1583.3	1580.8	2.5	1673.5	1676.4	-2.9
Longitudinal Acceleration (m/s <sup>2</sup> )	42.69	43.49	-0.80	21.33	22.33	-1.00
Velocity Vector Elevation (deg)	49.56	50.60	-1.04	48.18	49.19	-1.01
Velocity Vector Azimuth (deg)	99.86	100.24	-0.38	99.97	100.31	-0.34

CONFIDENTIAL

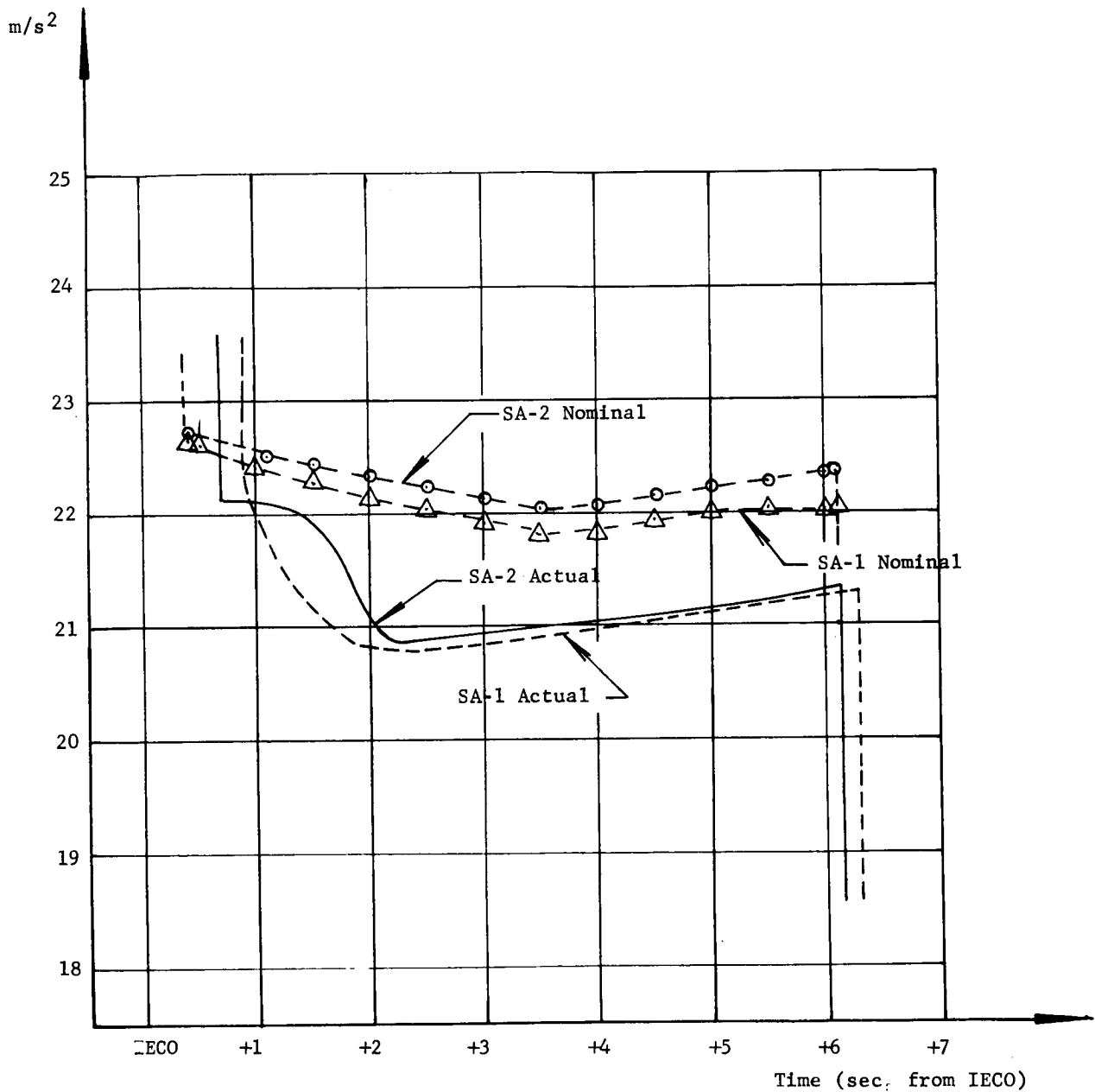
~~CONFIDENTIAL~~

Fig. 4-9 OUTBOARD ENGINE LONGITUDINAL ACCELERATION

~~CONFIDENTIAL~~

~~CONFIDENTIAL~~

## 5.0 PROPULSION

### 5.1 (C) SUMMARY

Over-all propulsion system operation during the flight test was very satisfactory. The total cluster performance averaged within approximately one percent of predicted. Individual engine performances were satisfactory with the exception of the engine at position 2 which performed approximately 3.6 percent below the predicted level. Examination of the data showed this engine to have had an abnormally long LOX lead (approximately 67 ms) in the gas generator, which caused erosion of the turbine. This erosion caused a decrease in turbine efficiency, resulting in a decrease in the engine performance level. The propellant tank pressurization systems functioned properly, resulting in satisfactory tank pressures during flight. All hydraulic systems operated well within the expected limits throughout powered flight.

The vehicle longitudinal thrust was 1.1% lower, total flow rate 2.4% lower, and specific impulse 1.4% higher than the corresponding predicted values. Cluster performance was derived by using telemetered and tracking measurements in a simulation of the actual trajectory. Individual engine performance was derived by a reconstruction of the flight. These two independent methods showed results which were in agreement within less than two tenths of one percent.

### 5.2 (U) INDIVIDUAL ENGINE PERFORMANCE

A schematic of the H-1 engine which was clustered for the SA-2 booster stage is shown in Figure 5-1.

Total thrust, total propellant flow, and specific impulse curves for each engine are shown in Figures 5-3 through 5-10. These curves indicate that the flight data deviated significantly from predicted data for several engines. The maximum deviation in engine thrust between that calculated from flight data and predicted values was approximately -3.6 percent (6.2% below nominal) which occurred on engine position 2. The deviations for the other engines were between +2.5 and -1.0 percent. The deviations of engine specific impulses were between +3.2 and -0.3 percent relative to predicted. These large deviations indicated that the flight data may have been in error. An investigation of the flight data revealed two facts: (1) turbine erosion on engine position 2 due to a long LPGG (liquid propellant gas generator) LOX lead time and (2) questionable combustion chamber pressure data.

~~CONFIDENTIAL~~

# H-1 ROCKET ENGINE

165 K

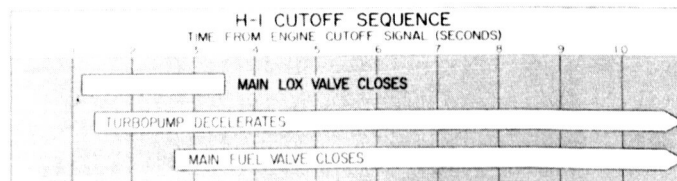
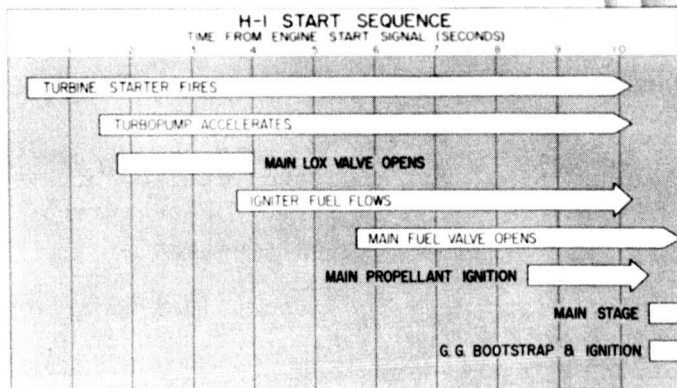
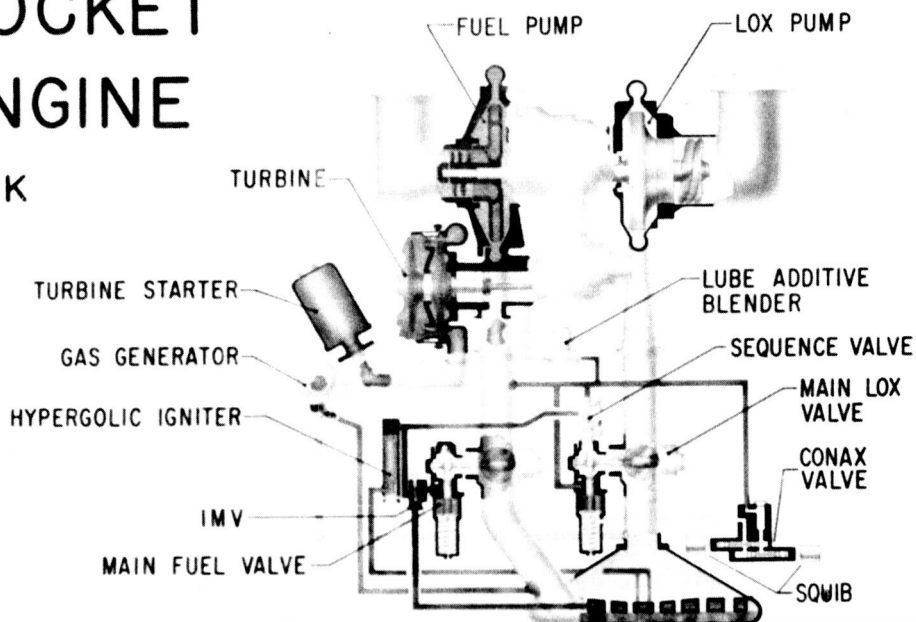


Figure 5-1 H-1 ENGINE SCHEMATIC

As shown in Table 5-I, the LPGG LOX lead time was extremely high for engine position 2. An evaluation of the flight data for this engine showed evidence of turbine erosion due to the long LPGG LOX lead time and accounts for the low thrust level.

As shown in Figures 5-3 through 5-10, the specific impulse and thrust from flight data for engine positions 7 and 8 were higher than predicted. The flight data showed positive pressures after engine thrust decay. Since ambient pressure at this altitude is close to 0 psia, the chamber pressure should reflect this value. This indicates that the Vibrotron transducers experienced a zero-shift and/or a sensitivity change. Flight data indicated that engine positions 6, 7, and 8 had an excessive zero-shift; whereas, the remaining engines had zero-shifts within the measurement accuracy of the transducers. The cause of these excessive zero-shifts has not yet been determined. These shifts may have been linear with time or a zero-shift during start or shutdown transition. From the indications of the specific impulse and thrust curves for engine position 7 (which had an approximate 9.5 psi zero-shift), the shift may have occurred during the flight.

Figure 5-2 shows the thrust build-up of all engines. The starting pairs by position numbers were 5,7; 6,8; 2,4; and 1,3 with a programmed 100 ms delay between pairs. The largest deviation from this programmed start sequence was on engine position 8. Engine positions 6 and 8 received the engine ignition signal at the same time, but the chamber pressure prime time for engine position 8 was 60 ms longer than the time for engine position 6. This longer prime time is due to the fact that the SPGG (solid propellant gas generator) on engine position 8 fired approximately 70 ms later (based on the LPGG injector pressure build-up) than the SPGG on engine position 6. Engine propellant valve opening times are shown in Table 5-I.

Engine main propellant valve closing times are shown in Table 5-I, and cutoff impulses are shown in Table 5-II. Engine position 8 produced the highest cutoff impulse. This is attributed to the fact that the main LOX valve on this particular engine was approximately 60 ms late (with reference to inboard engine valve operation) in starting to close. The cutoff impulses for the remaining engines were low as compared to nominal. These values of cutoff impulse on SA-2 will be modified if the chamber pressures are adjusted to compensate for the zero-shift. The main propellant opening and closing times were similar to the values from SA-1 flight.

Over-all performance of the engines was generally acceptable with the exceptions mentioned above. All engine subsystems and components

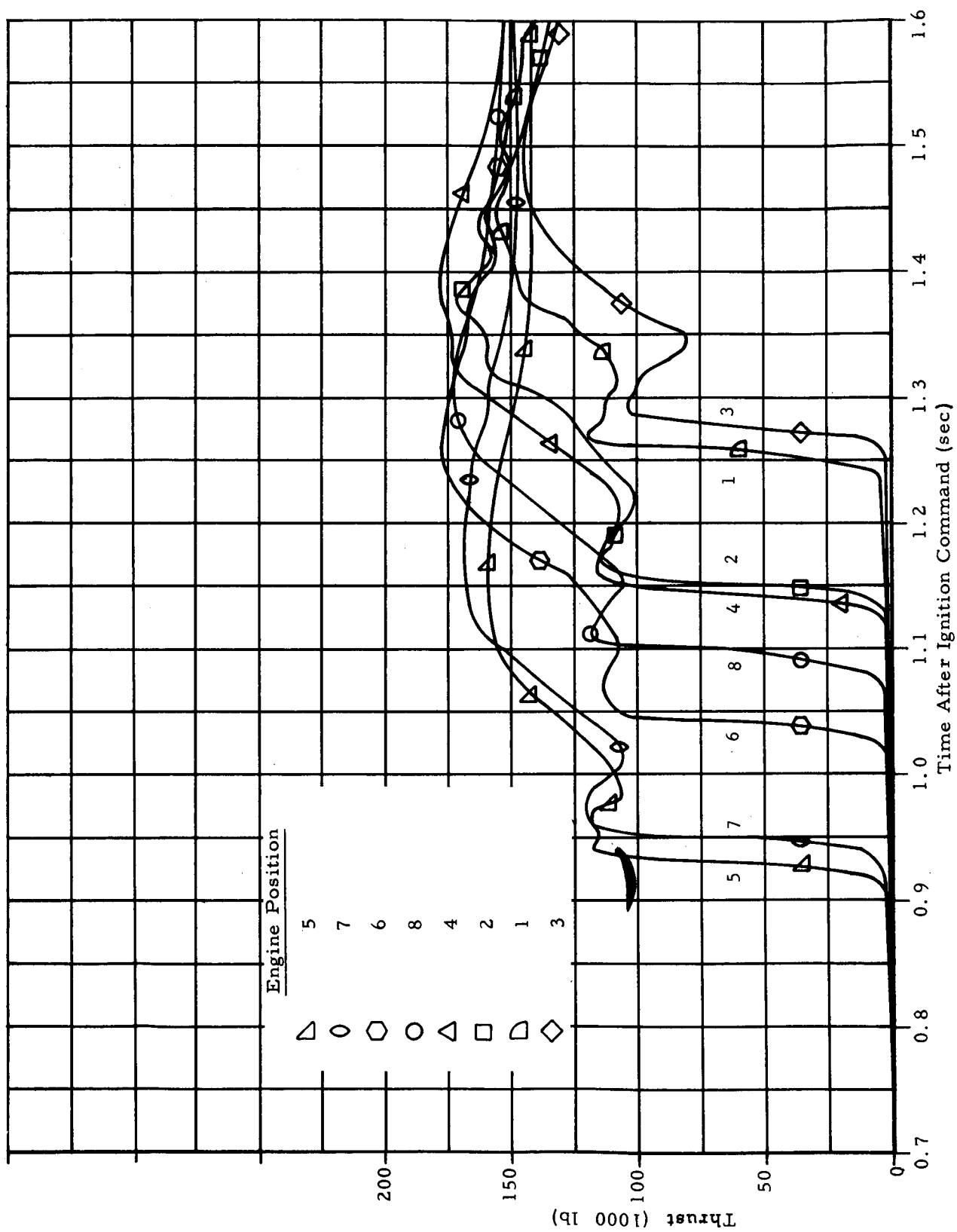


Figure 5-2 THRUST BUILD-UP

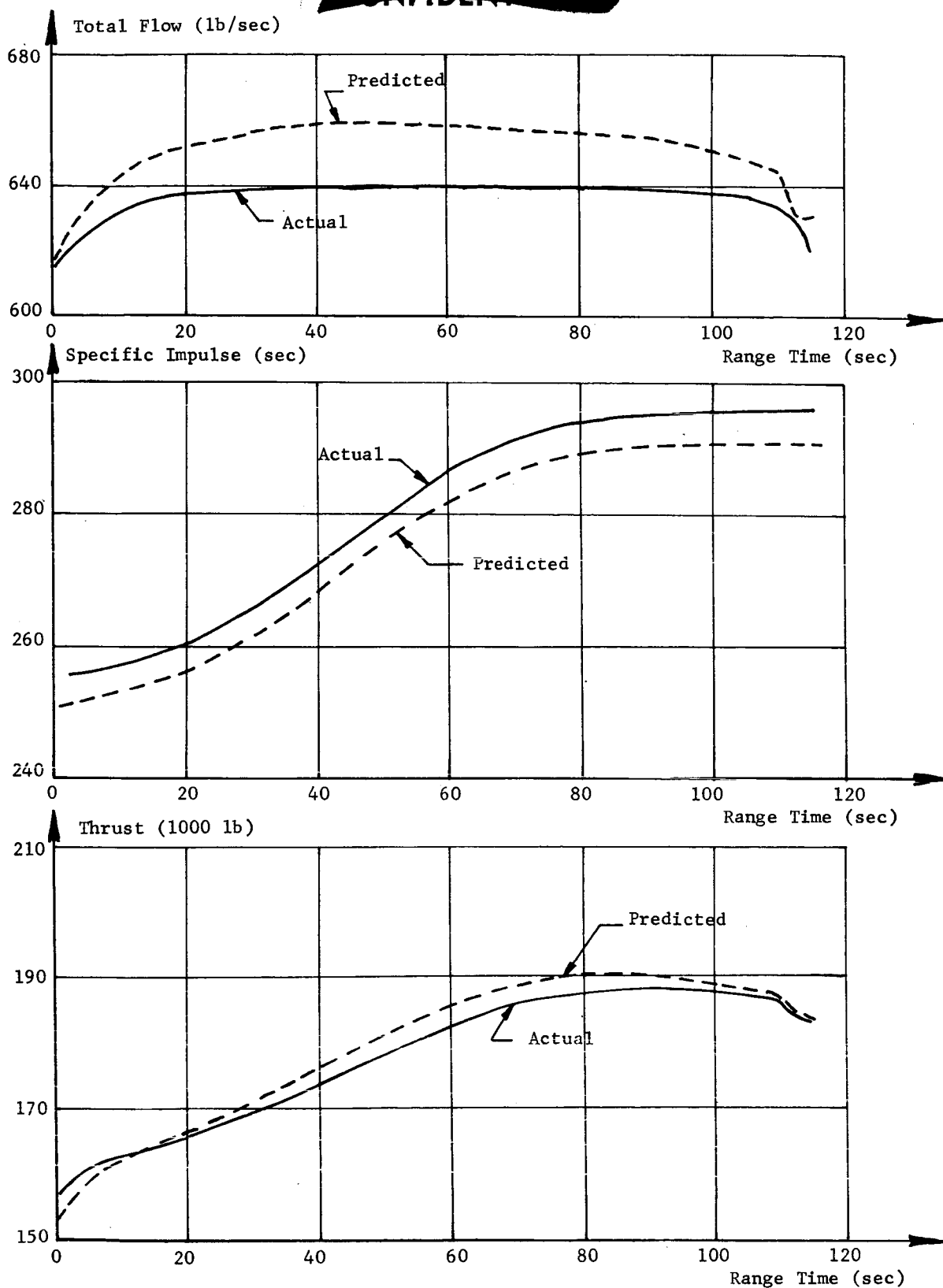


FIGURE 5-3 TOTAL FLOW, SPECIFIC IMPULSE AND TOTAL THRUST  
ENGINE POSITION 1

~~CONFIDENTIAL~~

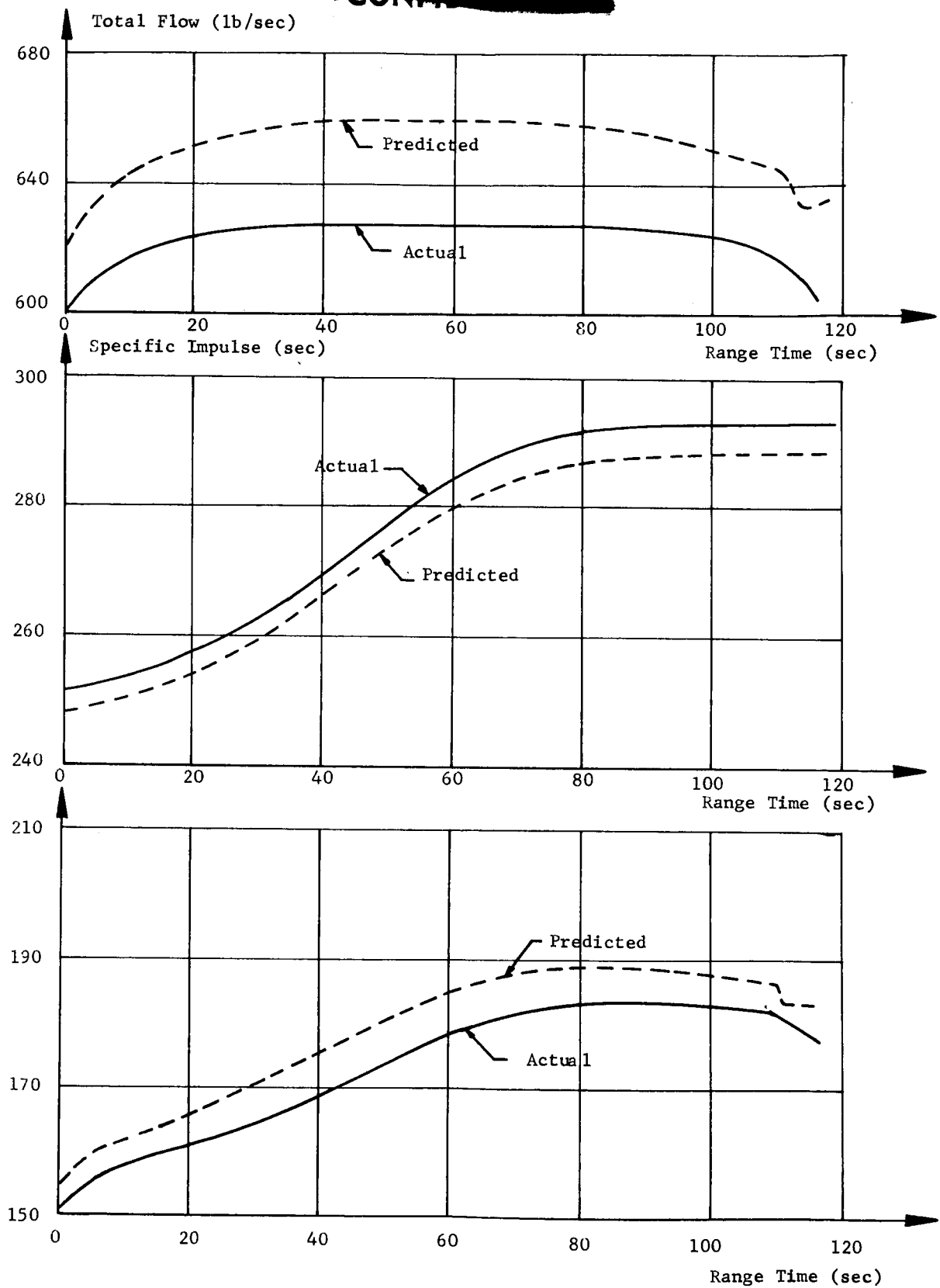
**CONFIDENTIAL**

FIGURE 5-4 TOTAL FLOW, SPECIFIC IMPULSE AND TOTAL THRUST  
ENGINE POSITION 2

**CONFIDENTIAL**

MPR-SAT-WF-62-5

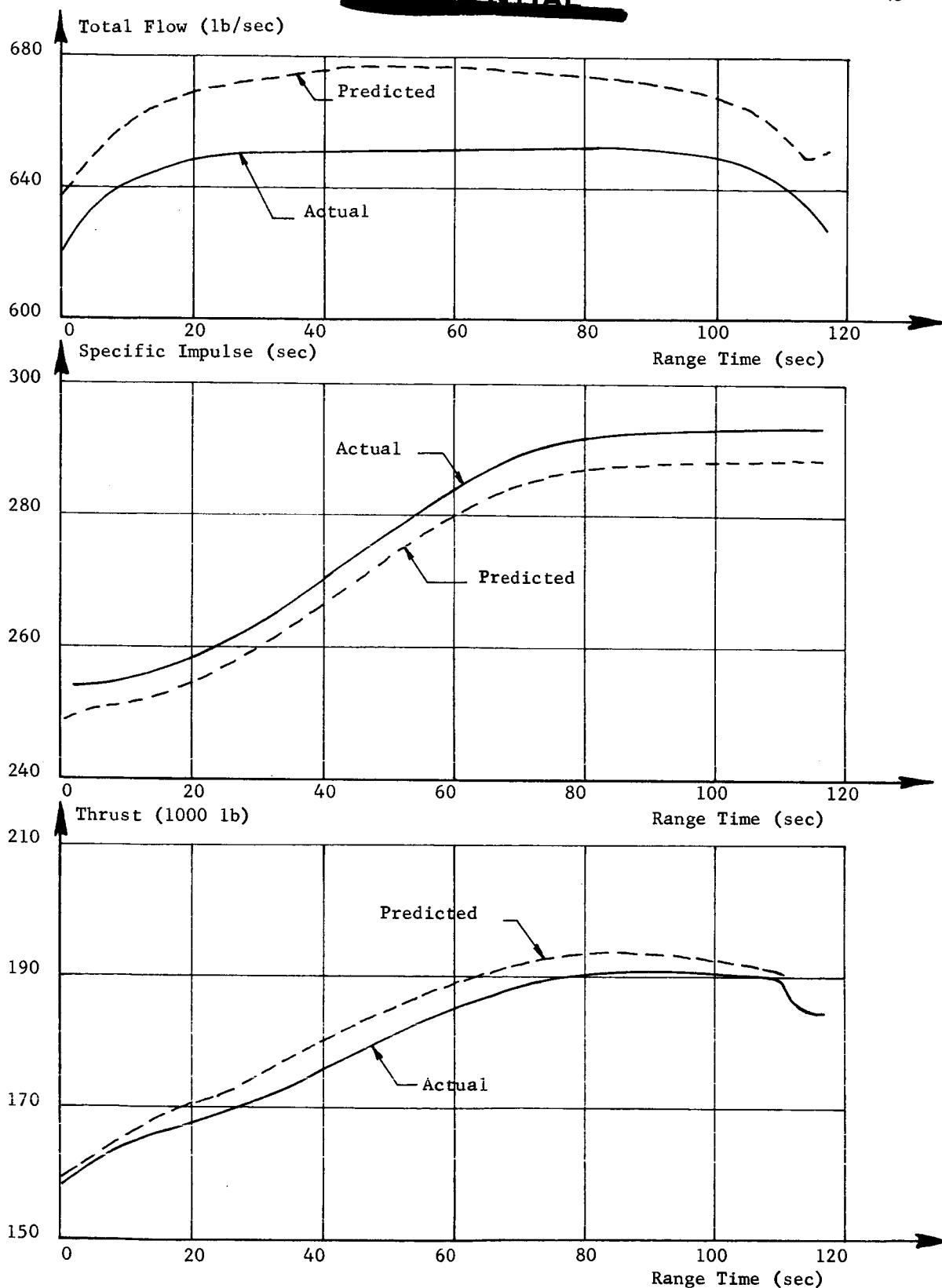


FIGURE 5-5 TOTAL FLOW, SPECIFIC IMPULSE AND TOTAL THRUST  
ENGINE POSITION 3

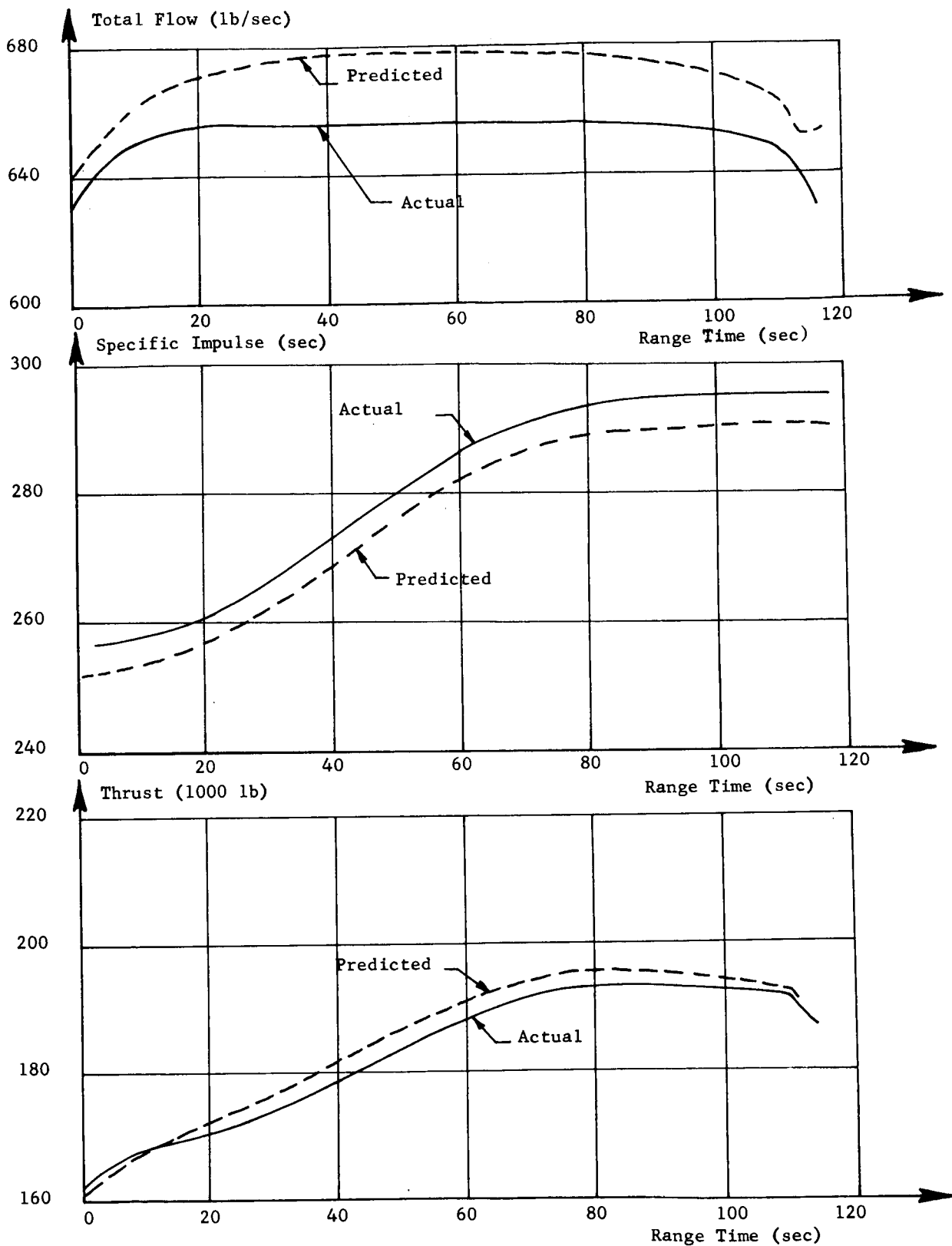
~~CONFIDENTIAL~~

FIGURE 5-6 TOTAL FLOW, SPECIFIC IMPULSE AND TOTAL THRUST  
ENGINE POSITION 4

~~CONFIDENTIAL~~

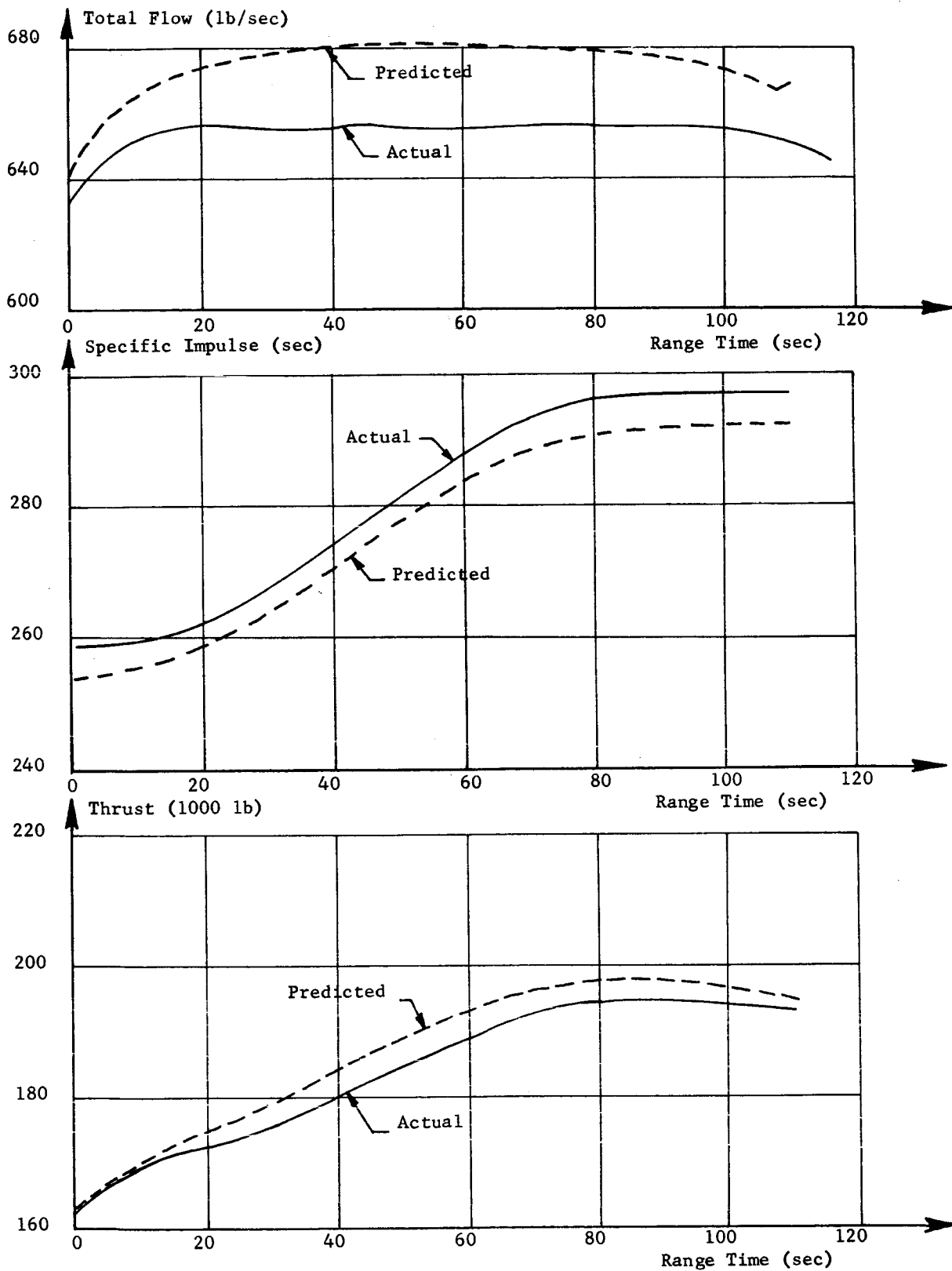


FIGURE 5-7 TOTAL FLOW, SPECIFIC IMPULSE AND TOTAL THRUST  
ENGINE POSITION 5

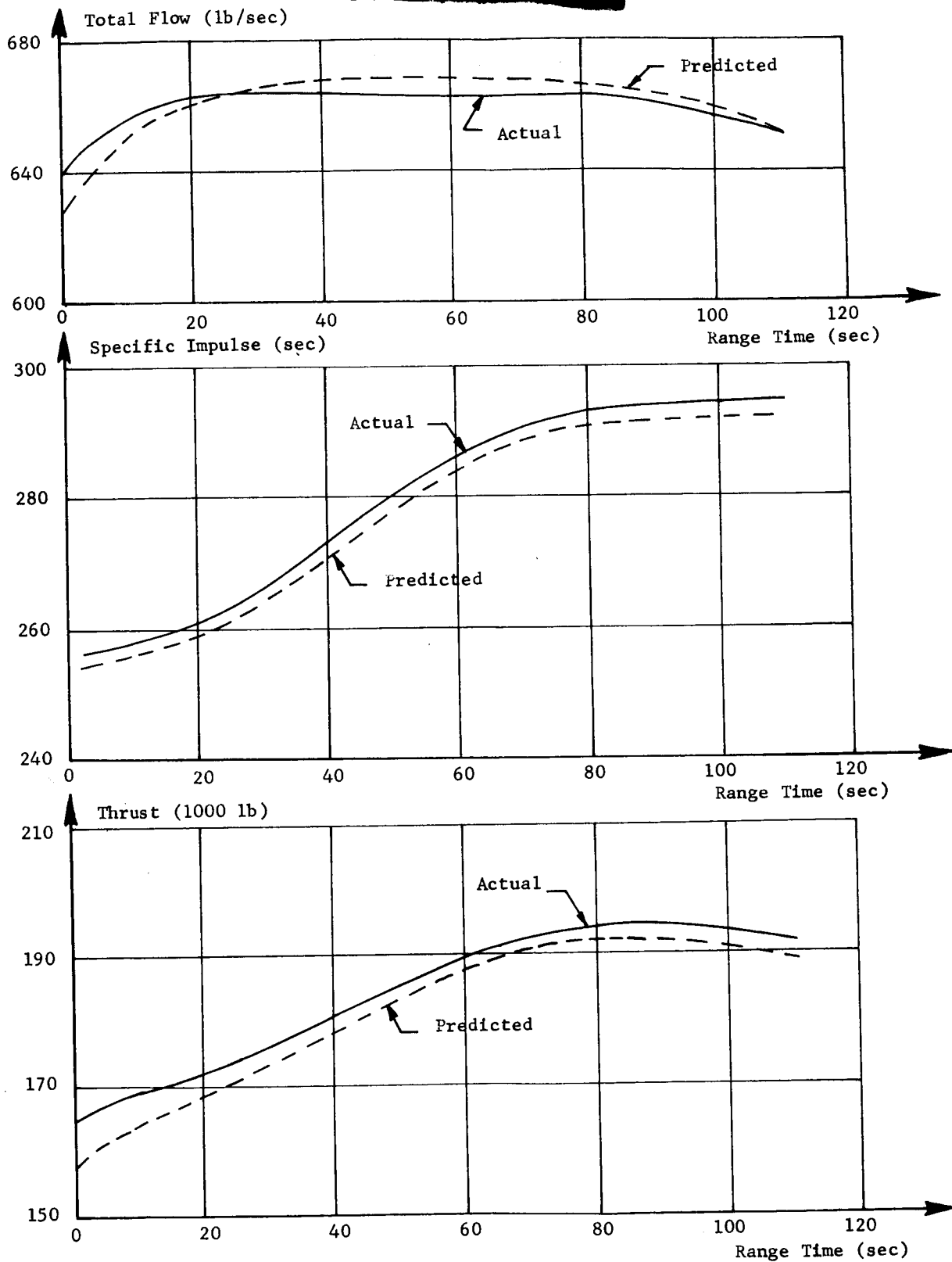


FIGURE 5-8 TOTAL FLOW, SPECIFIC IMPULSE AND TOTAL THRUST  
ENGINE POSITION 6

MPR-SAT-WF-62-5

~~CONFIDENTIAL~~

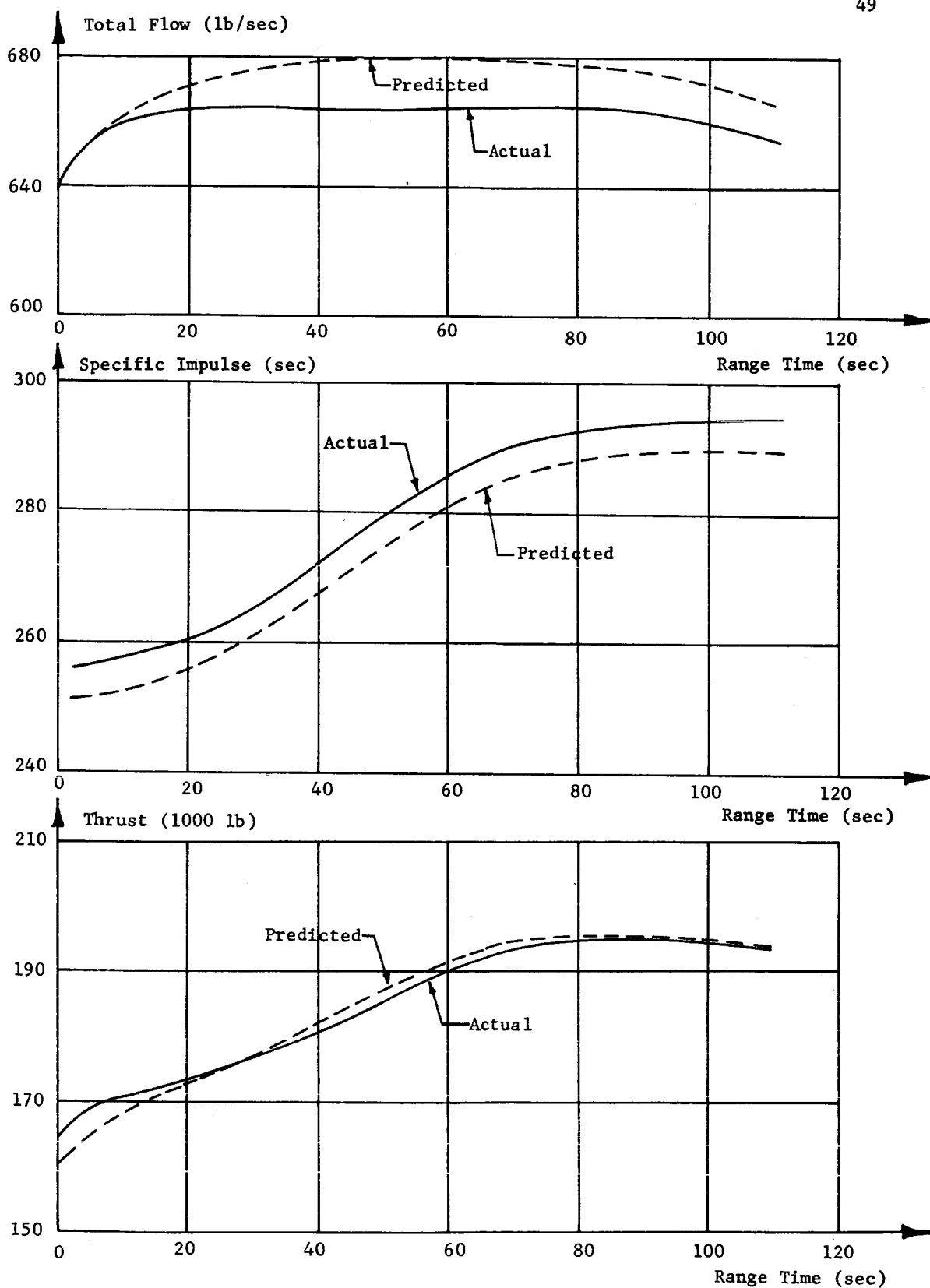


FIGURE 5-9 TOTAL FLOW, SPECIFIC IMPULSE AND TOTAL THRUST  
ENGINE POSITION 7

~~CONFIDENTIAL~~

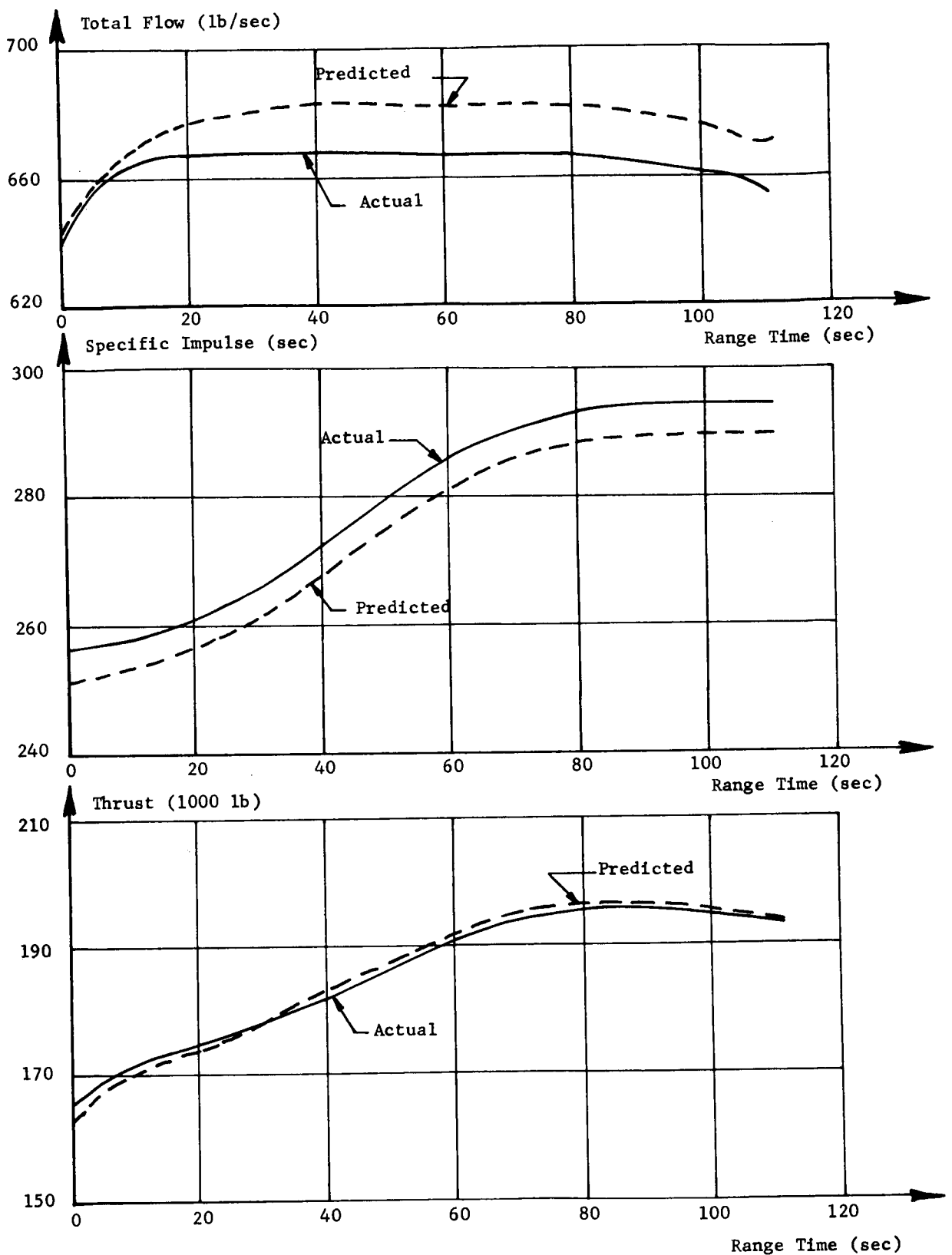


FIGURE 5-10 TOTAL FLOW, SPECIFIC IMPULSE AND TOTAL  
THRUST ENGINE POSITION 8

MPR-SAT-WF-62-5

TABLE 5-I ENGINE OPERATION TIMES

Engine No.	Ign. Signal Time After Ign. Command (ms)	GG LOX Lead (ms)	MLV Opening Time (ms)	MFV Opening Time (ms)	MLV Closing Time (ms)	MFV Closing Time (ms)
1	330	27	190	790	270	1300
2	240	67	230	690	240	1260
3	330	10	220	700	240	1120
4	240	36	220	680	250	1210
5	40	26	210	650	270	1210
6	130	37	200	780	260	1210
7	40	32	220	710	270	1200
8	130	30	220	690	280	1290

Note: Engines started in pairs with a predicted 100 ms difference in starting time as follows:

No. 5 and No. 7  
 No. 6 and No. 8  
 No. 2 and No. 4  
 No. 1 and No. 3

LEGEND: GG - Gas Generator  
 MLV - Main LOX Valve  
 MFV - Main Fuel Valve

~~CONFIDENTIAL~~

TABLE 5-II CUTOFF IMPULSE

Engine No.	Engine Cutoff Impulse (lb sec)	Comparison with Nominal (lb sec)
1	64,400	-7,000
2	60,800	-10,600
3	66,600	-4,800
4	65,200	-6,200
5	61,400	-10,000
6	63,500	-7,900
7	69,900	-1,500
8	82,500	+11,400

Notes: 1. The nominal cutoff impulse is  $71,400 \pm 5,200$  lb sec for a  $1\sigma$  confidence level.

2. All values in Table 5-II are based on chamber pressure decay data.

3. Calculated mean averages and  $1\sigma$  level values for SA-1 and SA-2 are:

SA-1:  $66,788 \pm 6,974$  lb sec

SA-2:  $72,450 \pm 6,588$  lb sec

~~CONFIDENTIAL~~

were evaluated, and the data indicated satisfactory operation with the exception that the gear case pressure was below the low limit. The gear case pressure limits for the H-1 engine have been set at 2 to 6 psi. Both SA-1 and SA-2 vehicles had engines which were below the low limit, three engines on SA-1 and one on SA-2. There appeared to be some similarity between the pressure level changes of the inboard engines of both vehicles. This was also noted for the outboard engines. Based on the deviation of inboard and outboard engine gear case pressure levels it was felt that the sudden change in pressure at approximately Mach one and the violation of the minimum pressure limit may be the result of an aerodynamic influence. However, since this deviation was not considered serious, it was felt that a change in the pressure limits was needed. The limits for later vehicles have been changed to a pressure range of 0.5 to 10 psi.

### 5.3 VEHICLE PROPULSION SYSTEM PERFORMANCE

Over-all propulsion system performance as reflected in vehicle performance was very satisfactory. Inboard engine cutoff occurred at 110.88 seconds after vehicle liftoff signal, and outboard engine cutoff occurred six seconds later at 116.88 seconds. Both the outboard engines and the inboard engines shut down smoothly within the expected time. Cutoff impulse for each group of engines is shown in Table 5-II.

Actual and predicted vehicle longitudinal thrust, total flow rate, mixture ratio, and specific impulse are shown in Figures 5-11 and 5-12.

Two analytical approaches were used to evaluate the vehicle propulsion system performance: flight reconstruction and flight simulation. Flight reconstruction is essentially a computer program which uses high quality propulsion system measurements (such as pump speed and inlet pressures) with a preflight prediction program to produce and reconstruct the propulsion parameters. Flight simulation is a computer program with a differential correction procedure used to obtain adjustments to the propulsion parameter inputs which will produce a trajectory which matches the actual trajectory.

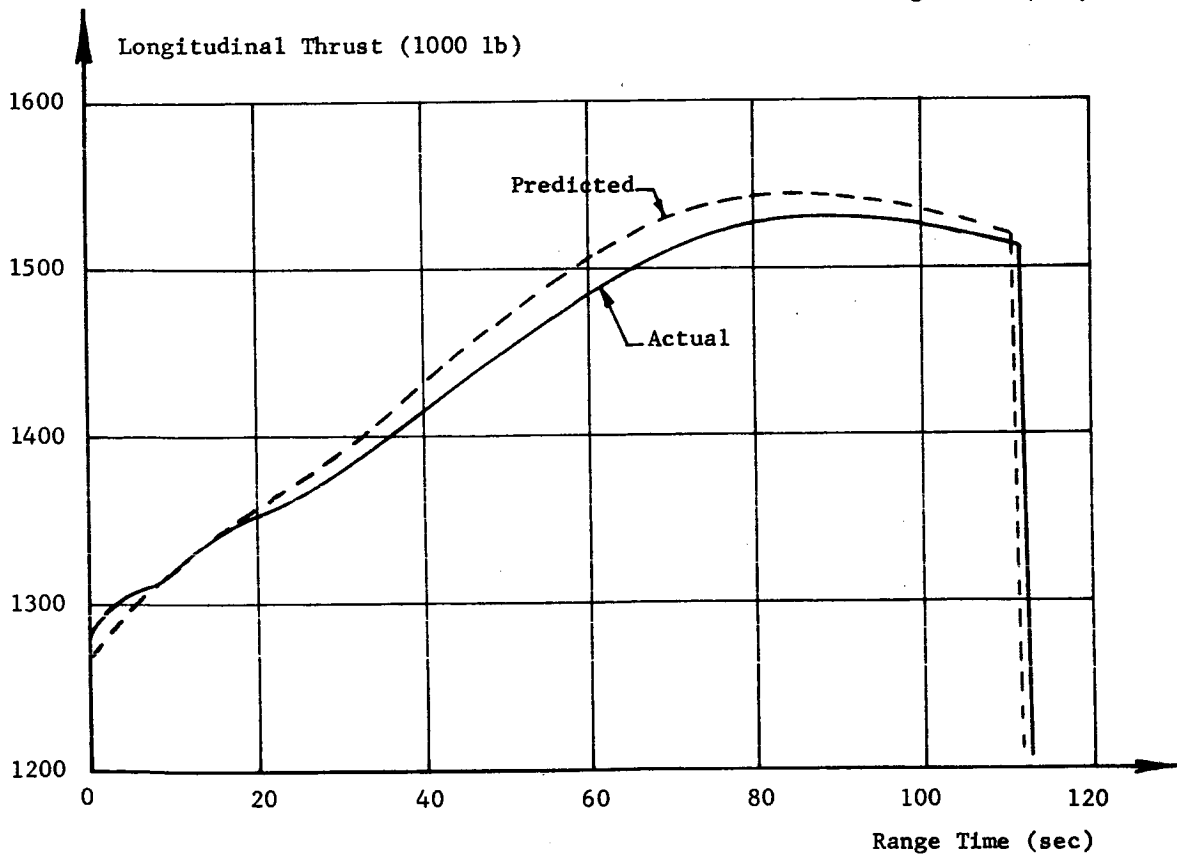
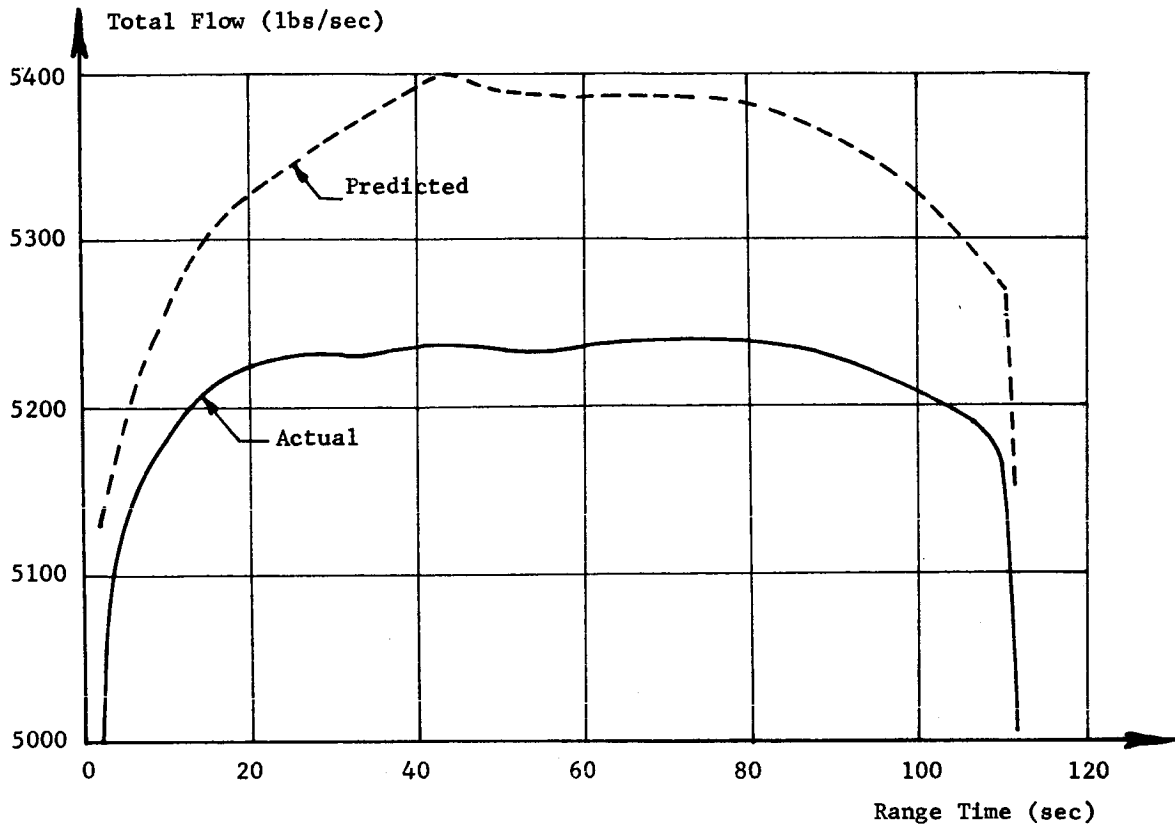
~~CONFIDENTIAL~~

Figure 5-11 VEHICLE TOTAL FLOW AND LONGITUDINAL THRUST

~~CONFIDENTIAL~~

MPR-SAT-WF-62-5

**CONFIDENTIAL**

55

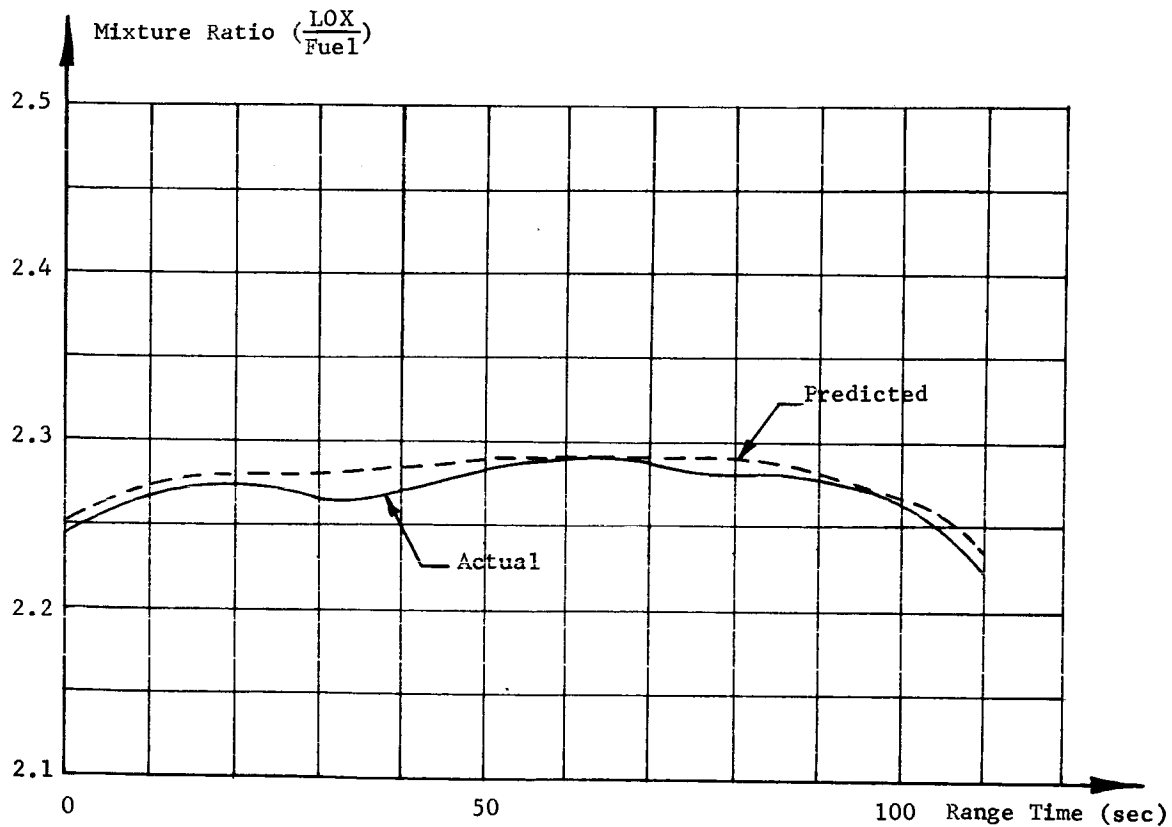
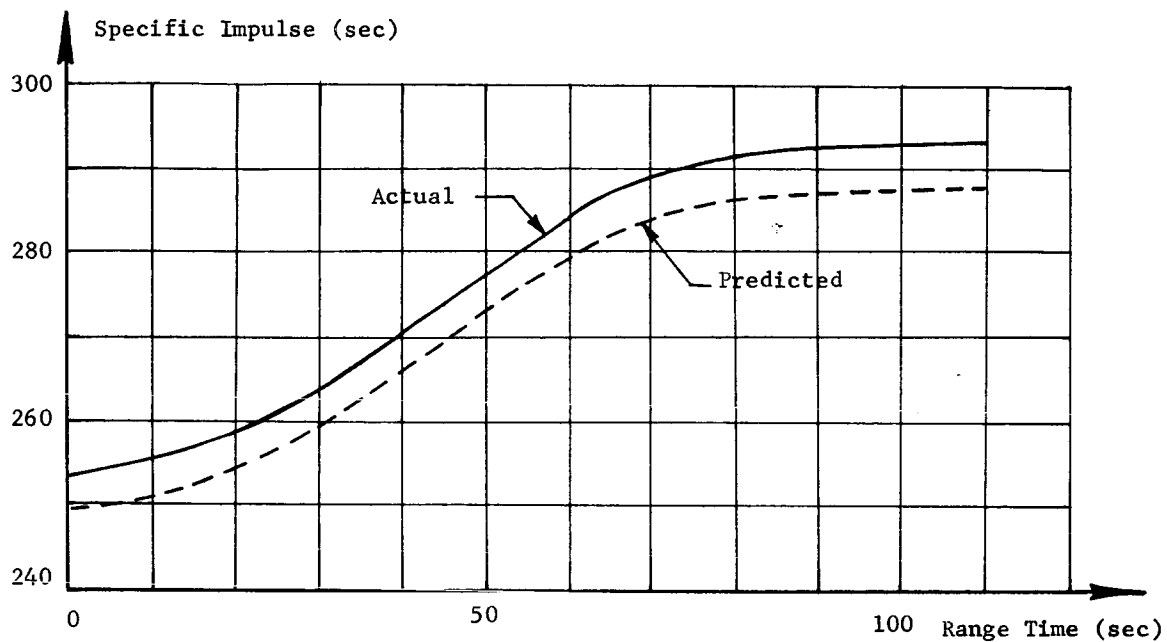


Figure 5-12 VEHICLE SPECIFIC IMPULSE AND MIXTURE RATIO

**CONFIDENTIAL**  
MPR-SAT-WF-62-5

The percent deviation from predicted along with the estimated accuracy limitations of each parameter from both approaches is shown below.

	Flight Reconstruction	Flight Simulation
Thrust	$-1.11\% \pm 0.25\%$	$-1.10\% \pm 0.10\%$
Total Flow Rate	$-2.38\% \pm 0.25\%$	$-2.51\% \pm 0.10\%$
Specific Impulse	$+1.30\% \pm 0.25\%$	$+1.44\% \pm 0.14\%$

The deviations shown above are computed by subtracting predicted from actual and dividing by predicted. The largest deviation between the two approaches is only 0.14% which is within the accuracy limitations of either approach.

#### 5.4 PRESSURIZATION SYSTEMS

##### 5.4.1 FUEL TANK PRESSURIZATION

The fuel tank pressurization system (Figure 5-13) operated satisfactorily during flight. Gaseous nitrogen, supplied by 48 high pressure spheres, showed a pressure of 3010 psig at liftoff and decayed as expected to approximately 2125 psig at 40 seconds. Beginning at 40 seconds flight time, the pressure showed a gradual rise to 2200 psig at 90 seconds, then decayed to 1875 psig at IECO.

Fuel tanks were initially pressurized during the automatic sequence which started with firing command. The time required to pressurize the tank was 19.0 seconds. Pressure in the fuel tanks was then maintained throughout powered flight by action of the pressure switch located in fuel tank F-1. Pressure in the tanks gradually decayed from 16.7 psig after initial pressurization to 15 psig at liftoff. A maximum pressure of 17 psig in the tanks was reached at 50 seconds, and a minimum of 14.3 psig at 94 seconds (see Figure 5-14).

Due to pressure decay in the high pressure spheres (see Figure 5-14) and a change in ambient pressure, varying nitrogen flows from the spheres were required throughout flight to maintain the required tank pressures. The flow was varied by changing the number of fuel tank pressurization valves which could be controlled by the fuel tank pressurization switch. Each of the four normally closed valves could be operated by the switch only while in the electrical circuit with the switch. A programmed tape, which was started at the time of

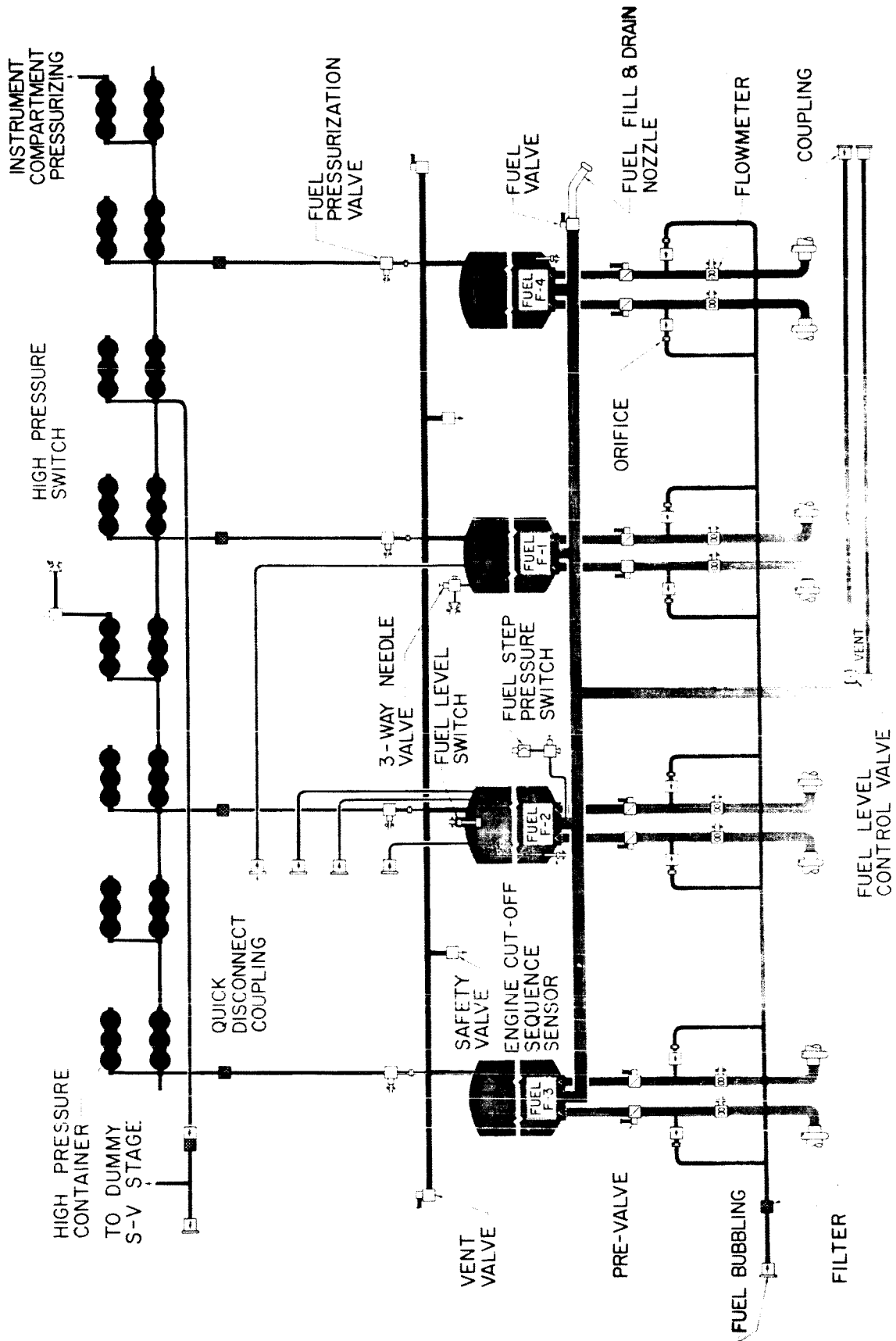


Figure 5-13 SA-2 FUEL SYSTEM

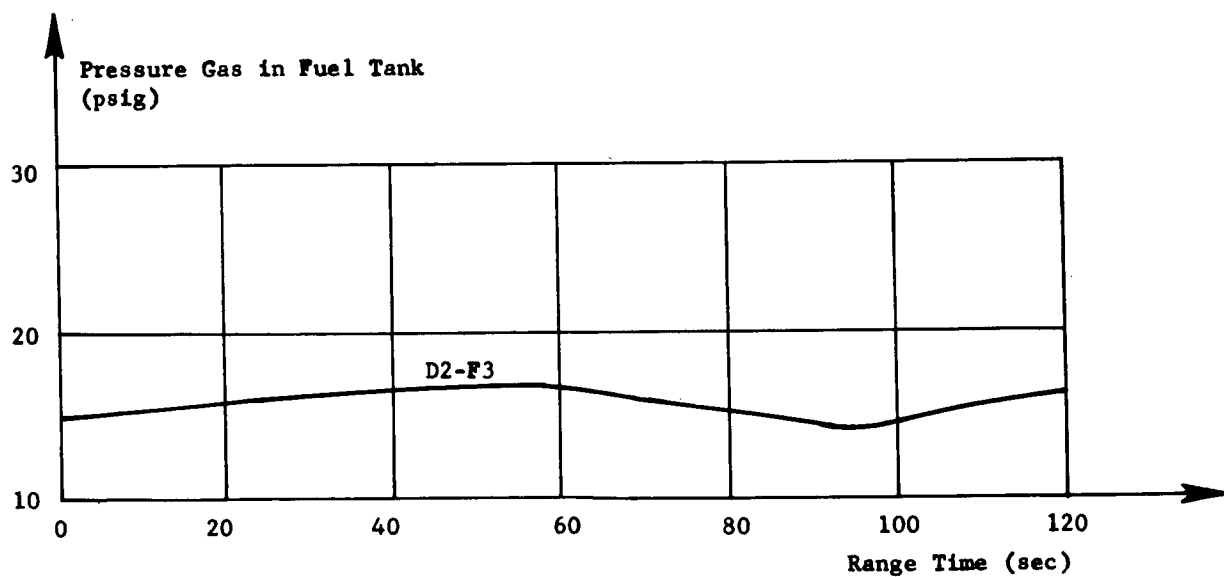
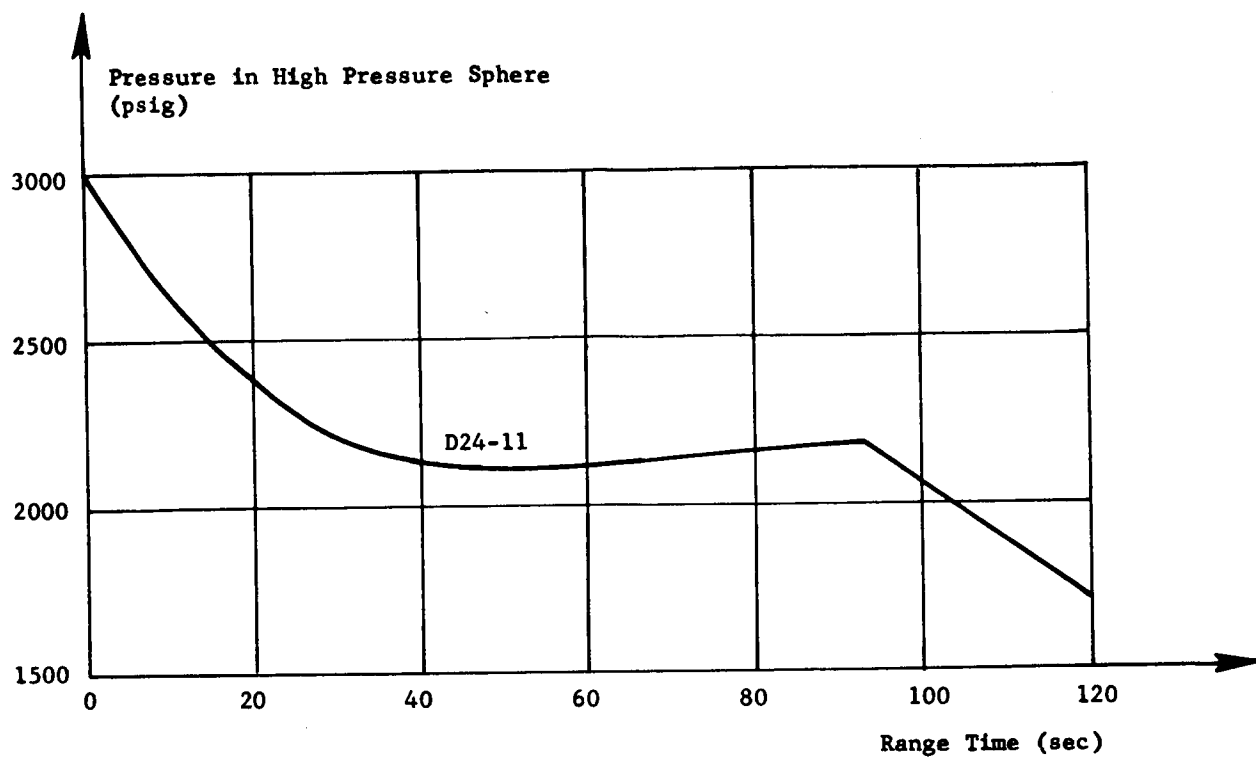


Figure 5-14 PRESSURE IN HIGH PRESSURE SPHERE AND PRESSURE GAS IN FUEL TANK

initial fuel tank pressurization, regulated the number of valves in the electrical circuit with the switch. The following table gives the times at which the pressurization valves had the capability of being controlled by the fuel tank pressure switch:

Liftoff	to	22	sec	--	4 valves in operation
22	to	31	sec	--	3 valves in operation
31	to	39	sec	--	2 valves in operation
39	to	76	sec	--	1 valves in operation
76	to	86.5	sec	--	2 valves in operation
86.5	to	104	sec	--	3 valves in operation
104	to	cutoff		--	4 valves in operation

Based on telemetered data, the fuel tank pressurization system performed as expected.

#### 5.4.2 LOX TANKS PRESSURIZATION SYSTEM (FIGURE 5-15)

Initial pressurization of the LOX tanks, which was the final function in the automatic sequence prior to ignition start timer, was provided by helium from a ground source. Pressurization was begun at approximately 120 seconds before liftoff and was stopped by the LOX tank pressure switch 86.7 seconds later at a pressure of 58.9 psia. The pressurizing time of 86.7 seconds was 8.7 seconds longer than the pressurizing time for Saturn SA-1.

Pressure in the center LOX tank was 57.7 psia at liftoff and rose to a maximum of 64.6 psia at 26 seconds flight time (see Figure 5-16). The pressure was slightly higher throughout powered flight than the center LOX tank pressure on Saturn SA-1. This is attributed to the use of more efficient, four-coil heat exchangers on SA-2 instead of two-coil heat exchangers as used on Saturn SA-1. The LOX tanks pressure curves show two distinct dips. These dips, which occurred in the center LOX tank at 2.3 seconds and 26 seconds flight time and slightly later in the outboard tanks, correspond with the opening of LOX pressure relief and vent valves. LOX relief valve #1 opened at 2.3 seconds when the pressure exceeded the control pressure switch setting of  $59.5 \pm 1$  psia and remained open until 113 seconds when the pressure dropped below the pressure switch setting. LOX relief valve #2 and the emergency vent valve opened at 26 seconds when the pressure

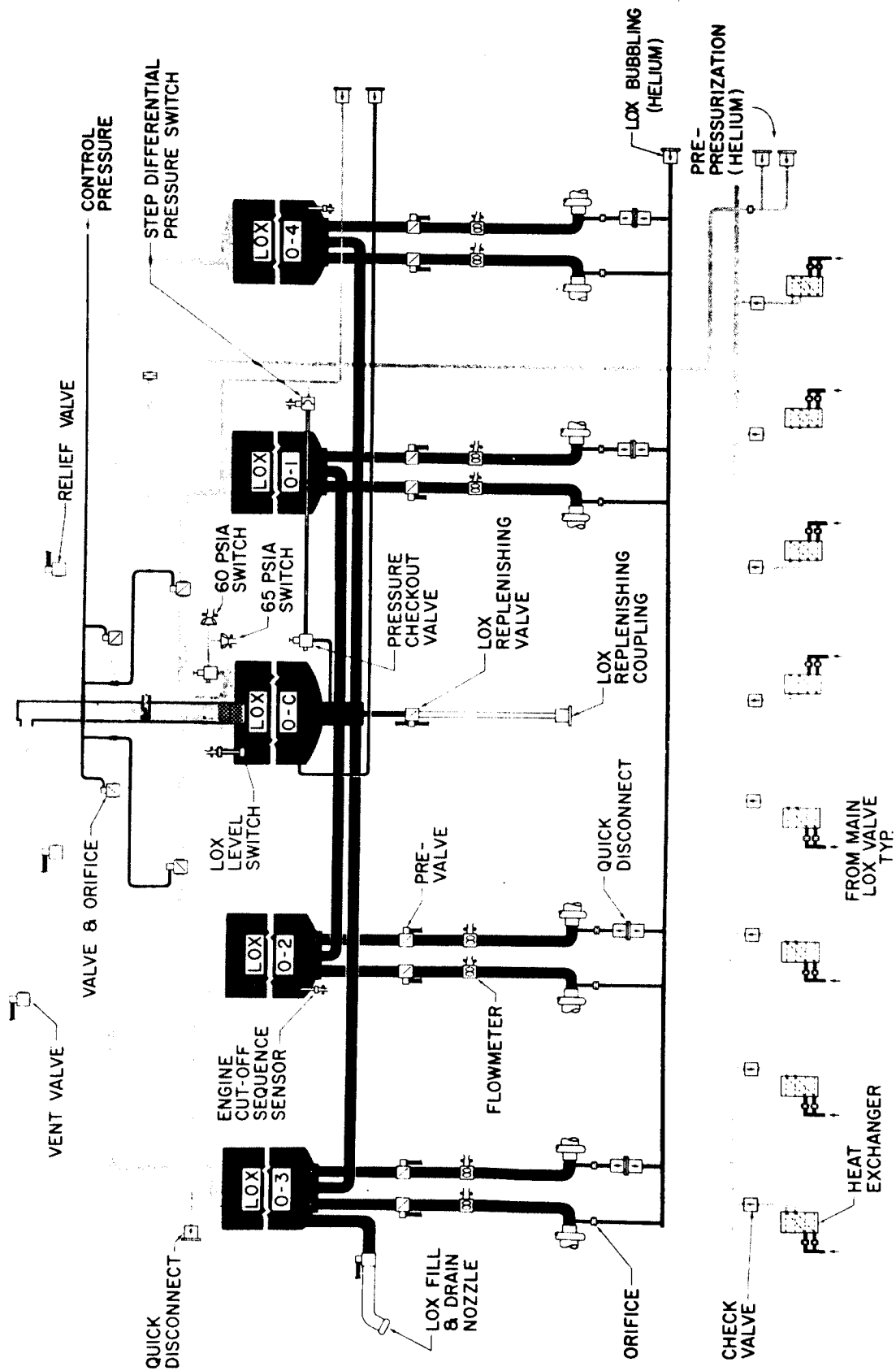


Figure 5-15 SA-2 LOX SYSTEM

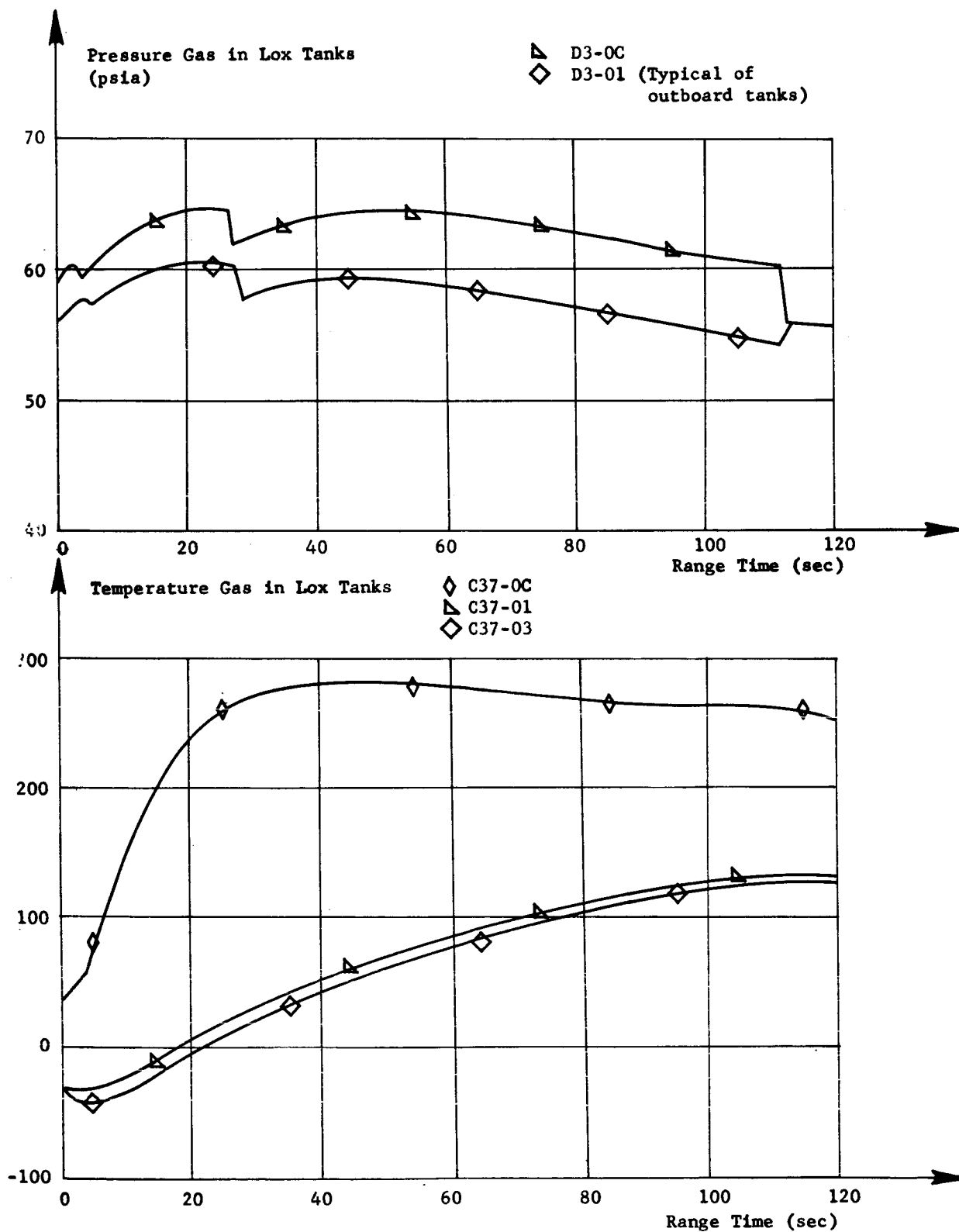


Figure 5-16 PRESSURE AND TEMPERATURE IN LOX TANK

exceeded the control pressure switch setting of  $65.5 \pm 1$  psia. LOX relief valve #2 and the emergency vent valve remained open for 0.4 seconds and did not open again during the flight.

The pressurization system was designed to maintain a differential pressure between the center and outboard LOX tanks. The differential pressure was necessary to cause depletion of the center LOX tank prior to depletion of the outboard tanks to prevent trapping of usable LOX in the center tank. The required differential pressure was maintained by orifices located in the pressurizing interconnect lines. The pressure drop across these orifices produced the necessary differential pressure. The differential pressure experienced in flight agreed very well with expected and reached a maximum of 6.2 psi at inboard engine cutoff.

At 112 seconds range time the center tank pressure decayed suddenly to a pressure equal to the pressure in the outboard tanks. This pressure decrease indicates that the center LOX tank was depleted by 112 seconds (0.7 second after IECO).

#### 5.4.3 CONTROL PRESSURE SYSTEM

The control pressure system (Figure 5-17) operated satisfactorily during flight. This system consists of a high pressure GN<sub>2</sub> supply (3000 psig), a 750 psig regulator, and a regulated pressure manifold from which is taken control pressure for the control valves, vent valves, relief valves, and prevalues. This manifold also supplies 750 psig pressure for gearbox pressurization and LOX seal and calorimeter purges.

Blockhouse records showed the high pressure supply sphere pressure to be 2860 psig at liftoff. This pressure gradually decayed over flight to 2300 psig at 120 seconds (see Figure 5-18). Regulated pressure was 785 psia at liftoff, and gradually decayed to 750 psia at 100 seconds range time. This decay is attributed to ambient pressure decay along with regulator creep.

#### 5.4.4 AIR BEARING SUPPLY

The purpose of the air bearing supply (Figure 5-19) was to provide clean gaseous nitrogen at a predetermined flow, temperature, and pressure to the air bearings of the ST-90 stabilized platform.

Prior to flight, the 0.5 cubic-foot sphere was charged and replenished to a pressure of approximately 3000 psig by ground support equipment. Sphere pressure was monitored during preflight by a high

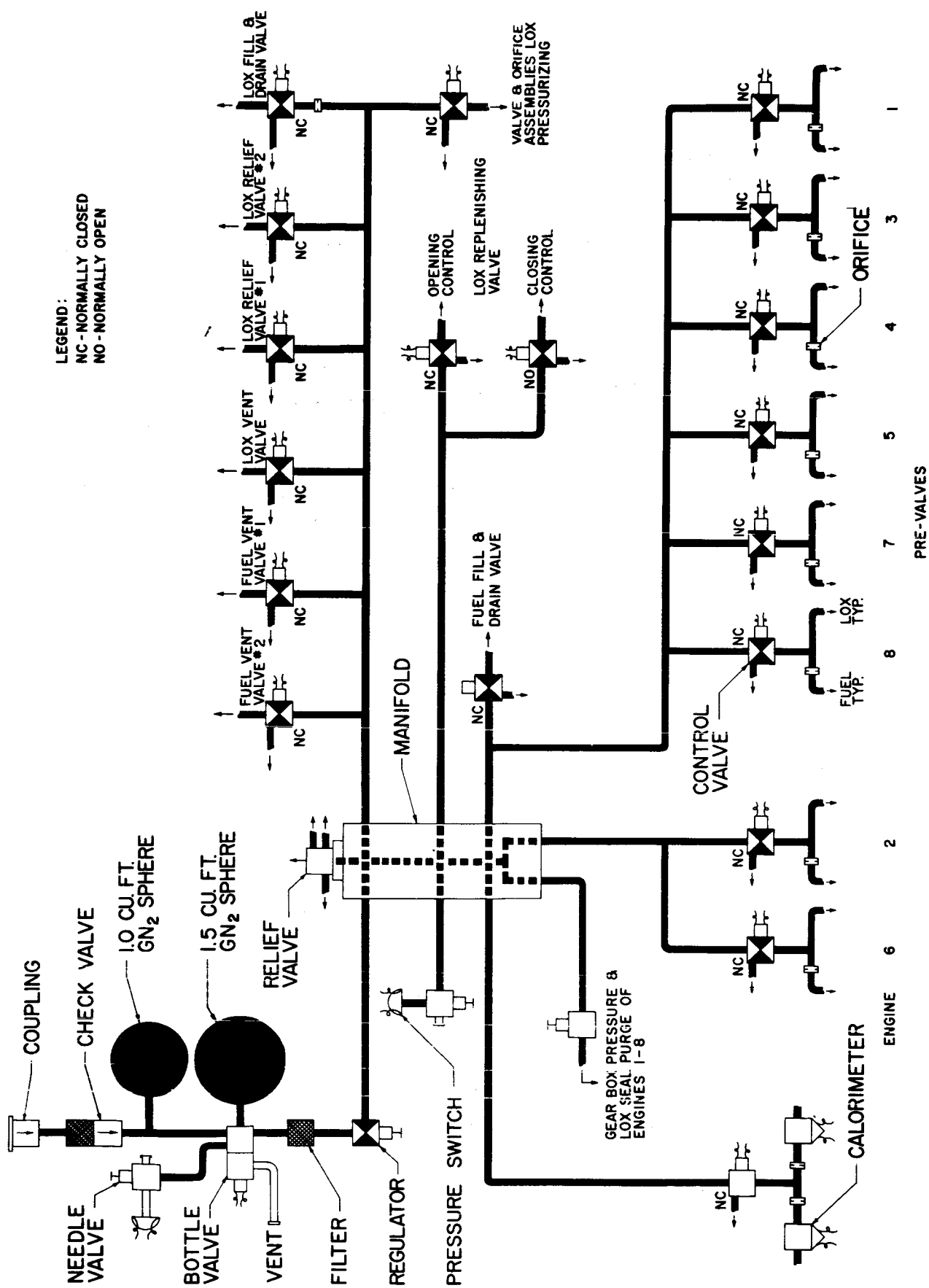


Figure 5-17 CONTROL PRESSURE SYSTEM SCHEMATIC

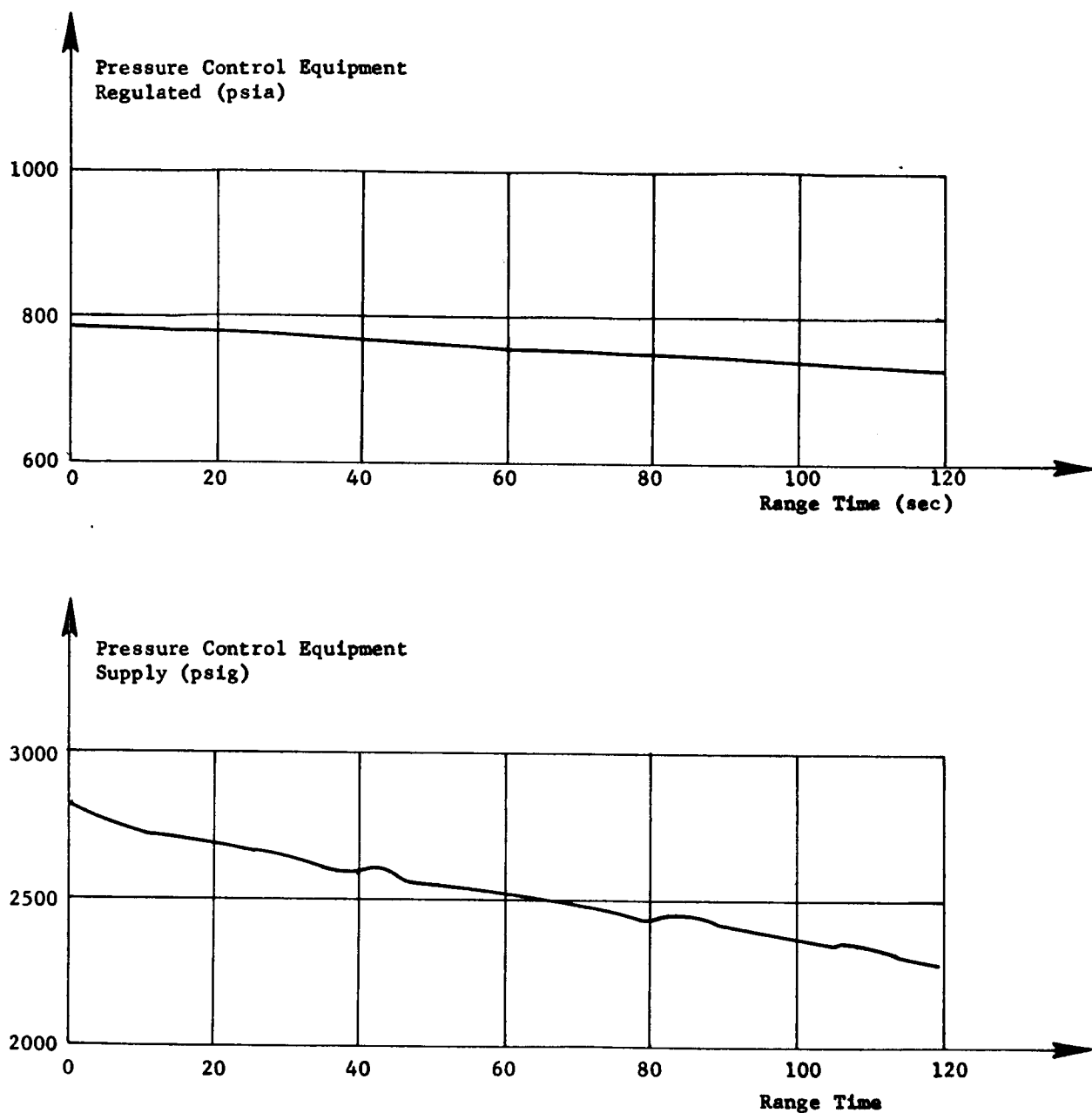


Figure 5-18 PRESSURE CONTROL EQUIPMENT, REGULATED AND PRESSURE  
CONTROL EQUIPMENT SUPPLY

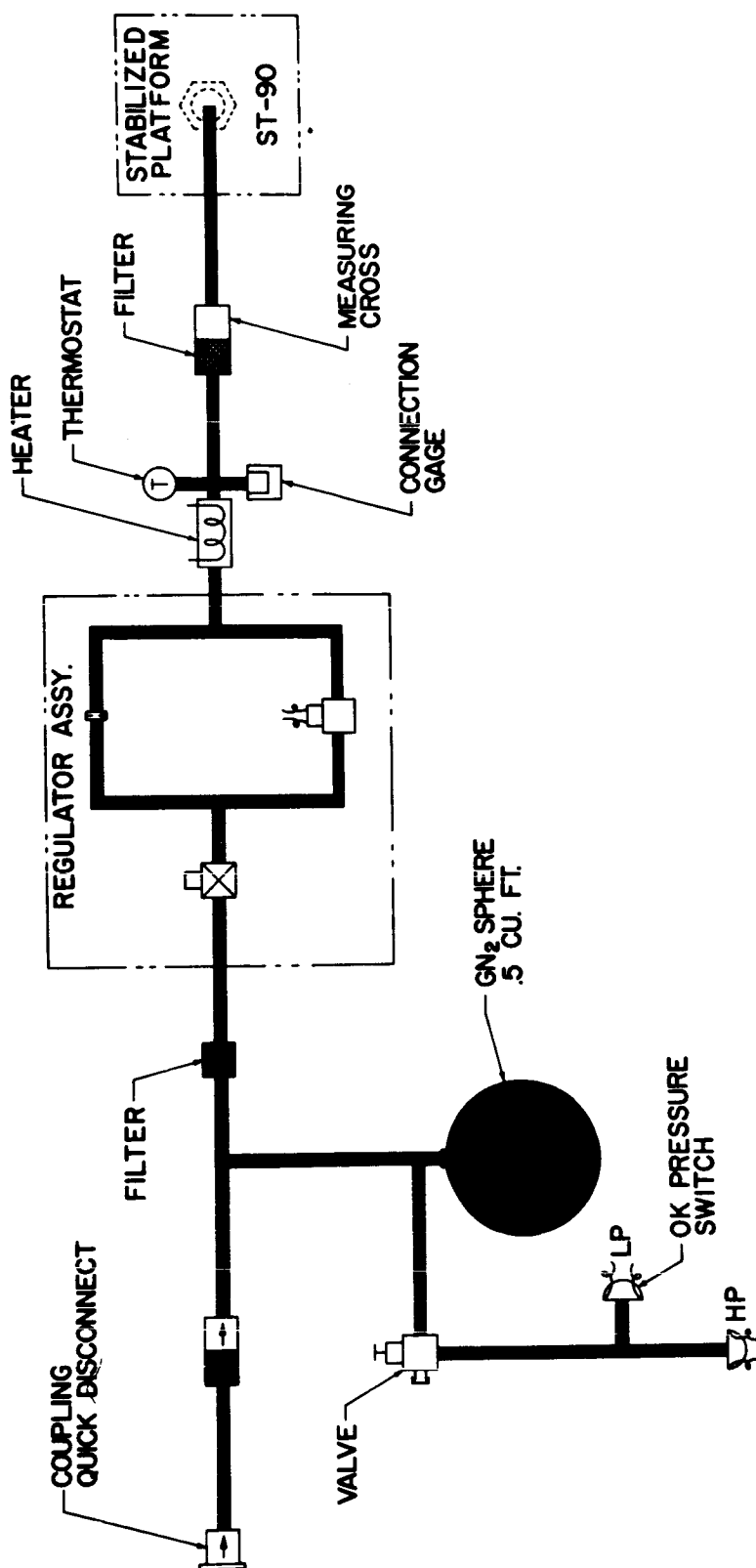


Figure 5-19 AIR BEARING SUPPLY SYSTEM SCHEMATIC

pressure OK switch set at an actuation pressure of  $2800 \pm 61$  psig and deactuation pressure of 2600 psig minimum. A low pressure OK switch was in the system to shutoff electrical power to the stabilized platform and close the solenoid valve in the regulator assembly if sphere pressure dropped below the switch setting. The switch was set to actuate on decreasing pressure at  $1375 \pm 33$  psig with a maximum actuation differential pressure of 70 psi. This assured an adequate flow of GN<sub>2</sub> through the orifice to the air bearings to prevent damage while the gyroscopes decelerated.

During stand-by and S-I stage flight, GN<sub>2</sub> flowed from the sphere through a filter to the pressure regulator where the high pressure GN<sub>2</sub> was regulated to a predetermined low pressure. From the pressure regulator the low-pressure GN<sub>2</sub> was directed through the orifice and the normally open solenoid valve in the regulator assembly to the thermostatically controlled heater where it was maintained at a constant temperature ( $25 \pm 1^\circ$  C). The GN<sub>2</sub> flowed from the heater through another filter to the air bearing of the ST-90 stabilized platform.

Blockhouse records show that the air bearing high pressure supply was maintained prior to launch at approximately 2975 psig which was within the redline limits of 3200 psig maximum and 2600 psig minimum. This pressure was also measured during flight (Figure 5-20) and decayed as expected to 2450 psig at 120 seconds. The low pressure air to the air bearing was constant throughout flight at approximately 32 psid.

Specifications for the air bearing inlet air temperature stated that the temperature must be maintained at  $25 \pm 1^\circ$  C. Blockhouse records show that this temperature was maintained within specified limits. As noted on SA-1, the blockhouse records show a cycling in the air temperature of approximately 10.5 cycle/minute which was the effect of a cycling of the thermostatically controlled inlet air heater.

## 5.5 VEHICLE PROPELLANT UTILIZATION

Vehicle propellants were utilized during the Saturn SA-2 flight test at a rate close to predicted. Inboard engine cutoff was given by the level cutoff probe in LOX tank 04 1.0 second later than predicted. The late cutoff was due primarily to performance dispersion. Performance parameters, which may cause deviations in consumption rates, are variables in engine calibration, container pressures, propellant densities, and propellant loading.

Fuel and LOX container levels for the latter part of powered flight are shown in Figures 5-22, 5-24, and 5-25. During this portion

of powered flight, the propellant level variations from predicted were the greatest. At inboard cutoff, the indicated LOX level in the 70-inch tanks was 31.0 inches; whereas the predicted level was 25 inches. The center tank depleted (gas breakthrough) at 112.5 seconds range time while predicted time was 107.4 seconds. The calculated fuel level was similar to predicted during the latter part of powered flight; however, the calculated level was approximately nine inches higher than predicted.

The center tank was scheduled to empty before inboard engine cutoff so that there would be no residual LOX transfer after inboard cutoff. The center tank emptied 0.7 seconds after inboard engine cutoff which is attributed to lower than predicted differential top gas pressure. At the predicted time of center tank gas breakthrough, the differential top gas pressure was 2.9 psid lower than predicted. There was approximately 205 pounds of residual LOX in the center tank at inboard cutoff. LOX in the center tank after inboard engine cutoff will be residual, since the six second time interval between inboard and outboard cutoff signal was based on the center tank being depleted at inboard cutoff.

The total LOX residual charged to late center tank gas breakthrough is 805 (+) pounds which includes 205 pounds center tank residual and 500 (+) pounds LOX transfer line residual. Out of 2000 pounds available LOX in the LOX transfer line, 600 pounds was predicted to be transferred to the outer tanks as usable LOX if gas breakthrough occurred before inboard engine cutoff. Since breakthrough occurred after inboard cutoff, the effect of the reduced outer tank head (reduction of acceleration on differential head between center and outer tanks) at this time created a much quicker and cleaner breakthrough than predicted. It is concluded that on SA-2 flight much more than 600 pounds of available LOX in the LOX transfer lines was transferred to the outer tanks as unusable LOX (600 + pounds).

A tabulation of vehicle weights at various times is shown in Appendix D. Since propellants are loaded according to the fuel density at tanking it is not necessary for the tanked LOX and fuel to agree with predicted; however, the total propellants loaded should and did correlate. The actual total weight deviations from predicted at inboard engine cutoff, outboard cutoff, and end of thrust decay (ETD) can be attributed to performance dispersion. The total propellant weight deviation at ETD was 6900 pounds of which 805 pounds may be attributed to late center tank gas blowthrough.

### 5.5.1 PROPELLANT UTILIZATION SYSTEM

The propellant utilization (PU) system (Figure 5-21) was carried on the SA-2 flight test to determine the performance and reliability of the system and was not a control feature of the Saturn first stage.

### 5.5.2 LIQUID LEVEL DISCRETE PROBE PERFORMANCE

Two discrete level probes were located at the bottom of each propellant container to obtain propellant level information toward the end of powered flight. With this propellant level information it should have been possible to calculate propellant consumption rates; however, over-all performance of the upper probes was unsatisfactory and propellant level never reached outer propellant tank lower probe level. One probe gave no signal, two probes gave late multiple signals, and one probe gave signal 16 seconds after cutoff. Even though over-all performance of the probes was unsatisfactory, fair agreement was obtained between the information from several discrete probes and the propellant utilization data.

### 5.5.3 CONCLUSIONS

The propellant utilization system performance was satisfactory although agreement with predicted consumption data decreased as powered flight progressed. The disagreement was attributed to performance dispersion and can be readily observed on the LOX and fuel level depletion plots.

The over-all liquid level discrete probe performance was unsatisfactory due to measurement failures, but the performance of 67 percent of the upper probes was satisfactory.

LOX container  $\Delta P$  transducer (Figure 5-26) indicates a slightly lower than predicted differential pressure except after 100 seconds where the differential pressure is higher than predicted. The fuel container  $\Delta P$  transducer (Figure 5-27) indicated a higher than predicted differential pressure throughout powered flight. The  $\Delta P$  ratio (Figure 5-28) calculated from the LOX and fuel container  $\Delta P$  data was lower than the predicted  $\Delta P$  ratio. A probable system malfunction saturated the ratio computer throughout powered flight.

Figures 5-22, 5-23, 5-24, and 5-25 depict the liquid level in LOX container #4, the center LOX tank, and fuel container #2. These levels were calculated using the container differential pressures, the vehicle longitudinal acceleration, and the propellant densities. Calculated LOX level was lower than predicted up to 100 seconds where the LOX

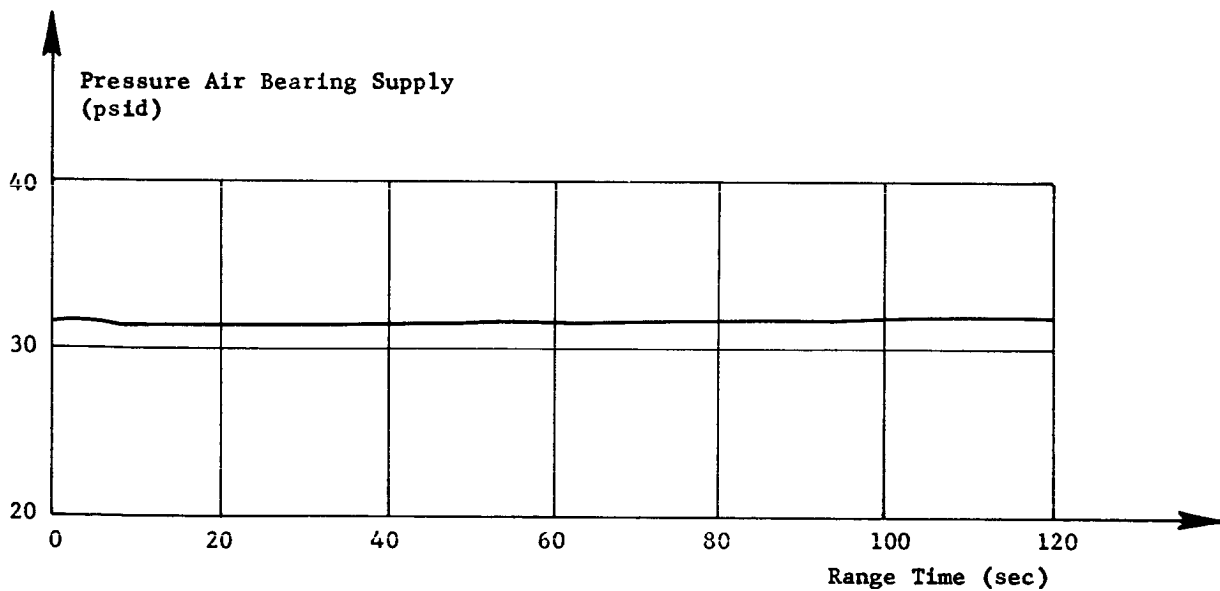
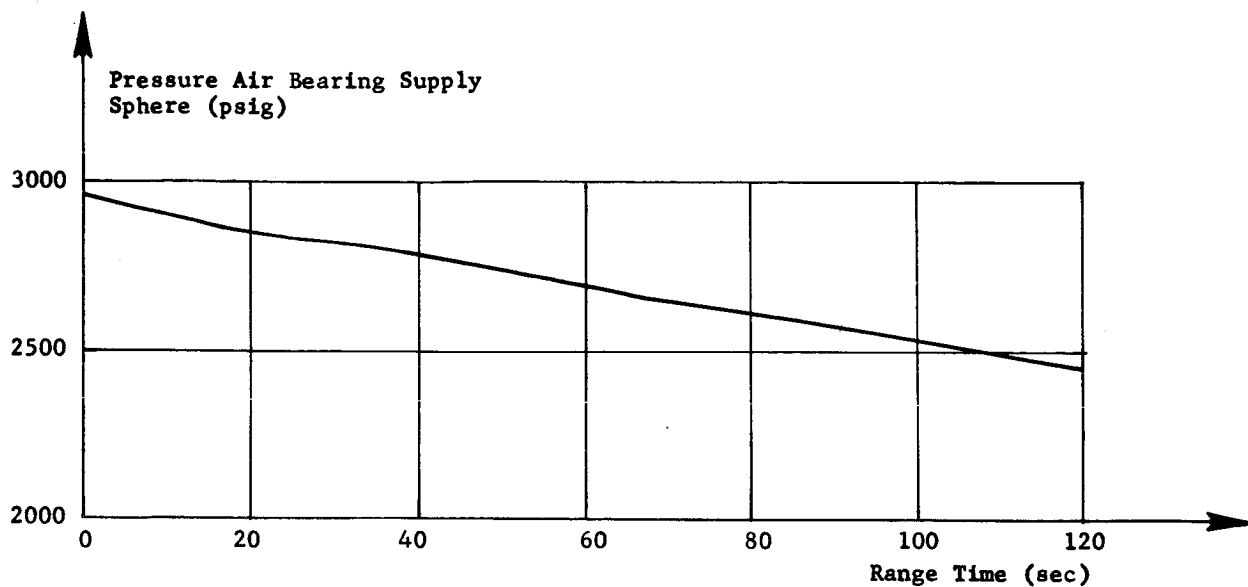


Figure 5-20 PRESSURE AIR BEARING SUPPLY SPHERE AND AIR BEARING SUPPLY

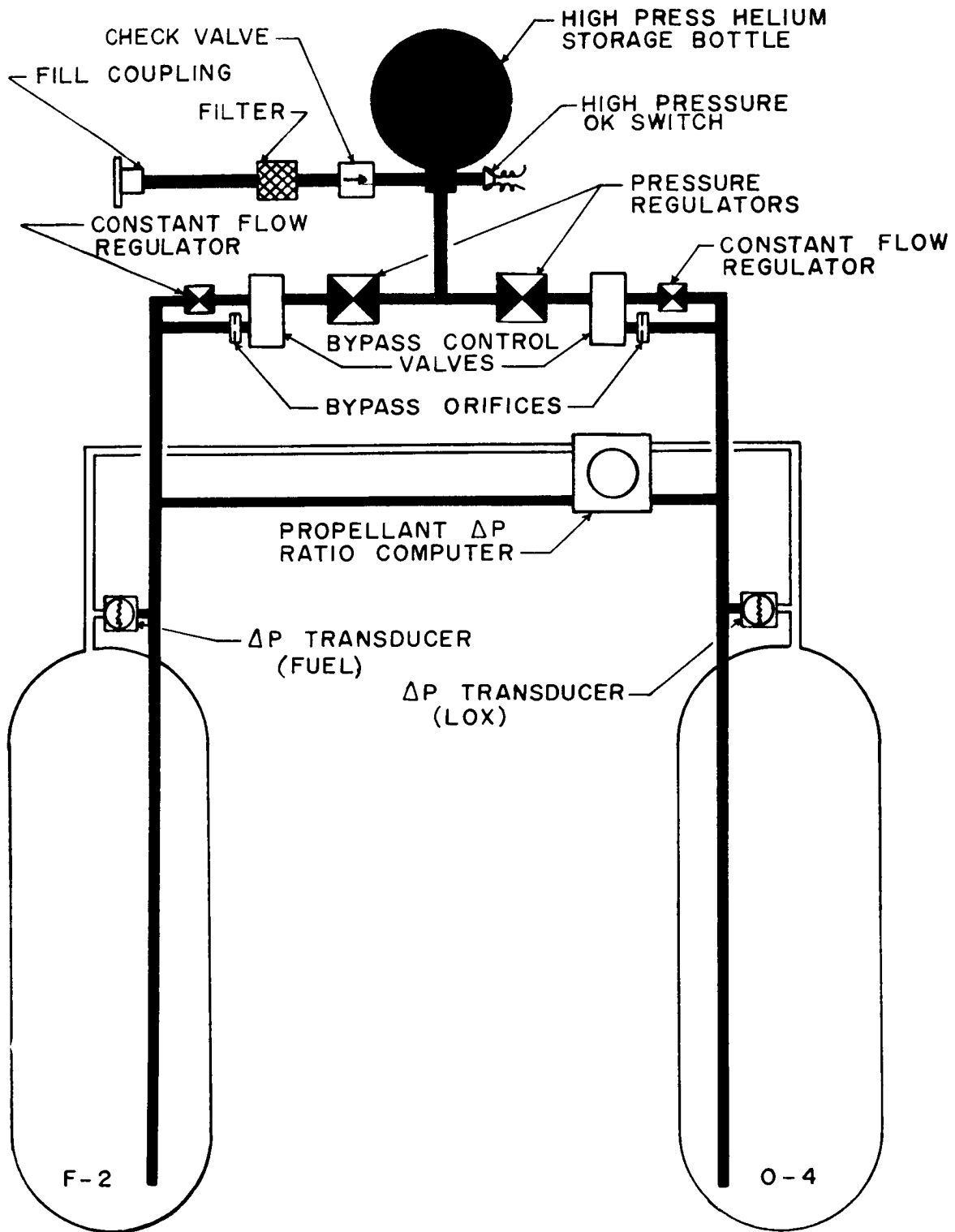


Figure 5-21 PROPELLANT UTILIZATION SYSTEM

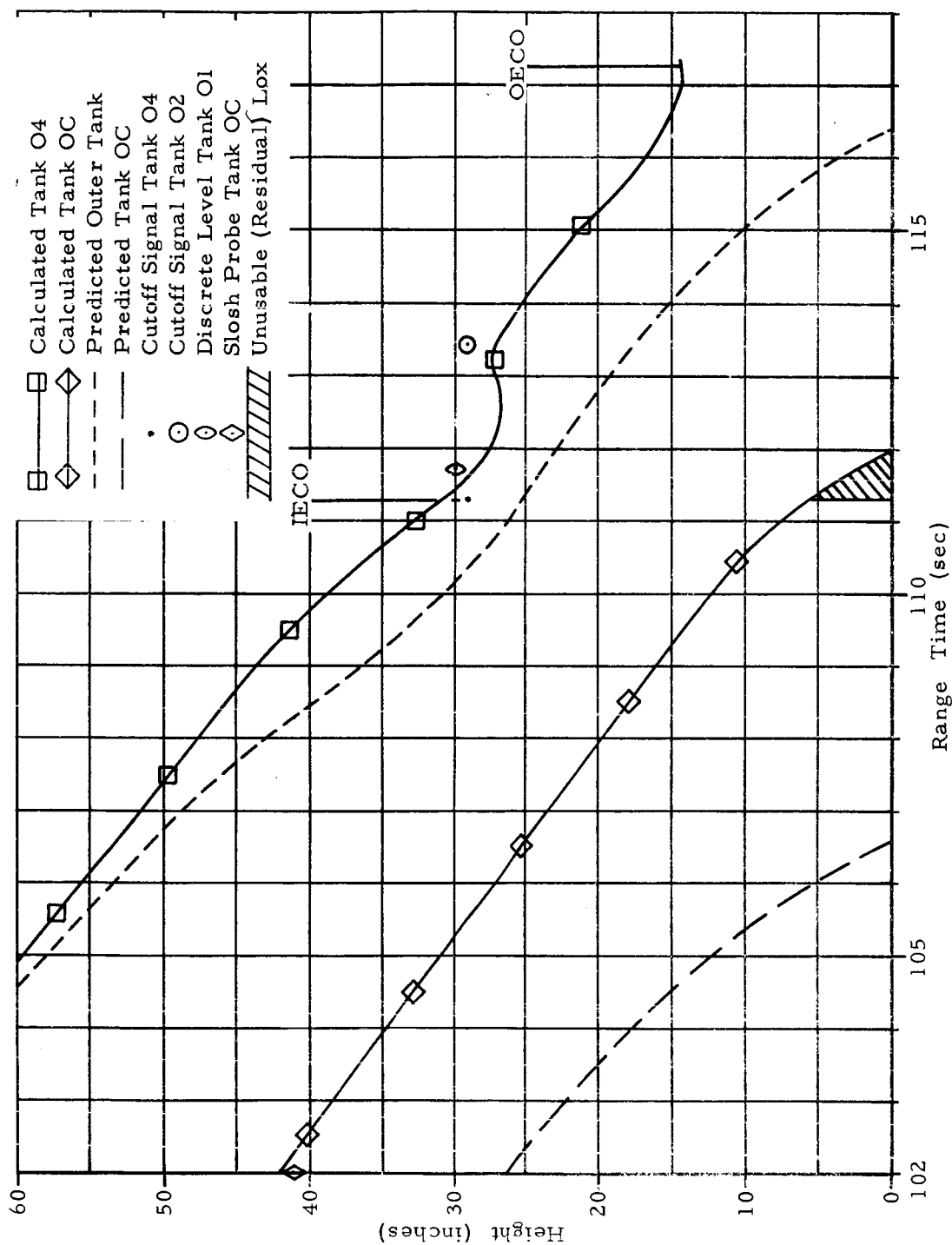


Figure 5-22 PROPELLANT HEIGHT ABOVE BOTTOM OF LOX TANK

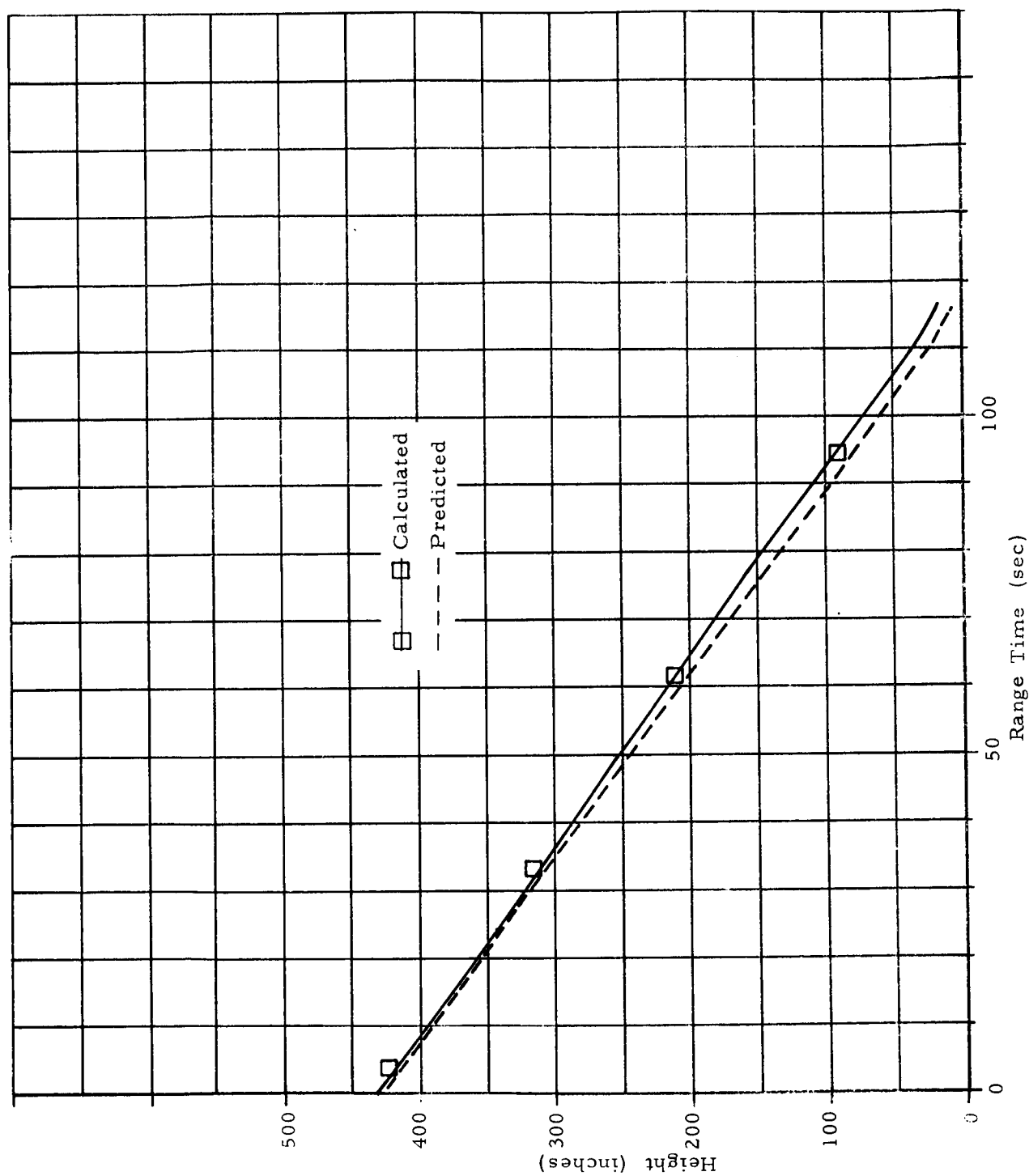


Figure 5-23 LIQUID HEIGHT ABOVE TANK BOTTOM - FUEL TANK F2

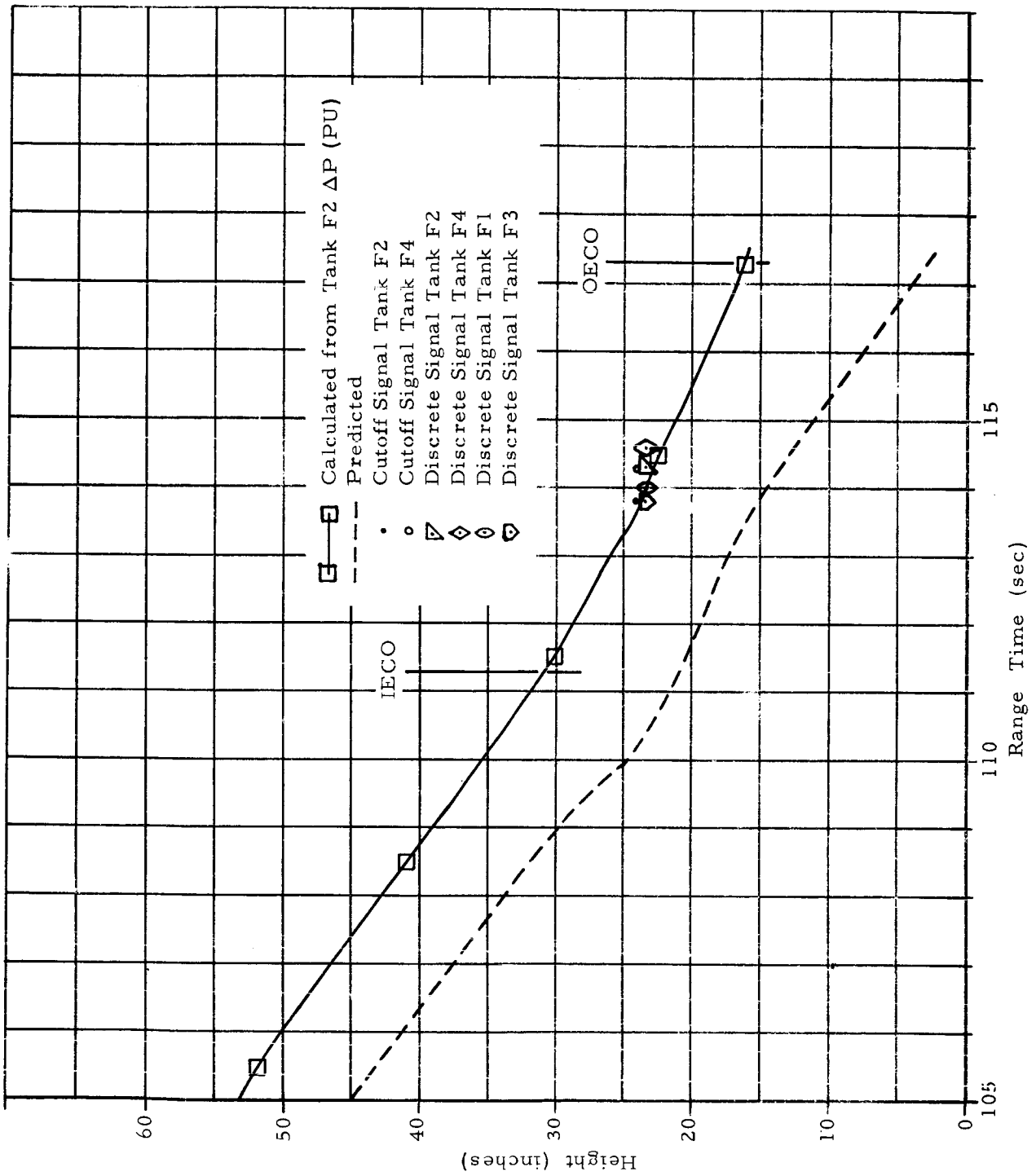


Figure 5-24 LIQUID HEIGHT ABOVE TANK BOTTOM - FUEL TANK F2

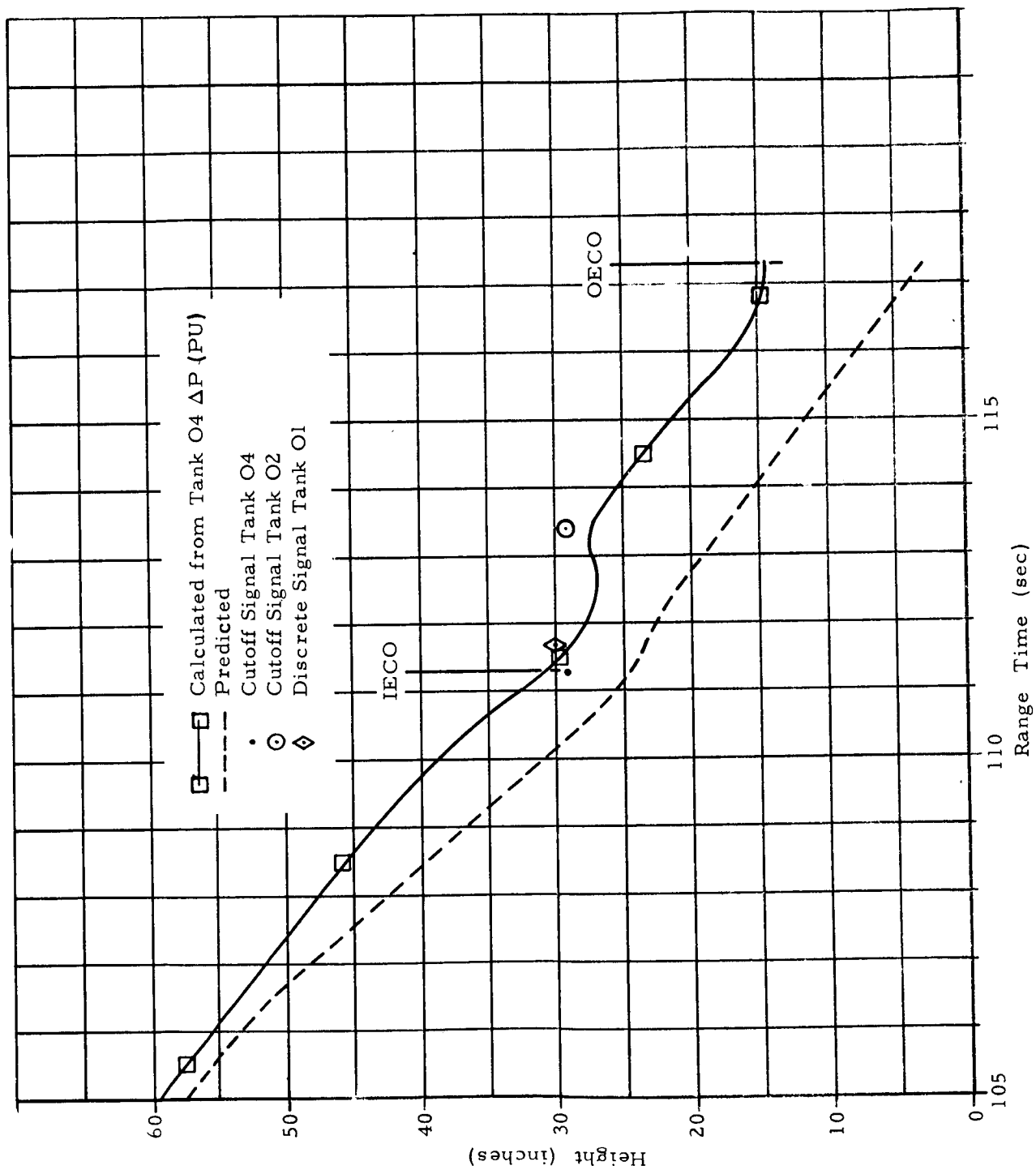


Figure 5-25 LIQUID HEIGHT ABOVE TANK BOTTOM - LOX TANK O4

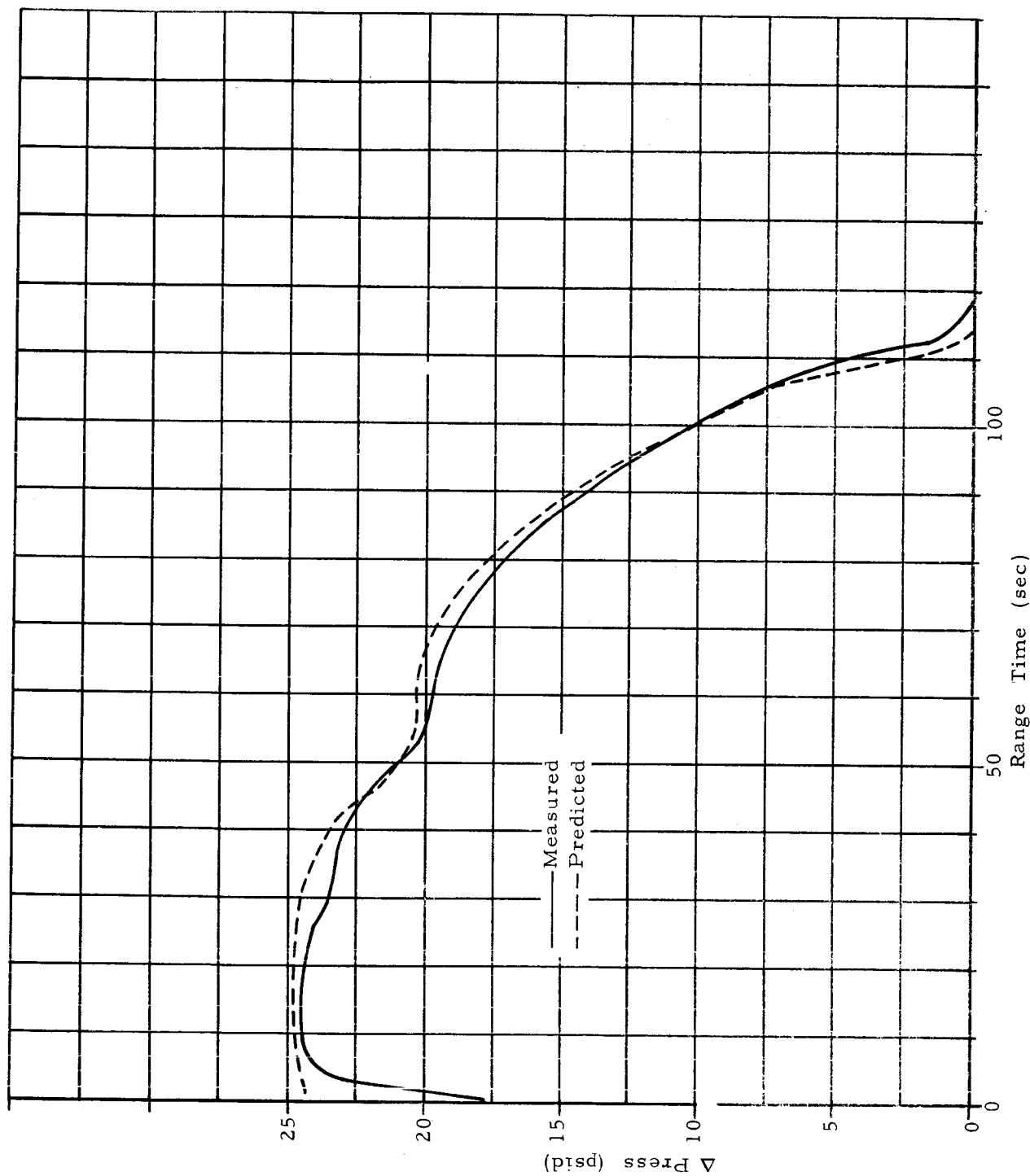
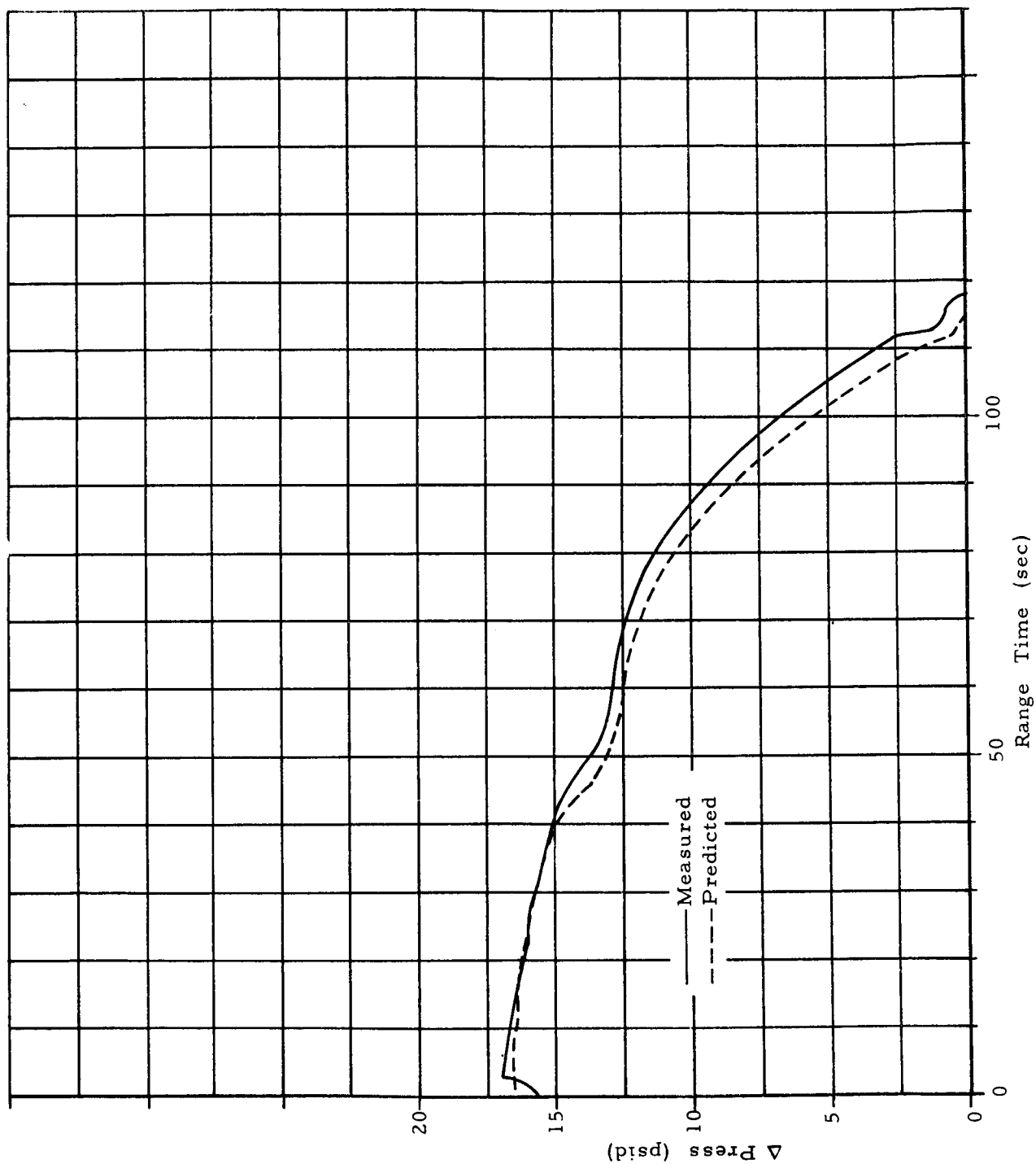


Figure 5-26  $\Delta$  PRESSURE PU COMPUTER, LOX, FINE

Figure 5-27  $\Delta$  PRESSURE PU COMPUTER, FUEL, FINE

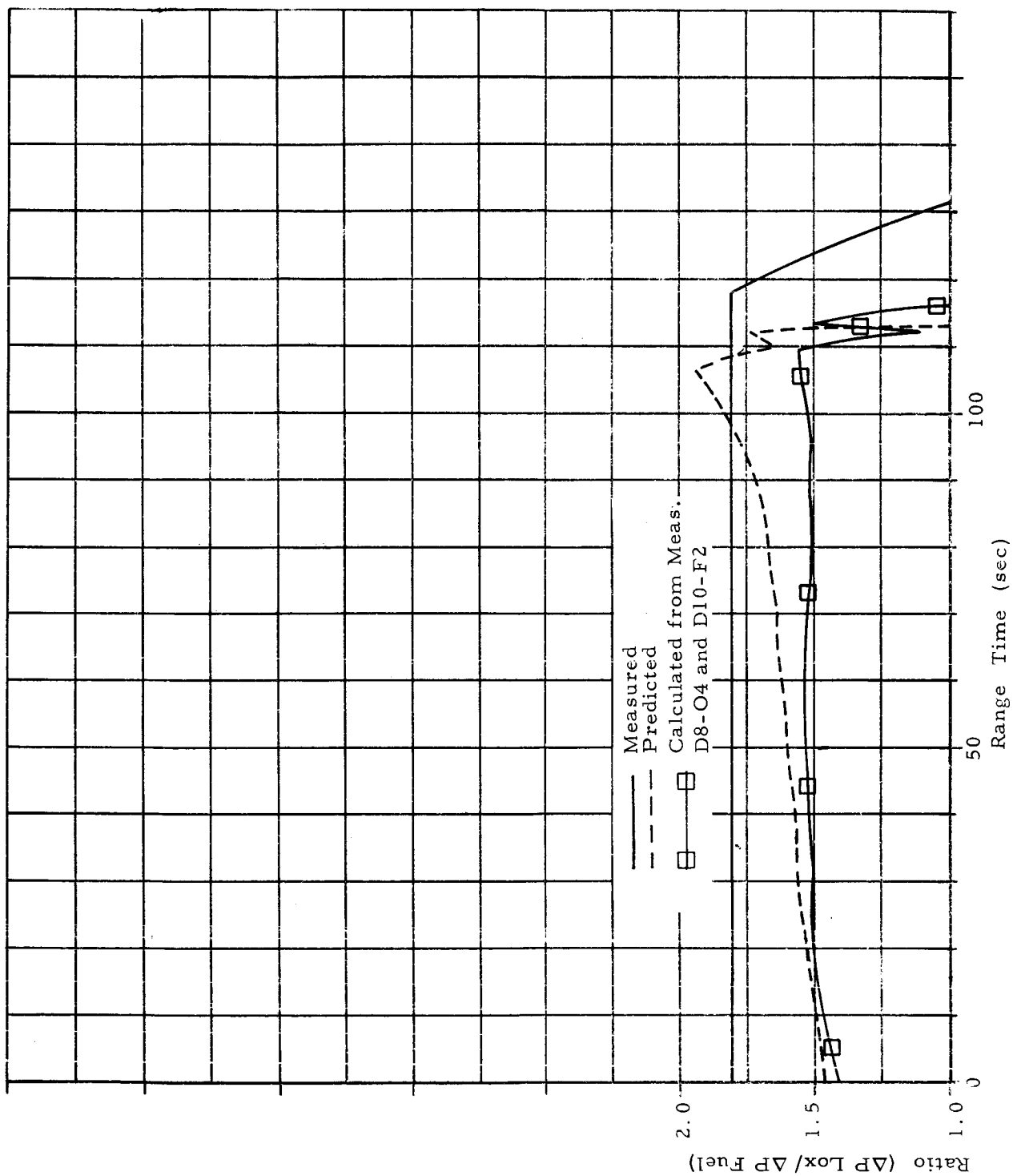


Figure 5-28 PROPELLANT UTILIZATION COMPUTER OUTPUT, FINE (A18-11)

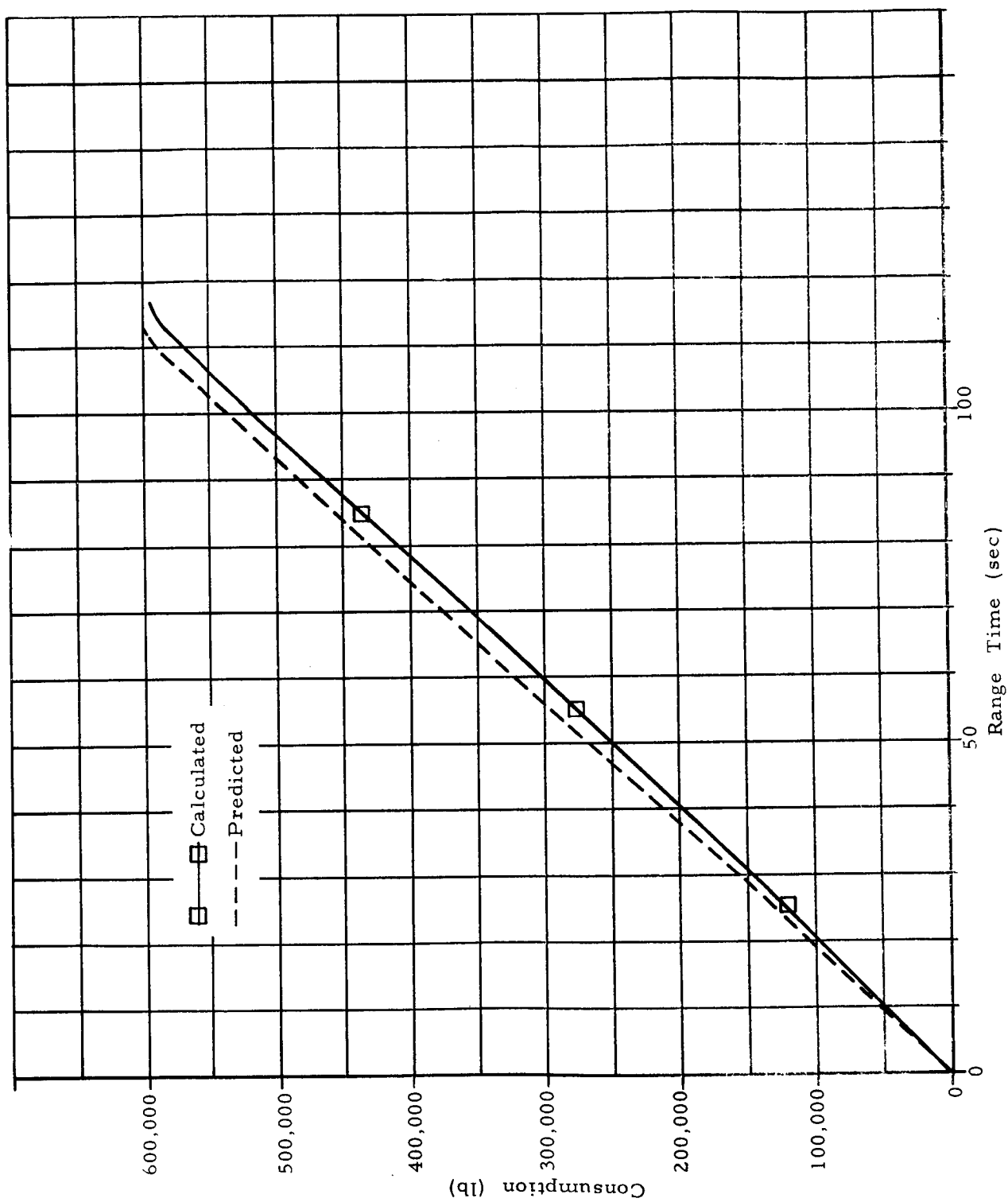


Figure 5-29 VEHICLE TOTAL PROPELLANT CONSUMPTION

level went above predicted (which is in agreement with the LOX  $\Delta P$  data). Calculated fuel level was continuously higher than predicted (which is in agreement with the fuel  $\Delta P$  data). Figures 5-24 and 5-25 also show the time and level of several other measurements (cutoff probes, level discrete probes, and slosh probes). It is noted that the PU system was not designed to give an exact level.

LOX and fuel container levels for the later part of powered flight are indicative of the rate of propellant utilization as well as the total utilization (Figures 5-26 and 5-27). During this portion of powered flight the propellant level variations from predicted were the greatest. However, for the comparison of propellant utilization the levels must be compared at predicted and actual inboard cutoff.

## 5.6 HYDRAULIC SYSTEM

The performance of all four hydraulic systems was well within the desired limits for proper operation. No malfunctions or major deviations from expected performance occurred.

The pressure of the hydraulic oil at the main pump outlet was monitored by a hydraulic "OK" pressure switch which actuated at a pressure of 2760 psig and deactuated at approximately 2500 psig. This device was originally intended to initiate cutoff on all engines at thrust commit if the oil pressure in any hydraulic package was below 2500 psig. This cutoff capability was eliminated prior to the SA-1 launch; however, the switch operation was monitored by an observer for both SA-1 and SA-2. On SA-1 the switches on hydraulic packages 2, 3, and 4 were observed to actuate and deactuate at random frequency between ignition command and thrust commit. This was due to the normal pressure pulsations from the hydraulic pump. On SA-2, an orifice (0.032 inches in diameter) was installed in the line between the pump outlet and the switch on each hydraulic package. No random flickering of the switch was observed on SA-2, indicating that the orifice successfully damped out the pressure pulsations between the pump and the switch.

The hydraulic source pressure and oil levels (Figure 5-30) indicate the over-all satisfactory performance of the hydraulic systems.

## 5.7 (C) MASS CHARACTERISTICS

Mass characteristics of SA-2, including predicted and actual values, are presented in Appendix D. The actual and predicted dry vehicle mass characteristics do not agree because of differences in actual and predicted water ballast and dry vehicle weights. Since

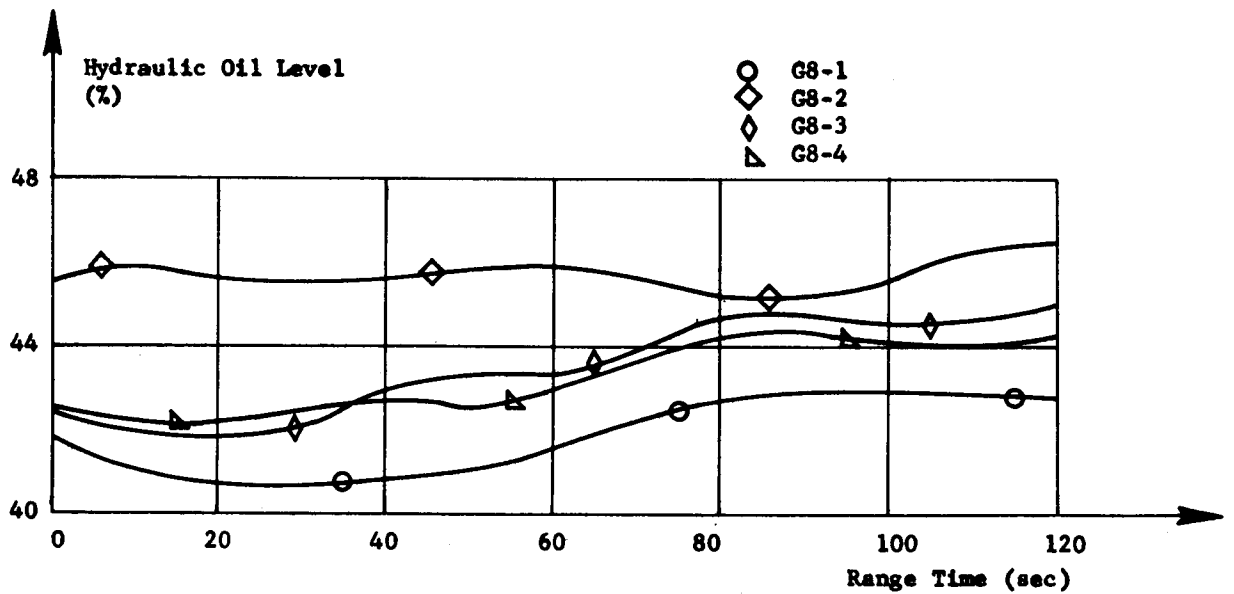
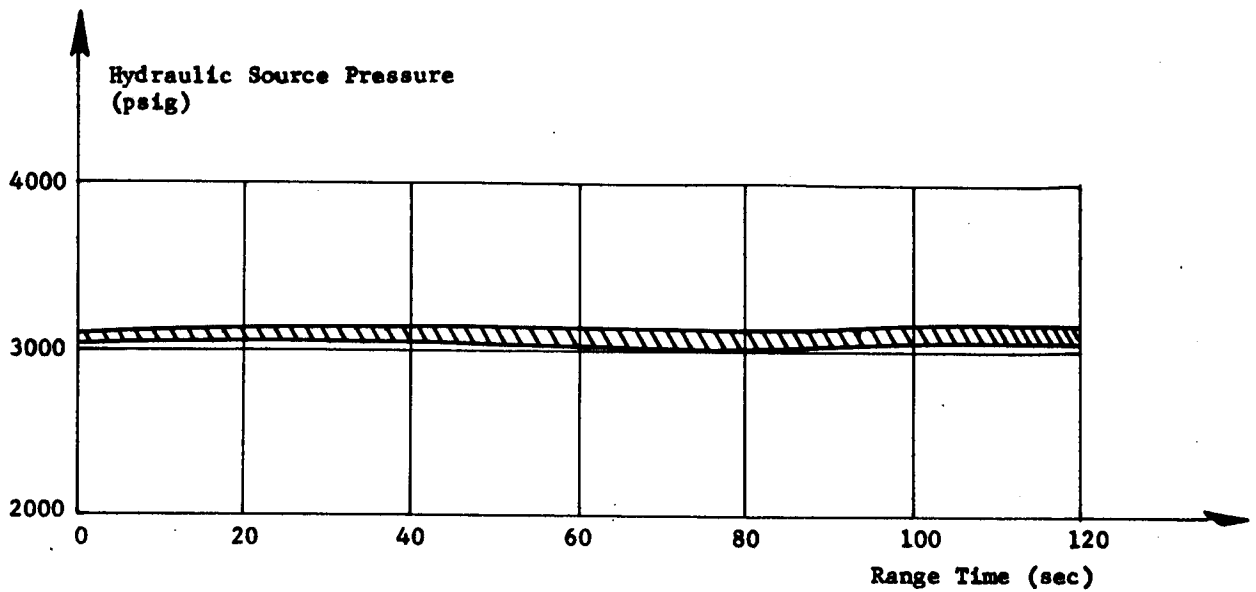


Figure 5-30 HYDRAULIC SOURCE PRESSURE AND HYDRAULIC OIL LEVEL

LOD did not weight the dry vehicle, a possible deviation of  $\pm 0.4\%$  (+ 1232 pounds) should be considered in addition to the deviation shown (921 pounds) in Appendix D.

The propulsion system performance as established by flight reconstruction and flight trajectory simulation agreed to within 0.2% making changes or adjustments of vehicle weights unnecessary for SA-2.

The total vehicle weights were:

Total Liftoff Weight:	925,679 lbs
Total Weight at IEEO:	347,158 lbs
Total Weight at OEEO:	330,832 lbs

## 6.0 (C) CONTROL

## 6.1 SUMMARY

The control system used for SA-2 was the same as on SA-1, with the exception of the tilt programmer, and the general performance was satisfactory.

The only observed discrepancy was found in the operation of the tilt programmer which introduced moderate disturbances into the vehicle control system approximately every 13 seconds. These disturbances were traced to the tilt programmer fine zero adjust mechanism. Although tests have shown that proper adjustment of this mechanism can satisfactorily reduce these disturbances, a new zeroing mechanism will be incorporated in SA-3.

No appreciable sloshing appeared towards the end of powered flight on SA-2 as occurred on SA-1. Additional baffles added to the bottom of the 70 inch propellant tanks on SA-2 were effective in reducing the sloshing amplitudes by a factor of approximately ten.

The maximum wind components determined by rawinsonde during the high Q region of flight were 31.7 m/sec tail wind in pitch and 13.6 m/sec from the right in yaw. Maximum control parameters of the SA-2 powered flight were as follows:

Parameter*	Magnitude	Time (sec)
Pitch Axis		
Attitude	2.8 deg	67.4
Angle of Attack (Free-stream)	-6.7 deg	98.3
Angular Velocity	-1.6 deg/sec	79.3
Normal Acceleration	-2.3 m/sec <sup>2</sup>	63.7
Actuator Positions	-4.9 deg	63.5
Yaw Axis		
Attitude	0.6 deg	70.9
Angle of Attack (Free-stream)	-2.4 deg	33.5
Angular Velocity	0.6 deg/sec	70.3
Normal Acceleration	-0.7 m/sec <sup>2</sup>	39.3
Actuator Positions	-1.4 deg	63.2
Roll Axis		
Attitude	0.9 deg	89.3
Angular Velocity	-0.8 deg/sec	112.1
Effective Engine Deflection	0.1 deg	89.4

\* For sign definition see page 6

~~CONFIDENTIAL~~

The Edcliff control accelerometers flown for operational study purposes on SA-2 indicate that closed loop operation could be satisfactory. Statham control accelerometers, which are planned for test on SA-3 and closed loop operation on SA-4, contain design improvements and should be even superior to the Edcliff instruments.

The control rate gyro package (a 3 axis Minneapolis Honeywell package) operated properly. Some vibration effects were evident in their outputs; however, with proper filtering this package could give satisfactory performance as an active control sensor. The rate gyro package located in the tail (a 2 axis Kearfott "measuring" package) on SA-2 also gave satisfactory results except possibly around liftoff. During this period a 3 cps oscillation was picked up by the tail rate gyros which has not, as yet, been identified with a basic body bending mode.

The Q-ball angle of attack system, flown as a passenger, operated satisfactorily at least between 30 and 80 seconds of flight and appears suitable for possible control applications. Possible measuring inaccuracies do not allow any definite conclusions concerning the later portion of flight.

## 6.2 S-1 CONTROL ANALYSIS

### 6.2.1 PITCH PLANE

During the powered flight phase, attitude control torques were obtained by swiveling the four outboard engines. Attitude control torques are not available after outboard engine thrust decay.

First motion occurred at 0.22 seconds range time, 3.83 seconds after ignition command.

Pitch attitude deviations were essentially zero prior to 33 seconds (Figure 6-1). Vertical flight was maintained until 10.4 seconds when vehicle tilting was started by the tilt programmer. Unlike SA-1, the pitch programming of SA-2 was provided by a cam device (located in the servo loop amplifier box) which was cut for a preselected tilting program. This program was based on the seven engine operating condition to minimize control requirements in case of an engine failure. Final tilt arrest was made at 99.5 seconds with a tilt angle of 43 degrees from the launch vertical.

The cam device used for SA-2 tilting program provided continuous tilting from the time of initiation to the end of tilt. The tilt rate varied from zero at the time of activation (liftoff) to a maximum of 0.66 deg/sec at 70 seconds. The cam was not shaped to give a smooth

~~CONFIDENTIAL~~

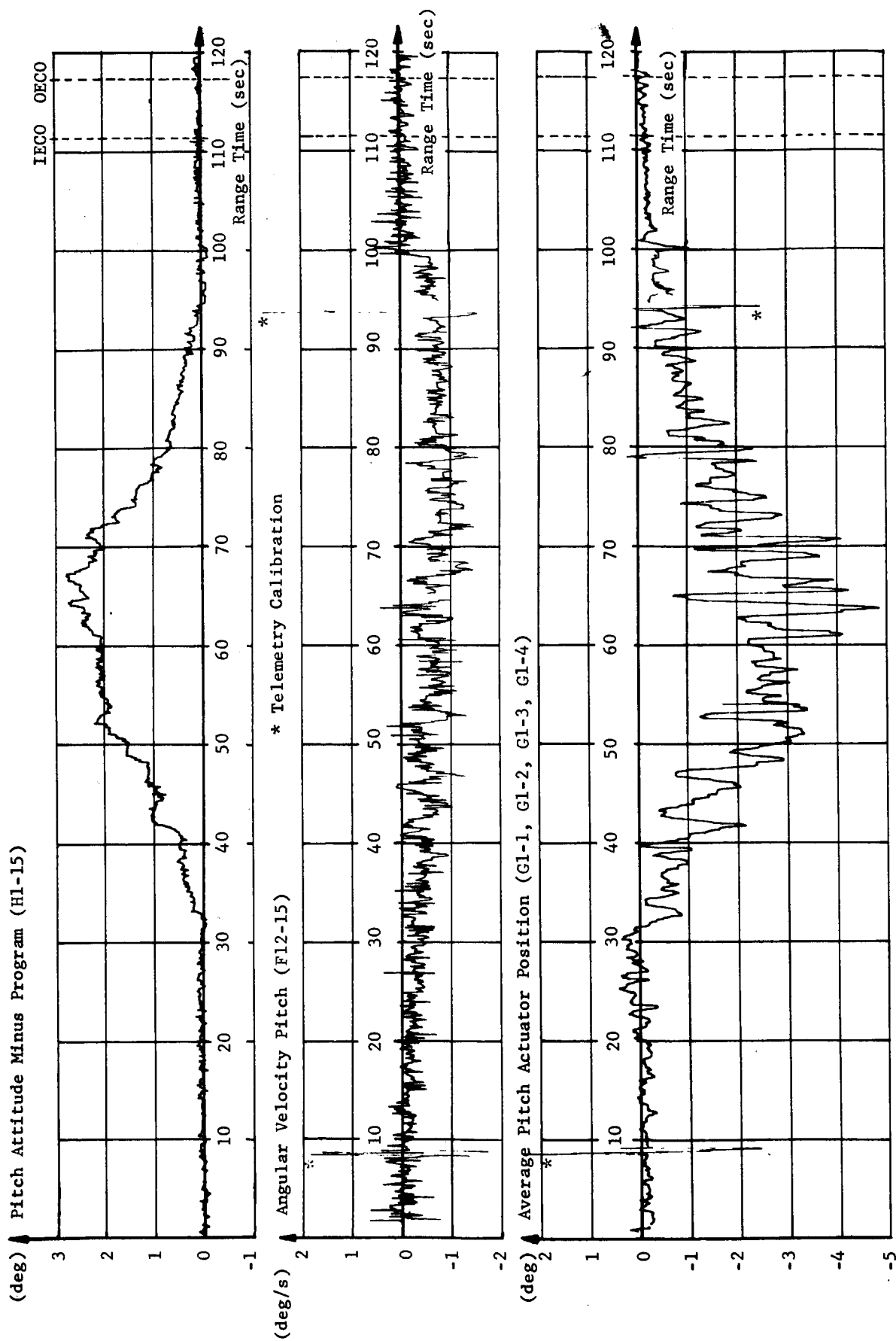


Fig. 6-1 PITCH ATTITUDE, ANGULAR VELOCITY AND ACTUATOR POSITION

~~CONFIDENTIAL~~

termination of tilt; therefore, a kick in the pitch actuator positions along with a sudden change in the pitch angular velocity was observed at 99.5 seconds (Figure 6-1). The tilt rate changed from 0.5 deg/sec to zero at this time. This will be corrected for SA-3 by gradually smoothing out the requested program at the end of the tilt program. Figure 6-2 shows the predicted tilting program together with the space-fixed pitch plane velocity vector angle.

The tilt angle measurement is inadequate for evaluation purposes due to the large measuring range (0 to 55 degrees). It is hoped that an improvement of this measurement can be made on future flights.

When the tilting program was arrested at 99.5 seconds the pitch local angle of attack was -8.0 degrees. This angle of attack was almost entirely due to the trajectory shaping. The angle of attack was reduced after this time (see Figure 6-3) by the gravity turn of the velocity vector.

Figure 6-3 shows a comparison of the pitch component winds from three sources of information - rawinsonde, rocketsonde and angle of attack winds. The angle of attack winds (solid line) were determined from attitude and angle of attack measurements made on-board the vehicle which were combined with trajectory angles and velocity components from tracking. Local angles of attack as measured by the U. S. Science (formerly Topp) indicators were used for this calculation after an appropriate correction for the upwash factor was made. Rawinsonde ceiling was 31.5 km (93.1 seconds) from a combination of T + 0 and T + 2 hour winds. Measurement of the T + 0 winds terminated at 23.25 km. Angle of attack winds after approximately 105 seconds are considered unreliable due to the low vehicle dynamic pressure. Rocketsonde wind measurements taken at T + 6 hours were obtained over the altitude range from 30.5 (91.7 seconds) to 42.5 km (104.4 seconds). The agreement between these measurements and the angle of attack winds was good throughout this period.

The maximum pitch plane wind component as measured by Rawinsonde was 31.7 m/sec at 66.0 seconds. This corresponds to an altitude of 13.5 km. The local pitch angle of attack at this time was -8.0 degrees. Approximately 41% of this angle of attack can be attributed to the winds and the fact that the control gains used do not correspond exactly with the drift minimum concept. The remaining portion is attributed to the fact that the tilt program is based upon the operation of only 7 engines.

Results for the pitch plane motion from a digital simulation are compared with telemetered attitude, free-stream angle of attack and average actuator position in Figure 6-4. The mathematical model used for this simulation includes the dynamics of the first elastic mode

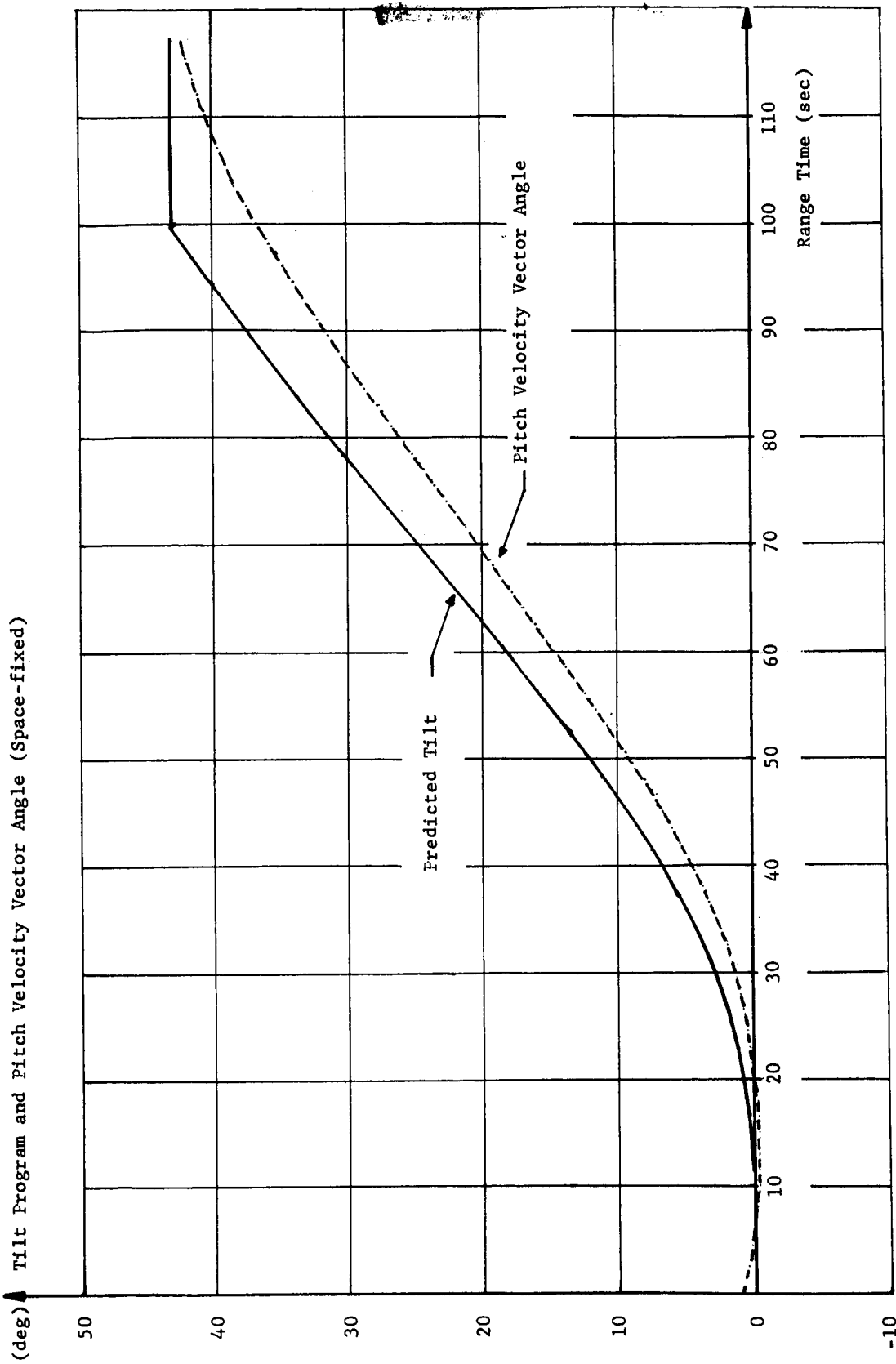


FIGURE 6-2 TILT PROGRAM AND PITCH VELOCITY VECTOR ANGLE

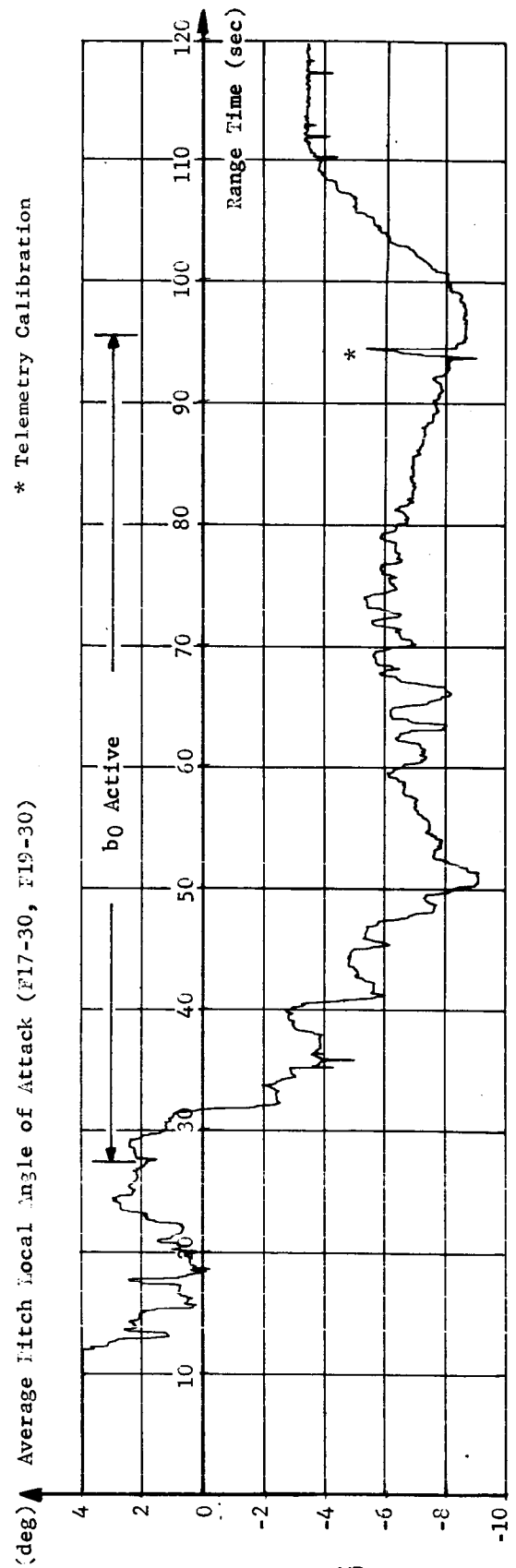
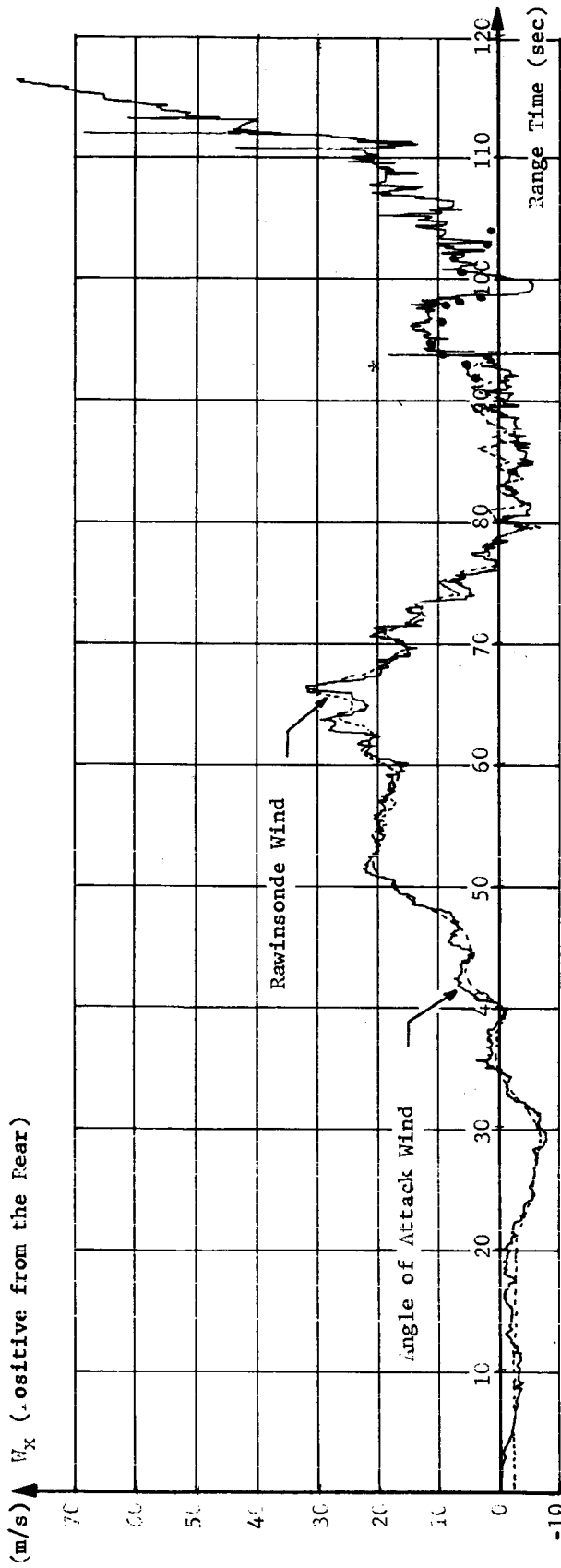


FIGURE 6-3 PITCH PLANE WIND COMPONENTS AND LOCAL ANGLE OF ATTACK

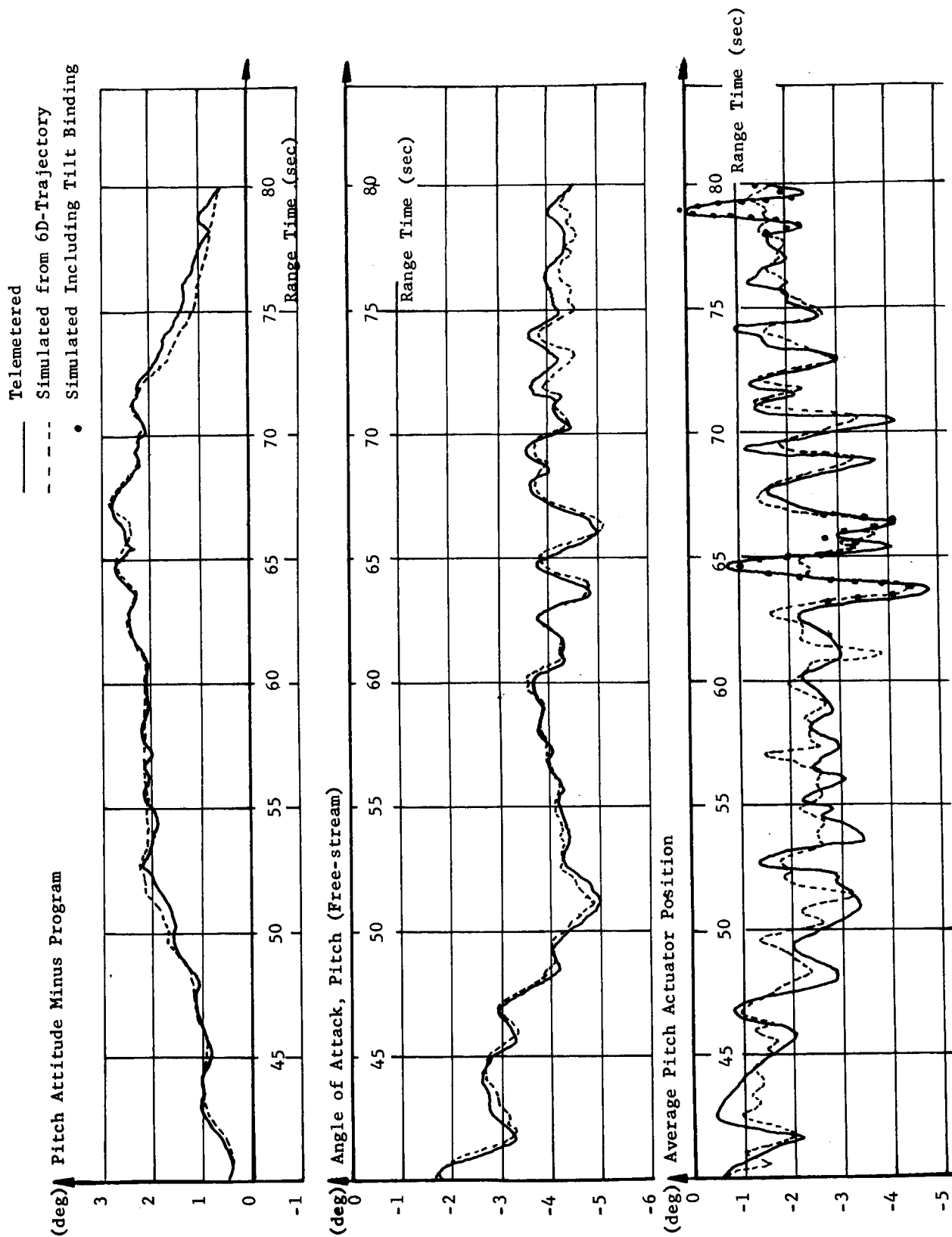


Fig. 6-4 PITCH ATTITUDE MINUS PROGRAM, FREE-STREAM ANGLE OF ATTACK (PITCH) AND AVERAGE PITCH ACTUATOR POSITION

~~CONFIDENTIAL~~

and the first sloshing mode. The control system filter network and swivel engine are represented by the appropriate transfer functions. Close agreement of the simulation trajectory with the tracking trajectory was obtained by using the best estimate of the actual weights and engine performance. As can be seen, the simulation gives a good representation of the actual control system action during the oscillations which are due primarily to wind gusts. Some of the small oscillatory motion appearing in the simulated engine deflections may be due to the calculated effect of propellant sloshing. No attempt was made to phase the sloshing in the calculations with the flight history and, since this does have an effect on the response, it may account for these small differences when comparing with the telemetered. The entire time history of the telemetered average engine actuator positions in pitch is shown in Figure 6-1.

There are several time periods in which distinct variations appear between telemetered and simulated pitch actuator positions. Six of these periods of deviation were probably direct results of loading of the tilt mechanism. The transients due to the tilt program interference are seen in the telemetered pitch actuator deflections (Figure 6-1) between 26 and 92 seconds of flight time. These transients occurred approximately every 13 seconds. The amplitude of the actuator deflection transients were a function of the tilt rate, with a maximum in the high dynamic pressure region. See Section 6.3.2 for a detailed description of the mechanism for these transients.

The SA-2 spare tilt mechanism has been placed in the Analog Flight Simulator at Astrionics Division. This simulator study resulted in peak actuator deflections of 0.5 deg which occurred, as in the SA-2 flight, every 13 seconds. To obtain deflections of the magnitude seen on the SA-2 flight, it was necessary to increase the tension on the fine zero switch actuating lever.

Two of these transients were also simulated with a digital simulation program by slowing the tilt rate for a short period and then increasing the rate so that the tilt angle would converge to the predicted value. The first simulation was made at 64 seconds. To match adequately the actual response of the actuators required a tilt rate of 0.4 deg/sec for 0.6 seconds beginning at 64.81 seconds and then switching to a rate of 0.9 deg/sec for 0.6 seconds was required, compared to a desired tilt rate at this time of 0.65 deg/sec. This results in a 0.12 deg maximum tilt deviation from the expected value. Similar results were obtained for the simulation at 78 seconds. The tilt rate was made to deviate from the expected rate, beginning at 77.9 seconds by about -0.2 deg/sec for 0.6 seconds and +0.2 deg/sec for 0.6 seconds resulting again in about 0.1 degree tilt deviation from the expected value. These results are shown as the solid dots in Figure 6-4.

~~CONFIDENTIAL~~

~~CONFIDENTIAL~~

At 63.5 seconds the maximum actuator deflection of -4.9 degrees occurred as a result of a wind gradient of 0.02/sec over an altitude increment of 400 meters. This gust as determined from the angle of attack winds had a velocity increment of 8.1 m/sec compared to 7 m/sec from rawinsonde winds. This resulted in 0.33 degree of actuator deflection per m/sec increment in wind velocity. This compares favorably with 0.38 degree per m/sec observed on SA-1. The maximum engine deflection experienced on the flight of SA-1 was -4.6 degrees at 62.9 seconds. The maximum winds in the pitch plane were only 5.1 m/sec less on SA-2 than were observed on the flight of SA-1. The general wind profile for the pitch component was actually very similar in both magnitude and direction (tail wind); hence, similar engine deflections were observed on both flights.

The telemetered pitch normal acceleration from the control accelerometer, which was close to the vehicle center of gravity is shown in Figure 6-5. This accelerometer was not in the control loop but was flown as a passenger for operational information. The accelerometer was located at station 879 on the web of the spider beam 44.5 inches from the longitudinal axis toward Fin position III. This measurement showed a considerable amount of high frequency (10 - 15 cps) oscillations. For comparison with calculated values shown in the lower portion of Figure 6-5 the telemetered acceleration was digitally smoothed from 0.01 second data using 31 point second degree polynomial smoothing. The calculated acceleration is based on telemetered angles of attack and engine positions and assumes a rigid body. The agreement between the two results is good except for the higher frequency oscillations (greater than approximately 1 cps) appearing in the telemetered acceleration. There also appears to be a slight bias in the telemetered values prior to 40 seconds. This could possibly be due to the smoothing process used if the noise had not been purely gaussian during this time period. A voltage shift in telemetry could also contribute to this effect since in reduction of the data only two in-flight calibration points are available and these are averaged for reduction purposes.

The maximum pitch acceleration observed was  $-2.3 \text{ m/sec}^2$  at 63.7 seconds. This accelerometer was located at station 879 on the web of the spider beam 44.5 inches from the longitudinal axis toward Fin position III.

Figure 6-6 shows an estimate of the pitch angle design criteria to be used for Block I vehicles SA-1 and SA-2 with eight engines operating on a seven engine tilt program. The values are considered estimates because constant factors have been used to account for the effects due to gusts and for aerodynamic parameter variations. The response due to the  $2\sigma$  steady-state winds has been increased by 25% to

~~CONFIDENTIAL~~

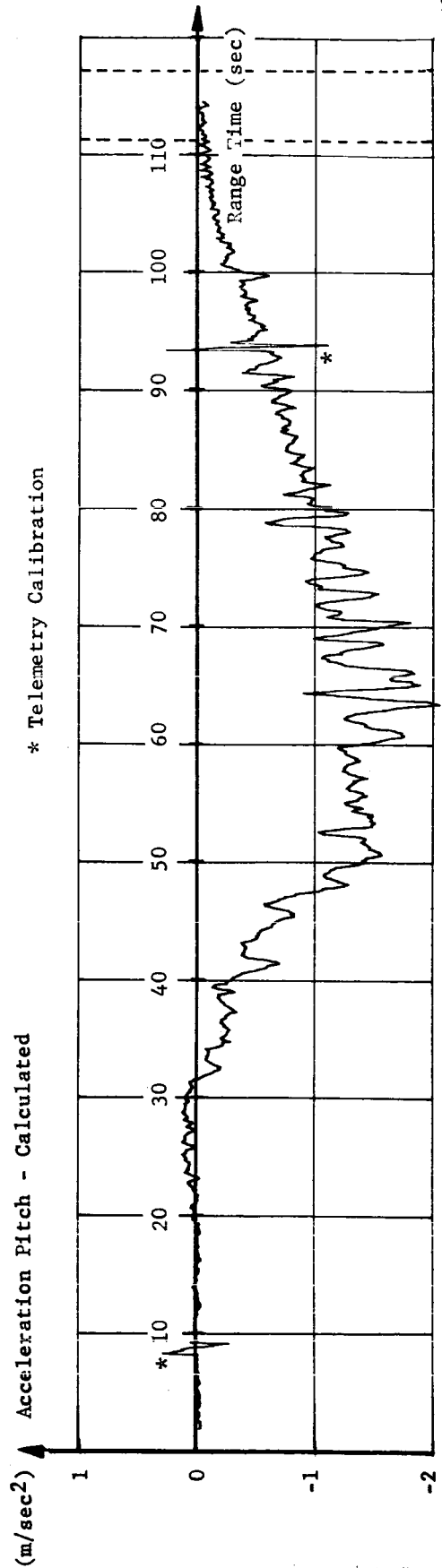
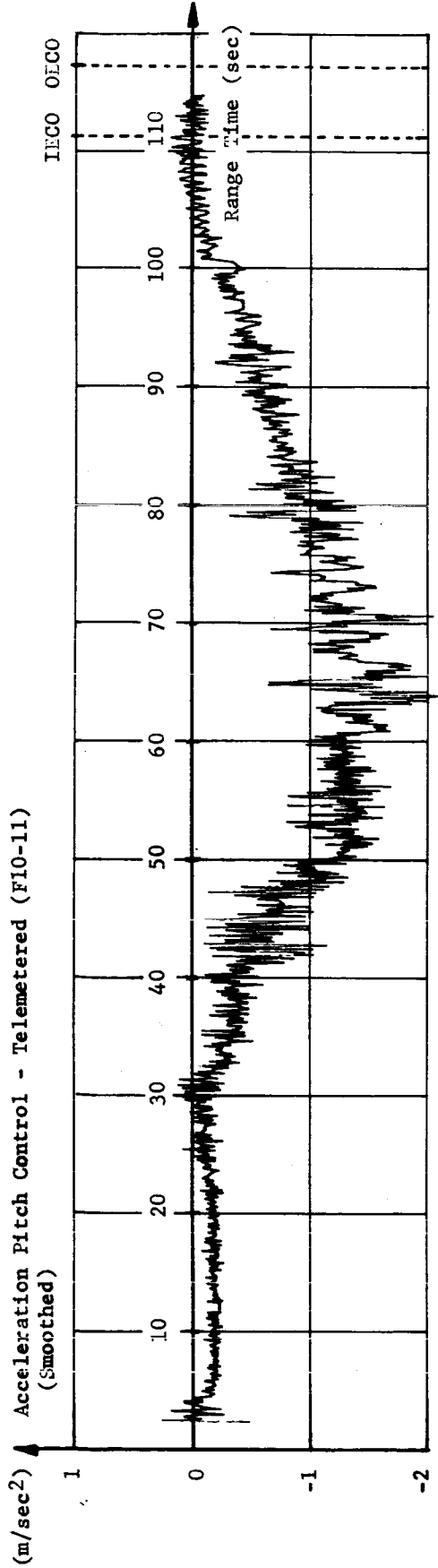


Fig. 6-5 PITCH NORMAL ACCELERATION

**CONFIDENTIAL**

account for the gusts. Variations in aerodynamic parameters have been accounted for by increasing the nominal response by 11%.

The solid lines in Figure 6-6 represent the design criteria as a function of time, and the circled points are the actual observed values from the SA-2 flight. Shown to the right of the figure are two bar graphs for each parameter which show an estimate of the budgeting for the various factors. The factors considered were:

1. Seven engine tilt program
2. Effect of control gains being different from drift minimum gains
3.  $2\sigma$  steady winds
4. Wind gusts
5. Stability ratio ( $C_L/B^0$ ) variations.

One bar graph represents the breakdown for the design value at 60 seconds, and the other represents an interpretation of the breakdown for the observed maximum values which occurred around 65 seconds.

The actual engine deflections approached the design limits even though the maximum wind in pitch was only 31.7 m/sec. The primary reason appears to be that the effect of the gusts is under-estimated for the design. There may also have been some small increase in the engine deflection due to the loading of the tilt programmer.

Even though the actual engine deflections approached the design limit, the angle of attack and resulting angle of attack - dynamic pressure product were well below the design values, and in this case the effect of the gusts was apparently adequately predicted.

**CONFIDENTIAL**

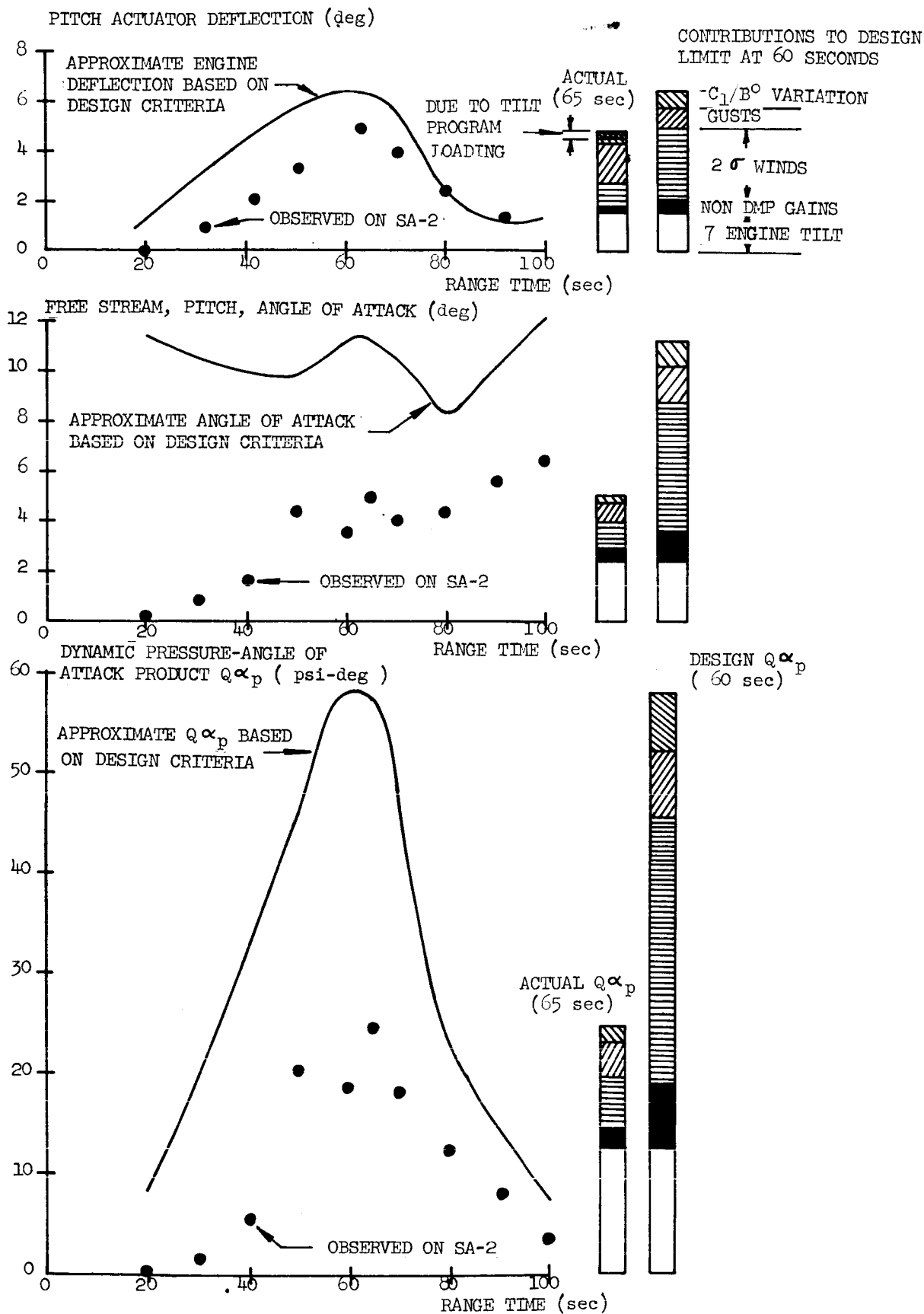


FIGURE 6-6 PITCH ANGLE DESIGN CRITERIA (8 ENGINES OPERATING ON 7 ENGINE TILT)

~~CONFIDENTIAL~~

### 6.2.2 YAW PLANE

Relatively small yaw attitude angles and engine deflections (Figure 6-7) were observed throughout the powered flight. Essentially all of the attitude deviations in this plane were due to winds.

Yaw plane wind components shown in Figure 6-8 were very light throughout the flight. The maximum yaw wind component was -13.6 m/sec (from right) at an altitude of 14.5 km (68 seconds).

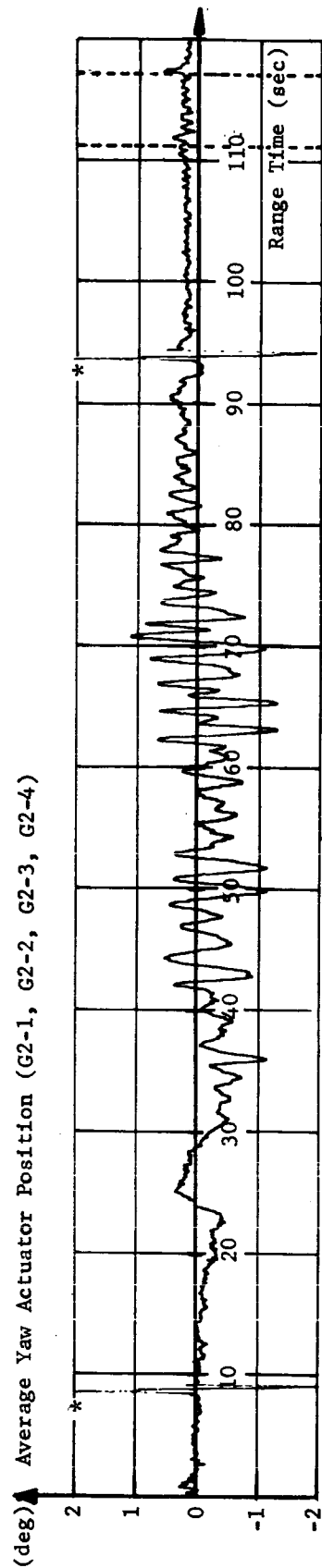
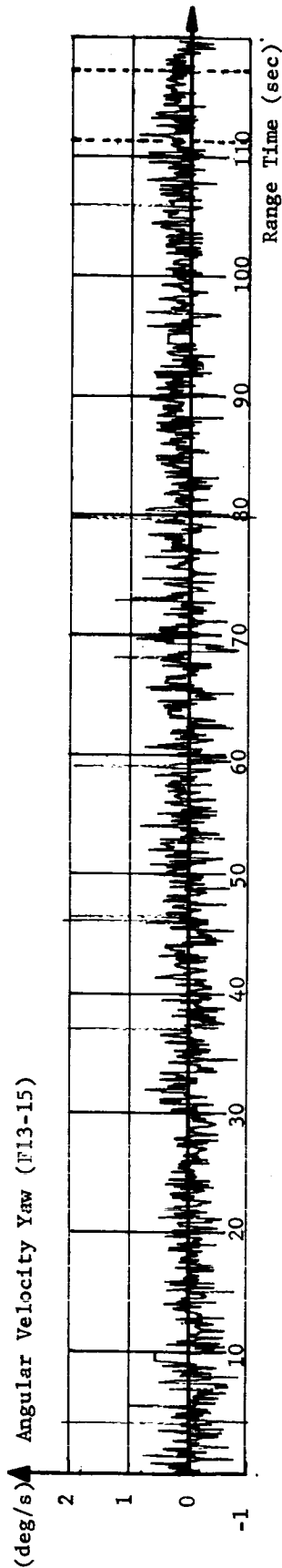
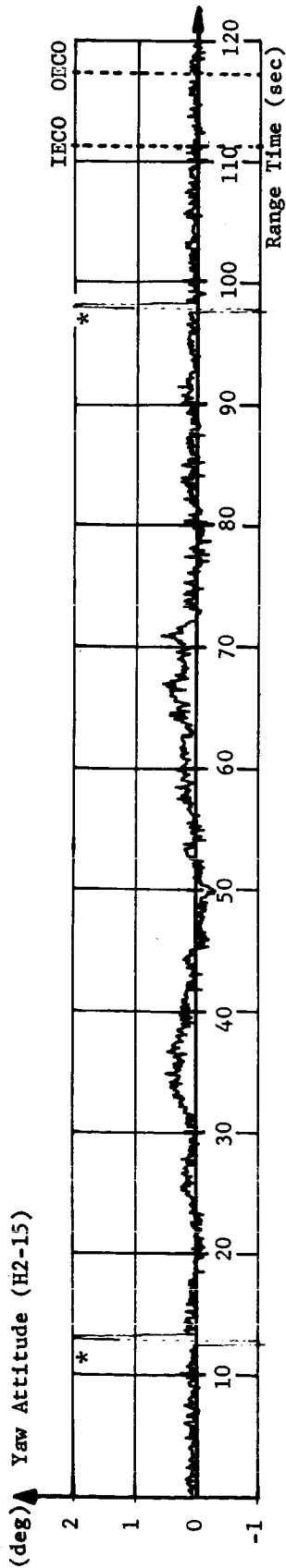
Rocketsonde measured winds are shown as solid points in the upper graph of Figure 6-8. Good agreement is obtained between the angle of attack winds (solid line) determined from onboard measurements and the externally measured wind velocity, at least to the end of rocketsonde data (104.4 seconds). The angle of attack winds determined from the local angle of attack indicators are considered unreliable after approximately 105 seconds due to the low dynamic pressure. Dynamic pressure at this time was 260 kp/m<sup>2</sup>. The dynamic pressure at which the angle of attack winds probably became unreliable on SA-1, based on rocketsonde winds obtained at a higher altitude, was 232 kp/m<sup>2</sup>.

Averages of the two local measured yaw angles of attack are shown in the lower portion of Figure 6-8. Yaw attitude angle, angular velocity and average actuator deflections in yaw are shown for the entire powered flight phase in Figure 6-7.

Yaw angular velocity (measurement Fl3-15) as shown in Figure 6-7 appears to have a non-constant bias. If the period at the beginning of flight is shifted into agreement with the derivative of the attitude angle and this constant shift applied over the entire power flight a discrepancy of approximately 0.2 deg/sec exists at cutoff. This discrepancy is probably the result of telemetry error.

Results for the yaw plane from the digital simulation of the flight from 40 to 80 seconds are shown in Figure 6-9. Virtually all of the oscillations appearing in the yaw actuator positions are the result of wind gusts. The greatest gust effects were experienced from 61 to 72 seconds with the largest oscillation in the actuator positions of  $\pm 1$  deg occurring at about 70 seconds. Pertinent data for three oscillations in yaw occurring during this period are shown in the table below.

~~CONFIDENTIAL~~



\* Telemetry Calibration

FIGURE 6-7 YAW ATTITUDE, ANGULAR VELOCITY AND ACTUATOR POSITION

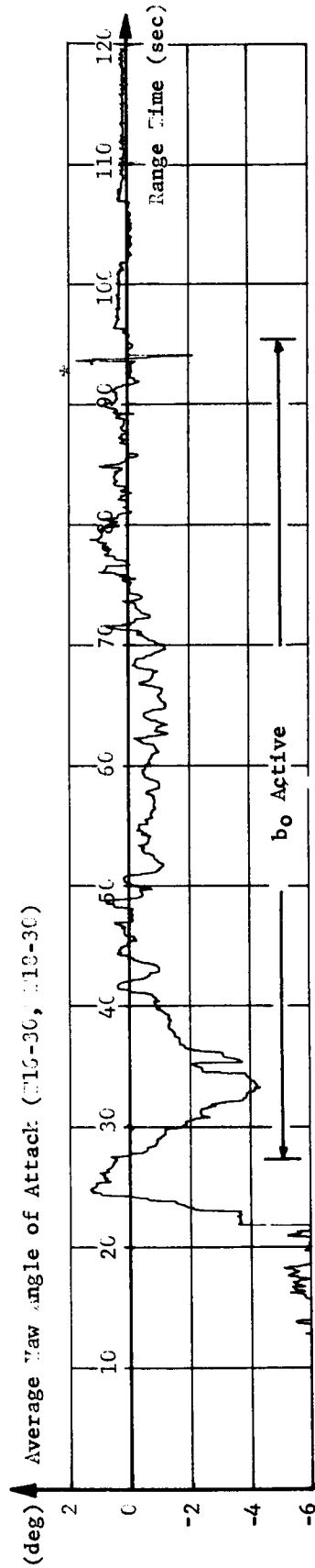
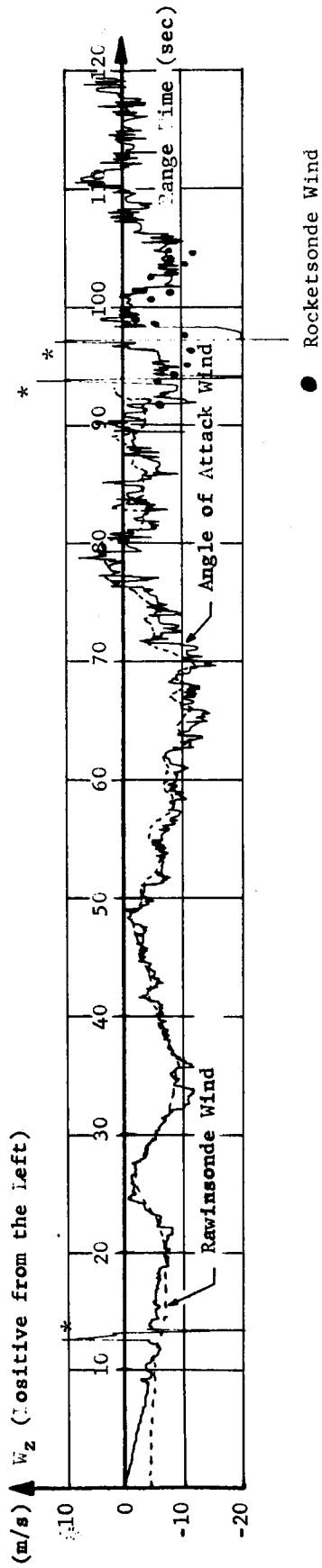


FIGURE 6-8 YAW PLANE WIND COMPONENTS AND LOCAL ANGLE OF ATTACK

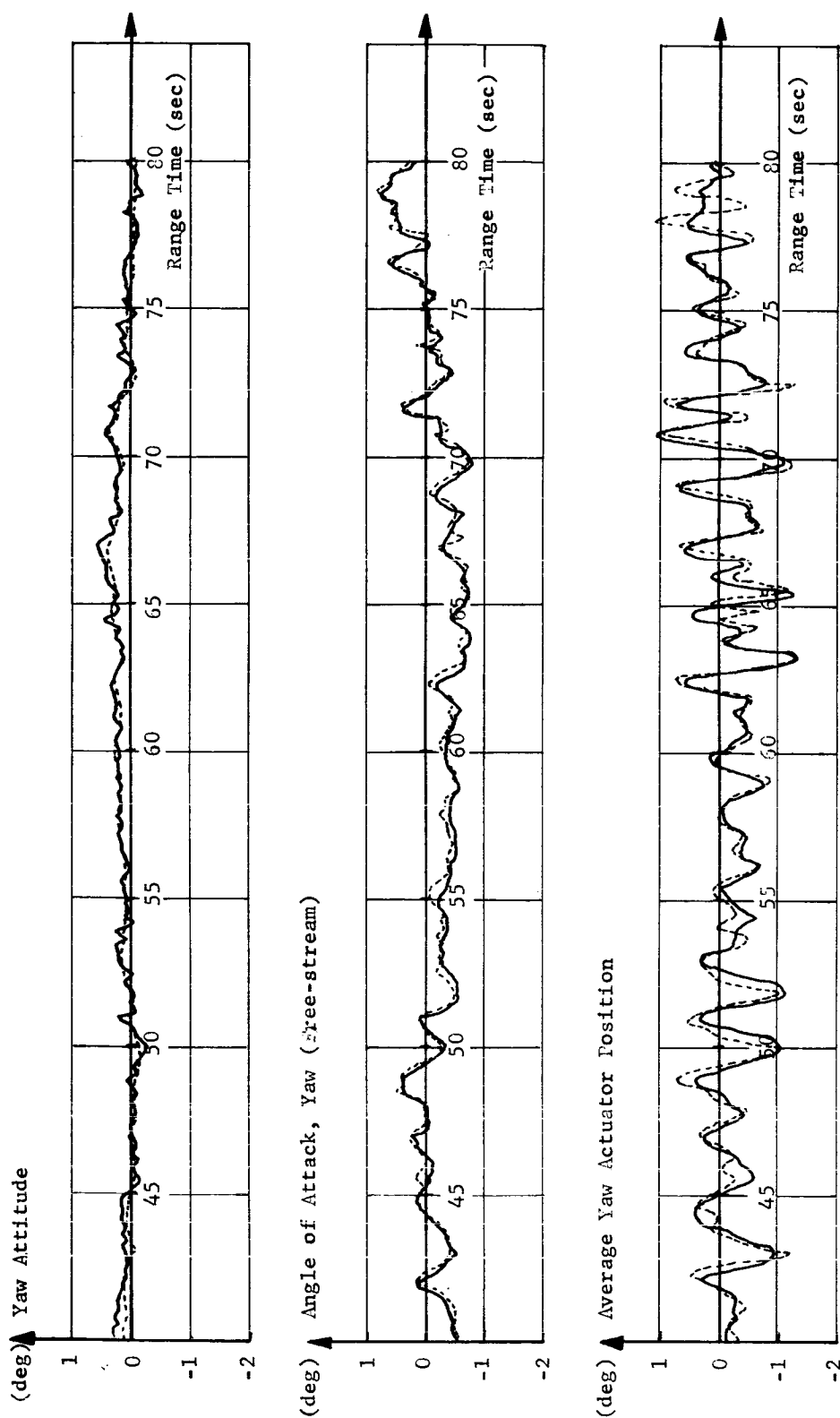


FIGURE 5-9 YAW ATTITUDE, FREE STREAM ANGLE OF ATTACK (YAW) AND AVERAGE YAW ACTUATOR POSITION

~~CONFIDENTIAL~~

Time of Actuator Excursion (sec)	Altitude Interval (m)	Wind Increment (m/sec)	Wind Gradient (1/sec)	Actuator Deflection per m/sec of Wind Increment (deg/m/sec)
62	265	3.7	.014	.30
69	258	5.3	.020	.36
70	220	6.8	.030	.32

The largest wind gradient of 0.030/sec (over an altitude increment of 220 m) as indicated by vehicle measurements occurred at an altitude of 16 km. Using a 250 m altitude increment, the maximum wind shear obtained from rawinsonde is 0.02/sec.

Telemetered normal accelerations as measured by the yaw control accelerometer (not in the control loop) are shown in the upper portion of Figure 6-10. The corresponding calculated acceleration is shown in the lower part of the figure. This accelerometer was located at station 879, close to the vehicle center of gravity. It was located, radially, 44.5 inches from the longitudinal axis toward Fin position IV. The telemetered measurement presented in Figure 6-9 was smoothed, using 0.01 second data, with a 31 point second degree polynomial. Except for the higher frequency oscillations (those greater than about 1 cps), agreement between the calculated and telemetered acceleration appears to be good.

### 6.2.3 ROLL PLANE

Roll attitude of the vehicle was maintained by differentially deflecting the outboard control engines in both pitch and yaw. This was accomplished by electrically mixing pitch and roll, and yaw and roll error signals in the control computer.

The roll attitude, angular velocity and averaged engine deflections in roll are shown in Figure 6-11. A roll angle of 0.6 degrees was reached 4 seconds after liftoff. This angle slowly decreased to zero by 25 seconds and remained small until 50 seconds. At this time a long period oscillation with an amplitude of  $\pm 0.6$  degrees started. After this the roll angle began a slow increase, reaching a maximum of 0.9 degrees at 89.3 seconds and remained near this value until IECO. This represents a forcing roll moment of 186,000 in lbs. At IECO the roll angle was reduced to approximately 0.3 degrees. This same roll angle trend as observed on SA-2 was also observed on SA-1. The magnitude of the roll angle, however, was somewhat less on the SA-1 flight.

~~CONFIDENTIAL~~

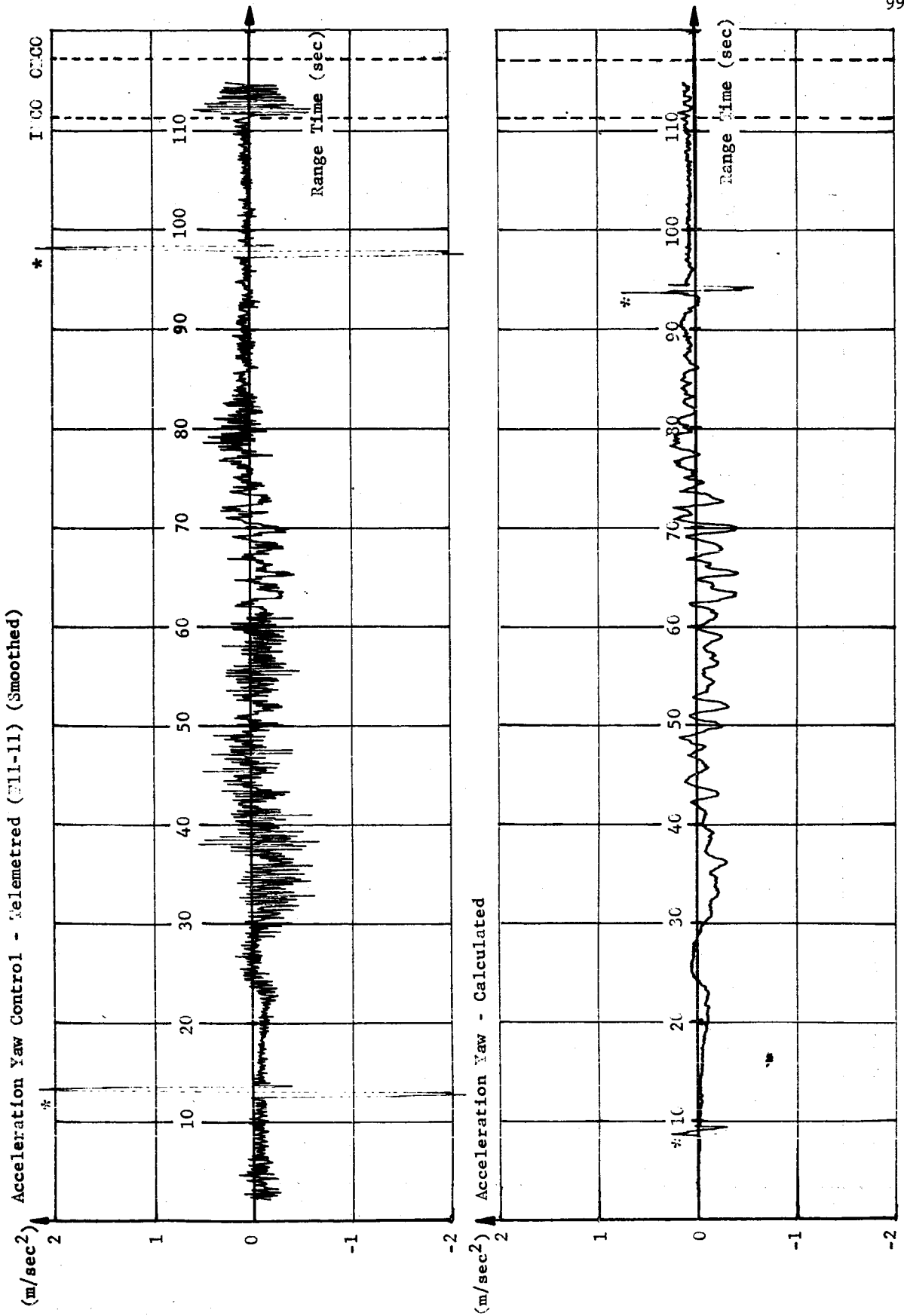
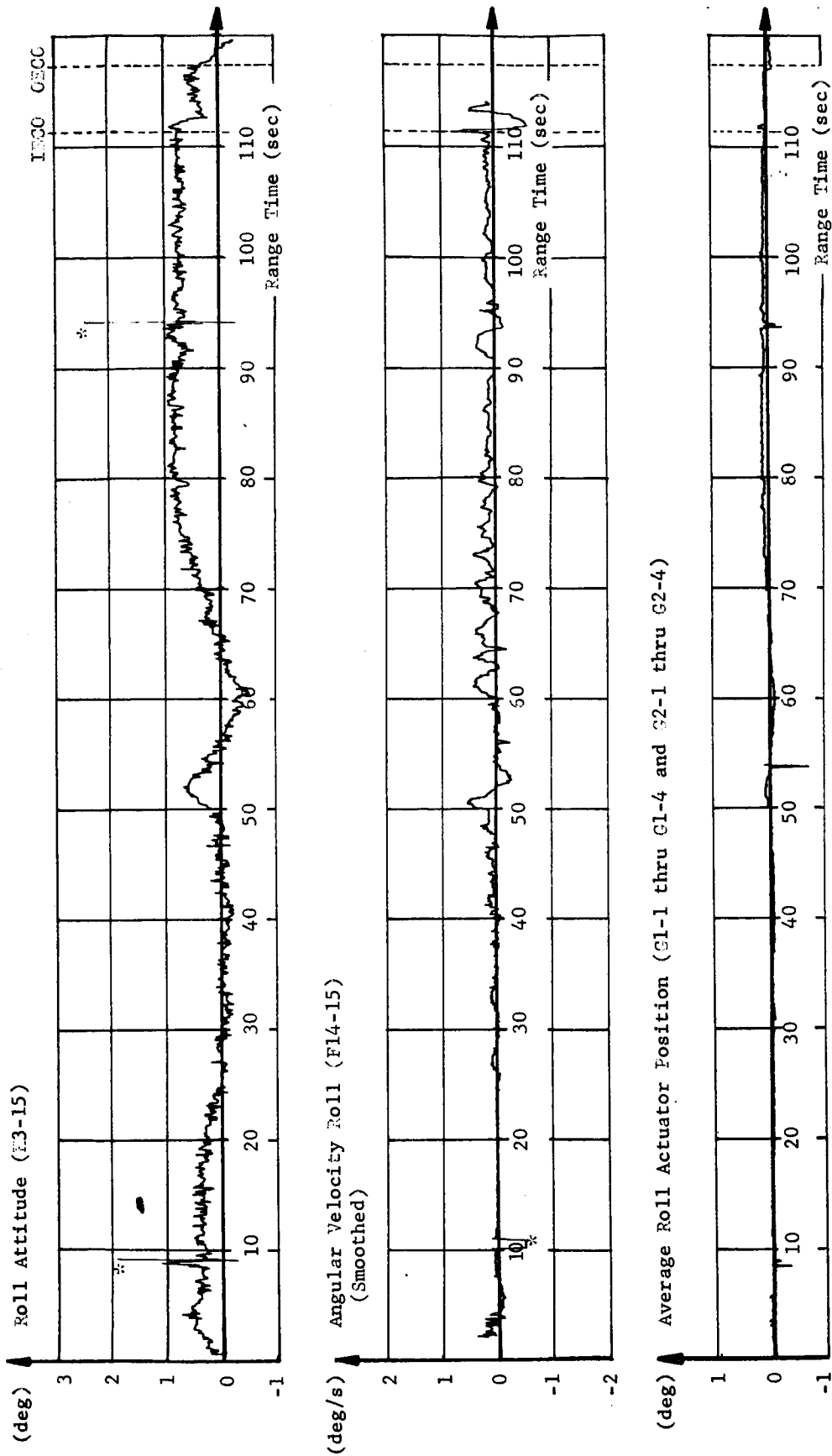


FIGURE 6-10 YAW NORMAL ACCELERATION



\* Telemetry Calibration

FIGURE 6-11 ROLL ATTITUDE, ANGULAR VELOCITY AND ACTUATOR POSITION

A divergent roll oscillation, due to propellant sloshing, which started around 90 seconds on the SA-1 flight did not occur on SA-2. Additional baffles added to the tanks of SA-2 sufficiently suppressed the propellant sloshing in this plane. The peak roll angular velocity during this period was  $\pm 0.1$  deg/sec compared to  $\pm 2.5$  deg/sec on the SA-1 flight.

A roll angular velocity of  $-0.8$  deg/sec, which was the maximum reached, occurred at 112.1 seconds. This apparently resulted from transients caused by inboard engine cutoff.

#### 6.2.4 ATTITUDE AFTER CUTOFF

The primary missions assigned to SA-2 concerned only the powered flight phase. However, some information may be obtained during free-flight which is of interest for future design configuration. Of interest for Block II vehicles is the effect of thrust vector angularity during engine cutoff and thrust decay.

Figure 6-12 shows the telemetered pitch and yaw angular velocities around OECO. The data is extremely erratic within the small values being considered. Interpreting the average of the data as well as possible, the period during cutoff and thrust decay results in less average angular velocity build-up than was observed on SA-1.

The average net thrust vector misalignment acting in pitch within the engine nozzles during the last portion of the thrust decay period was approximately  $0.1$  deg (considering the combined effect of all four outboard engines). The average net thrust vector angularity in yaw was approximately  $0.2$  deg. The resultant pitch angular velocity at the end of thrust decay was essentially zero because the thrust vector angularity within the engine nozzles just happened to counteract the engine deflection angles. In yaw a resultant angular velocity of only  $0.03$  deg/sec existed at the end of thrust decay.

It must be emphasized that these values for thrust angularity have a large degree of uncertainty associated with them due to the small deviations being analyzed.

There again was a pitching moment after OECO which lasted until the loss of telemetry due to destruct at 162.6 seconds. This moment caused a nose down pitch and was in the same direction and about the same magnitude as observed on SA-1. An average moment of 5900 in lbs was calculated from this motion. The yaw plane motion indicates no significant moment. The slight angle build-up shown in yaw was a result of the small angular velocity existing at the end of thrust decay after OECO (see Figure 6-13).

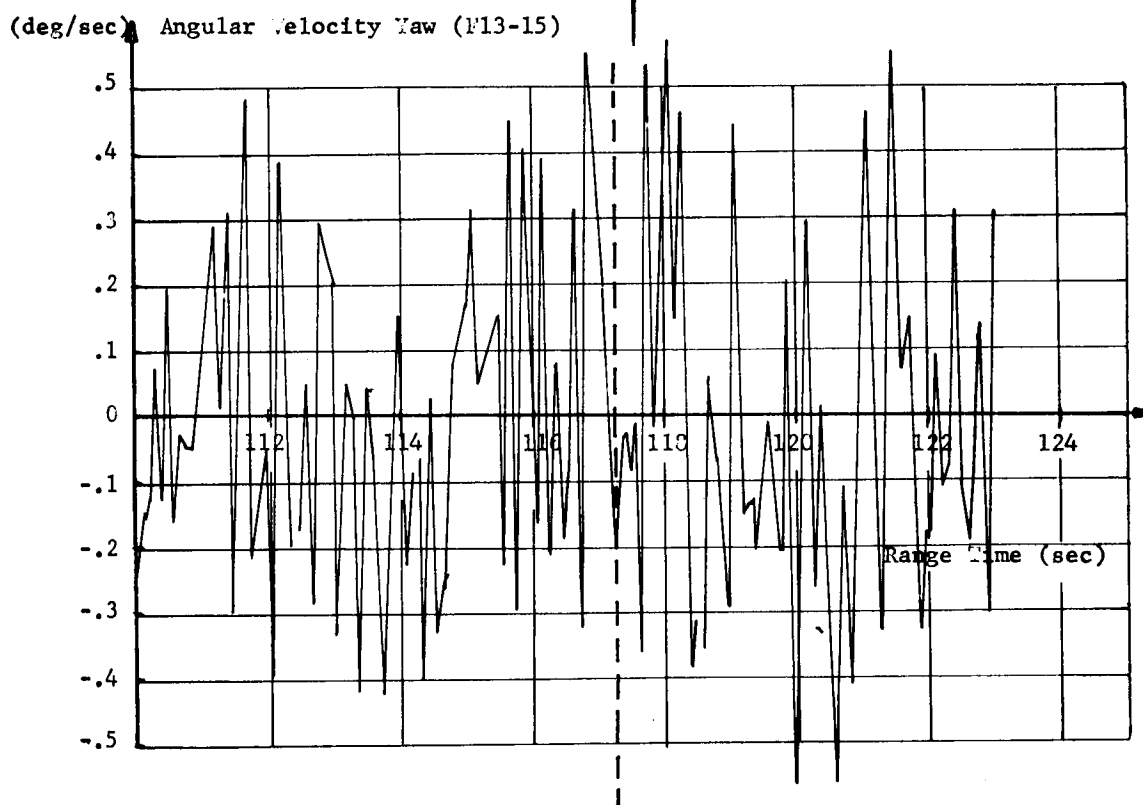
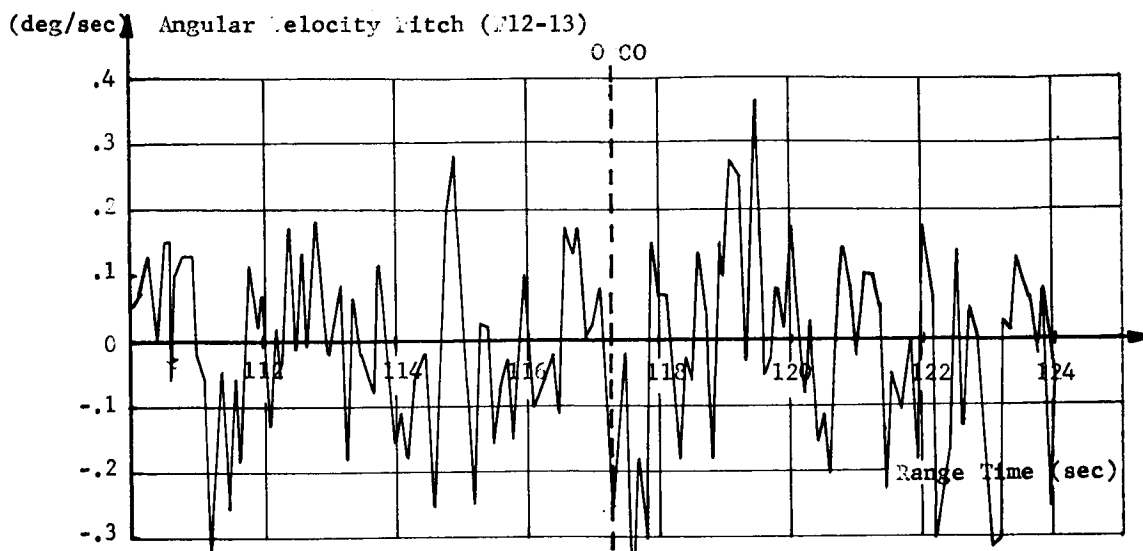


FIGURE 6-12 ANGULAR VELOCITIES DURING CUTOFF

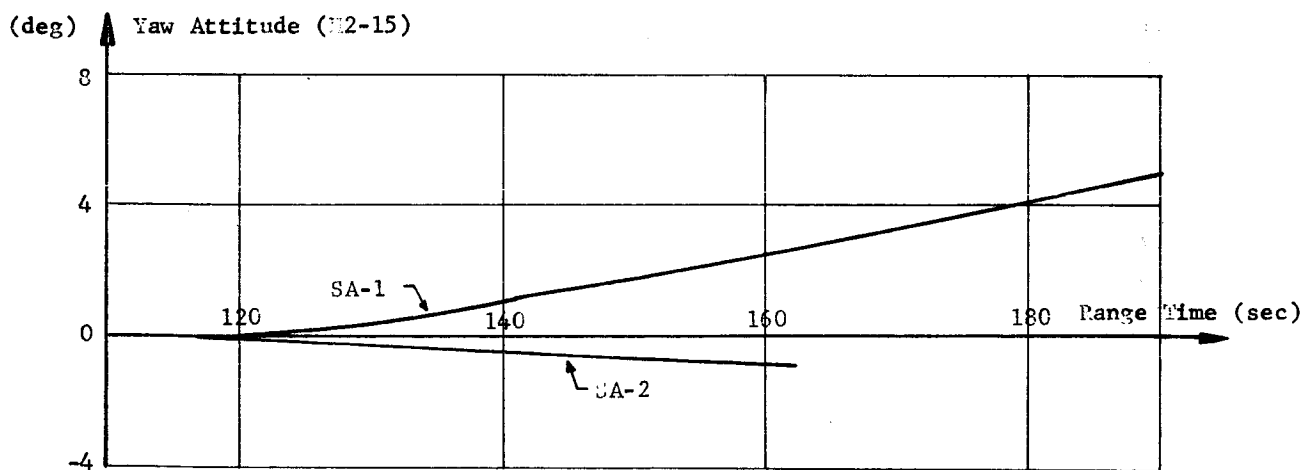
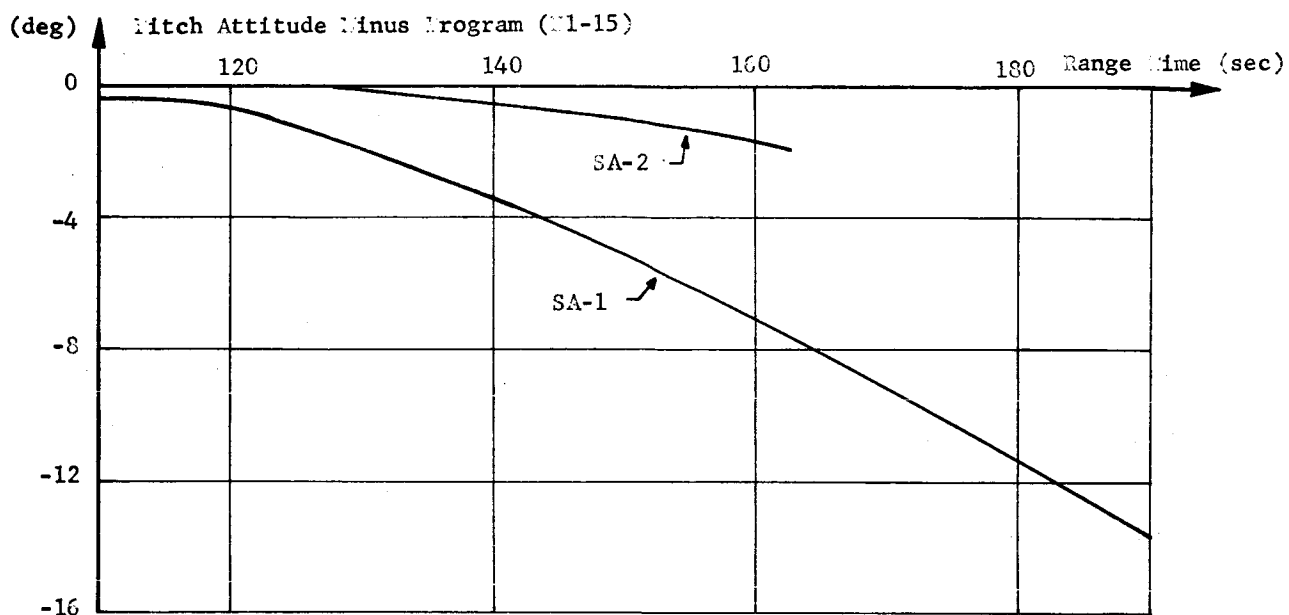


FIGURE 6-13 ATTITUDE ANGLES AFTER CUTOFF

~~CONFIDENTIAL~~

## 6.3 FUNCTIONAL ANALYSIS

### 6.3.1 CONTROL SENSORS

#### 6.3.1.1 CONTROL ACCELEROMETERS

Two Edcliff control accelerometers (pitch and yaw) were flown for operational study purposes on SA-2. The telemetered indications show proper operation of the equipment throughout the flight. A comparison made between the telemetered normal acceleration in pitch and yaw and calculated values of normal acceleration based on independent flight measurements shows good agreement ( $\pm 0.2 \text{ m/s}^2$ ). This is within the data reduction noise level of the measurements which were used in the calculation and comparison. The over-all operation of these sensors on this flight indicate that closed loop operation could be satisfactory; the appearance of some high frequencies in the telemetered data causes no concern since these would be filtered from the signal if used in active control operation.

The Statham control accelerometers planned for closed loop operation contain design improvements which make them superior to the Edcliff instruments (better static accuracy, more linear dynamic response, etc.). The Statham accelerometers will be flight tested at the earliest possible time.

#### 6.3.1.2 RATE GYROS

Rate gyro packages were located in both the instrument canister (a 3 axis Minneapolis Honeywell "control" package) and the tail of the S-I stage (a 2 axis Kearfott "measuring" package for pitch and yaw). Since the frequency response and phase characteristics of the two sets of instruments are quite dissimilar, some caution must be used when making comparisons of the outputs of the two packages. In general, it can be said that all of the instruments operated properly. Some vibration effects are evident in the output of each instrument in both packages in addition to the proper indications of the flight maneuvers of the vehicle. With proper filtering, the "control" package could give satisfactory performance as an active control sensor.

Shown in Figure 6-14 is a telemeter record of the two rate gyros located in the tail at Station 195. Pronounced oscillations, with a frequency of 3 cps, began at engine ignition in the yaw plane and had a maximum amplitude of  $\pm 0.3 \text{ deg/sec}$ . These oscillations decay to zero amplitude by 12 seconds. The same oscillations appear in the pitch plane rate gyro but are less defined, especially prior to liftoff. The source of these oscillations has not been identified.

~~CONFIDENTIAL~~

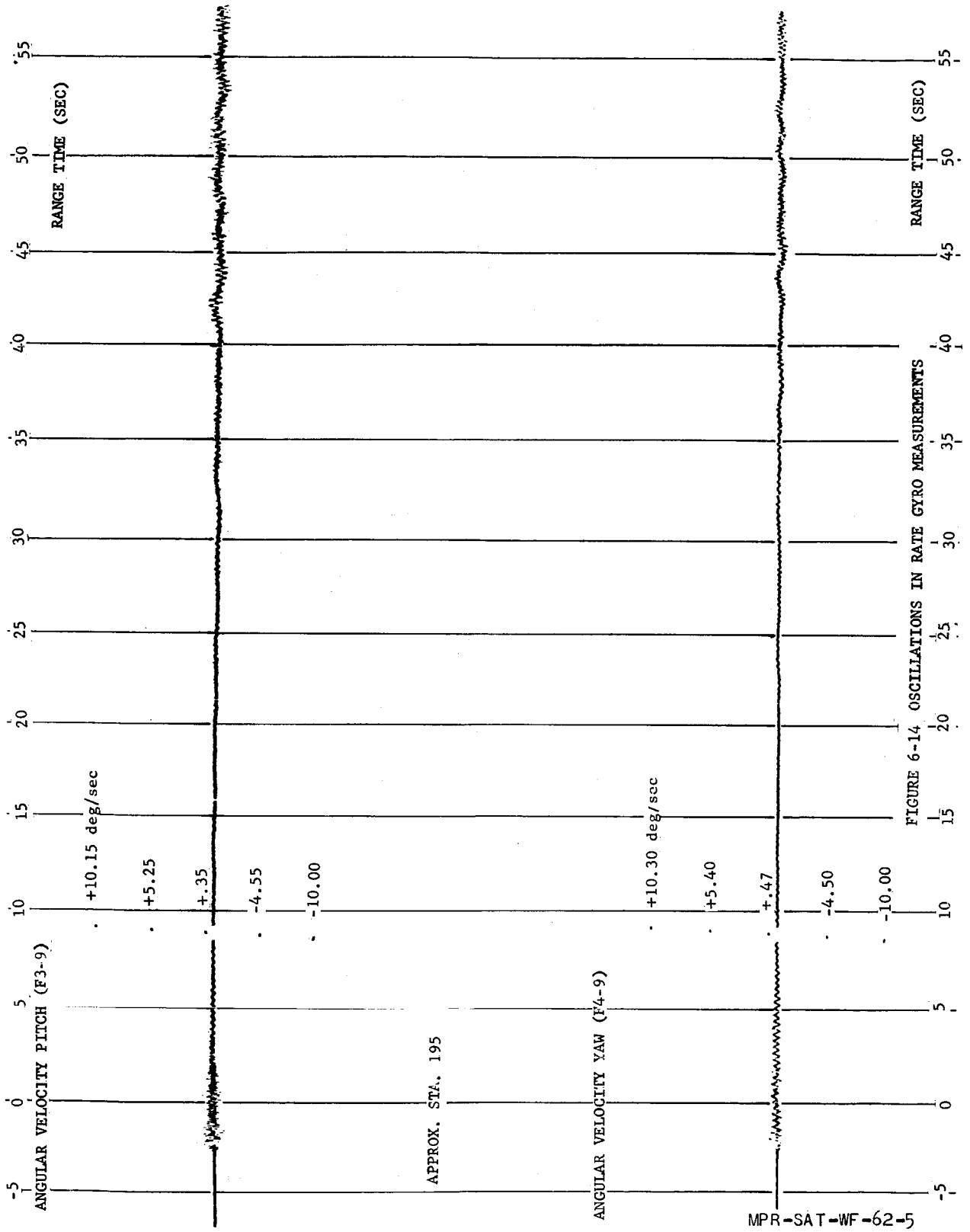


FIGURE 6-14 OSCILLATIONS IN RATE GYRO MEASUREMENTS

~~CONFIDENTIAL~~

The frequency of oscillations prior to liftoff might have been expected to be the first cantilever mode, but this frequency from SA-D tests was only 0.35 cps. Another possibility might have been the individual outer tank first mode. However, immediately after liftoff, this was approximately 2 cps according to the accelerometers mounted on an outer tank (see Section 9.4).

Accelerometers mounted on the center LOX tank at Station 250 indicate a lower frequency oscillation which lasts for a much shorter time span than appears on the rate gyro measurements. Although the two sets of measurements are located in different sections of the vehicle, this discrepancy in frequencies should be another indication that the rate gyros may not be sensing a true bending oscillation of the vehicle.

#### 6.3.1.3 ANGLE OF ATTACK METERS

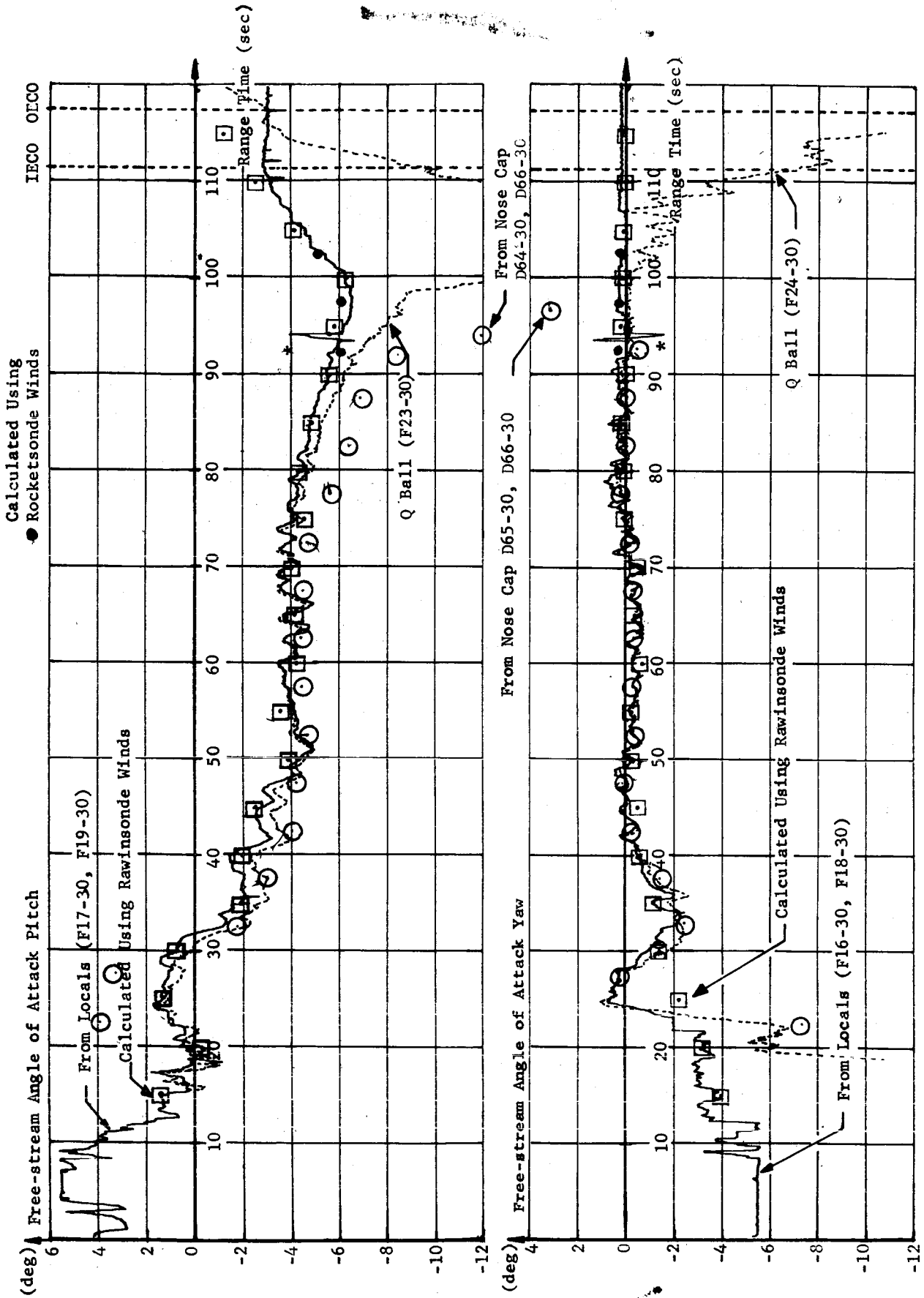
Four active control local angle of attack meters were on SA-2. An instrument type Q-ball angle of attack device was used for measuring purposes. Both systems operated satisfactorily.

The U. S. Science (formerly Topp) local angle of attack indicators used in the Jupiter program were employed for control purposes on SA-2. Four of these were mounted radially 90 degrees apart in the payload body surface (a Jupiter aft unit) at station 1841. Two of these indicators measured in the pitch plane and two in the yaw plane. These results as telemetered are shown in Figures 6-3 and 6-8. Since these indicators are located on the body they are influenced by the body upwash. The telemetered values may be converted to free-stream by means of a wind tunnel determined upwash factor which was verified by Jupiter flight tests. The resulting free-stream angles of attack are shown as solid lines in Figure 6-15.

Flown as a passenger on SA-2 was a model F-13 Q-ball angle of attack meter. This consisted of a set of six pressure orifices drilled in the spherical nose cap of radius 12.17 inches; four were used for differential pressure measurements and the other two sensed a dynamic pressure correction factor. This control sensing device is a forerunner of a model F-16 Q-ball angle of attack sensor scheduled to be flown as a passenger on SA-4.

The only difference between the model flown on SA-2 and that used on the SA-1 flight was a compensating servo device which allowed the dynamic pressure correction factor to be made to the differential pressures onboard the vehicle and a direct measurement of angle of attack telemetered. These measurements are shown as dashed lines in Figure 6-15.

~~CONFIDENTIAL~~



\* Telemetry Calibration

FIGURE 6-15 FREE STREAM ANGLES OF ATTACK

~~CONFIDENTIAL~~

The free-stream angle of attack was also calculated from the telemetered individual differential pressures and dynamic pressure correction factor. These are shown as circled points in Figure 6-15. The calculated angle of attack from the Q-ball differential pressures and the direct measurement of angle of attack from the Q-ball is in good agreement in the yaw plane prior to approximately 80 seconds. At this time, long period oscillations appear in the calculated values and reach an amplitude of  $\pm 2.4$  degrees by 95 seconds. The pitch plane agreement of the calculated angle of attack from the Q-ball and the direct telemetered Q-ball angle of attack is more biased than was observed in the yaw plane and is probably due to a telemetry bias in the differential pressure measurement (D64-30). The same oscillatory motion also starts at 80 seconds and continues to increase in amplitude. The phase and frequency of this motion is identical in the two planes and is believed to be due to the  $\Delta Q$  correction measurement (D66-30) rather than the differential pressures. Since these oscillations do not appear on the direct measurement of the angle of attack from the Q-ball, it can be assumed that this error occurs in the telemetering of the  $\Delta Q$  correction or that the telemetry transducer is not accurate enough for the low level of  $\Delta Q$  being sensed at this time.

Also shown in Figure 6-15 are calculated angles of attack based on rawinsonde winds (square points) and rocketsonde winds (solid points). The square points after 95 seconds do not include wind effects. The solid points calculated using rocketsonde winds indicate, by their close agreement with the no wind case, that since the winds were so small their effect on the angle of attack is almost negligible at this time.

Based on the comparison of the calculated angles of attack from rocketsonde wind data and the telemetered angles of attack from the U. S. Science indicators on both the SA-1 and SA-2 flights, it can be concluded that they functioned properly above a dynamic pressure of about  $250 \text{ kp/m}^2$ . This dynamic pressure was reached at about 105 seconds. Information from these indicators is probably unreliable after this time.

The nose cap angle of attack measurements as flown on this vehicle are expected to have an accuracy only on the order of 1 degree. However, even with this, a fairly large deviation between the direct measurement of the Q-ball pitch angle of attack and the pitch angle of attack determined from the locals begins at 80 seconds. The difference exceeds 1 degree shortly after 90 seconds. A similar deviation, but even larger in magnitude, was obtained using the calculated angle of attack from the differential pressure measurements. The yaw plane angle of attack obtained from the Q-ball does not start deviating

~~CONFIDENTIAL~~

~~CONFIDENTIAL~~

noticeably until about 100 seconds when its motion becomes quite erratic.

Although the comparisons above of the Q-ball angles of attack were made with angles of attack from other sources it should be pointed out that only the uncompensated differential pressures would be used as input to the control system if they were included in the control loop. Also the differential pressures will be sensed by a more refined system (Model F-16). Any error introduced by the dynamic pressure compensation factor used in arriving at an angle of attack in this present analysis would not be introduced into the control system. In addition, as of this time, accelerometers are considered the primary mode for control on Block II vehicles with angle of attack control only as a backup.

Based on the information from the flight of SA-2, the use of the Q-ball angle of attack system for control of the vehicle from 30 to at least 80 seconds of flight appears to be feasible. The reliability after 80 seconds could be judged only with improved accuracy in the measurement.

#### 6.3.2 TILT PROGRAMMER

A cam-type tilt program generator was flown on SA-2 (see Figure 6-16). The decision to use this device was based on a desire for a smooth and continuous tilt program. Its operation was satisfactory in reducing possible propellant sloshing excitation and in the generation of the desired tilt angle versus time. However, over-all performance was marred by the disturbance discussed below.

This programmer is the same device used in the Pershing missile program, with a cam defining the SA-2 tilt program.

A periodic disturbance occurred in the pitch actuator positions ( $\beta_p$ ) about every 13 seconds during the flight of SA-2. It was also apparent in the differential current ( $\Delta i_p$ ) and differential pressure ( $\Delta P_p$ ) measurements. The amplitude of the disturbance varied during flight in direct proportion to the tilting rate (see Figure 6-17). These values as obtained from the flight were influenced by the wind gusts so that the exact amount of engine deflection due to the tilt disturbance are actually somewhat smaller. The disturbance appears as a negative deflection of the actuator for about 0.5 seconds followed by a positive deflection for about 1 second. A superimposed 4 cps oscillation was also apparent only during each tilt disturbance and was probably due to gear tooth contacts superimposing small load changes on the main load disturbance. There were no unusual disturbances observed in the yaw plane either in the actuators or in any of the inputs to the control computer.

~~CONFIDENTIAL~~

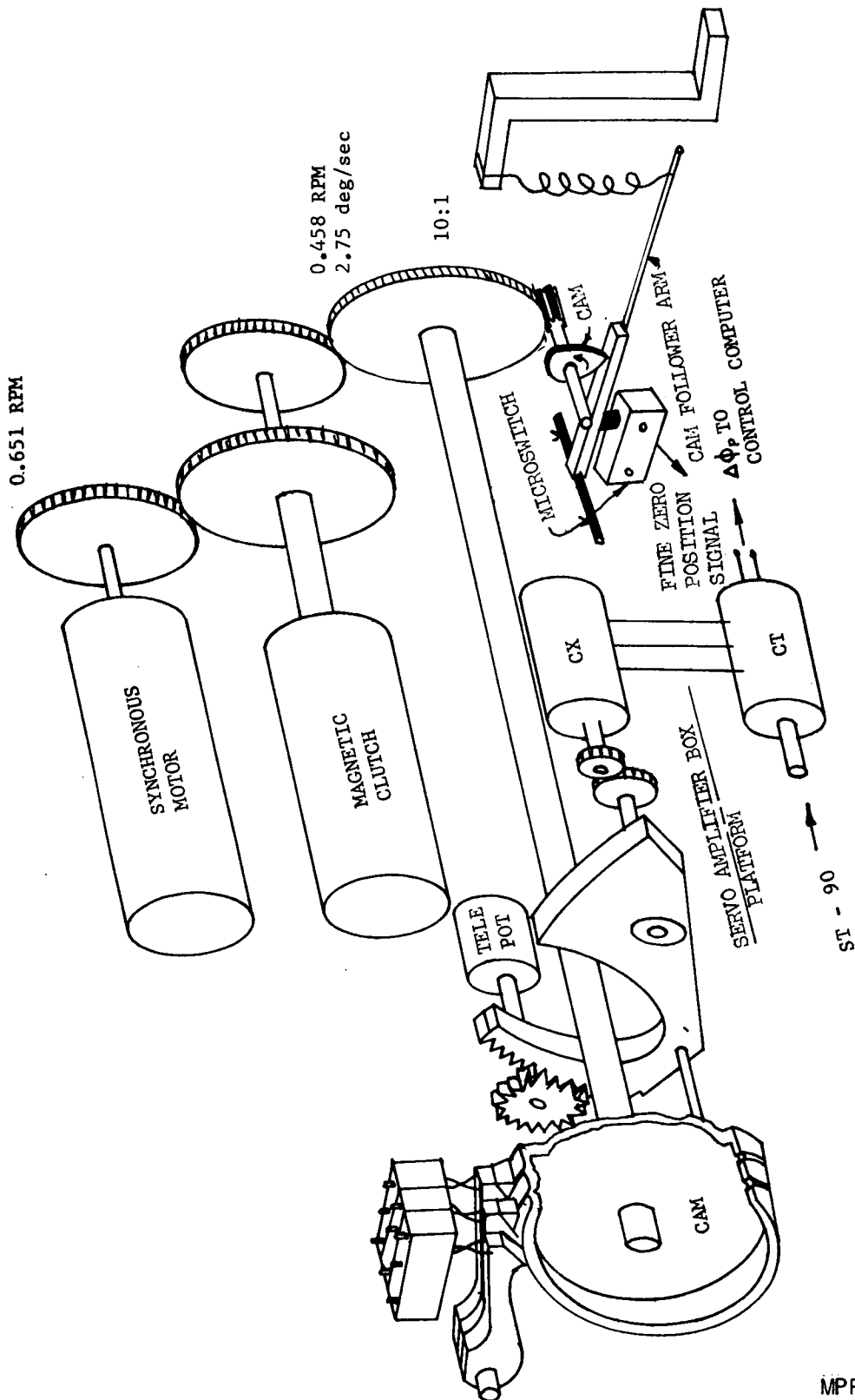


FIGURE 6-16 SCHEMATIC OF TILT PROGRAMMER, SA-2

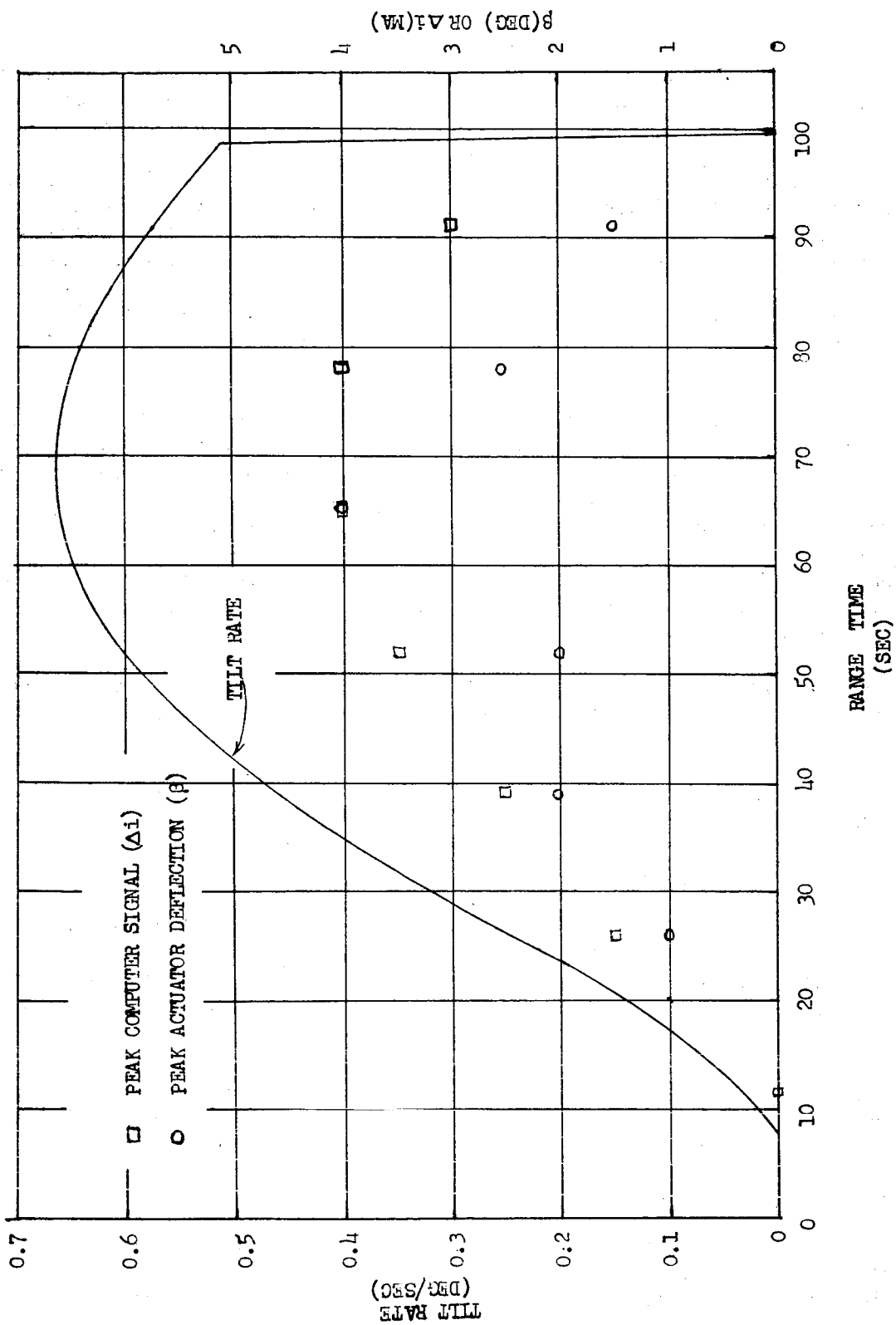


FIGURE 6-17 TILT RATE AND PEAK CONTROL SIGNALS

~~CONFIDENTIAL~~

An investigation of the tilt programmer mechanism disclosed a cam-driven micro switch which operated at the same time the disturbance appeared on the actuators (see Figure 6-16). The purpose of this switch (fine zero switch) is to furnish an accurate zero reference for the programmer prior to liftoff. The switch has no inflight function but continues to operate since it is connected directly to the gear train which drives the tilt cam. There is a 10:1 gear ratio between the tilt cam and the cam which operates the fine zero switch, giving a switch operation every 13.09 seconds. These intervals begin at liftoff since the gear train starts from zero position at that time. This sequence of switch operations coincides exactly with the disturbance observed on the pitch actuators.

The disturbance is created in the following manner. The cam which operates the fine zero switch experiences a resistive torque as it begins to close the microswitch. This torque is increased by a factor of ten (10:1 gear ratio) and transmitted to the tilt cam, reducing its rotation rate. As the fine zero cam rotates past the microswitch, it experiences a torque in the direction of rotation which increases the normal rotation rate of the tilt cam. This variation of the rotation rate of the tilt cam is then reflected on the pitch error signal to the control computer and produces the disturbances observed on the pitch actuators.

An analog study of the tilt problem was made which confirms that only 0.1 to 0.2 degrees of fluctuation are needed to produce the disturbance observed in the actuators measurements. It also indicates a small but detectable output from the pitch rate gyro could be expected. The simulation showed very clearly that any rapid changes in program input rate would have a significant effect on actuator operation (due to differentiation of the  $\Delta\phi_p$  signal) even though the magnitude of the fluctuation on  $\Delta\phi_p$  was very small.

This difficulty will be corrected on the present fine zero cam with a non-eccentric phenolic disk with a shorting bar. The micro switch will be replaced by a dual flyleg contactor which will give the necessary electrical signal for zeroing the system but which will not reflect a load change into the cam drive system.

An ST-90 tilting program measurement having a much higher resolution than the existing measurement is now under consideration, but introduction of this improvement before SA-5 is not likely.

### 6.3.3 CONTROL COMPUTER

The operation of the control computer on this flight was satisfactory. Comparisons of the telemetered computer outputs and calculations of the output values based on the static control equation gives

~~CONFIDENTIAL~~

an agreement in pitch within  $\pm 0.8^\circ$  (as expected); in yaw an agreement within  $\pm 0.5^\circ$  (as expected); and in roll within  $\pm 0.2^\circ$  (as expected) over the flight period. The comparatively large expected difference values in pitch and yaw are primarily due to normal flight maneuvers and are not accounted for in these comparison equations.

See also Figures 6-4 and 6-9 for a comparison of a digital simulation which does include some dynamics and the telemetered actuator deflections.

#### 6.3.4 ACTUATORS

Operation of the hydraulic actuators was satisfactory. An investigation of actuator loading during the flight of SA-2 was made by analyzing the differential pressure measurements. Thrust vector misalignment and inertial loads were determined on all actuators with the exception of the pitch actuator of engine 1. The  $\Delta P$  measurements on this actuator malfunctioned throughout the flight. An investigation of curtain and gimbal friction torques was not made since reliable data was not available for periods when these torques could be isolated.

The differential pressure measurements indicate that a maximum actuator load of about 3,000 pounds (design load, 12,000 lbs) occurred just prior to inboard engine cutoff (Figure 6-18). Variable loads up to 2,000 pounds appeared during the high Q region of flight. Thrust misalignment forces resulted in less than 400 pounds load on all actuators except engine 2 pitch; the force observed on this actuator was about 800 pounds (see Figure 6-19). The increase in actuator loads as a result of longitudinal acceleration can be easily traced on the vector diagrams. These load increases are due to the off planar location of the engine center of gravity. The maximum inertial loading occurred just prior to IECO, and the load force at this time was 2200 pounds. The inertial loading was greatest on the yaw actuators of engines 2 and 4 and the pitch actuator of engine 3. It appeared with smaller magnitude on the other actuators. The gravitational loading effect on the actuators before liftoff was not clearly indicated by the differential pressure measurements. The curtain loads, gimbal friction torques and errors in determining the exact null point of the delta P measurements are thought to account for the poor definition of the gravitational loads at this time.

The maximum demand on the actuator system occurred during the disturbance in pitch at 79 seconds. The disturbance required a maximum deflection rate of about 12.5 degrees per second which is well within the capabilities of the system. Lesser peaks occurred at 64-66 seconds due to a combination wind shear and a tilt disturbance and at 70.5 seconds due to another wind disturbance. The nominal level of demand was well less than one degree per second.

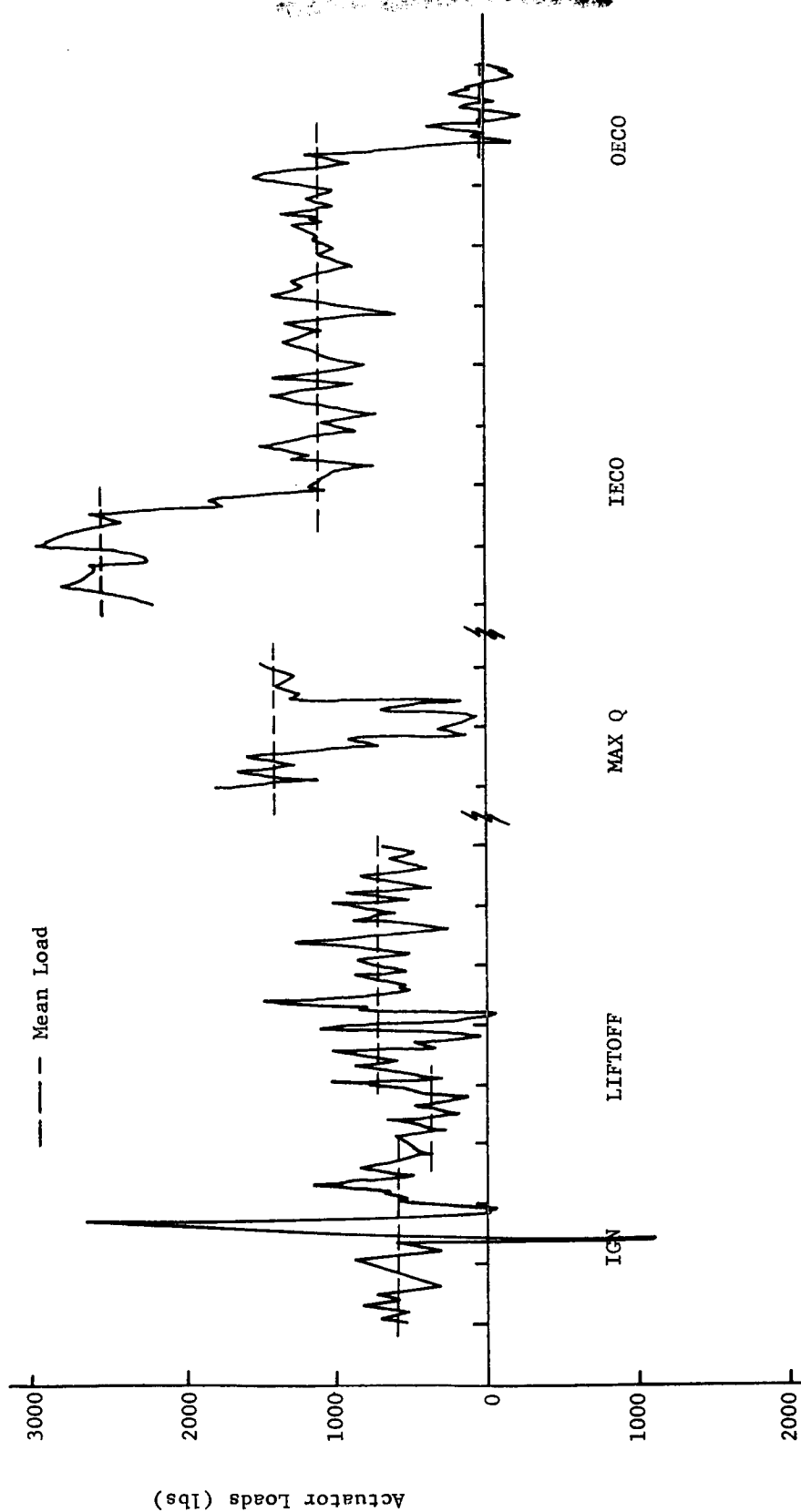


FIGURE 6-18 REPRESENTATIVE ACTUATOR LOADS

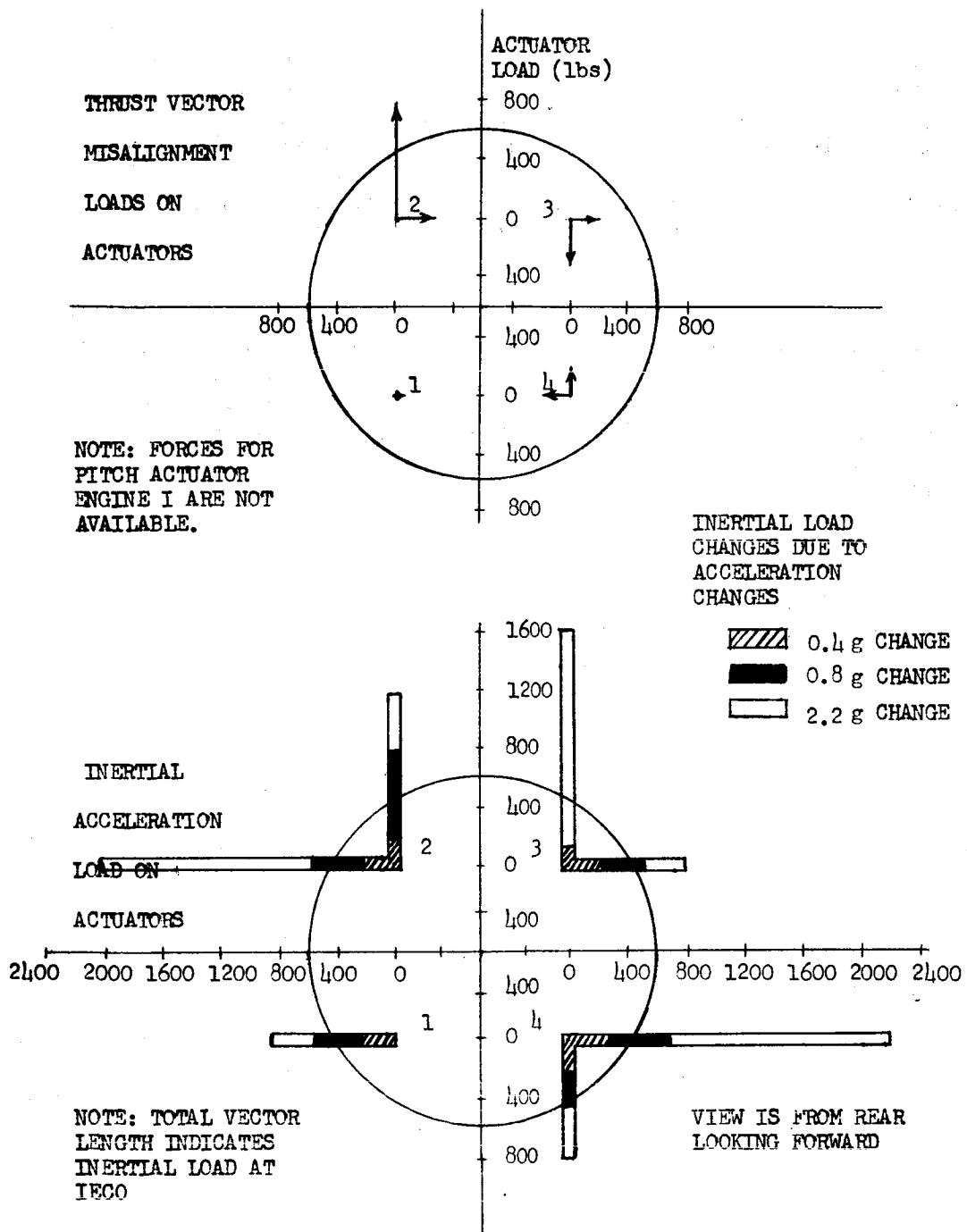


FIGURE 6-19 NON-CONTROL ACTUATOR LOADS

~~CONFIDENTIAL~~

#### 6.4 PROPELLANT SLOSHING

Sloshing was one of the few noticeable problems encountered on the SA-1 flight. As a result of the SA-1 flight, baffles were added in the lower portion of the outer tanks (see Figure 6-20) for subsequent Block I vehicles as a means of reducing this problem. These baffles proved effective since the sloshing at the end of powered flight observed on SA-2 was much smaller than SA-1, although another factor to consider is the lower excitation due to a smoother tilt program being used on SA-2.

During most of the flight prior to 90 seconds, a larger sloshing amplitude was indicated in the oscillations of the sloshing measurements on SA-2 than on SA-1. This is probably only due to an improvement in the instrumentation on SA-2 and does not indicate that the actual sloshing was greater. The largest amplitude oscillations observed on SA-2 occurred near 60 seconds. The following table shows these approximate peak to peak values.

Measurement No.	Double Amplitude (inches)
D5-F2 (outer fuel tank)	4.0
D6-0C (center LOX tank)	4.5
D6-04 (outer LOX tank)	5.0
D7-0C (center LOX tank)	4.0
D7-04 (outer LOX tank)	4.5

Additional accordion baffles were installed between the last three ring frames in the 70 inch fuel tanks and between the last four ring frames in the 70 inch LOX tanks. With the baffle configuration used in SA-1, the sloshing, if all tanks were oscillating in phase, theoretically went unstable after approximately 80 seconds when the fluid surface was on the smooth tank walls between the ring frames. However, with the changes made in the baffle configuration on SA-2, the all tanks in-phase sloshing mode remained stable until the fluid surface passed below the last ring frame; approximately 103 seconds in the 70 inch fuel tanks, 105 seconds in the 70 inch LOX tanks, and 97 seconds in the 105 LOX tank. The possible time for build up in the oscillations at the end of the powered flight was therefore much less. At inboard engine cutoff, due to the decreased sloshing frequency resulting from the decreased acceleration, the sloshing becomes stable again.

Sloshing was measured by means of differential pressure measurements in three of the nine propellant tanks. SLOSH measurements were made in the center 105 inch LOX tank, LOX tank 04, and fuel tank F2.

~~CONFIDENTIAL~~

Note: Numbers indicate station locations

\*  $\Delta P$  slosh probe  
Level C.O.

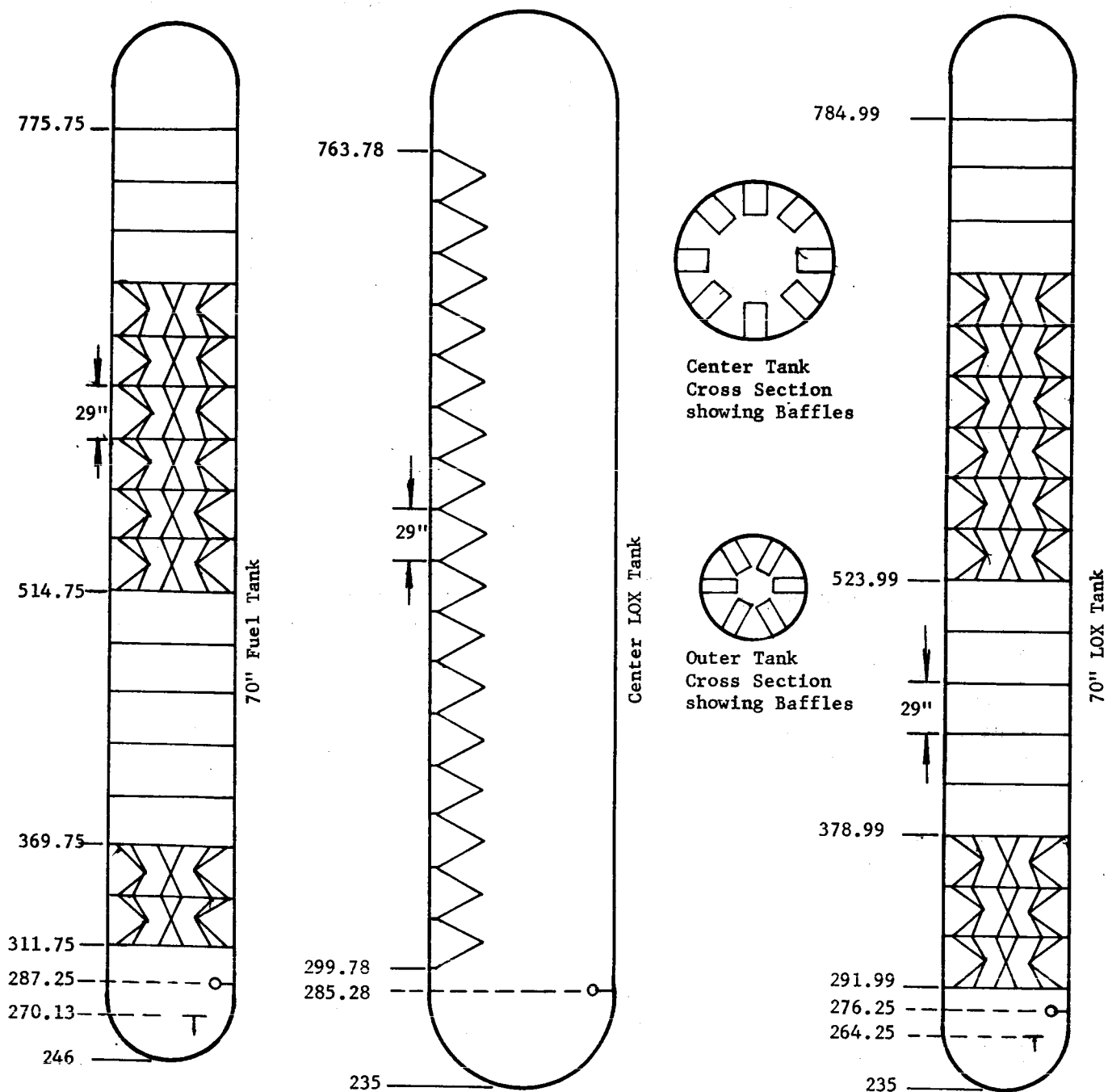
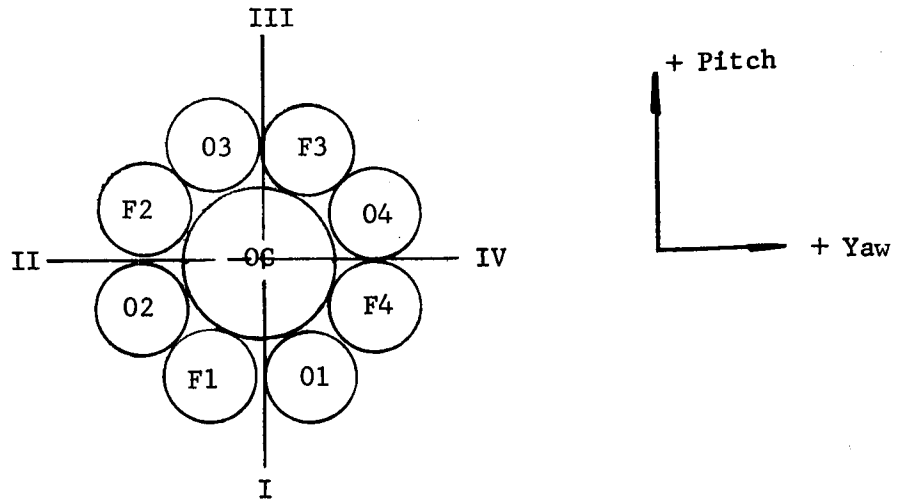


FIGURE 6-20 BAFFLE CONFIGURATIONS

~~CONFIDENTIAL~~

Locations of the tanks and the polarity of the measurements are shown below.



Several problems were encountered with the sloshing differential pressure measurements on the SA-1 flight. One problem was that some of the measurements did not begin functioning until late in flight, one as late as 62 seconds. This was improved to a satisfactory status on the SA-2 flight by increasing the helium purge rate through the sensing lines. The first apparently valid information was obtained on the SA-2 measurements beginning at the following times:

D5-F2	3 sec
D6-OC	15 sec
D6-O4	20 sec
D7-OC	14 sec
D7-O4	18 sec

At liftoff the purging of the sensing lines was transferred from ground to vehicle helium supply, decreasing the purge rate by a factor of three. This may have caused the slight delay in proper functioning of the sloshing measurements. Measurement D4-F2, pitch plane sloshing in the 70 inch fuel tank, did not function during the flight.

Another minor problem encountered with the sloshing measurements on SA-1 was exceeding the measuring range. Therefore, the measuring range was increased to  $\pm 1.0$  psid on SA-2. All measurements on SA-2 remained in range.

~~CONFIDENTIAL~~

The telemetered sloshing differential pressure measurements must be multiplied by a conversion factor to obtain the sloshing height in inches. This factor is a function of the liquid level in the tank, longitudinal acceleration and frequency of the oscillations. The converted propellant surface heights on SA-2 (solid line) are shown after 70 seconds in Figures 6-21 through 6-23. The results for the slosh amplitudes are extremely sensitive with respect to the fluid surface heights in the tanks and frequencies used. The results shown here are believed to be the best results at this time. The frequencies of oscillations observed in the sloshing measurements are compared with the predicted values in Figure 6-24.

The dashed lines in Figures 6-21 through 6-23 show the envelopes of the SA-1 slosh oscillations for a comparison with the sloshing on SA-2. This clearly illustrates the effectiveness of the baffles in the lower portion of the propellant tanks used on SA-2. The maximum sloshing amplitude measured in an outer tank on SA-2 before the end of the measurement was 0.4 inches compared to 3.5 inches on SA-1.

The only noticeable build-up rates in the sloshing measurements of the outer tanks after the liquid surface left the baffle are given below and compared with a predicted value.

Measurement No.	Rate of Damping ( $\sigma$ )	
	Flight	Predicted
D6-04	0.32	0.2
D7-04	0.28	0.2

The predicted value is based on all tanks oscillating in phase. The increased value of the observed damping rate over predicted may possibly be due to the inaccuracy of the linear model in this region.

The build-up of sloshing in the center LOX tank toward the end of powered flight was comparable to that on SA-1, but was somewhat smaller. No changes were made in the center LOX tank baffling arrangements.

Figures 6-25 and 6-26 show a comparison of polar plots of the propellant motion in the 70 inch LOX tank 04 and the center LOX tank from SA-1 and SA-2. The motion in the center tanks is somewhat similar near the end of the slosh measurement time for both vehicles, being essentially a pitch motion. The motion in the 70 inch tank is somewhat different. On SA-1 the polar plots indicate quite a predominant circular pattern which might be interpreted as a swirling or vortex motion of the fluid as the tank empties. This was not nearly as

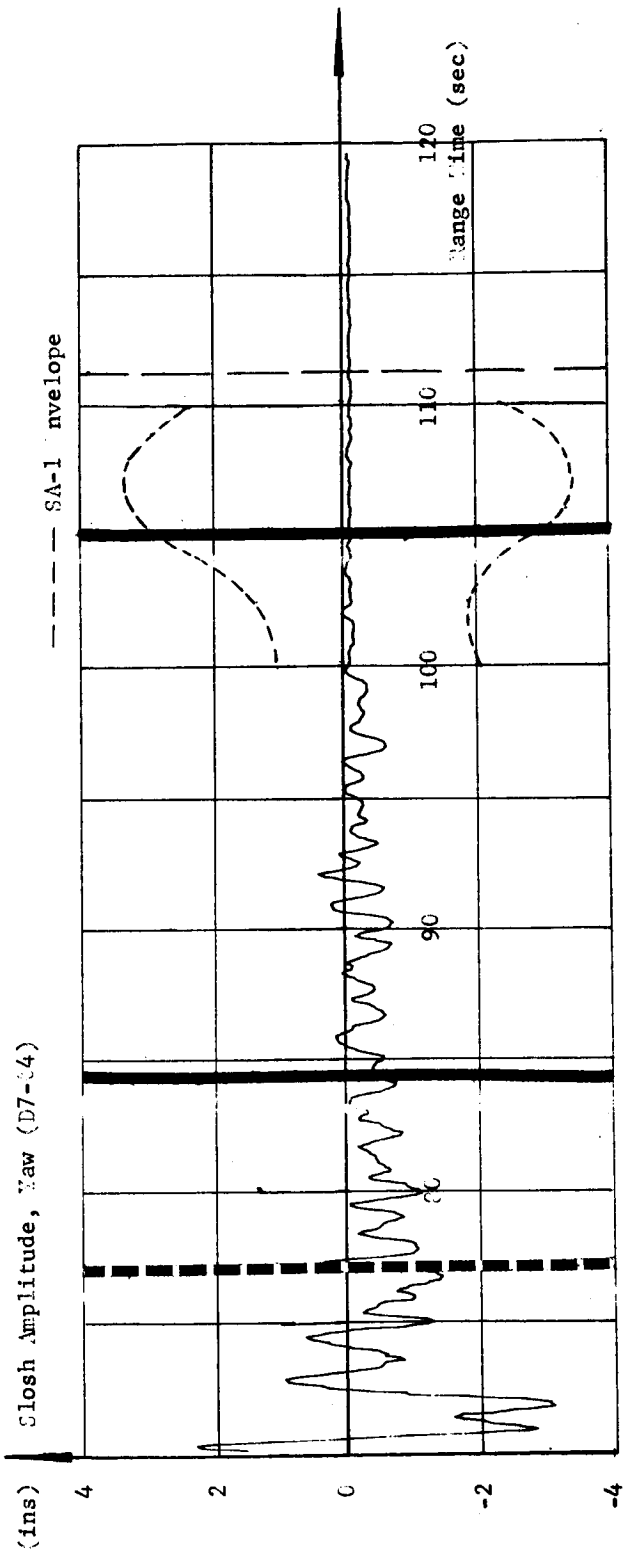
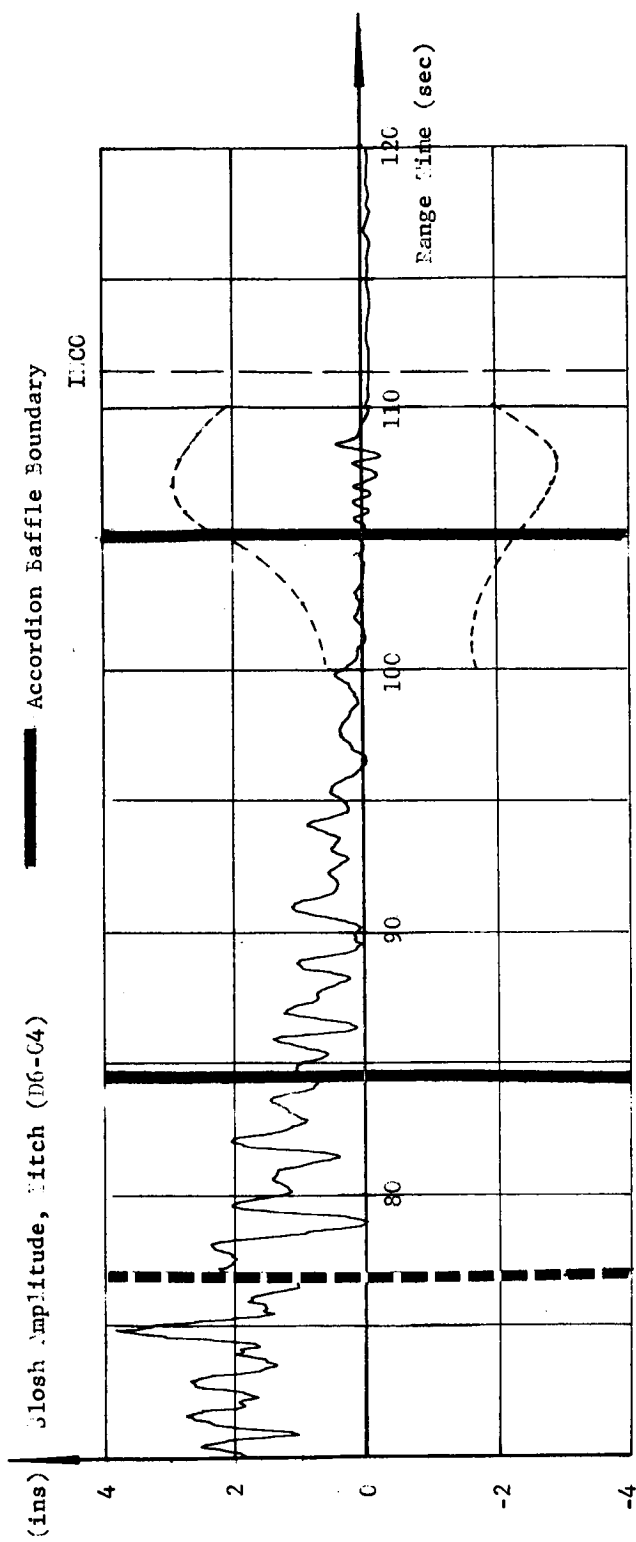


FIGURE 6-21 OUTER LOX TANK 04 TELEMETERED SLOSHING AMPLITUDES

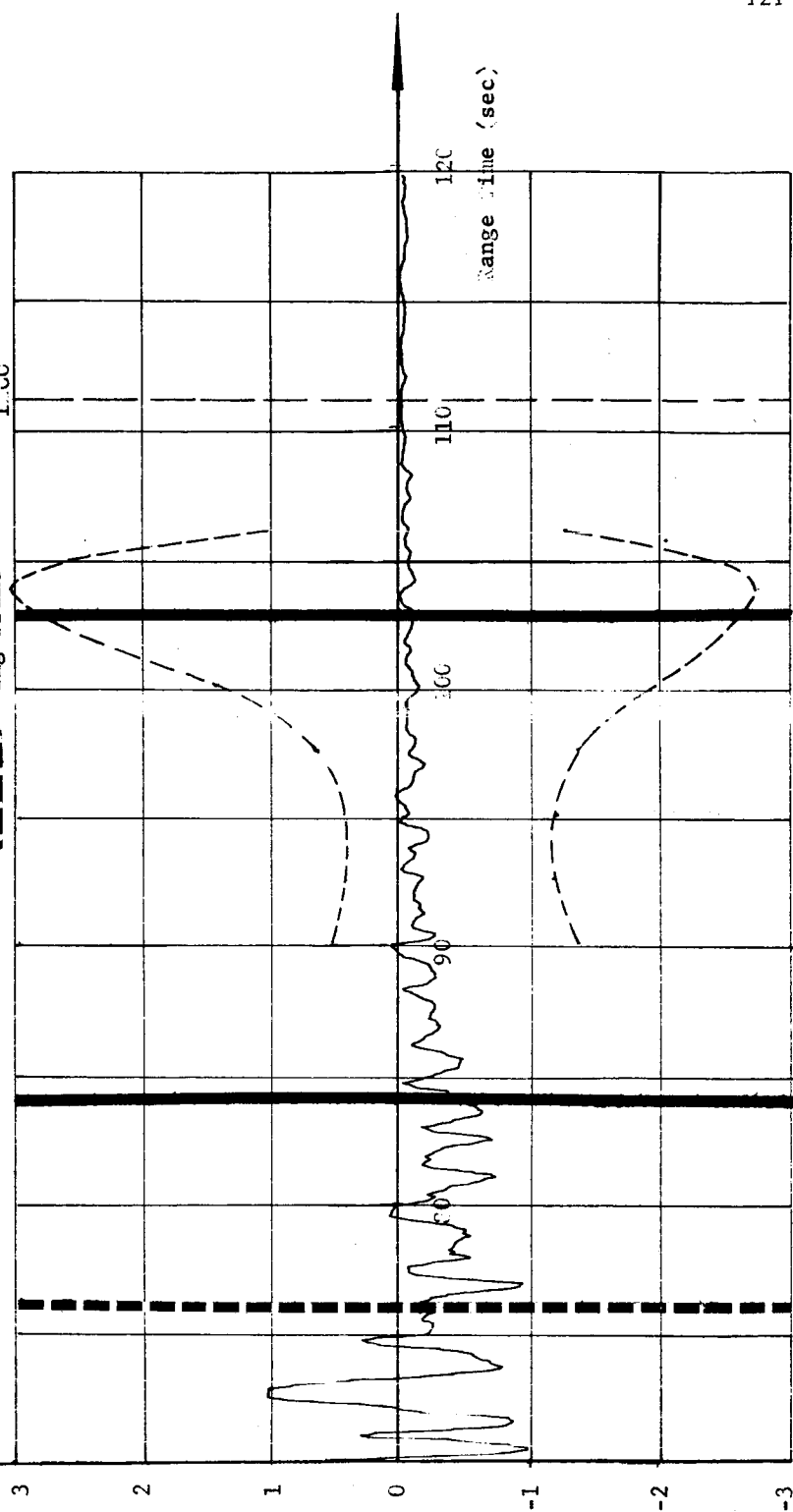
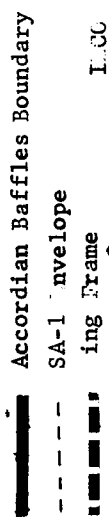
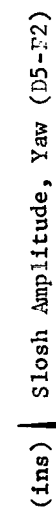
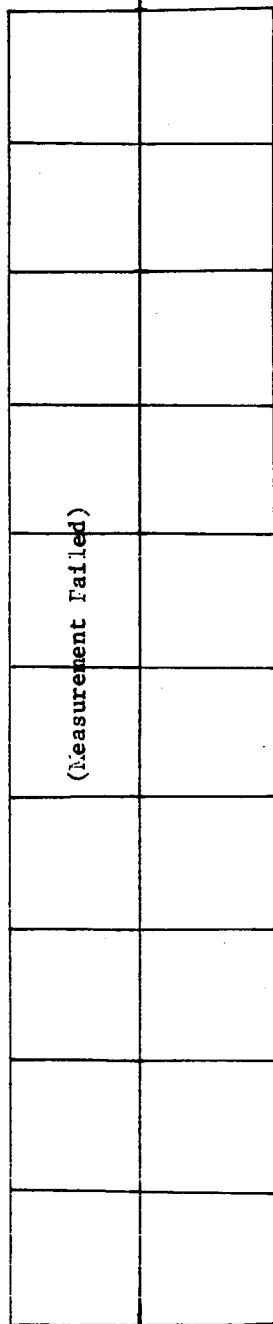
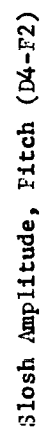


FIGURE 6-22 FUEL TANK F2 TELEMETERED SLOSHING AMPLITUDES

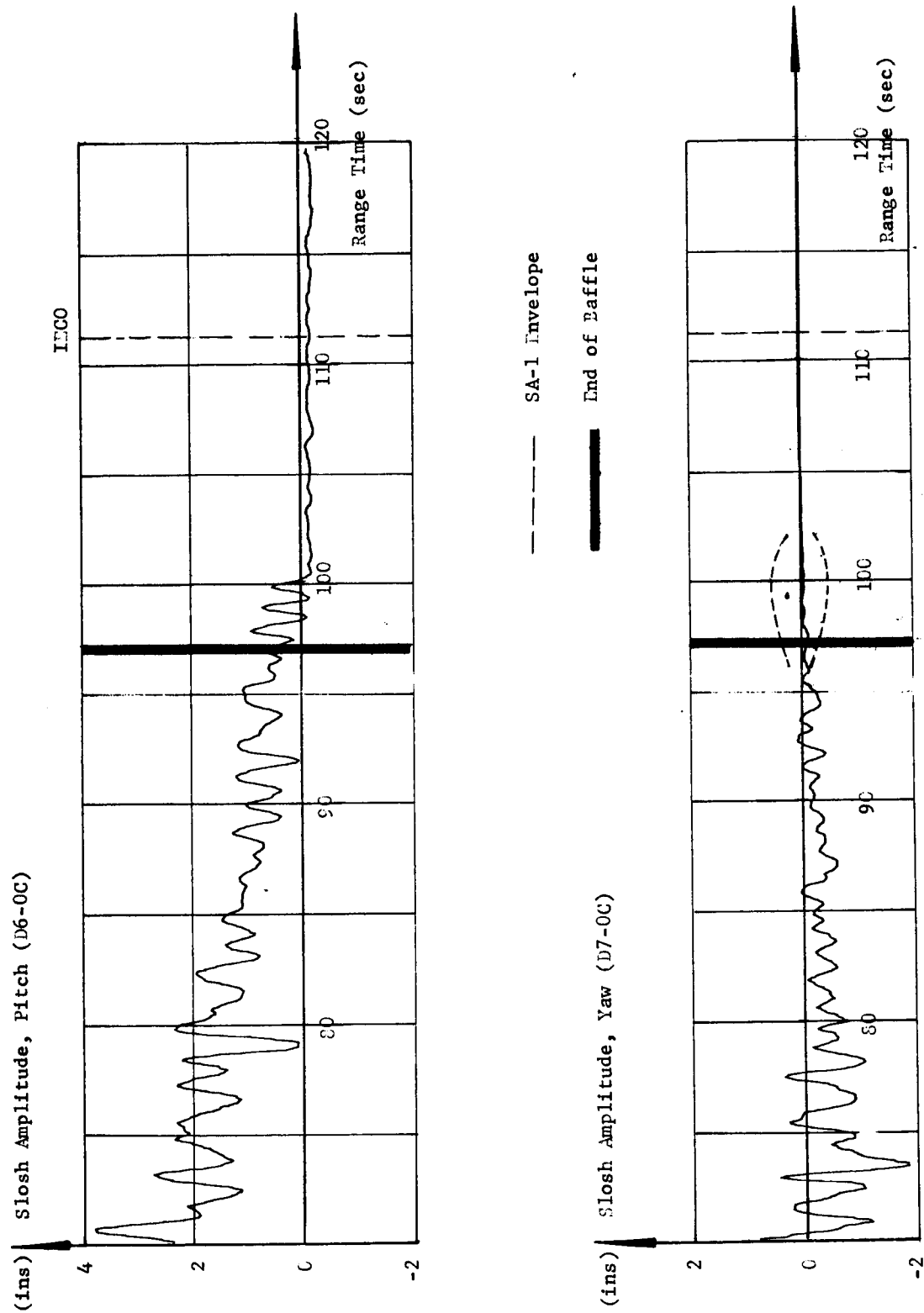


FIGURE 6-23 CENTER LOX TANK TELEMETERED SLOSHING AMPLITUDES

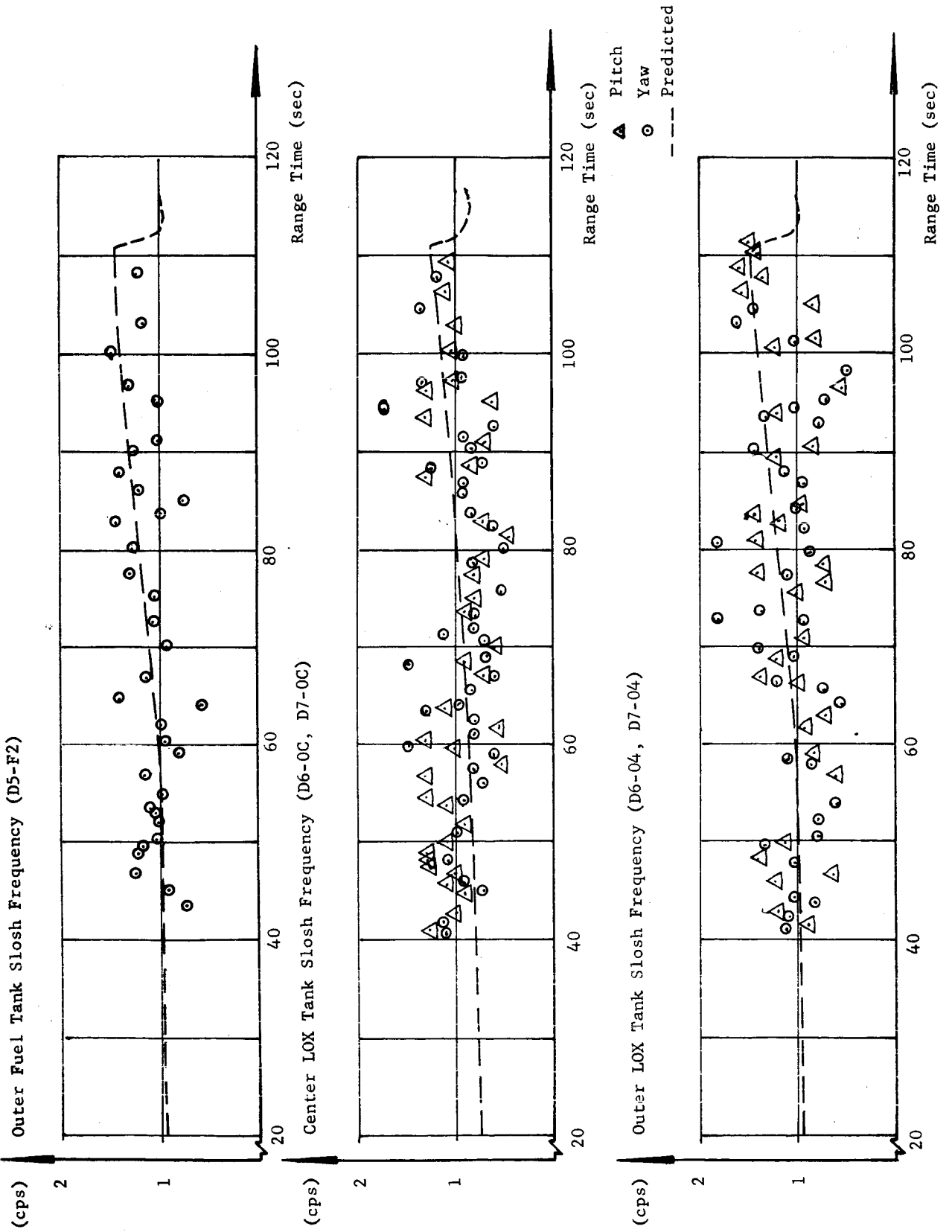
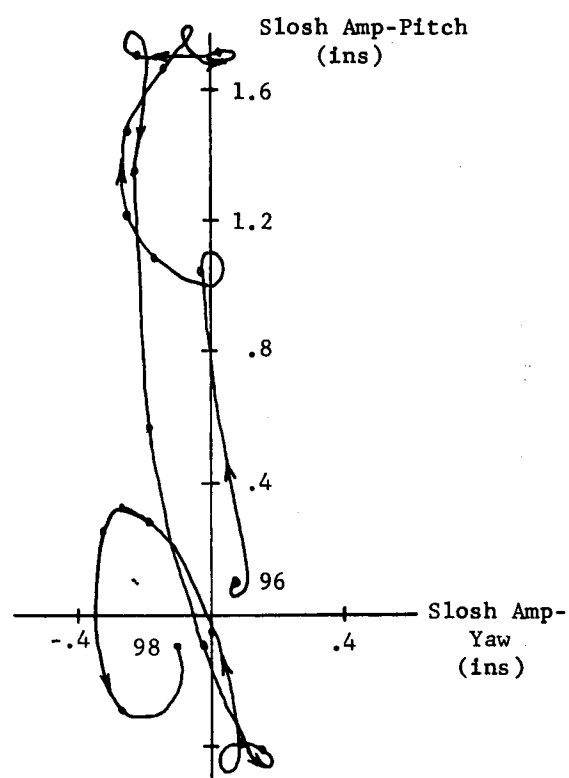
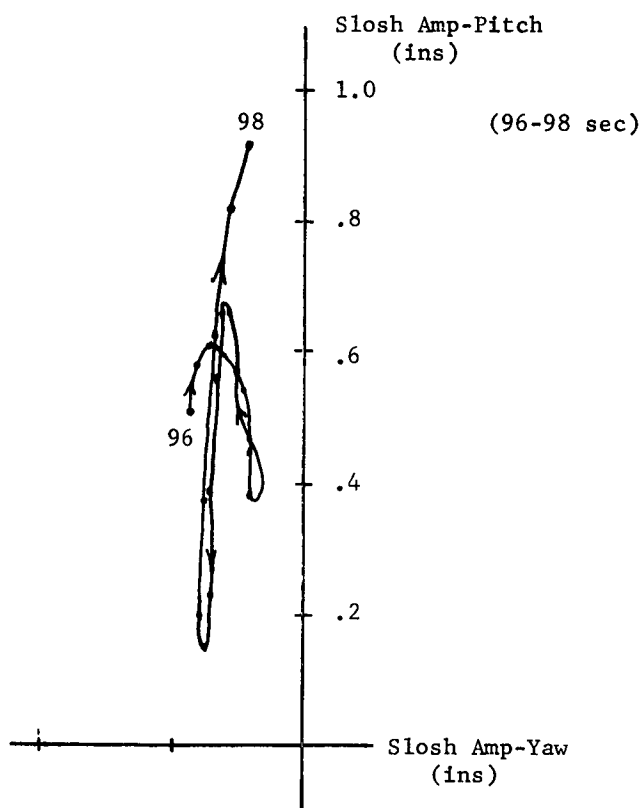
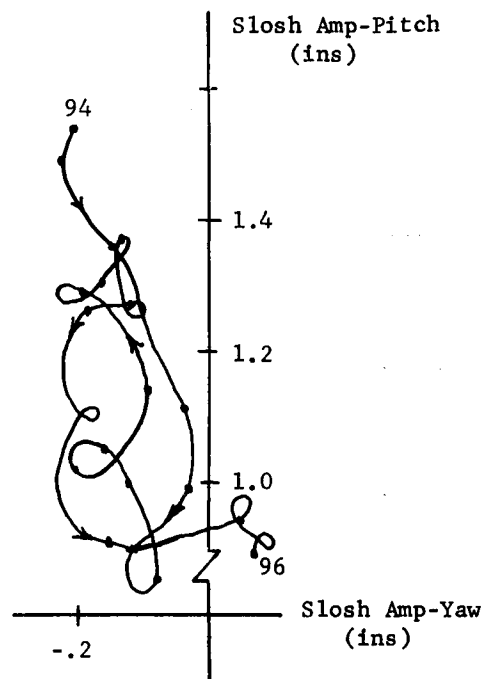
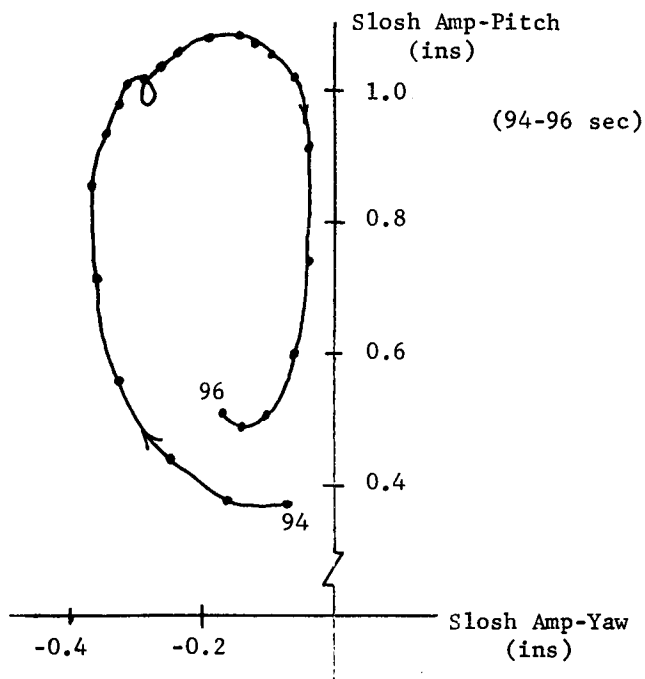


FIGURE 6-24 SLOSHING FREQUENCIES



105" LOX Tank

SA-2

105" LOX Tank

SA-1

0.1 sec Time Interval

Fig. 6-25 SPATIAL PLOTS OF SLOSHING MOTION

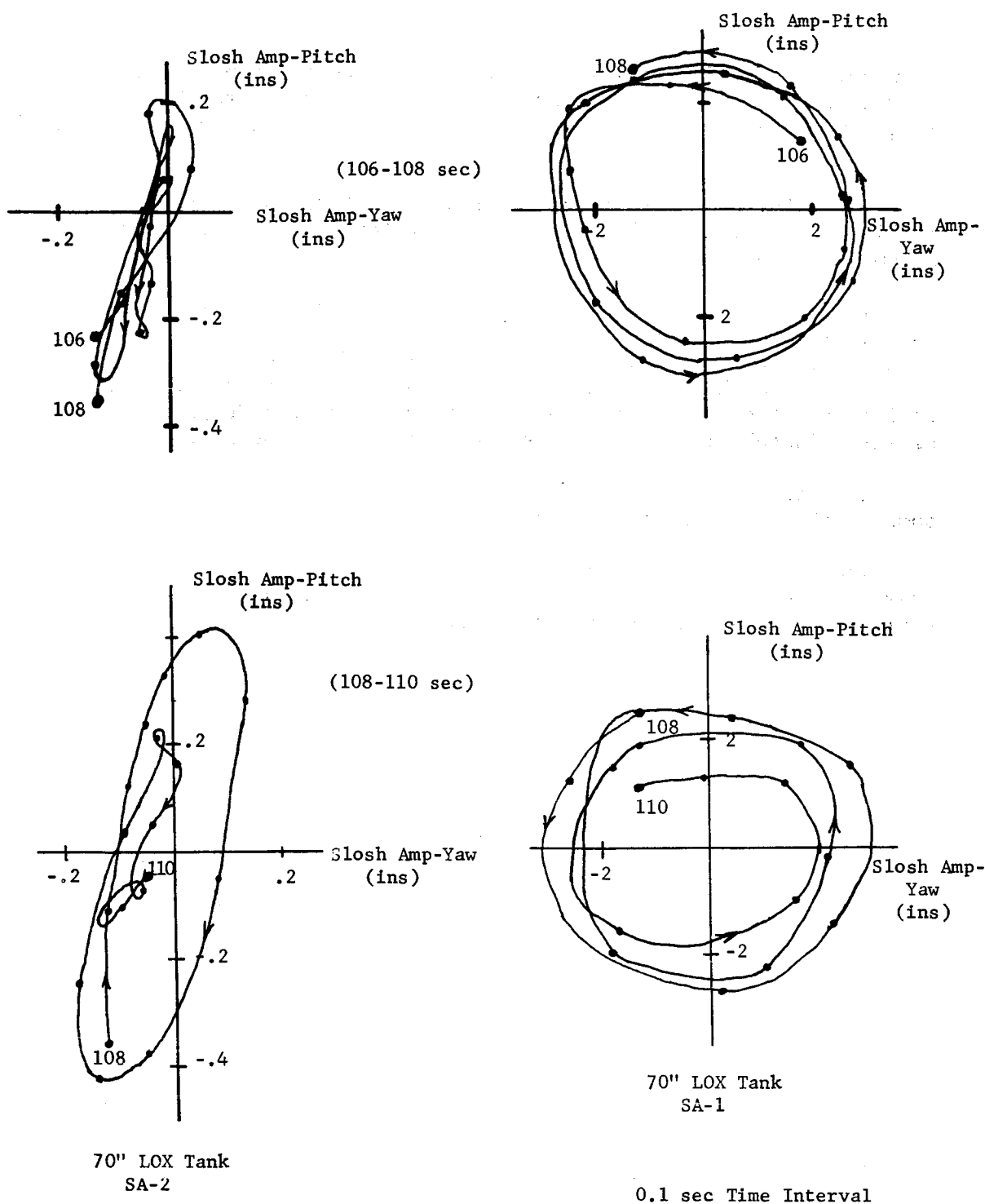


FIGURE 6-26 SPATIAL PLOTS OF SLOSHING MOTION

~~CONFIDENTIAL~~

pronounced on SA-2, being more elliptical. The apparent swirling or vortex motion on the SA-1 flight may have been aggravated by the much larger vehicle motions due to slosh interactions than those experienced on SA-2.

Vortexing probably occurs later on SA-2 than SA-1 because of a smaller excitation at the surface, the vortex action taking longer to become apparent.

The maximum amplitudes of the engine deflection oscillations due to the sloshing occurred at about 105 seconds and were  $\pm 0.15$  deg in pitch,  $\pm 0.1$  deg in yaw, and no noticeable effect in roll. On SA-1, in addition to the pitch and yaw reactions, there was a very extreme roll oscillation with a peak angular velocity of 2.5 deg/sec due to the sloshing instability. No such effect was observed on SA-2.

The ring frame and baffle locations as well as the locations of some of the measurements are shown in Figure 6-20.

The effect of sloshing on the inboard engine cutoff signal due to premature uncovering of the cutoff sensor on SA-2 is considered very small due to the low sloshing amplitudes.

~~CONFIDENTIAL~~

## 7.0 (C) GUIDANCE

### 7.1 SUMMARY

The Saturn SA-2 vehicle was flown without active path guidance. However, passenger hardware was on-board to establish the operational capabilities of the guidance equipment in the Saturn flight environment. The telemetered data as well as a trajectory comparison indicate satisfactory performance of the equipment.

### 7.2 DESCRIPTION OF GUIDANCE SYSTEM

The guidance hardware included three pendulous integrating gyroscopic accelerometers (AMAB-4) mounted on an ST-90 stabilized platform. These accelerometers were mounted to sense forces along a set of inertial axes oriented with respect to the stabilized platform X, Y, Z axes. The slant range axis was directed downrange and elevated 41 degrees from the launch site horizontal plane; the slant altitude axis was directed upward and 41 degrees counterclockwise from the local plumbline at launch; the positive cross range axis was parallel to the local horizontal plane at launch and normal to the slant range-slant altitude plane forming a right-handed Cartesian coordinate system. The platform axes were maintained in orientation by three AMAB-7 air bearing gyros. No second integrators were carried and the guidance measurements were in open loop.

Velocity Encoders and a Guidance Signal Processor Repeater were flown for the first time on SA-2. The encoders are mounted on the individual accelerometers and driven by the precession of the accelerometer measuring head. Each encoder generates two variable frequency output signals. The zero crossing of each signal indicate an incremental change in velocity of 0.1 m/sec. The polarity of the velocity increment is determined by the phase relation of the two signals.

The guidance signal processor accepts the two sine wave signals from the encoder, determines the phase of the signals, and the zero cross points and then sends a polarized, 350 millisecond pulse to the telemetry system. With each 64th incremental pulse the signal processor shifts the bias level of its respective telemeter channel. The bias shift is normally used as a coarse velocity count of 6.4 m/sec for data reduction purposes.

~~CONFIDENTIAL~~

### 7.3 OPERATIONAL ANALYSIS

#### 7.3.1 GUIDANCE INTELLIGENCE ERRORS

Guidance intelligence errors are defined as deviations in the guidance measurements resulting from platform and accelerometer errors. The intelligence errors are obtained by comparing the telemetered outputs of the guidance system with those calculated from trajectory data. The earth-fixed trajectory established from tracking data is mathematically transformed into inertial, space-fixed guidance indications. These calculated guidance velocities are then compared with the telemetered velocities to establish their agreement.

The guidance intelligence errors as presented in Figures 7-1 and 7-3 include errors in tracking and data reduction as well as guidance hardware errors. The errors shown are within the data noise level and one sigma hardware errors except for cross range. The results of a more extensive study of the cross range error will be published at a later time.

#### 7.3.2 ACCELEROMETER OUTPUTS

The inertial velocity outputs of the integrating accelerometers represent the vehicle motion as sensed by the guidance system. The telemetered inertial velocity data was compared with corresponding velocities calculated from external tracking data assuming the monitored alignment of the platform and accelerometers at liftoff. The comparison indicated a favorable agreement of the data. The small errors observed may be attributed to errors in telemetered data reduction, tracking, and guidance hardware errors. Monitored errors in alignment of the guidance accelerometers prior to liftoff were:

Slant Range	+0.001 deg about Z-axis
Slant Altitude	-0.012 deg about Z-axis
Cross Range	+0.014 deg about X-axis

where a positive angle represents a more positive output of the accelerometer.

The platform remained in its reference established at liftoff with essentially no errors greater than established one sigma deviations.

#### Slant Range Velocity

The outputs of the slant range accelerometer were compared with corresponding values calculated from earth-fixed trajectory data assuming the monitored alignment of the platform and accelerometers.

~~CONFIDENTIAL~~

These differences are plotted versus time in the upper portion of Figure 7-1. The small errors observed are the results of errors in the data compared and one sigma hardware errors. After the end of thrust, the telemetered slant range velocity remained 0.3 m/sec lower than the calculated velocity.

### Cross Range Velocity

The telemetered cross range velocity is plotted versus time in Figure 7-2. Some difficulty was experienced in the manual reduction of the cross range velocity telemeter trace (see Para 7.3.2), but valid cross range velocity measurements were obtained. The aiming azimuths of the vehicle and platform were 100.23 deg and 100 deg E of N respectively which is within the tolerance of .25°. This alignment difference produced a cross range velocity observed by the accelerometers and the external tracking. The overall velocity profile also reflects the changes in the cross range wind velocity.

Cross range guidance velocity was about 2.4 m/sec at 27 sec of flight when the angle of attack control coefficient,  $b_0$ , entered the control loop. This velocity represents an average acceleration of about 0.1 m/sec<sup>2</sup> in the cross range direction. The cross range velocity increased from 2.4 m/sec at 27 sec to 5.6 m/sec at 65 sec which corresponds to an average acceleration of 0.08 m/sec<sup>2</sup>. The velocity remained relatively constant from 65 to 90 sec when the  $b_0$  term was taken out of the control loop. A maximum cross range velocity was reached by the end of thrust and remained constant at about 7 m/sec (left) until time of destruct. The upper portion of Figure 7-3 presents the differences between the telemetered and calculated cross range velocities plotted versus time for Saturn SA-2. The differences oscillate with very small amplitudes until after 40 sec. From this time the differences increase to about 0.9 m/sec at outboard engine cutoff and remain constant to time of destruct. This difference corresponds to either a 0.02 deg misalignment of the platform or accelerometers around the X-axis or a 0.05 deg azimuth misalignment.

Telemetered outputs of the cross range accelerometer were simulated by assuming either an aiming azimuth error of 0.05 deg or that the cross range measuring axis was elevated by an angle of 0.02 degrees and then transforming the earth-fixed velocities into guidance velocities. The cross range velocity from the perturbed trajectories was compared with the values calculated from the same data with the monitored alignments. These differences obtained from the elevated cross range measuring axis are plotted as circled points, and the differences from the azimuth error are enclosed in triangles in Figure 7-3. The differences obtained from either of the perturbed transformations are

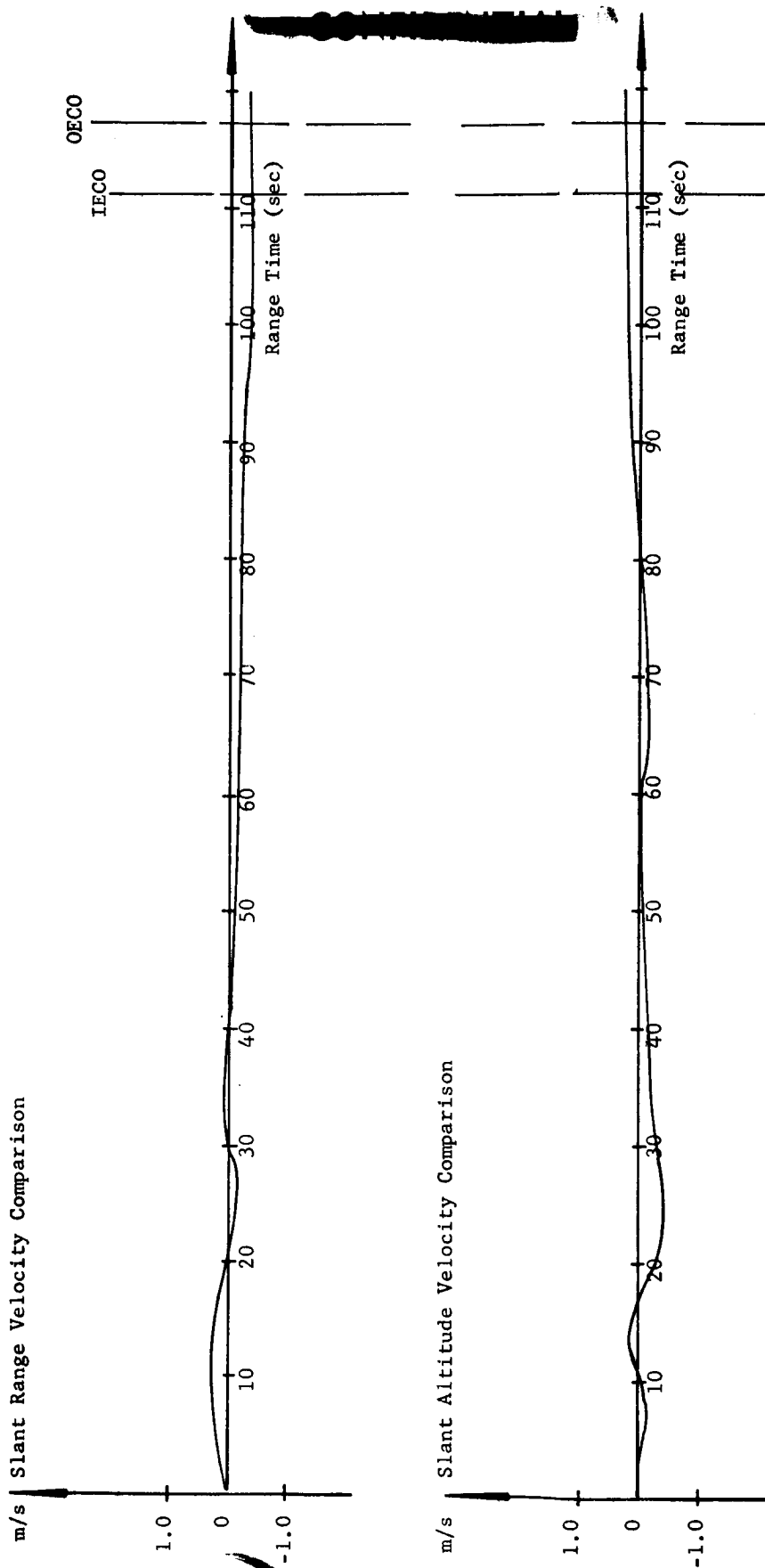


Fig. 7-1 GUIDANCE VELOCITY COMPARISON  
(TELEMETERED MINUS CALCULATED)

CONFIDENTIAL

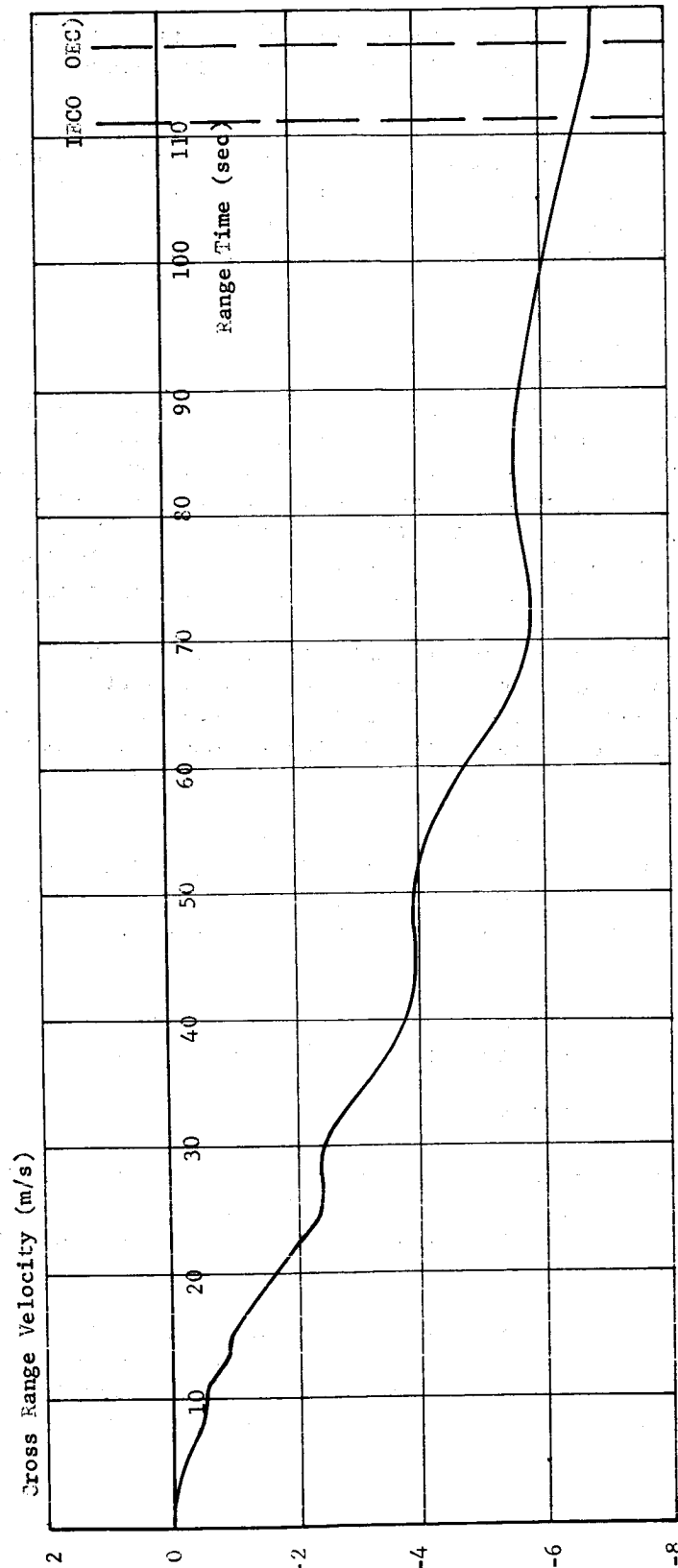


Fig. 7-2 CROSS RANGE GUIDANCE VELOCITY  
(TELEMETERED)

CONFIDENTIAL

~~CONFIDENTIAL~~

a very good approximation of the telemetered minus calculated velocity differences. Further study will be required to determine which is the more probable error.

The lower portion of Figure 7-3 presents a similar comparison for the SA-1 flight. Cross range differences for the two Saturn vehicles are very similar especially after 60 sec of flight when the observed error is more clearly distinguished from noise level of the compared data.

#### Slant Altitude Velocity

The telemetered slant altitude velocity was the output of the integrating accelerometer. Figure 7-4 presents the telemetered and precalculated slant altitude velocities plotted versus time. Telemetered velocity was generally lower than the precalculated values for the entire flight mainly as a result of approximately 2.3% lower flow rates. At the end of thrust the telemetered slant altitude velocity was 1050.4 m/sec or 10.0 m/sec lower than the precalculated value.

Differences between the telemetered and calculated slant altitude velocities are plotted versus time in the lower portion of Figure 7-1. The differences were within  $\pm 0.4$  m/sec for the entire flight and were essentially 0 at both inboard and outboard cutoffs. After the end of thrust the velocity difference remained constant at 0.2 m/sec.

Table 7-1 presents a comparison of the guidance velocities at some significant flight events. Telemetered values and those calculated from external tracking data are in close agreement although the cross range velocity error was too large to be attributed to errors in the data.

Most of the differences between the actual and precalculated values may be attributed to non-nominal flight conditions.

#### 7.3.3 FUNCTIONAL ANALYSIS

The Velocity Encoders and Guidance Signal Processor Repeater, which were flown for the first time on SA-2, operated satisfactorily. It should be noted that the two devices will not be used as active guidance components.

Oscillations with a frequency of 26 cps were observed in the accelerometer servo loop measurements as were noted in measurements on SA-1 and during static tests. The maximum amplitudes ( $\sim 50$  millivolts) occurred during the holddown period and the first six seconds of flight.

~~CONFIDENTIAL~~

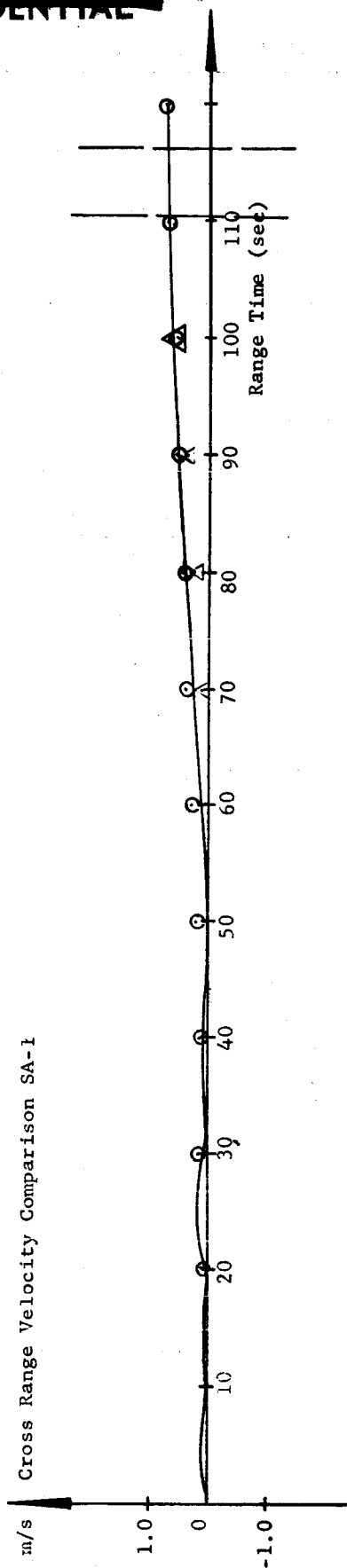
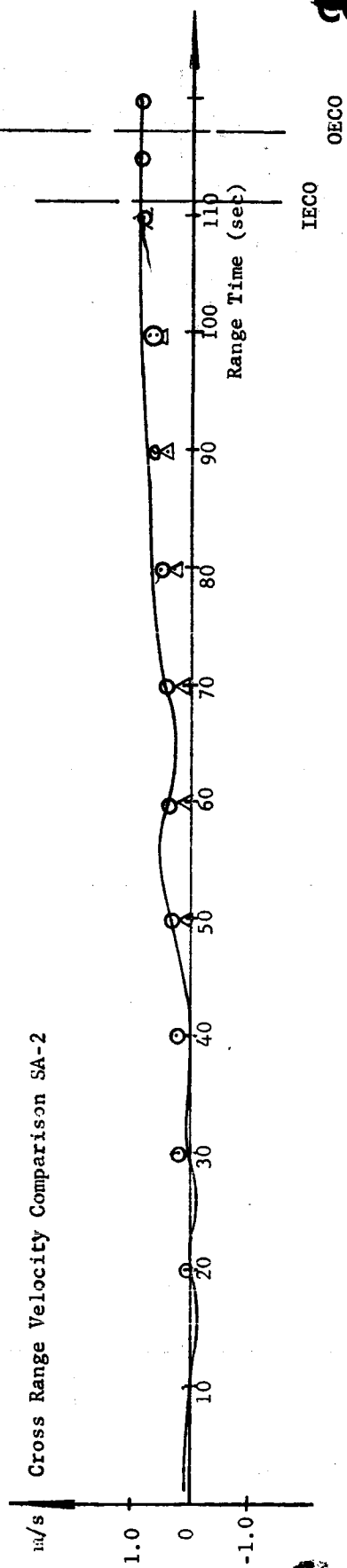


Fig. 7-3 GUIDANCE VELOCITY COMPARISON CROSS RANGE  
(TELEMETERED MINUS CALCULATED)

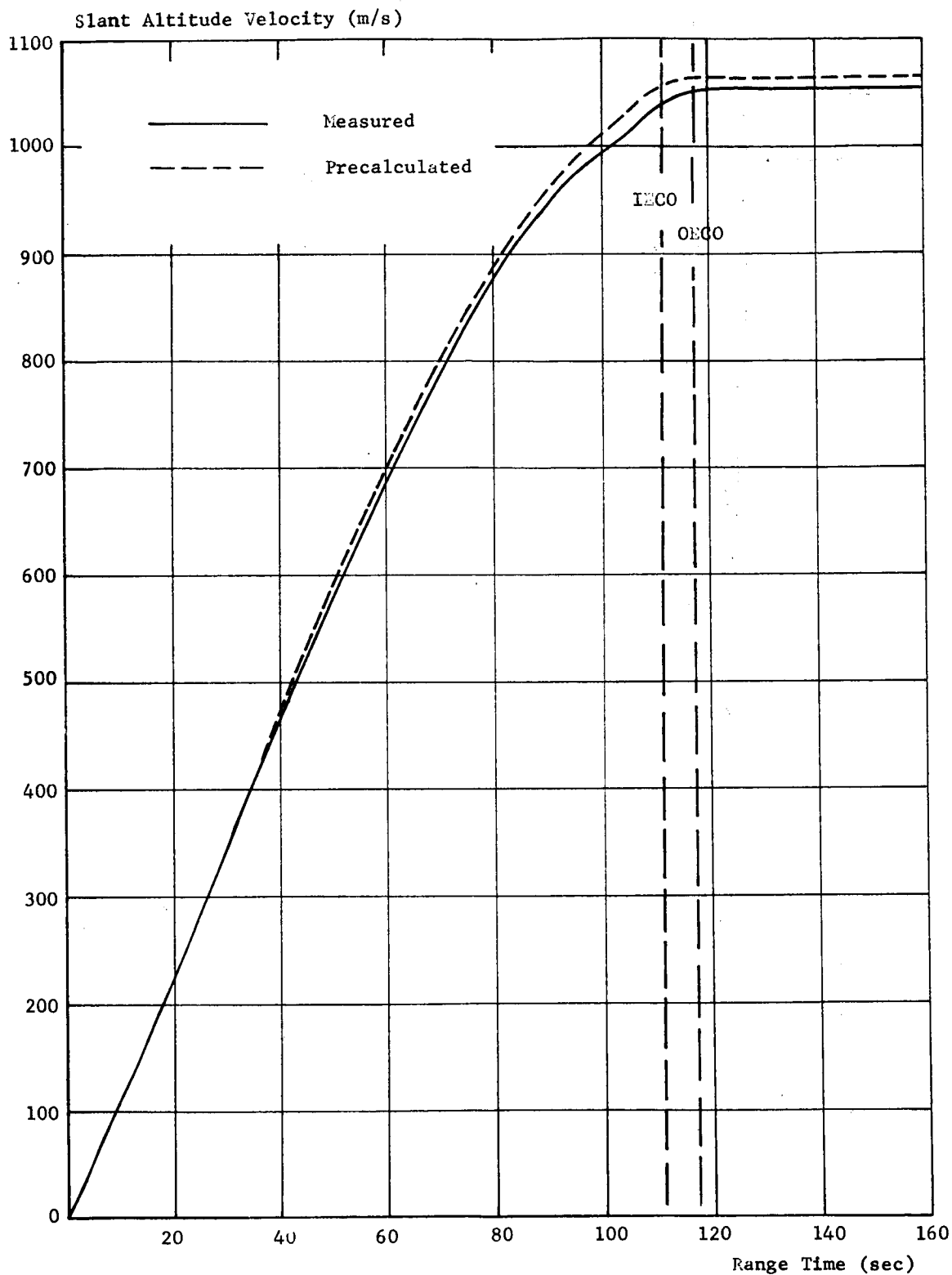


Fig. 7-4 SLANT ALTITUDE GUIDANCE VELOCITY  
(TELEMETTERED)

~~CONFIDENTIAL~~

MPR-SAT-WF-62-5

TABLE 7-1 GUIDANCE COMPARISONS

Flight Event	Slant Range Velocity (m/sec)			Cross Range Velocity (m/sec)			Slant Altitude Velocity (m/sec)		
	Telem	Calc	Precalc	Telem	Calc	Precalc	Telem	Calc	Precalc
Computer Preset	0.0	0.0	0.0	0.0	0.0	0.0	0.0	0.0	0.0
Inboard Engine Cutoff	2281.7	2281.9	2265.0	-6.7	-7.3	-1.7	1035.5	1035.2	1044.2
Outboard Engine Cutoff	2414.8	2415.1	2404.2	-6.9	-7.9	-1.9	1049.5	1049.2	1058.6
End of Thrust Decay	2422.2	2422.5	2412.7	-7.0	-7.9	-1.9	1050.3	1050.1	1059.5

~~CONFIDENTIAL~~

After this period the amplitude of the oscillations dropped to a low value and remained low in the slant altitude measurement. The oscillations in the cross range accelerometer servo loop signal increased in amplitude to near full scale of the measurement during the vibration peak around maximum dynamic pressure (high Q portion of the flight) and then decreased to a low level but somewhat higher than that in the slant altitude system.

The natural frequency of the accelerometers is 26 cps and, consequently, is a frequency inherent to some extent in the servo loop signals; however, the high frequency vibration environment in the instrument canister makes a definite contribution to the disturbance. It should be noted that the saturation point of the accelerometer servo loop is at least four times greater than the peak levels ( $\pm 50$  millivolts) indicated by the telemetered measurements.

Since the peak amplitude levels were near full scale on the measurements, the full scale range will be changed on subsequent flights to  $\pm 1^\circ$  (corresponds to  $\pm 125$  mv).

The peak overall composite vibration level measurement on the ST-90 platform was 0.844 "g" RMS (-2 to + 3 sec) along the Z-axis. The air bearing supply pressure was a constant 34 psid throughout flight, and the instrument compartment pressure was constant at 15 psia. The vibration levels and the pressure levels are satisfactory.

#### Guidance Velocity Measurements

The cross range velocity measurement as telemetered showed some undesirable characteristics. This can be readily seen by an examination of the sample of telemeter recording shown in Figure 7-5. Although there are a considerable number of pulses of both polarities evident on the recording, none are valid velocity indications in the cross range measurements. The extraneous pulses occur due to an actual relative motion between the accelerometer measuring head and the accelerometer mount frame and are probably a combination of actual motion of both. The independent motion of either would give an output signal. The condition demonstrated by the recording was at its worst during the holddown period of the vehicle; however, the Hangar D telemeter record indicated extraneous noise mixed in with the velocity signal just before cutoff.

Two approaches are being investigated for improving the cross range indications for SA-3 and SA-4. Either a stair-step presentation or a more frequent bias level shift would probably improve the data reduction effort.

~~CONFIDENTIAL~~

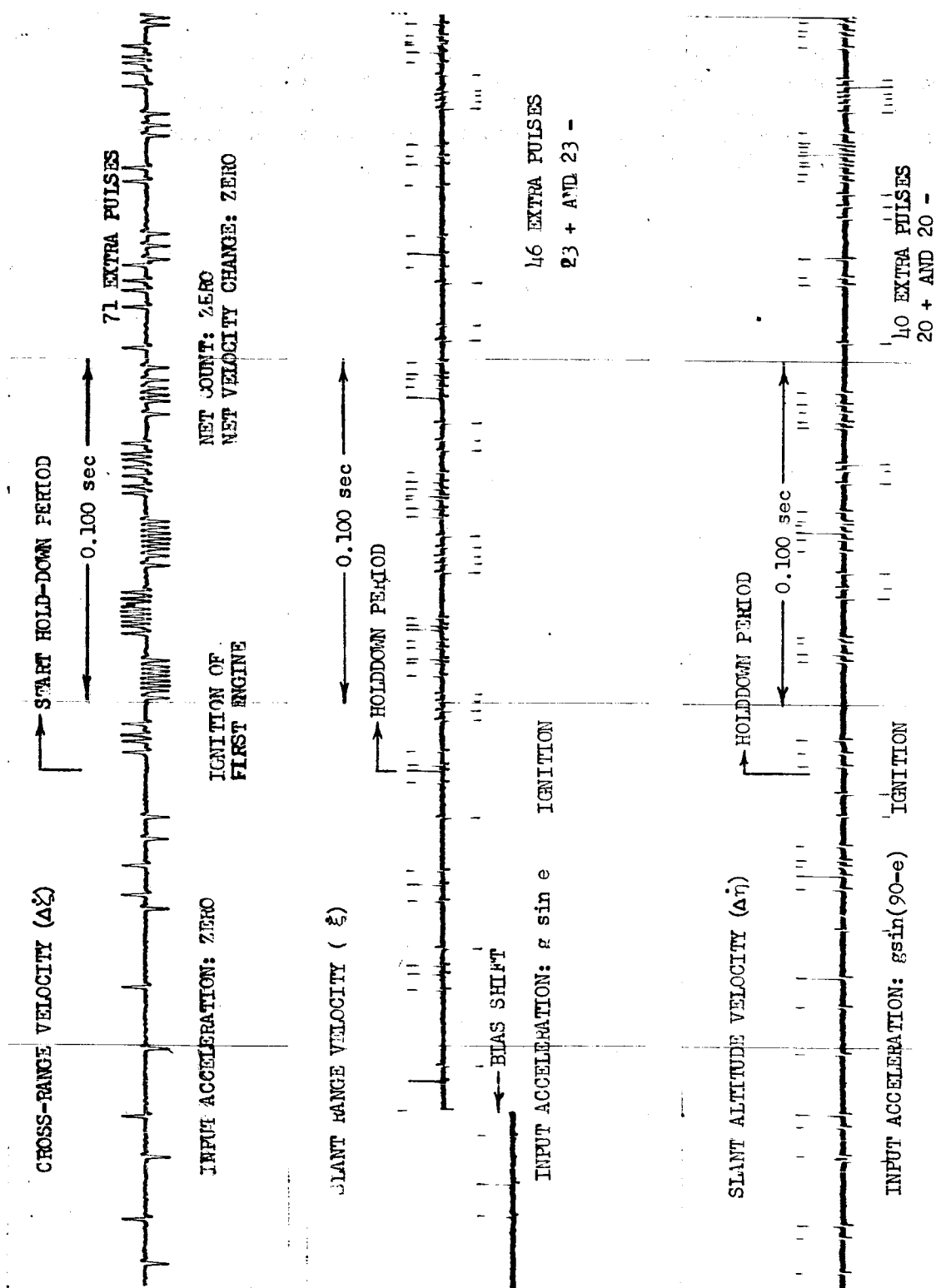


FIGURE 7-5 TELEMETERED VELOCITY INDICATIONS AT IGNITION

~~CONFIDENTIAL~~

The slant altitude and slant range velocity measurements also had some interference during holddown and the first four seconds of flight. After four seconds, practically no extraneous pulses were noted in these two measurements. The slant range and slant altitude velocity data was reduced manually with very little difficulty.

~~CONFIDENTIAL~~

## 8.0 (U) VEHICLE ELECTRICAL SYSTEM

### 8.1 SUMMARY

All vehicle networks performed as expected with only minor deviations.

### 8.2 POWER SUPPLY DESCRIPTION (FIGURES 8-1 AND 8-2)

The power supply for SA-2 consisted of two identical 28 volt, zinc-silver oxide batteries designated D-10 and D-20 and located in instrument canister 14 (canister and unit locations are shown on Figure 8-3). These batteries supplied power to 8 inflight distributors: a power distributor, control distributor, propulsion system distributor, and 5 measuring distributors. The capacity of these batteries is 2650 amp-min, which is approximately 6 times that required for normal flight.

#### Power Distributor

The two 28 volt batteries supply main power to the power distributor, located in canister 14, which is used to switch and distribute power as required for operating all inflight subsystems. Three busses (D-11, D-21 and 400 cycle) are used as junction points to distribute the power from the power distributor to the seven other distributors.

#### Control Distributor

This distributor, which contains busses to receive 28 volt power from the power distributor, distributes power to control the functions as required by the program device, flight sequencer, control computer and the pressurization system. Three-phase, 115-volt, 400 cycle ac power supply. The power supply converts this power to 60 volts dc and feeds it to the control distributor for distribution to the angle of attack meters and actuators. Three-phase, 115 volt, 400 cycle ac power is also distributed directly through the control distributor to the stabilized platform, servo amplifiers and guidance repeater. All of these components are thus integrated into the vehicle circuitry to accomplish vehicle control. This distributor is located in canister 15.

#### Propulsion System Distributor

The propulsion distributor contains the relays and circuitry which control the functions of all eight engines according to a preset, programmed sequence. This distributor is located in unit 9 of the vehicle.

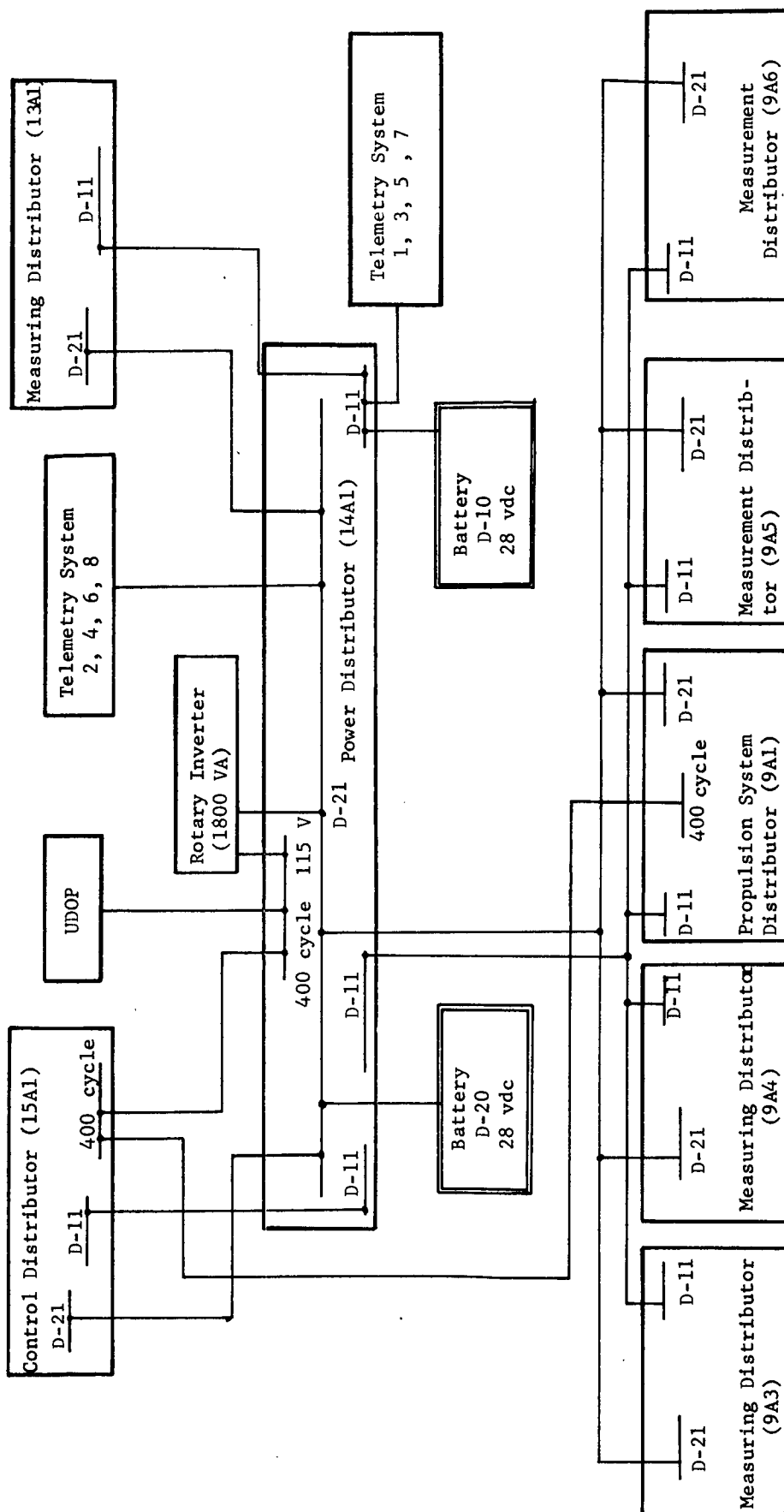


FIGURE 8-1 28 VOLT D.C. POWER SYSTEM

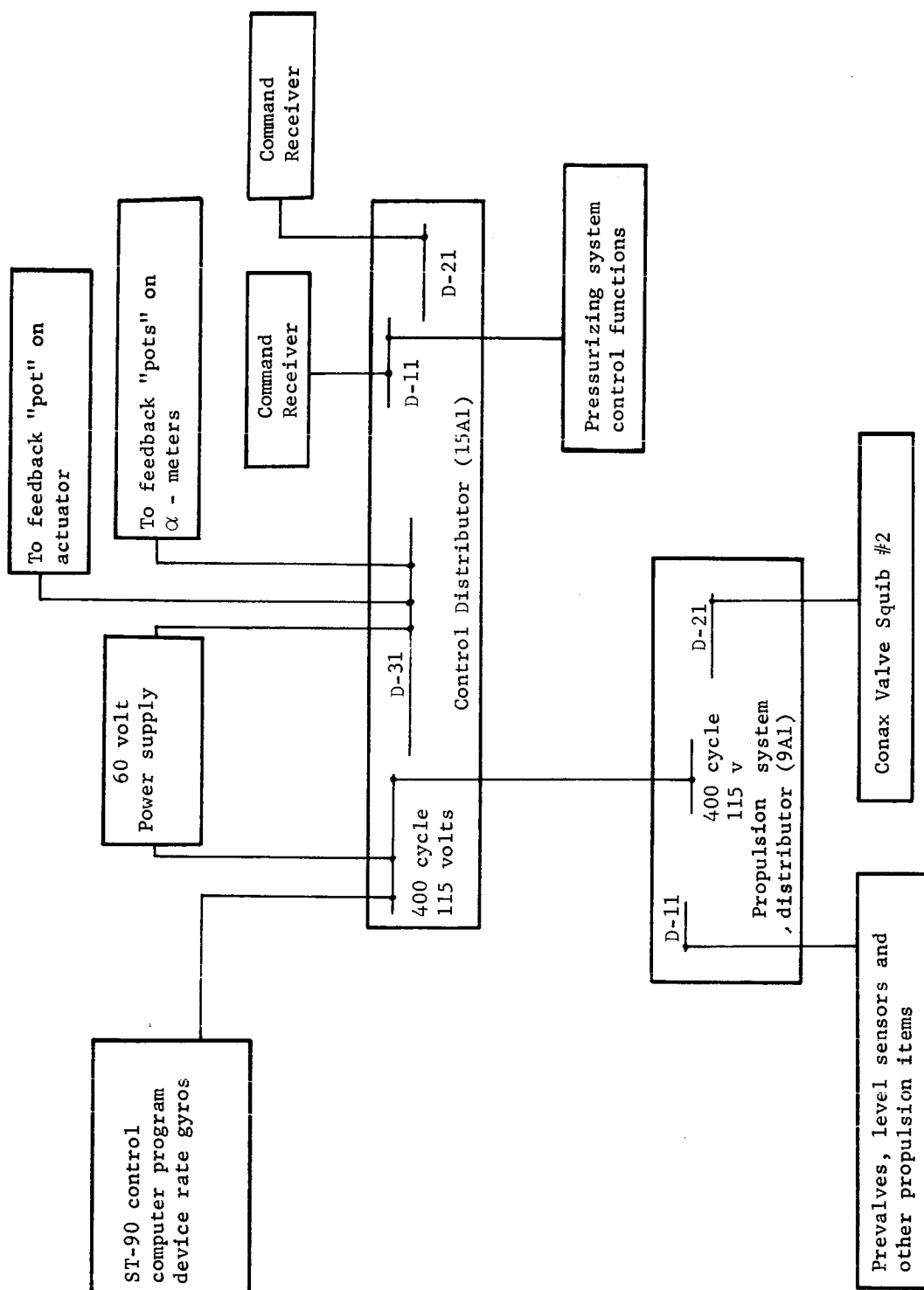


FIGURE 8-2 PROPULSION AND CONTROL DISTRIBUTOR NETWORK SYSTEM

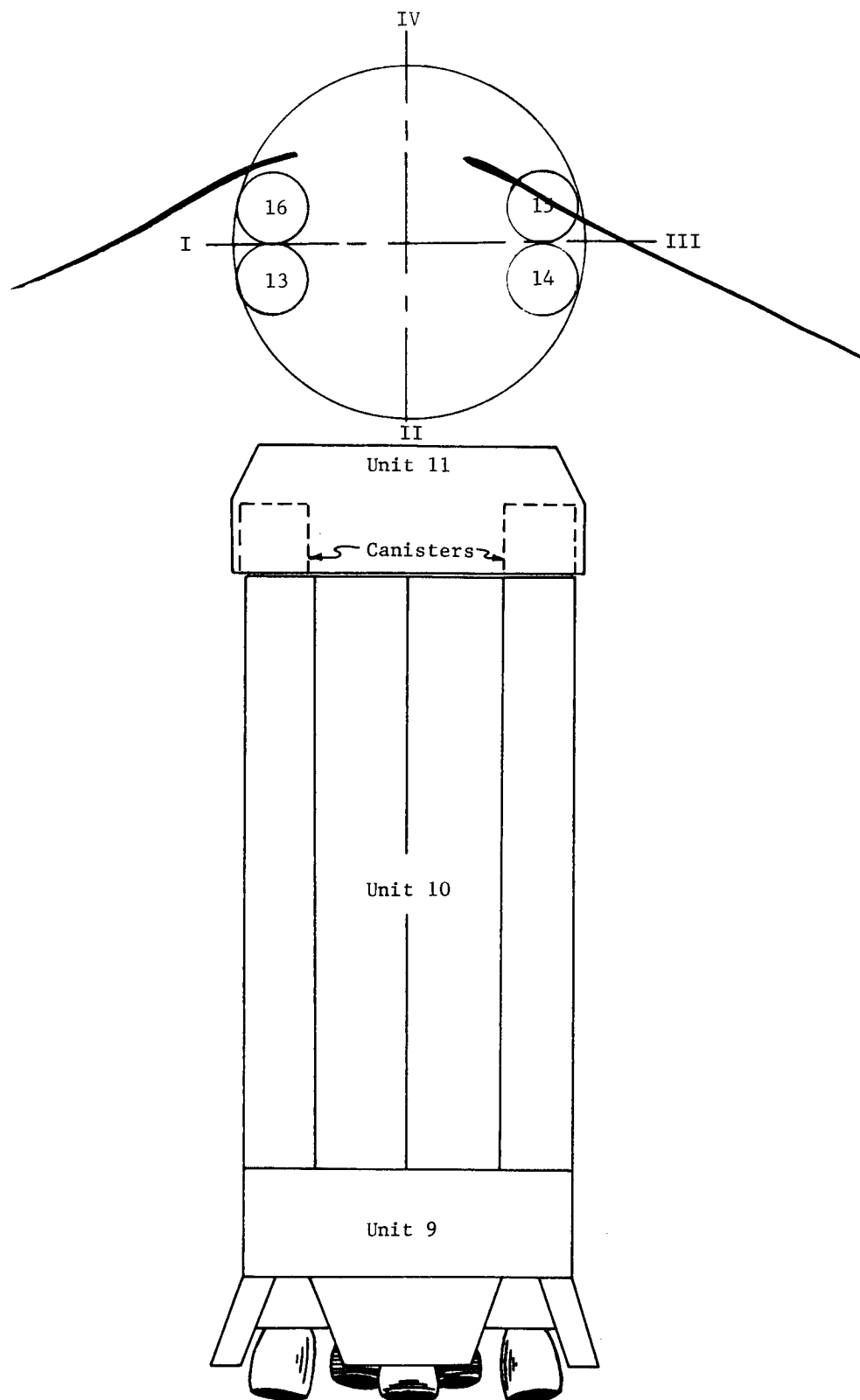


FIGURE 8-3 UNIT LOCATIONS

The propulsion distributor busses receive 28 volt power from the power distributor and distribute this power to the circuits and relays which control the engine functions. Part of the relays actuate fuel and LOX prevalues for controlling the flow of propellant to the engines. Some of the relays are used to activate the conax valves for engine cutoff. The engine cutoff relays are activated when signals are received from the flight sequencer or from sensors indicating low liquid level and low thrust. There are also relays which operate fuel and LOX fill-drain and replenishing valves.

### Measuring Distributors

The Saturn SA-2 vehicle was equipped with five measuring distributors. All five of these distributors are identical in configuration and size but differ electrically. The measuring distributors serve to distribute measurement signals to the telemeter channels from the engines, tail area, and the upper portion of the vehicle. The location and function of these distributors are:

Measuring Distributor 9A3 - located in unit nine - controls measurements which do not require signal conditioning on engines 1, 2, 5, 6, and a portion of the thrust frame area.

Measuring Distributor 9A4 - located in unit nine - controls measurements which do not require signal conditioning on engines 3, 4, 7, 8, and a portion of the thrust frame area.

Measurement Distributor 9A5 - located in unit nine - controls measurements which require signal conditioning on engines 1, 2, 5, 6, and a portion of the thrust frame area.

Measurement Distributor 9A6 - located in unit nine - controls measurements which require signal conditioning on engines 3, 4, 7, 8, and a portion of the thrust frame area.

Measurement Distributor 13A1 - located in canister 13 - controls all measurements located in the upper portion of the vehicle. It also controls all telemeter and tracking equipment.

The 28 volt dc power from the vehicle batteries is supplied through the power distributor to busses (D81 - D89) in the measuring distributor. This 28 volt supply is fed to the measuring power supplies, converted to a 5 volt output, and is routed to the measuring voltage busses. From these 5 volt busses, energy is supplied to the various measurement pick-ups throughout the vehicle. Busses D81 through D88 distribute 5 volt power through the vehicle measuring network to the measurements in the eight engine compartment areas. The D89 buss supplies 5 volt power to all the remaining measurements throughout the vehicle.

### 8.3 FLIGHT RESULTS

The voltage and current for battery D-20 and its corresponding buss (D-21) were constant at 27.5 volts and 120 amps.

The variable load over flight for battery D-10 and its corresponding buss (D-11) caused the voltage and current to vary from 27.5 volts, 112 amp at liftoff to 28.5 volts, 75 amps at end of flight. These voltages and currents are as expected with 0.5 volt increases both when the continuous lights and the angle of attack heaters were switched off. D-11 buss voltage also had slight fluctuations when the air bearing heater was cycled.

The frequency of the precision inverter on SA-2 was 399.987 cps, +0.021 cps over the flight period. The usual frequency disturbance -0.034 cps caused by ignition was within  $\pm .23$  cps. All frequencies are well within allowed tolerances.

Measuring voltages of the eight "slave" units off busses D81 thru D88 operated within the 5 volts  $\pm$  5% limits.

Main fuel and LOX valve position signals (start open, open, and closed) operated satisfactorily.

Cutoff signals (inboard and outboard) and flight sequence signals were as expected.

## 9.0 (U) STRUCTURES AND VIBRATION

### 9.1 SUMMARY

The original instrumentation for SA-2 included 8 strain measurements on the truss members and 8 strain measurements on LOX pins (mounting stud). From these measurements, pitch and yaw moments and longitudinal forces were computed at various significant flight times. The results compared well with predicted values. Of the original 16 strain measurements, one LOX pin measurement (on the pitch axis) was inoperative, precluding calculation of yaw moment into outer tanks; however, from assumed values for this measurement calculations of longitudinal loads were made without appreciable error.

Instrumentation for detecting vehicle body bending consisted of 10 bending accelerometers at three stations along the vehicle; however, one of these measurements (outer LOX tank yaw measurement) was inoperative throughout the flight, and another (nose pitch measurement) yielded questionable data at certain times during the flight. The vehicle at several times in flight vibrated in a first bending mode. This frequency ranged from 2.2 cps at liftoff to 3.0 cps at cutoff. These frequencies were present in both pitch and yaw directions, but in all cases larger amplitude existed for the oscillations of the yaw accelerometers. The first bending acceleration was very low throughout flight and did not exceed 0.045 g's single amplitude at any time. Some frequency content of approximately 8.6 cps to 9.4 cps at flight times of 35 seconds to cutoff was evident in the results of the correlation study performed on these measurements. These frequencies are in the range of the vehicle second bending mode. Lower amplitudes exist for these frequencies than for the fundamental modes. Many more frequencies in the range of 2 cps to 11 cps were present which cannot be thoroughly identified primarily because of lack of instrumentation and low response of measurements taken. These could be coupled frequencies caused from the cluster arrangement of the booster.

Vibration levels recorded during the SA-2 flight were of the same general order as those measured on SA-1. An accurate comparison of these data cannot be accomplished by direct inspection, however, since the telemetry bandwidths used on the two flights differed considerably. Three principle sources of excitation were considered in the analysis of the vibration data. These were: (1) mechanical excitation, which originates with engine ignition, (2) acoustical excitation, due to the sound field generated by the propulsion system, and (3) aerodynamic excitation which is most influential as Mach 1 and Max Q are approached.

## 9.2 BENDING MOMENTS AND NORMAL LOAD FACTORS

### 9.2.1 INSTRUMENTATION

Instrumentation for determining bending moments and normal load factors consisted of eight truss strain gauges (E 13-11 thru E 20-11) and eight LOX tanks stud strain gauges (E 21-01 thru E 21-04 and E 22-01 thru E 22-04). These gauges were located at stations 929 and 869 respectively (see Figure 9-1). The telemetered data was obtained as decommutated oscillograph traces and also in digitized form. Flight evaluation consisted of determining the instantaneous longitudinal load and bending moments about the pitch and the yaw axis for numerous time slices.

Data for obtaining bending moment and normal load factor distribution was also available from the 10 bending accelerometers located along the vehicle (Ref. para. 9.4).

### 9.2.2 RESULTS

Strain gauge measurements at vehicle station 979 indicated that the SA-2 vehicle experienced the highest bending moments at  $t = 63.5$  seconds and  $t = 65.3$  seconds. Figures 9-2 and 9-3 present the bending moment distributions for these time points. The dotted curve is labeled a "design" curve. This is the calculated moment for the SA-2 vehicle for an engine "hard-over" case used in the original design effort. The curve labeled actual was calculated using actual measured SA-2 flight input data; such as Mach number, dynamic pressure, angle of attack, and gimbal angles. This curve is generated from a vehicle beam analysis which takes into account design aerodynamic force distribution and inertia effects.

The strain gauge moment is shown by an asterisk at the gauge location station 979. The normal load factors for the bending moments depicted are compared with the accelerometer readings from the flight.

Strain gauges on the studs of the 70 inch LOX tanks (station 869) indicated the amount of bending moment experienced by the outer tanks to be that shown on Figures 9-2 and 9-3 as the "telemetered value". This bending moment was also calculated by applying values from the actual bending moment curve to the Saturn Internal Loads Distribution Analysis. The difference between this calculated value and the telemetered value was only 3% of the total bending moment at station 869 for the  $t = 63.5$  seconds time point (4% for  $t = 65.3$  seconds). This near perfect agreement substantiates the accuracy of both the vehicle beam analysis and the internal loads analysis.

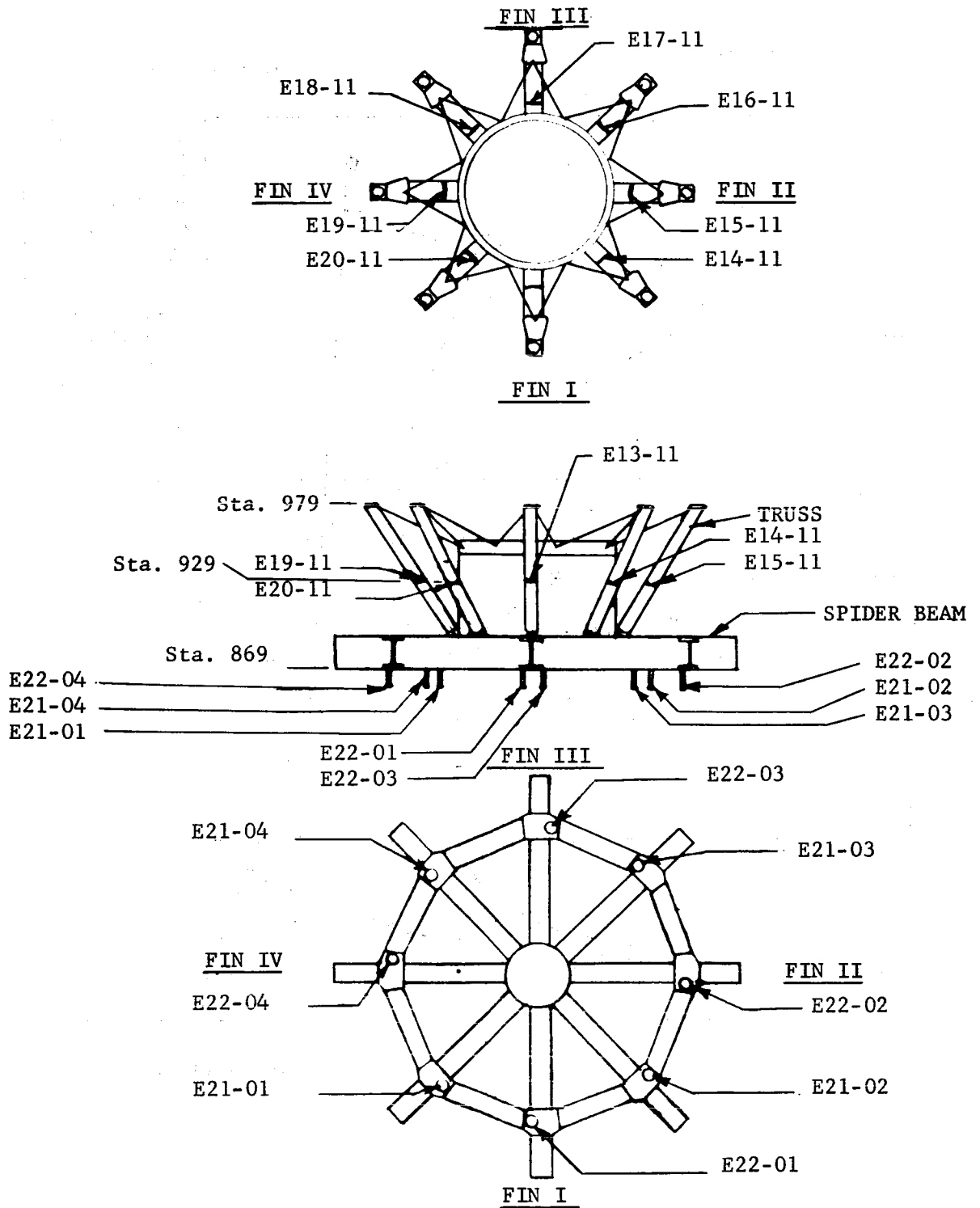


Figure 9-1 SA-2 STRAIN GAGE LOCATION

⊙ Accelerometer Reading - g's

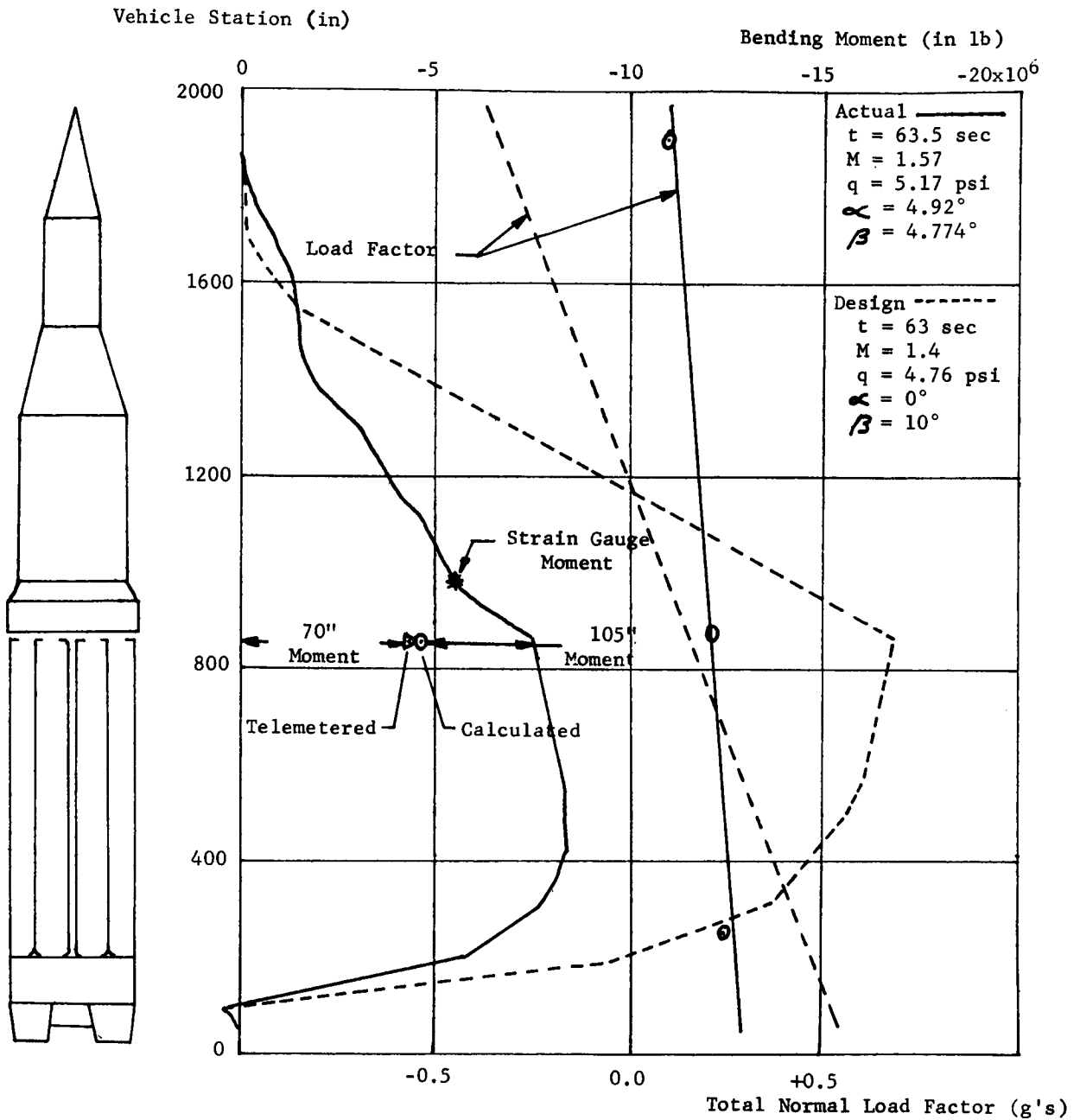


Figure 9-2 Bending Moment Comparison and Normal Load Factors (63.5 sec)

⊙ Accelerometer Reading -g's

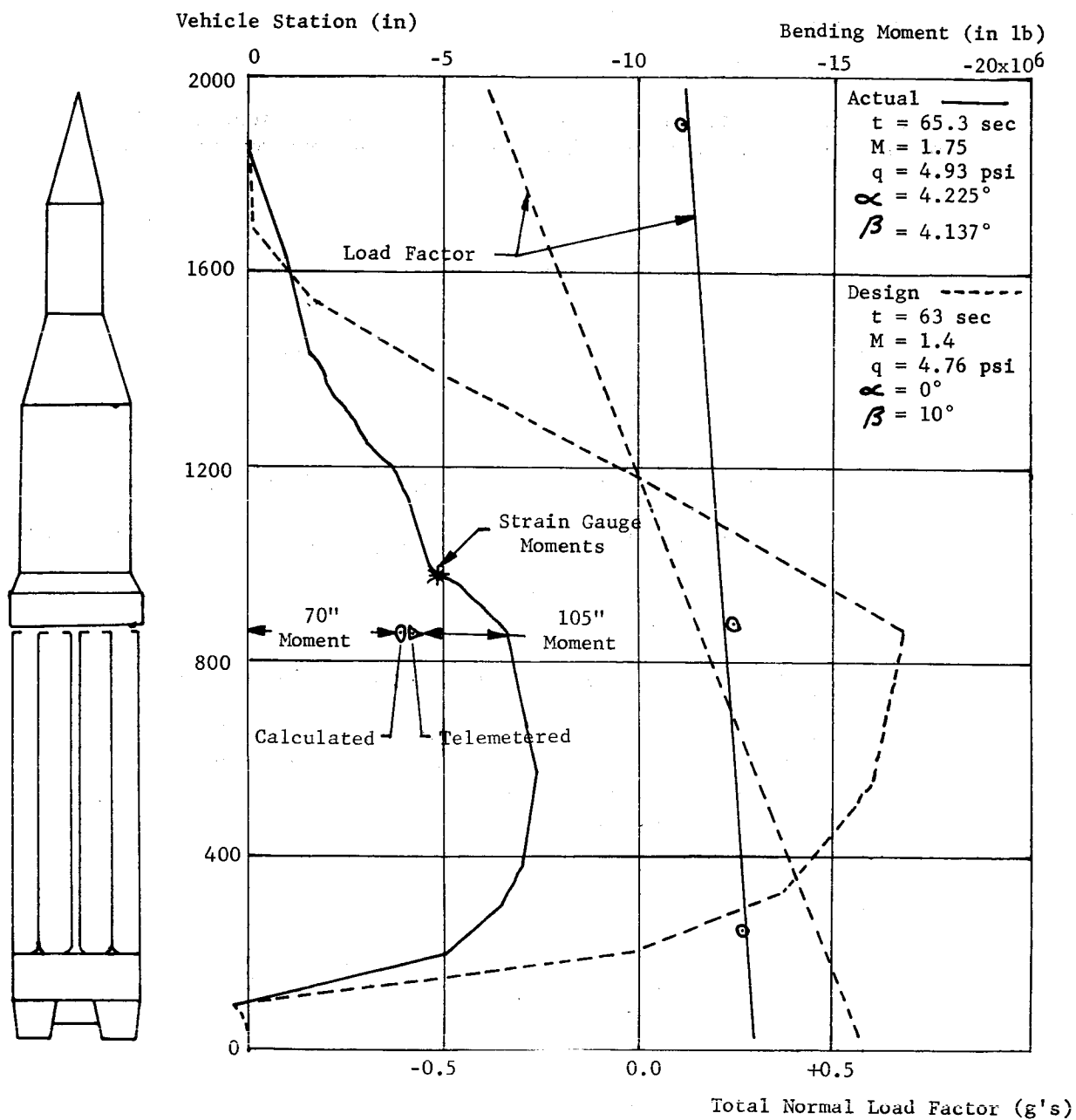


Figure 9-3 Bending Moment Comparison and Normal Load Factors (65.3 sec)

### Calculation of Longitudinal Load and Moments

#### 1. At Station 979

Although the strain measurements were taken at station 929, the following equations determine longitudinal load and moment values at station 979:

$$M_{yaw} = 5.055 \left[ \epsilon_{15} - \epsilon_{19} + 0.707 (\epsilon_{14} + \epsilon_{16} - \epsilon_{18} - \epsilon_{20}) \right]$$

$$M_{pitch} = 5.055 \left[ \epsilon_{13} - \epsilon_{17} + 0.707 (\epsilon_{14} + \epsilon_{20} - \epsilon_{16} - \epsilon_{18}) \right]$$

$$L = 0.06245 \sum \epsilon_n + P$$

where:

$M_{yaw}$  = Moment about an axis through Fins I and III, inch-kips

$M_{pitch}$  = Moment about an axis through Fins II and IV, inch-kips

$\epsilon_n$  = Differential strain measurements E 13-11 thru E 20-11, micro-inches per inch

$L$  = Total longitudinal load at station 979, kips

$P$  = Weight of structure above station 979 and water ballast, kips (This load was lost when the gauges were set to a zero reading; the value for this load is 221 kips).

#### 2. At Station 869

The following equations determine the amount of longitudinal load and moment which is introduced into the top of the 70 inch LOX tanks by the spider beam assembly:

$$M'_{yaw} = 2.592 \left[ \epsilon_{22-02} - \epsilon_{22-04} + 0.707 (\epsilon_{21-02} + \epsilon_{21-03} - \epsilon_{21-01} - \epsilon_{21-02}) \right]$$

$$M'_{pitch} = 2.592 \left[ \epsilon_{22-01} - \epsilon_{22-03} + 0.707 (\epsilon_{21-01} + \epsilon_{21-02} - \epsilon_{21-03} - \epsilon_{21-04}) \right]$$

$$L' = 0.026 \sum \epsilon'_n + P'$$

where:

- $M'_{yaw}$  = Moment in 70 inch LOX tanks about an axis through Fins I and III, inch-kips
- $M'_{pitch}$  = Moment in 70 inch LOX tanks about an axis through Fins II and IV, inch-kips
- $\epsilon'_n$  = Differential strain measurements E 21-01 thru E 21-04 and E-22-01 thru E 22-04, micro-inches per inch
- $L'$  = Total longitudinal load introduced into the top of the 70 inch tanks, kips
- $P'$  = Load introduced into 70 inch LOX tanks before ignition of engines, kips (This load was lost when the gauges were set to a zero reading; the calculated value for this load is 88 kips).

A program was written, using the RPC-4000 computer, to standardize the strain measurements and solve the equations above.

#### Strain Gage Measurement Adjustments

Four days before the SA-2 flight date, each strain gauge was set to a zero reading with a total of 221 kips ( $= 2.21 \times 10^5$  lb) of load existing above station 979; however, the telemetry data recorded the 30 seconds just prior to engine ignition indicated that the gauges might have drifted. An average of each truss strain gauge during this time interval indicated a total of 8 kips (instead of 0 kips) of compressive load from the dummy stages. The actual strains used in the equations were obtained as follows:

(a) The average of 100 strain readings recorded prior to ignition was computed for each strain gauge. This average constituted a "drift" value for each strain gauge.

(b) These "drift" values were subtracted from their respective strain measurements recorded at any time point during flight to obtain differential strain values for use in the calculation of bending moments and longitudinal load at stations 979 and 869. Hence, the zero readings were essentially reset (the 8 kip load was subtracted out), and any moment present prior to ignition was neglected. (Note: Low wind velocity just before liftoff generates extremely small bending moments at station 979.)

(c) Strain gauge number E 22-02 was not active during flight. It was assumed, for total longitudinal load calculation purposes, that its value was the same as gauge number E 22-04. This missing gauge was located at the Fin II position; therefore the assumption does not affect the calculation of the pitch moment reacted by the 70 inch LOX tanks.

#### Time Point Evaluated

Moments and longitudinal loads were calculated in 2/10-second intervals for the following time slices:

<u>Seconds from Range Zero</u>	<u>Significant Event</u>
-5.0 - 3.0	Ignition and Liftoff
35.0 - 40.0	Max Yaw Normal Acceleration
42.0 - 56.0	Mach 1
56.0 - 62.0	Max "Q"
62.0 - 71.0	Intermediate Time Slice
98.0 - 101.0	Stop Tilt Program
105.5 - 122.0	First and Second Cutoff

Additional time points were considered for the construction of the longitudinal load vs time curve.

#### Moment Loads

Maximum bending moment at station 979 occurred at 63.6 seconds range time. Figure 9-4 presents bending moments for a time slice around this maximum moment and includes the time point for Max "Q" (59.0 seconds). The moment values due to external imposed loads vary so much (zero moment just 1.25 second after the maximum moment) that it is impossible to detect any natural bending frequencies. One point of interest is that the amount of moment load introduced into the top of the 70 inch LOX tanks is very close to the value for the moment at station 979. This is in very close agreement with values calculated by the Saturn Internal Loads Analysis (see Figures 9-2 and 9-3).

Around the time point of maximum yaw normal acceleration (Figure 9-5), the strain gauges on the truss members indicated oscillations of about  $2\frac{1}{2}$  cycles per second about the yaw axis.

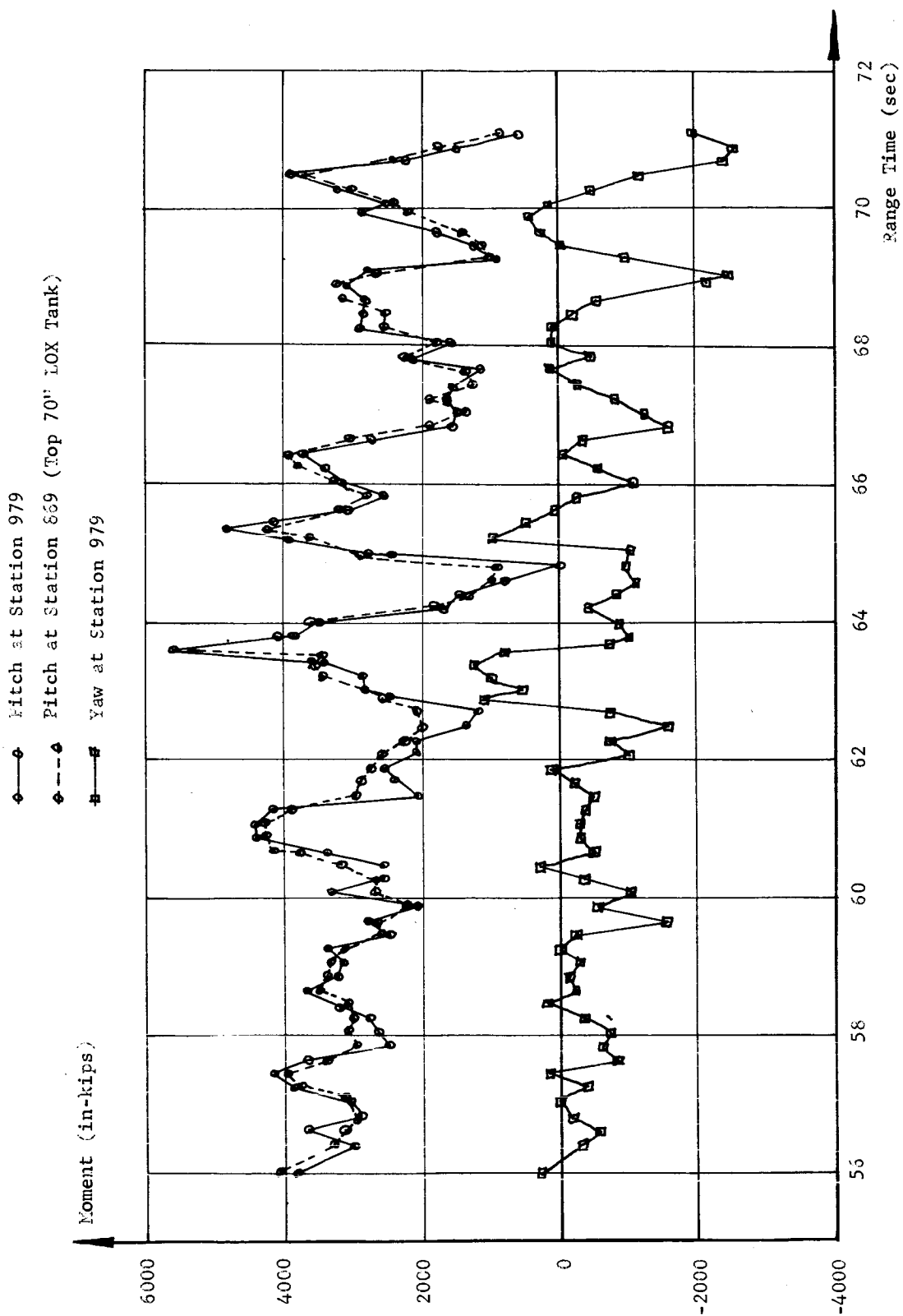


Figure 9-4 PITCH AND YAW BENDING MOMENTS AT STATION 979  
AND PITCH BENDING MOMENT AT STATION 869

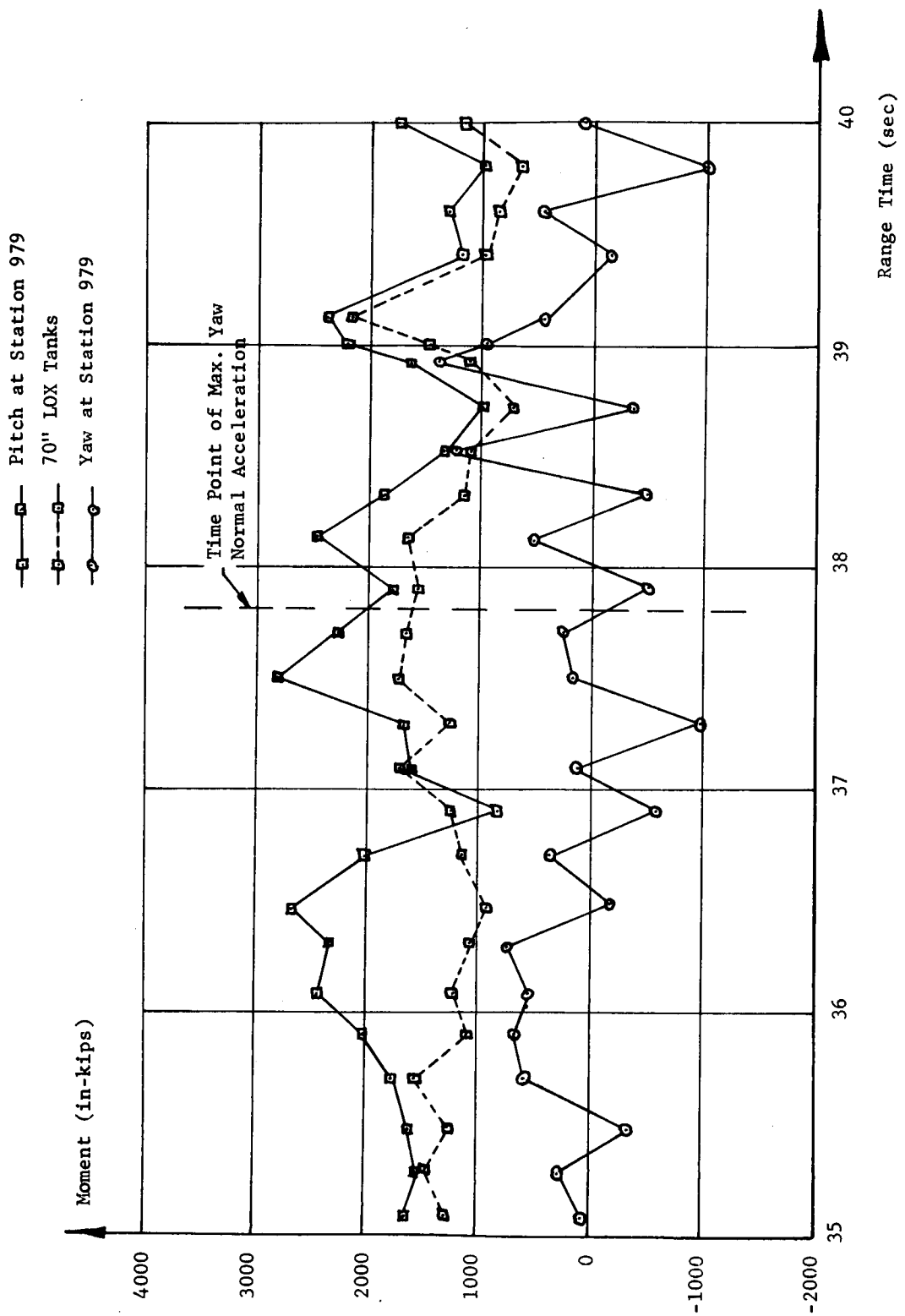


Figure 9-5 MOMENT LOADS AT STATION 979 AND MOMENT REACTED BY 70" LOX TANKS

### 9.3 LONGITUDINAL LOADS

Multiplication of the actual telemetered strain by the calibration factor results in the loads shown in Figure 9-6 (circled points). This curve indicates that the gauges possibly drifted prior to liftoff, since the gauges should have been reading zero at time points before ignition. The solid line on Figure 9-6 was obtained by using the differential strains and adding the 221 kips of load which was lost when the gauges were set to zero. The calculated load was determined from SA-2 thrust and acceleration data and theoretical drag data. Only the five points indicated on the graph were considered.

The amount of longitudinal load introduced to the top of the 70 inch LOX tanks is also presented in Figure 9-6 (dotted line). Two points of interest which should be brought out about this load are: (1) the load at the top of the 70 inch LOX tanks is reduced when the inboard engines are ignited; and (2) a total of 60 kips of load remains on the 70 inch tanks after cutoff. This load after cutoff is due to aerodynamic heating of the outer tanks and is in close agreement with expected values.

During firing of the engines, before launch command, dynamic forces arise in the deflecting masses of the system. These forces can be amplified and cause large vibrations of the vehicle. It was expected that a staggering time of 100 milliseconds between engine pairs would keep the vibrating force lower or equal to twenty percent of the maximum static thrust. Figure 9-7 shows the results of an investigation made to see if the actual staggering times of the engines still kept the vibrating force below the value above. The frequencies of the system were measured by strain gauges located on the holddown structure. From these frequency measurements and from single engine thrust curves the maximum vibrating force was obtained as shown by the maximum theoretical response (calculated) on Figure 9-7. These results show that the maximum response was twelve percent of the maximum static thrust.

### 9.4 BENDING OSCILLATIONS

Instrumentation to detect vehicle bending frequencies and deflections consisted of three pitch and three yaw accelerometers located at stations 250 (center LOX tank), 875 (spider beam), and 1900 (nose cone). In addition to these three positions on the vehicle proper, accelerometers were located on fuel tank #1 and LOX tank #1 at vehicle station 830 in both pitch and yaw directions (Figure 9-8). The measuring range of these ten low frequency accelerometers (0-25 cps) was  $\pm 0.5$  g's. These measurements were monitored continuously throughout the SA-2 flight.

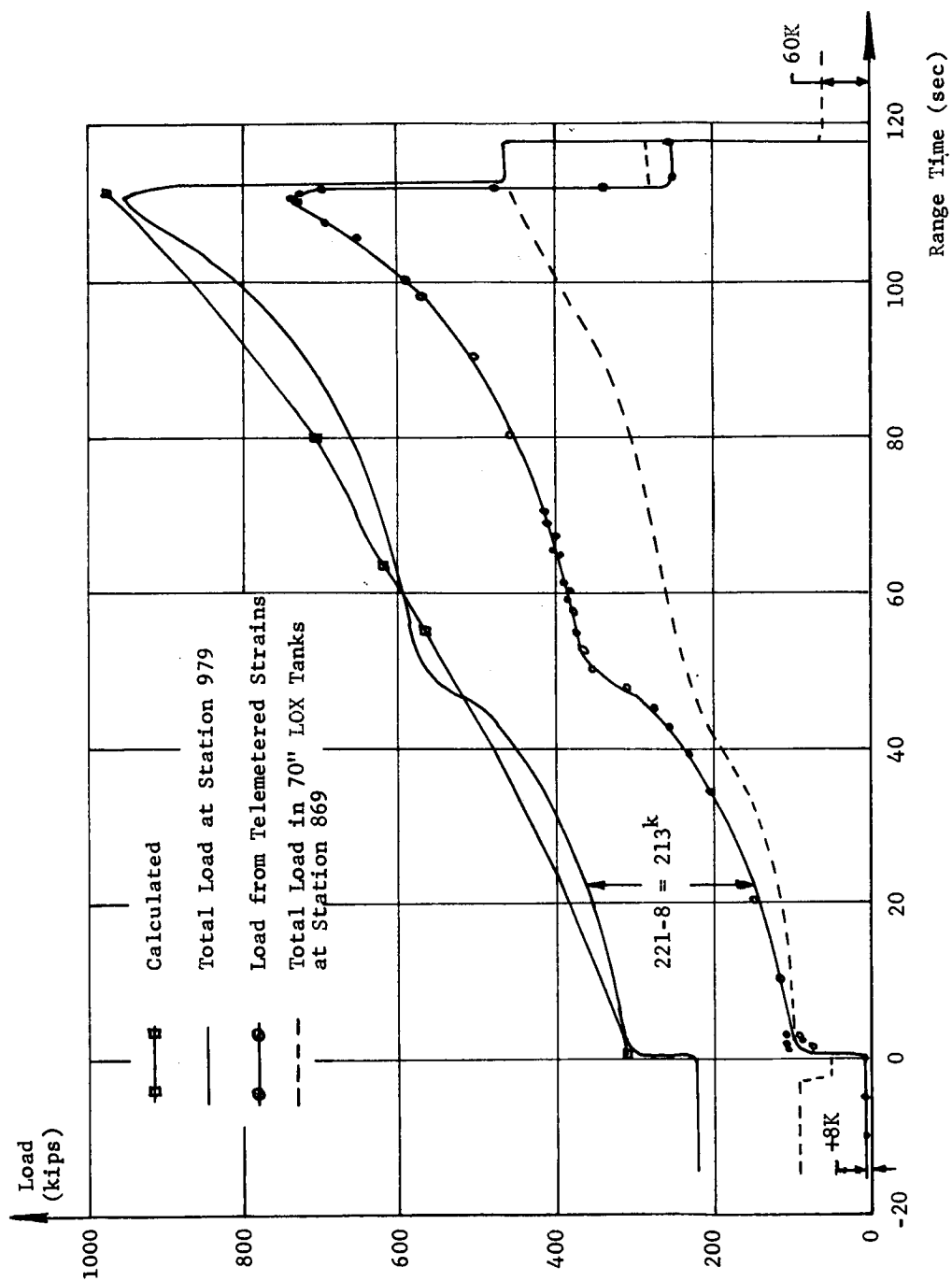


Figure 9-6 LONGITUDINAL LOAD AT STATION 979 AND 869

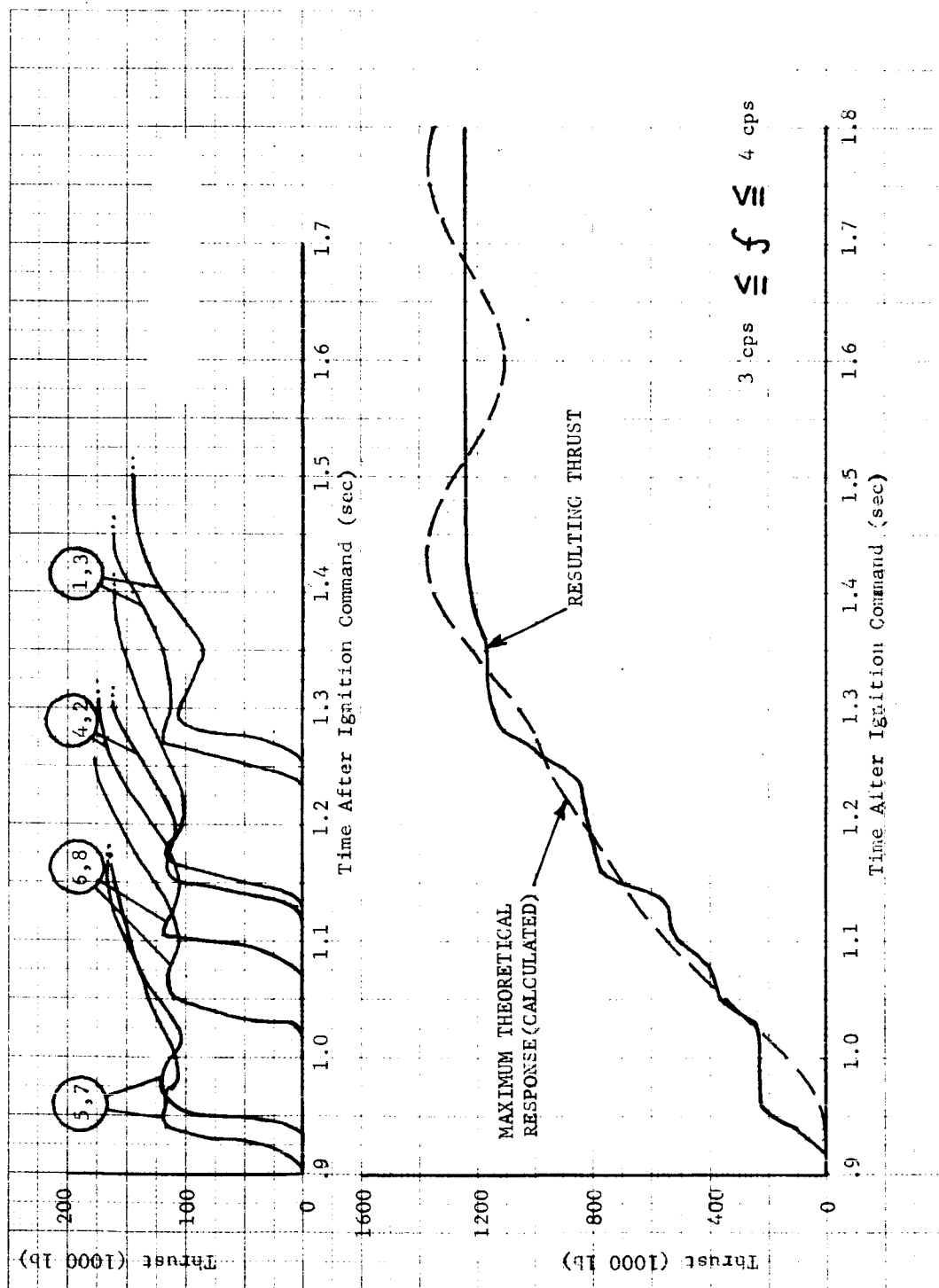


FIGURE 9-7 MAXIMUM DYNAMIC RESPONSE

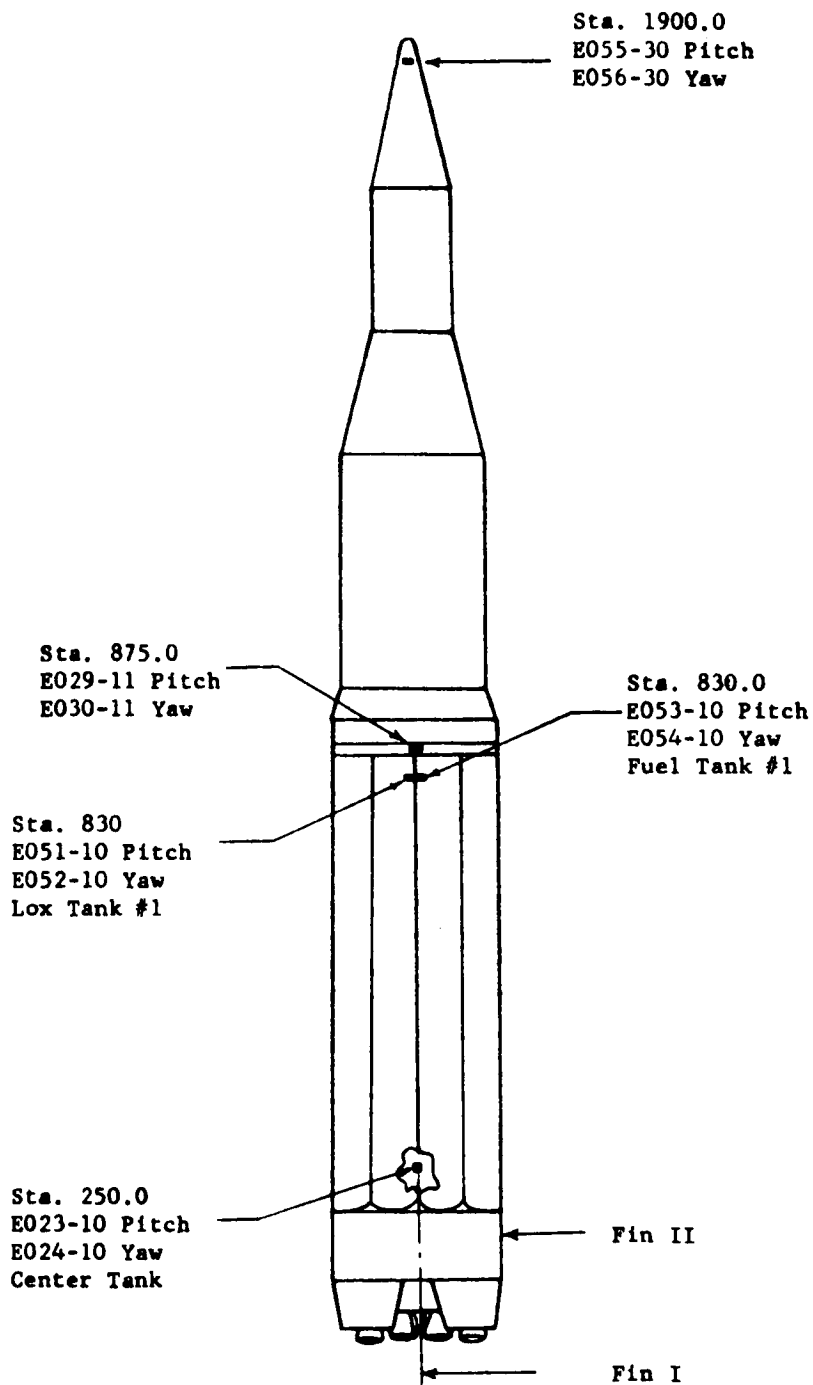


Figure 9-8 Bending Mode Accelerometer Locations

Two accelerometers were not operating properly during the flight. The outer LOX tank yaw measurement (measurement number E 52-10) showed no response at any time during the flight. The nose pitch accelerometer (measurement number E 55-30) had no response between 65 seconds and 117 seconds and looks questionable at other time points on the oscillograph trace. All other measurements appear to respond properly and have correct polarity as reported before flight.

The frequencies presented as flight results vary slightly in accuracy depending upon the length of the time slice. The accuracy also depends upon how many analyses were performed within the same time slice. All frequencies presented are considered to have an accuracy of  $\pm .12$  cps.

The oscillographs showed some higher frequency content of approximately 60-100 cps throughout the flight but with larger amplitudes at lift-off and cutoff. This is probably local structural vibration picked up at the upper limits of the accelerometers. Some frequencies in the control frequency range of .25 cps to .50 cps, and low amplitude responses caused by propellant slosh in the 1.25 cps to 1.50 cps range were also present at some time points.

The low bending frequencies responded with small accelerations throughout the oscillograph trace. In addition to these small "g" levels, an over-riding of high frequencies on the low frequencies made a visual analysis of the oscillograph records impractical. A correlation program originated for other studies has been adapted to determine frequency, phasing and amplitudes for measurements of this type. This program adaptation was performed after the SA-1 flight evaluation. With the exception of about two time points in flight, the detection of the correct frequency, phasing, and amplitudes for even the fundamental mode would have been impossible without the use of this correlation program. The following evaluation was accomplished with the correlation program on the IBM 7090 computer.

The SA-2 over-all vehicle frequencies, phase, and relative amplitudes are compared to both SA-D test results and theoretical calculations. The SA-D test results are contained in Reference I. Theoretical calculations are included in Reference II. These theoretical calculations considered the vehicle as a single beam with an effective booster EI of  $300 \cdot 10^{10}$  lb in<sup>2</sup>. Outer fuel and LOX tank frequencies are compared to calculations presented in Reference III. In these calculations the tanks were considered to be simply supported.

The trend of the vehicle first mode frequency versus flight time follows closely to that of the SA-D test results (Figures 9-9 and 9-10). This frequency range was approximately 2.2 cps at liftoff to 3.0 cps at cutoff.

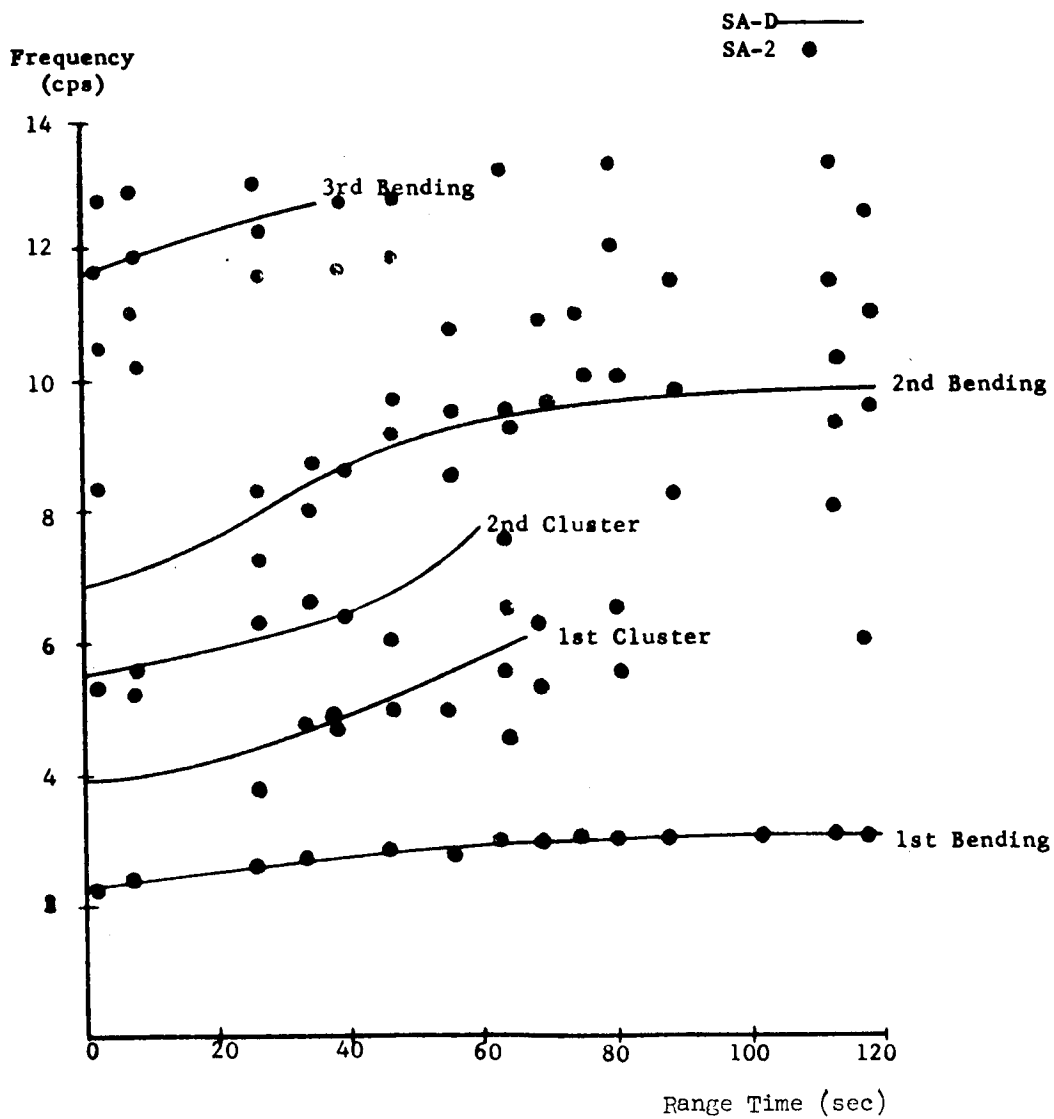


Figure 9-9 SA-2 System Frequency Trend

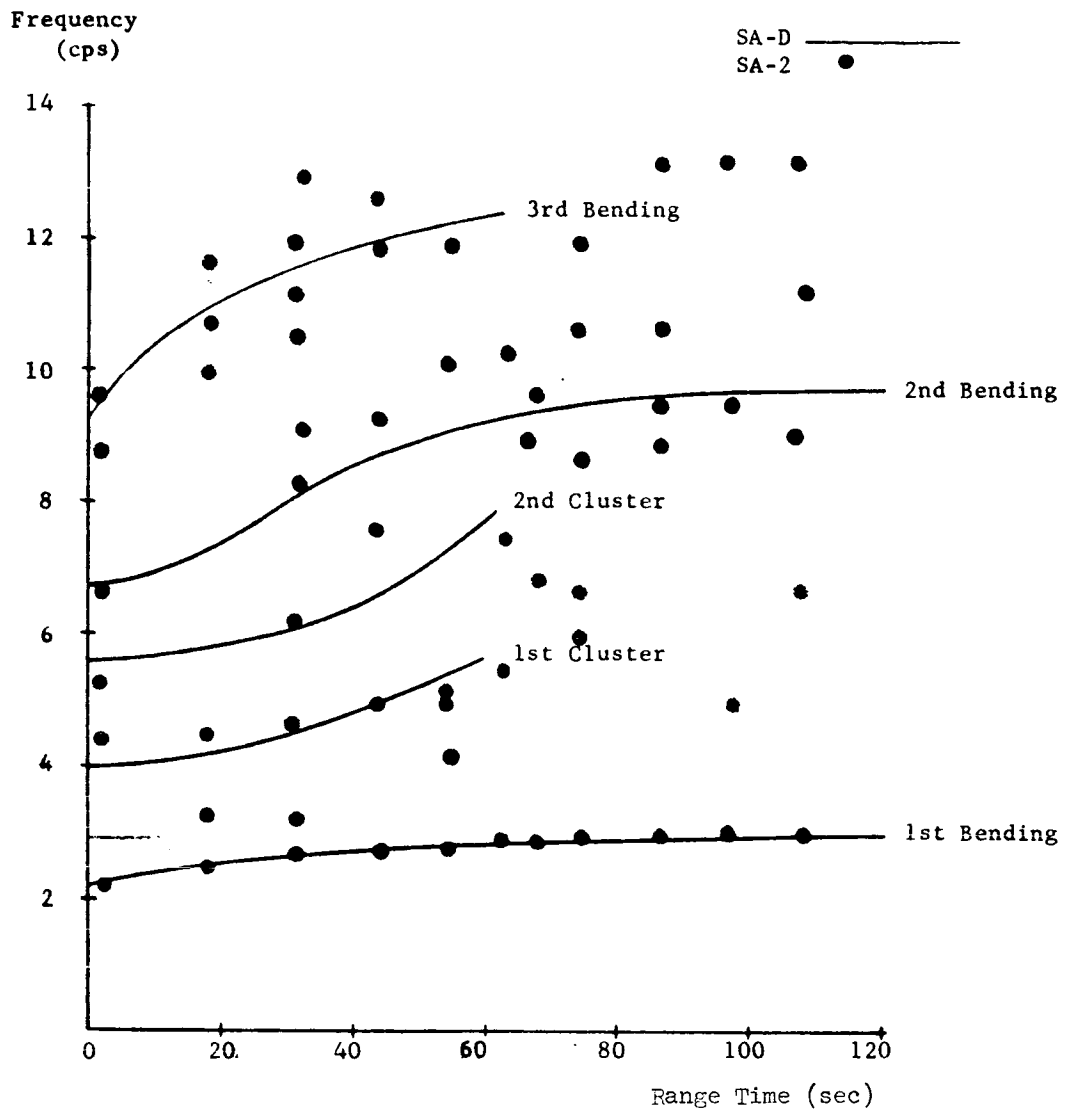


Figure 9-10 SA-2 System Frequency Trend

Several frequencies existed in the range of the first three vehicle bending modes but with the limited instrumentation and very low response; no accurate identification could be assigned to many of these vibrations (Figures 9-9 and 9-10). However, at two times in flight sufficient excitation existed to cause the vehicle to respond in a second mode. Even though each of the three accelerometers responded with low amplitude, a comparison of SA-2 flight frequency, phasing, and relative amplitude shows a close agreement with calculations and the measured second mode of the SA-D test vehicle (Figures 9-15 and 9-16).

The other frequencies shown in Figures 9-9 and 9-10 are predominant frequencies, but all can not be identified with known natural frequencies of the system. Some trends are present which follow SA-D results, and other trends are present which are probably coupled tank, vehicle torsion, and vehicle bending modes for which no comparison data is available.

The three accelerometers located to give vehicle acceleration in the yaw direction responded more strongly throughout flight than those in the pitch direction. Predominant responses occurred within five seconds (sometimes closer) to time points chosen for calculation and SA-D testing. Other time points with weaker responses were evaluated and found to have good first mode characteristics but are not shown, since no test or calculated modes are available for comparison. It is also felt that sufficient evidence is portrayed in the figures to show first mode bending. Since the pitch accelerometer located on the nose cone (Sta. 1900) was not operating from about 65 seconds to 117 seconds, only four time points showed enough response for comparison with SA-D tests and calculations for the pitch direction. With the limited instrumentations it is more difficult to identify higher modes, but it is felt that frequencies and mode shapes shown in Figures 9-15 and 9-16 are second bending frequencies. It should be noted that the low frequency responses in natural bending were very low in amplitude. At no time in flight did a natural bending frequency (0-10 cps) give an acceleration of more than .045 g's single amplitude, which was less than 9% of the measuring range of the accelerometers. This g level was attained at inboard engine cutoff. The next strongest response occurred at about 35 seconds at a magnitude of .043 g's single amplitude. Both of these g levels were taken from the yaw measurements on the nose cone, which showed higher accelerations than any other point on the vehicle. An envelope of maximum g levels is shown for first mode in Figure 9-17. When converting acceleration to deflection at these fundamental frequencies, a maximum amplitude was found to be .06 inches. This occurred at liftoff on the nose in the yaw direction. There were high frequencies (60-100 cps) present which gave much larger magnitudes at liftoff and cutoff, but this was probably local structure vibrations and was not associated with vehicle bending frequencies.

The outer tank frequencies are compared with the calculated results in Figures 9-18 and 9-19. Although over-all vehicle frequencies and local structural frequencies were present on the outer tanks, the frequencies shown were predominant in this range of the frequency spectrum. No mode shapes for the outer tanks were determined since only one accelerometer was installed in each direction.

To establish bending mode shapes, time slices were analyzed throughout the flight and the results showed predominant frequencies common to the accelerometers at stations 250, 875, and 1900. To substantiate these frequencies as being the vehicle natural bending frequencies, a comparison to SA-D test results showed the proper phasing and relative amplitudes close to the SA-D modes (Figures 9-11 thru 9-16). An investigation of the control accelerometer responses also showed the same frequency content, correct phasing, and close amplitude when compared to the bending accelerometer results.

## 9.5 TORSIONAL OSCILLATIONS

SA-2 was not adequately instrumented for determining torsional oscillations. The roll rate gyros measured rigid roll plus or minus the torsional oscillations. The dominant frequencies measured by the rate gyro were well below the fundamental torsional natural frequency and imply that any torsional compliance was negligible.

## 9.6 VIBRATION

### 9.6.1 INTRODUCTION

Three main sources of excitation are responsible for the vibration environment of the Saturn vehicle. These are mechanical, acoustical, and aerodynamic. The mechanical source begins with engine ignition and, after the transients at ignition, does not change significantly until cutoff. The acoustical source begins with the sound field generated by the engines at ignition. This source has a maximum at lift-off and becomes negligible after Mach 1. The aerodynamic source begins as the vehicle's velocity increases and is most influential during transition at Mach 1 and at maximum dynamic pressure.

Vibration data received from the SA-2 flight was obtained by two telemetry systems. The first system, identical to the system used on the SA-1 vehicle, was FM-FM with a maximum frequency response of 1050 cps. The second system, single side band, had a frequency response of 3000 cps; consequently, the composite data received from the two systems cannot be directly compared. This should definitely be considered when data with different frequency responses are being evaluated.

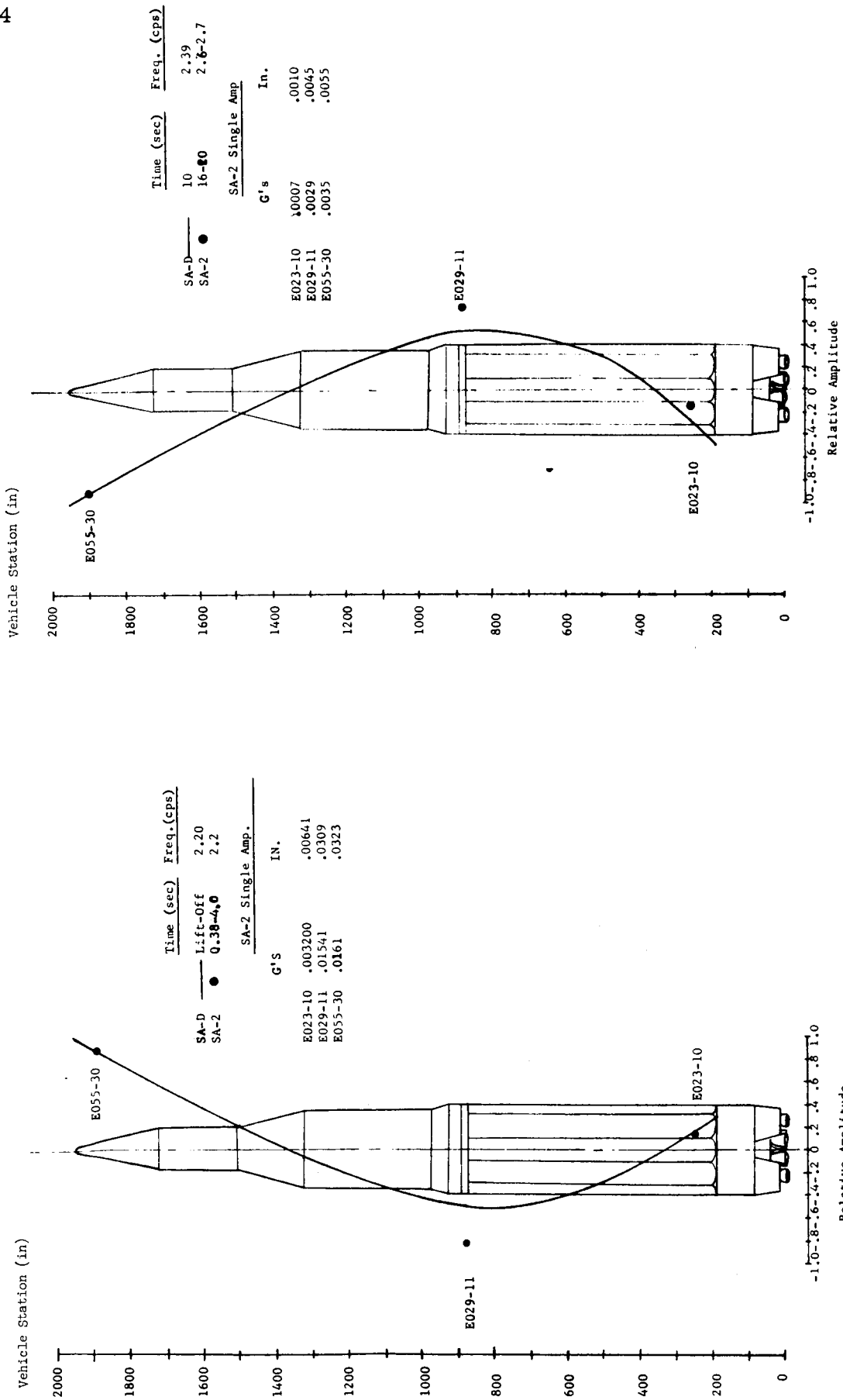


Figure 9-11 SA-2 Bending Mode - First Mode, Pitch

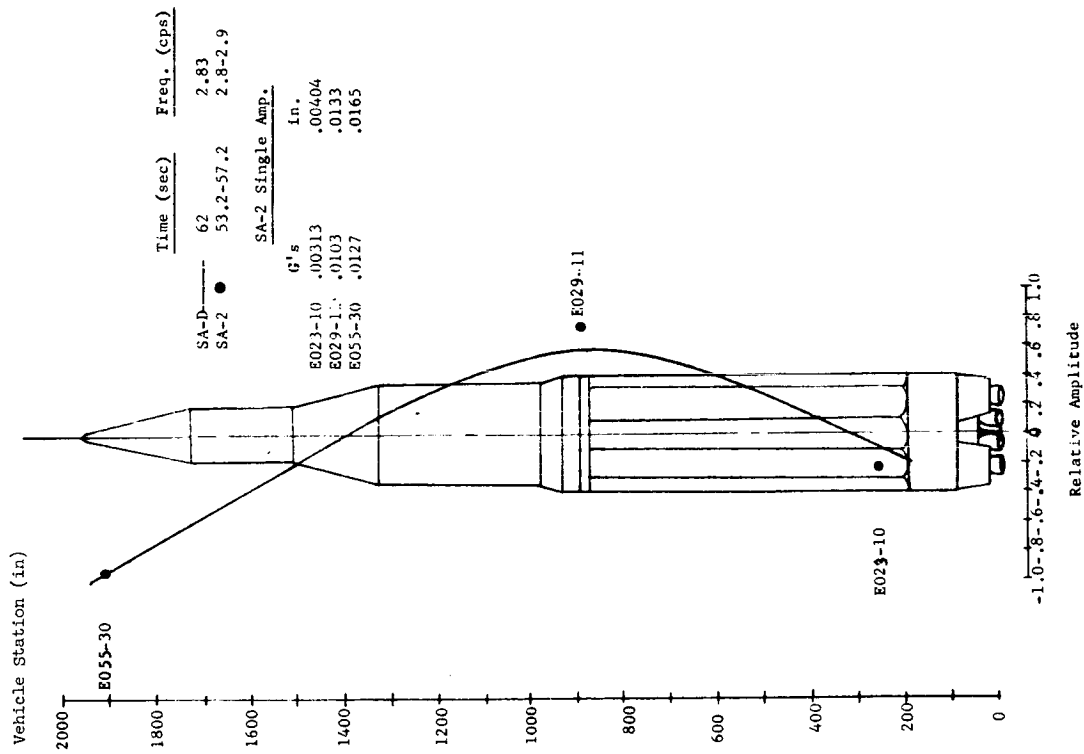
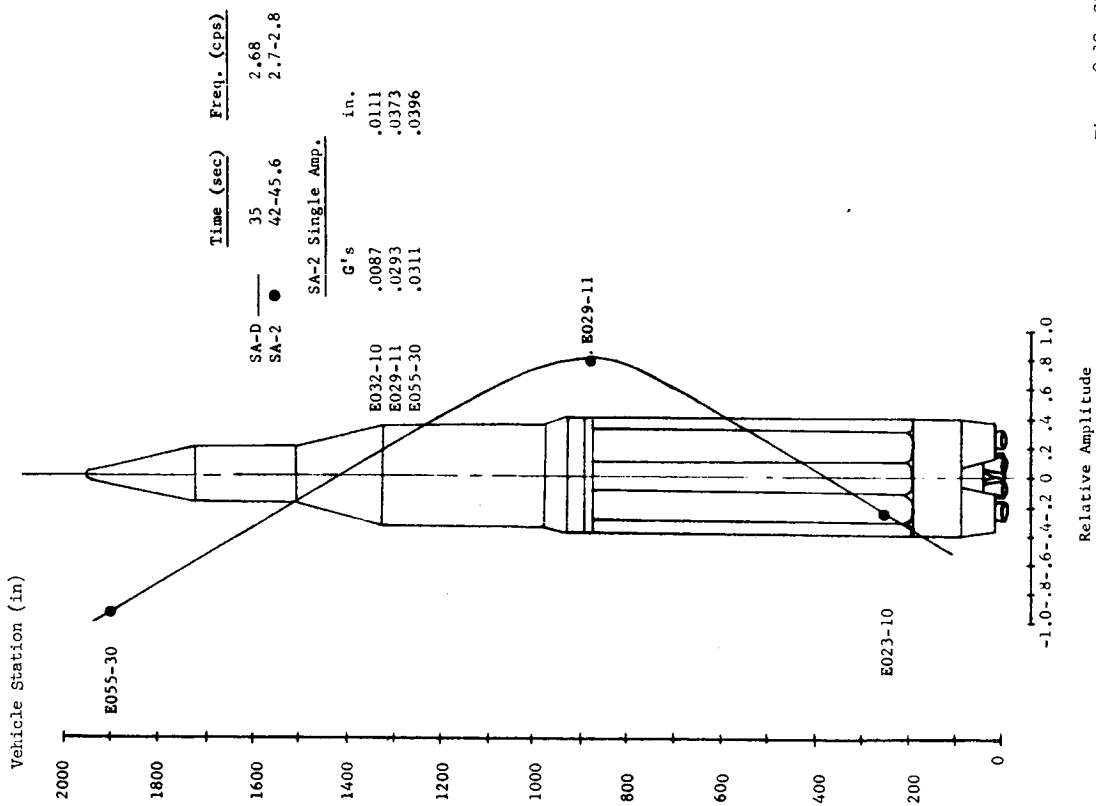


Figure 9-12 SA-2 Bending Mode - First Mode, Pitch

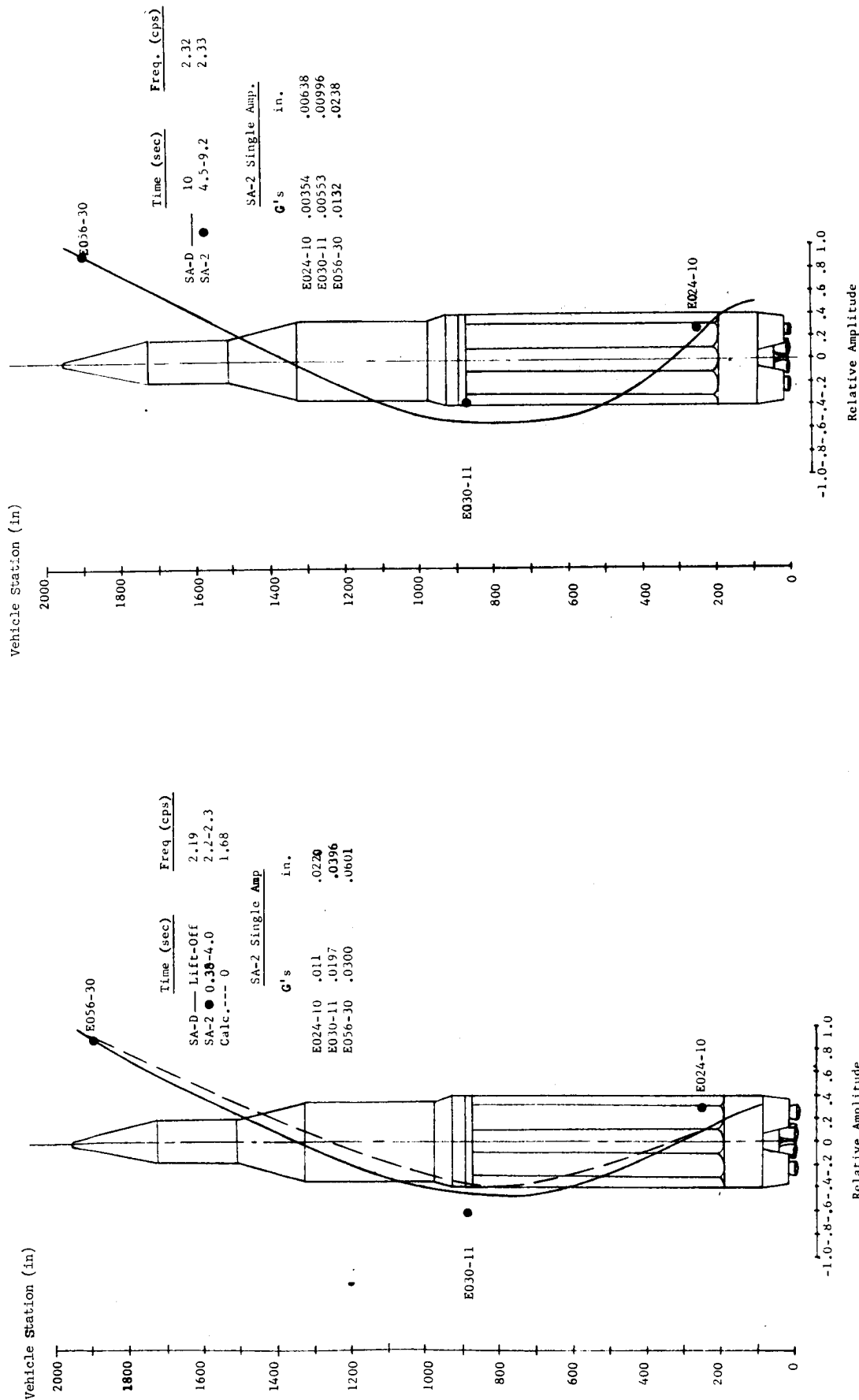


Figure 9-13 SA-2 Bending Mode - First Mode, Yaw

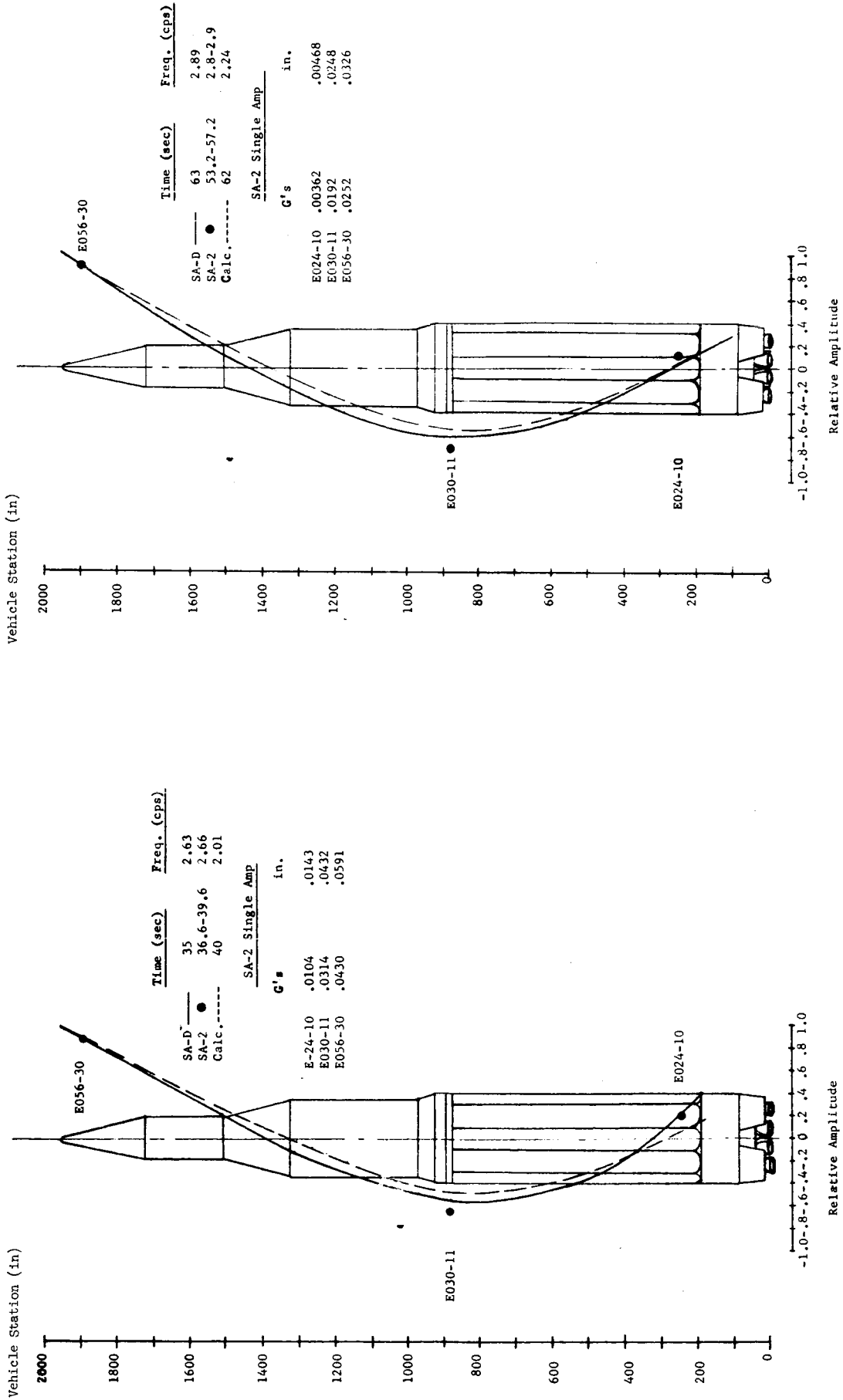


Figure 9-14 SA-2 Bending Mode - First Mode, Yaw

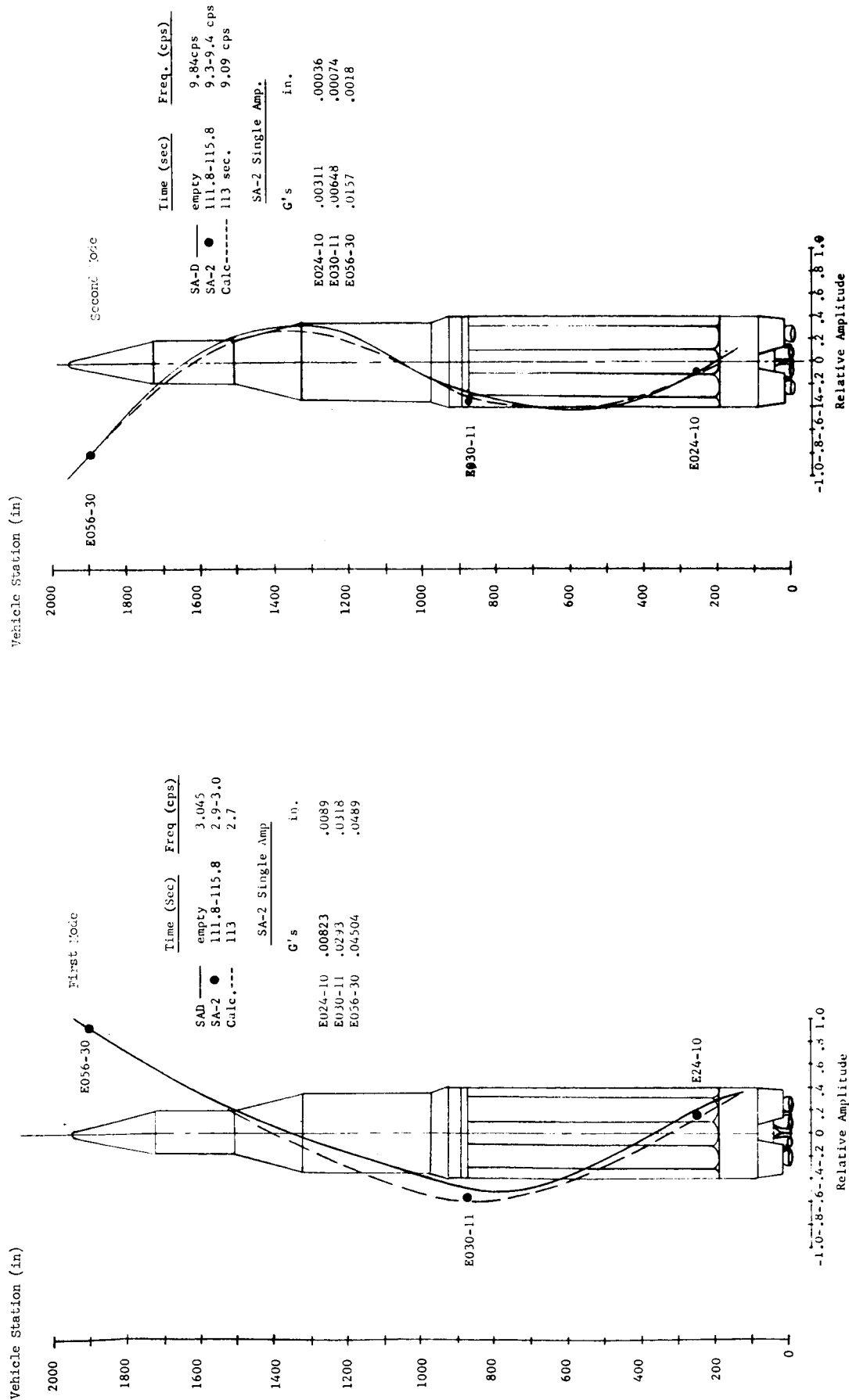


Figure 9-15 SA-2 Bending Mode - First and Second Mode, Yaw

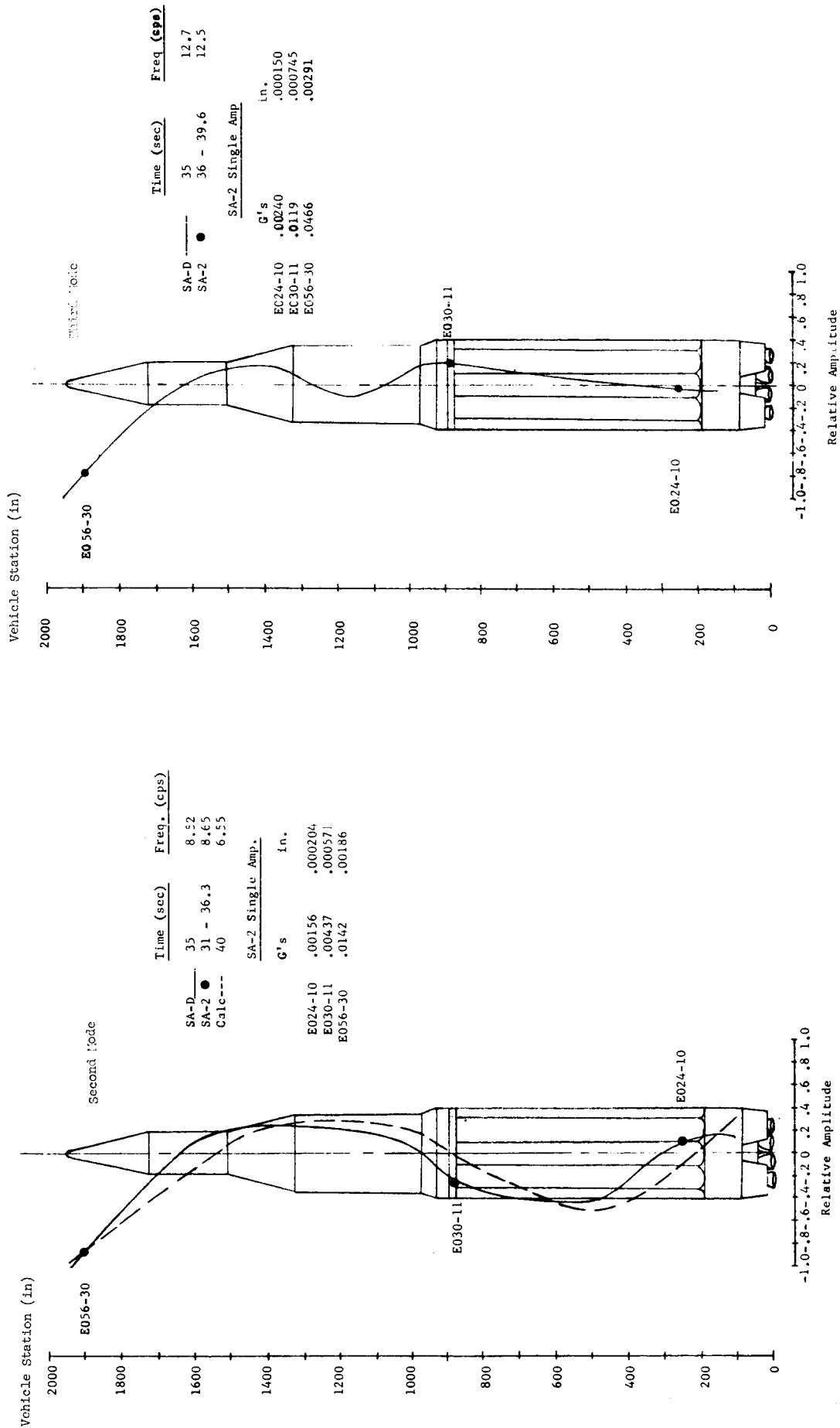


Figure 9-10 SA-2 Bending Mode - Second and Third Mode, Yaw

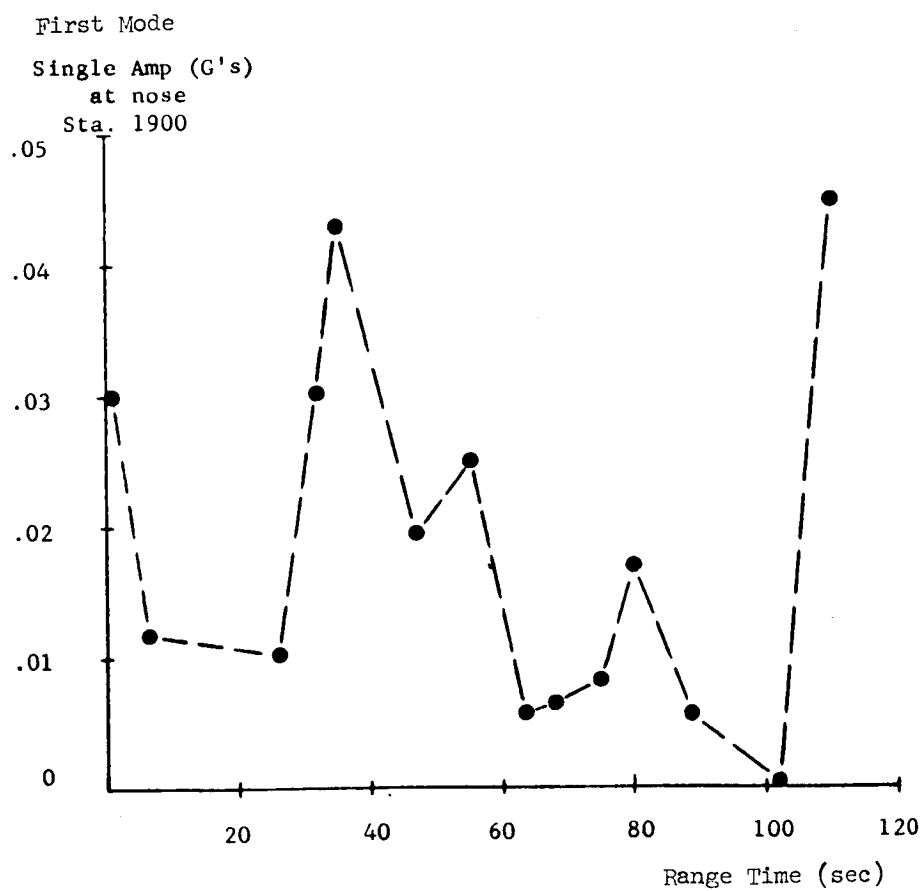


Figure 9-17 SA-2 Nose Acceleration Envelope

Note: Calculations based on tanks as being simply supported.

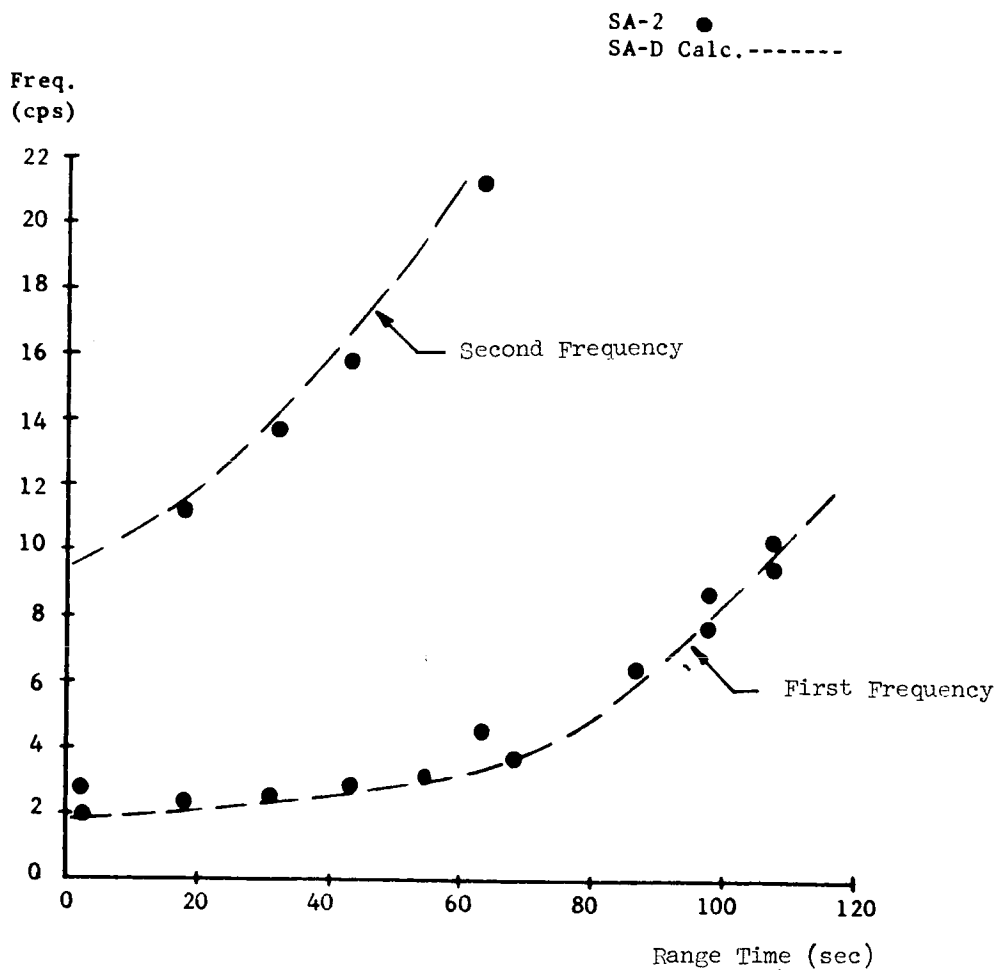


Figure 9-18 SA-2 Outer Tank Frequencies - Fuel Tank, Pitch

Note: Calculations based on tanks as being simply supported.

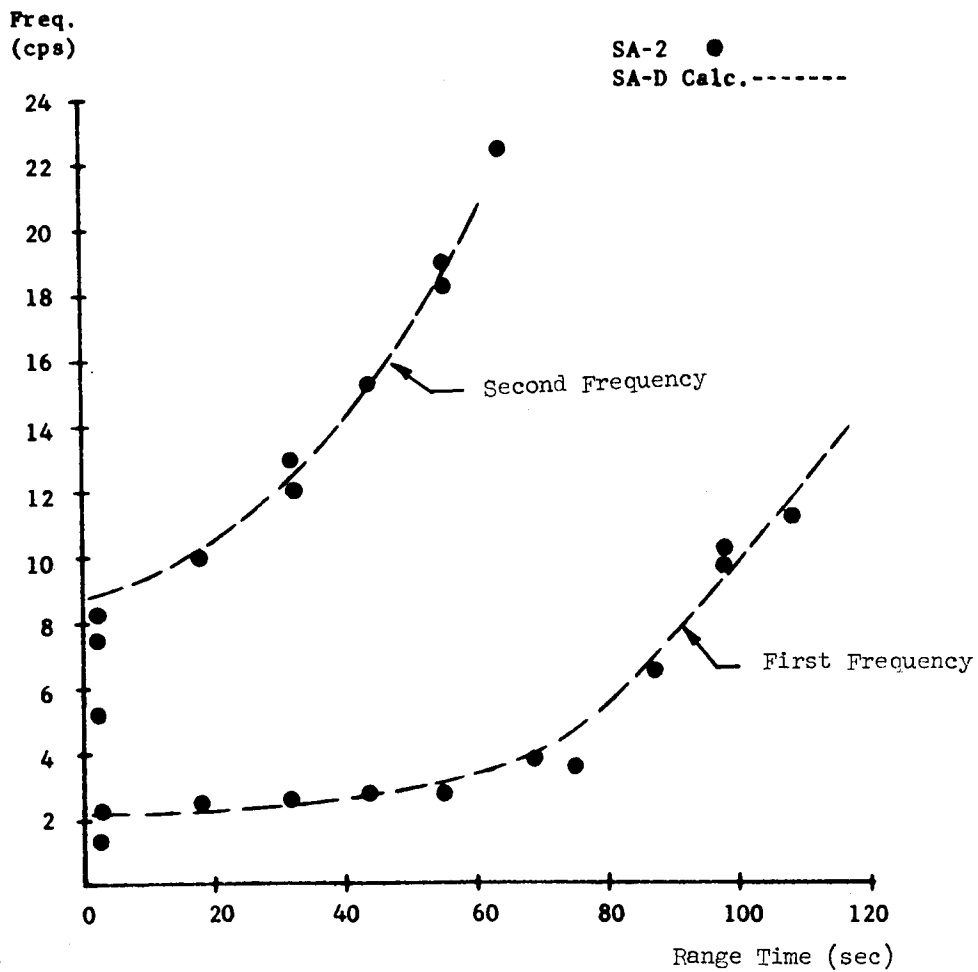


Figure 9-19 SA-2 Outer Tank Frequencies - LOX Tank, Pitch

A total of 58 vibration measurements was monitored during the SA-2 flight, excluding the bending mode measurements. The 58 measurements were located as follows:

Location	No. of Measurement
Upper Structure	5
Canister No. 15	2
Canister No. 14	1
Thrust Frame	3
Engines	16
Center Tank	2
Actuators	24
Gimbal Point Support	2
Fuel Suction Line	1
Prop. Unit Distributor	1
Radiation Shield	1

Table 9-I indicates the location, sensitive axis and linear frequency range of the vibration measurements.

Vibration measurements on the hydraulic actuators were recorded on a time shared basis. The twenty-four measurements occupied six telemetry channels, allowing four measurements on each channel. The four segment commutator had a rotational period of 12.4 seconds which allowed each measurement 3.1 seconds of transmission in each period of revolution. This method allowed only one measurement on each telemetry channel to be recorded during the times of ignition, liftoff, Mach 1, Max Q, and both inboard and outboard engine cutoffs.

Vibration summary curves are presented to indicate a time history of the vibration during flight.  $G_{RMS}$  values were plotted versus range time. An example is shown in Figure 9-20. The points were then connected by a faired curve which is to indicate the approximate RMS vibration level at any time during powered flight. The RMS acceleration level of all the vibration measurements obtained at the times noted is presented in Table 9-II. Since the actuator measurements were commutated, the RMS levels for these measurements could not all be obtained exactly at the times noted. However, the RMS levels for the actuator data were obtained as closely to the indicated times as the commutation period would permit. Summary graphs of 10 cps analyses are presented for the time periods indicated. The limit of linear frequency response for each measurement is indicated by an asterisk and a vertical line intersecting the summary curve. Complete time history composite vibration traces are included for all continuous measurements. These traces have been compressed such that the entire

MEAS. NO.	DESCRIPTION	DIRECTION OF SENSITIVITY	FREQUENCY RESPONSE (CPS)
E1-11	Vibration Upper Structure	Longitudinal	3000
E2-11	Vibration Upper Structure	Pitch	3000
E3-11	Vibration Upper Structure	Yaw	3000
E4-15	Vibration ST-90	Long.(Y axis)	3000
E5-15	Vibration ST-90	Lat.(Z axis)	3000
E6-9	Vibration Thrust Frame	Longitudinal	3000
E7-9	Vibration Thrust Frame	Pitch	3000
E8-9	Vibration Thrust Frame	Yaw	3000
E11-2	Vibration Thrust Chamber Dome	Lateral	3000
E11-4	Vibration Thrust Chamber Dome	Lateral	3000
E11-6	Vibration Thrust Chamber Dome	Lateral	3000
E11-8	Vibration Thrust Chamber Dome	Lateral	3000
E12-1	Vibration Turbo Gear Box	Lateral	3000
E12-2	Vibration Turbo Gear Box	Lateral	3000
E12-3	Vibration Turbo Gear Box	Lateral	3000
E12-4	Vibration Turbo Gear Box	Lateral	3000
E33-1	Vibration Thrust Chamber Dome	Longitudinal	3000
E33-3	Vibration Thrust Chamber Dome	Longitudinal	3000
E33-5	Vibration Thrust Chamber Dome	Longitudinal	3000
E33-7	Vibration Thrust Chamber Dome	Longitudinal	3000
E34-1	Vibration Pitch Actuator	Pitch	1050
E34-2	Vibration Pitch Actuator	Pitch	1050
E34-3	Vibration Pitch Actuator	Pitch	1050
E34-4	Vibration Pitch Actuator	Pitch	1050
E35-1	Vibration Pitch Actuator	Yaw	1050
E35-2	Vibration Pitch Actuator	Yaw	1050
E35-3	Vibration Pitch Actuator	Yaw	1050
E35-4	Vibration Pitch Actuator	Yaw	1050
E36-1	Vibration Yaw Actuator	Pitch	1050
E36-7	Vibration Yaw Actuator	Pitch	1050
E36-3	Vibration Yaw Actuator	Pitch	1050
E36-4	Vibration Yaw Actuator	Pitch	1050
E37-1	Vibration Yaw Actuator	Yaw	1050
E37-2	Vibration Yaw Actuator	Yaw	1050
E37-3	Vibration Yaw Actuator	Yaw	1050
E37-4	Vibration Yaw Actuator	Yaw	1050
E38-1	Vibration Pitch Actuator	Longitudinal	1050
E38-2	Vibration Pitch Actuator	Longitudinal	1050
E38-3	Vibration Pitch Actuator	Longitudinal	790
E38-4	Vibration Pitch Actuator	Longitudinal	790
E39-1	Vibration Yaw Actuator	Longitudinal	1050
E39-2	Vibration Yaw Actuator	Longitudinal	1050
E39-3	Vibration Yaw Actuator	Longitudinal	790
E39-4	Vibration Yaw Actuator	Longitudinal	790
E40-1	Vibration Gimbal Point Support	Longitudinal	3000
E40-7	Vibration Gimbal Point Support	Longitudinal	3000
E41-8	Vibration Turbine Starter Flange	Longitudinal	3000
E42-2	Vibration Fuel Cracking Valve	Longitudinal	3000
E43-4	Vibration Hydraulic Package	Longitudinal	3000
E44-8	Vibration Fuel Pump Inlet Flange	Longitudinal	3000
E45-8	Vibration Suction Line	Longitudinal	3000
E46-9	Vibration Prop. Unit Distr. 9A1	Longitudinal	3000
E47-1	Vibration Radiation Shield	Longitudinal	3000
E48-14	Vibration Instrument Panel	Lateral	330
L40-20	Sound Intensity		3000

TABLE 9-I SA-2 FLIGHT VIBRATION MEASUREMENTS

MEAS. NO.	DESCRIPTION	DIRECTION	GRMS						LEVELS	
			-3.61 sec.	.22 sec.	20 sec.	48.7 sec.	62 sec.	111.3 s		
E1-11	Vibration Upper Structure	Long't	2.1	2.0	1.9	1.7	1.5	1.3/0.6		
E2-11	Vibration Upper Structure	Pitch	1.6	1.9	1.0	1.1	0.9	0.9/0.3		
E3-11	Vibration Upper Structure	Yaw	2.8	2.7	2.3	2.3	2.2	2.1/1.0		
E4-15	Vibration ST-90	Long(Y Axis)	1.0	0.85	0.1	0.3	0.3	0.3/0.2		
E5-15	Vibration ST-90	Lat (Z Axis)	0.9	0.65	0.1	0.3	0.2	0.2/0.2		
E6-9	Vibration Thrust Frame	Long't	2.1	1.8	1.1	1.2	1.2	2.6/1.2		
E7-9	Vibration Thrust Frame	Pitch	2.5	2.2	1.0	1.2	1.1	2.1/1.2		
E8-9	Vibration Thrust Frame	Yaw	2.6	2.4	1.3	1.4	1.6	1.4/1.7		
E11-2	Vibration Thrust Chamber Dome	Lateral	7.8	4.5	5.5	5.2	4.9	3.9/7.5		
E11-4	Vibration Thrust Chamber Dome	Lateral	9.2	5.7	3.7	3.2	3.2	3.5/3.5		
E11-6	Vibration Thrust Chamber Dome	Lateral	9.5	5.2	4.5	4.6	4.5	5.3/1.0		
E11-8	Vibration Thrust Chamber Dome	Lateral	6.8	4.5	4.0	3.8	3.7	4.2/1.0		
E12-1	Vibration Turbo Gear Box	Lateral		14.4	13.75	14.5	15.5	17.9		
E12-2	Vibration Turbo Gear Box	Lateral	20.3	17.7	18.2	17.6	17.4	19.2/17.9		
E12-3	Vibration Turbo Gear Box	Lateral	13.25	13.9	14	13	13.8	15.5/16.1		
E12-4	Vibration Turbo Gear Box	Lateral	21.2	18	21.6	22.2	22.8	19.9/18.7		
E33-1	Vibration Thrust Chamber Dome	Long't	8.3	4.2	4.9	5.7	5.8	5.1/8.7		
E33-3	Vibration Thrust Chamber Dome	Long't	9.7		6.7	4.7	4.5	5.1/5.5		
E33-5	Vibration Thrust Chamber Dome	Long't	11.2	4.2	4.4	4.8	5.1	4.5/5.3		
E33-7	Vibration Thrust Chamber Dome	Long't	11.7	4.6	4.6	4.5	4.5	4.4/1.4		

TABLE 9-II SA-2 FLIGHT VIBRATIONS

MEAS. NO.	DESCRIPTION	DIRECTION	G RMS LEVELS				
			-3.61 sec.	.22 sec.	20 sec.	48.7 sec	62 sec
E34-1	Vibration Pitch Actuator	Pitch		13.0	9.0	12.2	11.3
E34-2	Vibration Pitch Actuator	Pitch		12.4	11.3	12.4	13.6
E34-3	Vibration Pitch Actuator	Pitch		13.6	9.6	9.0	13.6
E34-4	Vibration Pitch Actuator	Pitch		8.8	7.1	7.9	11.6
E35-1	Vibration Pitch Actuator	Yaw			6.2	13.6	12.4
E35-2	Vibration Pitch Actuator	Yaw			8.8	10.2	11.9
E35-3	Vibration Pitch Actuator	Yaw			5.4	10.7	7.9
E35-4	Vibration Pitch Actuator	Yaw			7.1	12.7	5.7
E36-1	Vibration Yaw Actuator	Pitch			5.1	6.2	10.7
E36-2	Vibration Yaw Actuator	Pitch			10.7	10.7	11.3
E36-3	Vibration Yaw Actuator	Pitch			4.8	5.7	5.9
E36-4	Vibration Yaw Actuator	Pitch			5.7	10.2	
E37-1	Vibration Yaw Actuator	Yaw	4.5		6.8	6.8	7.1
E37-2	Vibration Yaw Actuator	Yaw	13.6		10.2	11.3	10.2
E37-3	Vibration Yaw Actuator	Yaw	5.1		6.5	6.5	6.5
E37-4	Vibration Yaw Actuator	Yaw	11.3		7.9	8.5	6.5
E38-1	Vibration Pitch Actuator	Long't		12.4		12.4	11.3
E38-2	Vibration Pitch Actuator	Long't			5.9		
E38-3	Vibration Pitch Actuator	Long't		13.0	11.0	10.2	10.7
E38-4	Vibration Pitch Actuator	Long't			7.4	12.2	12.7
E39-1	Vibration Yaw Actuator	Long't			4.8	5.4	6.5
E39-2	Vibration Yaw Actuator	Long't	9.3		6.2	6.5	6.5
E39-3	Vibration Yaw Actuator	Long't			9.6	10.5	11.0
E39-4	Vibration Yaw Actuator	Long't	14.4			9.5	9.5

TABLE 9-II SA-2 FLIGHT VIBRATIONS

[illegible]

TABLE 9-II SA-2 FLIGHT VIBRATIONS

flight history for each measurement can be observed in one display. This type of presentation is especially useful in noting any changes in vibration level during times of liftoff, Mach 1, max Q, or inboard and outboard engine cutoffs.

The term "vibration mainstage" used with reference to SA-2 flight refers to the sustained vibration level occurring after the vehicle has left the acoustically reflective influence of the earth's surface and before the transonic conditions are reached. This term should not be confused with the mainstage term as used in propulsion. When referring to vibration data received from static firings, "vibration mainstage" is the sustained vibration level occurring after ignition and existing until cutoff.

#### 9.6.2 STRUCTURAL VIBRATIONS

Measurements E6-9, E7-9, and E8-9, (Figures 9-21 through 9-23 and 9-42 through 9-46) sensitive to vibrations in the long't, pitch and yaw directions respectively, were located on the upper thrust frame adjacent to the Fin I side of the center barrel. The vibration levels of this group of measurements remained fairly constant throughout the flight. A smooth build-up occurred at ignition with a transient response noted only on measurement E6-9. The liftoff levels remained constant until 4 seconds, then decreased and remained at a constant level throughout the flight with the exceptions of small transients at 4.75 seconds and cutoff. The predominant frequencies were 400, 800, 1225 and 1600 cps. At liftoff, in addition to the frequencies above a predominant frequency occurred at 275 cps.

##### Gimbal Point Support (Figures 9-22 and 9-44)

Measurements E40-1 (engine no. 4 gimbal support point) and E40-7 (engine no. 7 support point) both sensitive in the longitudinal direction exhibited the same trends. Therefore, the following analysis applies to both measurements unless stated otherwise.

There was no shock transient at ignition; however, the composite vibration during the first .4 seconds after ignition was 1.4 times higher than the mainstage level. The vibration level subsequent to this period appeared uniform throughout with no apparent increase during the Mach 1 and Max Q periods. Narrow bandwidth analyses of E40-1 indicated predominant frequencies of 375 cps and 775 cps.

Measurement E40-7 exhibited predominant frequencies of 775 cps and 1575 cps. These major frequencies were present throughout the time history as may be observed in Figure 9-22. Inboard engine cutoff

resulted in a slight shock transient on E40-7 which quickly decayed. The vibration following cutoff was negligible indicating that the operation of the outboard engines had no influence on the vibration characteristics of the inboard engine support point. Outboard engine cutoff resulted in a shock transient in E40-1 which quickly damped out.

#### Heat Shield (Figures 9-22 and 9-45)

Measurement E47-1 was located on the heat shield; the accelerometer was positioned off Fin II outboard of engine 6 and measured vibration in the longitudinal direction. During holddown and liftoff, the composite record was clipped in the positive direction for a duration of about 9.5 seconds. The level slowly decreased until about 35 seconds at which time it gradually increased until it reached a maximum at about 54.5 seconds. This level was maintained during Max Q from which it decreased to a constant value by about 64 seconds. The constant level was maintained up to IECO after which it dropped rapidly. This decreased level was maintained up to OECO after which it decayed at a steady rate.

During holddown and liftoff most of the energy was in the frequency range from 400 cps to 1600 cps. At mainstage the energy was fairly well distributed throughout the frequency range of 63 cps to 1600 cps. From 48 to 64 seconds the energy between 400 and 3000 cps remained unchanged while the low frequencies increased slightly above mainstage values. After IECO most of the energy was between 315 and 630 cps.

#### Upper Structure (Figures 9-23 and 9-46)

Measurements E1-11, E2-11, and E3-11 were located on the spider beam and measured vibrations in the longitudinal, pitch, and yaw directions respectively. All these measurements had very uniform composite levels with most of the energy being concentrated in the frequency range of 300 cps to 2000 cps. In measurements E1-11 and E3-11, the composite trace was clipped during powered flight. E2-11 showed a slight increase at Mach 1. All measurements decreased after inboard engine cutoff and no effect was noted at outboard cutoff.

### 9.6.3 PROPULSION SYSTEM VIBRATION

#### Gear Box (Figures 9-24, 9-27 and 9-43)

Measurements E12-1, -2, -3, and -4 were mounted on the turbo gear box of engines 1, 2, 3, and 4 respectively and sensed acceleration in the lateral direction. In view of the problems encountered with the gear boxes during the static test of SA-3, these measurements were analysed very carefully. All the records indicated a transient at ignition followed by a smooth transition into mainstage within 2 seconds.

The mainstage levels were very uniform throughout powered flight with the exception of El2-2. Measurements El2-3 and 4 appear to be clipped in the positive direction.

The mainstage level of El2-2 was uniform up to approximately 45 seconds. From 45 seconds upwards in time a 5 cps fundamental developed slowly, becoming predominant by 85 seconds. The low frequency signal persisted until inboard cutoff, at which time it immediately terminated. The level between inboard and outboard cutoff was uniform and similar to the level before 45 seconds.

Since the lower cutoff frequency of the single sideband telemetry system used to transmit these measurements was approximately 30 cps, the validity of the 5 cps signal of El2-2 was questioned. A cursory test of the telemetry system was made which indicated that an output of approximately 4-6 cps can be obtained when an input signal outside the passband (30 to 3000 cps) is applied to the telemetry channel. Therefore the 5 cps signal is considered to be due to the telemetry system. A more detailed investigation of this phenomenon is being undertaken.

None of the measurements showed a change in level due to Mach 1, Max Q, or inboard engine cutoff (with the exception that the 5 cps signal on El2-2 terminated at first cutoff as noted above). All the records indicated a transient at outboard engine cutoff. On several measurements this transient was followed by a decay and then a second transient of lower amplitude.

Narrow bandwidth summary graphs, given in Figures 9-24 and 9-27, show almost identical spectra with the exception of El2-4 which, for no known reason, had significantly higher levels at most discrete frequencies. The summary graphs were kept to the same scale for comparison purposes, with the consequence that the curves for El2-4 went off scale. Their maximum GRMS amplitudes were as follows:

Freq. \ Time	-2 to 3	20 to 25	45 to 50	60 to 65
1200 cps	3.9	5.3	5.2	5.4
2000 cps	9.6	12.0	11.6	14.0

Table 9-III gives all discrete frequencies which occurred in the 16 narrow bandwidth analyses, the number of analyses in which they occurred, the number of times when this occurrence exceeded a value of 2.0 GRMS, and a possible source which would have the same frequency and be capable of producing that magnitude of vibration. These frequencies were normalized to a constant pump speed of 6000 RPM since the actual

TABLE 9-III COMPILATION OF DISCRETE FREQUENCIES NOTED  
IN TURBO PUMP MEASUREMENTS NORMALIZED TO  
A PUMP SPEED OF 6000 RPM

Freq.	Frequency of Occurrence	Frequency of Occurrence Above 2.0 GRMS	Possible Source
225	1	0	Rotational Freq. of Intermediate Shaft
400	16	0	(1) Vehicle Main Power Supply (2) Fuel and LOX Pump Lead-In Blade Passing Freq.
480	15	0	Rotational Freq. of Turbine Shaft
800	16	11	(1) Harmonic of 400 cps (2) LOX Pump Impeller Blade Passing Freq.
875	15	0	No Source Known
1000	15	4	Fuel Pump Impeller Blade Passing Freq.
1075	12	0	No Source Known
1200	16	4	Harmonic of 400 cps
1300	13	0	No Source Known
1400	12	0	No Source Known
1500	16	2	No Source Known
1600	16	4	Harmonic of 400 and 800 cps
1700	8	0	No Source Known
1800	6	0	No Source Known
1850	1	0	No Source Known
1900	5	0	No Source Known
2000	15	7	Harmonic of 400 and 1000 cps
2150	9	1	No Source Known
2180	7	0	No Source Known
2290	10	0	No Source Known
2400	15	15	Harmonic of 400 and 800 cps
2490	12	2	No Source Known

pump speed varies considerably. These discrete frequencies are forced frequencies rather than structural resonant frequencies because they vary with the pump speed. The amplitudes of these frequencies, however, could be either magnified or attenuated by the structure of the gear case. Due to the small scale on the summary graphs, good accuracy was not possible and some frequencies given in Table 9-III do not show on the summary graphs because of their small amplitudes.

#### Combustion Chamber Dome - Lateral (Figures 9-25, 9-27, and 9-44)

All the composite data received from the lateral measurements (E11-2, -4, -6, and -8) on the Combustion Chamber Dome appeared very uniform. All data showed a pronounced high amplitude vibration at ignition. Every measurement showed a rapid decrease of vibration into the steady state mainstage condition. Measurement E11-2 indicated a gradual increase in composite vibration until approximately 50 seconds after range zero, then gradually diminished until engine burnout. Measurement E11-4 showed a gradual decrease in mainstage composite vibration throughout flight.

There were no noticeable effects on any measurement at liftoff Mach 1, or Max Q. The measurement on the outboard engines showed no change in vibration during the time of inboard engine cutoff.

#### Combustion Chamber Dome - Longitudinal (Figures 9-26, 9-27, and 9-45)

As a group the vibration levels of all measurements (E33-1, -3, -5, and -7) with the exception of E33-3 remained relatively constant throughout the flight. A slight build-up occurred at ignition which diminished within 1.5 seconds. The mainstage level remained constant with no noticeable change in the vibration level at Mach 1 or Max Q.

At inboard engine cutoff a vibration build-up was experienced but rapidly decreased to the noise level. Inboard engine cutoff was noted as a transient response on the outboard engine. The outboard engines also experienced this build-up and decay phenomenon at cutoff. Transient responses, indicative of shock inputs, occurred intermittently throughout the flight.

Vibration measurement E33-3 showed deviations from a pattern which would normally be expected for the flight envelope. On the composite trace a vibration transient response appeared at ignition then rapidly diminished to a low level. The narrow band analysis did not show the characteristic resonance frequencies during this period of low level vibration. The level started to build-up at a very slow, smooth, even rate until a maximum value was reached at approximately 33 seconds.

The level decreased until approximately 50 seconds, then throughout the remainder of the flight no abnormal deviations were noted. The low magnitude and slow build-up cannot be construed as a malfunction in the telemetry and data reduction system. Therefore, the data must be considered as valid until other reasons are uncovered. A continuing effort will be required for full interpretation of the data from this measurement.

#### Turbine Starter Flange (Figure 9-28 and 9-44)

Measurement E41-8 was located on the turbine starter flange on engine no. 8 and measured in the longitudinal direction. A high magnitude shock transient occurred at ignition. From the initial transient decay until cutoff the entire time-history data exhibited erratic response which was apparently caused by a low frequency component. This phenomenon is characteristic of the single side band telemetry circuit as explained in the gear case section (9.6.3). Neglecting the effect of the low frequency, there is no increase in levels at either Mach 1 or Max Q. Narrow band analysis indicates predominant frequencies of 500 cps, 1300 cps and 1025 cps. However, the 1025 cps frequency is the natural frequency of the transducer mounting bracketry. Therefore, the actual response of the turbine starter at this frequency may be greatly magnified.

#### Fuel Cracking Valve (Figures 9-28 and 9-44)

Measurement E42-2 was located on the fuel cracking valve on engine number 2 and measured in the longitudinal direction. From ignition until 2 seconds after ignition the time-history exhibits very erratic response. After 2 seconds the data levels off into a steady state condition. This irregularity of data may have been due to saturation of the system at ignition and the subsequent recovery characteristic. The remainder of the time-history until 33 seconds appears relatively uniform. However, after 33 seconds the response again appears erratic but of a different characteristic from that noted at ignition. This type of irregularity appears to have a large low frequency component which continues until outboard engine cutoff. This low frequency phenomenon is characteristic of the single side band telemetry system as explained in the gear case section (9.6.3). Neglecting the effect of the low frequency, predominant frequencies of 375 cps, 850 cps, and 1625 cps are indicated throughout the powered flight.

#### Hydraulic Package (Figures 9-28 and 9-43)

Measurement E43-4 was located on the hydraulic package of engine number 4 and measured in a lateral direction. A slight shock transient appeared at ignition and quickly damped out into steady state vibration.

This steady state condition continued throughout the entire powered flight with no increase in vibration at either Mach 1 or Max Q. Maximum energy was concentrated in the 900 cps to 1500 cps frequency range throughout the time history. This is illustrated in Figure 9-34. No transient response or depletion of vibration was indicated as a result of inboard engine cutoff. Outboard cutoff did not indicate a shock transient but did result in rapid decay of the vibration.

#### Fuel Suction Line (Figures 9-29 and 9-45)

Measurement E45-8 was located on the fuel suction line which supplied engine number 8 and measured vibration in the longitudinal direction. For about 1.3 seconds after ignition, transients occurred, then the vibration level diminished to a steady state. This level was constant during mainstage with a very slight build-up at Mach 1 and Max Q. At inboard engine cutoff the level was the same as the mainstage value. About .5 seconds after IECO the vibration level fell off for about .3 sec, built up momentarily and then decreased steadily.

The frequency ranges in which most of the energy was contained during ignition and holddown were 200 cps to 500 cps and 1000 cps to 2000 cps. These frequency ranges contained most of the energy from ignition to IECO. At IECO the energy dropped in a proportional amount so that the aforementioned frequency ranges still were predominant up to OECO after which they died out.

#### Fuel Inlet Flange (Figures 9-29 and 9-43)

Measurement E44-8 was located on the fuel inlet flange of engine number 8. The composite vibration record showed that transients occurred for about one second after ignition, then the level remained fairly constant for the holddown and liftoff conditions. These levels persisted through mainstage, Max Q, and Mach 1. Immediately following inboard engine cutoff the level decreased for about .3 seconds and then increased back to the mainstage value. After this return the level decreased at a steady rate.

Most of the energy during the ignition and holddown conditions was in the 250 to 500 cps range. During mainstage the 100 cps filter began to show a slight increase. The energy was apparently shifting from the 80 cps filter to the 100 cps filter. After inboard engine cutoff most of the energy was at a frequency of 80 cps. It should be noted that the energy at Mach 1 and Max Q was located at the same frequencies as it was for holddown.

#### 9.6.4 COMPONENT VIBRATION

##### Hydraulic Actuators (Figures 9-30 through 9-41)

A total of twenty-four vibration measurements were recorded on the hydraulic actuators. All measurements were time shared on a four segment commutator; consequently, the data from each measurement appeared only at specific time intervals during flight.

Tilting of the vehicle in pitch was cam operated on the SA-2 flight. This was programmed in lieu of the "step input" type gimballing which was used on the SA-1 vehicle. The data exhibited erratic response which may be attributed to improper functioning of the cam during the SA-2 flight. The cam was loading periodically, thus causing a sudden kick when it released (see Page 83 ). An investigation is being continued to determine if any correlation exists. It is also noted that the pitch and yaw  $\beta$  graphs for the outboard engines revealed large changes of gimbal angles in very short periods of time. These high magnitude rate of changes correlate very closely to transients which occur frequently in the actuator data. A few typical transients are shown in Figure 9-38. The composite data from most of the actuator measurements was relatively unstable throughout powered flight. Vibration at engine ignition was normal with low amplitude transients occurring on each measurement which was transmitted during the ignition period. Typical samples are shown in Figure 9-39. Vibration levels were not affected by liftoff, Mach 1, Max Q, or inboard engine cutoff. Figure 9-39 displays data samples from the mainstage period during times of the most uniform vibration. Note the erratic appearance of most of the measurements. This is typical for most of the actuator data received from the flight of the SA-2 vehicle.

##### ST-90 Gyro Platform (Figures 9-40, 9-41 and 9-46)

Measurements E4-15 and E5-15 were mounted on the ST-90 gyro platform and sensed vibration in the longitudinal (Y) and yaw (Z) directions respectively. Since the orientation of the gyro platform was space-fixed, the sensitive axes of the subject measurements coincided with the vehicle major axes only in the launch orientation.

Both measurements indicated an ignition transient and decayed to mainstage level by approximately 7 seconds. The measurements slowly increased, E4-15 reaching a maximum at 43 seconds. This measurement decreased momentarily and then increased to a lesser peak at 57 seconds. From 57 seconds upwards in time, the level of E4-15 diminished steadily until IECO at which time a low level transient occurred. Measurement E5-15 reached a maximum by about 45 seconds and maintained that level until approximately 65 seconds, at which time it decreased at a

constant rate. A small increase in level occurred at IECO followed by a decay. The vibration level recorded on E5-15 was higher than that recorded by E4-15 throughout powered flight. Transients appeared on the composite trace of E5-15 before ignition and throughout recorded flight. The transients occurred approximately every six seconds and persisted for approximately 0.5 seconds at each occurrence. The magnitude of these transients varied, but at least one transient occurred every six seconds throughout the record. Less predominant transients were observed on E4-15. The transients which could be detected on this measurement occurred at the same time as those recorded on E5-15.

Low frequency analyses of the measurements indicated a 26 cps signal on E5-15. This signal was most predominant during the holddown period. A lower level signal of the same frequency was also present on E4-15 during holddown (see Page 136).

#### Instrument Panel (Figures 9-41 and 9-46)

Measurement E48-14 was located on the center of the instrument panel in canister number 14. The flight composite showed a build-up at ignition with a transient approximately 6 times the mainstage value. The composite level during liftoff was 5 times the mainstage level. The liftoff vibration level remained relatively constant for approximately 4.5 seconds then smoothly decreased to the mainstage level. The composite level did not show any pronounced change at Mach 1, Max Q, and IECO. At outboard engine cutoff a small magnitude transient was noted.

The narrow band analysis indicated a predominant frequency of 680 cps during liftoff. Throughout the remaining portion of the flight, the predominant frequencies are 150, 200 and 730 cps. The 1/3 octave band analysis shows the presence of beats on the 20 cps center frequency between 60 and 66 seconds. The beats did not appear at any other time.

#### Propulsion Unit Distributor (Figures 9-41 and 9-42)

Measurement E46-9 was in fuel tank 4 attached to the propulsion unit distributor and measured vibration in the longitudinal direction. The vibration level during ignition, holddown, and liftoff was relatively high; it then slowly decreased to a steady state value by about 6 seconds from range zero. The level remained constant up to 33 sec, then increased at Max Q. After Max Q the level tapered off at a constant rate. At about .3 sec after IECO there was an increase in level. About .2 sec after OECO the level increased for about .3 sec. After this slight transient occurred, the level tapered off.

During ignition, holddown, and liftoff most of the energy was contained in the 400-1600 cps frequency range. At mainstage most of the energy was at 500 and 630 cps. As the level increased to Mach 1, these frequencies showed contributions: 400, 500, 630, 1250, and 1600 cps. This energy distribution was maintained through Max Q. After Max Q most of the energy showed up at 500 and 630 cps for the remainder of powered flight.

#### 9.6.5 DISCUSSION OF VIBRATION DATA

The composite data received during the flight of the SA-2 vehicle has in general the appearance of amplitudes higher than the data received during the flight of the SA-1 vehicle. This is believed to have resulted from the extended frequency bandwidths used in the telemetry system of the SA-2 vehicle. All SA-1 vibration data was received on an FM-FM telemetry system with a maximum frequency response of 1.050 KC. Vibration data from the SA-2 flight was received by both FM-FM telemetry and single side band. The single side band system transmits more vibration energy by virtue of its increased frequency bandwidth of 3 KC.

A direct comparison of the over-all vibration levels occurring during the SA-1 and SA-2 flights is not possible at this time; however, a preliminary review of narrow bandwidth data indicates that the vibration levels on the two flights were generally on the same order of magnitude. Vibration levels on the SA-1 flight were found to be generally lower than the levels obtained during static test. Vibration test levels for Saturn have been determined from static firing data. The SA-2 flight vibration levels are considered to be generally below these specified levels.

A comprehensive comparison will be made of all vibration data from the flights of the SA-1 and SA-2 vehicles. The results of this investigation will be presented in the near future.

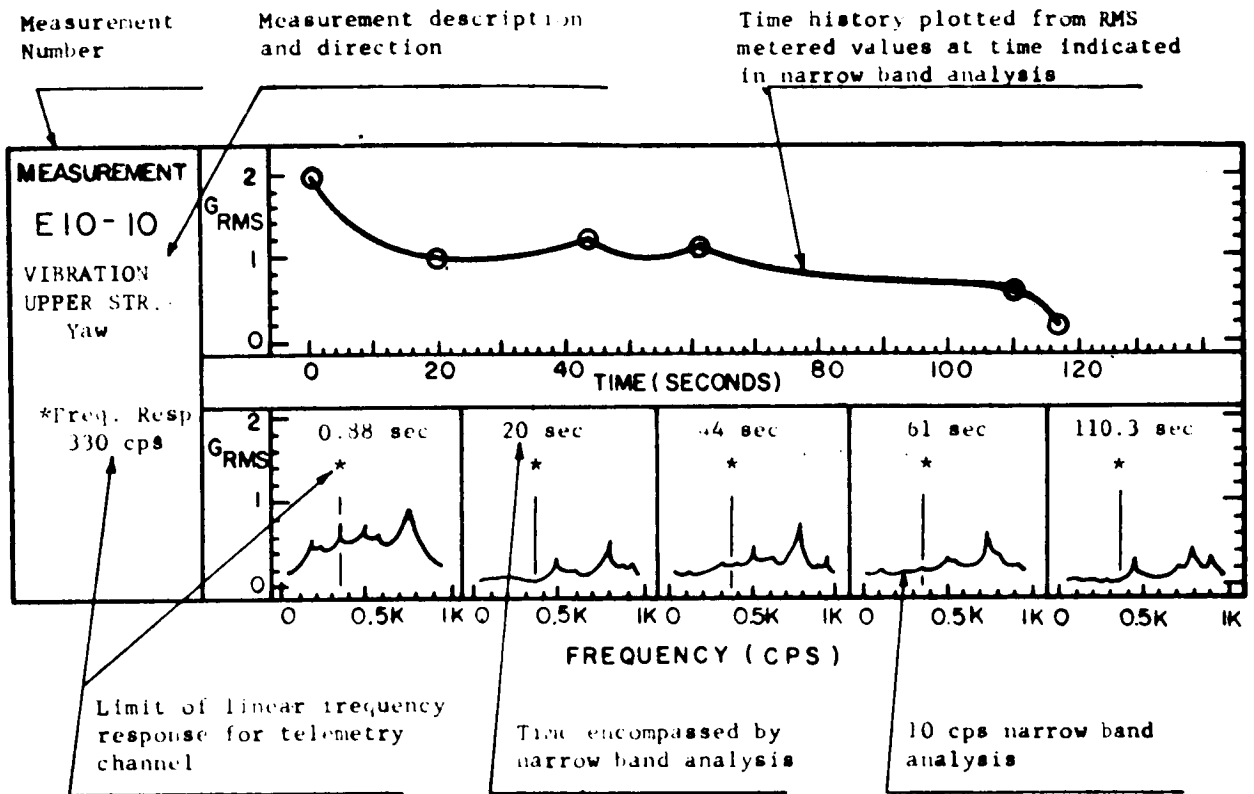


Figure 9-20 Explanation of Data in Vibration Summary Curves

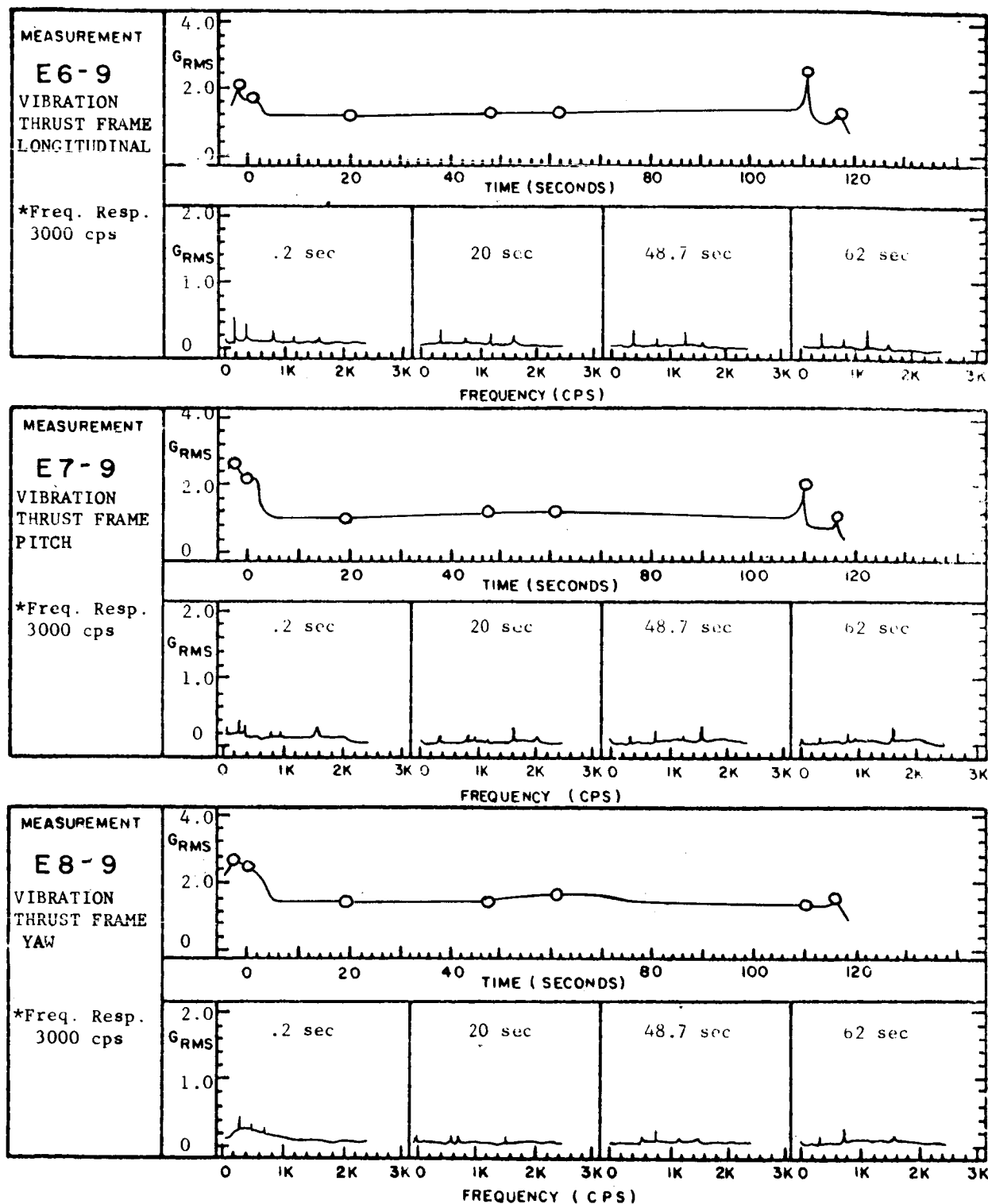


Figure 9-21 SA-2 Flight Vibration Data

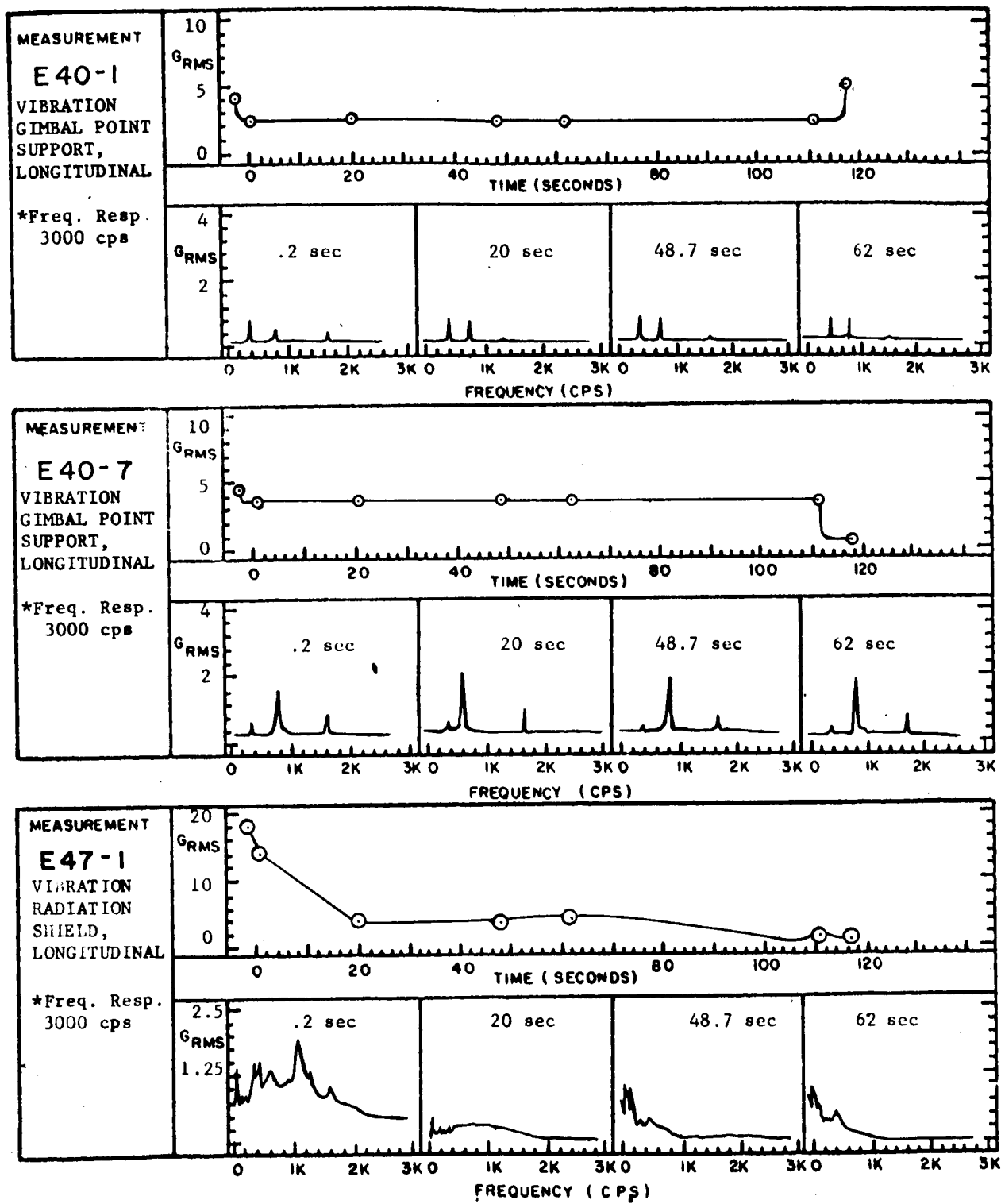


Figure 9-22 SA-2 Flight Vibration Data

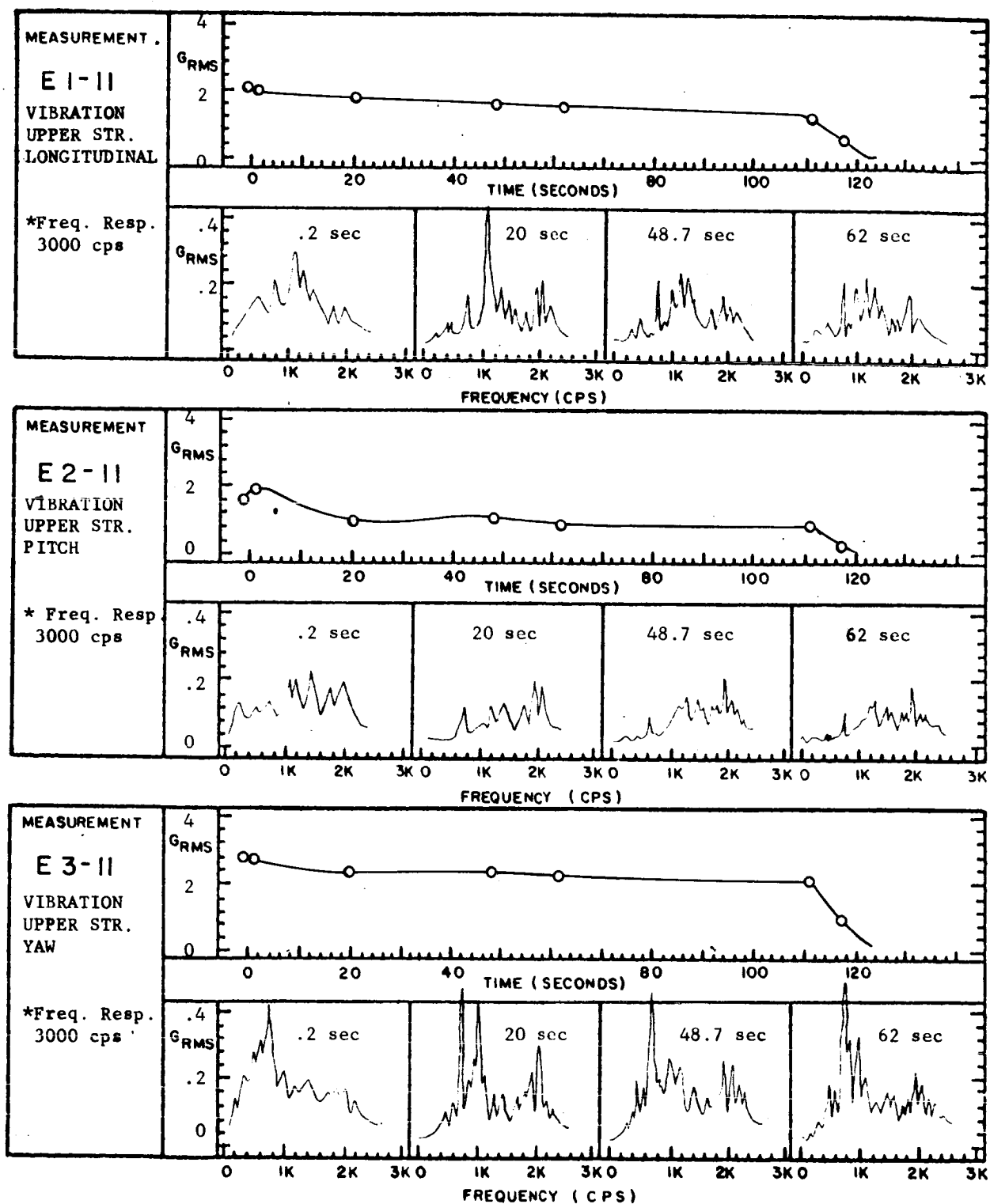


Figure 9-23 SA-2 Flight Vibration Data

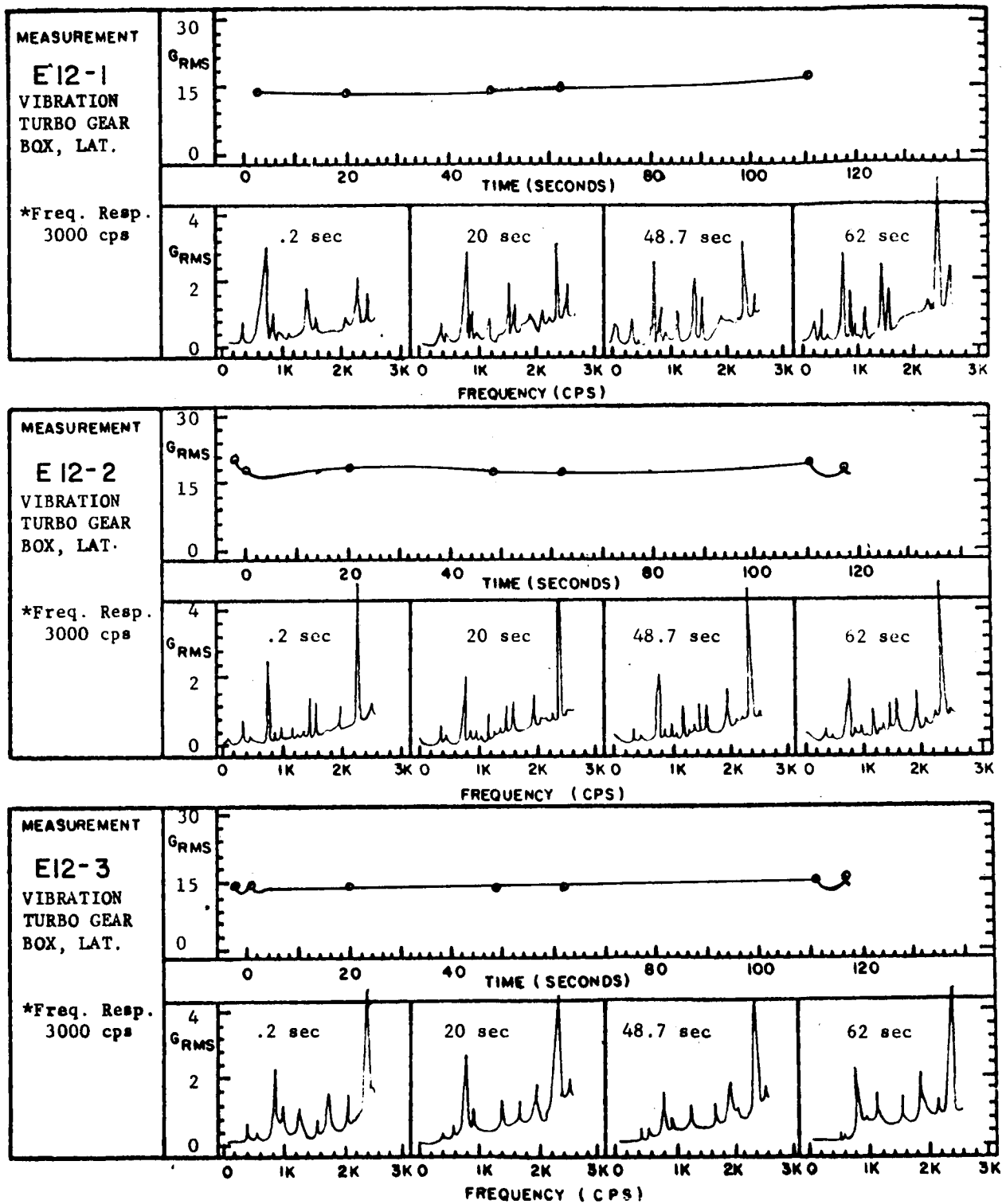


Figure 9-24 SA-2 Flight Vibration Data

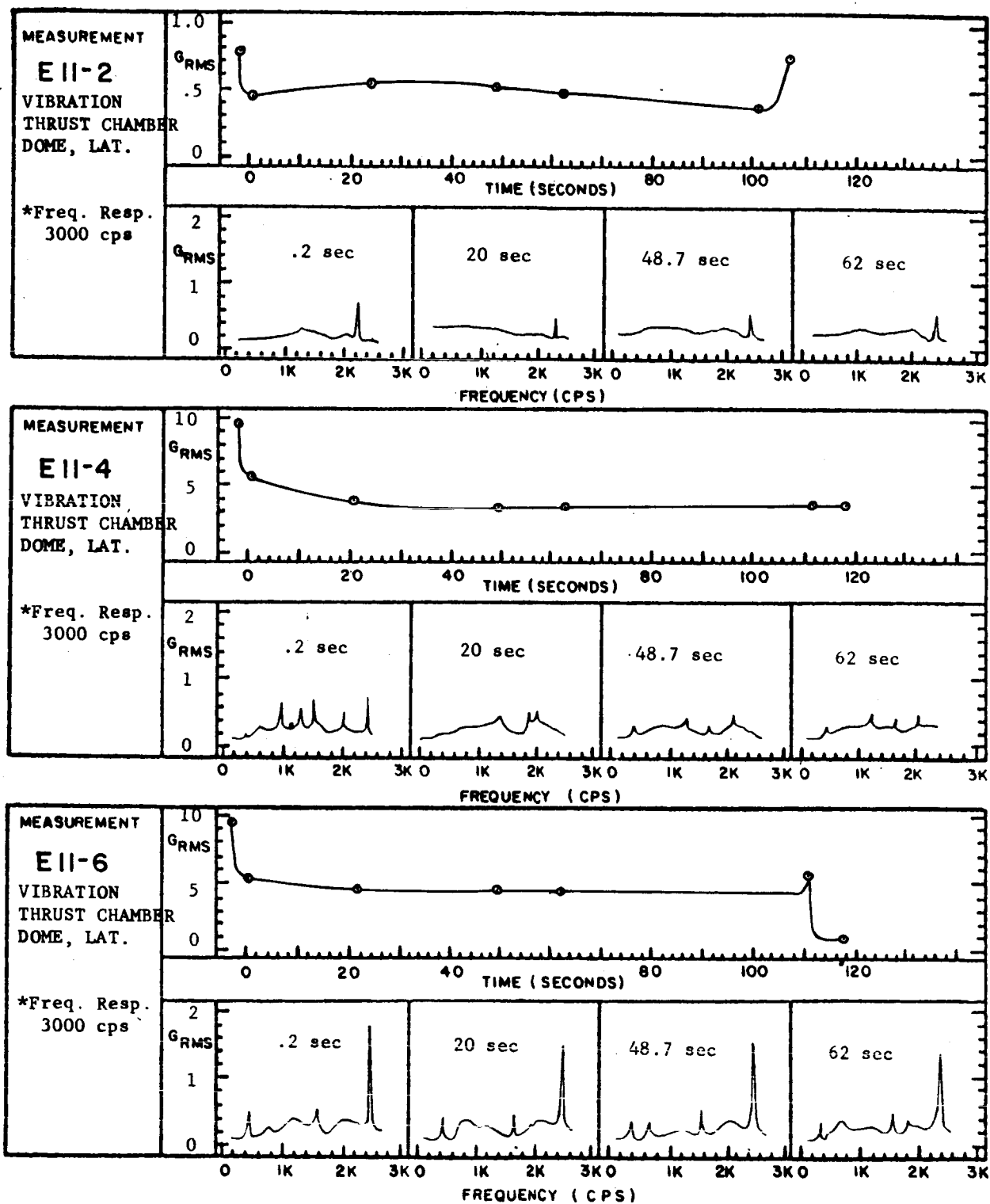


Figure 9-25 SA-2 Flight Vibration Data

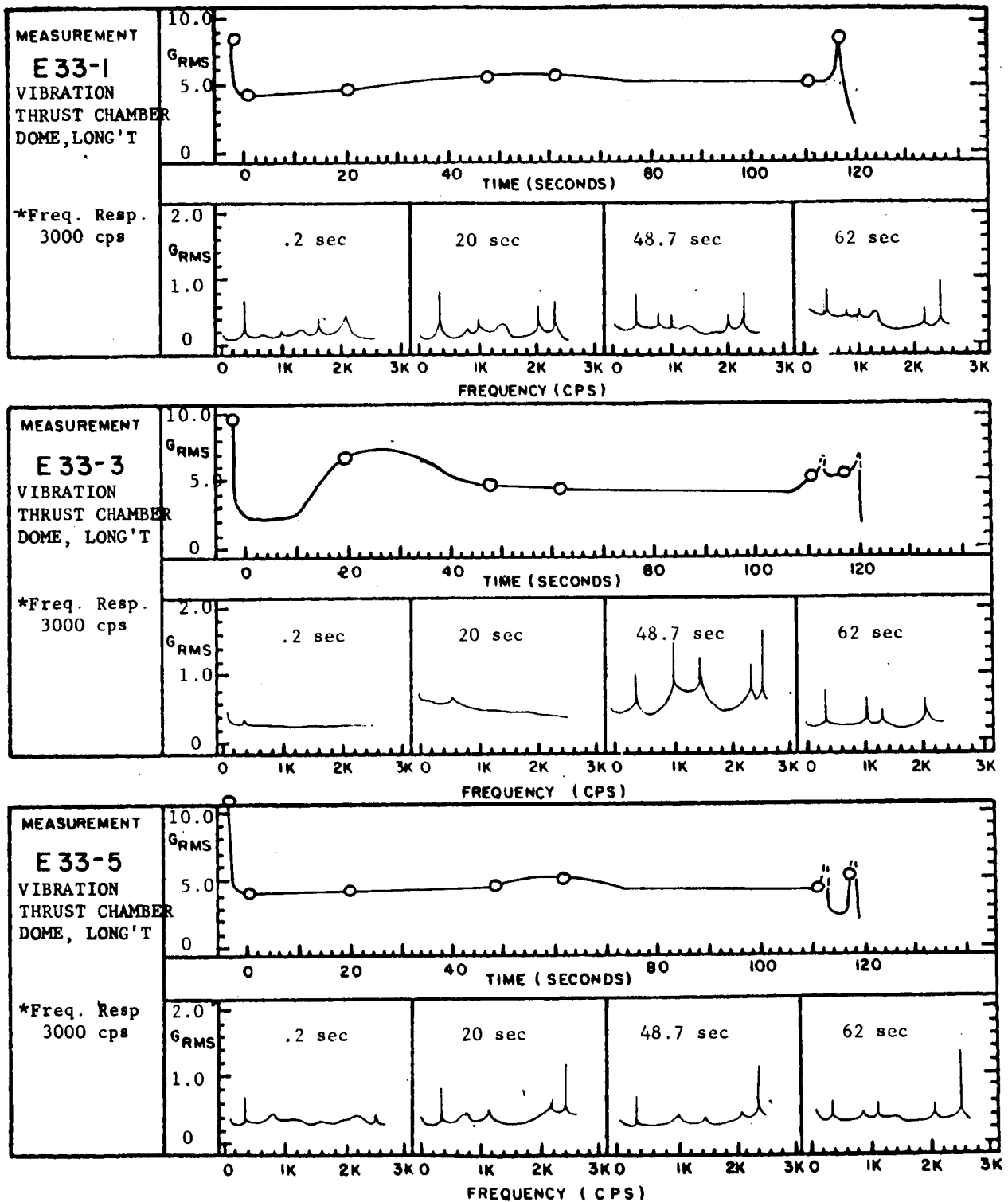


Figure 9-26 SA-2 Flight Vibration Data

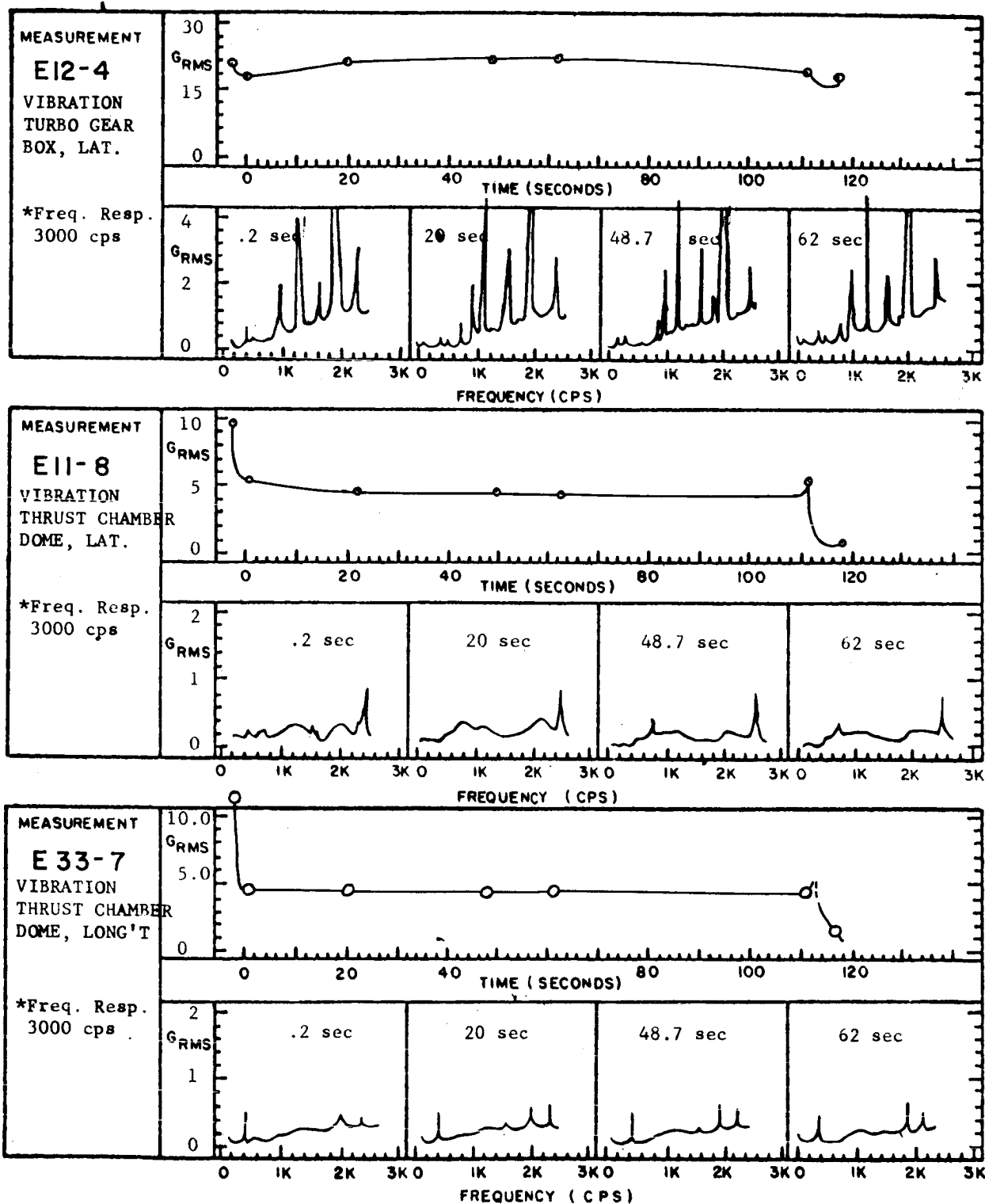


Figure 9-27 SA-2 Flight Vibration Data

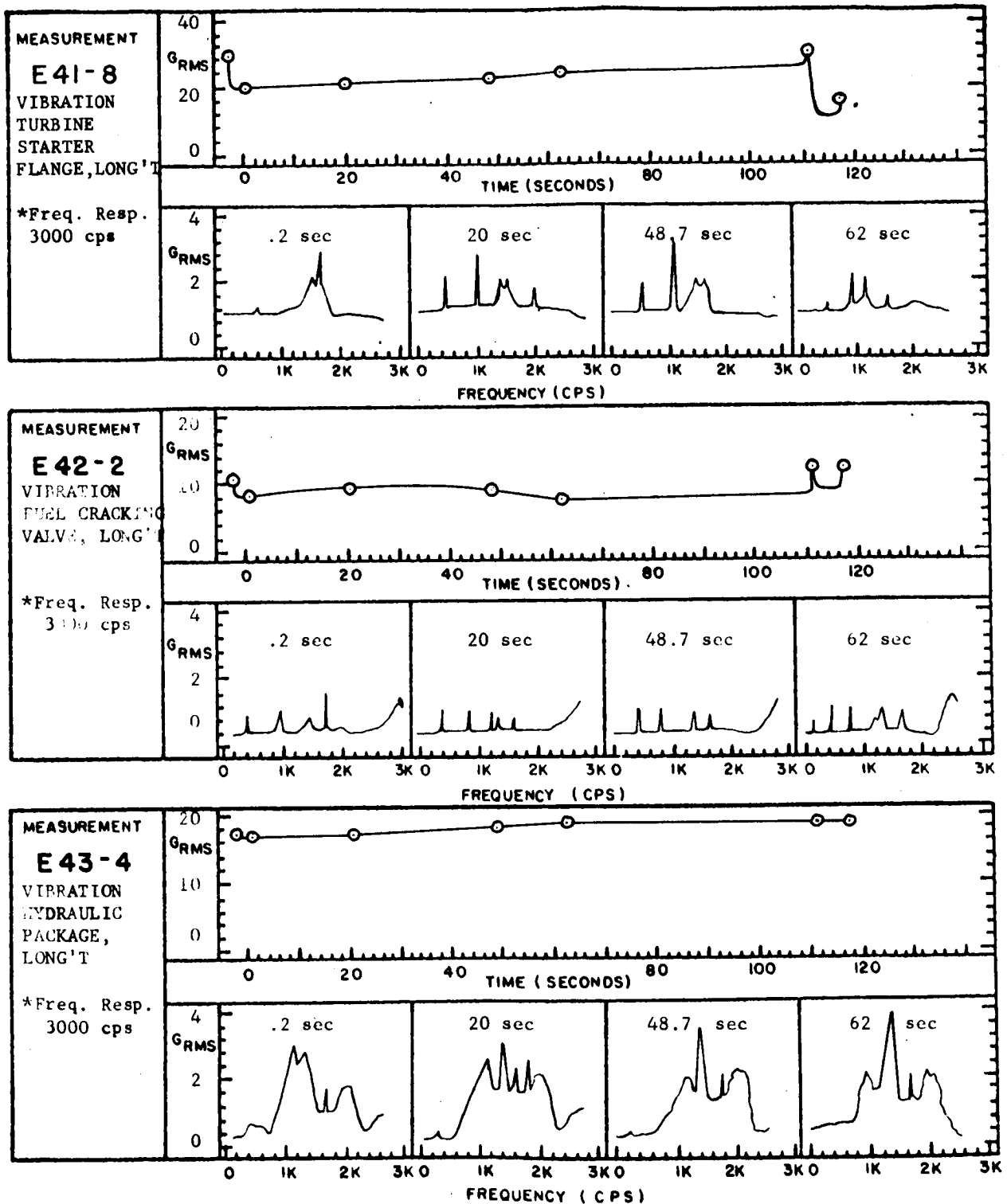


Figure 9-28 SA-2 Flight Vibration Data

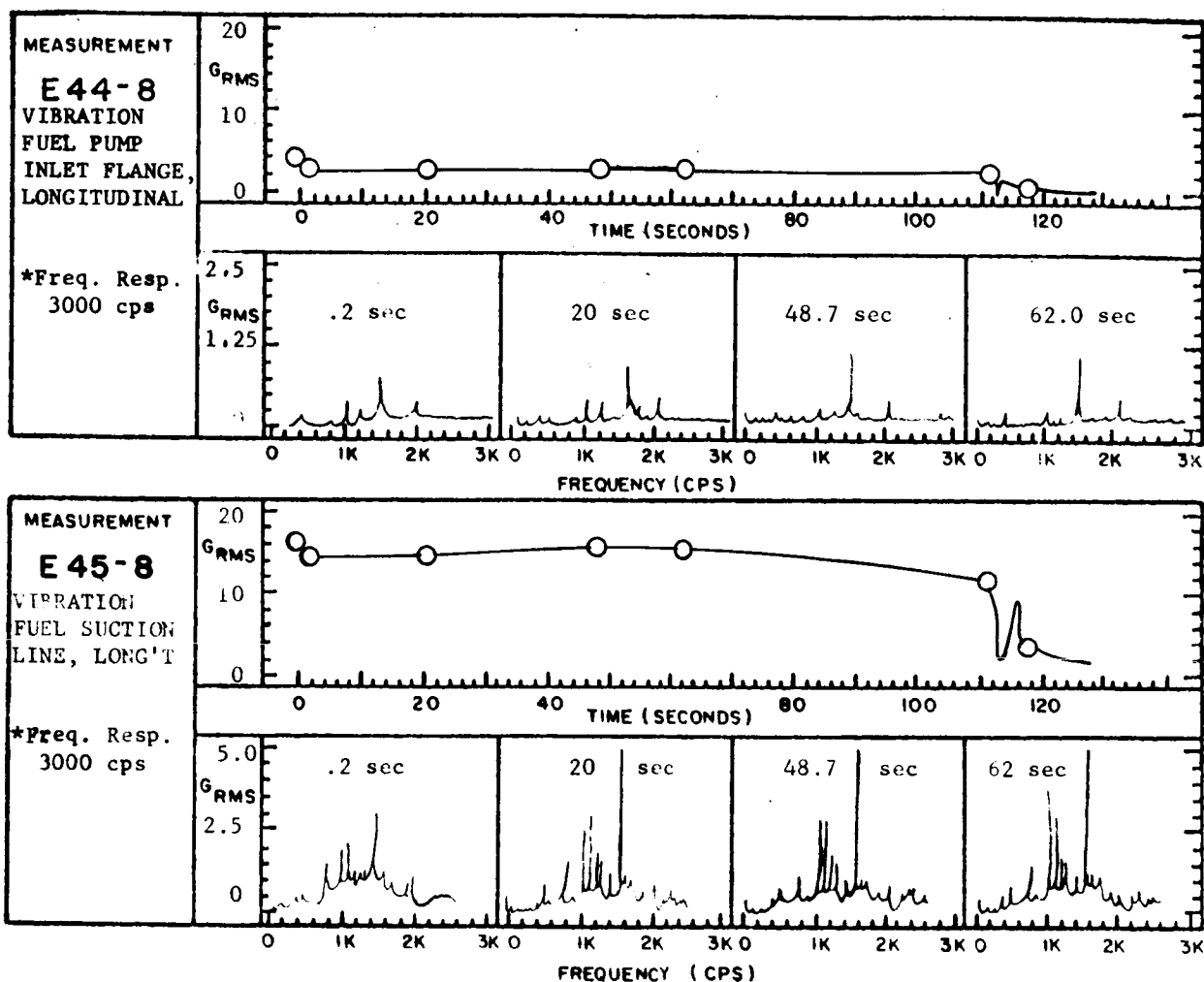


Figure 9-29 SA-2 Flight Vibration Data

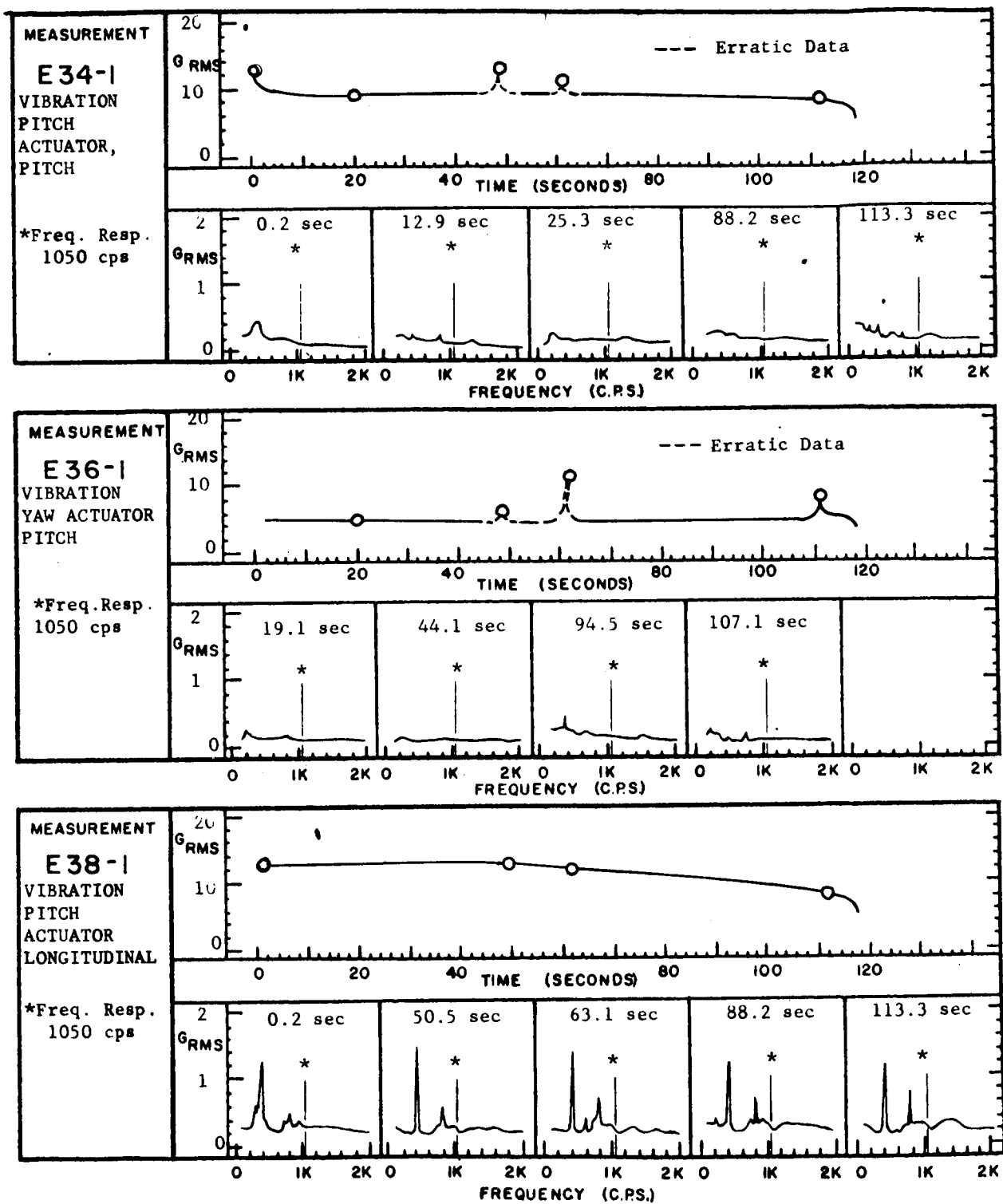


Figure 9-30 SA-2 Flight Vibration Data

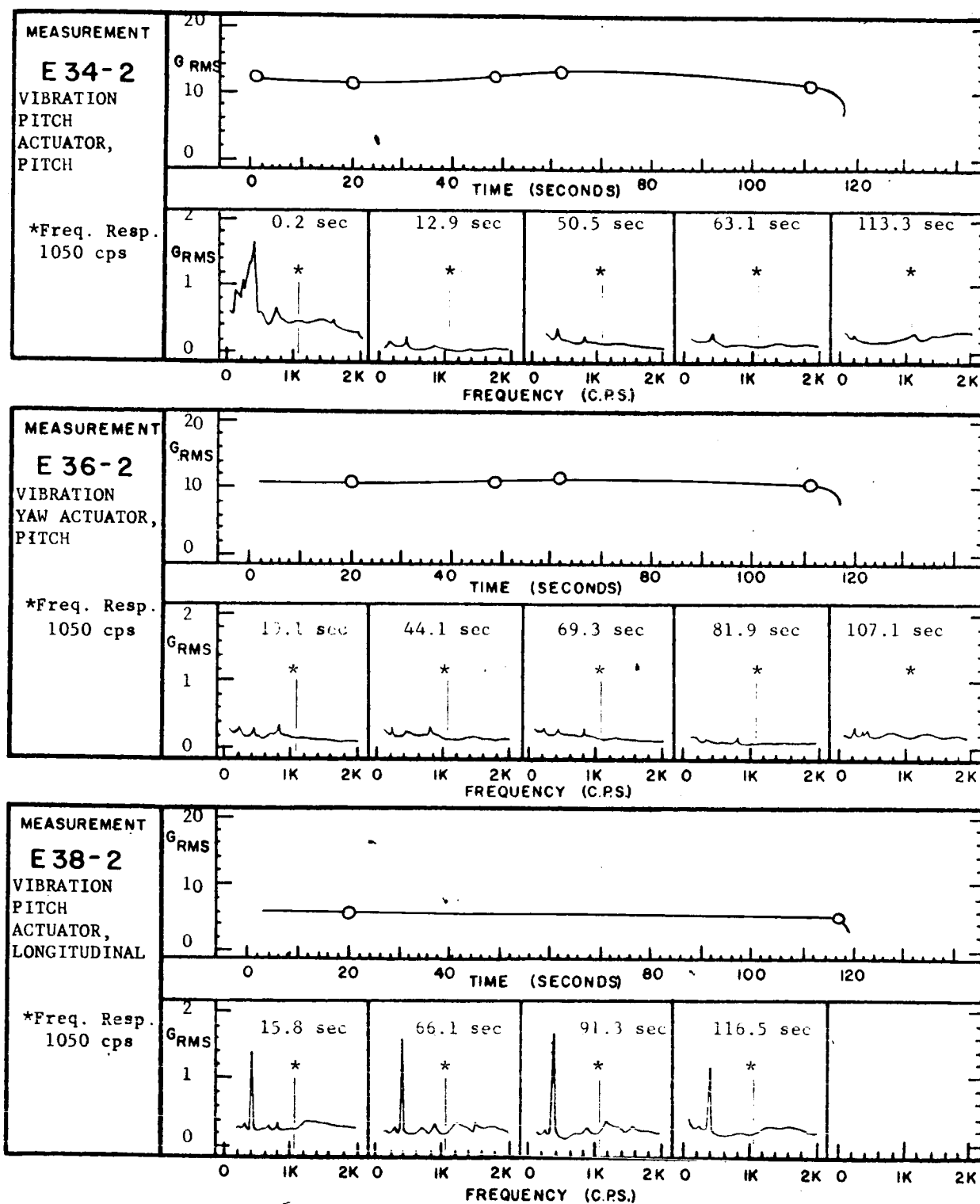


Figure 9-31 SA-2 Flight Vibration Data

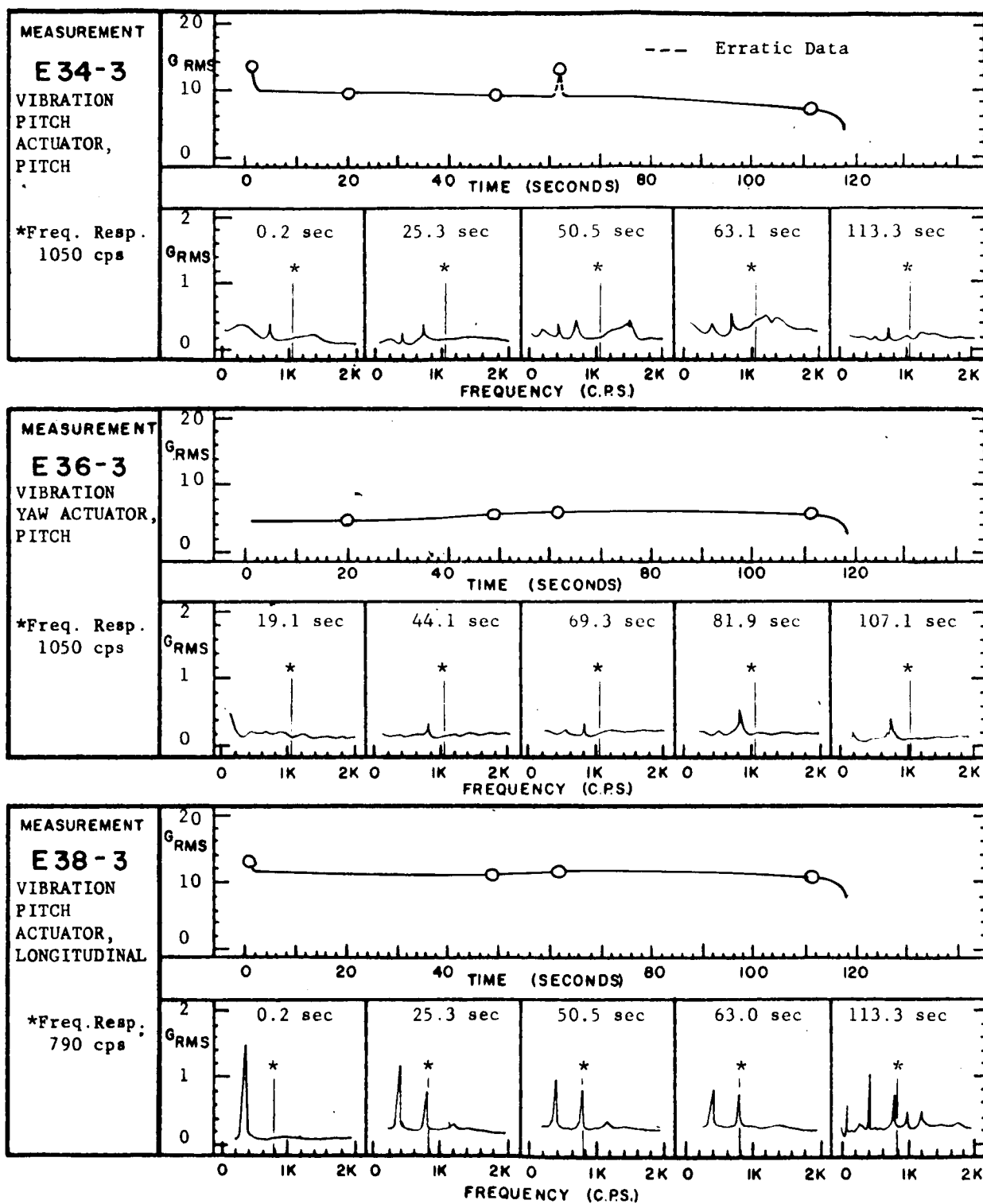


Figure 9-32 SA-2 Flight Vibration Data

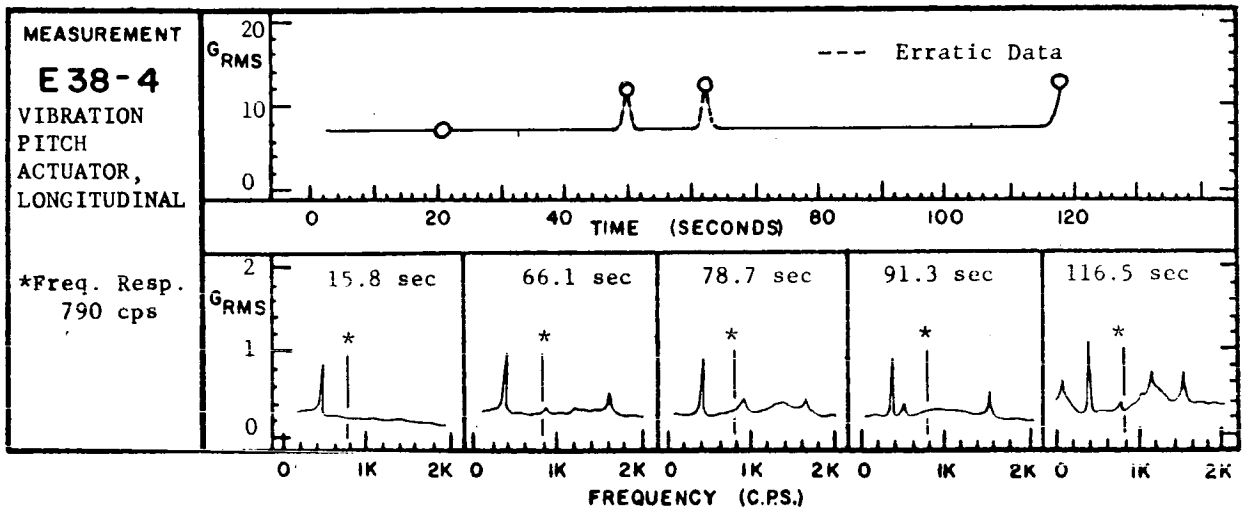
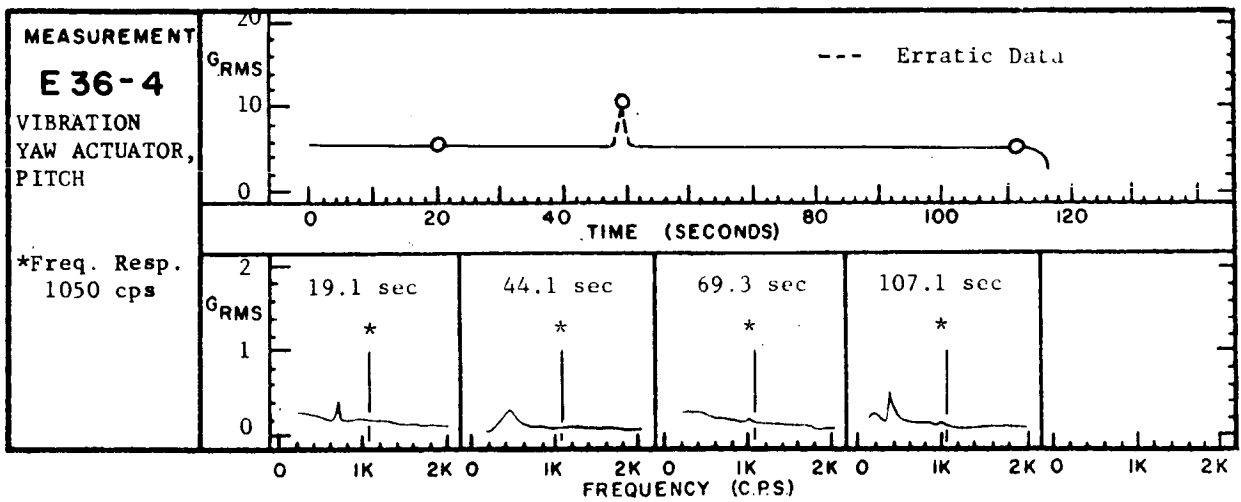
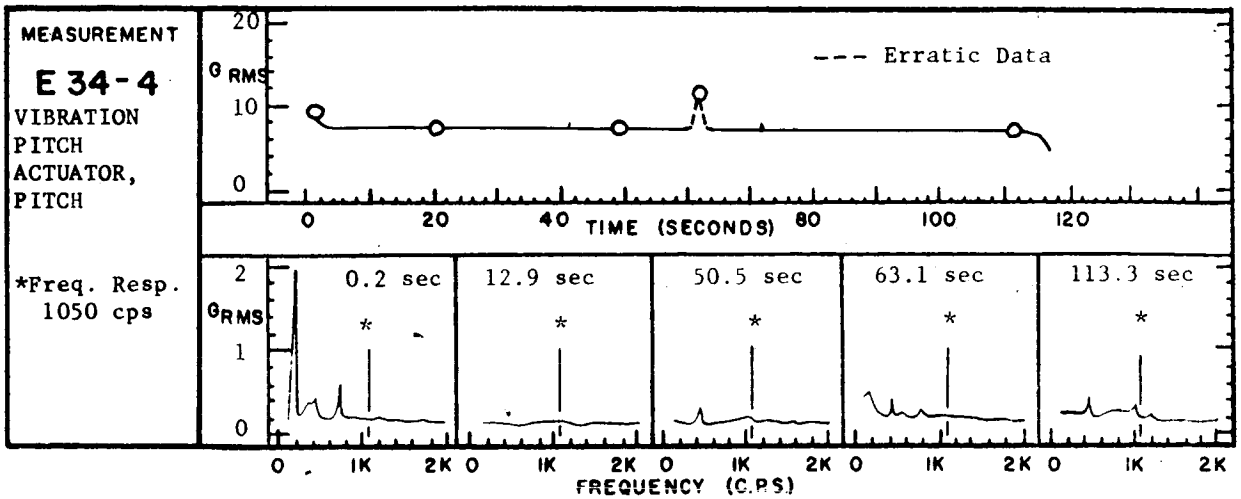


Figure 9-33 SA-2 Flight Vibration Data

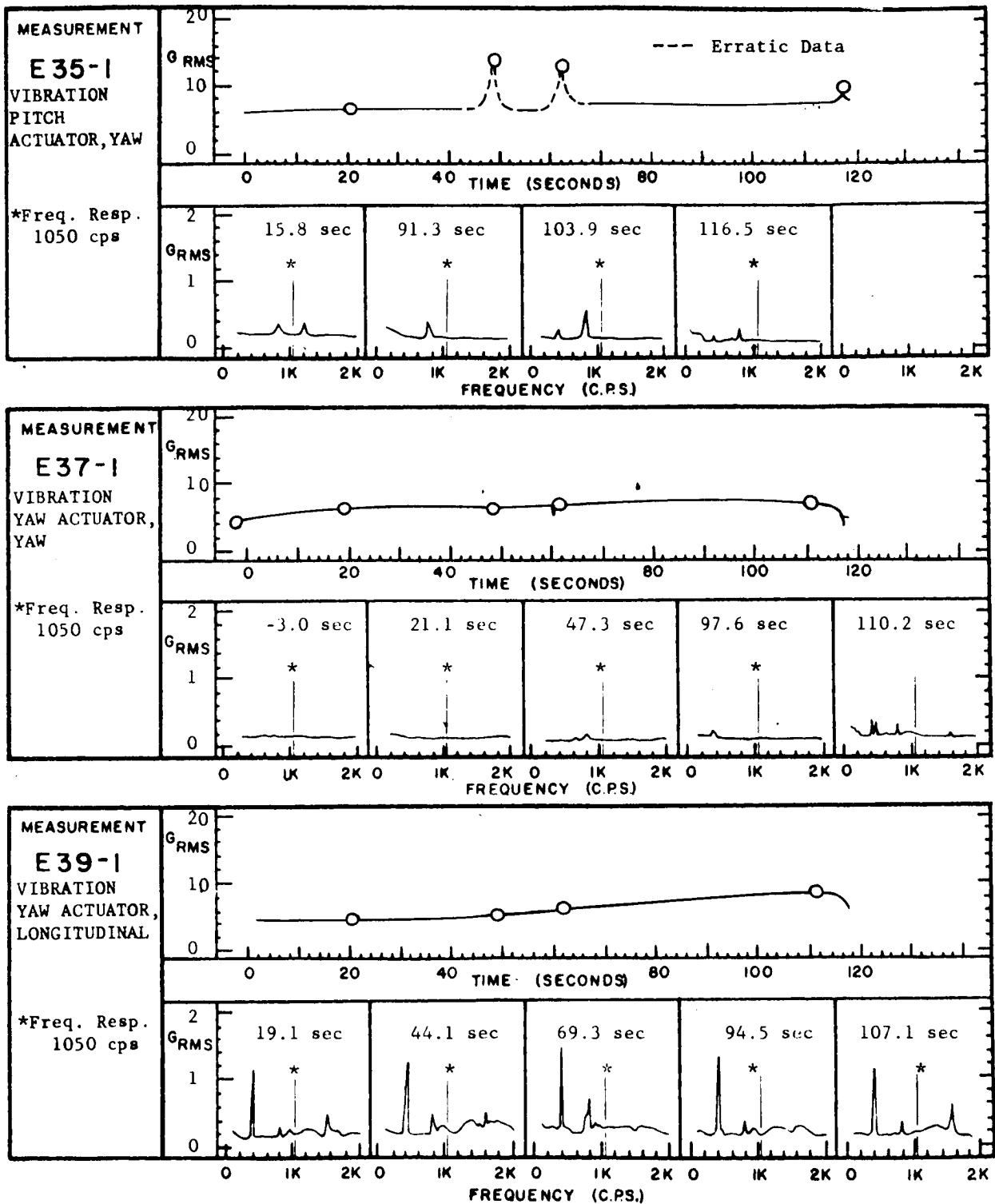


Figure 9-34 SA-2 Flight Vibration Data

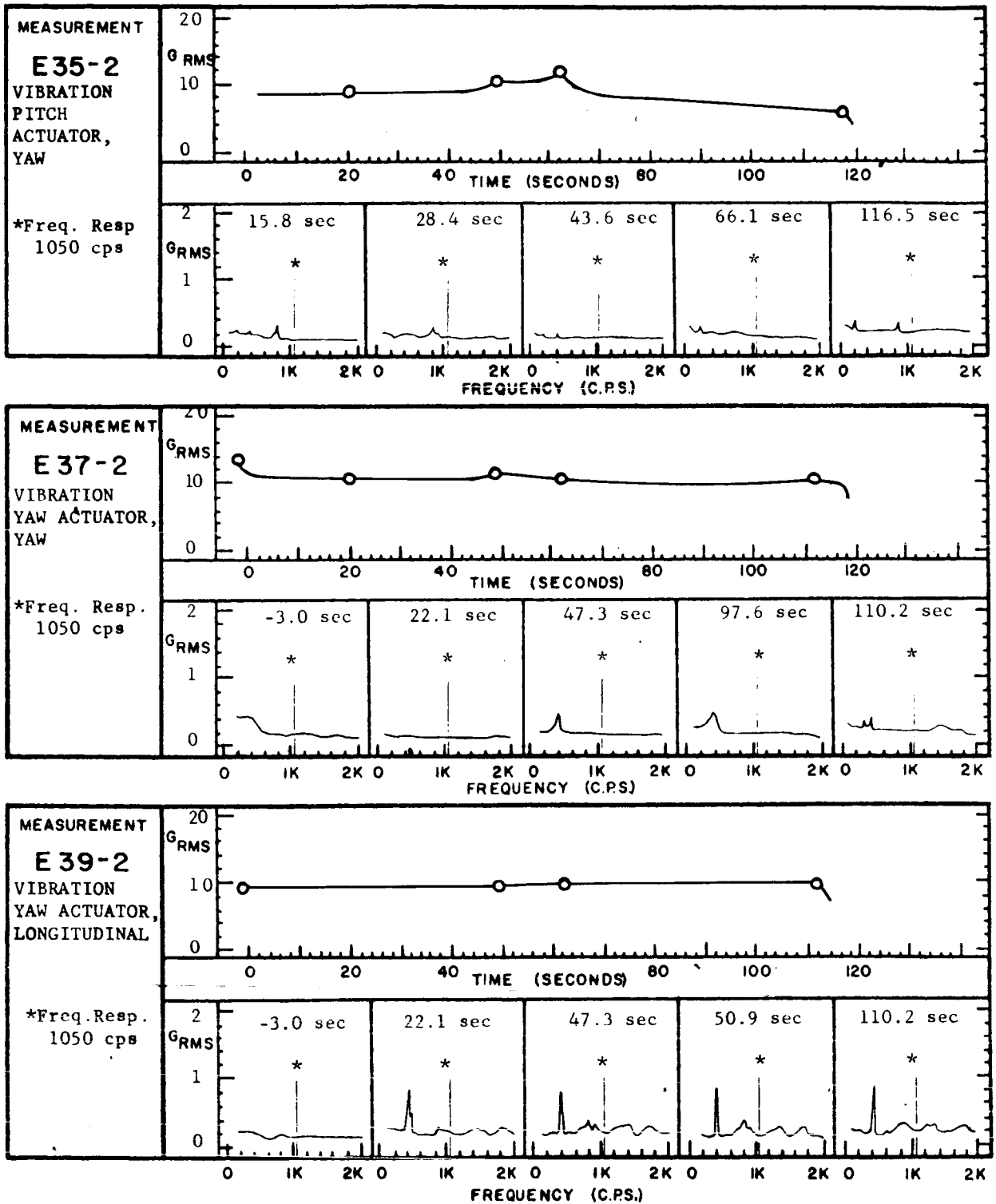


Figure 9-35 SA-2 Flight Vibration Data

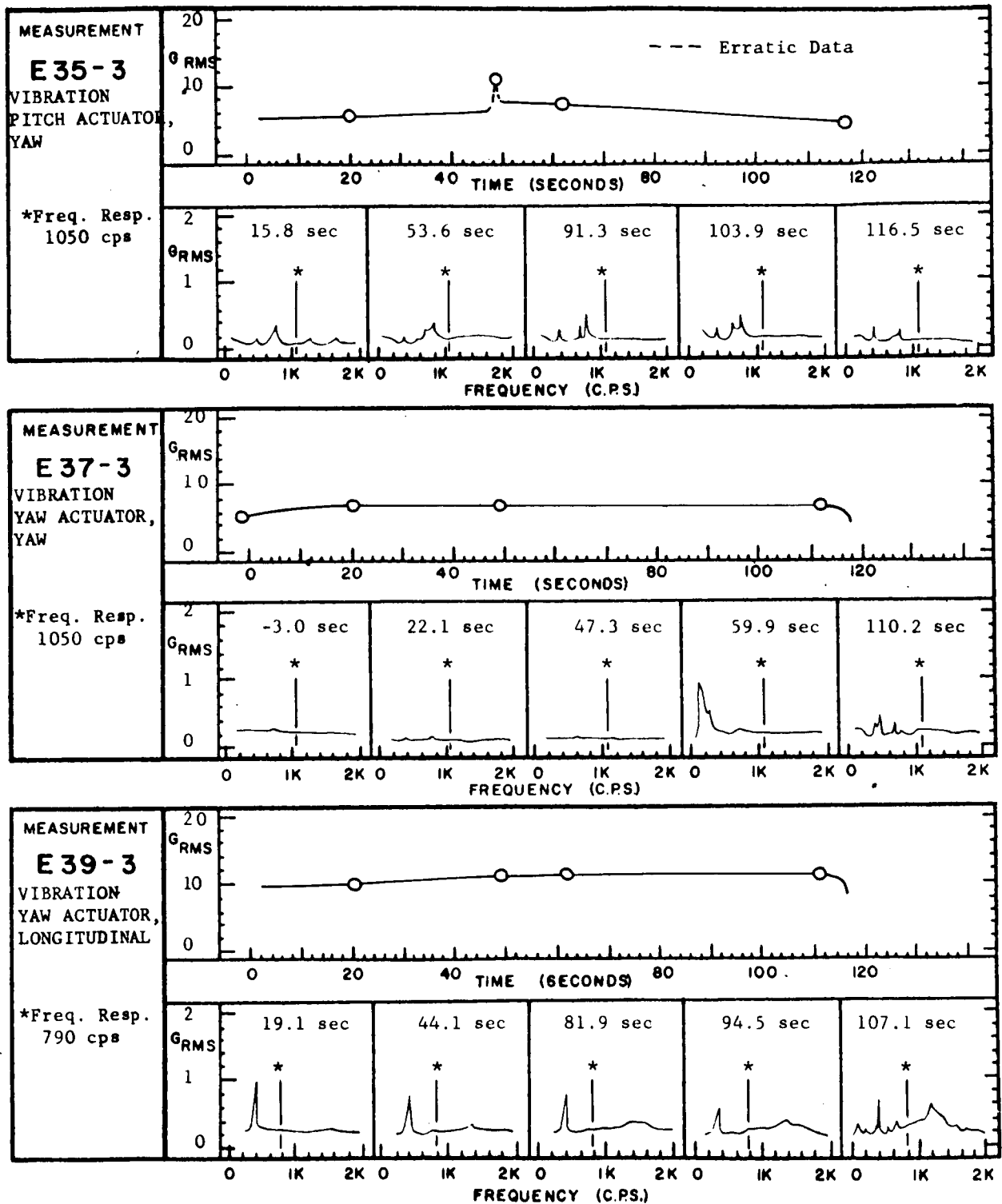


Figure 9-36 SA-2 Flight Vibration Data

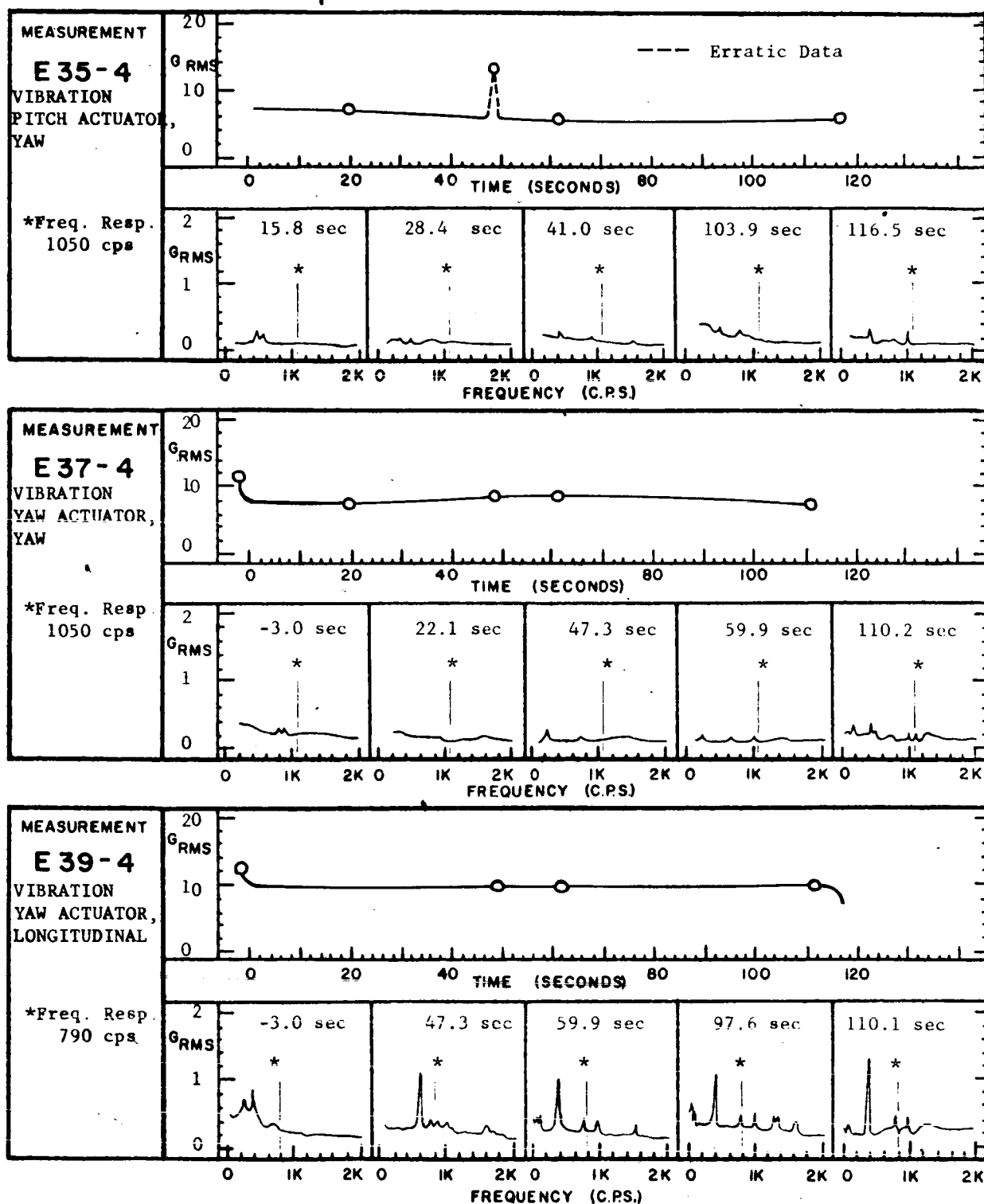


Figure 9-37 SA-2 Flight Vibration Data

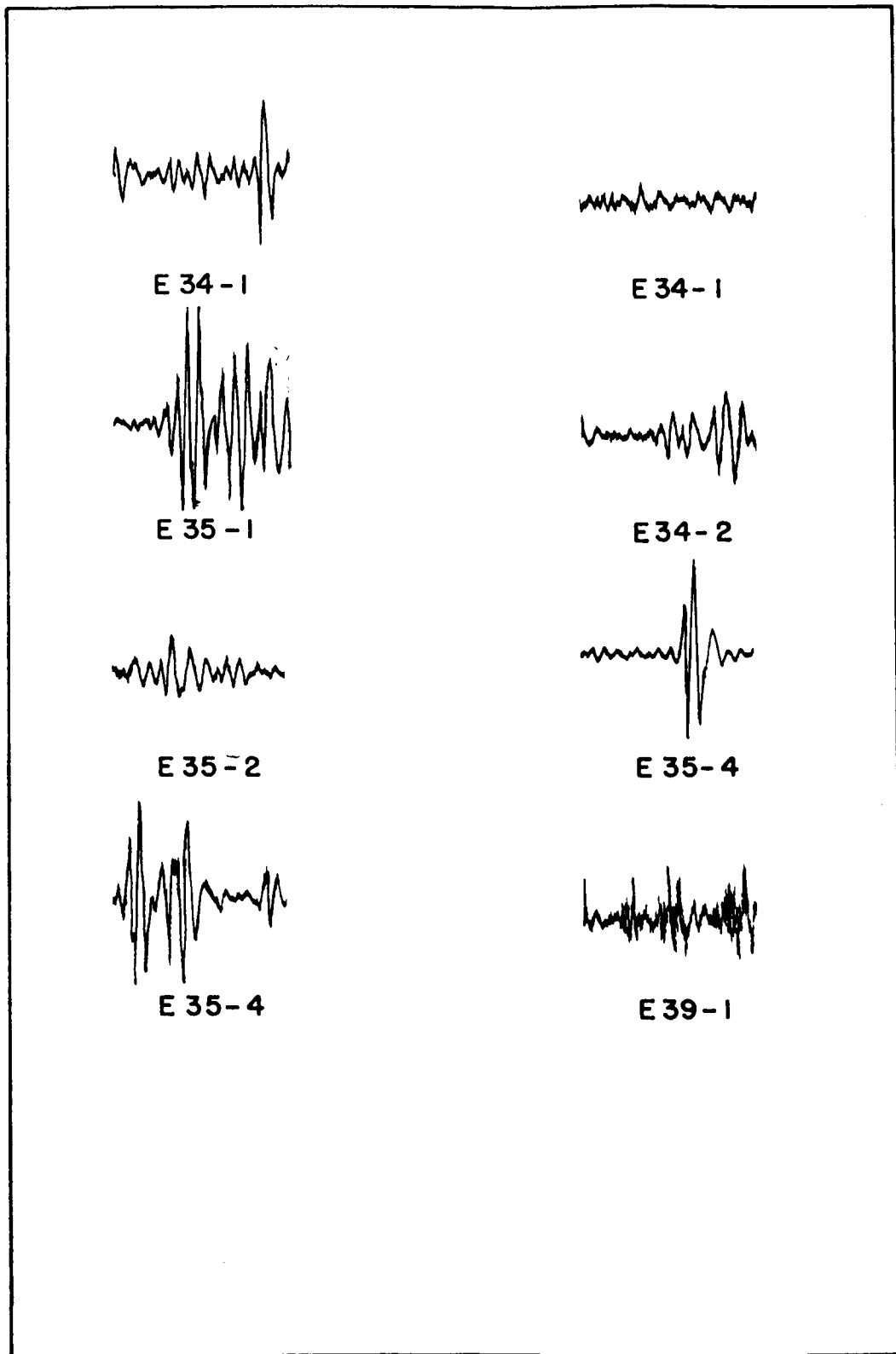


Figure 9-38 Typical Transients in Actuator Data

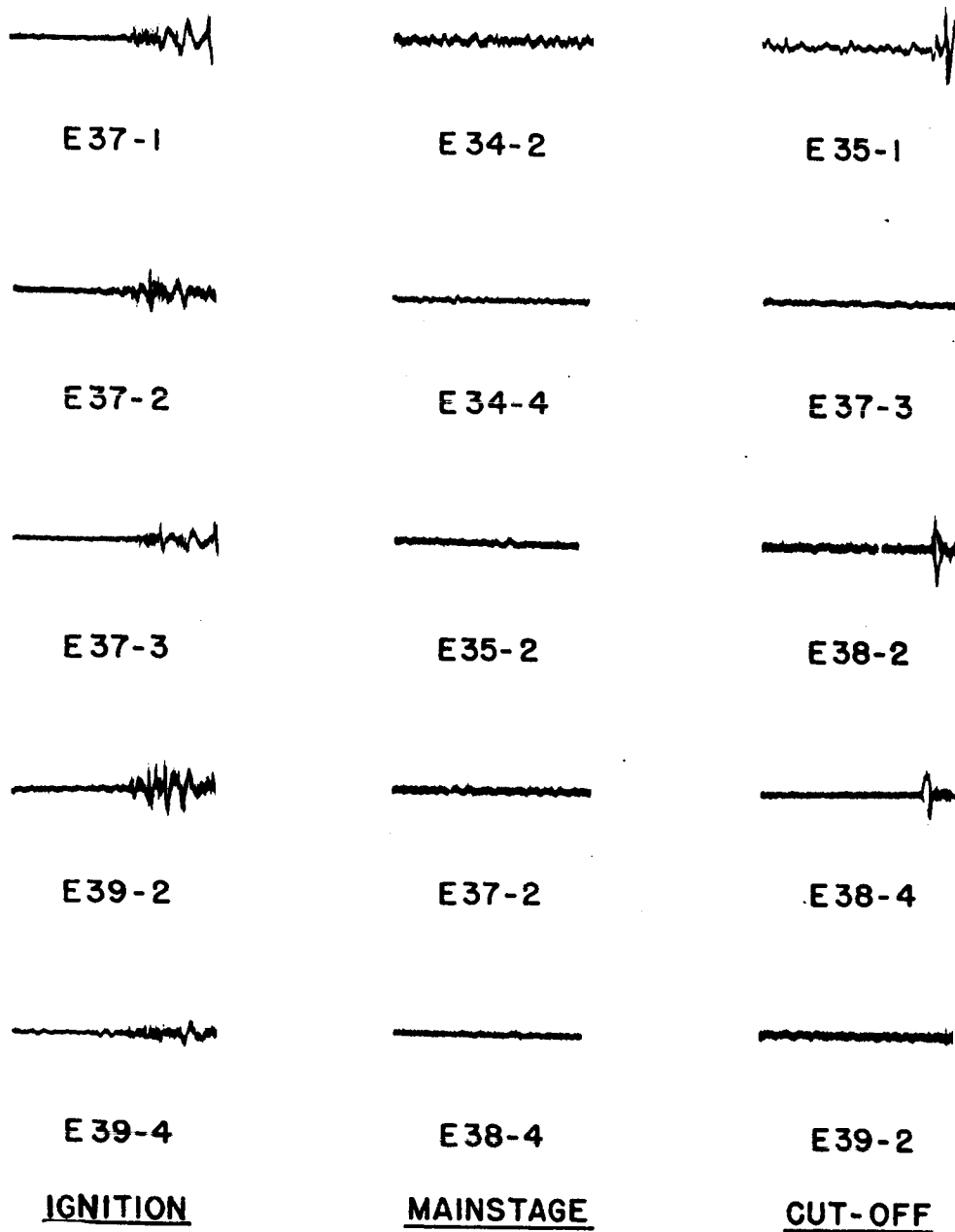


Figure 9-39 Hydraulic Actuator Data

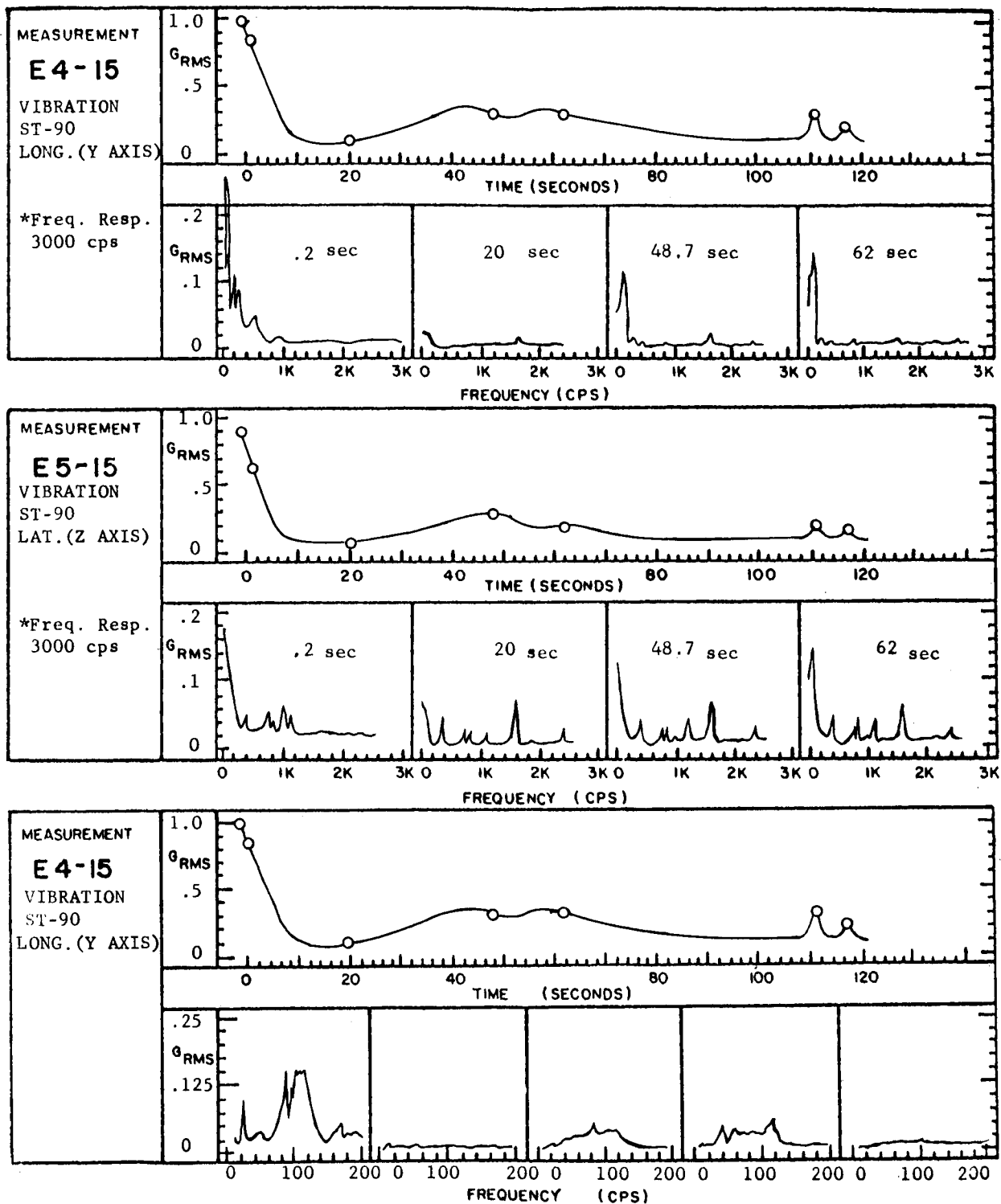


Figure 9-40 SA-2 Flight Vibration Data

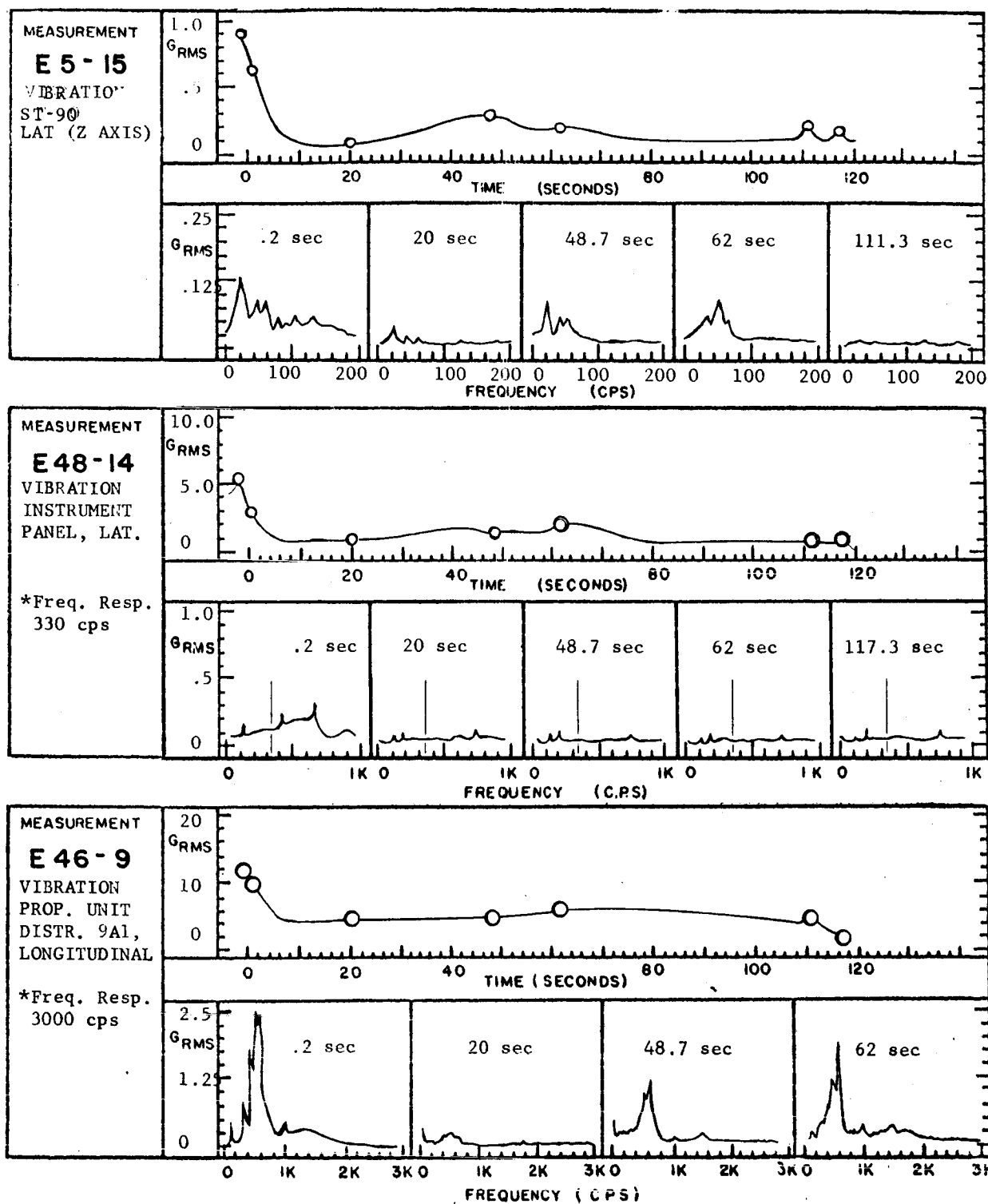


Figure 9-41 SA-2 Flight Vibration Data

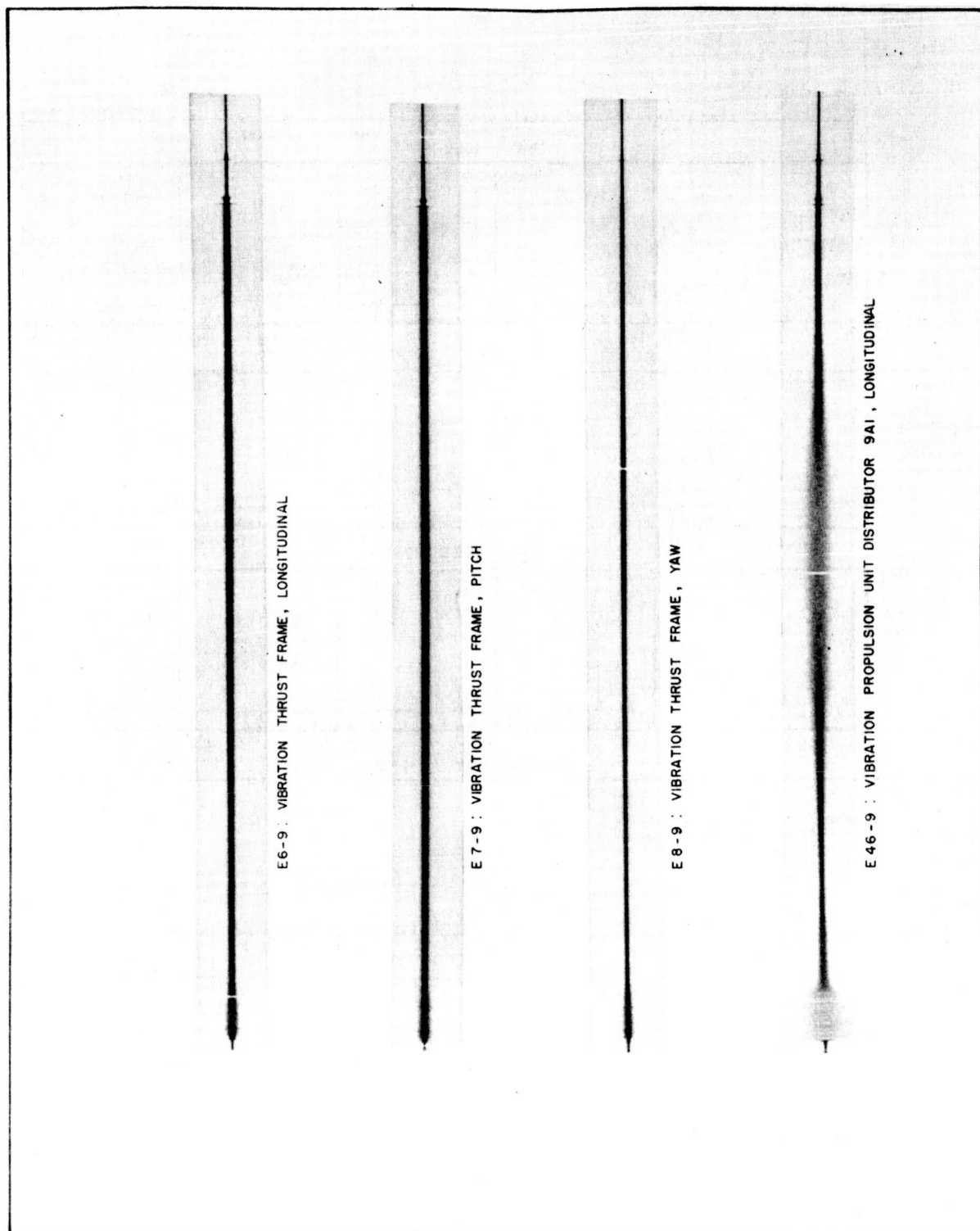


Figure 9-42 SA-2 Composite Vibration Traces

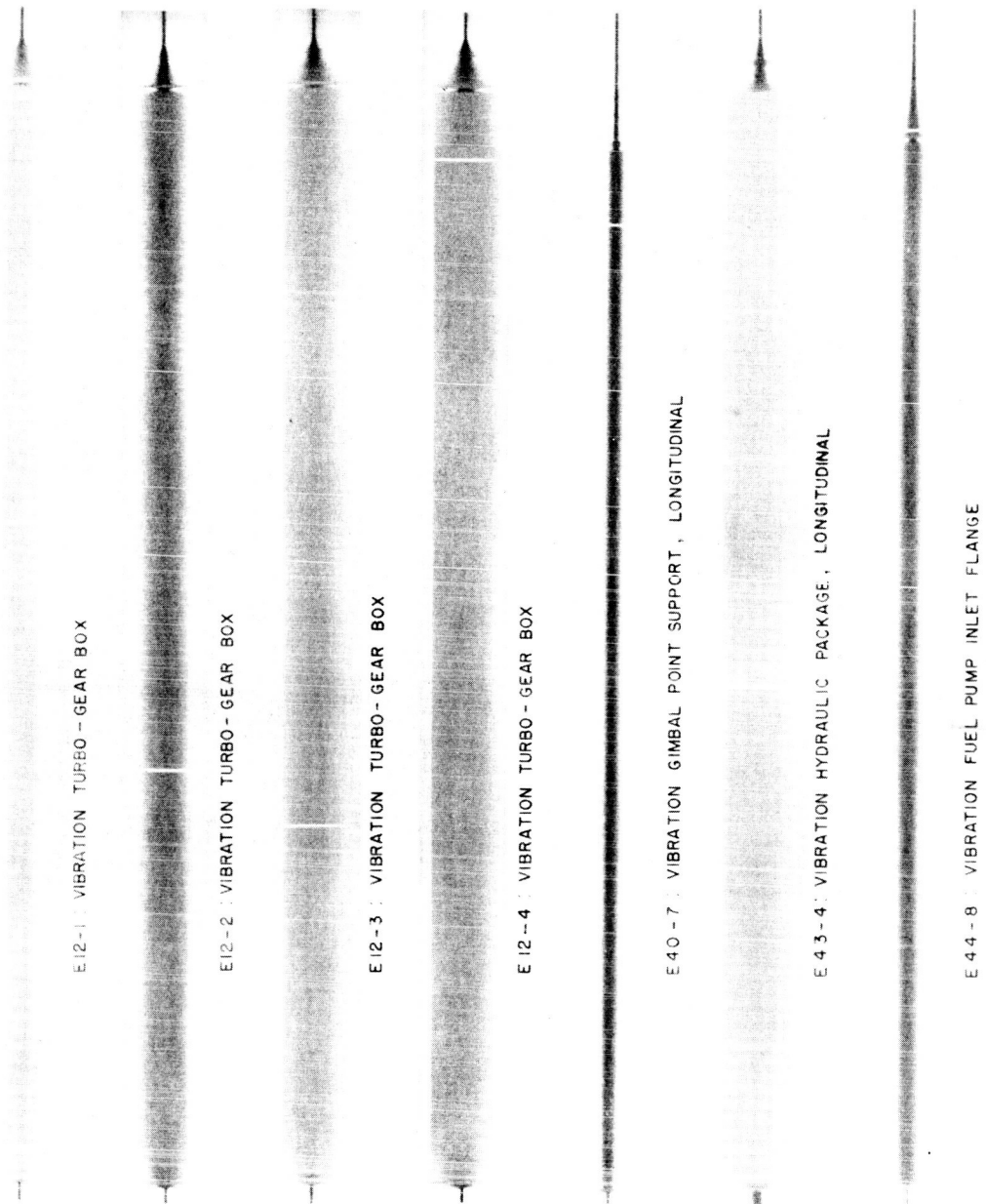


Figure 9-43 SA-2 Composite Vibration Traces

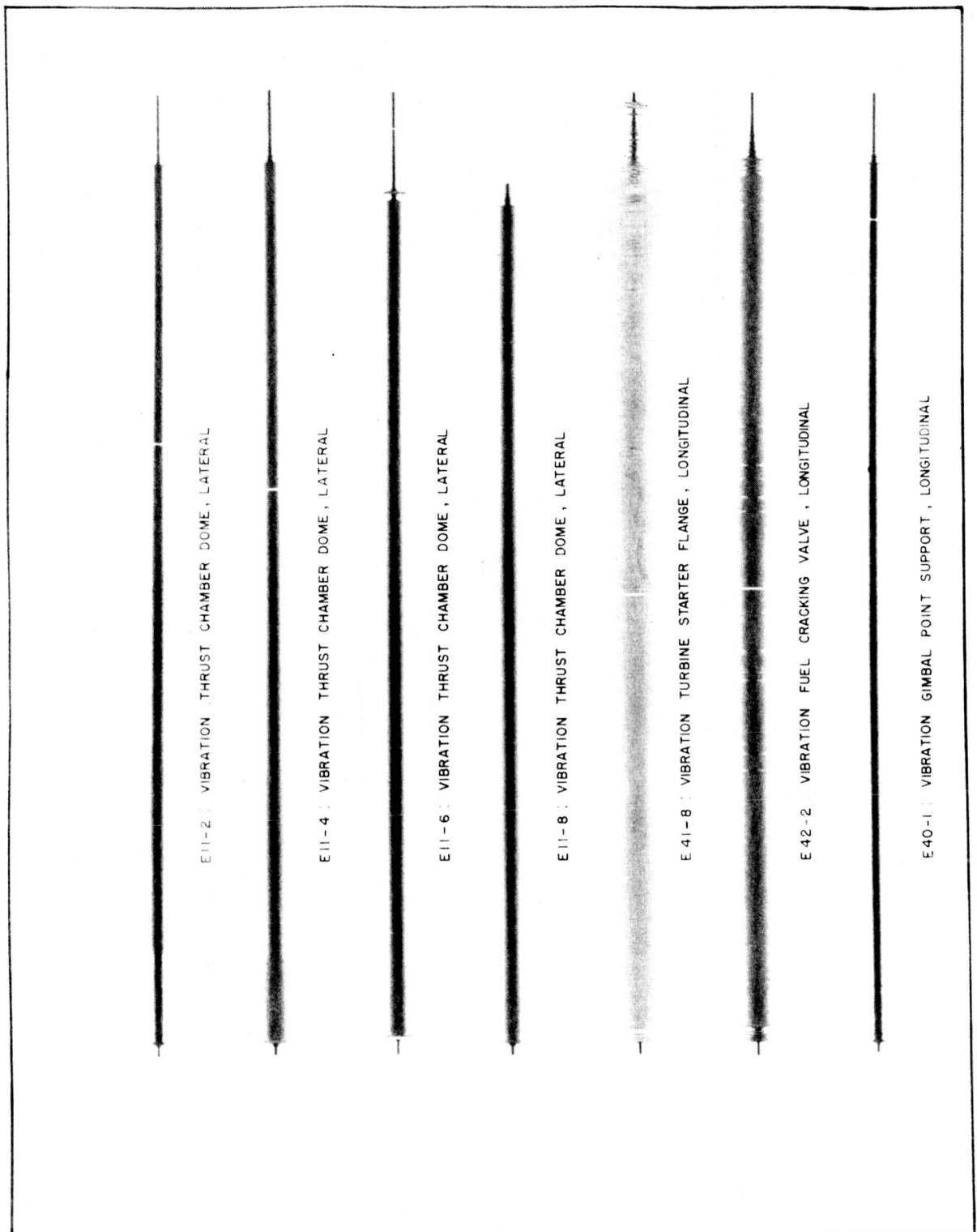


Figure 9-44 SA-2 Composite Vibration Traces

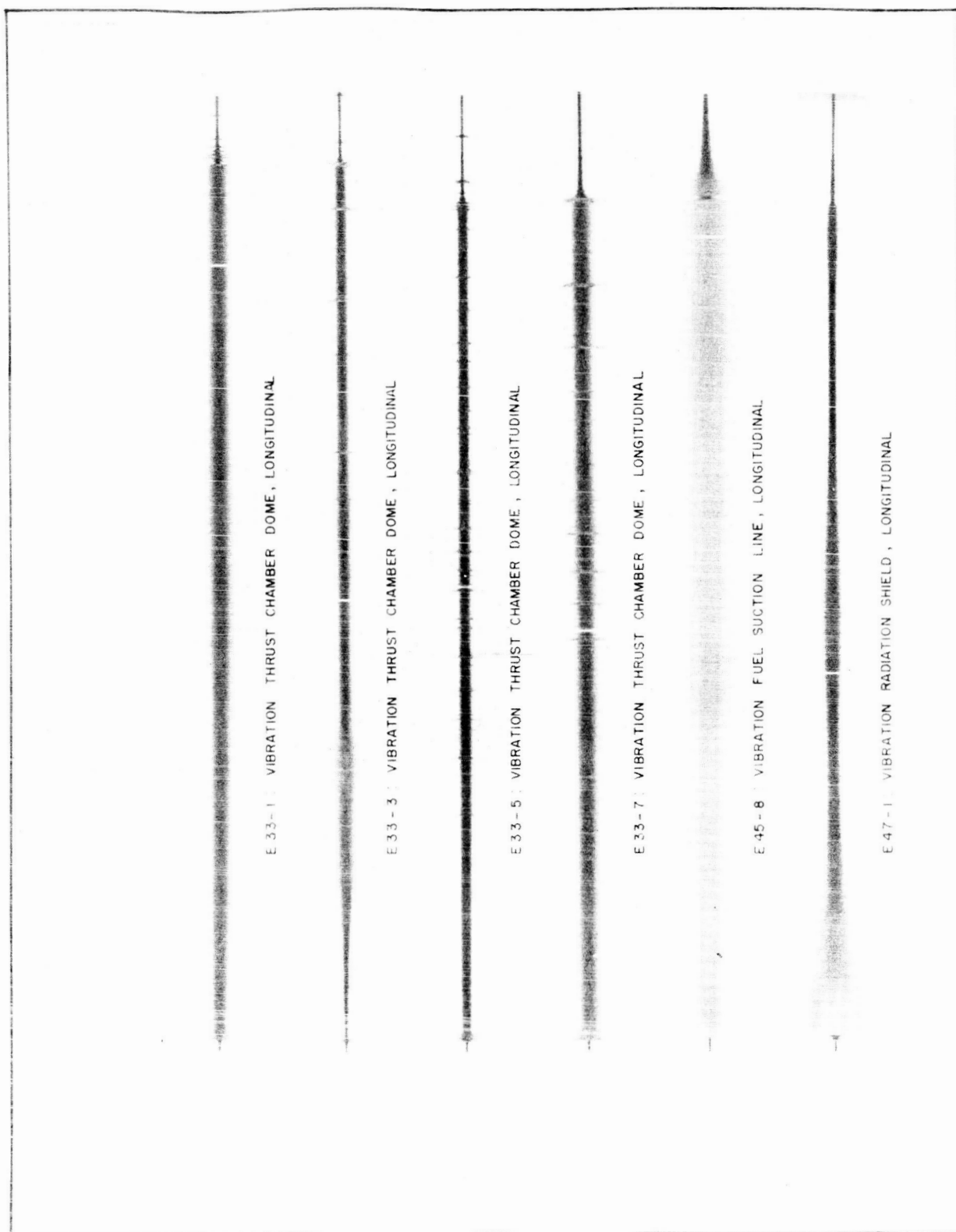


Figure 9-45 SA-2 Composite Vibration Traces

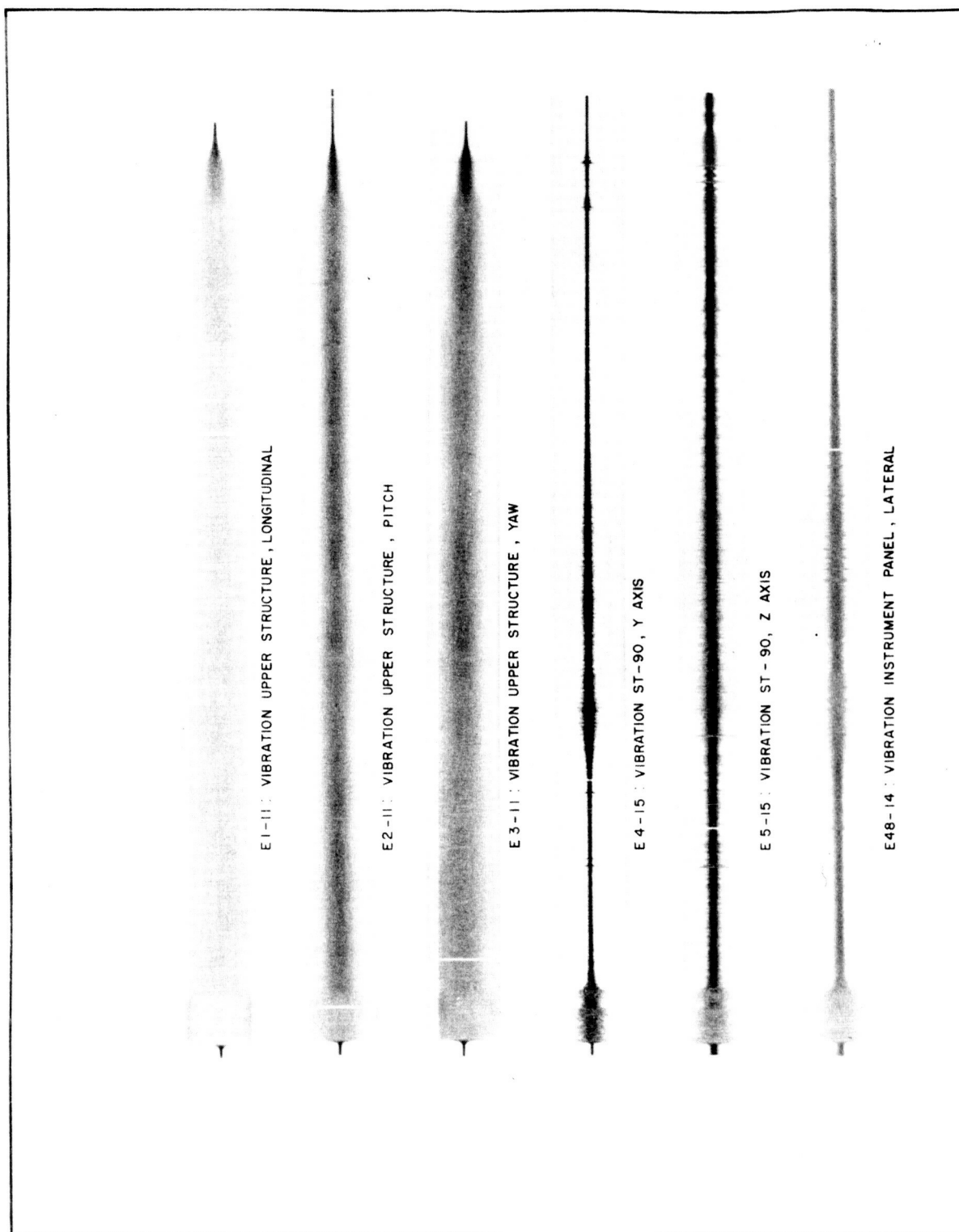


Figure 9-46 SA-2 Composite Vibration Traces

## 9.7 VEHICLE ACOUSTIC MEASUREMENT (FIGURE 9-47)

The SA-2 flight vehicle had one acoustic measurement, L40-20 which was a flush mounted microphone located on Fin position III at station 1200.

A time-history of the over-all sound pressure level in db, RE 0.0002 microbar, was made and the results are shown in Figure 9-47. This illustration describes in detail the variation in over-all sound pressure level versus range time.

The over-all level for on pad conditions was 152.0 db, and as the vehicle lifted off the launch pad, the level dropped rapidly to 136.8 db at 15 seconds. The over-all level then gradually began to increase until a peak of 150 db was reached at 46 seconds. At this time, the over-all level dropped suddenly to 145.8 db. Changes in local flow conditions and pressure fluctuation are believed to have caused this situation. Another peak level of 150.6 db was reached just before Max Q. The over-all level then gradually decreased for the duration of the flight.

In examining the 10 cps bandwidth analysis, on pad condition indicated that most of the energy was contained from 50 cps to 400 cps with a peak level at 200 cps. At 50 seconds the energy was shifted to a broad band spectrum from 50 cps to 1300 cps with approximately equal energy distribution throughout this band.

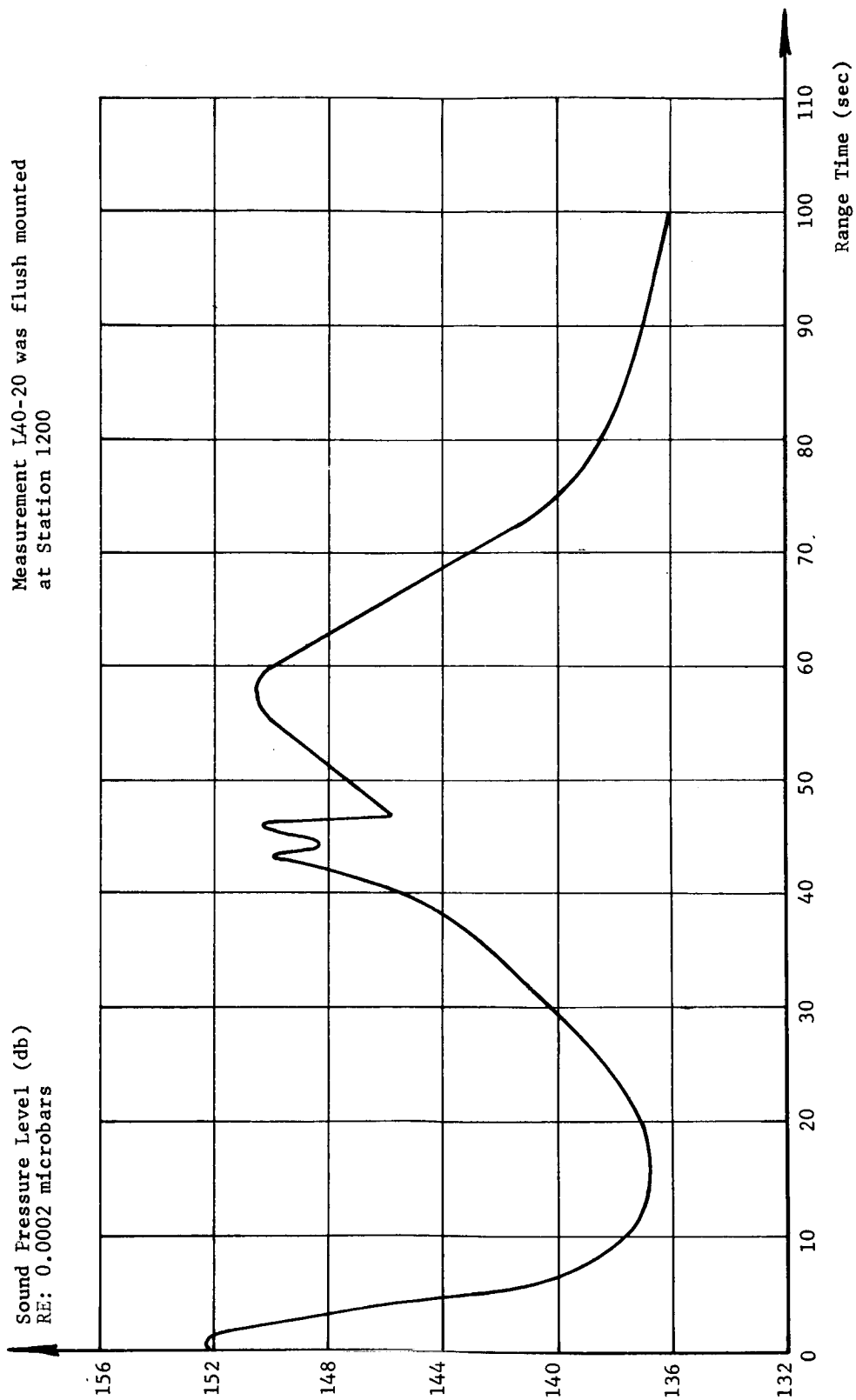


FIGURE 9-47 OVERALL SOUND PRESSURE LEVEL (FLIGHT)

## 9.8 ANALYSIS OF GROUND ACOUSTIC MEASUREMENTS

### 9.8.1 SUMMARY

Sound measurements made of the SA-2 vehicle were used to determine the dynamic environment created during launch. These measurements were made in a manner similar to those for SA-1; in the near-field, mid-field, and far-field; such that both specific environmental characteristics were known and general acoustic evaluations could be made. To obtain a better description of the noise within launch complex 34, additional measurements were made during the SA-2 launch.

The measurement records for this launch show two distinct phases with respect to time: (1) From the time the rocket engines reach full thrust (approximately  $T - 2$  seconds) until the booster is about one vehicle length above the pad (approximately  $T + 2$  seconds), the characteristics of the noise are relatively constant. Data during this time frame are referred to as representing "on pad" conditions. (2) After approximately  $T + 2$  seconds, the noise field is characterized by "in-flight" conditions where the data changes with time as the vehicle moves away from the measuring stations. The maximum sound level recorded during this second time frame is given as "launch maximum".

### 9.8.2 NEAR-FIELD DATA

Four measurements were made on the vehicle itself with the microphone signals transmitted to the blockhouse through trailing wires which were cut when the vehicle was approximately 38 m above the pad.

The results of the near-field acoustic measuring program are shown below compared with the SA-1 results. For SA-2, these values were recorded between ignition and approximately  $T + 4.5$  seconds within a hundred feet of the vehicle, giving an indication of the magnitude of the sound pressure at some critical points on the launch complex.

## NEAR-FIELD ACOUSTIC MEASUREMENTS

Microphone Location	Over-all Sound Pressure Level DB (Re: 0.0002 micro bars)			
Vehicle Environment Meas.	On Pad		Launch Max.	
	SA-1	SA-2	SA-1	SA-2
Umb. Pole, Sta. 860	148	143		145
Umb. Pole, Sta. 167	153	152		167
On Vehicle Meas.				
Outside Shroud, Sta. 167		153		156
Inside Shroud, Sta. 167		138		135
Outside Can. No. 13, Sta. 889		144		141
Inside Can. No. 13, Sta. 900		130		130
GSE Environmental Meas.				
Small Utility Room	113	108		
Large Utility Room	119	112		
Outside Control Building		133		139
Inside Control Building				110

## 9.8.3 MID-FIELD DATA

The mid-field data represents measurements ranging from .046 to .457 km from the launch site. The results obtained from these measurements are shown below. The maximum levels were measured at angles of 70 to 90 degrees from the deflected jet stream, and the lowest levels were measured nearest the jets. The static test environments indicated that the directivity of the maximum levels were 50 to 70 degrees from the jet stream.

## MID-FIELD ACOUSTIC DATA

Microphone Location	Over-all Sound Pressure Level DB (Re: 0.0002 Micro Bar)			
Meas. Made in a Plane .0018 km Above Pad Level	On Pad		Launch Max.	
	SA-1	SA-2	SA-1	SA-2
.046 km, AZ182°*	154	149		
.091 km, AZ182°		140		
.183 km, AZ 82°		141		138
.183 km, AZ102°		132		143
.183 km, AZ162°		130		140
.183 km, AZ182°		134		140
.183 km, AZ198°		139		145
.183 km, AZ122°	141	140	145	142
.183 km, AZ242°	143	144	141	142
.183 km, AZ262°		141		142
.183 km, AZ282°		134		142
.183 km, AZ302°		123		
Meas. Made 6 ft. Above Grade Level at Microphone Location				
.091 km, AZ182°		139		131
.183 km, AZ162°	129	135	141	148
.183 km, AZ198°	130	138	141	146
.366 km, AZ122°		117		136
.366 km, AZ142°		117		139
.366 km, AZ162°	123	122	132	137
.366 km, AZ182°	129	126	138	137
.366 km, AZ198°	130	128	135	139

## 9.8.4 FAR-FIELD DATA

To determine the variation of sound levels, frequency, spectral characteristics, and effects of meteorological conditions over the acoustic ray path; ten data collection points were established. These points were chosen to fall along three azimuths running through the major population centers of Brevard County as shown in Figure 9-48. Figure 9-49 shows the over-all sound pressure level for two of the far-field positions with respect to range time. The maximum over-all sound pressure levels measured at each far-field monitoring point are shown below compared to those values recorded for SA-1.

---

\*Flame path azimuth (132°)

## FAR-FIELD ACOUSTIC DATA

Over-all Sound Pressure Levels  
DB (Re: 0.0002 Micro Bar)

Station	Range (km)	SA-1	SA-2
A	26.4	94	100
B	10.3	102	109
C	1.52	122	126
D	4.50	122	122
E	15.77	102	107
F	22.04	93	103
G	24.26	86	100
H	9.02	84	121
I	21.72	-	102
J	16.55	105	105

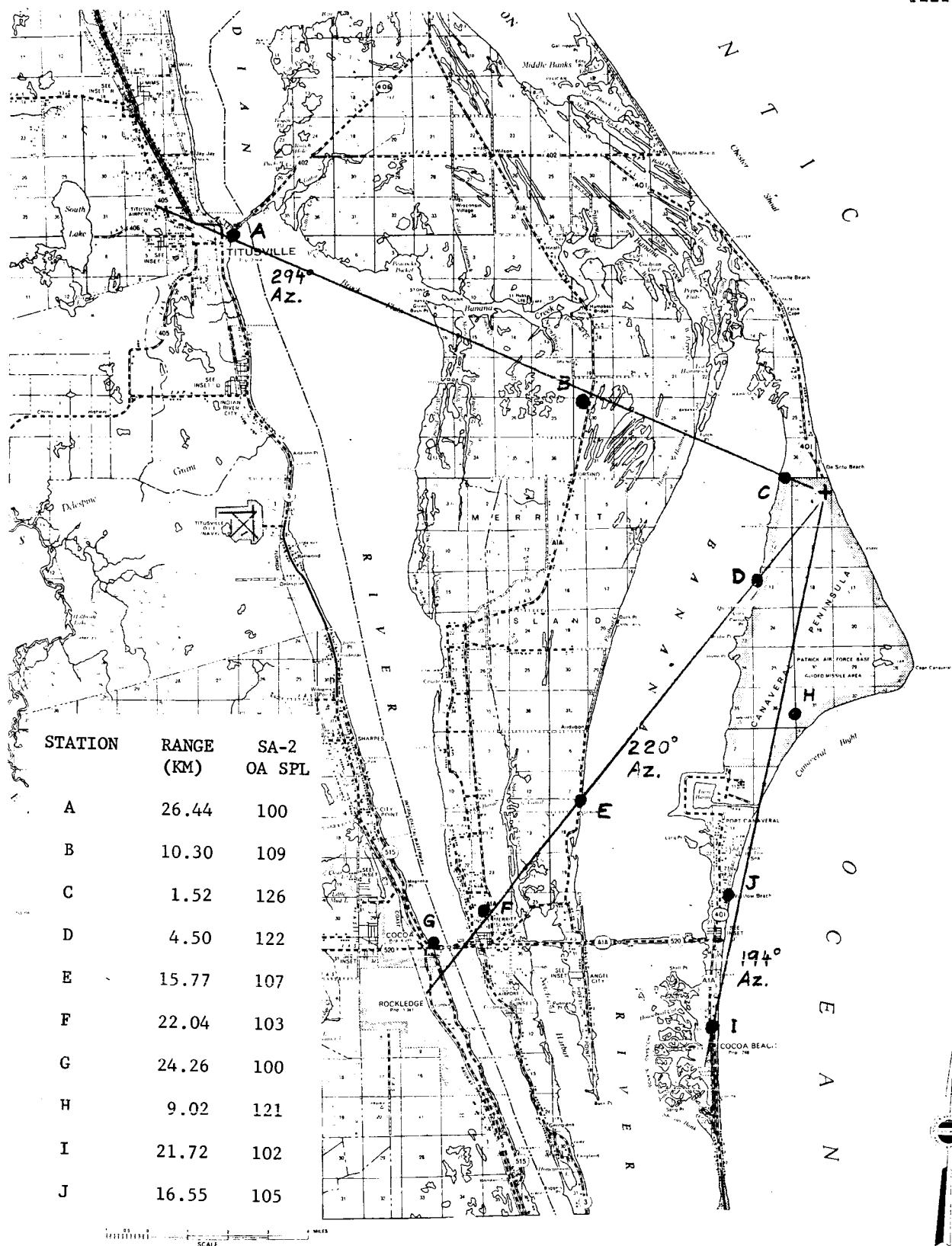


Figure 9-48 FAR FIELD ACOUSTIC MEASURING POINTS MPR-SAT-WF-62-5

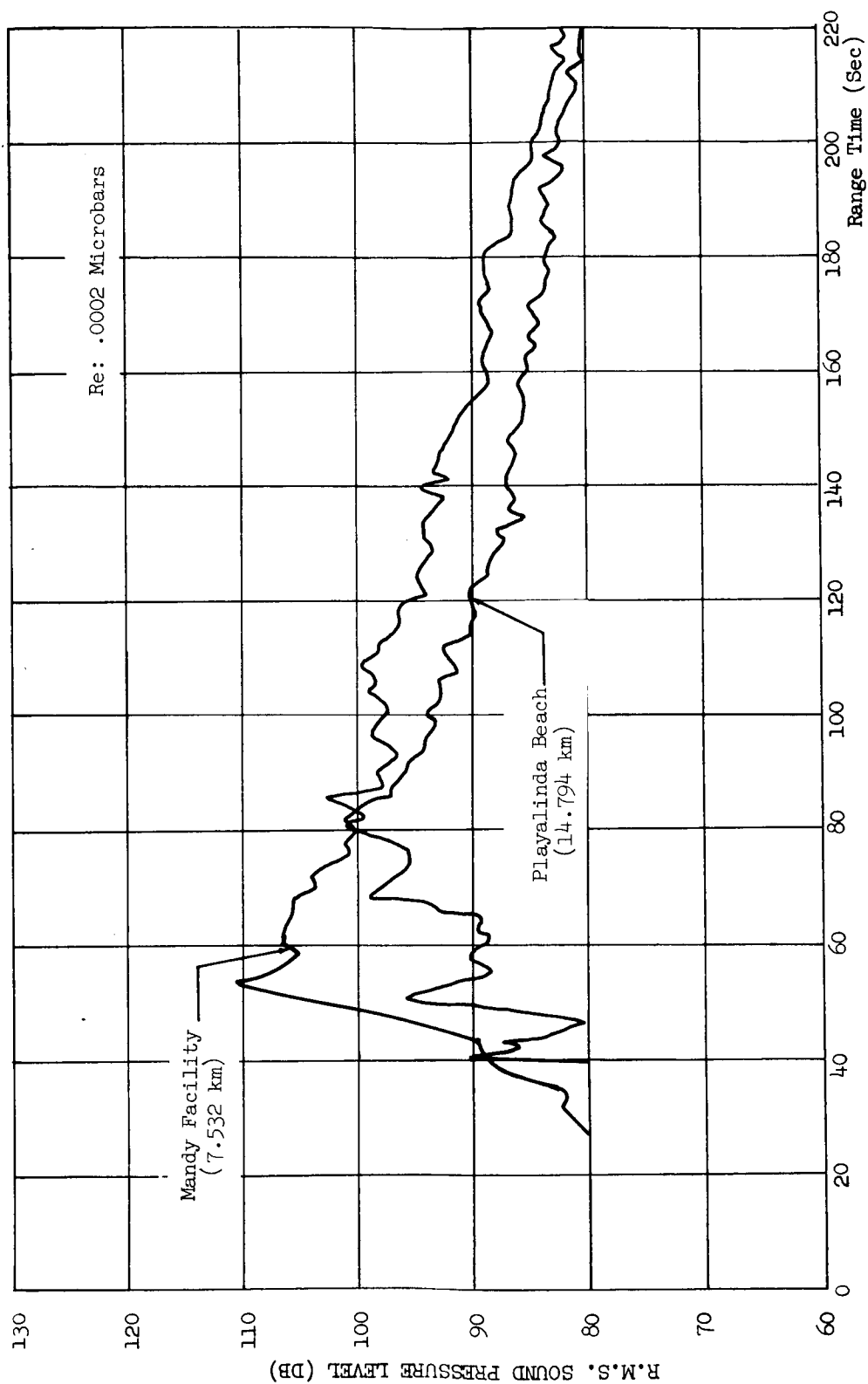


Figure 9-49 OVERALL R.M.S. SOUND PRESSURE LEVEL

## 10.0 (U) ENVIRONMENTAL TEMPERATURES AND PRESSURES

### 10.1 SUMMARY

The thermal environment of SA-2 was quite similar to that encountered by the SA-1 vehicle. Total heat flux to both the heat shield and the flame shield was in good agreement with that measured on the SA-1 flight. The heat shield and flame shield thermal insulation scheme for the SA-1 and SA-2 vehicles was the same, and measurements made forward of the heat shield indicate that the insulating material is more than adequate. No fires or other abnormal heat sources occurred in the engine compartment.

Base pressures measured on the SA-1 and SA-2 vehicles are in good agreement. Any differences between the SA-1 and SA-2 results can be considered within the accuracy of the telemetered data.

Instrument canister pressures were maintained between 10 and 17 psia during flight by controlling the vent rate of the gases. An auxiliary pressurization system, to provide GN<sub>2</sub> from the fuel high pressure spheres if the canister pressure dropped to 12 psia, was not required during the SA-2 flight. Temperatures in the canisters were all within an acceptable range (50 to 104° F) during both prelaunch and the flight. Temperature of the ST-90 ambient air was 73° F at liftoff which was slightly out of tolerance (77 ± 3.6° F).

### 10.2 TAIL SECTION

#### 10.2.1 ENGINE COMPARTMENT

The engine compartment experienced no extreme temperature environment during the flight. Ambient air temperature within each engine area was measured with gas thermocouples, and no temperatures above 65° F or below -45° F were experienced. However, as noted on SA-1 some of these measurements showed a gradual temperature drop after 90 seconds flight time (see Figure 10-1).

Nine thermocouples measured bulk temperatures of various structural members within the engine compartment (Figure 10-2). All of these measurements were within a range of +50 to -35° F with the exception of the tail shroud temperature measurement C60-2, which rose to 145° F at OECO. The rise in temperature of the tail shroud was due to aerodynamic heating.

Thirty-two thermocouples were located on the firewall to indicate the existence of fires in one or more engine areas prior to liftoff.

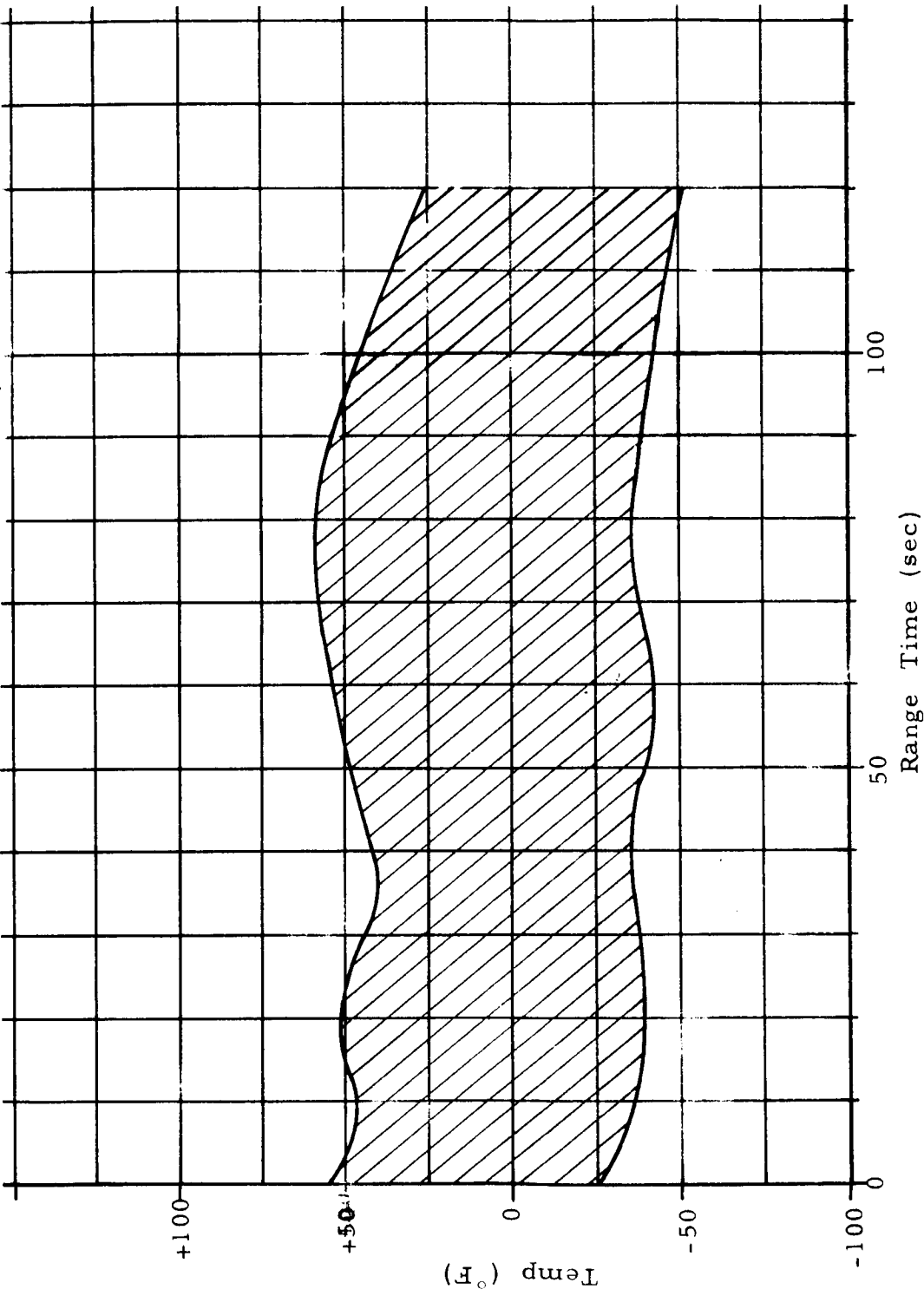


FIGURE 10-1 RANGE OF AMBIENT AIR TEMPERATURE  
IN ENGINE COMPARTMENTS

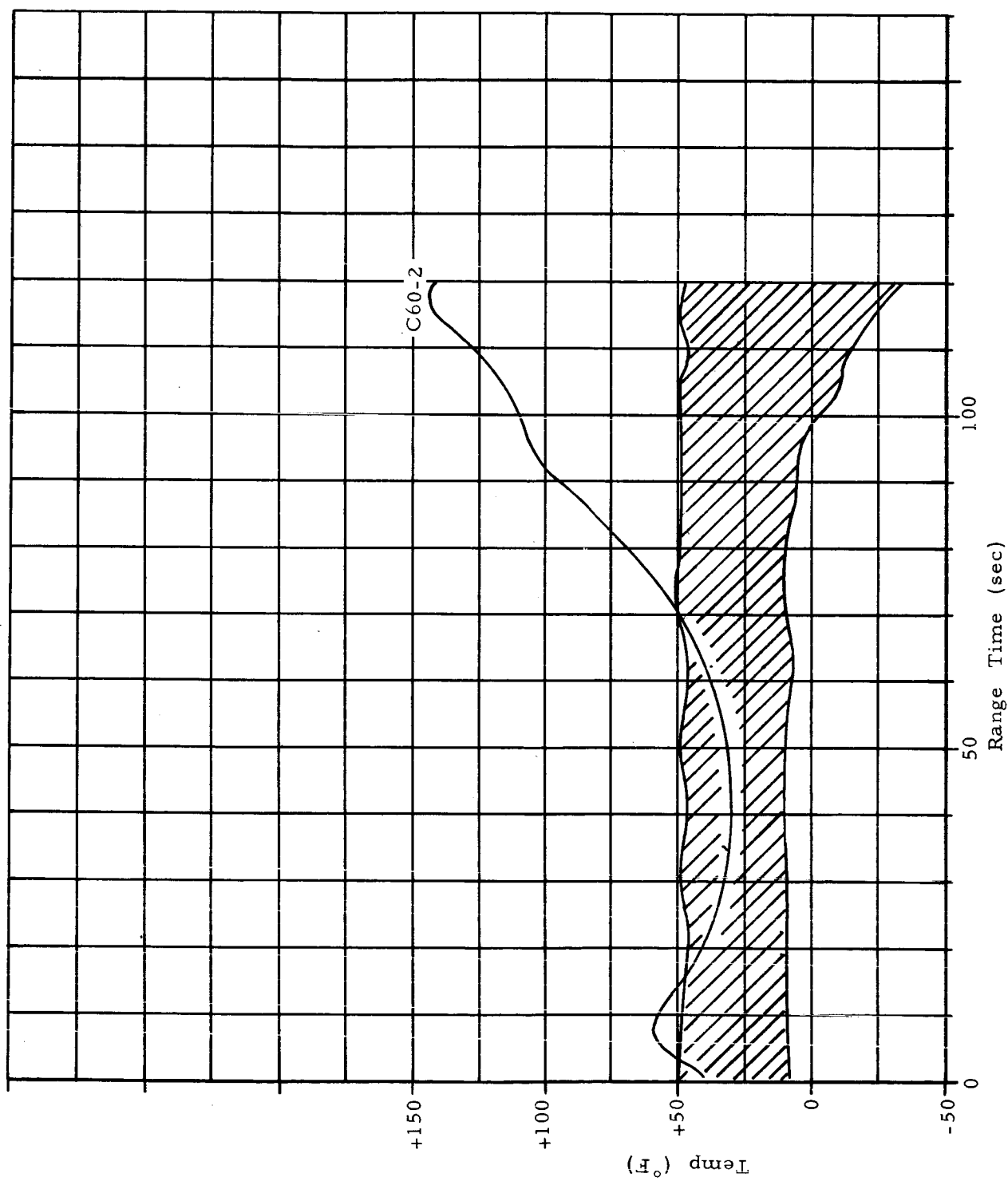


FIGURE 10-2 BULK TEMPERATURE OF STRUCTURAL MEMBERS IN ENGINE COMPARTMENT

This system consisted of four circuits of eight thermocouples each with each thermocouple wired in series within the circuit. The thermocouples were monitored in the blockhouse prior to liftoff and would have given cutoff if any excessive rise in temperature had occurred.

One measurement was mounted above the firewall to monitor air temperature near the thrust frame. The ambient temperature in this area was between 0 and -25° F throughout flight.

Locations of temperature measurements in the engine compartment are shown in Figure 10-3.

#### 10.2.2 BASE ENVIRONMENT

Base pressure was measured on the SA-2 base by four measurements (D25-4, D25-7, D38-4 and D38-7). Three of these measurements, D25-4, D25-7 and D38-4, were located on the heat shield at Station 54 while measurement D38-7 was mounted on the flame shield between the four inboard engines and sensed the ambient pressure aft of the flame shield. This measurement (D38-7) was located 3.5 inches from the vehicle centerline toward Fin position I. Measurement D25-4 was located 62 inches from the centerline, 30 degrees off Fin position IV toward I. Measurement D25-7 was located 66 inches from the vehicle centerline, 2 degrees from Fin position III toward IV. Measurement D38-4 was located 140 inches from the centerline, 45 degrees between Fin positions I and IV. A schematic showing the locations of both the pressure and the temperature instrumentation is shown in Figure 10-4.

Three total heating calorimeters (measurements C76-3, C63-1, and C77-5) were mounted on and in the vicinity of the heat shield to measure the base heating in this area. In addition, shielded and unshielded gas temperature probes (measurements C10-2, C10-4, C10-7, C65-3, and C93-7) measured the temperature of the circulating gas in the vicinity of the heat shield (see Figure 10-4). Temperature measurements on the flame shield included a total calorimeter, measurement C78-8 and a gas temperature probe, measurement C67-7. These measurements were mounted on the flame shield to measure the incoming flame thermal radiation and hot exhaust gas convective heating.

Six base temperature measurements (C79-2, C65-3, C76-3, C93-7, C64-4, and C77-5) were mounted at a stand off distance of nine inches on both the SA-1 and the SA-2 vehicles.

It should be noted that the three shielded temperature measurements, C10-2, C10-4 and C10-7, (see Figure 10-5) are expected to indicate the same temperature levels as the unshielded measurements. This is due

# SATURN VEHICLE SA-2

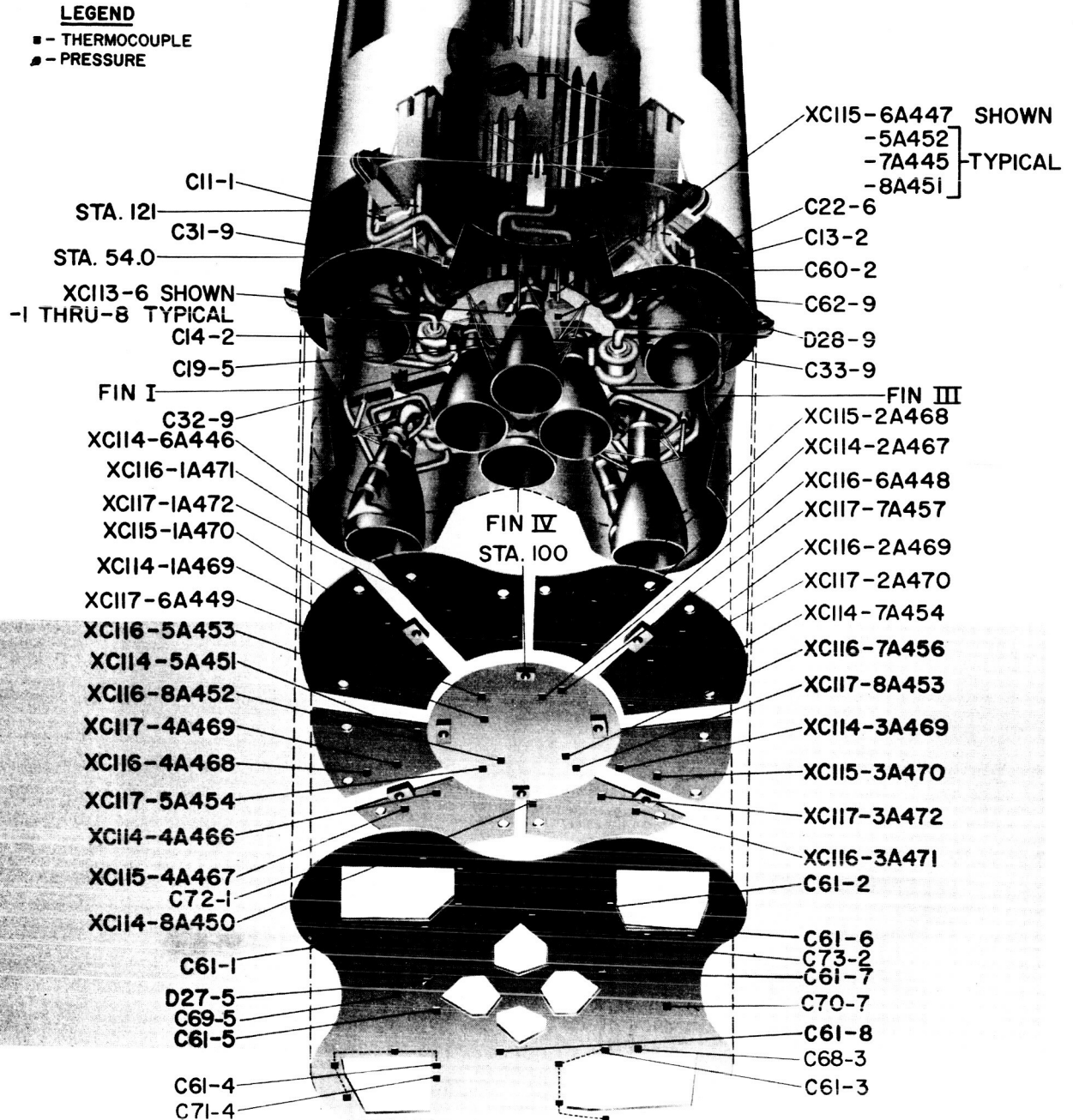


FIGURE 10-3 S-I STAGE FLIGHT MEASUREMENTS

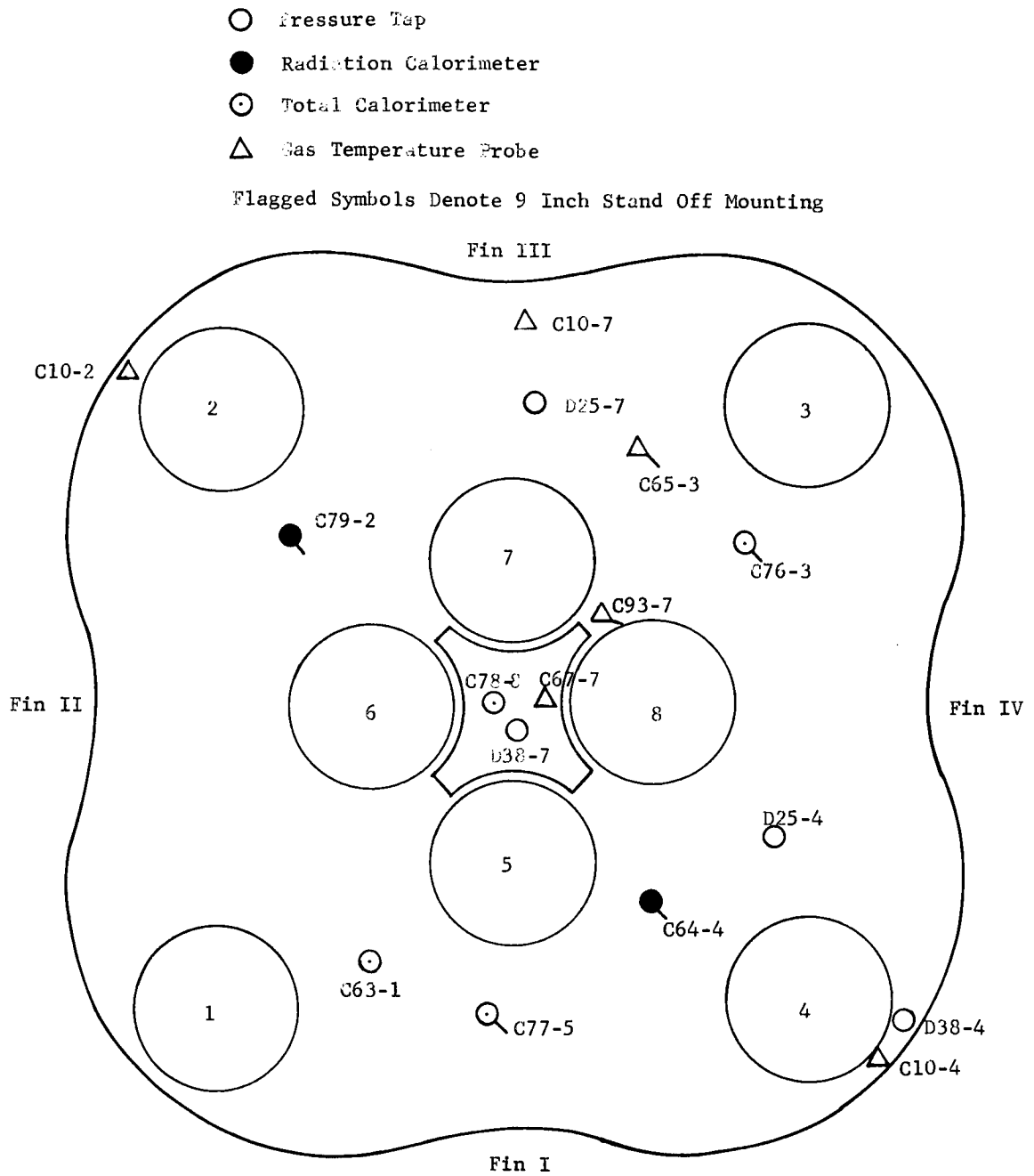


FIGURE 10-4 HEAT SHIELD INSTRUMENTATION LOCATION FOR SATURN SA-2 FLIGHT TEST

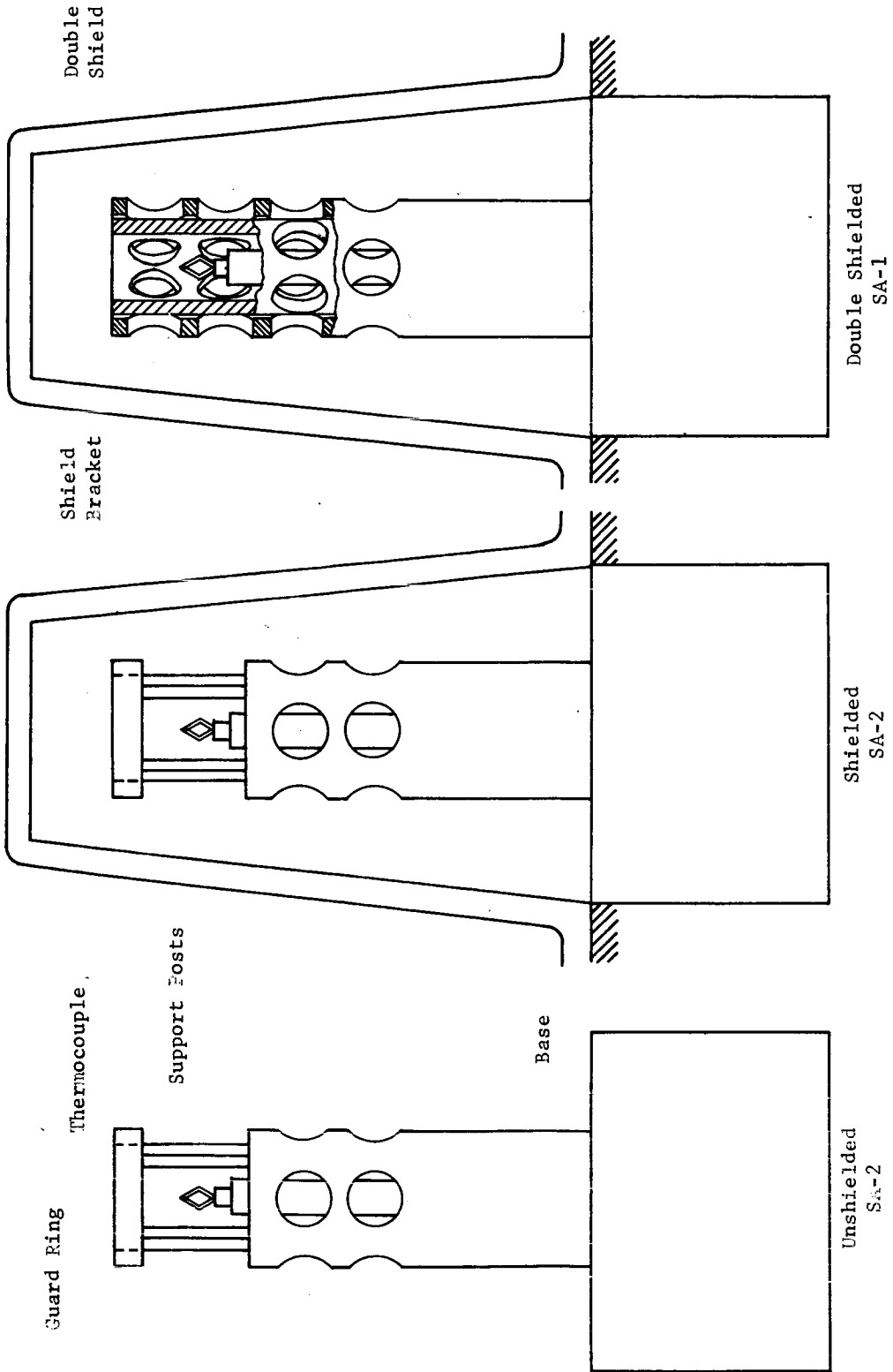


FIGURE 10-5 GAS TEMPERATURE PROBES FOR SA-1 AND SA-2

to the fact that the shields were fabricated of a  $1\frac{1}{4}$  inch, U-shaped, sheet metal bracket and the thermocouple wire used was platinum rhodium which has a high reflectivity. Therefore, the values indicated by these measurements are expected to fall within the  $\pm 5\%$  accuracy level assigned to the temperature levels and not be influenced by the presence of the bracket.

The thermocouples on the cold side (forward side) of the heat shield were C68-3, C69-5, C70-7, C71-4, C72-1, and C73-2 (see Figure 10-3). Two thermocouples (C20-5 and C21-5) were used to measure structural temperature of the back side of the flame shield and the flame shield struts (see Figure 10-6).

### Base Pressures

Base pressure instrumentation identical to that flown on SA-1 was also flown on SA-2. Telemetered base pressures were converted to the form base-minus-ambient-pressure and plotted versus time in Figure 10-7. All three measurements on the heat shield (D25-4, D25-7 and D38-4) were consistent throughout the powered phase of the flight. At approximately 53 seconds of flight all three heat shield readings reached the largest deviation from ambient pressure,  $P_b - P_a$  being equal to approximately -0.6 psia.

The largest magnitude of  $P_b - P_a$  occurred in the center star region where extreme values ranged from -3.4 psia at 35 seconds to 2.5 psia at 105 seconds. A sharp decrease in the base pressure occurred at the time of inboard engine cutoff (111.29 seconds) as expected.

The individual readings were compared to those obtained from SA-1 data (shown as solid dots on all figures). Although data from measurements D25-7 and D38-4 individually displayed the same trend as SA-1 readings, measurement D25-4, located between the inboard and outboard engines, showed a deviation from SA-1 results. SA-2 data indicates a minimum value of approximately -0.5 psia at 55 seconds while SA-1 had a positive reading of about +0.5 psia at the same period of flight. Since the two curves appear to be almost identical except for polarity, the calculations were re-checked for a possible error. As no error was found, it must therefore be concluded at this time that this discrepancy is simply due to telemetry and/or measurement error. When compared to SA-1 data, SA-2 base pressures appear to be much closer to expected values since they indicate a more uniform pressure distribution across the heat shield. No significant angle of attack effects on the base pressure distribution as suggested in the SA-1 Flight Evaluation Report were indicated by the SA-2 data. Any differences between SA-1 and SA-2 results can apparently be considered within the accuracy of the telemetered data.

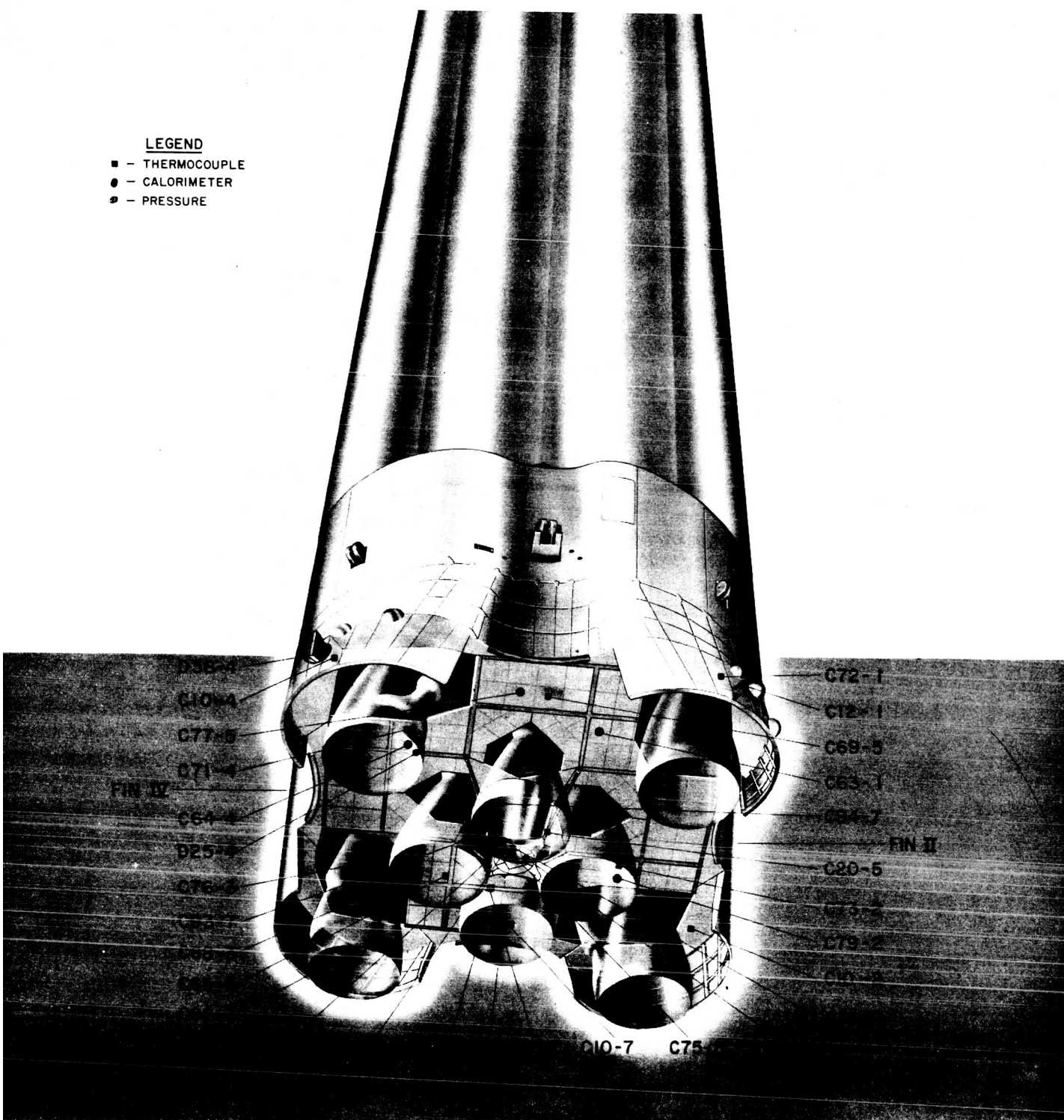


FIGURE 10-6 S-1 STAGE FLIGHT MEASUREMENTS

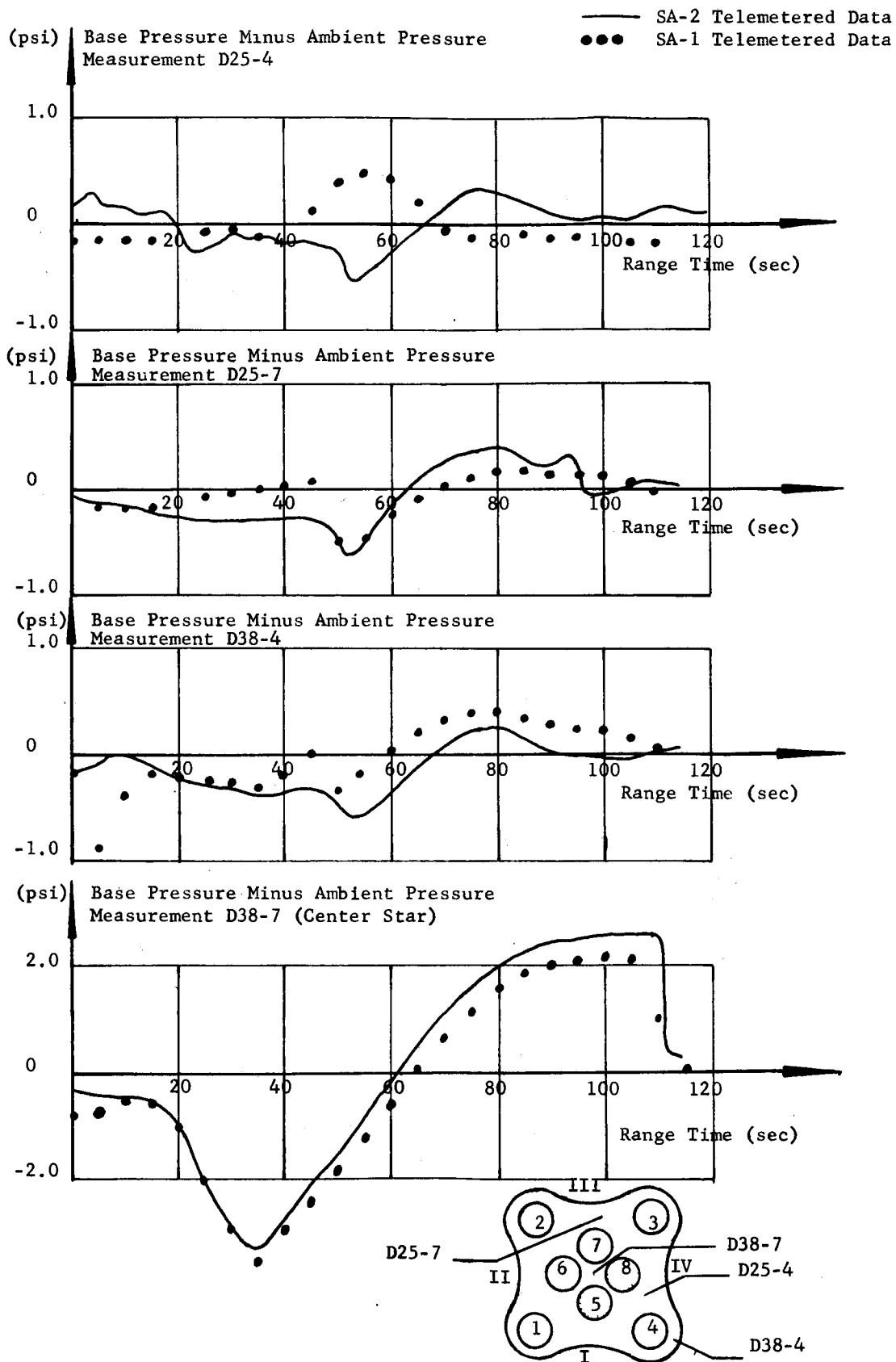


Fig. 10-7 BASE PRESSURE MINUS AMBIENT PRESSURE VERSUS TIME

Average values of base to ambient pressure ratio,  $P_b/P_a$ , on the heat shield are plotted versus Mach number in Figure 10-8 and compared to SA-1 results. Wind tunnel test data from the Rocket Test Facility, AEDC, are also shown in the figure. Also plotted versus Mach number are values of  $P_b/P_a$  from the flame shield (center star), measurement D38-7. Flight test results have an error band based on a possible 2% error on base pressure measurements ( $\pm 0.4$  psia). An average base pressure coefficient was also computed from heat shield base pressure measurements (see Figure 10-9) and similar comparisons were made. Results showed good agreement in all cases.

The pressure difference between the flame shield measurement D38-7 and the heat shield measurement D25-4 located nearest the flame shield reached a maximum pressure differential of -2.9 psi at approximately 35 seconds (Figure 10-10). The pumping effect created by the inboard engines at the lower altitudes accounts for the flame shield pressure being lower than the base pressure. After 60 seconds of flight the exhaust gases from flow reversal toward the flame shield causes the flame shield pressure to decrease at a slower rate than does the base pressure. At approximately 78 seconds corresponding to an altitude of 20 km these reversed gases become choked, and the flame shield pressure remains constant until inboard engine cutoff. Choking flow occurred roughly at the same time and altitude as in SA-1, and this figure is in general agreement with AEDC wind tunnel data.

Included in Figure 10-10 are the differences between the individual base pressure measurements and the lower compartment pressure measurements. The maximum pressure load on the heat shield is approximately 1.0 psi on the area encompassed by measurement D25-4 and occurs at 55 seconds of flight.

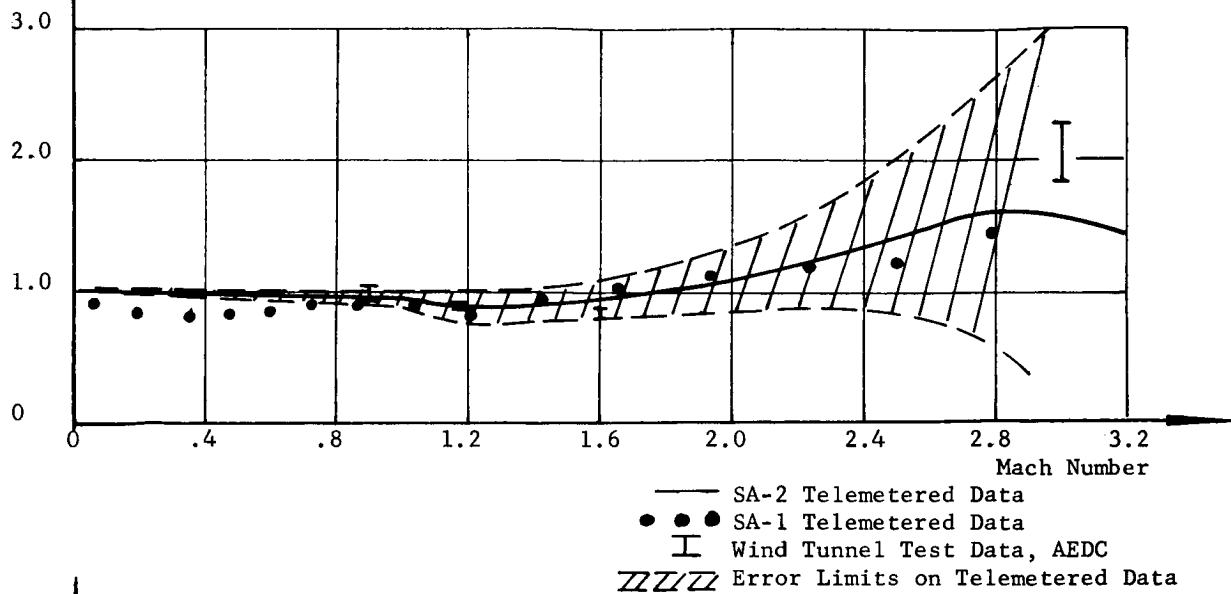
Figure 10-11 shows the differential pressure between the upper and lower compartment indicating the pressure load on the fire wall. Very little pressure differential existed between the two compartments on SA-1; however, a maximum load of 0.9 psi is indicated on the SA-2 flight.

Figure 10-11 also presents individually the upper and lower compartment pressure measurements minus the ambient pressure. The pressure differential trend appears to be the same on SA-1 and SA-2 with the exception of the upper compartment pressure differential which was considerably lower in SA-2.

#### Base Temperatures

Temperatures on the base of the SA-2 vehicle were measured by a series of shielded and unshielded thermocouples (see Figure 10-5). The locations of the thermocouples and the total and radiative calorimeters

Pb/Pa Average on Heat Shield  
(D25-4, D25-7, D38-4)



Pb/Pa On Flame Shield (D38-7)

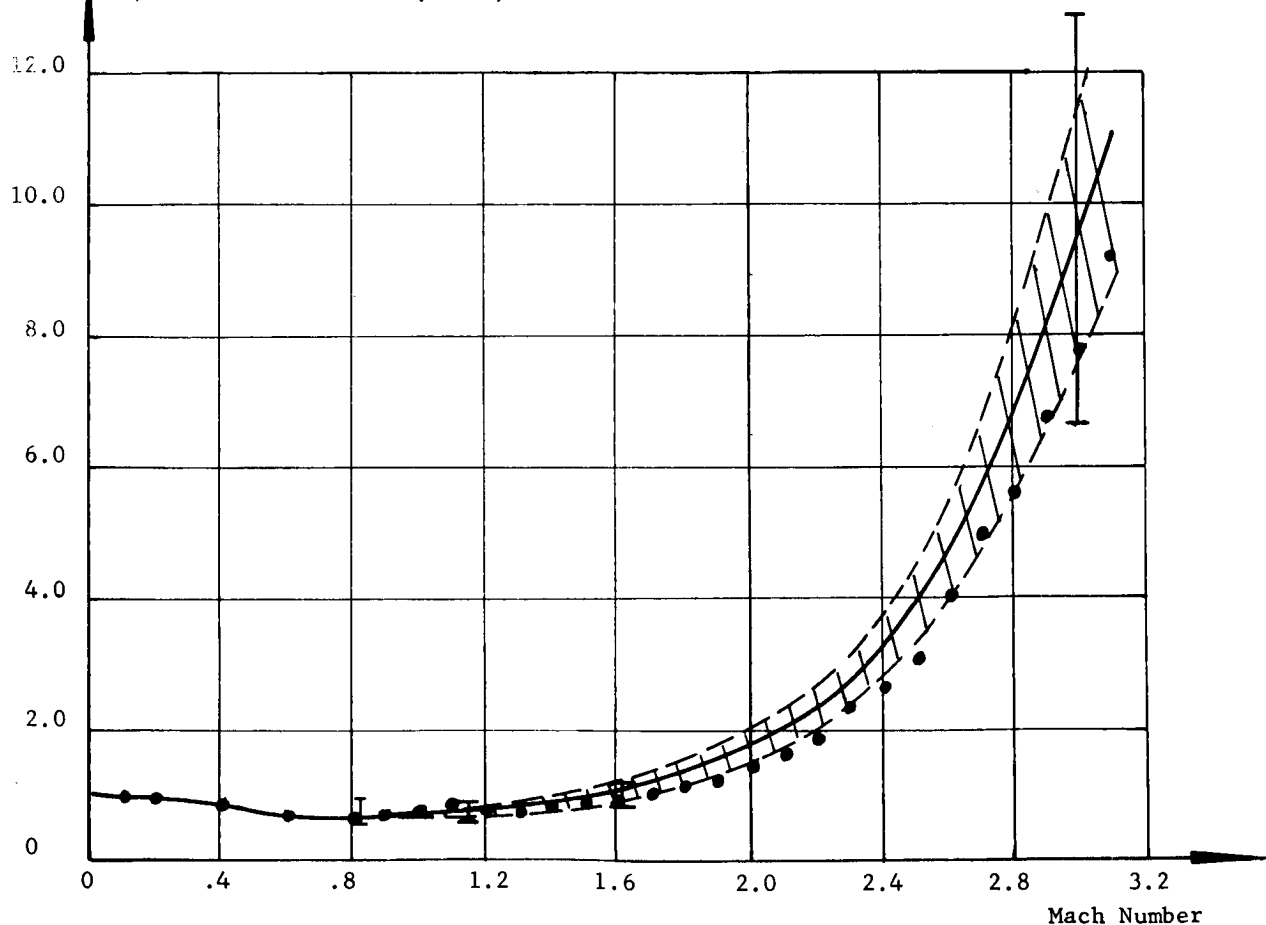


FIGURE 10-8 RATIOS OF BASE PRESSURE TO AMBIENT PRESSURE VERSUS MACH NUMBER

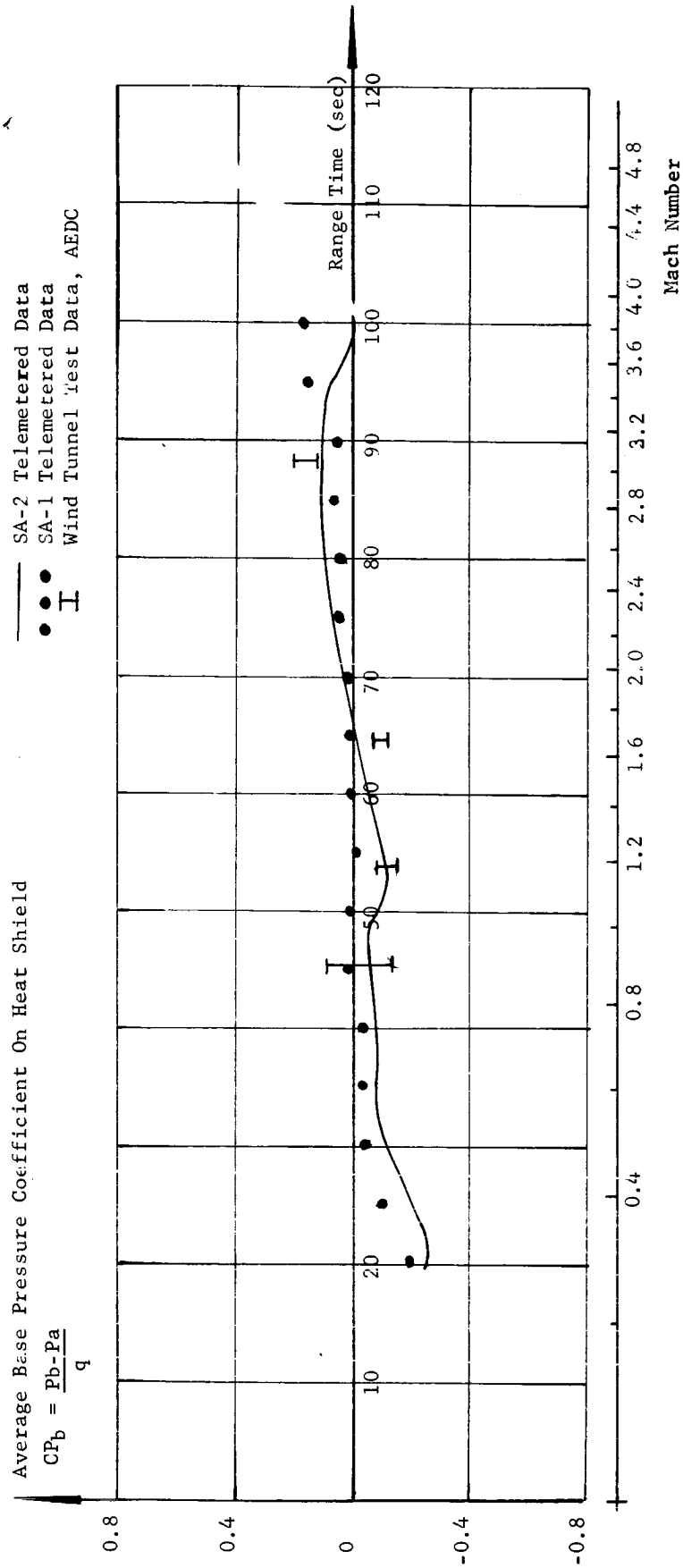


FIGURE 10-9 BASE PRESSURE COEFFICIENT VERSUS TIME

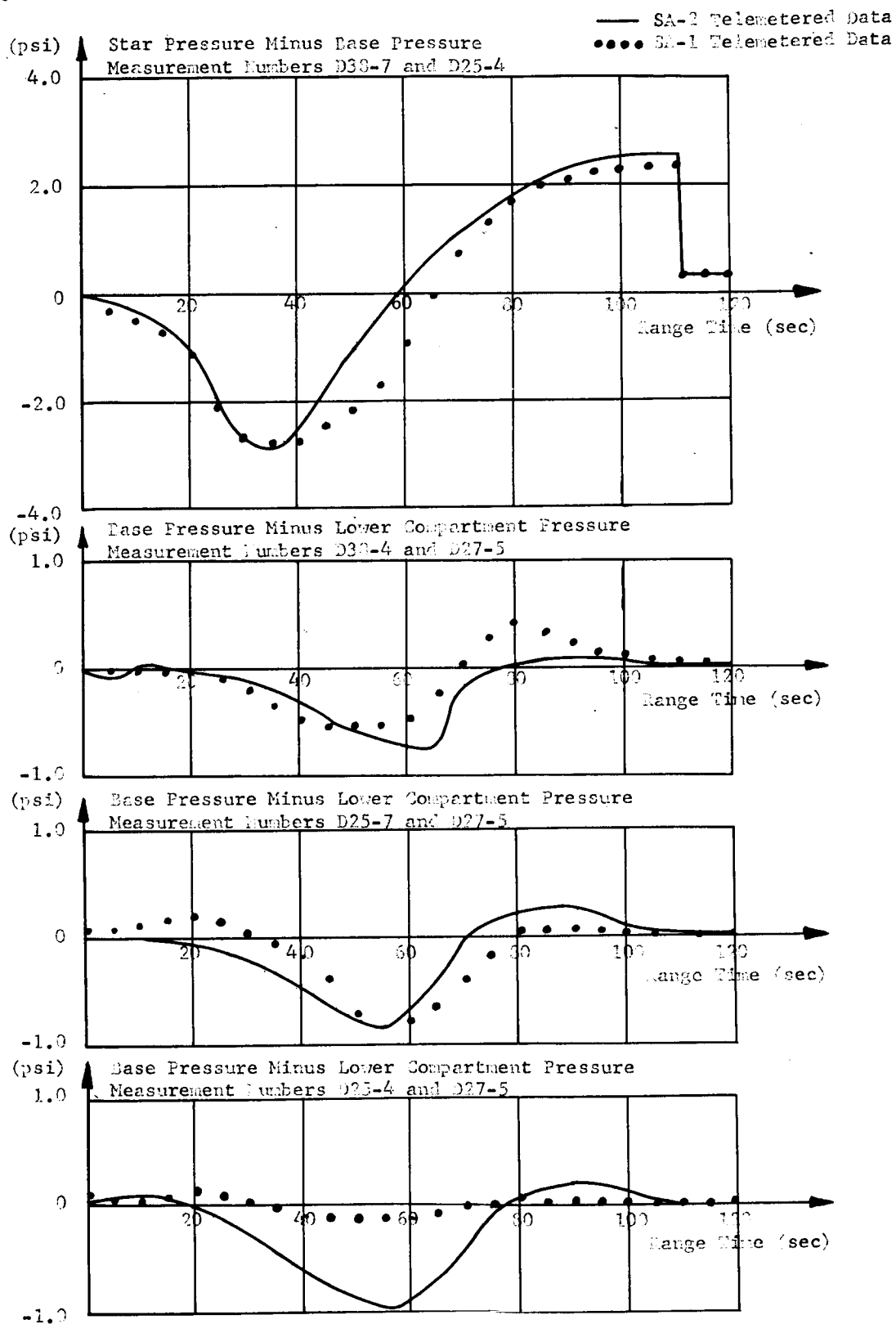


FIGURE 10-10 STAR AND BASE PRESSURE MINUS LOWER COMPARTMENT PRESSURE

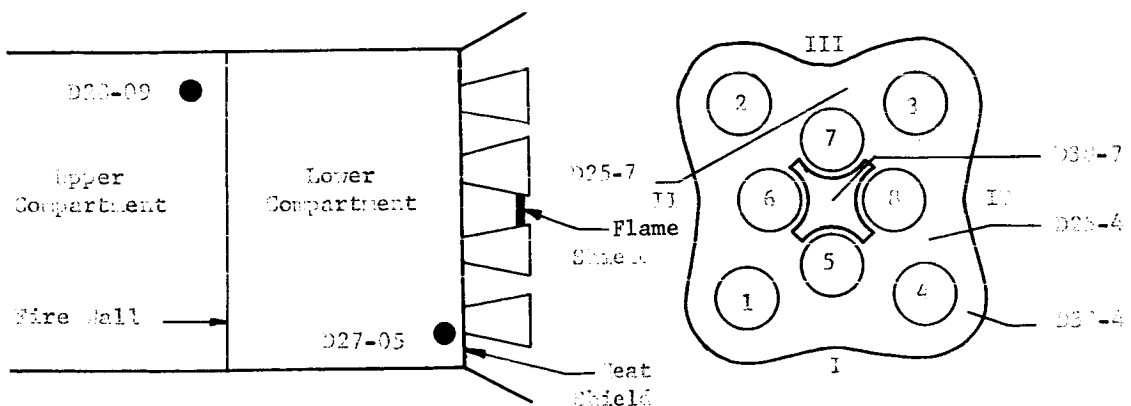
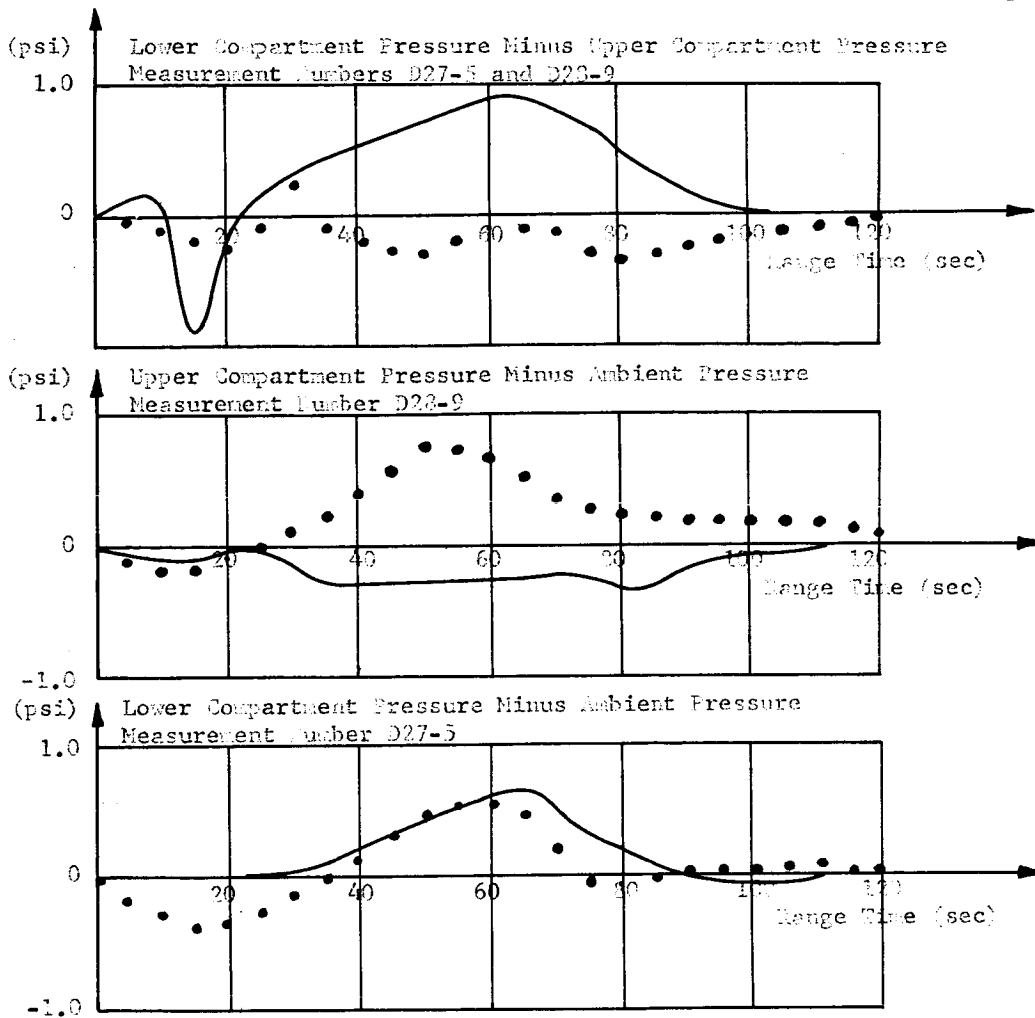


FIGURE 10-11 COMPARTMENT PRESSURE DIFFERENCES

are shown in the sketch of the vehicle base (see Figure 10-4). Flagged symbols on the sketch indicate that the measurement was mounted nine inches aft of the heat shield. Temperatures measured on the SA-2 vehicle base are more representative of the environment than those measured on the SA-1 flight as the temperature probes used on the SA-1 vehicle (see Figure 10-5) were enclosed in a double walled radiation shield which resulted in a slower measurement response. Consequently, a correction factor was required to determine the approximate temperature on the SA-1 vehicle at any given time.

In comparing the gas temperature measurements, C65-3, for SA-1 and SA-2 (Figure 10-12) it is seen that reasonably good agreement was obtained; however, the measurement on SA-2 did show a maximum temperature of 2100° F at approximately 85 seconds flight time, which is slightly higher than the SA-1 corrected measurement. Gas temperature, C93-7, (Figure 10-13) indicated a maximum value of 1400° F on the SA-2 flight which was approximately 350° F higher than was indicated on the SA-1 flight. Figure 10-14 shows a comparison of gas temperature measurements, C10-2, C10-4, C10-7, and C65-3. The measurements near the shroud scoops, C10-2 and C10-4, are lower due to the flushing action of the scoops. The temperatures are normal except for a rapid increase in temperature for measurement C10-2 to 1200° F at about 25 seconds which was unexpected. Temperatures near the valley flow deflector, measurements C10-7 and C65-3, are somewhat higher than those near the shroud scoops since the area is not as well flushed. With the exception of measurement C10-2, the temperature data show a general increase in temperature to approximately 80 seconds where maximum temperatures appear to occur. Further increase in time and altitude bring about an over-all decrease in temperature to IECO. IECO is clearly defined in these data by a sharp drop in the temperature level.

Shown in Figure 10-15 is the gas temperature measurement, C67-7, which was located on the flame shield. This gas temperature probe extended approximately three inches above the surface of the flame shield. The maximum temperature measured by this probe was 3280° F at approximately 50 seconds of flight. After 65 seconds this gas temperature probe measured 2700° F. Gas temperatures of the order of  $\frac{1}{2}$  to  $\frac{1}{3}$  of combustion chamber temperatures are to be expected in the region of choked flow and the temperature level observed on the flame shield falls within this limit agreeing with model test results.

#### Heating Rates

Four total heat sensing calorimeters, measurements C78-8, C76-3, C63-1 and C77-5, were located on the SA-2 vehicle base (see Figure 10-4). Data measured by these calorimeters were evaluated by two independent groups using different techniques. The solid and the dashed curves in

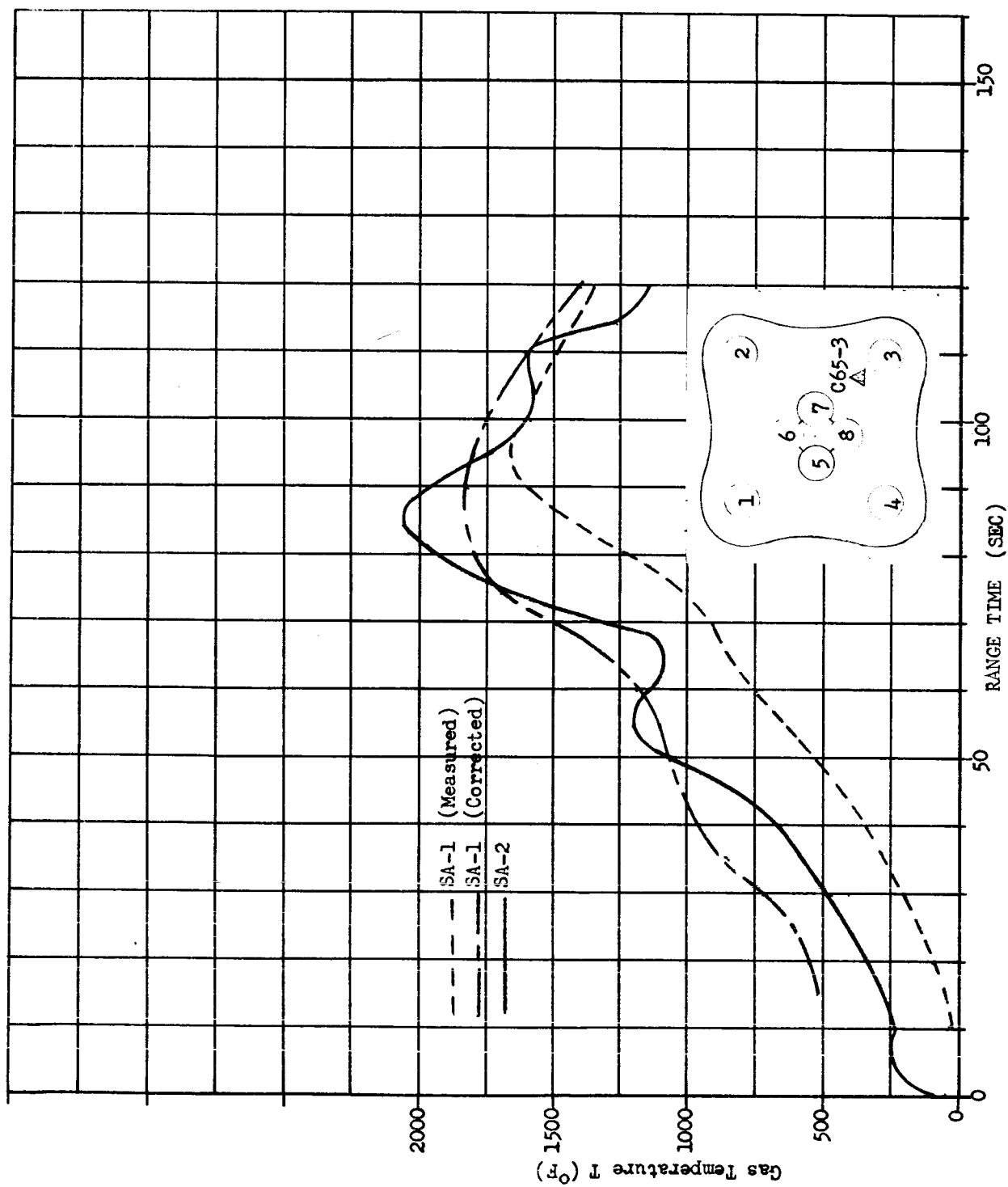


FIGURE 10-12 GAS TEMPERATURE MEASURED 3 INCHES BELOW HEAT SHIELD

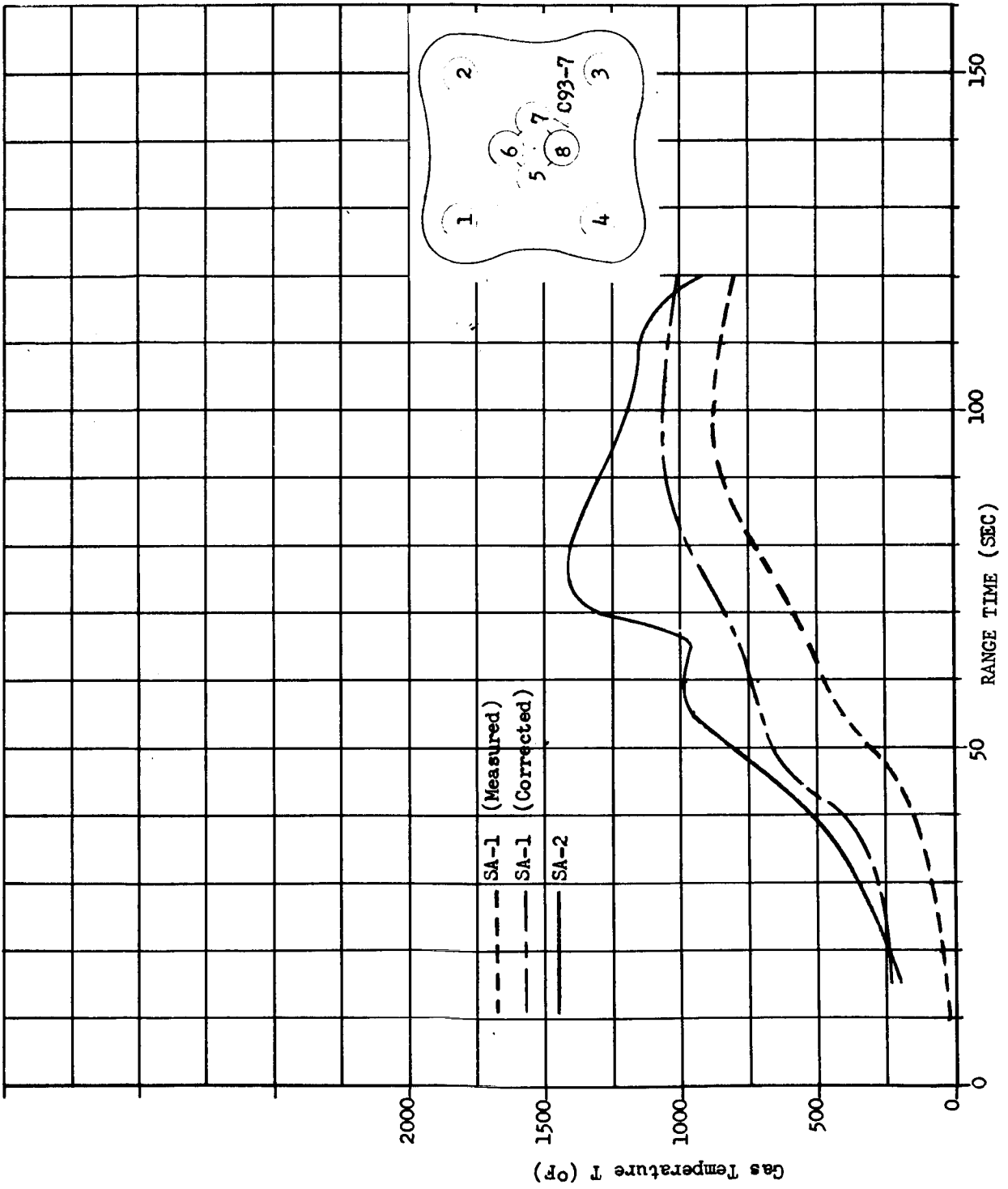


FIGURE 10-13 GAS TEMPERATURE MEASURED 3 INCHES BELOW HEAT SHIELD

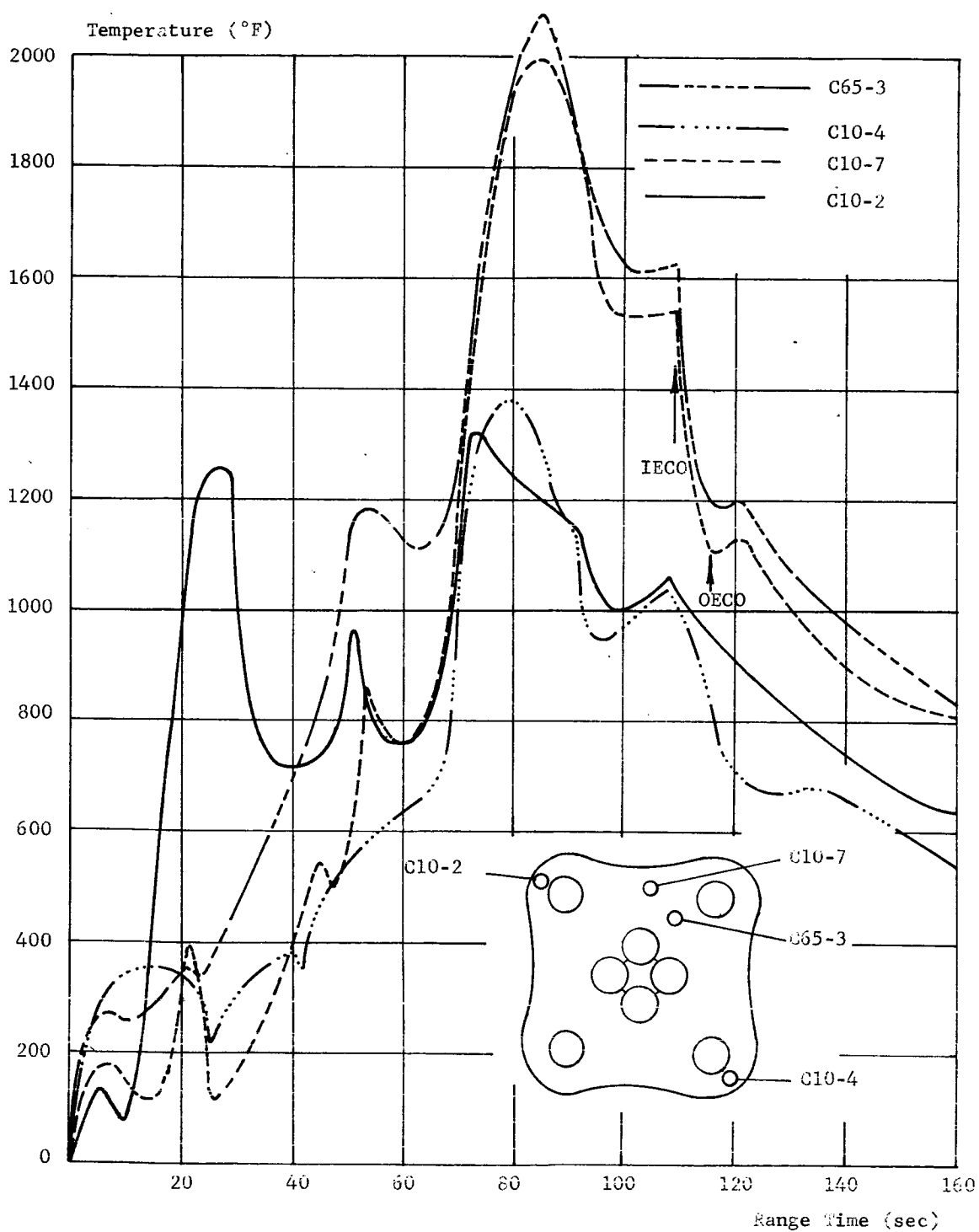


FIGURE 10-14 HEAT SHIELD GAS TEMPERATURE

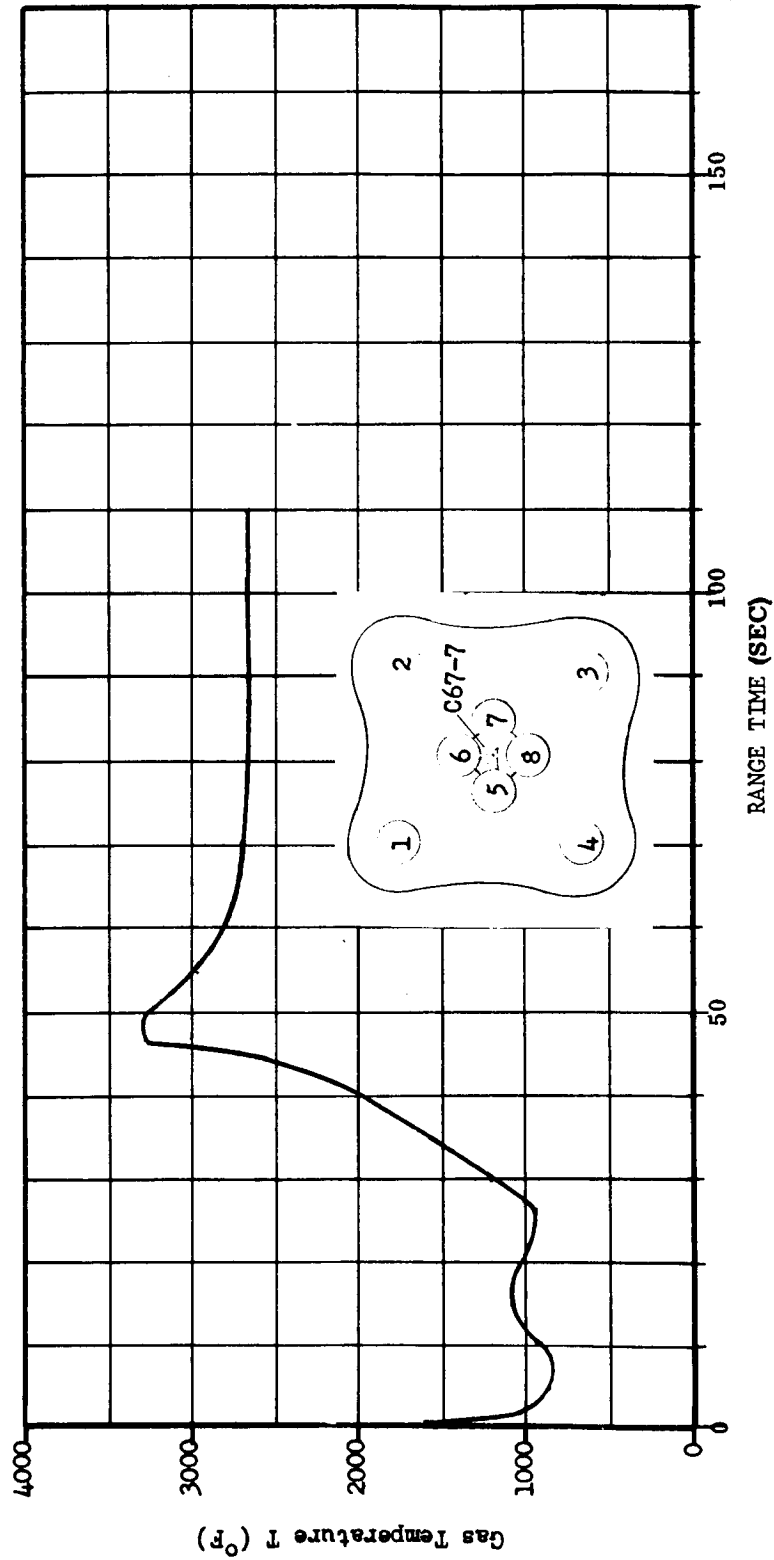


FIGURE 10-15 GAS RECOVERY TEMPERATURE MEASURED 3 INCHES BELOW FLAME SHIELD

Figures 10-16 and 10-17 were evaluated by determining the loss coefficient of the calorimeter slugs using laboratory calibration techniques. This technique has been utilized in the evaluation of static test data showing good agreement with measured temperature values. The circled data points shown in the figures were obtained by the determination of the loss coefficient of the slugs after engine cutoff (i.e.  $q=0$ ) using a method suggested by Hottle and others. Good agreement is obtained between the two techniques for all flight intervals.

Comparison between the total heat flux (radiation plus convection) measured by the heat shield calorimeters for the SA-1 and the SA-2 flights, in general, shows close agreement (see Figure 10-16). The total integrated heat input (area under the curves) to the SA-2 calorimeters is approximately the same as that to the SA-1 calorimeters. However, calorimeter measurement C63-1 on SA-2 was approximately 20% higher than the corresponding SA-1 calorimeter.

The difference of approximately 20% for calorimeter measurement C63-1 on SA-1 and SA-2 is due to the difference in the way the calorimeters were mounted on the two vehicles. On the SA-1 vehicle the calorimeter was recessed approximately 0.3 inches from the heat shield surface; whereas on SA-2 the calorimeter was mounted approximately flush with the surface. For this reason the heating rates measured by C63-1 during the SA-2 flight are more indicative of what would be encountered by the heat shield surface.

The difference in transient total heating rates measured by C77-5 during the two flights at approximately 50 seconds supports the possibility that the calorimeter on the SA-1 was shielded by the opaque turbine exhaust gases (from inboard engines) during this time. The trend indicated by the SA-2 calorimeter is more nearly what would be expected in this region than that of SA-1.

In conclusion the heat shield total calorimeter measurements on SA-1 and SA-2 indicate that the over-all base thermal environment for the two vehicles was approximately the same indicating that the heat shield thermal protection is more than sufficient.

The comparison between the total heat flux to the flame shield measured during the SA-1 and SA-2 flights is shown in Figure 10-17. This comparison shows the heat flux at liftoff to be slightly less severe on SA-2 than on SA-1. This conclusion is based on the data obtained using the laboratory calibration technique. The integrated total heat input for the two flights is in good agreement. Again it should be noted that good agreement is obtained between the two methods of evaluating the total calorimeter data.

The heat protection tape on the heat shield come loose in some areas after liftoff (see Page 280).

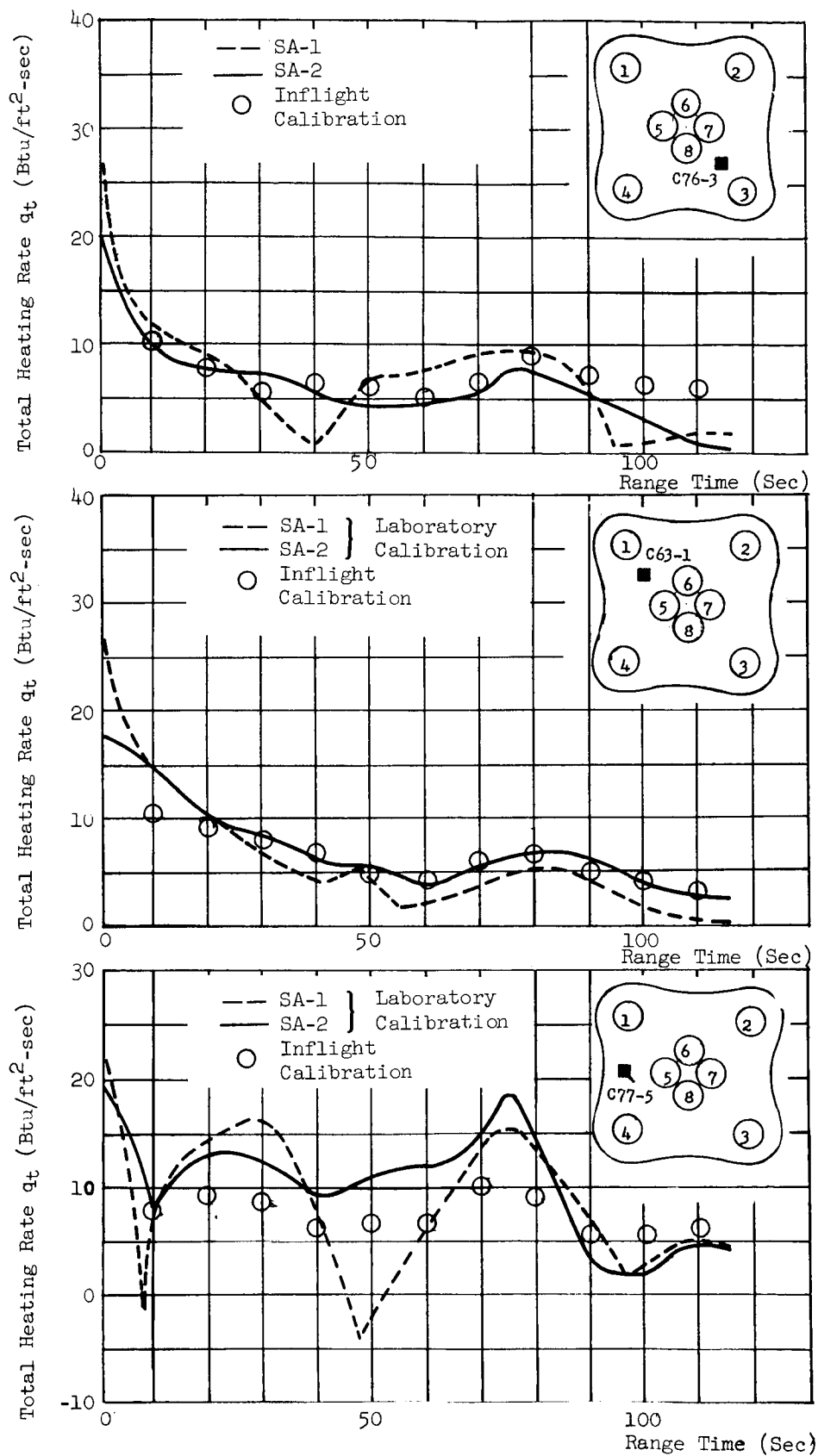
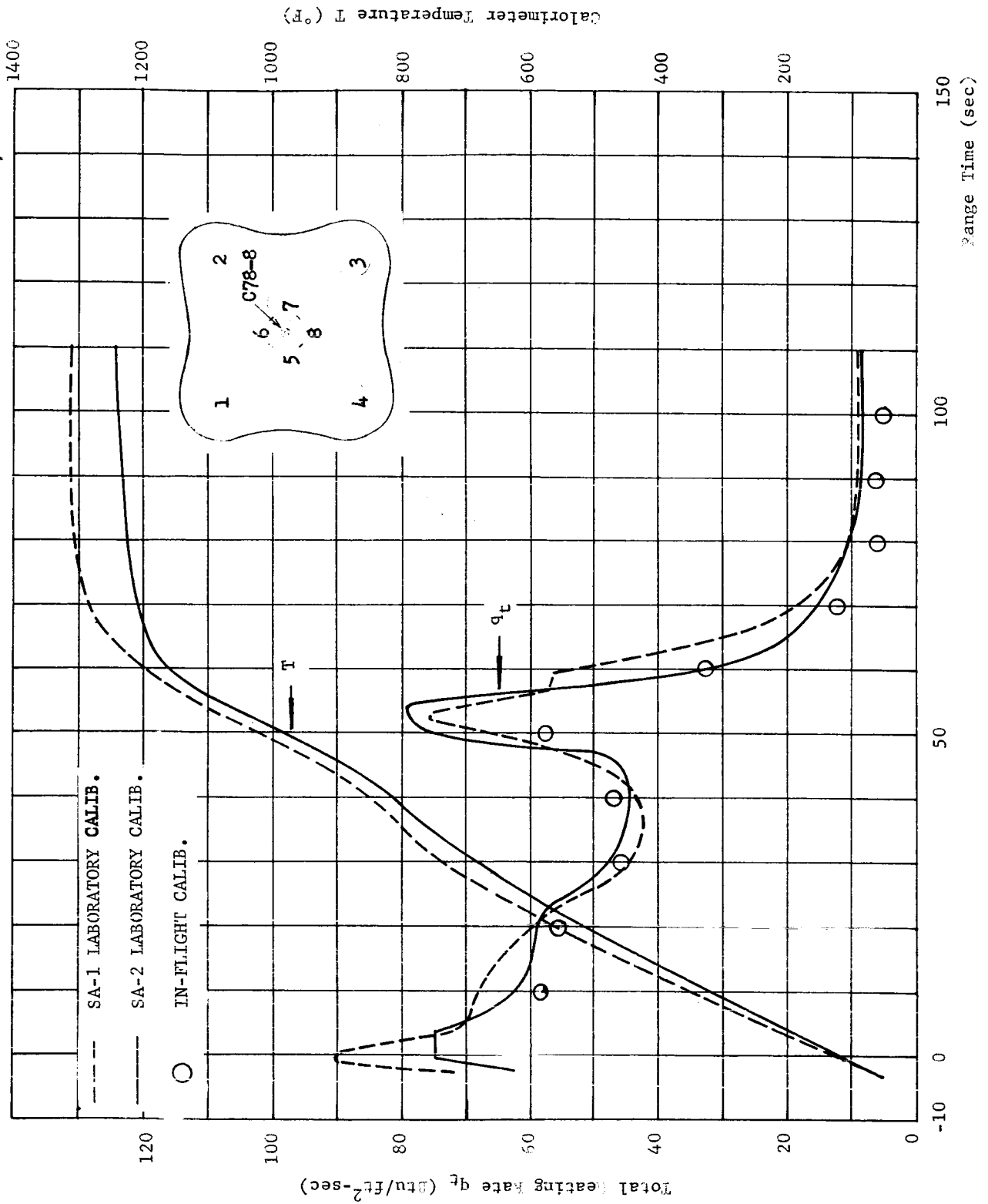


FIGURE 10-16 TOTAL HEATING RATE OF THE HEAT SHIELD

FIGURE 10-17 MEASURED FLAME SHIELD HEATING RATE  $q_t$  AND TOTAL CALORIMETER TEMPERATURE T

In conclusion, base heating environment on SA-2 was similar to that on SA-1. Due to the uncertainty involved in dividing the total heating rate to the base into components (radiation and convection) only the total heating rate curves are presented. A breakdown of the total heating rates will be formulated and presented at a later date.

Thermocouples C20-5 and C21-5 (Figure 10-18) were used to measure the structural temperatures of the flame shield support strut and seal support respectively. The support strut was covered with asbestos and wrapped with reflective tape; therefore measurement C20-5 was not expected to show any temperature rise. On the other hand, there is no reason for the temperature of the strut to decrease as shown by C20-5, so measurement C20-5 must be regarded as possibly being unreliable until further analysis can be made.

The flame shield seal support was not insulated on SA-2, and measurement C21-5 shows an expected typical response. On SA-1 the seal support was heavily insulated; therefore, measurement C21-5 indicated very little temperature rise. A valid comparison between SA-1 and SA-2 for respective measurements C20-5 and C21-5 cannot be made past 85 seconds flight time because of the malfunction of these measurements on SA-1 at approximately this time in flight.

Measurements C68-3, C69-5, C70-7, C71-4, C72-1, and C73-2, shown in Figure 10-19 were used to monitor the skin temperatures of the forward side of the heat shield. These measurements essentially show the same general range of temperatures which were measured on SA-1 with the exception of C70-7. All of these measurements exhibit a slight decrease in temperature after about 100 seconds flight time. This trend indicates that no heat is penetrating the heat shield insulation. Measurement C70-7 indicates a temperature rise from 50° at liftoff to approximately 200° F at about 90 seconds. The temperature rise indicated by C70-7 is not verified by other measurements in the engine compartment, but the temperature-time history of C70-7 does show a response pattern similar to the measured base gas temperatures. However, the base pressure data for the first portion of the flight indicates that a leak would be out of the engine compartment rather than into the compartment (see Figure 10-10). As time permits, additional studies on C70-7 will be made. Measurement C75-8 was used to measure the skin temperature on the flame shield forward side and indicates temperatures similar to those of SA-1 flight (see Figure 10-20).

Thermocouples C12-1 and C92-3 (Figures 10-21 and 10-22) were used to measure the temperature of the outboard engine shroud stringer and skin respectively. These measurements differ from the respective SA-1 measurements primarily because larger portions of the X-258 thermal protection material were cut out from around the thermocouple mounting

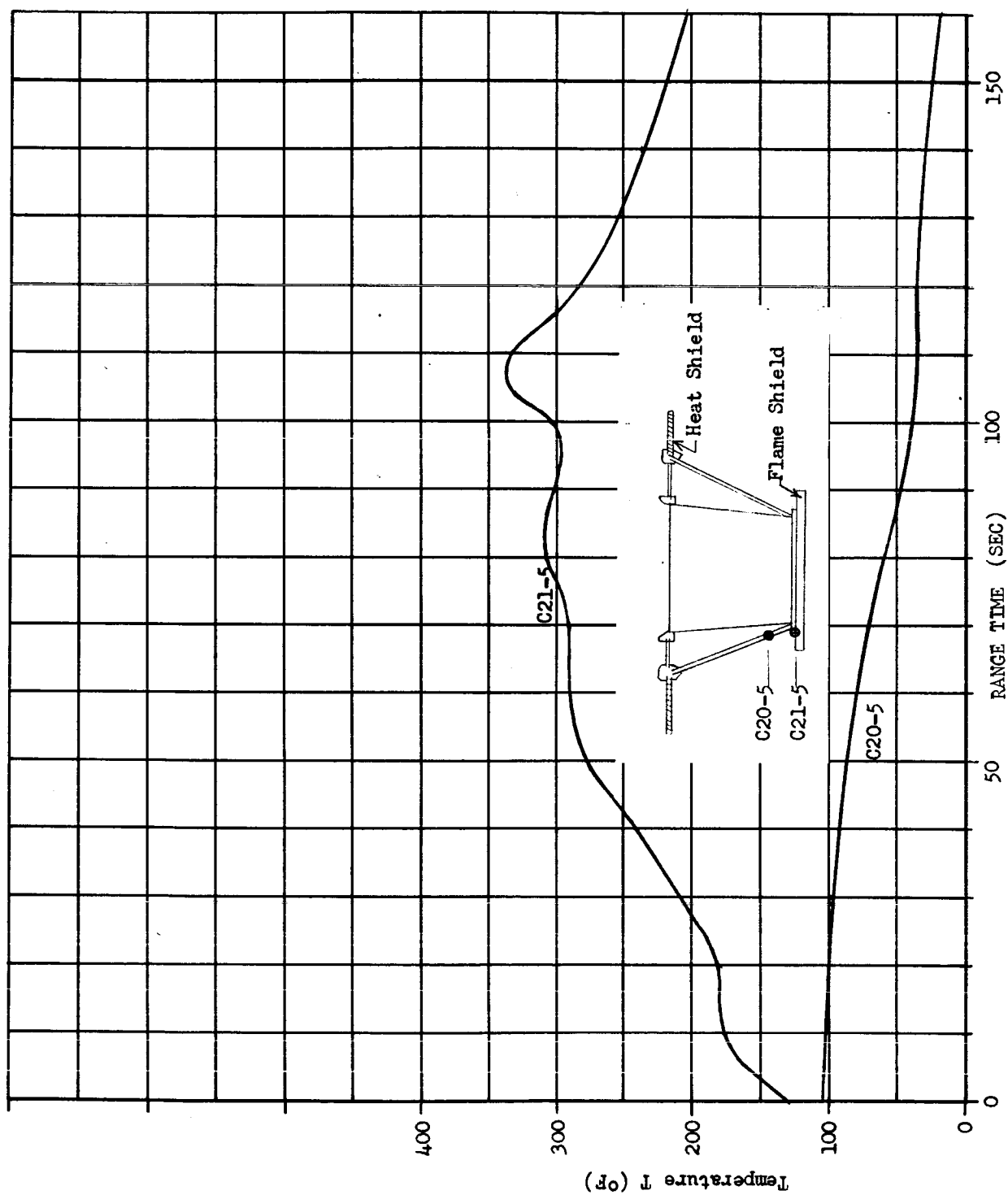


FIGURE 10-18 TEMPERATURE, AFT OF FLAME SHIELD, CONDUCTION THERMOCOUPLE

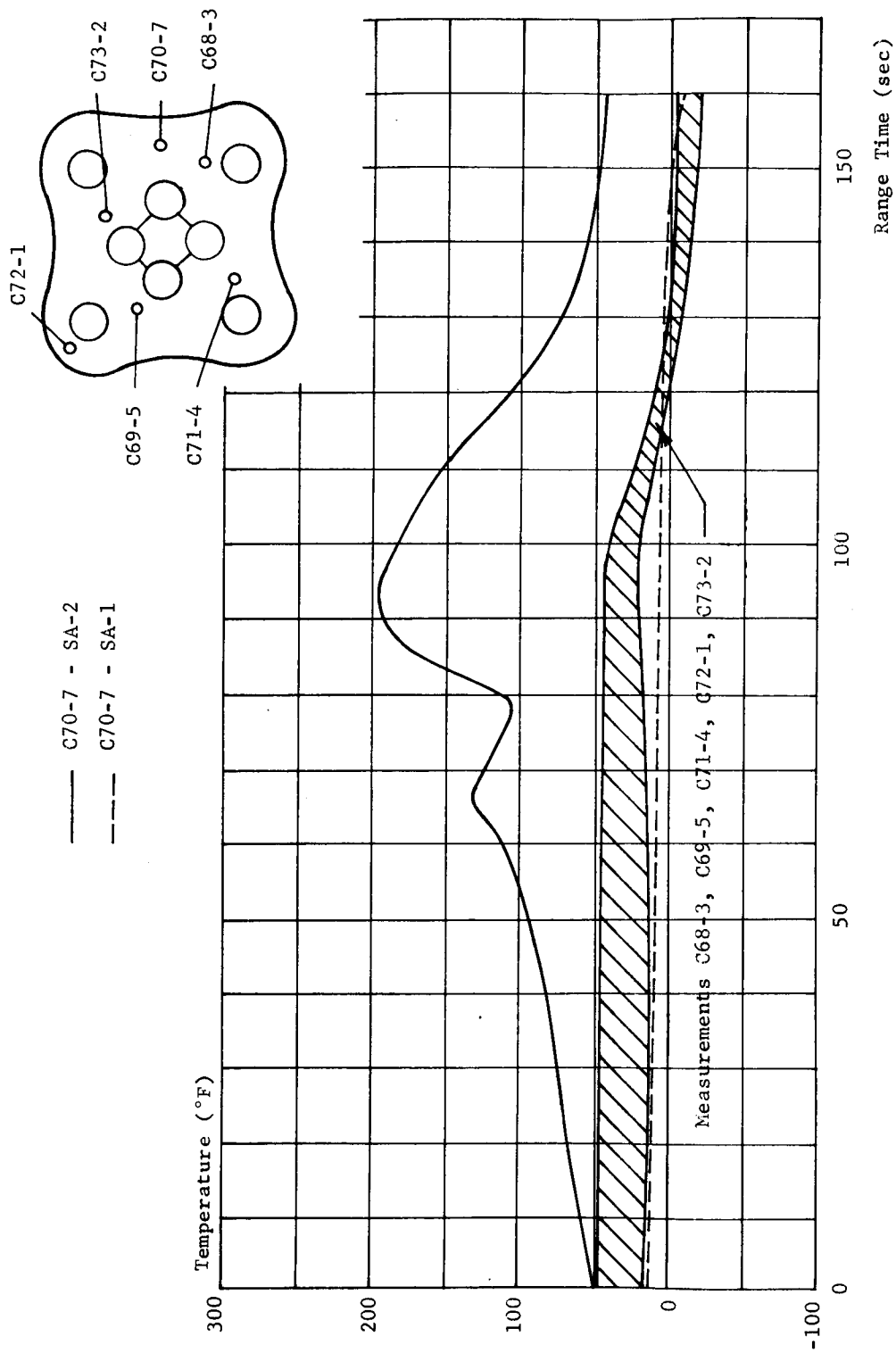


FIGURE 10-19 FORWARD SIDE HEAT SHIELD TEMPERATURE

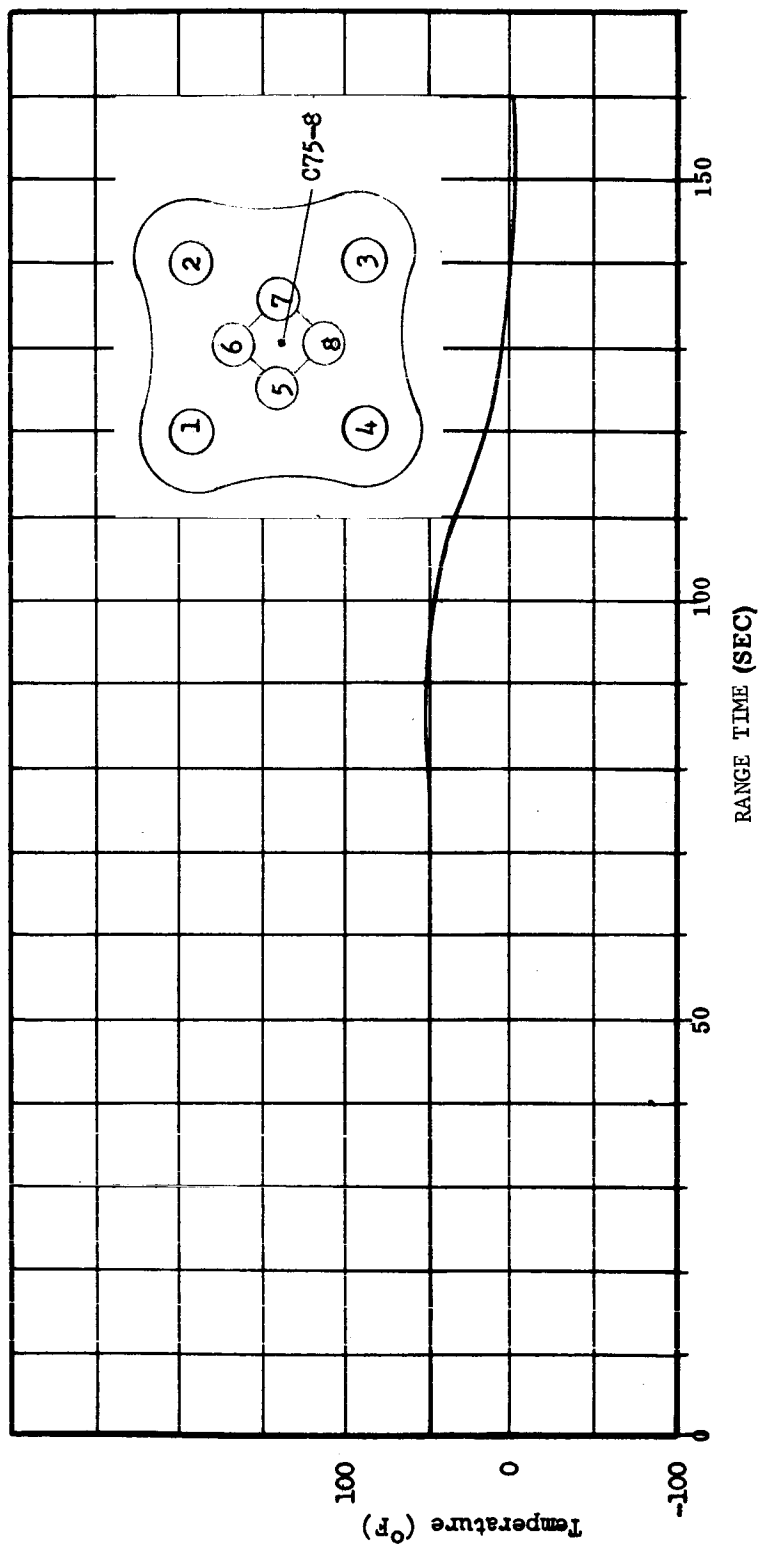


FIGURE 10-20 FORWARD SIDE FLAME SHIELD TEMPERATURE

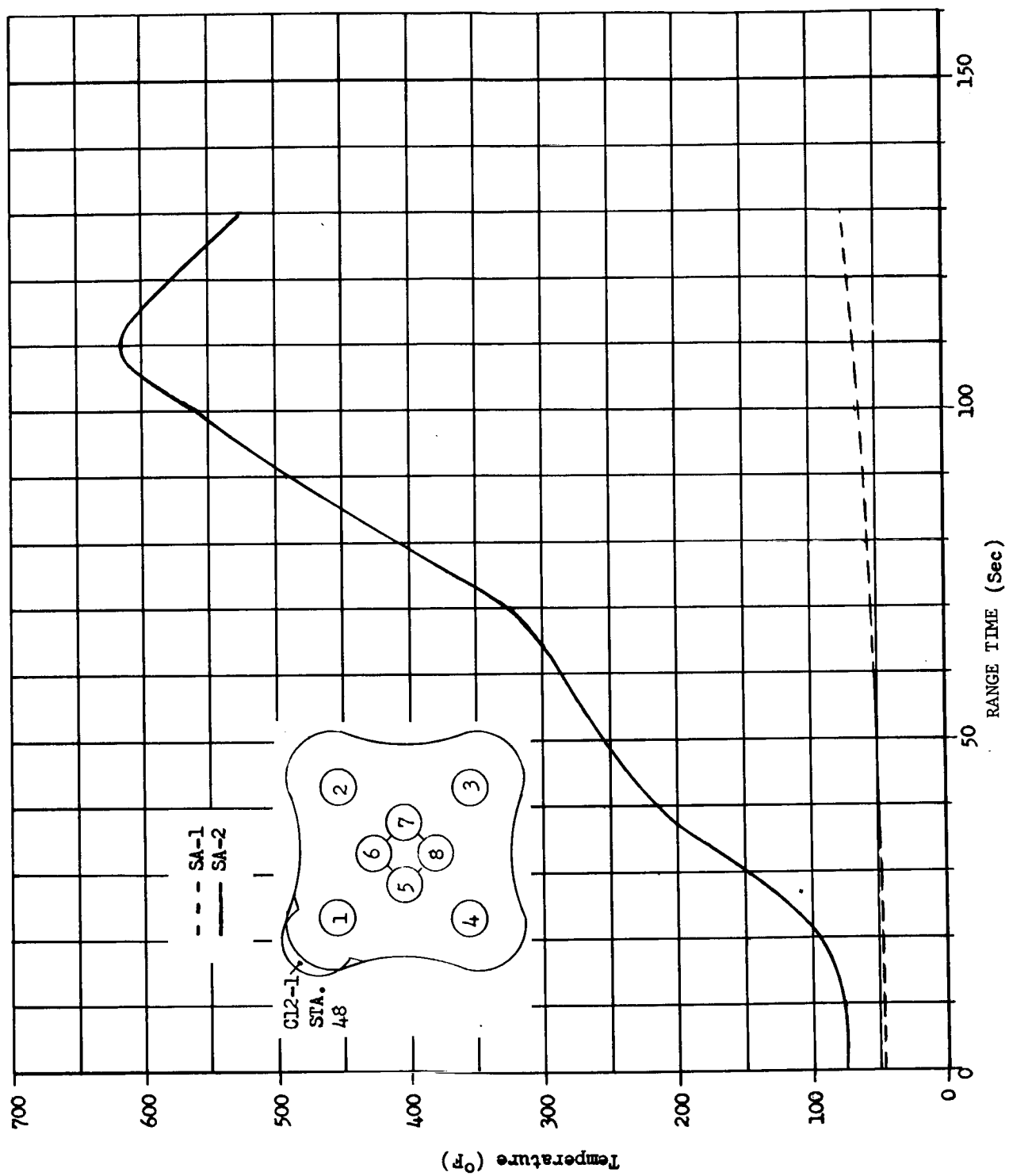


FIGURE 10-21 OUTBOARD ENGINE SHROUD STRINGER TEMPERATURE

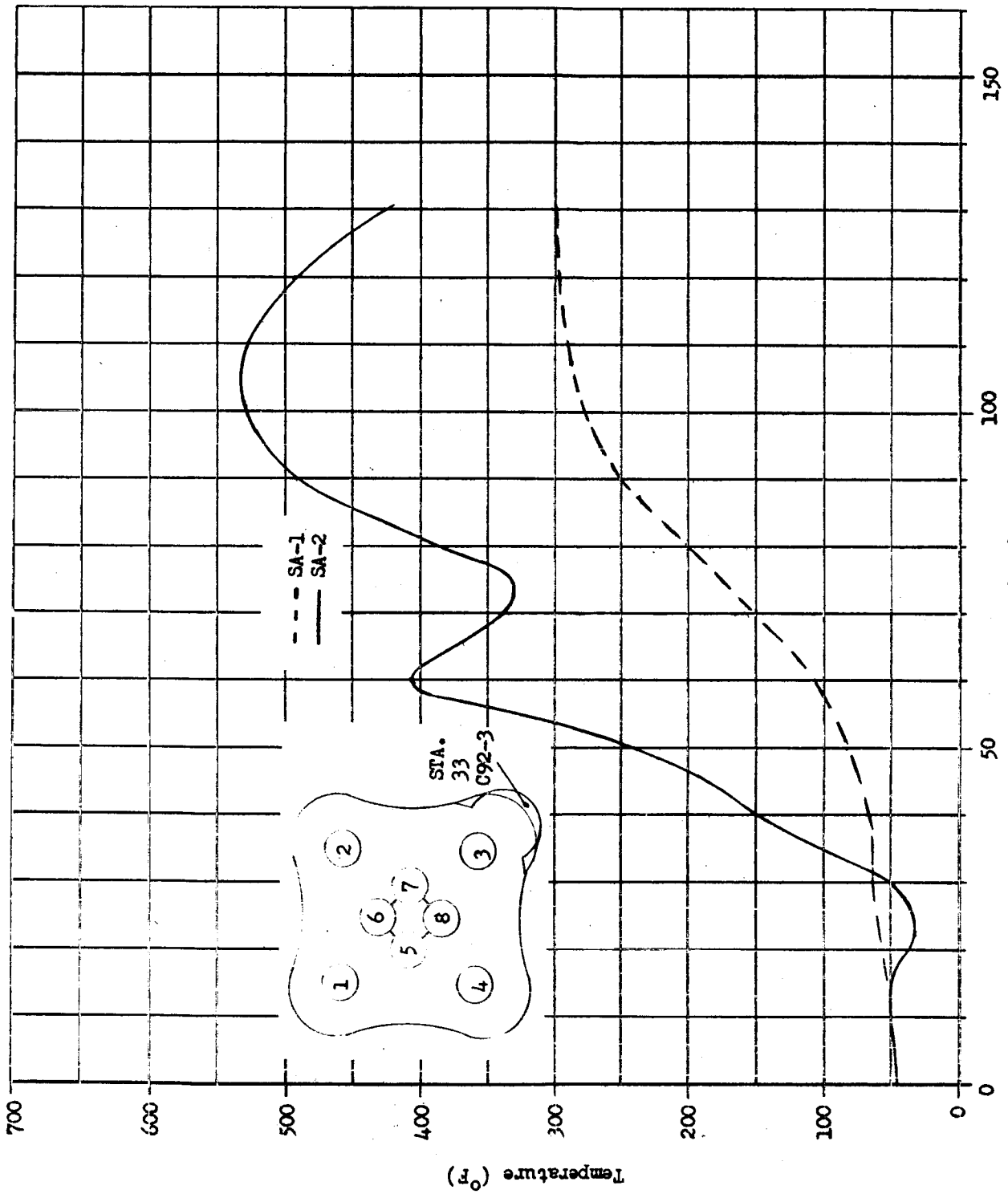


FIGURE 10-22 OUTBOARD ENGINE SHROUD SKIN TEMPERATURE

region than on SA-1, exposing measurements C12-1 and C92-3 more directly to base heating on SA-2. Although measurements C12-1 and C92-3 are located on the shroud stringer and skin respectively, they show similar temperature-time histories. This is attributable to the fact that both measurements are subject to essentially the same base heating, but the stringer has a relatively larger mass while the skin is influenced by aerodynamic heating.

### 10.3 SKIN (SEE FIGURES 10-23 to 10-30)

The skin temperatures at various positions on the propellant tanks for the SA-2 vehicle were measured by ten thermocouples located as shown in Figure 10-23. Generally, the skin temperatures measured on the propellant tanks during the SA-2 flight were in good agreement with those measured during the SA-1 flight. However, the following differences between the skin temperatures measured during the two flights were noted:

1. Measurement C48-03 at station 745.0 on SA-2 indicated a temperature at liftoff which was approximately 55° F higher than was measured by that measurement on SA-1; however, good agreement was obtained after approximately 60 seconds flight time.

2. The temperature-time histories measured by C45-03 on SA-1 and SA-2 show similar trends; however, the magnitudes of the temperature measured on SA-2 were lower than those measured on SA-1. The maximum temperature difference was 70° F and occurred at cutoff.

Although the causes of the aforementioned differences are not immediately apparent, it is suspected that the deviations were the results of secondary effects such as measurement error, sloshing of LOX, frost, etc. As pertains to the over-all vehicle performance, the role of the aforementioned temperature differences is considered to be negligible.

### 10.4 INSTRUMENT CANISTERS (SEE FIGURES 10-31 AND 10-32)

#### 10.4.1 CANISTER PRESSURE

Instrumentation and guidance components located in the canisters required the canister pressure to be maintained between 10 and 17 psia during flight. Pressure was maintained within this range by controlling the venting rate of the gases.

The instrument compartment pressurization system for SA-2 was identical to SA-1. The system utilized an absolute pressure regulator located in the return duct of the cooler package. The regulator was set to maintain canister pressure at  $16.2 \pm 0.5$  psia until the cooler package was retracted from the vehicle at T-25 seconds.

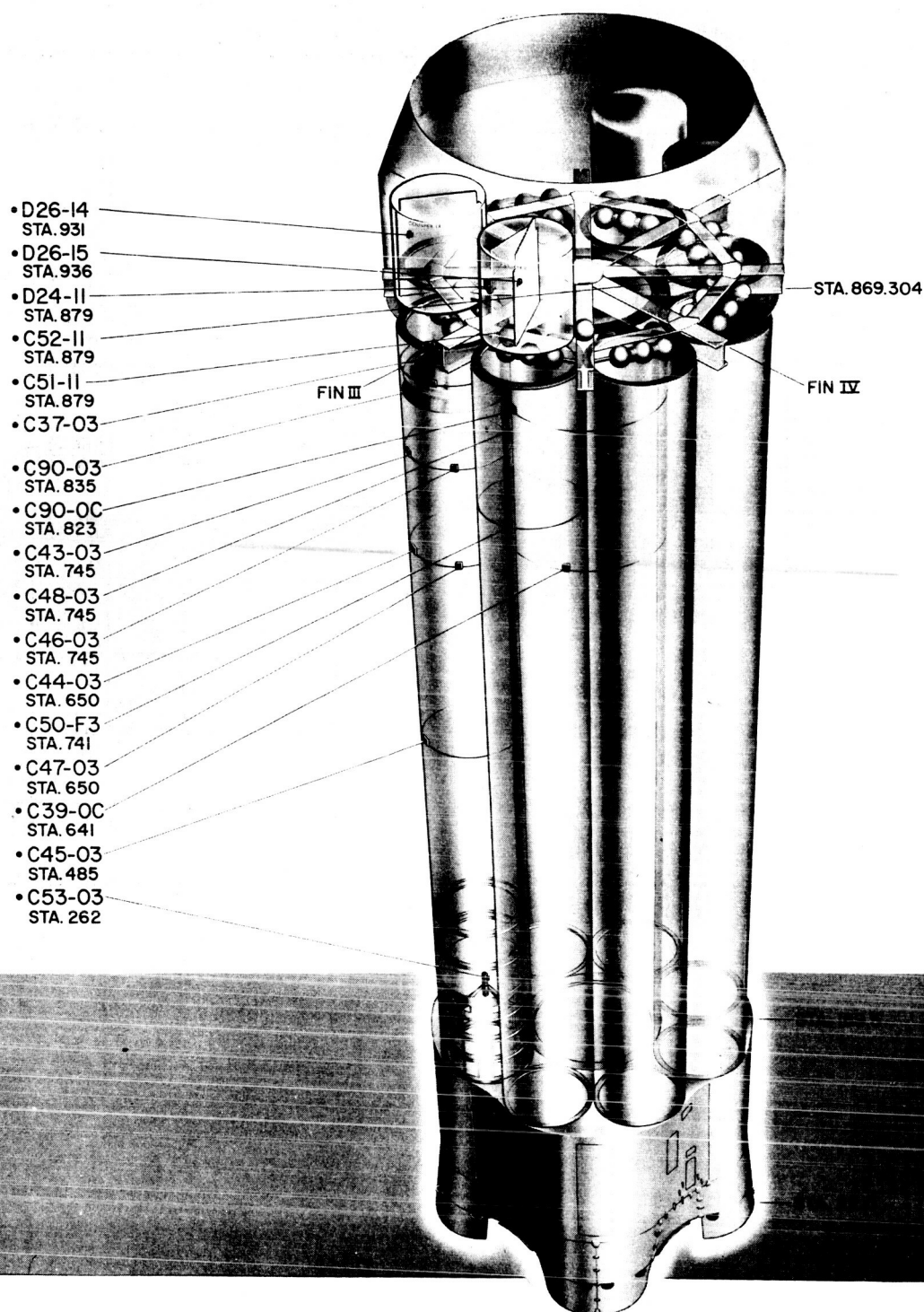


Figure 10-23 S-1 STAGE FLIGHT MEASUREMENTS

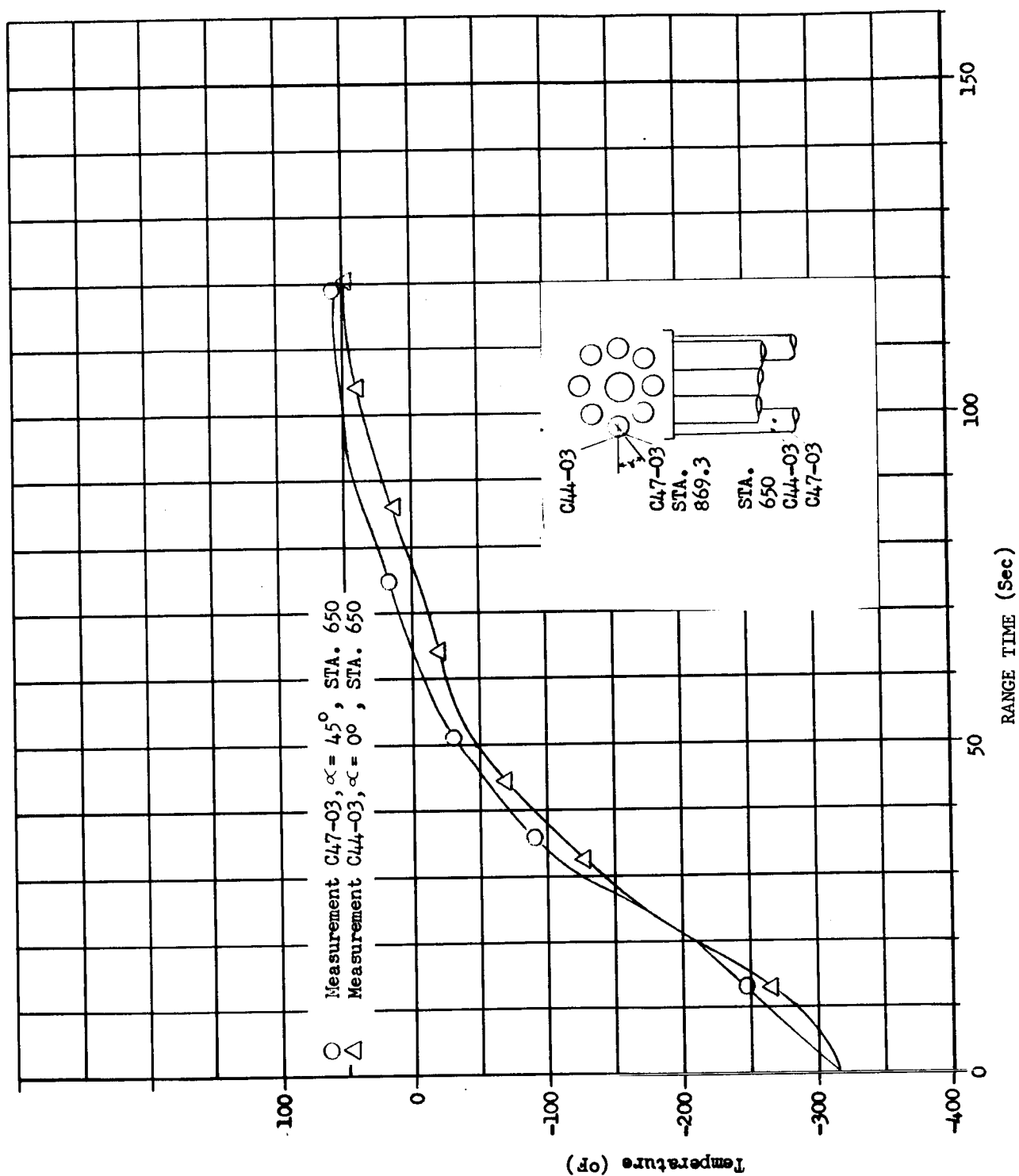


FIGURE 10-24 OUTBOARD LOX TANK SKIN TEMPERATURE

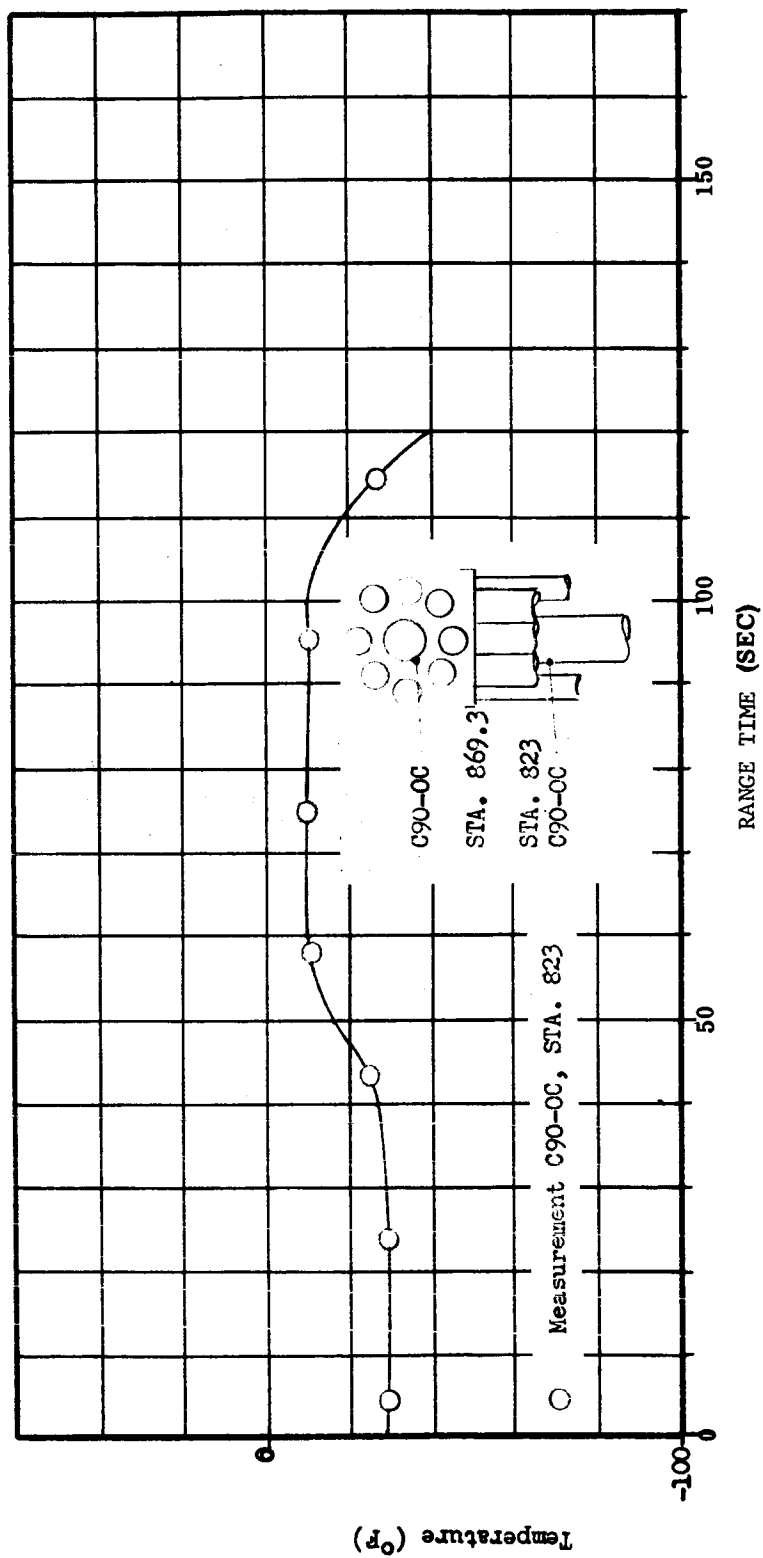


FIGURE 10-25 CENTER LOX TANK GROUND TEMPERATURE

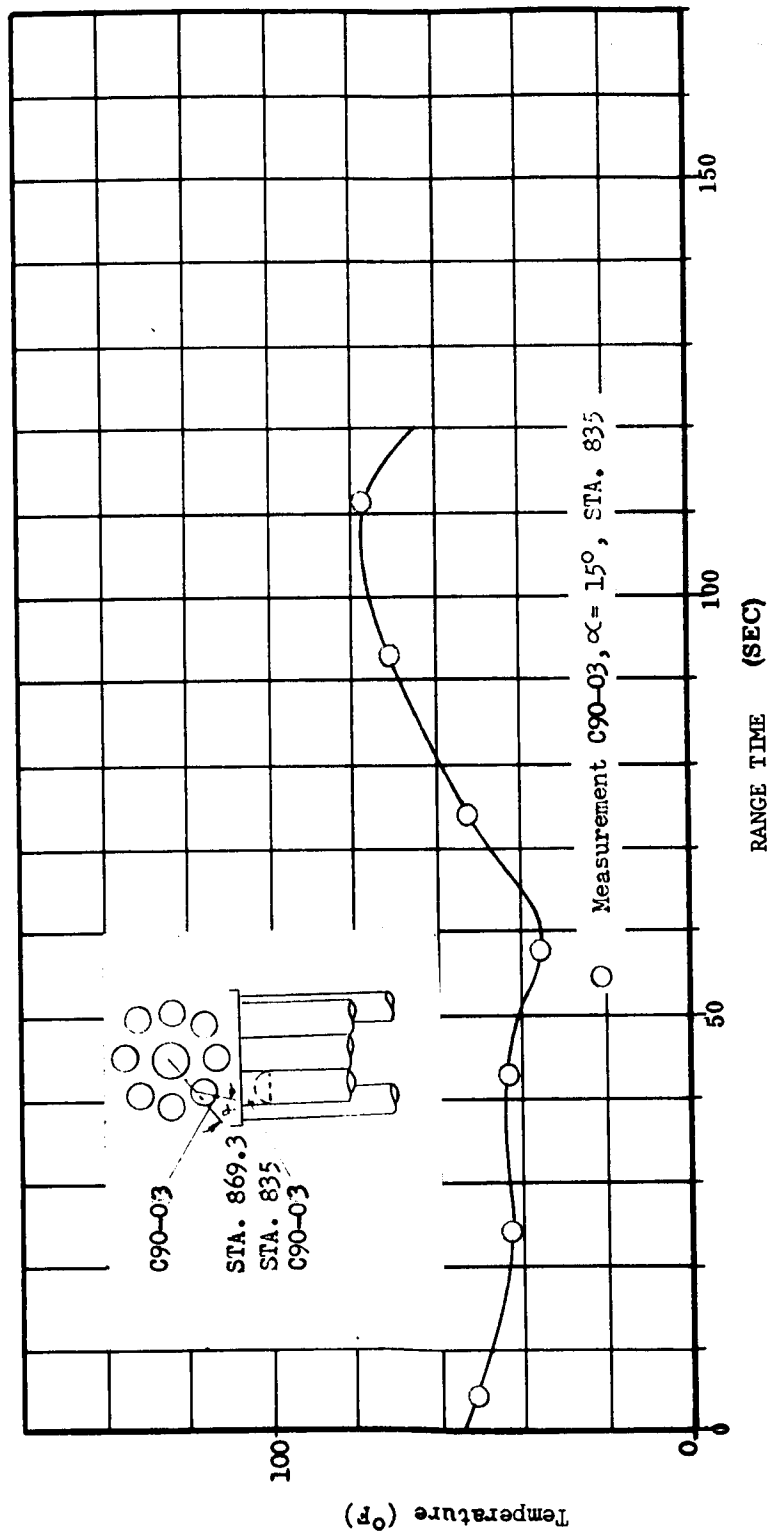


FIGURE 10-26 OUTBOARD LOX TANK SHROUD TEMPERATURE

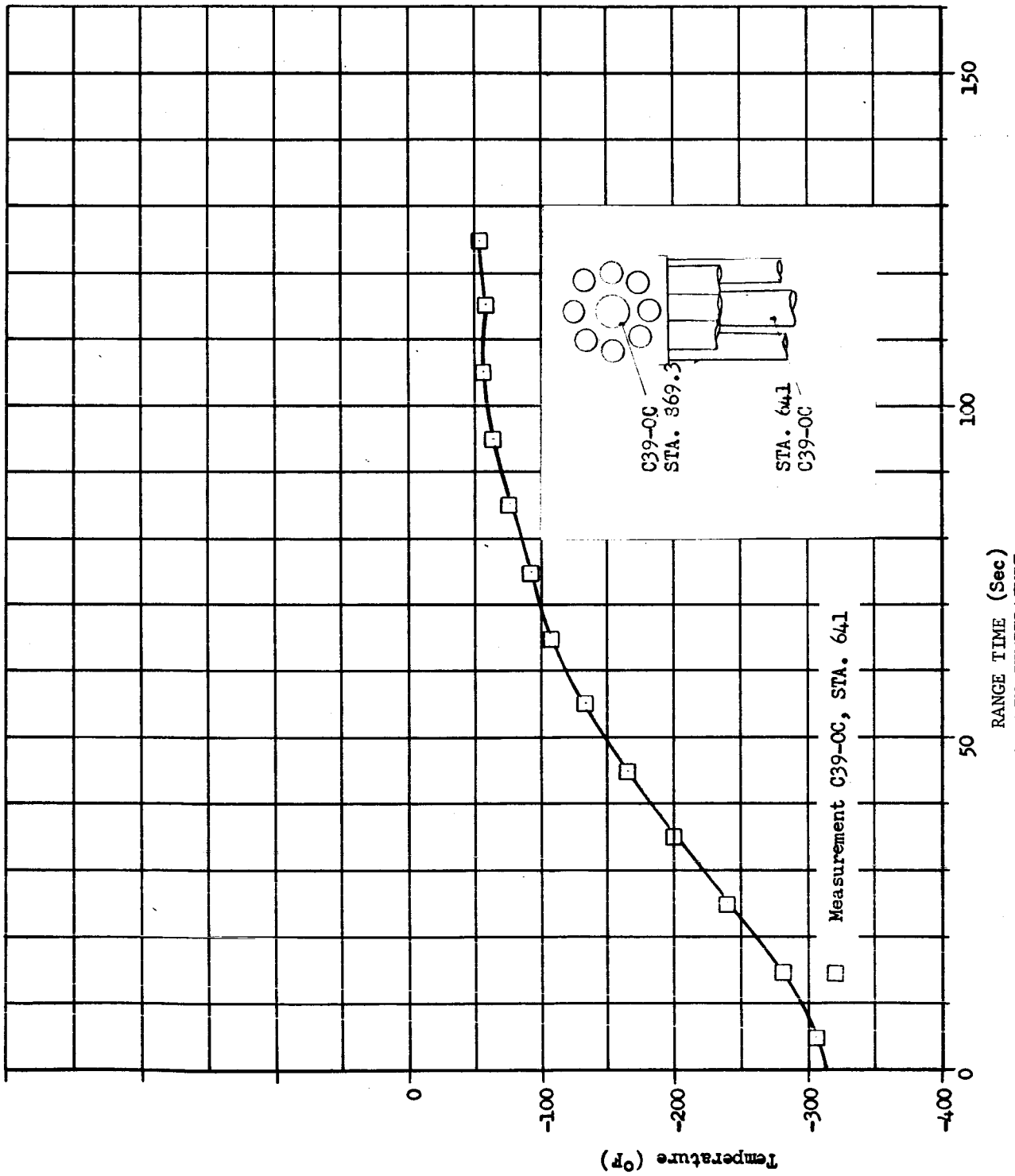


FIGURE 10-27 CENTER LOX TANK SKIN TEMPERATURE

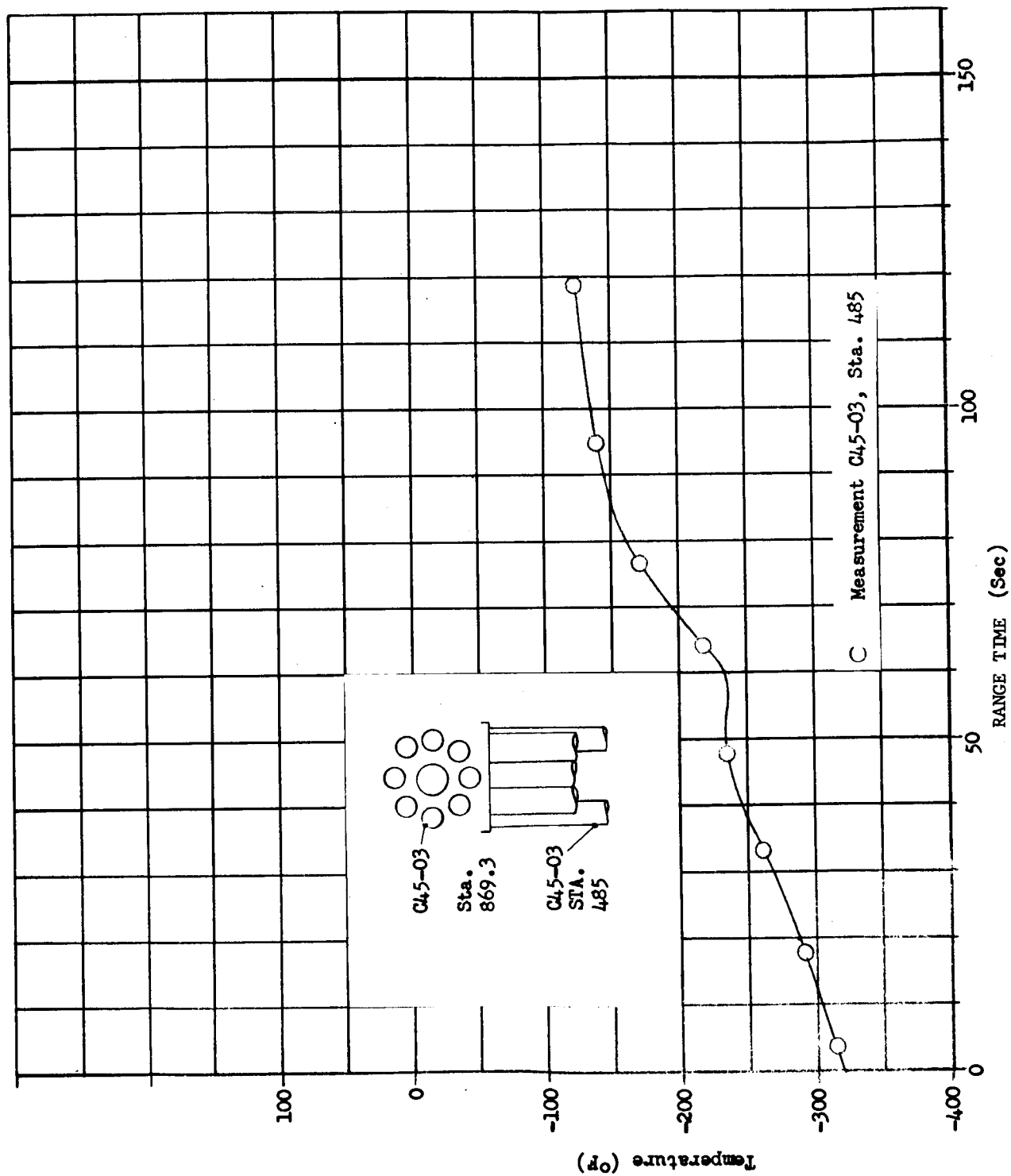


FIGURE 10-28 OUTBOARD LOX TANK SKIN TEMPERATURE

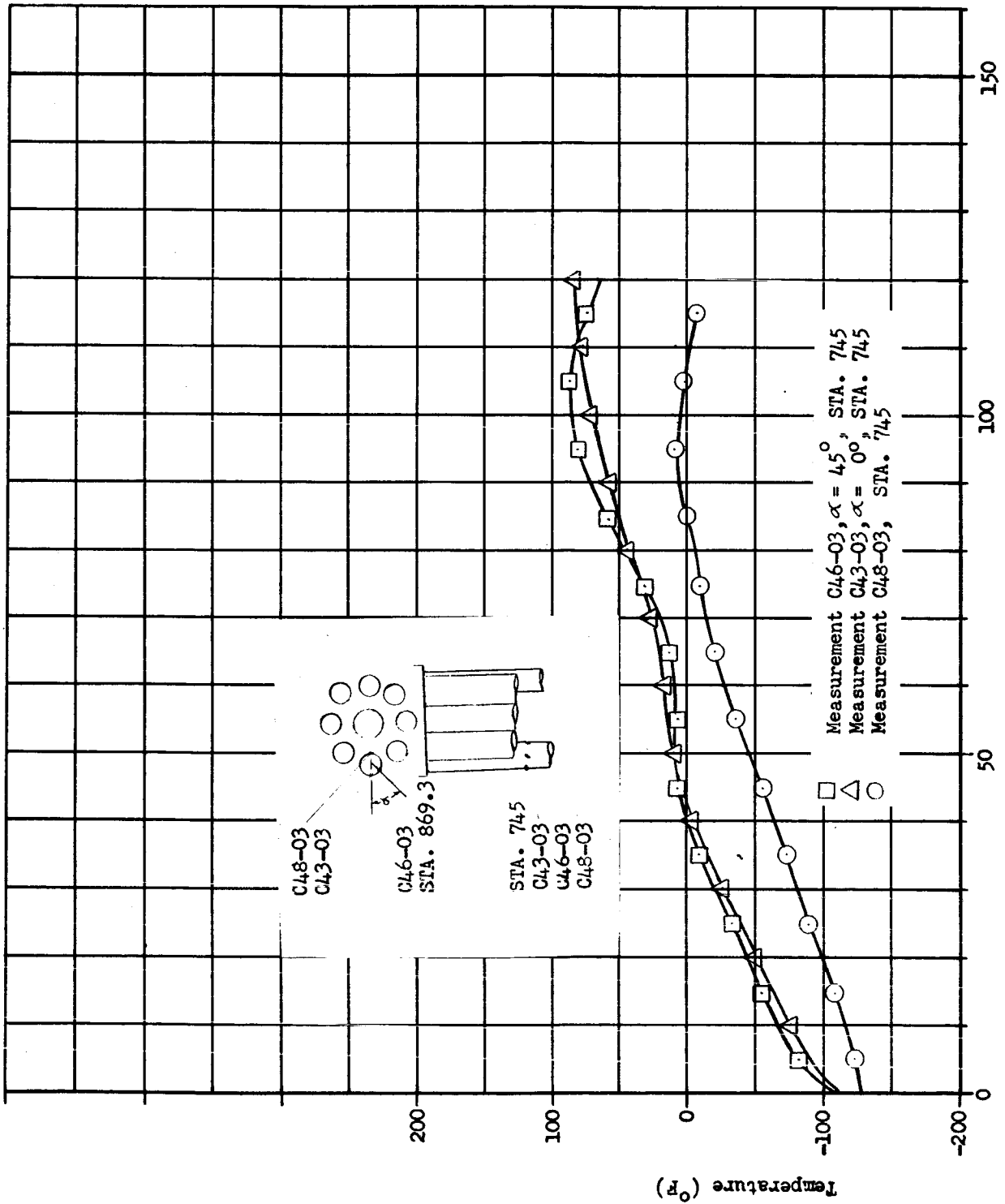


FIGURE 10-29 OUTBOARD LOX TANK SKIN TEMPERATURE

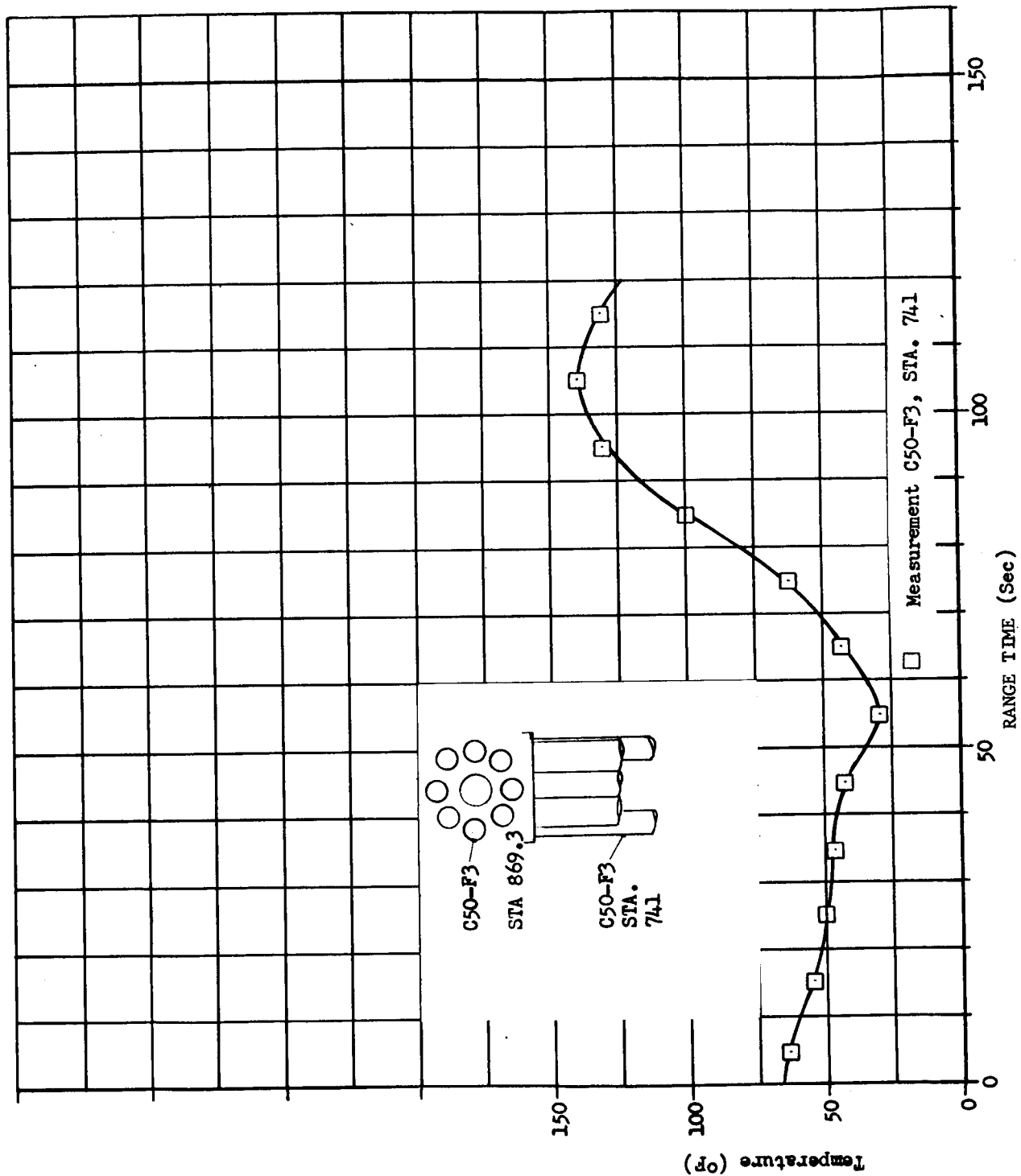


FIGURE 10-30 FUEL TANK SKIN TEMPERATURE

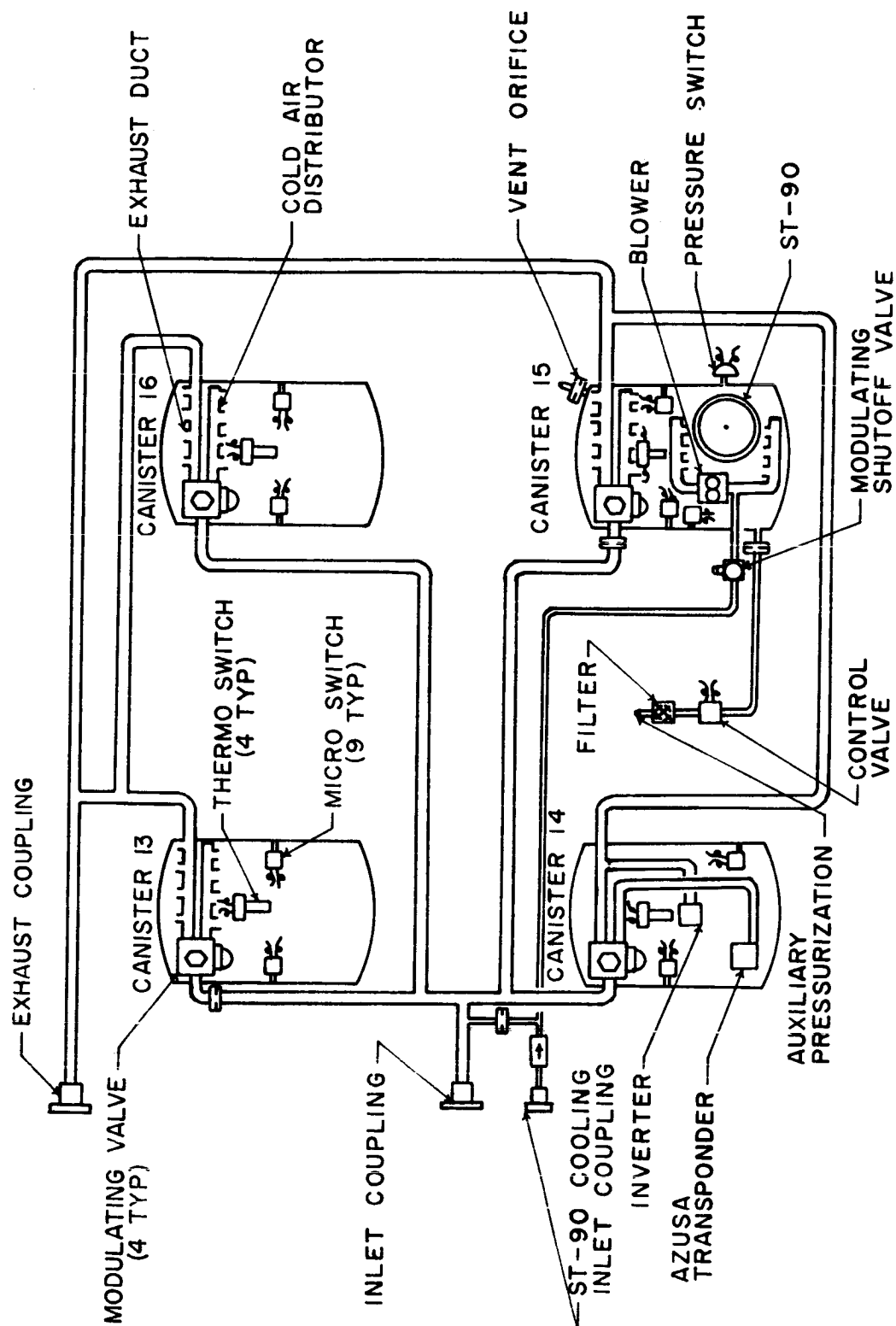


FIGURE 10-31 INSTRUMENT CANISTER COOLING SYSTEM

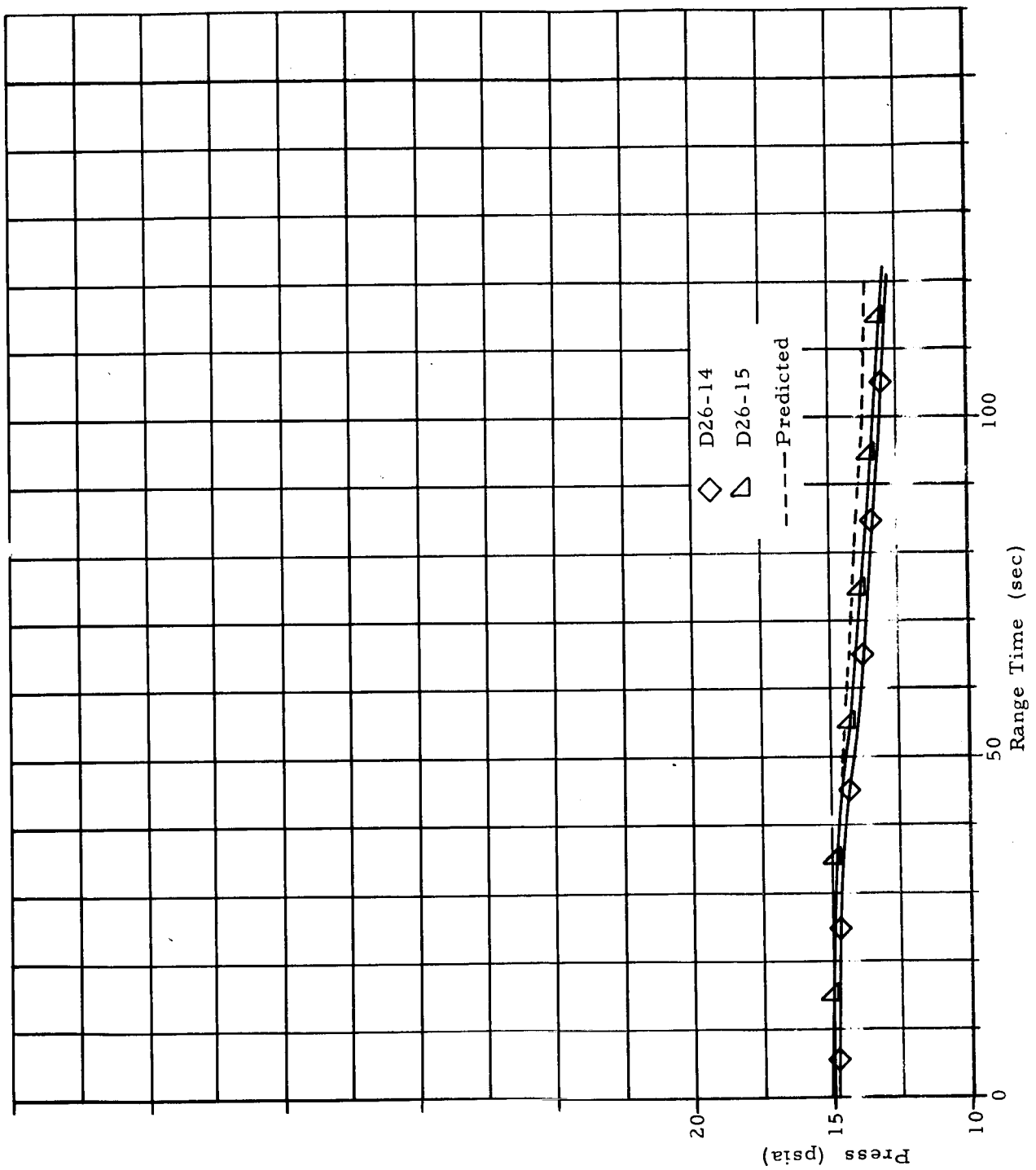


FIGURE 10-32 PRESSURE INSTRUMENT COMPARTMENT

An orifice plate (0.375 inches in diameter) was installed on canister #15 to allow gases to vent from the canisters during flight and prevent a pressure build-up in the canisters. It was sized to permit a slight decay in pressure over flight but assure that the pressure would remain within the allowable limits.

The canisters were equipped with an auxiliary pressurization system which was provided to supply GN<sub>2</sub> from the fuel high pressure spheres should a malfunction or structural leak occur. This system was set to energize if the canister pressure dropped to 12 psia, and buildup the canister pressure to 14 psia where it would de-energize.

The pressure in two canisters (#14 and #15) was measured during flight. The characteristic pressure decay of these two measurements (approximately 2 psia from 0 to 120 seconds flight time) compares very closely with SA-1 flight data and with SA-2 predicted data. Since the pressure dropped to a minimum of 12.6 psia at 160 seconds flight time, it is apparent that the auxiliary pressurization system was never operative.

#### 10.4.2 CANISTER TEMPERATURE

Temperature in the four canisters was controlled by an external cooler package mounted on top of the long cable mast. As programmed, the long cable mast retracted from the vehicle at T-25 seconds before ignition. There was no canister cooling during flight. The acceptable range of canister temperature is 50 to 104° F. All canisters were within this range at liftoff; however, the temperature in canisters #14 and #15 was slightly lower than the temperature in canisters #13 and #16. The Azusa blower in canister #14 and the ST-90 cooling system in canister #15 were responsible for these slightly lower temperatures.

The temperature of the ST-90 ambient air was 73° F at liftoff which was slightly out of tolerance ( $77 \pm 3.6^\circ$  F). This deviation is attributed to improper calibration procedure and is not considered to be significant. SA-1 blockhouse data showed a cycling in this temperature of approximately 1.7 cycle/minute, which was believed to be from the operation of the modulating ball valve. No cycling was evident in this measurement on SA-2.

## 11.0 (U) AERODYNAMICS

## 11.1 SUMMARY

An analysis of SA-2 telemetered data was performed to determine the aerodynamic static stability ratio, gradient of the normal force coefficient, and the center of pressure location. Results showed good agreement with predicted values and flight results. A more accurate and refined curve fitting procedure was used for data reduction on the flight analysis of SA-2 than was originally used on SA-1. The aerodynamic parameters above were then re-calculated for the SA-1 flight using the new analysis techniques and are presented in the figures herein for comparison.

Telemetered surface pressure readings were plotted in the form of surface pressure to ambient pressure ratio versus Mach number. These surface pressure measurements were made for the first time on SA-2. They are generally in good agreement with predictions from wind tunnel tests.

## 11.2 RATIO OF GRADIENTS OF ANGULAR ACCELERATION (STABILITY RATIO)

The ratio of the gradients of angular acceleration (or stability ratio) was determined from the average pitch plane outboard engine deflection ( $\beta_p$ ) and the free-stream angle of attack ( $\alpha_p$ ).

$$\frac{C_1}{B^O} = - \frac{\beta_p}{\alpha_p}$$

where

$C_1$  = angular acceleration due to unit angle of attack

$B^O$  = angular acceleration due to unit outboard engine deflection

The values of  $\frac{C_1}{B^O}$  obtained for the SA-2 vehicle basically show good agreement with predicted values and SA-1 flight results when plotted versus time (Figure 11-1). The deviations between SA-1 and SA-2 values between 30 and 48 sec of flight are considered to be due to errors caused by using questionable small engine deflection and angle of attack values and do not mean that SA-2 was more stable than SA-1 or the predicted values over this period of flight. An estimate of the possible error margin in the flight determined stability ratio is also shown in Figure 11-1.

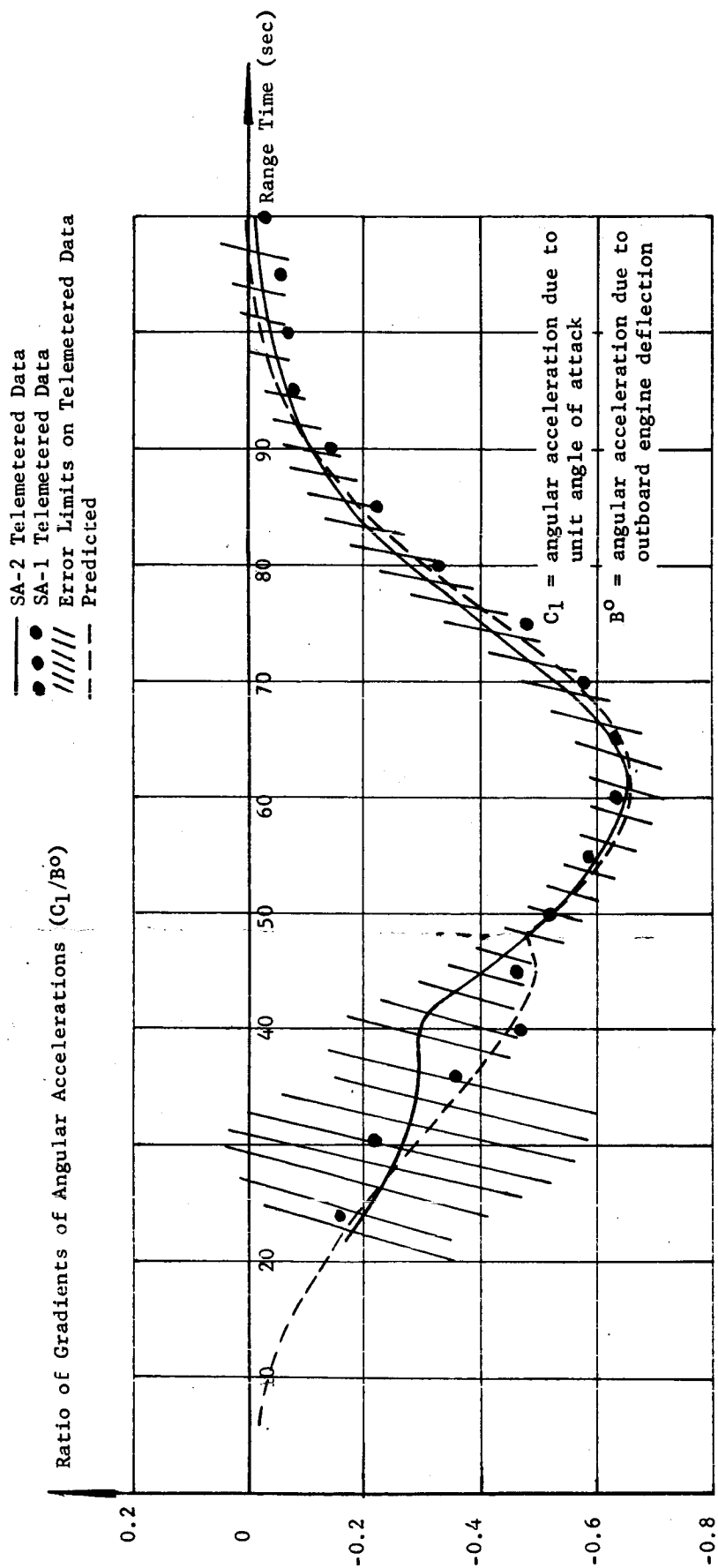


FIGURE 11-1 RATIO OF GRADIENTS OF ANGULAR ACCELERATIONS VERSUS RANGE TIME

### 11.3 GRADIENT OF NORMAL FORCE COEFFICIENT AND CENTER OF PRESSURE LOCATION

The gradient of the normal force coefficient ( $C_z'$ ) was obtained using telemetered values of angle of attack, normal acceleration, and engine deflection;

$$C_z' = \frac{m\ddot{\gamma}_p - \Sigma F\beta}{qS\alpha_p}$$

where

$C_z'$  = gradient of normal force coefficient

$m$  = mass of vehicle

$\ddot{\gamma}_p$  = normal acceleration, pitch

$F$  = individual outboard engine thrust corrected for cant angle

$\beta$  = individual outboard engine deflection

$\Sigma F\beta$  = total normal thrust component due to deflections of engines

$q$  = free-stream dynamic pressure

$\alpha_p$  = free-stream pitch angle of attack

$S$  = reference (cross-sectional) area

Calculated and predicted values of  $C_z'$  are shown with SA-1 results for comparison in Figure 11-2.

The center of pressure location of the vehicle (plotted versus Mach number in Figure 11-2) was determined from the relationship

$$\frac{CP}{D} = \frac{CG}{D} \left[ 1 + \frac{1}{C_z' q S \alpha_p} (\Sigma F\beta) \right]$$

where;

$\frac{CP}{D}$  = center of pressure location from sta. 100 (calibers)

$\frac{CG}{D}$  = center of gravity location from sta. 100 (calibers)

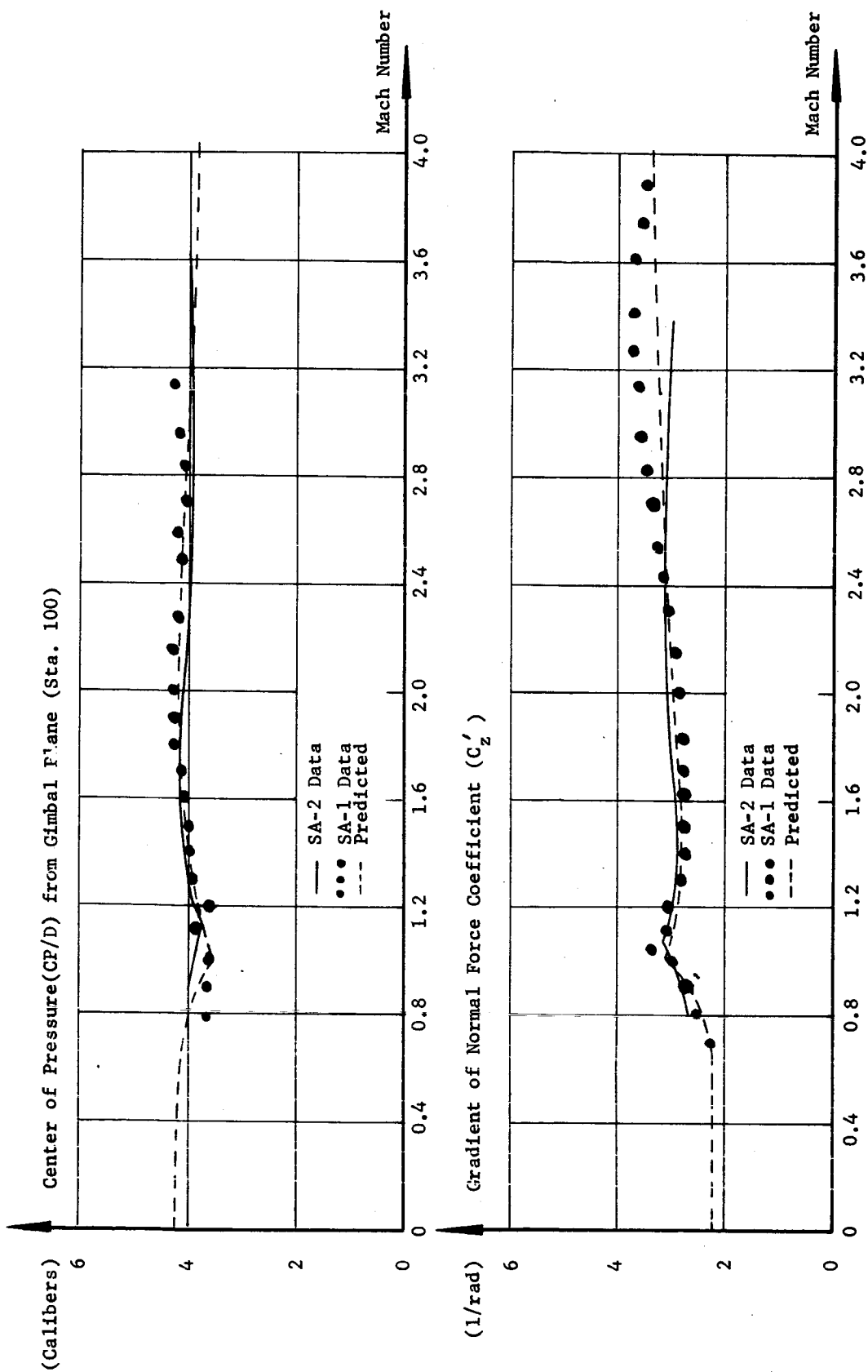


Fig. 11-2 CENTER OF PRESSURE LOCATION AND GRADIENT OF NORMAL FORCE COEFFICIENT VERSUS MACH NUMBER

Values of  $C_z'$  and  $\frac{C_P}{D}$  below Mach 0.8 and above Mach 3.0 are not considered reliable because of the wide scatter of data due to the small values of dynamic pressure and normal accelerations. Both  $C_z'$  and  $\frac{C_P}{D}$ , however, displayed excellent agreement with predicted values and SA-1 results in the region from about Mach 1.0 to Mach 2.8.

#### 11.4 SURFACE PRESSURES

##### 11.4.1 STATION 205 MEASUREMENTS

All four surface pressure pick-ups at station 205 are located on the fillets of the flared-out region adjacent to the extreme lower portion of the fuel and LOX tanks. Figure 11-3 is a plot of surface to ambient pressure ratio versus Mach number for all four individual measurements and also shows their approximate radial location at this station.

Values of surface pressure to ambient pressure ratio showed a steady increase with Mach number except measurement D78-10 which peaked at a Mach number of about 1.1 to a value of 1.3 and then gradually decreased to values slightly below 1.0. Predicted values, based upon unpublished wind tunnel test data from the Experimental Aerodynamics Branch, Aeroballistics Division, are shown on the graphs for the locations corresponding to measurements D78-10 and D79-10 as circled points and indicate close agreement with flight data up to a Mach number of 1.1. Wind tunnel tests were conducted in the transonic section of the MSFC 14 inch tunnel on a 0.007782 - scale model of the SA-5 vehicle. Although Saturn Block II model test data was used for comparison purposes, it is believed that there will not be a significant pressure difference between the two configurations for the two particular locations considered on the booster.

Flight results are slightly higher than the wind tunnel results for measurement D79-10, but the same upward trend is seen in both with increasing Mach number. Measurement D78-10 is the only one of the four measurements at station 205 which did not show an increase in pressure ratio with increasing Mach number. It also disagrees with the wind tunnel data and therefore the flight measurement is probably not valid. Additional flight test measurements will be needed to verify this result. All wind tunnel test results shown are for a pitch angle of attack of 4 deg which is within 0.5 deg of those attained in the SA-2 flight for the Mach numbers in question.

##### 11.4.2 MEASUREMENTS AT STATIONS 860 AND 863

Pressure ratios (surface to ambient) obtained from the four measurements located at stations 860 and 863 are plotted versus Mach

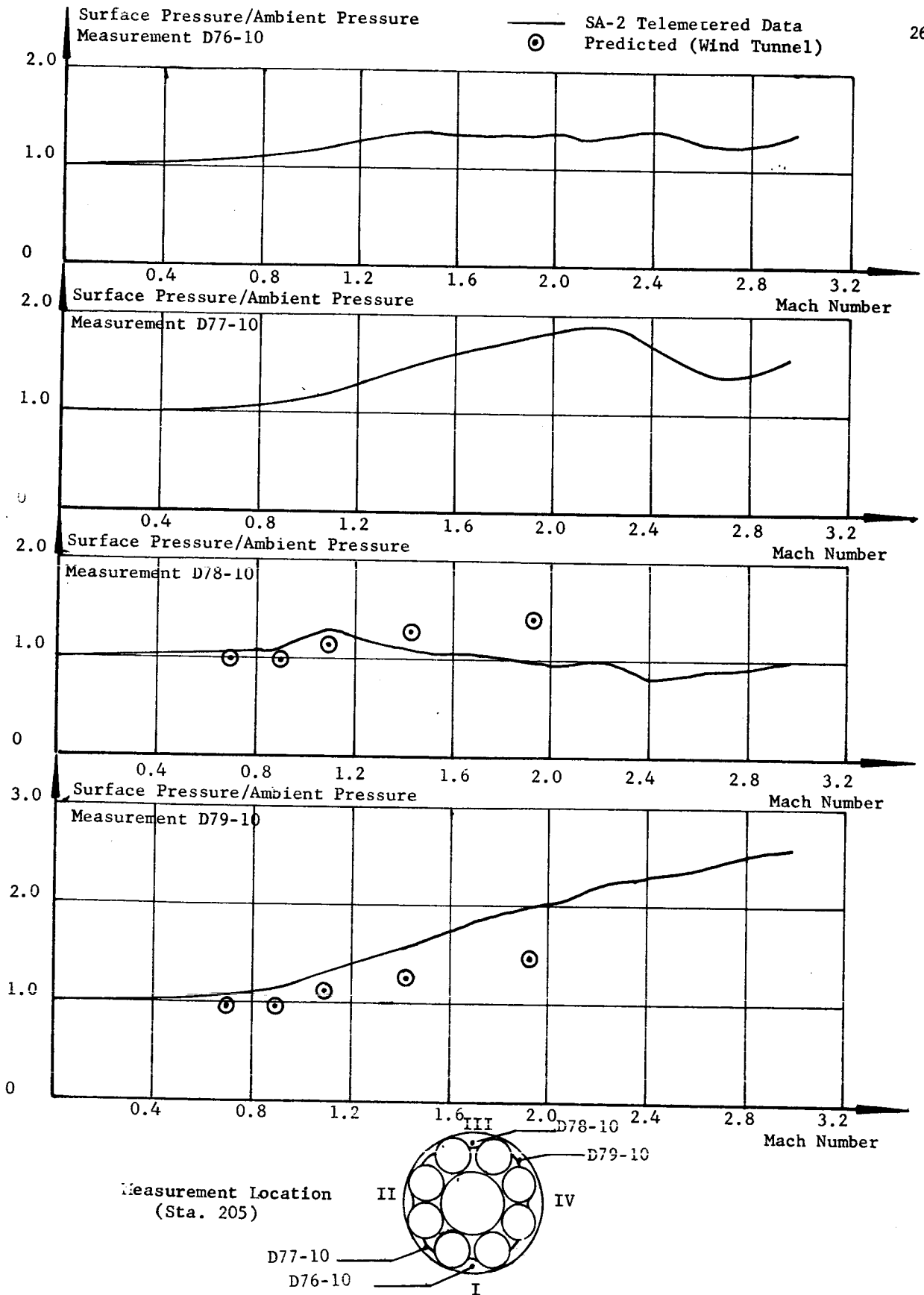


Fig. 11-3 RATIOS OF SURFACE PRESSURE TO AMBIENT PRESSURE VERSUS MACH NUMBER

number in Figure 11-4, and a sketch is included indicating the radial location of each individual measurement. Surface pressure measurements D80-F1 and D82-F3, situated at station 863, were located on the extreme upper portion of the fuel tanks facing the external free-stream flight conditions. Surface pressure measurements D81-F1 and D83-F3 were located facing the center of the cluster at station 860 slightly above the fuel tanks (Figure 11-4). Observed flight readings from all locations indicate very close agreement with each other, dropping gradually from a value of 1.0 at liftoff to approximately 0.4 at Mach 3.0. Wind tunnel test data ( $\alpha = 4^\circ$ ) corresponding to measurement D82-F3 nearly coincided with telemetered SA-2 data and is shown as circled points in Figure 11-4. Wind tunnel data coinciding with the stations above was available only for this one radial location.

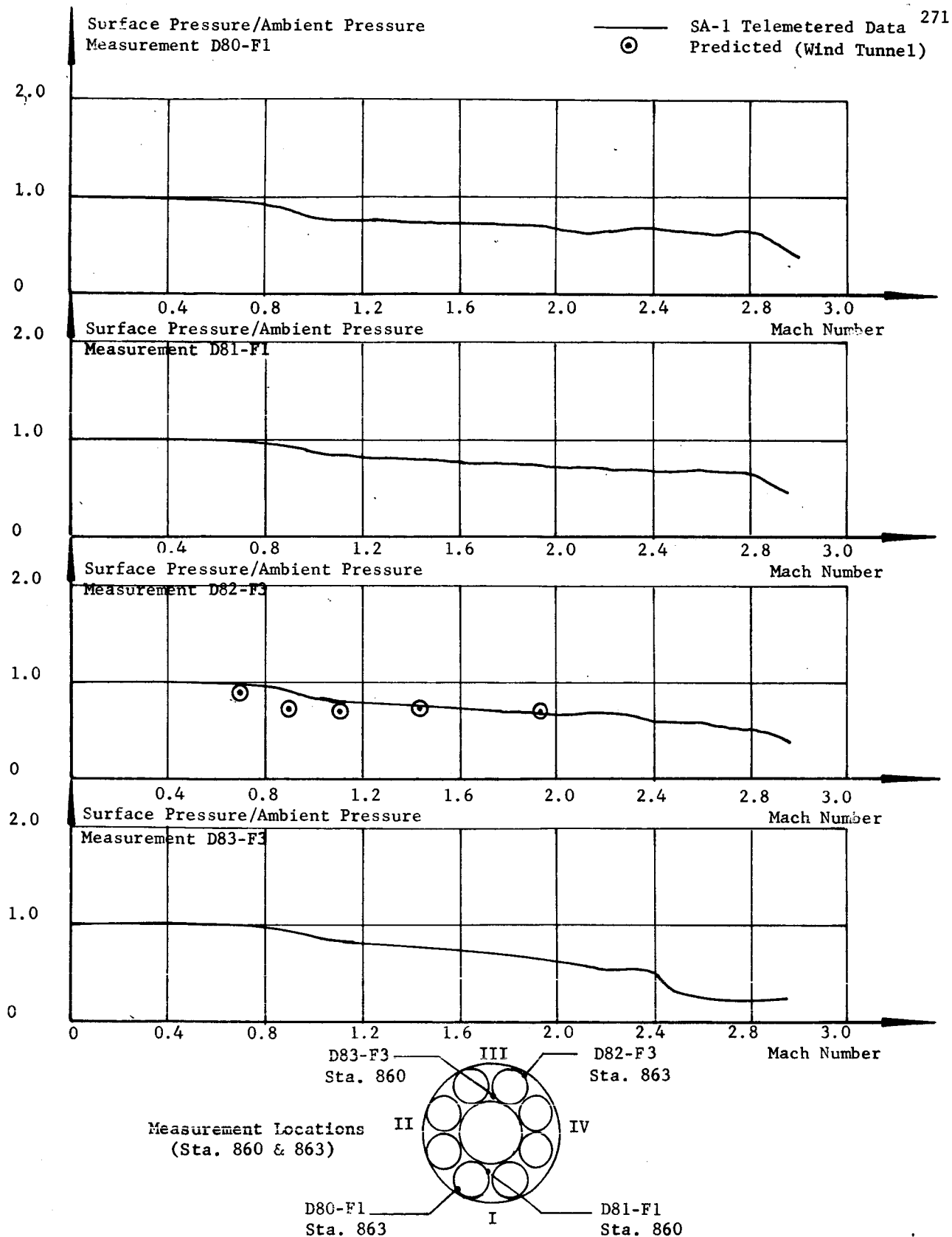


Fig. 11-4 RATIOS OF SURFACE PRESSURE TO AMBIENT PRESSURE VERSUS MACH NUMBER

## 12.0 (U) INSTRUMENTATION

### 12.1 SUMMARY

Over-all reliability of the SA-2 measuring system was 98.5 percent. Of the 526 flight measurements, four were completely unusable, three questionable, and one had to be altered before use.

All commutators performed satisfactorily with no deviations from normal operation.

All preflight and inflight calibrations were satisfactory.

Transmitted RF power from telemetry links 1 through 8 was sufficient to produce good data during a flight time of approximately 162.6 seconds. Indications are that the entire system performed without significant fallacy.

The telemetry records received were good with the exception of Cape telemetry no. 3 (Mercury Control Center). The records from the two Cape stations (Cape telemetry no. 2 and Hangar D) showed strong signals except from link 1 which measured low by about 20 to 25 dbm.

The only usable UDOP signal strength record received was from station 1.11 (Titusville - Cocoa Airport). Azusa and Radar signals were good.

Photographic coverage was good except for the lack of complete aircraft coverage of Project High Water. The requirements for aircraft coverage will be re-evaluated.

Real time data was received from the Green Mountain tracking station for the first time.

The telemetry signal was received at T+98 sec at an elevation angle of about  $-1.8^{\circ}$ . The UDOP signal was received at T+107 sec at an elevation angle of about  $-1.2^{\circ}$ . Everything functioned well at the facility except that the higher sub-carrier frequencies on "comp time" were lost.

### 12.2 MEASURING ANALYSIS

#### Measurement Malfunctions

There were 526 flight measurements made on this vehicle. Of these measurements, four were found to be completely unusable, three were questionable, and the data from one had to be altered to make it usable.

Pressure measurement D4-F2,  $\Delta P$  Fuel Sloshing, Pitch Plane, gave no data. This is an unbonded strain gauge pressure transducer. This malfunction could be in the dc amplifier of this measurement or an open leg of the bridge circuit of pressure transducer.

The pressure data from D14-8, Pressure Turbine Inlet, was about 10 percent below normal for this measurement. This is derived from the performance of the combustion chamber, fuel pump inlet, and LOX pump inlet pressures made on this engine.

Pressure measurement D12-4, Pressure Fuel Pump Inlet, showed erroneous data during the later part of the flight. The data was in error approximately 14 psi from normal at the time of inboard engines cutoff. This pressure transducer was a gauge type, but reacted as an absolute type for this flight. It is suspected that the air vent to the back of the pressure transducers diaphragm was sealed. This seal would produce the data which was obtained. Data from this measurement are usable if corrected with the ambient atmospheric pressure corresponding to the time readings.

The bending mode accelerometer E52-10 did not operate.

Two of the discrete liquid level measurements, A2-02 and A2-04, did not function. The two respective probes located below these measurements functioned normally, indicating that the liquid level had passed them.

Two other discrete probes, A3-0C and A2-03, produced questionable data. Measurement A3-0C should have produced a signal between inboard and outboard engines cutoff, based on the flow data and the pressure measurements D6-0C, D7-0C, and D3-0C. There was one signal from this measurement at 145.1 sec. The probe A2-03, which is the upper probe in LOX tank number 3, also should have produced a signal. The flow data and other discrete level measurements indicate this.

In an effort to correct these liquid level measurements, a new and more reliable type of liquid level measurement will be used on SA-3 and subsequent vehicles. These new instruments will consist of twelve optical probes spaced at equal intervals of the length of the tank. Only two impedance type probes were used at the bottom of each tank on SA-1 and SA-2.

#### Measurement Performance

Over-all reliability of the SA-2 measuring system was 98.5 percent; this is assuming eight measuring failures.

The dc flowmeter converters performed on an average of less than 0.5% within the range of its ac flowmeter counterpart. The LOX ac and dc flowrate measurements compared on an average of 0.23 gps. There was no measurable difference between the ac and dc fuel flowrate measurements.

Temperature measurements for this flight gave 100 percent performance.

The new instrumentation flown on this vehicle performed as expected. The strain gauge type pressure transducers which were used on the  $\Delta P$  sloshing measurements showed a large improvement over those flown on SA-1. A new design which was made on the ac amplifiers used on the Thrust Chamber Dome vibration measurements also showed an improvement.

### 12.3 TELEMETRY SYSTEMS ANALYSIS

#### Telemetry System Description

Data transmission for flight testing Saturn vehicle SA-2 was effected by eight Radio Telemetry System links and a TM Auxiliary Equipment Assembly. The systems utilized in this flight test were as follows: (see Table 12-I).

- A. Two XO-4 systems (links 5 and 6)
- B. Three XO-4B systems (links 3 and 4) -- Triple FM subsystems were used in conjunction with these systems. This was the first time that triple FM has been flight tested.
- C. One XO-6B system (link 1) -- This system was a high capacity commutation system used to transmit static - and low-frequency data.
- D. Two XO-7 systems (links 7 and 8) -- These systems were single-sideband systems used to transmit vibration data. This was the first time that this type system has been flight tested.
- E. A modified XO-4, PAM/FM/FM system was also used for transmitting prelaunch data; however, it should be noted that this system was located in the service room and was not a flight item.

#### Commutation

Commutators "A" and "B" on link 4 and commutator "A" on links 5 and 6 were 30 channel by 10 samples/second, electronic, solid-state commutators. Link 1 used a high-data-capacity electronic commutator. Mechanical commutators were used for the remaining commutation requirements. All commutators performed satisfactorily with no deviation from normal operation.

TABLE 12-1 SATURN SA-2 TELEMETRY SYSTEMS

Telemetry Link #	Frequency In Megacycles	System Type	Data Handling Capacity Continuous Channels	Capacity Commuted Channels	Remarks
1	242.0	XO-6B PAM/FM/FM	0	216	
2	246.3	XO-4B PAM/FM/FM Tripple FM	20	54	Commutator D, a 4 channel vibration commutator located in the TM auxiliary equipment assembly was connected to channel 18. Triple FM channels 2 thru 8 replaced Channel 17.
3	248.6	XO-4B PAM/FM/FM Tripple FM	19	62	Commutator C, an 8 channel flowrate commutator, was connected to channel 13. Commutator D, (see explanation above). Triple FM (see explanation above).
4	249.9	XO-4B PAM/FM/FM Tripple FM	19	62	Commutator C, Commutator D, and Triple FM (see explanation above). Commutators A & B on this link were solid state electronic commutators.
5	252.4	XO-4 PAM/FM/FM	15	29	Commutator D, (see explanation above). Commutator A on this link was a solid state electronic commutator.
6	253.8	XO-4 PAM/FM/FM	14	33	Commutator D, (see explanation above). Commutator E is identical to commutator D. Commutator A (see explanation above).
7	256.2	XO-7 SS/FM	15	0	15 Vibration data channels with 50 cps to 3000 cps frequency response. 2 Volt peak-to-peak preflight calibration signal must be used for reference level.
8	259.7	XO-7 SS/FM	15	0	Identical to link 7.
Total Channels:			117	456	

### Preflight Calibration

All preflight calibrations were applied to the links through the preflight calibrator in the TM Auxiliary Equipment Assembly. All preflight calibrations were normal and satisfactory.

### Inflight Calibration

All inflight calibrations were applied to the links through the inflight calibrator in each individual system. All inflight calibrations were satisfactory.

### Telemetry System Performance

This section contains information regarding links 1, 3, 7, and 8. Also, information has been included which is intended to acquaint the reader with single-sideband FM (SS-FM) transmission. There will undoubtedly be more information, to delineate the performance of SA-2 telemetry, derived from the studies now in progress.

- A. Link One. An analysis of all signal strength records indicates that transmitted RF power from link 1, the high-capacity commutator, was approximately -20 dbm from the predicted signal strength for this link. Maximum attenuation points occurred at T+37.5 seconds (-77 dbm) and T+52.5 seconds (-73 dbm). Low signal-to-noise ratios were evidenced, but they were not materially degrading to the analog records in the vicinity of the times mentioned above. There are indications that the transmitter, the RF power amplifier, or the power supply section of the link may have malfunctioned just prior to launch and caused a reduction in the amount of RF power which was generated.
- B. Link Three. Analysis of link 3 indicates that channel 5 of commutator "A" received a negative polarity (with respect to common) data input. In the interest of future evaluations, it is felt that attention should be focused to this channel because of synchronization problems associated with negative polarity inputs in some types of data reduction equipment.
- C. Links Seven and Eight (Single-Sideband FM). Because the single-sideband FM (SS-FM) system is still in its infancy, it is felt that some information regarding it should be presented in this document. The system employs balanced-modulator, frequency-translation techniques, and very sharp skirt mechanical filters. The system accommodates data of 50 cps to 3 kc/sec bandwidth and a maximum peak-to-peak amplitude of five volts.

This system is preflight calibrated by a swept-frequency sine wave which starts at 3 kc/sec, proceeds to zero cps, and then recovers to 150 cps over a 10-second duration. The preflight calibration establishes a 2-volt peak-to-peak signal which is used for reference purposes when it is demodulated in the ground receiving equipment.

Any information found in data reduction which falls outside the 50 cps to 3 kc/sec bandwidth should be regarded as spurious data. The amplitude variation of the data can be influenced a maximum of 2 db by the SS-FM system. An evaluation in progress presently indicates that the performance of links 7 and 8 was as anticipated. No deviations from expected behavior have yet been discovered.

#### 12.4 R. F. SYSTEMS ANALYSIS

##### Telemetry

The telemetry records received were good with the exception of Cape Telemetry No. 3 (Mercury Control Center). This record showed fluctuations due to ground antenna scanning.

The records from the two Cape stations (Cape Telemetry No. 2 and Hangar D) showed strong signal and compared favorably to predicted figures. An exception to the above was link 1 which measured about 20 to 25 dbm lower than the other seven links. This occurred at all three telemetry stations including the one on G.B.I. A possible explanation for this is low power output of the transmitter.

During powered flight, there were two brief but significant drops in the signal. These were very similar to those experienced during the SA-1 flight and are presumably caused by nulls in the antenna pattern. There was again a correlation among the links on the two separate antenna systems.

The period of disturbance before and during cutoff was characteristic of flame effects. Reduction in signal began at about 85 seconds. Noise fluctuations which were superimposed on the regular pattern began at about 95 seconds. The magnitude of the fluctuations appears to be directly proportional to the reduction in signal level. These rapid fluctuations increased to a maximum of 15 to 20 dbm while the signal level dropped about 25 dbm. At IECO there was a sudden increase in signal of approximately 15 dbm followed by more fluctuations which smoothed out by OECO. After OECO, the signal recovered to its former level less about 5 dbm due to increased range. The signal decreased gradually to destruct and was lost at 162.56 seconds.

The GBI telemetry station began receiving signal at about 45 seconds, shortly before visual horizon. The signal reached a maximum at about 85 seconds then gradually decreased and was lost at destruct. No flame attenuation was evidenced at this viewing angle. Figure 12-1 shows the maximum and minimum signal strength recorded at Cape Telemetry 2 and GBI along with the predicted values.

#### UDOP

The only usable UDOP signal strength record received was from station 1.11 (Titusville - Cocoa Airport). The signal was low at liftoff (-110 dbm) and increased to a maximum of about -61 dbm at 65 seconds. Between 90 and 100 seconds there was a drop of about 10 dbm. This may possibly be due to flames but is more likely attributed to the antenna pattern. Signal was lost at destruct.

#### AZUSA

The Azusa signal strength recording was good and compared favorably with predicted values. Signal was lost at 162.5 seconds.

#### Radar

Good track was obtained by radar from launch to destruct. At that time all stations continued on skin track. The record from Cape station 1.16 showed several short drops from 80 to 93 seconds. The maximum of these was about 25 dbm. There were some fluctuations in signal shortly before IECO which may possibly be due to flame effects. The GBI station (3.16) picked up signal at about 50 seconds. After increasing to full level the signal remained fairly uniform until destruct.

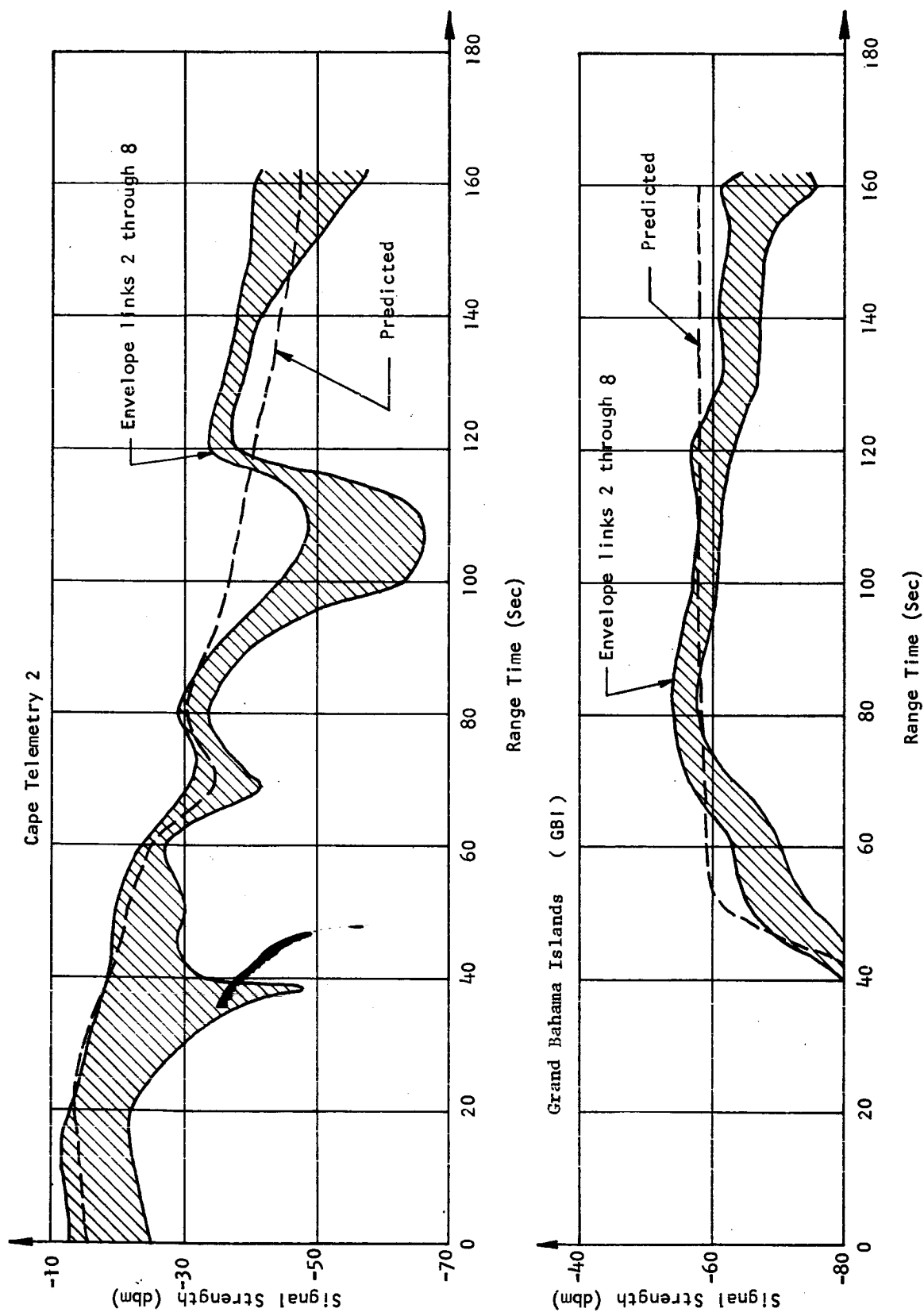


Fig. 12-1 TELEMETRY SIGNAL STRENGTH; CAPE TELEMTRY 2 & GBI

## 12.5 PHOTOGRAPHIC COVERAGE

Engineering Sequential Camera Coverage (ESCC) was utilized to record conditions surrounding the vehicle prior to and during the flight test. The film was used to record vehicle motions during ignition, liftoff, and flight. It was also used to record ground support equipment (GSE) operation, propulsion systems operation, heat shield environment, and various malfunctions which occurred.

Generally, the ESCC for SA-2 flight test was comparable to that obtained on SA-1. Eighty-one cameras were utilized to fulfill ESCC requirements. Four cameras did not operate. Two of these were to have been used for cloud coverage at twilight conditions.

The remaining 77 cameras gave good results. Sixteen cameras were located on the launch table to observe the vehicle and ground support equipment through ignition and liftoff. Five of these cameras were mounted under the torus ring to photograph engine operation during ignition and liftoff. The heat shield was also photographed by these cameras. This film showed that the heat protective tape separated from the heat shield in several areas after ignition.

The remaining eleven cameras were located on top of the launch table and were used to record the operation of each of the four retractable support arms, each of the four holddown arms, each of the short cable masts, and one in-board engine turbine exhaust. One camera, designated to view the short cable mast located at Fin IV, recorded the premature disconnect of the fuel injector manifold GN<sub>2</sub> purge line. This occurred at approximately two seconds before liftoff.

A rippling in the tail shroud and considerable vibration was observed on the film covering the areas around the retractable support arms and holddown arms. Since shroud undulation was observed on SA-1 during ignition, a checkered pattern was painted on the shroud of SA-2 to facilitate a detailed analysis of the skin undulation.

Fixed cameras, located off the launch table, recorded several interesting events during ignition and after liftoff. The long cable mast (LCM) appeared to operate satisfactorily during retraction. After the vehicle had attained approximately 300 feet altitude, however, the LCM failed in the same general area as the LCM of SA-1 due to the heat and blast of the vehicle exhaust. The retractable support arms appeared to have operated satisfactorily during ignition and liftoff; however, camera coverage showed that the retractable support arms returned to the hold position after liftoff. Exhaust smoke and debris obscured the camera view and prevented a determination of the exact time of

the return. The LOX fill and drain mast, part of the GSE, retracted satisfactorily, but failed shortly after liftoff in the area directly below the coupling assembly. This appeared to be a structural failure due to heat and exhaust blast of the vehicle. The LOX vent valve was observed venting at 2.3 seconds flight time. This occurred at approximately the same flight time on SA-1.

The tracking camera coverage was not completely satisfactory. A 400 inch lens was the longest focal length lens used on a tracking camera and did not give the detailed coverage on SA-2 that a 500 inch lens gave on SA-1. Therefore, it was impossible to determine whether or not the skin discolored near the end of powered flight. Tracking cameras which photographed the vehicle through the early part of flight showed a sudden change in the outboard engine flame at approximately 15 seconds flight time. The outboard engine aspirators direct the fuel-rich turbine exhaust gases around the main chamber exhaust which produces a dark area in the flame near the chamber exit. Until 15 seconds flight time the dark area in the flame is approximately five feet long. It then is suddenly reduced to approximately two feet in length. This same change was noted on SA-1 at this time in flight.

Film from one tracking camera, which was exposed to photograph the flame pattern during flight, also showed considerable detail of the heat shield and tail shroud area. It showed that the heat protective tape on the heat shield was separated from the heat shield in certain areas but did not appear to be torn or to fall loose from the vehicle through approximately 50 seconds of flight time. After this time the vehicle image became too small to permit detailed observation of components in the tail.

Engineering tracking cameras were utilized to record the cloud formation after the vehicle explosion. The image size from the camera with the 400 inch focal length lens was so small at the time of the explosion that a detailed analysis of the vehicle breakup could not be made. Pieces of the vehicle could be seen after the explosion, but the image size was so small that the pieces could not be identified.

Two Fixed Cameras were utilized to record the sway of the vehicle caused by wind loads. Data from these cameras were to be used to correlate with data from strain gauge measurements; however, the image size was too small and the collimators were misaligned for these cameras and no usable data were obtained.

Limited useful data was obtained from the aircraft coverage of the vehicle in flight. On the basis of the poor coverage obtained from aircraft on both SA-1 and SA-2 flight tests, the requirements for aircraft coverage will be re-evaluated and possibly replaced by more

long range tracking cameras for future flights.

Photographs of various items and events are distributed throughout this report.

## 12.6 SA-2 DATA ACQUISITION AT GREEN MOUNTAIN TRACKING STATION

### Background

An attempt was made to provide real time flight data of SA-2 to the Computation Division. Primary importance was placed upon real time data; however, of almost equal importance was the obtaining of SA-2 telemetry data prior to first engine cutoff. UDOP data was to be provided on magnetic tape with "Comp time" as the time reference. Preparations were made at the Green Mountain tracking station for receiving and re-transmitting the telemetry data as well as recording it on magnetic tape.

### Telemetry

Telemetry signals were received with a tri-helix antenna and fed to a low noise multi-coupler amplifier. The multi-coupler fed 8 receivers, one for each telemetry link. The detected output of each receiver was used to modulate spare flight telemetry transmitters, one for each link, as well as being recorded on magnetic tape. The outputs of the transmitters were fed in pairs to yagi antennas which transmitted the signal to the Computation Division and the Astrionics Division. See Figure 12-2.

### UDOP

The UDOP signal was received with a 19 ft. dish using a helical feed and fed to the UDOP receiver. The 50 mc reference signal for the UDOP system was transmitted to Green Mountain from the Astrionics Division. The 50 mc signal was derived from an Atomicon with an output frequency of 10 mc, which was multiplied to 50 mc. The doppler beat from the UDOP receiver was recorded on magnetic tape with "Comp time" as the time reference. See Figure 12-2.

### Results

The telemetry signal was received at  $T + 98$  sec at an elevation angle of about  $-1.8^\circ$ . At  $T + 109$  sec. the telemetry signal level was at -80 dbm and got as high as -77 dbm at the time of destruct.

The UDOP signal was received at  $T + 107$  sec at an elevation angle of about  $-1.2^\circ$ . The average signal level of the UDOP signal was -80 dbm.

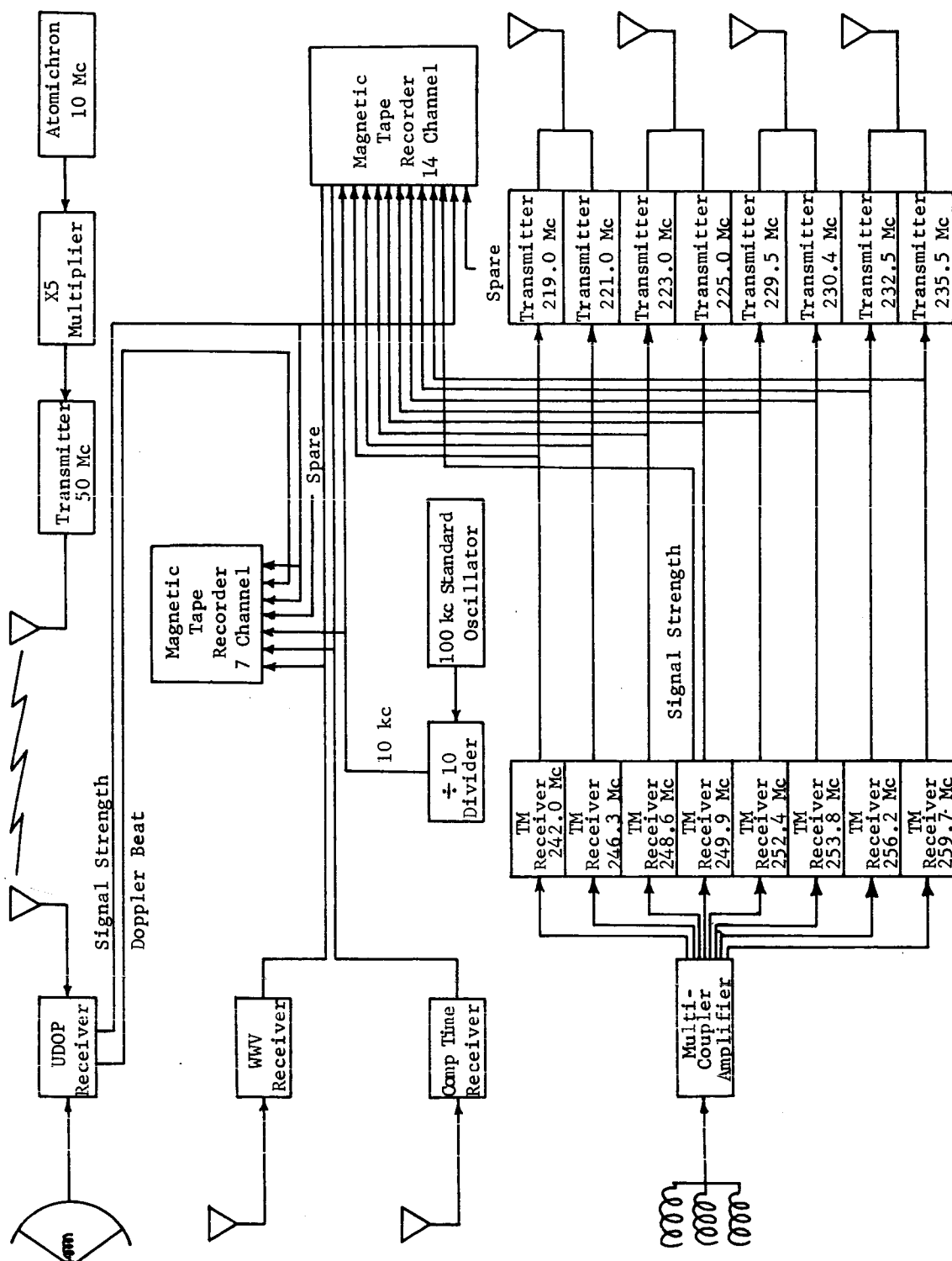


Fig. 12-2 SYSTEM BLOCK DIAGRAM

The signal was held until destruct.

Everything functioned well at the facility except the higher subcarrier frequencies on "Comp time" were lost.

It is of particular interest to note the received times of both the telemetry and UDOP signals,  $T + 98$  sec. and  $T + 107$  sec. respectively. If one calculated the expected time for receiving the signal using a true earth radius of approximately 6370 km and line-of-sight geometry, the expected time for receiving the signals would be approximately  $T + 125$  sec. However, if one uses line-of-sight geometry and earth radius equal to  $4/3$  true earth radius, the calculated expected time for receiving the signals would be  $T + 109$  seconds, which agrees closely with the received time of the UDOP signal. See Figure 12-3.

Calculations based on the  $4/3$  radius principle were made prior to the firing of SA-2, and the hope of receiving the telemetry signal prior to first cutoff depended upon this theory. Experiments conducted by others indicated that below 2 Kmc and above 50 mc, radio wave propagation was not limited by line-of-sight paths but only as a first approximation. It has long been recognized that radio frequency energy is bent around the curvature of the earth by both refraction and diffraction; however, path losses do become unpredictable. Theory states that below 2 Kmc a  $4/3$  radius is a good approximation. However, there are other factors involved such as atmospherics. It is also possible that instead of the  $4/3$  radius used for both the telemetry and UDOP frequencies that  $5/3$  may apply to the telemetry frequencies and  $4/3$  to the UDOP frequency.

It would be of interest on future firings to correlate actual received times with times calculated on various earth radii, depending on the carrier frequency. The same could be done for other receiving stations.

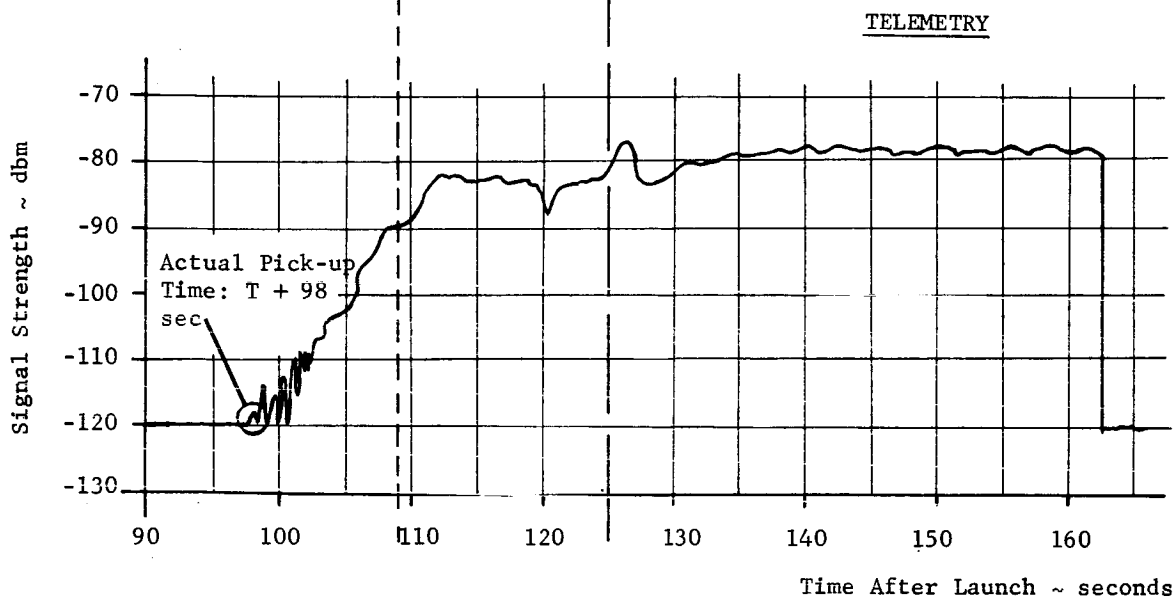
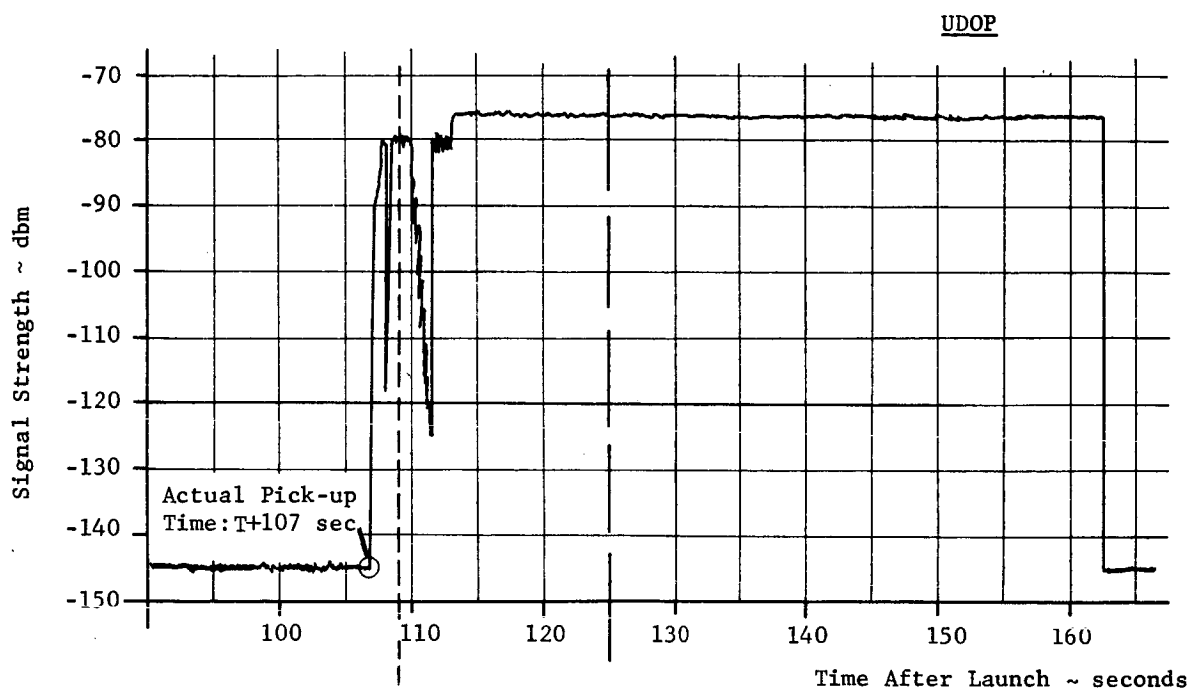


Fig. 12-3 TELEMETRY AND UDOP SIGNAL STRENGTH PLOT

~~CONFIDENTIAL~~

## 13.0 (C) SUMMARY OF MALFUNCTIONS AND DEVIATIONS

The flight test of Saturn SA-2 did not reveal any malfunctions or deviations which could be considered a serious system failure or design deficiency. However, a number of minor deviations did occur and are summarized here for documentary purposes.

Corrective measures were recommended by the divisions for some of the items listed. These are marked with an asterisk. Each item listed shows the section of the report where the occurrence is explained in detail.

1. Quick disconnect fitting on 500 psi GN<sub>2</sub> line at Short Cable Mast failed (Para 3.2.3).\*
2. Low thrust on Engine at position no. 2 (Para 5.2).
3. 1.61 seconds longer than expected burning time (Para 5.3).
4. Deviation of 0.9 m/sec in cross range velocity (Para 7.3.2).
5. Loading of tilt cam every 13.1 seconds (Para 6.3.2).\*
6. Loose heat tape noted on heat shield before liftoff (Para 12.5).\*
7. 26 cps oscillations in Instrument canister no. 15 (Para 7.3.3).
8. Low pressure in gear case on some of engine positions (Para 5.2).
9. Specific Impulse of vehicle again higher than expected (Para 5.3).
10. Q-ball angle of attack drifted out of suitable measuring tolerance after 80 seconds (Para 6.3.1).
11. Higher noise level in gear box on Engine no. 4 (Para 9.6.3).
12. Eight measurements failed to operate properly during the flight (Para 12.2).

~~CONFIDENTIAL~~

## (U) REFERENCES

1. Experimental Vibration Program on a Full Scale Saturn Space Vehicle, MTP-P&VE-S-62-3, dated April 26, 1962.
2. Preliminary Vibration Analysis of Saturn SA-1 (Case V), DSF-TM-2-60, dated April 21, 1960.
3. Predicted Bending and Torsional Vibration of Saturn SA-D in Dynamic Test Tower, IN-M-S&M-S-61-13, dated June 1, 1961.
4. Memorandum to Distribution from Director, Aeroballistics Division, Saturn C-1 Vehicle SA-2 Test Flight: Trajectory Corridor to be Flown by SA-2, dated April 18, 1962.

## APPENDIX A

## (U) SYSTEM DESCRIPTION

## A.1.0 LAUNCH CHARACTERISTICS

Saturn vehicle SA-2 was launched April 25, 1962, at 0900:34.41 EST from Launch Complex 34, Cape Canaveral, Florida, with a firing azimuth of 100 degrees east of North (see Figure A-7).

The geographical coordinates of Complex 34 are:

Geodetic Latitude	28.521529 degrees
Longitude	80.561357 degrees

## A.2.0 SA-2 VEHICLE DESCRIPTION

Saturn SA-2, the second of the C-1 series of Saturn launch vehicles, represents the second United States launch vehicle in the 1.5 million pound thrust class. With a total length of approximately 163 feet and measuring more than 21 feet in diameter at the base, SA-2 was powered by eight Rocketdyne H-1 liquid propellant rocket engines developing a total sea level thrust of more than 1.3 million pounds. The total vehicle weight was approximately 927,000 lbs at liftoff with approximately 608,000 lbs of propellant consumed during the S-I powered phase of flight.

SA-2 was the same basic configuration as the Saturn SA-1 vehicle flight tested in October 1961. The vehicle was made of a live S-I stage, a dummy S-IV stage, a dummy S-V stage, and a dummy payload. A diagram of the overall Saturn configuration including some of the more important vehicle dimensions is presented in Figure A-1. SA-2 mass characteristics are presented in Appendix D.

## A.2.1 S-I STAGE

The S-I stage was the only active stage of the SA-2 Saturn vehicle. Propulsion was provided by a unique arrangement of eight clustered H-1 rocket engines. Propellants were supplied to the engines from a cluster of nine propellant tanks. Most of the SA-2 instrumentation, including guidance and control components, were located in the S-I stage. The SA-2, S-I stage was essentially the same as the S-I stage flown on SA-1, with the only important change between the two vehicles being the adding of additional anti-slosh baffles to the outer propellant tanks.

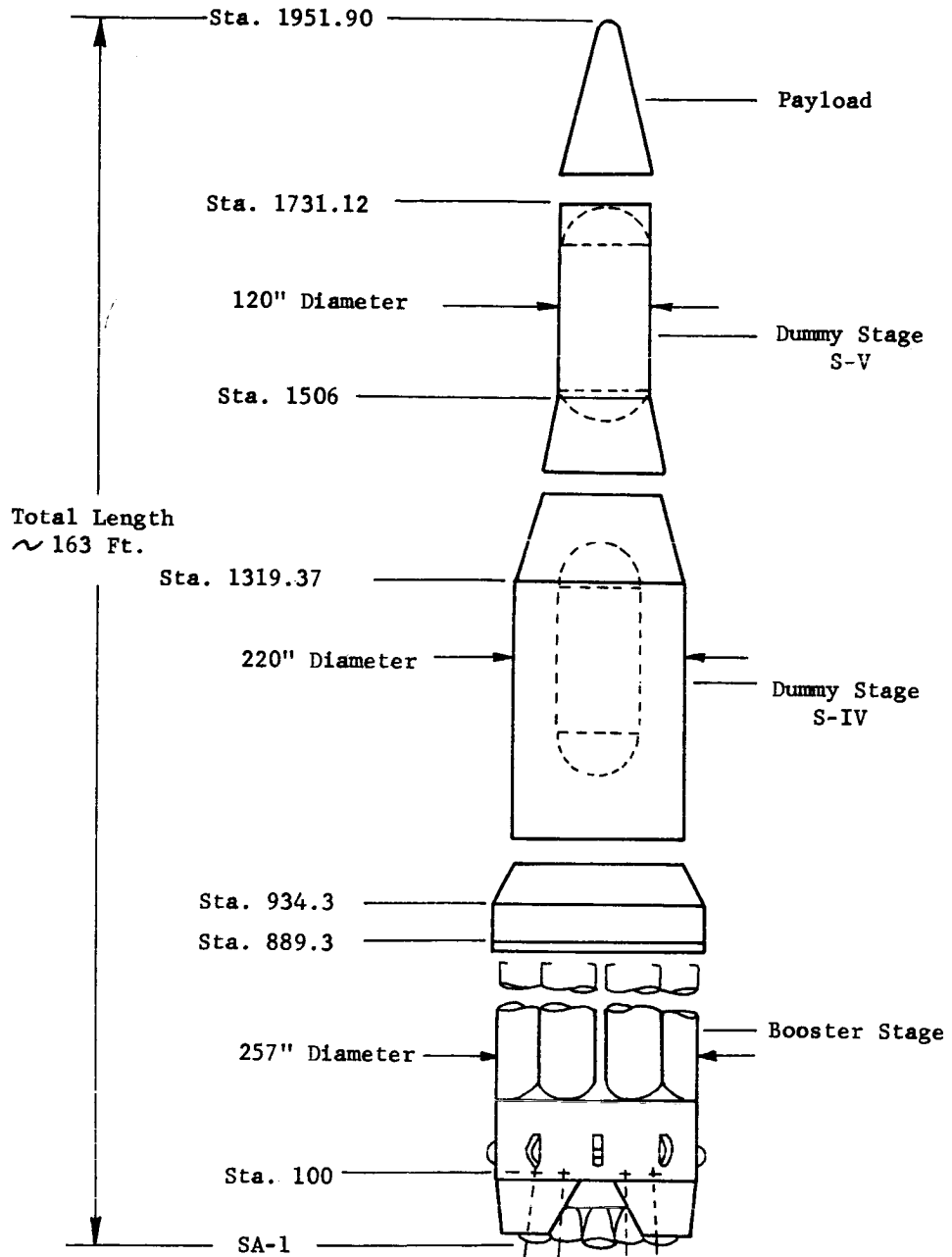


FIGURE A-1 SATURN CONFIGURATION

## Propulsion

The S-I or booster stage of the SA-2 vehicle was powered by eight clustered H-1 liquid propellant engines. Engines 1 through 4 are designated outboard while engines 5 through 8 are designated inboard. The four inboard engines are fixed mounted on a 64 inch diameter with a 3° cant angle. The four outboard engines are gimbal mounted to provide pitch, yaw, and roll control with a null position cant angle of 6°. The outboard engines have a maximum gimbal angle of 7° in the pitch and yaw planes.

The SA-2 flight test was the second flight flown with "Engine-Out" capability. "Engine-Out" was to be initiated by one pressure sensor each in the eight high pressure fuel lines (just down stream of fuel pump outlets). If the normal pressure of about 780 psia is reduced to a value of 670 psia the sensor would start the cutoff sequence for that engine. Should thrust termination occur in an engine or engines, the LOX and fuel supply of that engine or engines would be routed to the remaining engines through the respective interchange lines (see Figure 5-13, Page 57 and Figure 5-15, Page 60 of the main report). The LOX and fuel level cutoff sensors would then effect a longer burning time.

The "Engine-Out" system has provisions for cutting off only one engine during the first 10 seconds after liftoff. At liftoff plus 10 seconds the "Engine-Out" mode switches to a multi-engine out system. During the flight of SA-2 it was not necessary to make use of this capability. Measured engine parameters indicated that the pressure in the high pressure fuel lines was above cutoff switch setting (nominal setting of  $700 \pm 10.5$  psia. However, the wide tolerances of this gauge allows minimum cutoff switch operation at 656 psia). Engine #2, which was low for SA-2, was approximately 710 psia after thrust commit (switch not activated until after thrust commit due to chamber pressure transition). During the holddown period cutoff can be given by the fuel line pressure, Rough Combustion Monitor, or the fire detection system.

The H-1 engine is a fixed thrust, single start type, bi-propellant rocket engine. It is a derivative of the Thor-Jupiter-Atlas family of rocket engines manufactured by Rocketdyne Division of North American Aviation. The SA-2 version of the engine produces a nominal 165,000 pounds of thrust and has a nominal sea level specific impulse of 252.7 lb sec/lb.

Liquid oxygen (LOX) and RP-1 fuel are the propellants used as the main power source. A hypergolic fuel mixture is used for combustion chamber ignition, and a solid propellant charge provides initial gas to spin the turbine.

Major components of the H-1 engine are a thrust chamber assembly, turbopump assembly, gas generator assembly, hydraulic system (outboard engines only), and a hypergolic ignition system. The H-1 engine has no thrust or chamber pressure control.

The exhaust gases from the turbine are handled differently in the outboard and inboard engines. In the case of the outboard engines the exhaust is routed rearward through the heat exchanger and into an aspirator. The aspirator is welded around the periphery of the expansion nozzle exit to form an integral part of the thrust chamber. Use of the aspirator on the gimbaled engines allows removal of the hot gases from the engine compartment without the need for flexible joints in the turbine exhaust ducts. The exhaust gas from the inboard engine turbine is routed laterally from the heat exchanger through the outer vehicle skin, then ejected rearward.

Propellants were supplied to the engines by use of suction lines from an arrangement of nine propellant tanks. These tanks consist of four 70" LOX tanks, four 70" fuel tanks, and one 105" LOX tank. The 70" fuel and LOX tanks are mounted alternately around the circumference of the center LOX tank. Each outboard tank (LOX and fuel) supplies propellant to one inboard and one outboard engine. The center LOX tank is used to supply the outboard tanks through the LOX interchange system and does not supply LOX directly to any engine.

LOX tank pressurization is provided by gaseous oxygen (GOX). The GOX is obtained by passing LOX through a heat exchanger (one for each engine). Pressurization of the fuel tanks is provided by gaseous nitrogen ( $\text{GN}_2$ ) supplied from 48 storage spheres located atop the propellant tanks.

Eight outriggers and a spider beam assembly support the outer propellant tanks. The LOX tanks form the basic structure with the fuel tanks mounted to allow for thermal contraction of the S-T stage structural elements. All four fuel tanks are interconnected at the base through the fuel interchange system. Baffles used to prevent propellant sloshing in the tanks may be seen on Page 117. As a result of the SA-1 flight test additional baffles were installed at the bottom of the outer propellant tanks. As seen on Page 117 the baffles were added to the outer LOX tanks between stations 291.99 and 378.99 and to the fuel tanks between stations 311.75 and 369.75. The baffles were added in order to reduce the sloshing amplitude during the period of flight from 80 to 105 seconds.

A propellant utilization (PU) system was flown as a passenger on this flight to obtain flight data for performance evaluation of the system. The system utilized two (one for LOX and one for fuel) differential pressure transducers for propellant weight information. Signals from the transducers were sent to a computer for mass ratio determinations.

### Guidance and Control

Active inertial guidance was not incorporated in SA-2. However, in anticipation of future guided flights, partially active guidance components were carried as passengers only. Several components (i.e., ST-90 stabilized platform, program device, angle of attack transducers, etc.,) from the Jupiter Missile Program were utilized with relatively minor modifications for control and sequencing.

The ST-90 stabilized platform was used to provide the attitude reference signals for control of the four gimbal engines. Angular rate information for vehicle damping was obtained by electrical differentiation of the attitude signal in the Flight Control Computer. First and second bending mode influences on the control system were suppressed by phase shaping and/or attenuation of those frequencies in the computer. Angle of attack information\* is derived from four local type transducers (see Fig. A-4 for location) and fed into the Flight Control Computer. The computer filters, amplifies and/or attenuates, shapes, sums these signals, and issues commands to the eight hydraulic actuators for proper positioning of the control engines. This gives vehicle control in pitch, yaw, and roll.

In order to obtain information necessary for the development of the guidance and control system of future Saturn C-1 vehicles several items were test flown on SA-2. These items were as follows:

- a. Three ST-90 mounted AMAB-4 Accelerometers which provide 3 axes velocity information in digital form.
- b. A Guidance Signal Processor - Repeater which processes the digital velocity signals and conditions them for telemetering.
- c. A 3 Axes Control Rate Gyro Package which provides attitude rate information as a. c. signals.
- d. A Control Signal Processor which converts the attitude rate information to d. c. control signals and conditions them for telemetering.
- e. Pitch and Yaw Control Accelerometers which measure lateral vehicle accelerations, converts the signals to d. c. control signals and conditions them for telemetering.
- f. A Q-ball Transducer which measures pitch and yaw angles-of-attack and dynamic pressure, converts the signals to d. c. and conditions them for telemetering.

---

\*For artificial stabilization

The tilt program for the SA-1 vehicle was accomplished by a step input method. Pitch actuator deflections of 2 degrees resulted from the tilt program commands, as expected. Even though this did not have any appreciable effect on the stability of the vehicle, a "smooth" tilt program was introduced on the SA-2 vehicle. The tilt program for SA-2 is based on the engine out concept; that is, the tilt angle is designed for seven engines thrust operating from liftoff.

### Structure

The booster structure consists basically of a thrust frame on which the eight engines are mounted, five LOX containers (designed as load carrying members), four fuel containers (flexible mounted to allow for shrinkage), and at the top of the containers a transitional structure extending to the base of the second stage.

### Heat and Flame Protection

#### (1) Firewall

Location: Lower end of thrust frame (see Figure A-5)

Function: Prevents fires originating in engine compartment from spreading into propellant tank area

#### (2) Heat Shield

Location: Station 54, (46" from engine gimbal point) covers entire area within shrouds (see Figure A-5)

Function: Provides (1) lateral support for shrouding and (2) protection to all equipment forward of Station 54 (structures, engines, etc.,) from flames and heat flux of engines.

#### (3) Flame Shield (Star or Base Plate)

Location: Exit of inner engine nozzles (see Figure A-5)

Function: Provides heat and flame protection for engine compartment principally by recirculating hot exhaust gases in base region.

### Instrumentation

SA-2 carried a telemetry system composed of eight separate R-F links. Two single side band units were flown for the first time on

SA-2. These units were used to transmit high frequency information for the vibration and accoustical measurements. These units allow accurate frequency measurements up to 3 kc. The telemetry units and antennas were located in the Adapter Section at the top of the S-I stage. The instrumentation program for the S-I stage was as follows:

<u>Type Measurement</u>	<u>Total Number (S-I Stage)</u>
Propulsion	76
Temperature	145
Pressure	125
Strain and Vibration	77
Flight Mechanics	13
Steering Control	21
Stabilized Platform	5
Guidance	3
Signals	21
Volt, Current and Frequency	<u>21</u>
Total Measurements (S-I)	507

#### A.2.2 S-IV DUMMY STAGE (FIGURE A-2)

The S-IV dummy second stage for Saturn SA-2 carried water ballast (89,525 lb) to simulate the weight and aerodynamic characteristics of the live S-IV stage. Dimensions of the S-IV stage are given in Figures A-1 and A-2. The instrumentation on this stage was a sound intensity measurement at station 1200.

#### A.2.3 S-V DUMMY STAGE (FIGURE A-3)

The S-V dummy third stage was basically a Centaur cruiser tank modified by increased skin gages. The tank carried water ballast (102,000 lb) to simulate upper stage weight. Dimensions of the S-V stage are given in Figures A-1 and A-3. The only in-flight measurement on this stage was the pressure of the S-V dummy ballast.

#### A.2.4 DUMMY PAYLOAD (FIGURE A-4)

SA-1 carried a Jupiter type nose cone and aft unit as dummy payload. An adapter section was required to mate the aft unit to the S-V stage. Four local angle of attack meters and two bending accelerometers were mounted on the aft unit as instrumentation. Other instrumentation on the dummy payload included one dynamic pressure measurement and ten measurements associated with the test of the Q-ball angle of attack transducer.

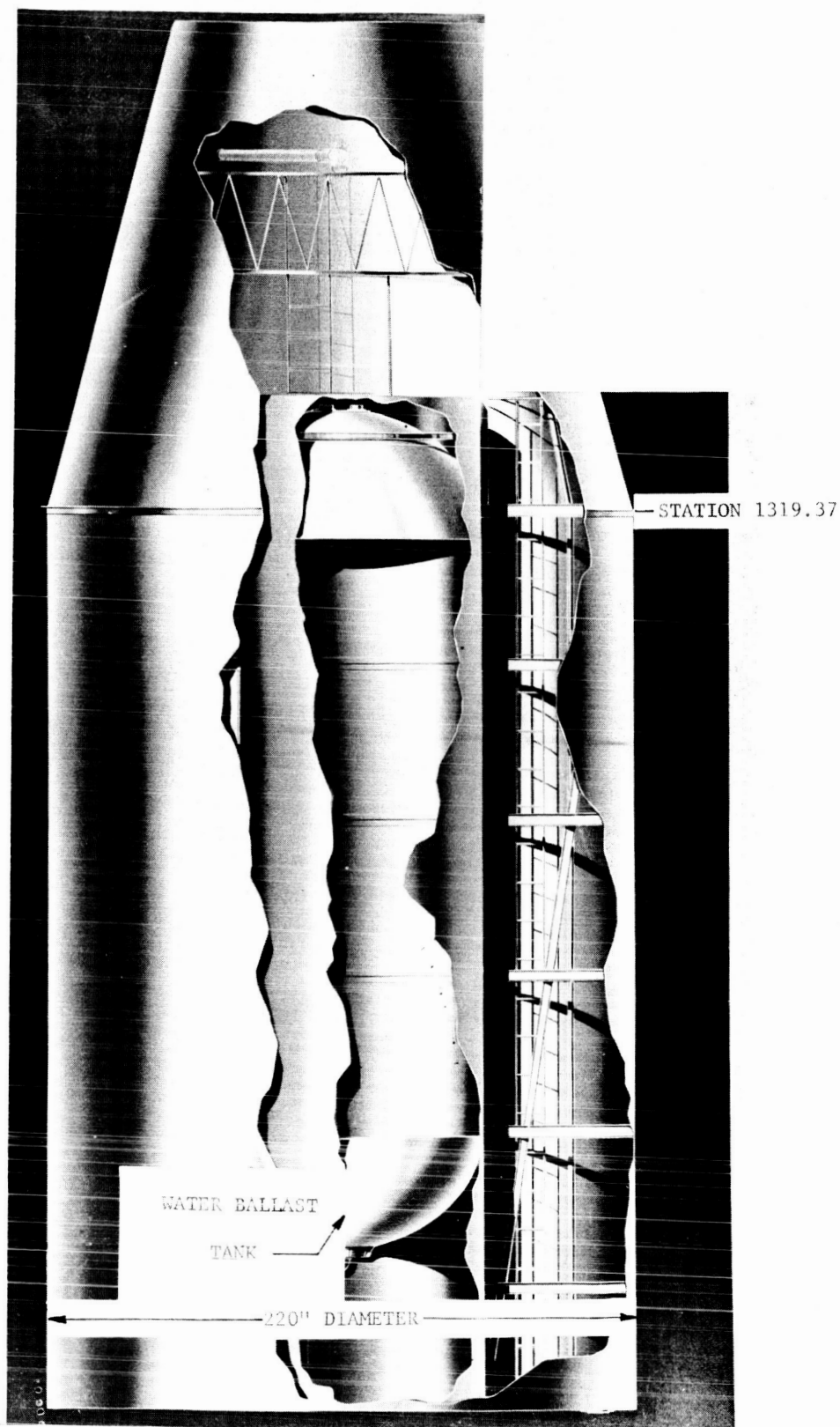


FIGURE A-2 DUMMY SECOND STAGE, SATURN SA-2

MPR-SAT-WF-62-5

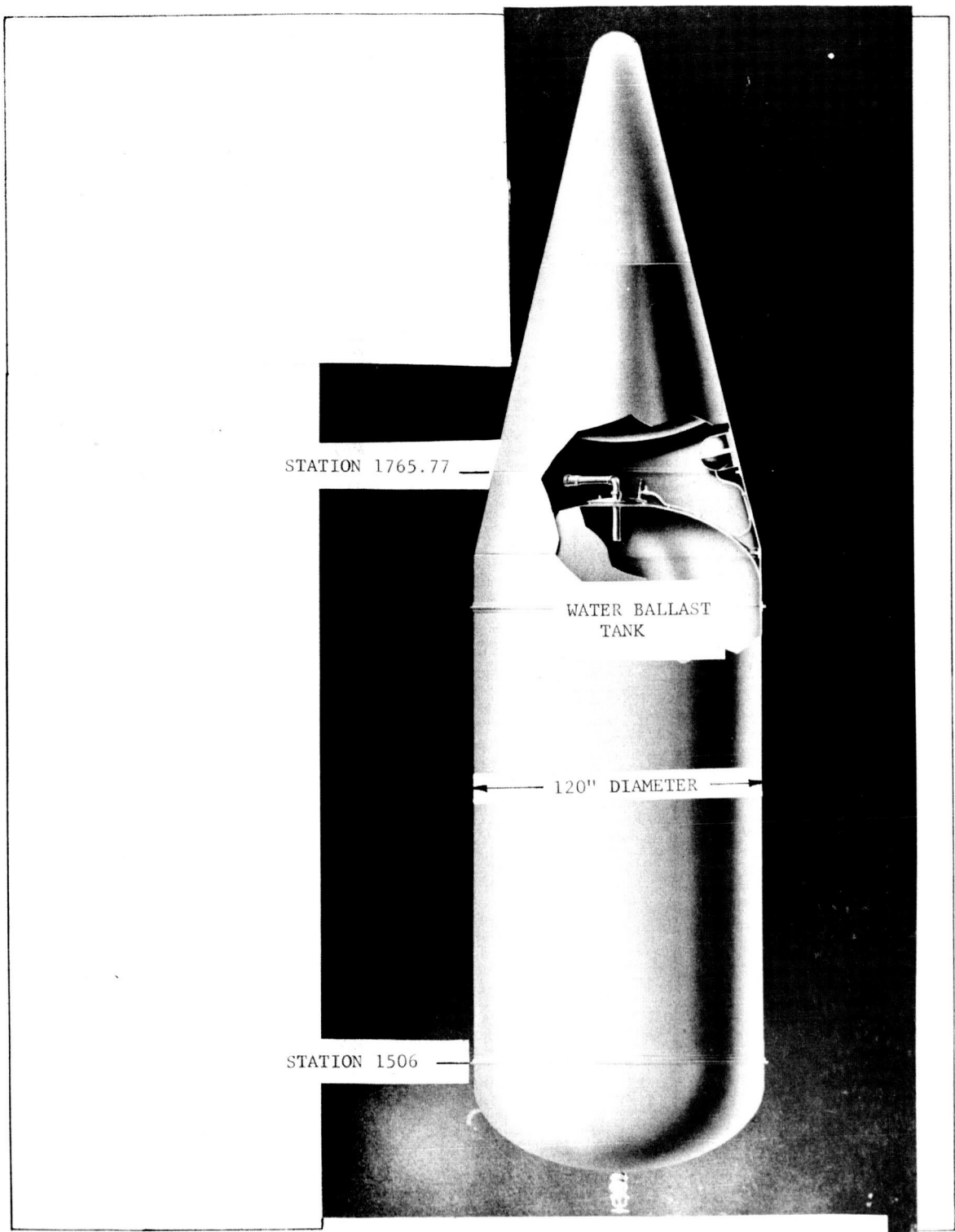


FIGURE A-3 DUMMY THIRD STAGE, SATURN SA-2

MPR-SAT-WF-62-5

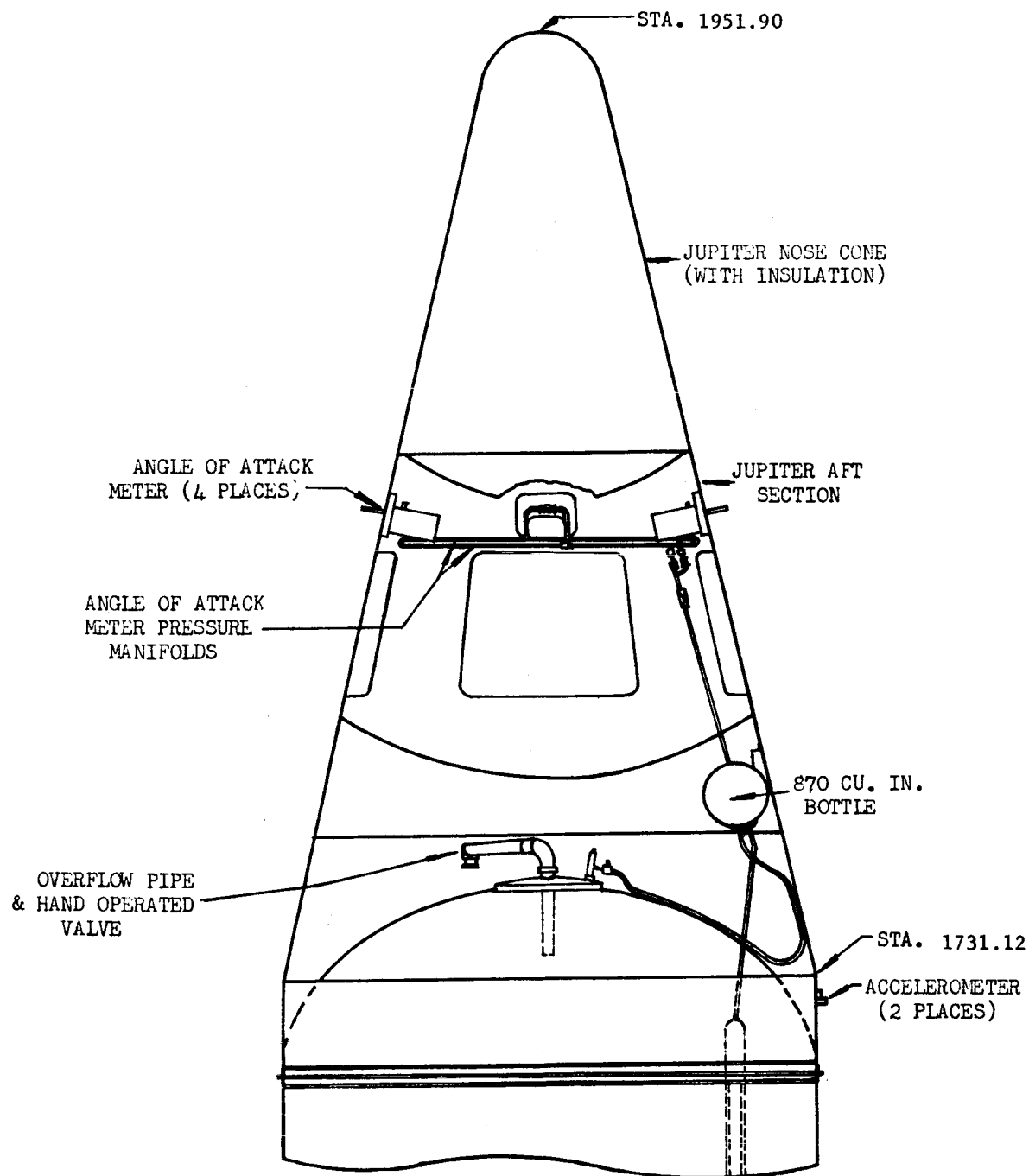


FIGURE A-4 DUMMY PAYLOAD, SATURN SA-2

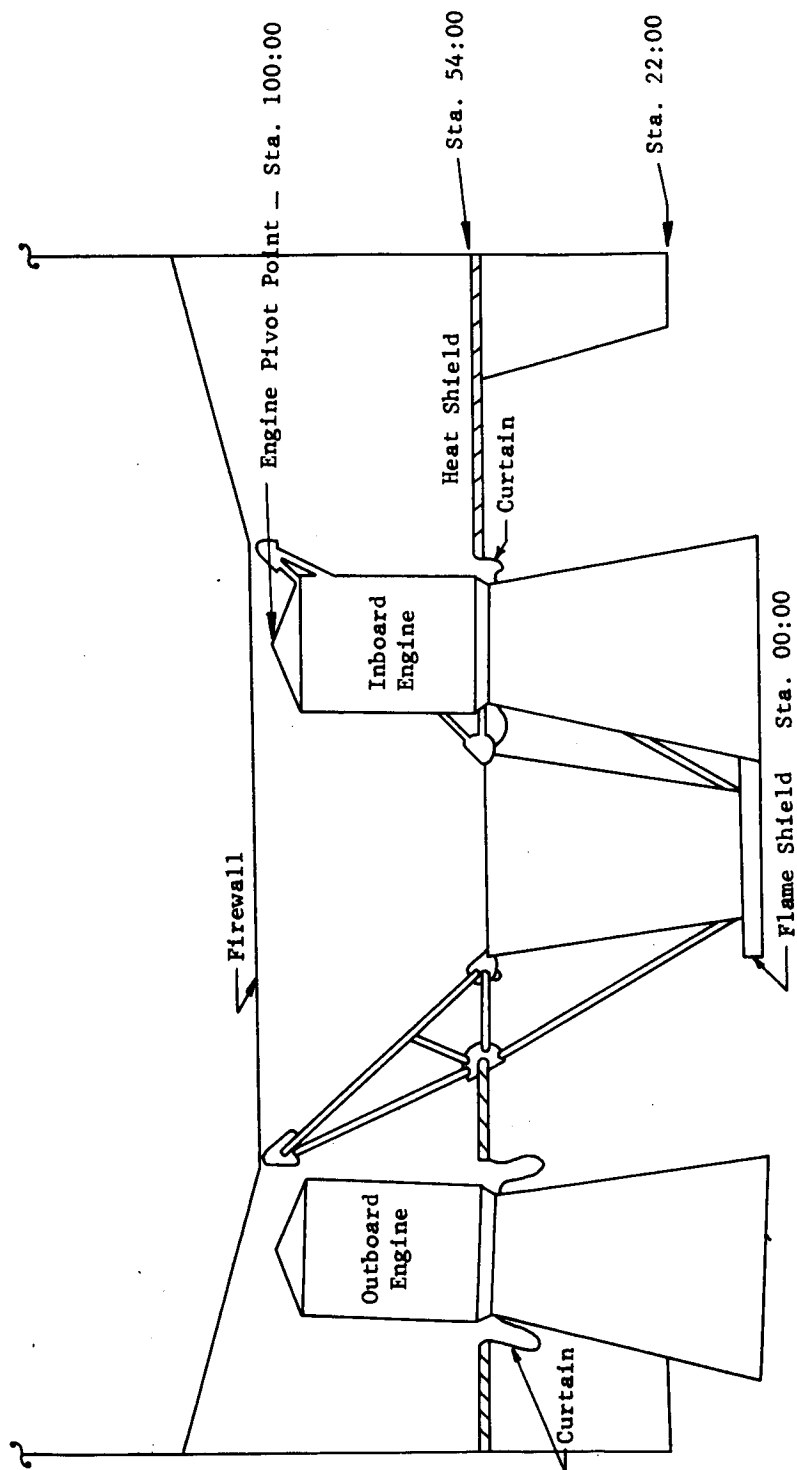


FIGURE A-5 ENGINE COMPARTMENT LAYOUT

### A.3.0 GROUND SUPPORT EQUIPMENT (FIGURE A-6)

#### A.3.1 SHORT CABLE MAST ASSEMBLY

Number : 2

Location: Fin II and Fin IV

Function: Provides (1) means of routing electrical cables and pneumatic lines from launcher to vehicle, (2) quick disconnect of these cables and lines 0.3 seconds before liftoff, and (3) successful release to initiate support arm retraction.

#### A.3.2 LONG CABLE MAST ASSEMBLY

Number : 1

Location: 30° from Fin II toward Fin I

Function: Provides (1) means for mounting equipment; routing and connecting electrical cables, pneumatic lines, LN<sub>2</sub> line, and two air conditioning ducts to the vehicle booster instrument compartment; and (2) rapid disconnect prior to liftoff.

Operation: Automatically retracted prior to liftoff.

#### A.3.3 SUPPORT ARMS

Number : 4

Location: 45° off fin lines

Function: Support the vehicle on the launch table. After thrust buildup is complete, support is no longer needed; therefore, on release of the short masts, the support arms begin to retract. During the retraction period, combustion instability and low thrust are monitored continuously. Any malfunctioning engine is cut off immediately. A malfunction stops the sequence and initiates support arm return. The remaining engines are cut off when the supports have returned. Successful retraction of the support arms initiates launch commit and vehicle holddown arm release.

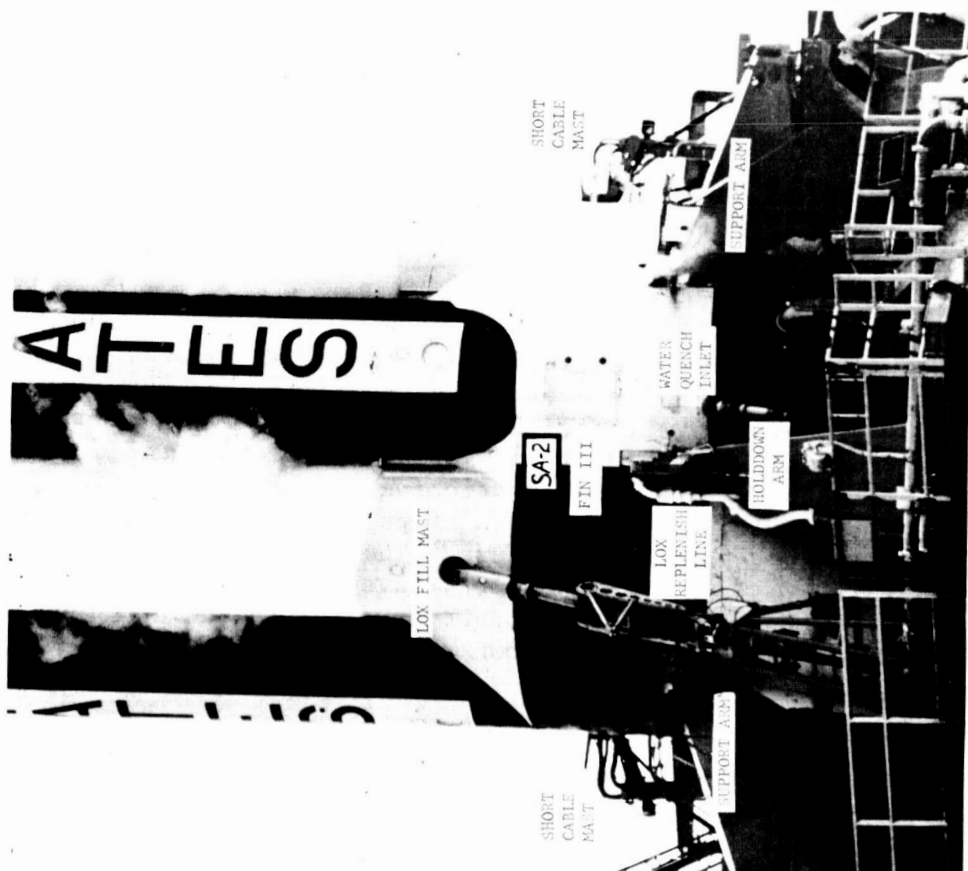


Figure A-6 GROUND SUPPORT EQUIPMENT

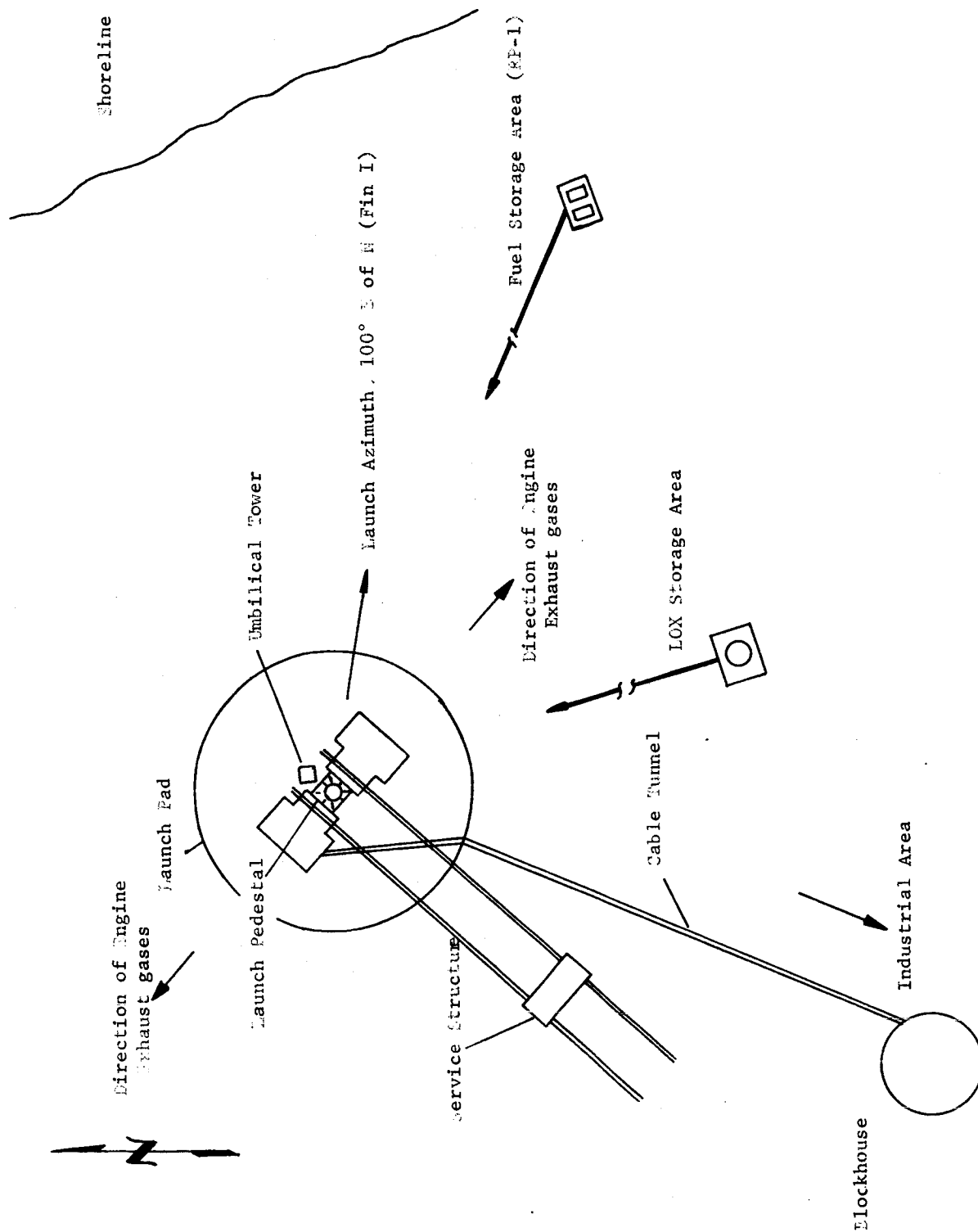


FIGURE A-7 SATURN LAUNCH COMPLEX 34

#### A.3.4 HOLDDOWN ARMS

Number : 4

Location: On fin lines

Function: Secure vehicle to launch table during the holddown period. Release vehicle after monitoring systems show "go" position and launch commit is given.

#### A.3.5 FUEL AND LOX FILLING MAST ASSEMBLIES

Position: Fuel fill 30° from Fin I toward Fin II: LOX fill 30° from Fin III toward Fin II.

Function: Supply the final links in the fuel and LOX filling systems to the vehicle storage tanks.

#### A.3.6 BOATTAIL CONDITIONING SYSTEM

The purpose of the boattail conditioning system is to provide a controlled atmosphere in the vehicle boattail area during various periods while the vehicle is on the launch pad. A controlled atmosphere is necessary for personnel safety and vehicle protection. The function of the system is threefold:

- (1) Air Purge - with LOX tanks empty, supply oil-free air at 10° - 21° C at rate of 1900 SCFM for personnel. With LOX tanks full, air temperature is at 21° C.
- (2) Gaseous Nitrogen Normal Purge - At T-5 sec gaseous nitrogen is supplied at 1800 SCFM.
- (3) Gaseous Nitrogen Deluge Purge - Used for vehicle malfunction requiring shutdown. Rate of supply is 5400 SCFM at -46° C.

#### A.3.7 HIGH PRESSURE BATTERY

Function: Source of all  $\text{GN}_2$  and  $\text{H}_2$  used for checkout, servicing, and launching.

#### A.3.8 LOX REPLENISHING SYSTEM

Function: Provides LOX topping for booster tanking system.

#### A.3.9 LIFTOFF SWITCH INSTALLATION

Number : 4

Location: Mounted on forward portion of each holddown arm

Function: Provides means of completing electrical circuit to recorder located in blockhouse for recording time of vehicle liftoff from launch pedestal.

#### A.3.10 WATER QUENCH SYSTEM

- Function: (1) Conveys water to tail section spray nozzle system for combating fires in boattail section.
- (2) Supplies conditioned air to tail section spray nozzle system.

#### A.4.0 GROUND INSTRUMENTATION

Three ground instrumentation systems were utilized during the flight. These were telemetry receivers, optical systems, and tracking systems.

##### A.4.1 TELEMETRY RECEIVERS

Telemetry stations used to record signals received from the onboard telemetry transmitters were as follows:

##### NASA Stations

Hangar D  
Blockhouse 34

##### RCA Stations

Station Location	Station Number
Cape	Tel 2
Cape	Tel 3
GBI	3.0

Each receiver station contains a minimum of one receiver, one panadapter, and two 7-channel recorders.

•

#### A.4.2 OPTICAL SYSTEMS

##### Documentary Cameras

A documentary history of significant events and vehicle activities was recorded on film. These cameras were located in appropriate positions to record the desired activities.

##### Engineering Sequential Cameras

Fixed and tracking engineering sequential cameras were used to monitor significant vehicle events and to provide information for vehicle performance evaluation. Wide camera coverage was obtained on the launch table. Four cameras were used to view the four retractable support arms; four cameras viewed the two short cable masts, and five cameras, located on the torus ring, covered ignition of the eight engines. Other cameras were used to view the complete vehicle, launcher, and a portion of the pad area during ignition and liftoff, and to record vehicle motion, structural integrity, and flame effects. In addition to the fixed and tracking cameras, long focal length tracking telescopes were used as follows:

Type	Locations
Recording Optical Tracking Instrument (ROTI)	Melbourne Beach and Vero Beach
Intercept Ground Optical Recorders (IGOR)	False Cape, Williams Point, Cocoa Beach, and Patrick AFB
Metric Cameras	False Cape, East Cape, West Cape, South Cape, Cocoa Beach, PAFB

#### A.4.3 TRACKING

The following tracking systems were used for the SA-2 test flight:

- a. UDOP
- b. Azusa
- c. S-Band Radar
- d. C-Band Radar

All SA-2 tracking beacons were located in Instrument Canister No. 14. The antennas for this equipment were located in the vehicle skin as follows:

- |    |                                   |   |
|----|-----------------------------------|---|
| a. | UDOP (2)<br>Station 919           | 7° off Fin II toward Fin I<br>7° off Fin IV toward Fin III        |
| b. | Azusa (1)<br>Station 911.3        | 29° 30' off Fin IV toward Fin I                                   |
| c. | S-Band Radar (2)<br>Station 911.3 | 20° 40' off Fin IV toward Fin I<br>25° 5' off Fin IV toward Fin I |
| d. | C-Band Radar (1)<br>Station 911.3 | 33° 45' off Fin IV toward Fin I                                   |

## APPENDIX B

## (U) REDLINE VALUES

Redline values are limits on special measurements which are obtained to assure safe engine and vehicle operating conditions. These measurements are monitored in the blockhouse, and count-down procedure could be stopped if these measurements show values outside the required range. These redline values are shown in Table B-1.

Three turbine spinner case temperatures exceeded the required limits, but this occurred at approximately T-345 minutes and was within the required limits by T-330 minutes. The gas generator (GG) LOX injector purge pressure for engine position 5 was below the minimum allowable pressure. This particular measurement is checked at T-20 minutes to see if the value is within the required limits. Four other GG LOX injector purge pressures were at the minimum allowable pressure, those being on engine positions 1, 2, 3, and 6. The temperature of LOX pump bearing #1 for engine position 1 showed a shift from 137° F at T-72 minutes to 99° F at approximately T-43 minutes. This temperature was above the minimum required. Two gear case lubricant temperatures (engine positions 1 and 2) dropped near the minimum required value, but this occurred at approximately T-207 minutes for engine position 1 and T-93 minutes for engine position 2 and remained at this low value for only a short time. The remaining measurement values which had redline limits were within their limits throughout preflight operations, transition, and liftoff.

TABLE B-1

Meas. No.	Measurement	Redline	Observed Value	
			Engine Position	Minimum
XC1	Temp LOX Pump Brg. #1	0° F minimum	1	95° F
			2	112° F
			3	114° F
			4	132° F
			5	124° F
			6	118° F
			7	118° F
			8	125° F
			Engine Position	At Ignition Command
XC54	Temp LOX Pump Inlet	-290° F minimum -280° F maximum at ignition command	1	-286.6° F
			2	-284.8° F
			3	-284.8° F
			4	-286.6° F
			5	-285.9° F
			6	-285.7° F
			7	-287.0° F
			8	-284.4° F
			Engine Position	Maximum
XC59	Temp Hydraulic Oil	210° F maximum	1	90.5° F
			2	77.0° F
			3	81.5° F
			4	81.5° F

TABLE B-1 (CONT.)

<u>Meas. No.</u>	<u>Measurement</u>	<u>Redline</u>	<u>Engine Position</u>	<u>Observed Value</u>	
				<u>Minimum</u>	<u>Maximum</u>
XC89	Temp Gear Case Lubricant	105° F minimum 145° F maximum	1	105.3°	F 115.7° F
			2	105.3°	F 119.7° F
			3	111.2°	F 118.4° F
			4	107.4°	F 118.2° F
			5	108.6°	F 119.3° F
			6	109.6°	F 115.5° F
			7	113.9°	F 122.0° F
			8	111.9°	F 118.4° F
XC113	Temp Turbine Spinner Case	40° F minimum 75° F maximum At start of 10% LOX tanking (approx.) to T-350 minutes) to T-20 minutes	1	56.3°	F 73.4° F
			2	58.1°	F 73.0° F
			3	53.6°	F 75.6° F
			4	56.5°	F 73.0° F
			5	56.7°	F 73.0° F
			6	59.4°	F 76.3° F
			7	60.8°	F 75.4° F
			8	57.2°	F 71.6° F
XD2-F3	Press Gas in Fuel Tank	23 psig maximum		16.75 psig (max)	
XD3-OC	Press Gas in LOX Tank	50 psig maximum		45.7 psig (max)	
XD24-11	Press Gas in High Press Spheres	2600 psig minimum 3200 psig maximum		3012 psig (liftoff)	

TABLE B-1 (CONCLUDED)

<u>Meas. No.</u>	<u>Measurement</u>	<u>Redline</u>	<u>Engine Position</u>	<u>Observed Value</u>	
				<u>At T-20 Minutes</u>	
XD35	GG LOX Injector Pressure (checked at T-20 minutes)	25 psig minimum 55 psig maximum	1	25	psig
			2	25	psig
			3	25	psig
			4	42	psig
			5	21	psig
			6	25	psig
			7	30	psig
			8	38	psig
XD39-11	Press Air Bearing Supply Sphere	2600 psig minimum 3200 psig maximum		<u>Minimum</u>	<u>Maximum</u>
				2980 psig	2985 psig
XD40-9	Press Control Equipt Supply Sphere	2600 psig minimum 3200 psig maximum		<u>Minimum</u>	<u>Maximum</u>
				2985 psig	3012 psig
XG8	Level Hydraulic Oil	18% minimum 68% maximum	<u>Engine Position</u>	<u>At Liftoff</u>	
			1	42.8%	
			2	44.0%	
			3	45.9%	
			4	44.1%	

## APPENDIX C

## (U) GROUND SEQUENCE EVENTS

Event	Predicted Time Nominal (sec)	Actual Time* (sec)
Firing Command	-374	-370.41
Fuel Vent No. 1 Closed	-372	-370.41
Fuel Vent No. 2 Closed	-372	-370.39
Fuel Pressurizing Command	-372	-370.39
Fuel Pressurizing Valve No. 1 Open	-372	-370.34
Fuel Pressurizing Valve No. 2 Open	-372	-370.34
Fuel Pressurizing Valve No. 3 Open	-372	-370.34
Fuel Pressurizing Valve No. 4 Open	-372	-370.34
Fuel Pressurized	-359	-351.31
Open LOX Vent and Relief No. 1	-125	-121.50
Open LOX Relief No. 2	-125	-121.50
LOX Vent Open	-125	-121.22
LOX Vent Closed	-125	-120.94
LOX Pressurizing Valve Open	-125	-120.75
LOX Relief No. 2 Closed	-125	-119.39
LOX Relief No. 1 Closed	-125	-117.82
LOX Pressurized	-35	-34.06
Power Transfer Command	-35	-34.05
Power Transfer Complete	-25	-33.98
Long Mast Eject Command	-25	-25.16
Long Mast Retracted	-2	-7.95
Ignition Start Timer	0	-0.00
Ignition Command	0	0.0
Eng. No. 5 Igniter No. 1 Energized	0	+0.04
Eng. No. 5 Igniter No. 2 Energized	0	+0.04
Eng. No. 7 Igniter No. 1 Energized	0	+0.04
Eng. No. 7 Igniter No. 2 Energized	0	+0.04
Eng. No. 6 Igniter No. 1 Energized	+0.10	+0.13
Eng. No. 6 Igniter No. 2 Energized	+0.10	+0.13
Eng. No. 8 Igniter No. 1 Energized	+0.10	+0.13
Eng. No. 8 Igniter No. 2 Energized	+0.10	+0.13
Eng. No. 2 Igniter No. 1 Energized	+0.20	+0.24
Eng. No. 2 Igniter No. 2 Energized	+0.20	+0.24
Eng. No. 4 Igniter No. 1 Energized	+0.20	+0.24
Eng. No. 4 Igniter No. 2 Energized	+0.20	+0.24
Eng. No. 1 Igniter No. 1 Energized	+0.30	+0.33
Eng. No. 1 Igniter No. 2 Energized	+0.30	+0.33
Eng. No. 3 Igniter No. 1 Energized	+0.30	+0.33
Eng. No. 3 Igniter No. 2 Energized	+0.30	+0.33

\* Times referenced to ignition command

## (U) GROUND SEQUENCE EVENTS (CONT)

All Igniters Energized	+0.30	+0.35
All Engines Running	+2.15	+1.38
Thrust OK Timer	+3.30	+3.34
Thrust Commit	+3.31	+3.37
Retract Support Timer	+4.40	No Operation
Short Mast No. 2 Valve No. 1 Open	+3.32	+3.44
Short Mast No. 2 Valve No. 2 Open	+3.32	+3.44
Short Mast No. 4 Valve No. 1 Open	+3.32	+3.44
Short Mast No. 4 Valve No. 2 Open	+3.32	+3.44
Retract Support Command	+3.40	+3.47
Retract Valve No. 4 Open	+3.40	+3.62
Retract Valve No. 3 Open	+3.40	+3.63
Retract Valve No. 2 Open	+3.40	+3.65
Retract Valve No. 1 Open	+3.40	+3.66
Support No. 4 Not Supporting	-	+3.69
Support No. 3 Not Supporting	-	+3.71
Support No. 2 Not Supporting	-	+3.71
Support No. 1 Not Supporting	-	+3.72
Launch Commit	+3.67	+3.74
H.D. Release Valve No. 1 Open	+3.67	+3.81
H.D. Release Valve No. 2 Open	+3.67	+3.81
H.D. Release Valve No. 3 Open	+3.67	+3.81
H.D. Release Valve No. 4 Open	+3.67	+3.81
Holddown No. 1 Released	+3.77	+3.82
Holddown No. 2 Released	+3.77	+3.82
Holddown No. 3 Released	+3.77	+3.82
Holddown No. 4 Released	+3.77	+3.82
Liftoff No. 1	+3.77	+3.94
Liftoff No. 2	+3.77	+3.94
Liftoff No. 3	+3.77	+3.94
Liftoff No. 4	+3.77	+3.94
Liftoff	+3.77	+4.02

## APPENDIX D

TABLE D-I MASS CHARACTERISTICS COMPARISON (REF. PARA. 5.6)

Event	Range Time Seconds	Weight		Longitudinal C.G. (X-Sta)		Radial C.G.		Pitch Moment of Inertia Kg-M-Sec <sup>2</sup>	Roll Moment of Inertia Kg-M-Sec <sup>2</sup>
		Pounds	% Dev	Inches	Dev in.	Inches	Dev in.		
Dry Vehicle	Act	307,980	0.2	1,108	1	0.2	.1	2,526,529	26,926
	Pred*	307,059		1,109		0.3		2,515,497	26,776
Ignition Command	Act	943,543	0.0	675	1	0.1	0	5,503,011	151,665
	Pred*	943,253		674		0.1		5,493,891	151,447
Liftoff	Act	926,673	0.0	674	1	0.2	0	5,502,045	148,713
	Pred*	927,237		673		0.2		5,490,237	148,635
Inboard Engine Cutoff	Act	347,158	1.9	1,012	14	0.2	0	3,304,500	36,395
	Pred*	340,762		1,026		0.2		3,182,441	34,619
Outboard Engine Cutoff	Act	330,832	2.1	1,049	16	0.2	0	3,009,862	32,124
	Pred*	323,915		1,065		0.2		2,874,643	30,301
End Thrust Decay	Act	329,598	2.3	1,052	18	0.2	0	2,986,377	31,932
	Pred*	322,127		1,070		0.2		2,840,806	29,858

\* Predicted mass characteristics are those reported in P&VE-E-62-7 dated April 19, 1962.

Notes: Pred dry weight includes 191,525 pounds of water  
Act. dry weight includes 192,000 pounds of water

TABLE D-II SA-2 VEHICLE WEIGHTS

Event	Ignition Command		Liftoff		Inboard Engine Cutoff		Outboard Engine Cutoff		End of Thrust Decay	
	Pred	Flight	Pred	Flight	Pred	Flight	Pred	Flight	Pred	Flight
Range Time (sec)	-3.26	-3.61	0.41	0.41	110.32	111.29	116.32	117.29	118.91	119.84
Weights (lb)										
Dry Vehicle	307,059	307,980	307,059	307,980	307,059	307,980	307,059	307,980	307,059	307,980
LOX	438,741	437,584	427,101	425,315	16,582	21,556	5,344	10,623	4,851	10,148
Fuel	194,192	195,382	189,811	190,681	10,753	13,712	5,172	8,262	4,373	7,506
Gas in LOX	1,305	630	1,372	736	3,606	2,943	3,690	3,000	3,690	3,000
Containers										
GN <sub>2</sub>	898	907	898	907	898	907	898	907	898	907
Hydraulic Oil	60	60	60	60	60	60	60	60	60	60
TOTAL	942,255	942,543	926,301	925,679	338,958	347,158	322,223	330,832	320,931	329,601

- NOTES: 1. GOX vented accounted for.  
 2. No gas vented from fuel containers.  
 3. Fuel consumed includes one-half pound/sec lube fuel flow per engine.  
 4. Ice accumulation (approximately 1000 pounds at liftoff) not included.  
 5. Dry vehicle weight includes 192,000 pounds water ballast.  
 6. Ignition weight does not include jacket prefill.  
 7. Predicted propellant weights based on fuel density of 50.00 lb/ft<sup>3</sup>.  
 Flight propellant weights based on fuel density of 50.22 lb/ft<sup>3</sup>.

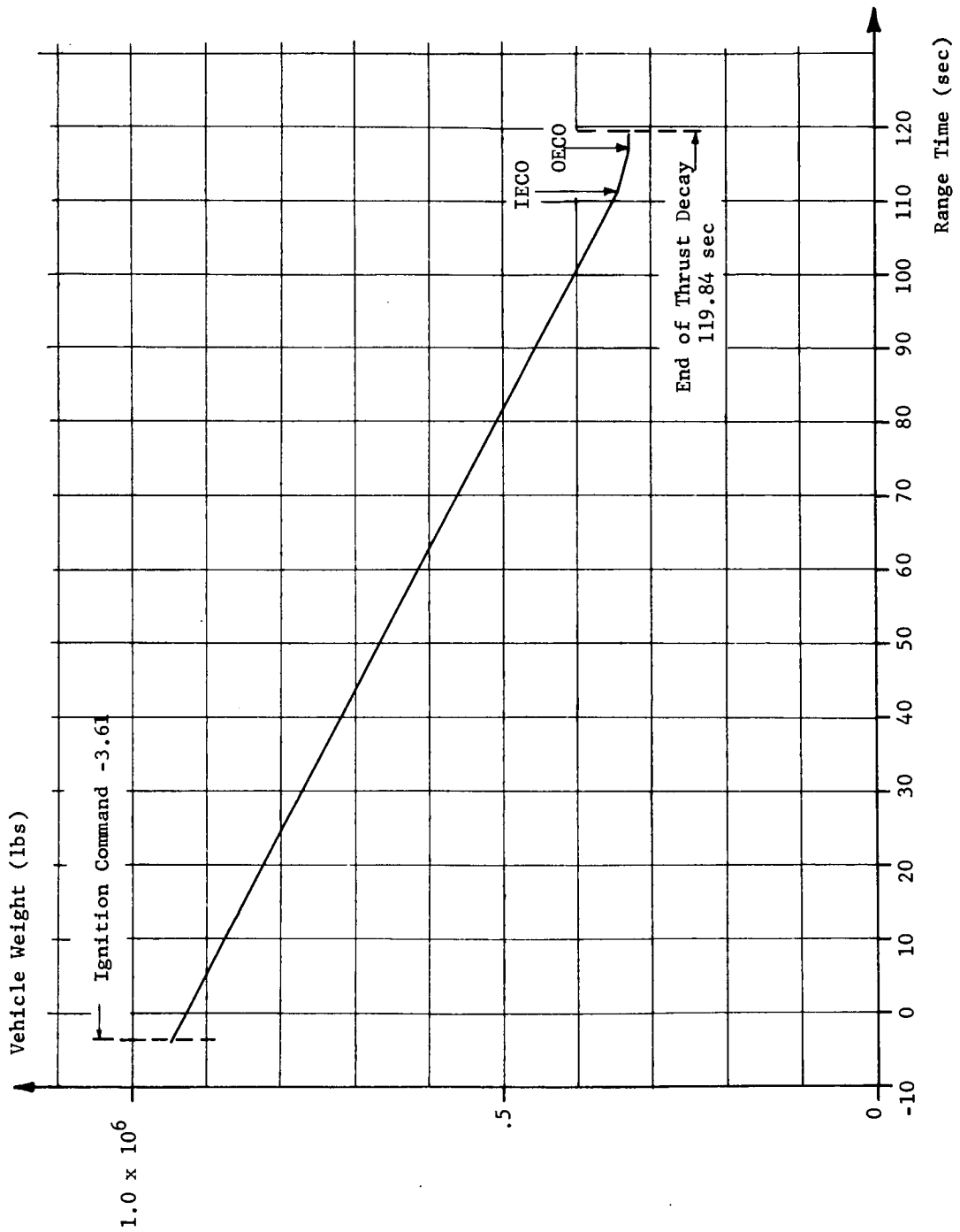
~~CONFIDENTIAL~~

Fig. D-1 VEHICLE WEIGHT VERSUS RANGE TIME

~~CONFIDENTIAL~~

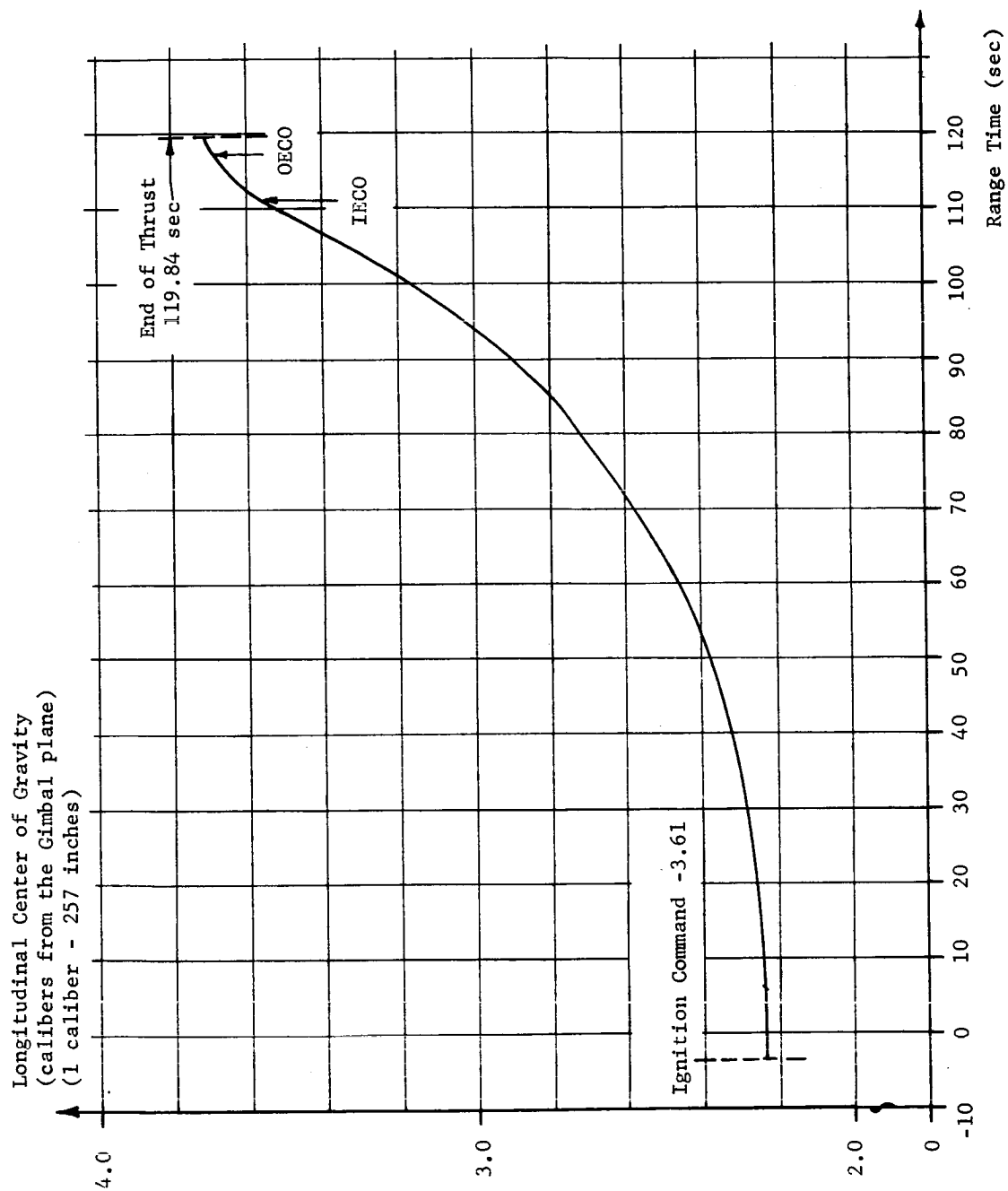


Fig. D-2 LONGITUDINAL CENTER OF GRAVITY VERSUS RANGE TIME

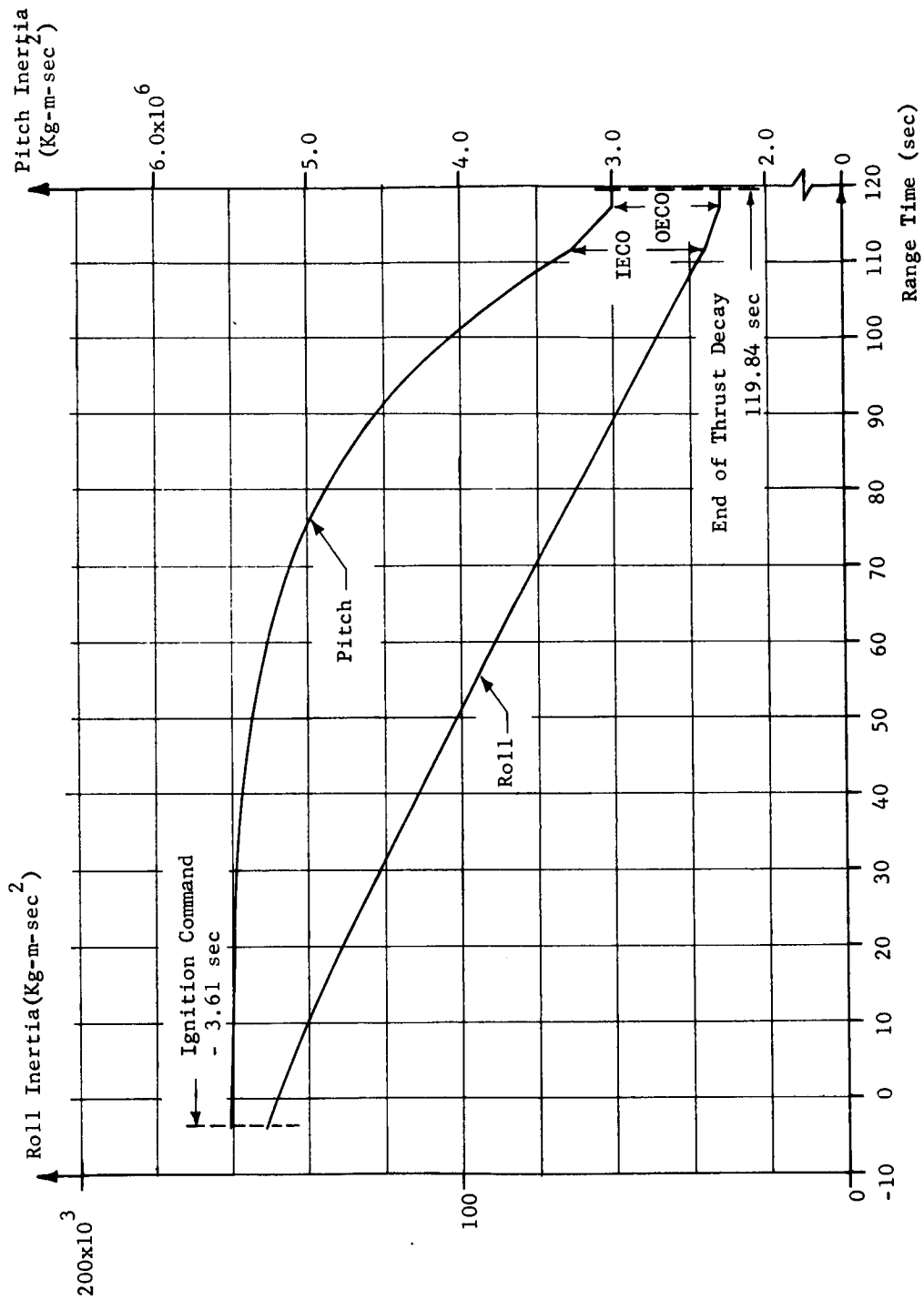
~~CONFIDENTIAL~~

Fig. D-3 ROLL AND PITCH MOMENT OF INERTIA VERSUS RANGE TIME

~~CONFIDENTIAL~~

## APPENDIX E

## (U) ATMOSPHERIC SUMMARY FOR SA-2

## E.1 INTRODUCTION

This appendix contains information concerning the more important portions of the atmospheric environment for the flight of Saturn SA-2. The atmospheric data are given in a form which will allow easy comparison with other space vehicle flights at the Atlantic Missile Range. For ready reference, winds and thermodynamic data are presented in graphic form as a function of altitude and vehicle flight time. This appendix gives the general weather situation for the flight area including the surface observations at launch time and upper air conditions (as measured by rawinsonde and rocketsonde) soon after flight time.

## E.2 GENERAL SYNOPTIC SITUATION AT LAUNCH TIME

Pressure Distribution and Fronts. At launch time a large maritime tropical air mass, centered near Bermuda, dominated the southeast coast of the United States, including the launch area. A weak low pressure area was centered over East Texas and Arkansas. A dissipating stationary front extended from southern Georgia to central Mississippi.

The core of the low pressure area tilted eastward with increasing altitude, and at 500 mb (6 km) a small cyclonic circulation was centered over the Mississippi-Alabama area.

Jet Streams and Associated Weather. The pressure distribution at launch time caused a jet stream with winds of about 40 m/sec to move eastward across the central Gulf and through the Florida Straits, at about 12 km altitude.

The dissipating front caused several scattered showers in the Gulf States, but none were reported in peninsular Florida. Scattered (0.3 or less sky cover) cumulus and stratocumulus clouds, with bases near 1 km, were reported in the launch area during countdown, and 2 to 4 tenths of the sky was covered by high thin cirrostratus (ice-crystal) clouds. Light (less than 5 m/sec) south to southeast surface winds prevailed in the launch area.

## E.3 SURFACE OBSERVATIONS AT LAUNCH TIME

Blockhouse Observations. At launch time recording instruments at the blockhouse showed the surface temperature to be 24.6°C (76.3°F), relative humidity 59 percent, pressure 1020.5 mb (10,406.2 kp/m<sup>2</sup>), and

the wind southerly (170°) at 2.6 m/sec. One-tenth stratocumulus clouds were observed at 1 km altitude, and 0.3 cirrostratus (ice-crystal) clouds were visible, but none of these clouds were reported near the flight path.

Launch Pad Observations. A recording anemometer on the launch pad, 13.4 m above ground level and 38 m north of the launch pedestal, showed the winds to be averaging 3.5 m/sec from the south (swinging from 157 to 235°) prior to launching (Figure E-1). SA-1 launch pad winds averaged 7 m/sec from about 75° and were steady. The launch blast caused the winds to vary quickly reaching maximum peaks of 12 m/sec and to shift through all directions during the first minute after firing. Winds returned to prelaunch conditions about 1 minute after T-0. Wind disturbances at launch were less severe.

Surface wind data for SA-2 were improved over SA-1 by recording synchronized time measurements on the pad and service structure anemometer records.

Service Structure Observations. A recording anemometer on the service structure, 95 m above ground level and 207 m southwest of the Saturn launch pedestal, showed the wind to be quite steady from the south-southeast at 4 m/sec before and during launch - no effects from the launch blast could be detected. During SA-1 launch the winds on the service structure were moderately disturbed (dropping from 9.2 to 4.1 m/sec 10 seconds after T-0), but the effects were not severe.

Recording instruments on the ground near the pad show the launch time temperature to be 76.7°F (24.8°C), relative humidity 52 percent, and the air pressure 30.15 inches (1021.0 mb = 10,411.3 kp/m<sup>2</sup>). 13.4 m (44 ft) above the ground, on the service structure, the launch time temperature was 73.4°F (23.0°C), and the relative humidity was 55 percent. 79.2 m (260 ft) above the ground, on the service structure, the launch time temperature was 70.0°F (21.1°C), and the relative humidity was 60 percent. The launch blast did not cause any deflection of the service structure instrument readings.

#### E.4 TIME AND SPACE VARIATIONS BETWEEN MISSILE FLIGHT PATH AND UPPER AIR MEASUREMENTS BY RAWINSONDE AND ROCKETSONDE

Rawinsonde Path. A rawinsonde was released 5 km south of the Saturn pedestal 8 minutes after the SA-2 launch. The rawinsonde drifted 57 km east-northeast of the Saturn launch pedestal and burst at 23,250 m altitude 1 hour 27 minutes after SA-2 launch time, thus ending the observation. At that time, it was 46 km east-northeast of the position reached by SA-2 when SA-2 was at the same altitude. A second rawinsonde was released 2 hours 38 minutes after SA-2 launch time. This followed a path which

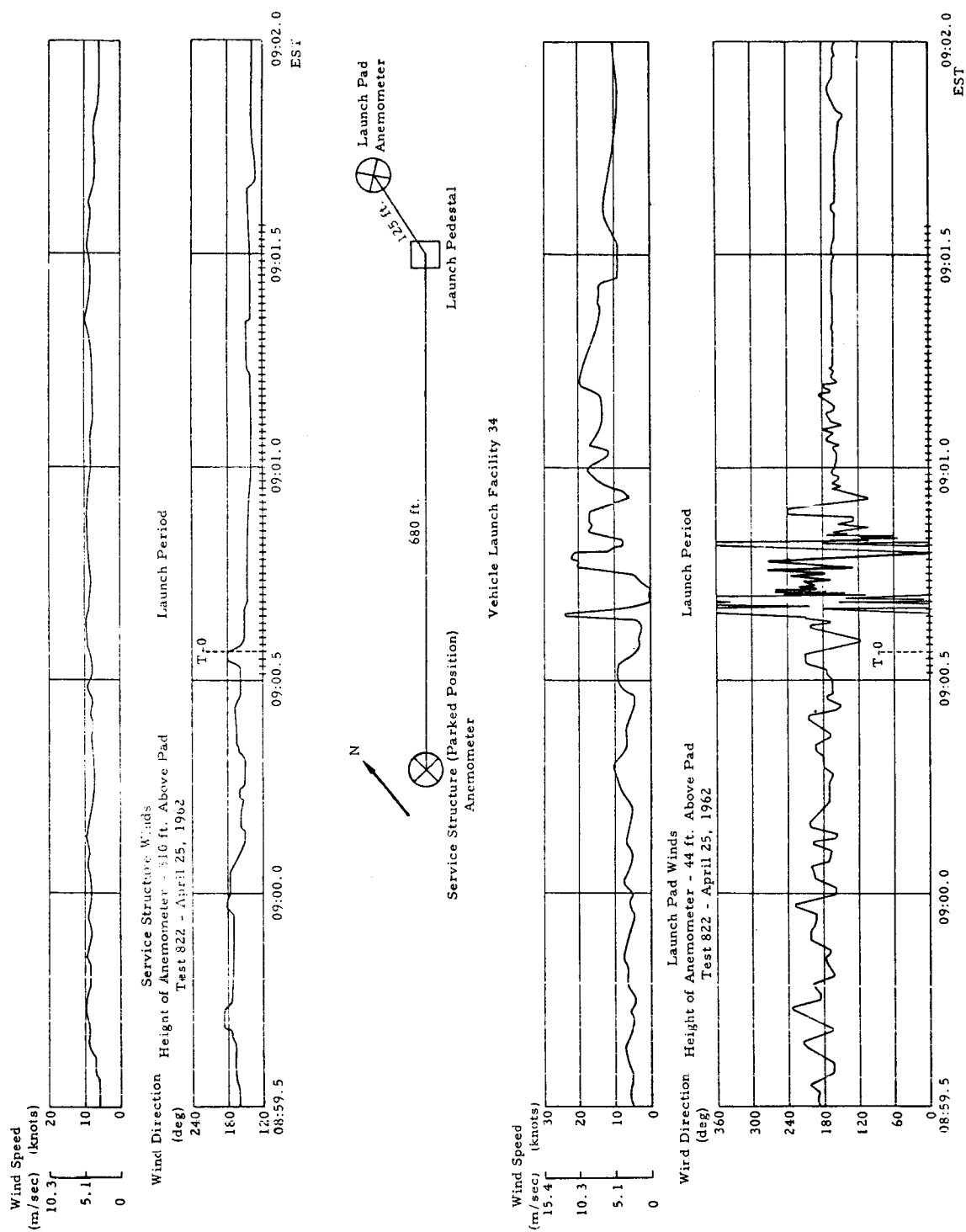


Figure E-1 LAUNCH SITE WIND MEASUREMENTS (ANEMOMETER)  
 FOR SATURN (SA-2) LAUNCH

differed slightly from the T-0 rawinsonde. It burst at 31,500 m altitude 3 hours 41 minutes after SA-2 launch time. At that time, it was 47 km east-northeast of the Saturn launch pedestal, and it was 38 km northeast of the position reached by SA-2 when SA-2 was at the same altitude.

The Rocketsonde Path. A meteorological rocket was fired on almost the same heading as SA-2. Its parachute target was acquired 46 km east-southeast of the SA-2 pedestal, at an altitude of 34,750 m, 4 hours 15 minutes after the SA-2 launch. At that time, it was 35 km east-southeast of the position reached by SA-2 when SA-2 was at the same altitude. The rocketsonde target drifted about 3 km eastward where it was lost, at 26 km altitude, 4 hours 20 minutes after SA-2 liftoff. Another rocketsonde was fired 6 hours 7 minutes after T-0. Data from this second rocketsonde are shown between 35 and 42.5 km altitude.

## E.5 WIND DATA

Wind Speed and Direction. The rawinsonde and angle-of-attack wind measurements are in very close agreement as to wind speed and direction (Figure E-2). They show the wind to be south-southeast about 4 m/sec at the surface, then shifting to westerly from 5 to 19 km altitude. The highest wind speed observed was 33.6 m/sec from the west-southwest at 13.5 km (33 m/sec by angle-of-attack), which is about 66 seconds of flight time. The highest wind speed observed for the SA-1 flight was 47 m/sec from the west-southwest at 12 km altitude (64 seconds of flight time) - 40 percent greater. SA-2 wind measurements above 19 km indicated that winds were light (less than 10 m/sec) and variable up to 30 km. The angle-of-attack shows a wind of 15 m/sec from the west-southwest at 33.5 km, which is the fastest wind measured above 17 km altitude.

Wind Components. Cross range components (Fig. E-3) were mostly from the right. The strongest cross range component was 13.3 m/sec from the right at 12 km altitude, which is about 63 seconds of flight time. This is less than half of the corresponding strongest cross range component in the high dynamic pressure region for SA-1 which was also from the right. The strongest tailwind component was 31.8 m/sec which occurred at 14 km altitude at about 66 seconds of flight time. A tailwind component of 36 m/sec was recorded for SA-1 near 12 km; therefore the vehicle pitch plane winds were approximately the same for both vehicle launches.

Wind Shear. Pitch and yaw component wind shears computed over 1000 m intervals of altitude (Figure E-4) as well as the pitch and yaw component shears for 250 m intervals (Figures E-5 and E-6) are for the modulus of the shear (i.e. the absolute shear values). It is recommended that 1000 m shears be used for comparative study purposes in preference to 250 m shears whenever possible because they are more accurate. The extreme 1000 m layer rawinsonde pitch component wind shear of 0.0101

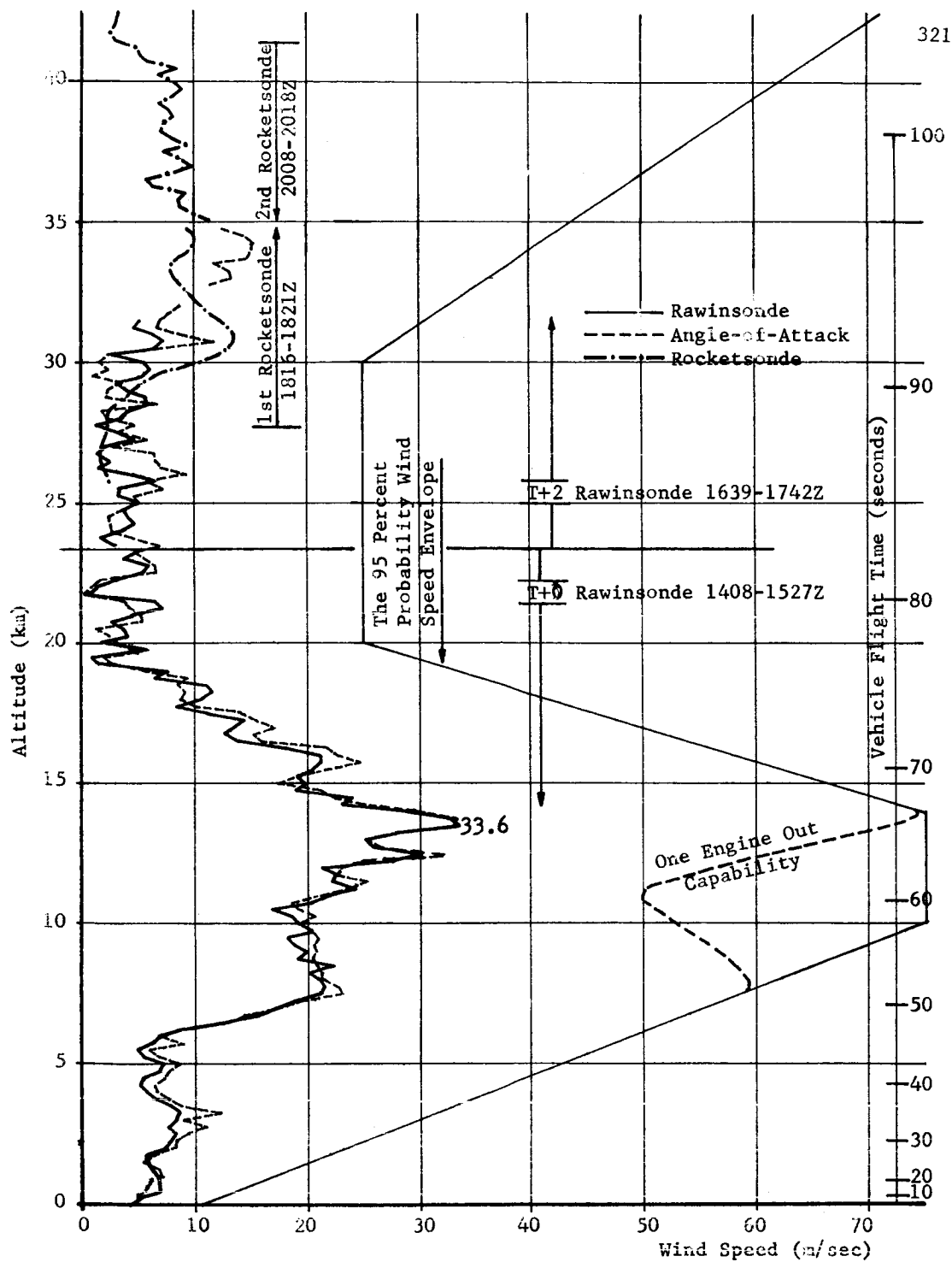


Figure E-2 SA-2 WIND SPEED BY RAWINSONDE,  
ANGLE-OF-ATTACK AND ROCKETSONDE

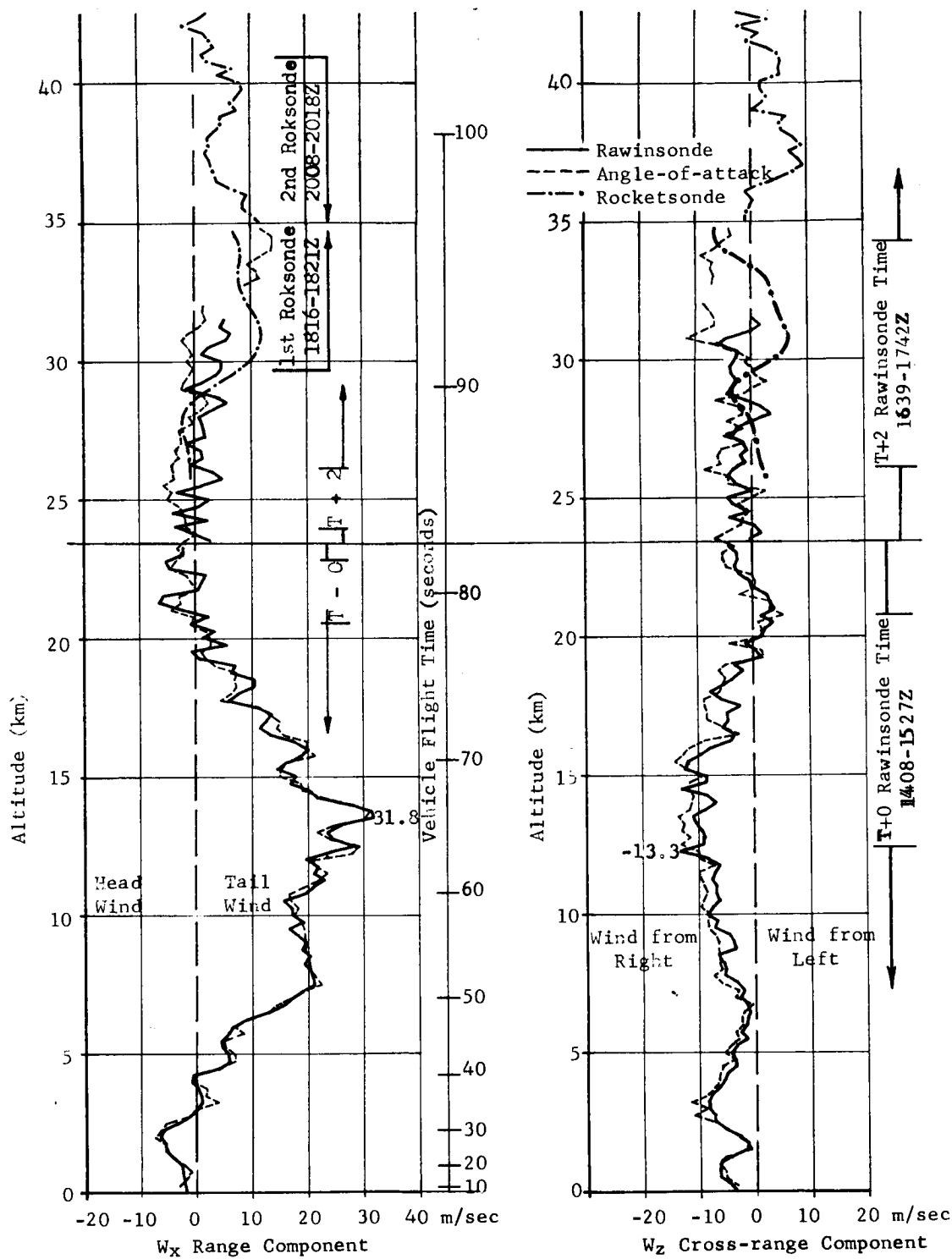


Figure E-3 SA-2 WIND COMPONENTS BY RAWINSONDE MEASUREMENT, ANGLE-OF-ATTACK AND ROCKETSONDE

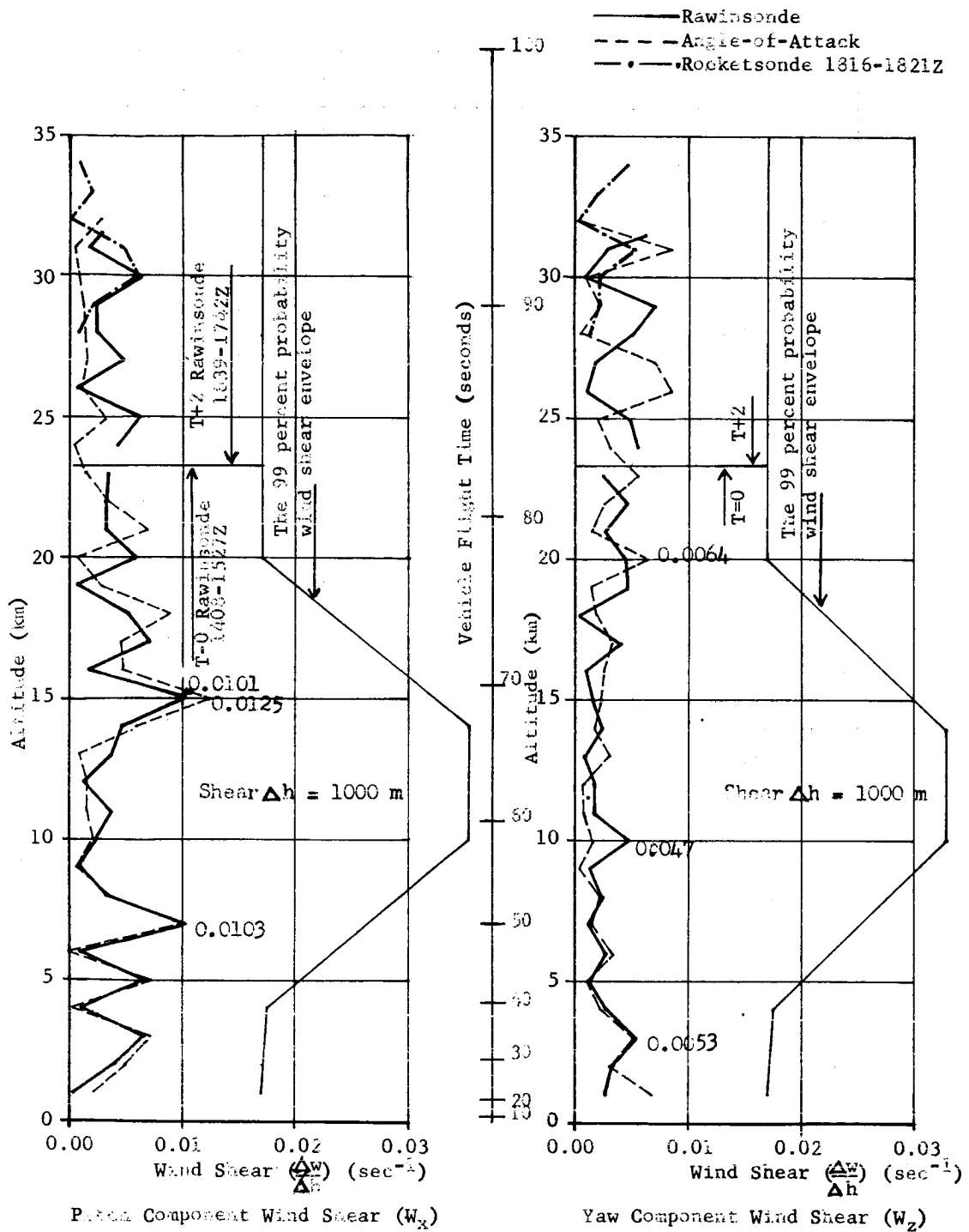


Figure E-4 PITCH AND YAW COMPONENT WIND SHEAR (1000 m)

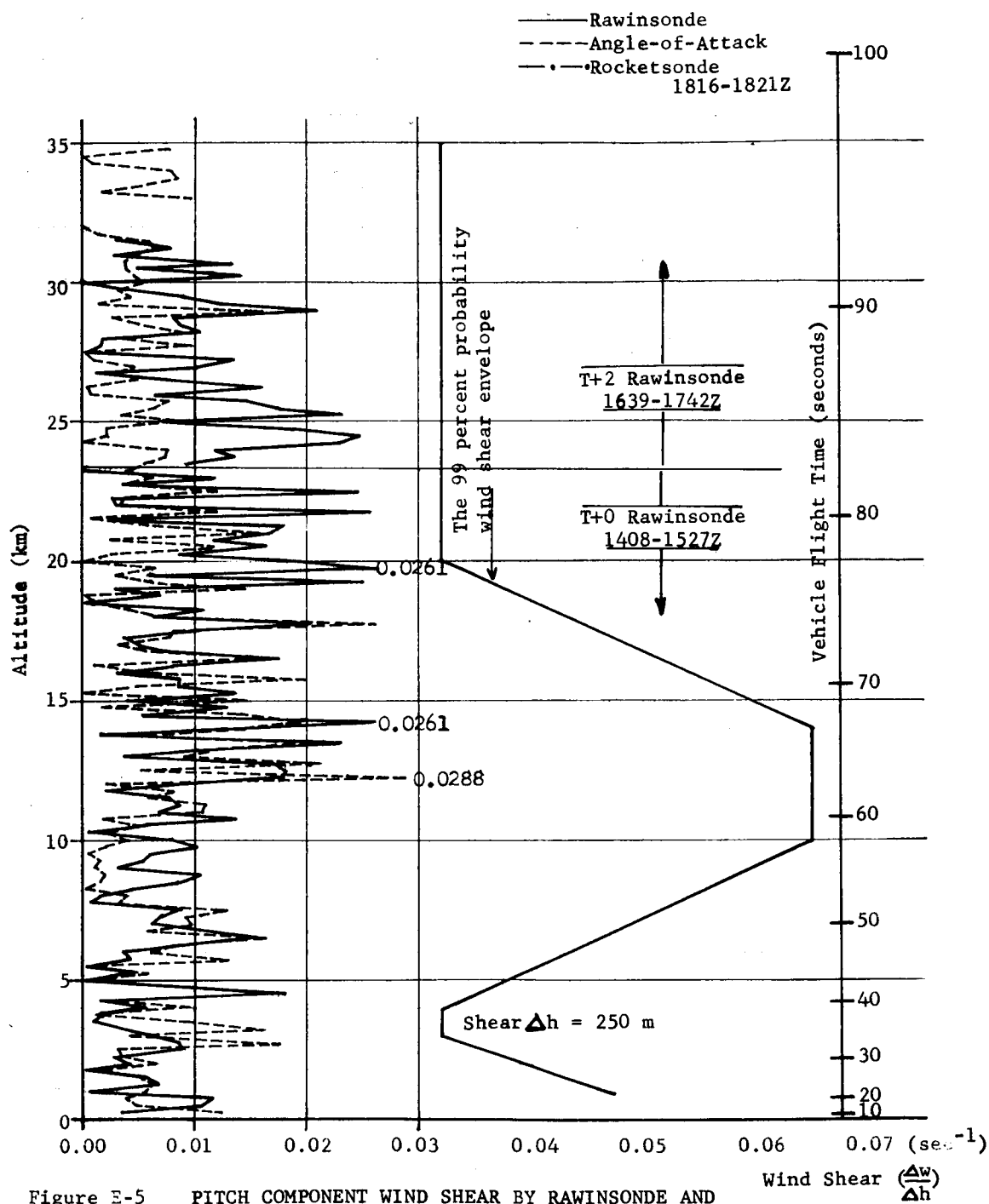


Figure E-5 PITCH COMPONENT WIND SHEAR BY RAWINSONDE AND ANGLE-OF-ATTACK MEASUREMENT ( $W_x$ ) (250 METERS)

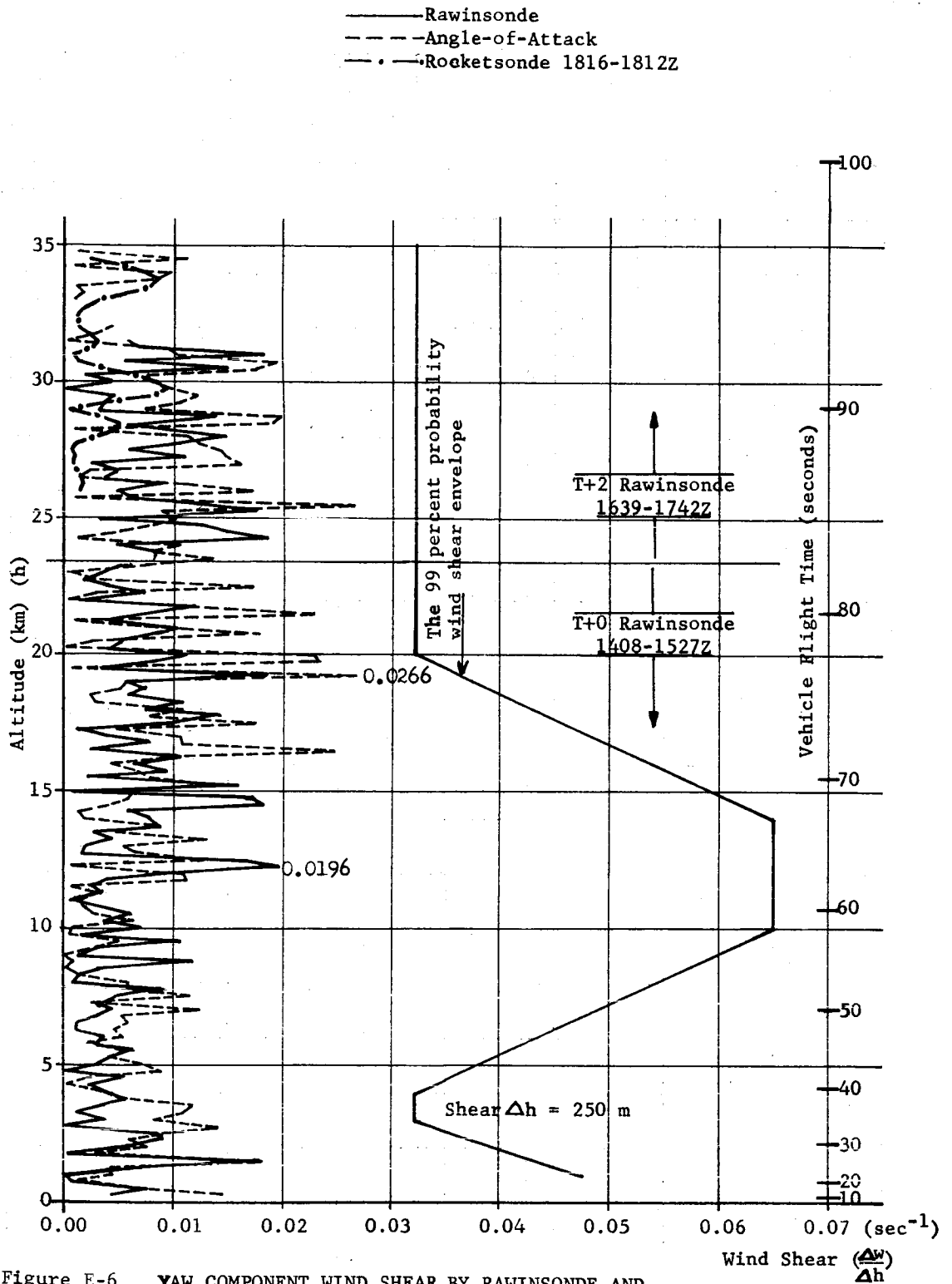


Figure E-6 YAW COMPONENT WIND SHEAR BY RAWINSONDE AND ANGLE-OF-ATTACK MEASUREMENT ( $W_z$ ) (250 METERS)

( $\text{sec}^{-1}$ ) occurred at 15 km altitude. (This is one-third less than the extreme 1000 m shear experienced by SA-1). The greatest 1000 m interval shear in the yaw plane was  $0.0047 (\text{sec}^{-1})$  which occurred at 10 km. (The extreme yaw plane shear for SA-1 was three times as strong). The component wind shears for 250 m and 1000 m intervals during SA-2 flight are decidedly less than design criteria at all altitudes.

#### E.6 THERMODYNAMIC DATA

Pressure does not vary from normal (PAFB Reference Atmosphere) more than 2 percent below 30 km altitude (Figure E-7). The other thermodynamic quantities are more erratic. The greatest deviation of temperature (Figure E-8) is 2.7 percent at 14 km, which is almost 2 standard deviations above normal at this altitude. Density (Figure E-8) is 3.7 percent below normal at this altitude. The greatest deviation of density is 3.8 percent below normal at 13 km. Density exceeded 2 standard deviations above normal in the 4 to 6 km region.

The greatest deviation of the optical refractive index (Figure E-7) occurs at 1.5 km altitude where it is  $50(n-1)10^6$  units above normal. This is more than twice the greatest deviation of the SA-1 refractive index. This sharp increase in the refractive index was caused by a layer of cool, dense, and extremely dry air at this altitude. The humidity varied widely to cause still other, although lesser, shifts of the refractive index at other altitudes.

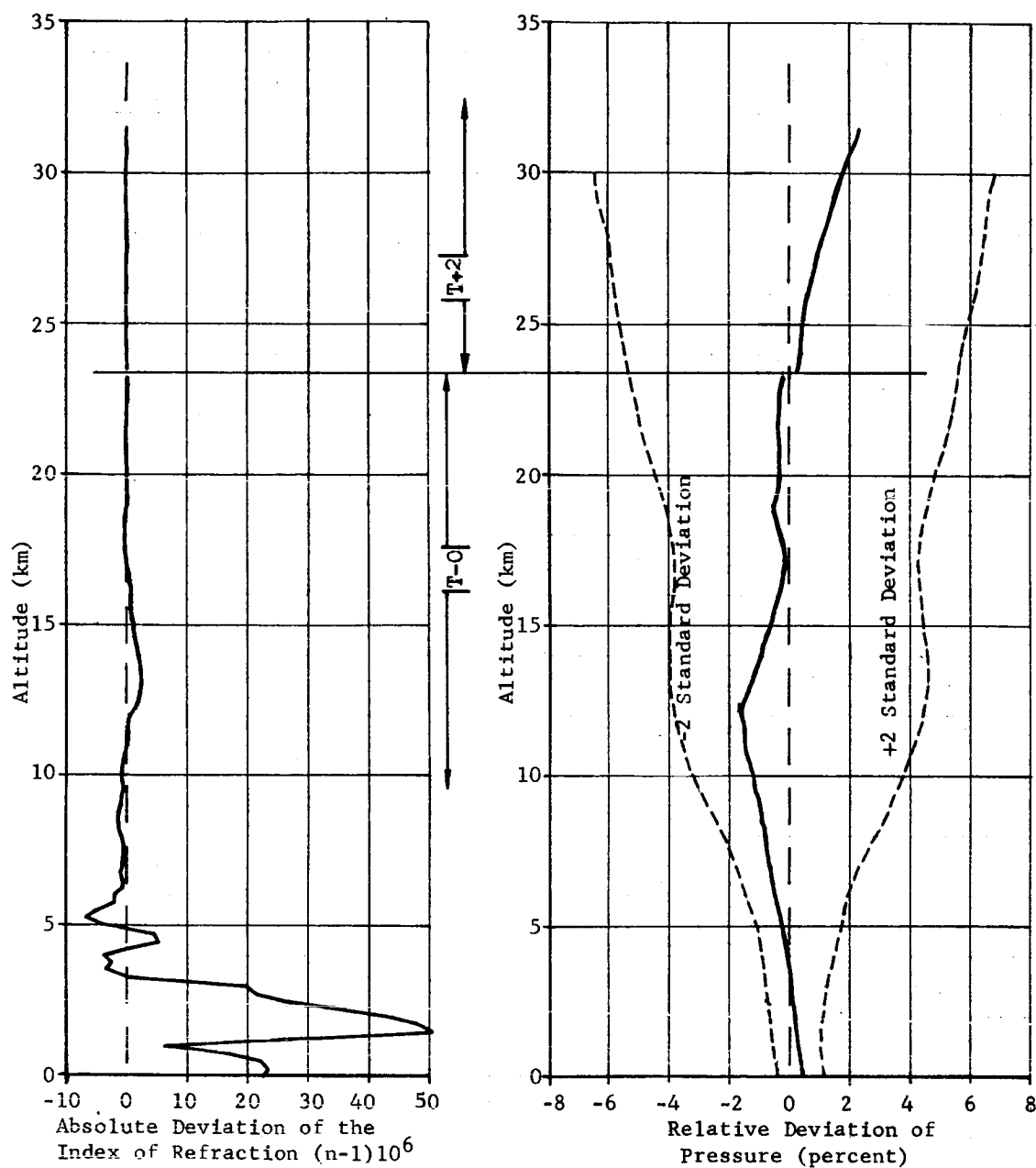


Figure E-7 SA-2 ABSOLUTE DEVIATION OF OPTICAL REFRACTIVE INDEX  
AND RELATIVE DEVIATION OF PRESSURE  
FROM PAFB REFERENCE ATMOSPHERE

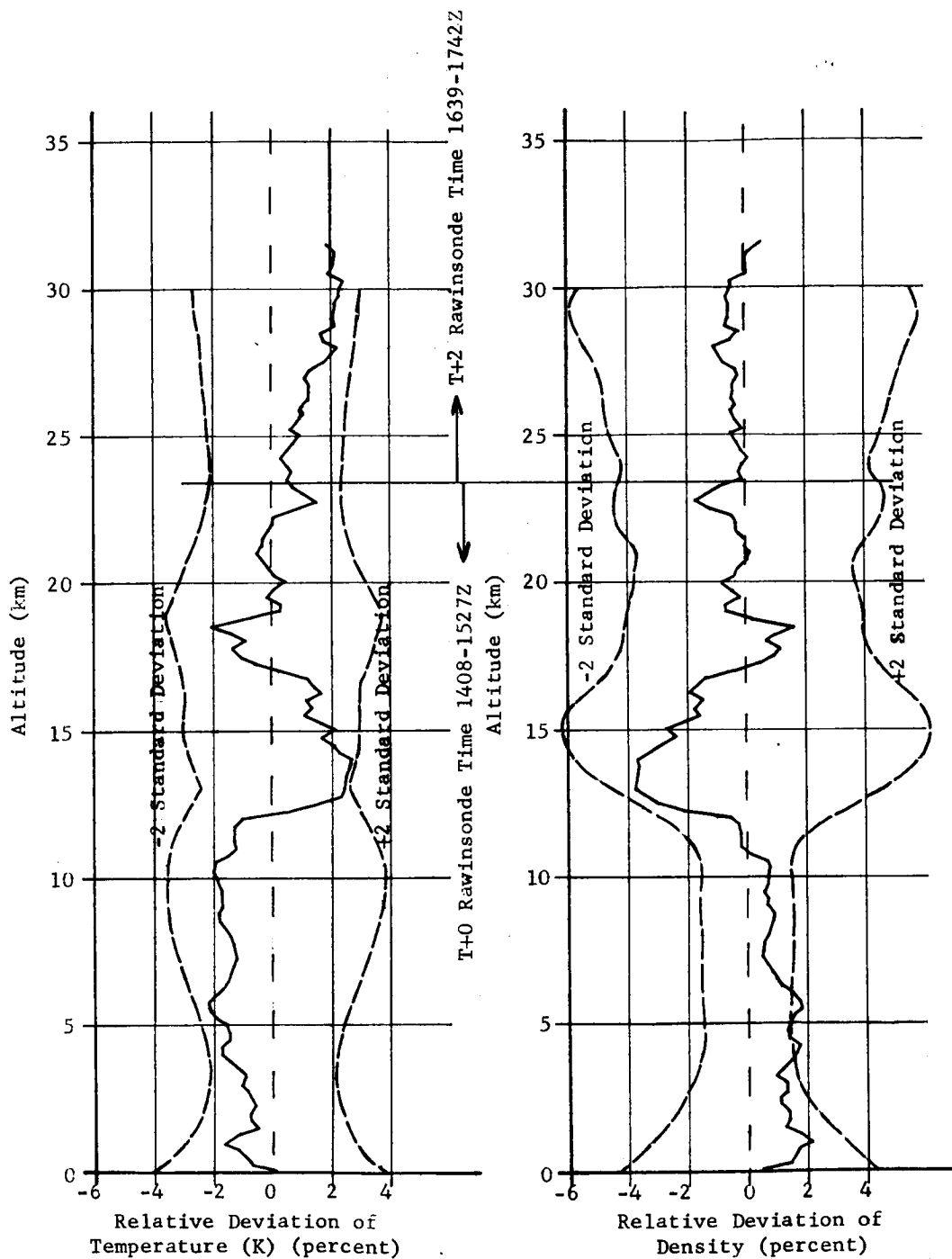


Figure E-8 SA-2 RELATIVE DEVIATION OF  
TEMPERATURE AND DENSITY FROM  
PAFB REFERENCE ATMOSPHERE

## APPENDIX F

## (U) DATA REDUCTION

## F-1 TELEMETRY DATA

Analog flight tapes were received from the range by aircraft approximately 7 hours after launch. As was the case on SA-1 flight, an insufficient number of tapes were available to allow concurrent operation of the various reduction systems. The reduction systems are the telemetry ground station, the MicroSadic, the RCC Cycle Counter, and the vibration equipment. Approximately one hour was expended in making tape copies in order that these data reduction systems could have input tapes. Receipt of additional analog tapes from the range approximately 9 hours after launch satisfied the input tape requirements of all data reduction systems.

Telemetry Ground Station

The telemetry ground station was employed in a real time experiment conducted during the SA-2 flight and in the production of oscillographs from the analog tape received from the range after the flight.

The real time experiment consisted of receiving the flight telemetry signals from Astrionics Division's installation on Green Mountain and displaying selected parameters in real time to the evaluation working group in the Saturn Evaluation Complex located in the Computation Division. The display consisted of the platform altitude positions and engine cutoff signals and was completed by use of a Sanborn recorder and closed circuit television. The real time experiment was considered a complete success. Signal was acquired at approximately 100 sec flight time and lost at destruct command at approximately 162 seconds. The received signal was of sufficient quality for digital reduction.

Upon receipt of the range recorded flight tape, the telemetry ground station was employed in producing nine sets of twenty groups of oscillograph records for the evaluation working group. These groups are made to display all the measurements in a flight system on a single oscillograph rather than the arrangement of measurements by telemetry links. The oscillograph groups were available as previously scheduled to members of the evaluation working group at 7:30 AM the day following launch. The telemetry ground station has since been used to make expanded records to show graphically areas of particular interest.

### MicroSadic

The MicroSadic was used to digitize the PAM/FM/FM telemetry and the FM/FM telemetry not devoted to frequency dependent measurements and vibration measurements. As was the case in SA-1, the telemetry was exceptionally clean to loss of signal, and no difficulty was encountered in digitizing any of the data except for a brief period of noise in Link 1. This noise occurred at approximately 52 seconds flight time and was evidently peculiar to Link 1 since no difficulty was experienced with the other links. A total of 10 PAM/FM/FM channels were reduced. These channels consisted of the large commutator package on Link 1, eight 30 segment commutator packages on the remaining flight links, and one 30 segment commutator on the Y telemeter channel which measured GSE performance. A total of 328 commutated measurements were digitized, linearized, calibrated in the 7090 Computer, and plotted on the magnetic tape plotter.

Six telemetry links were used to carry FM/FM information. Of these, five were flight links and one was Y telemeter. The channel capacity of three of the five flight links was expanded by use of triple FM. No difficulties were experienced in digitizing any of the FM/FM information. One PAM/FM/FM channel was rerun several days after the initial run, since the initial run was found to be in error in the order of 3% due to operator error. Several runs were made of bending mode accelerometer measurements to filter out superimposed high frequencies. Digitizing of all telemetry data was complete approximately 8 hours after receipt of the telemetry tape. This represents a considerable increase in performance over the SA-1 flight. A total of 70 FM/FM measurements were processed, tabulated, and plotted.

### RCC Cycle Counter

The RCC Cycle Counter was used to digitize those telemetry measurements which are functions of frequency rather than of measuring voltage. These measurements, a total of 33, consist of vibrotron measurement of combustion chamber pressure, turbine RPM, inverter frequency, and multiplexed AC flow rates. Initial reduction of all these measurements had been accomplished by 7:30 AM on the day following launch, and the plotted and tabulated results gave the first indication of marginal operation of engine 2. The only difficulty encountered in the Cycle Counter reduction was malfunctioning of the tape translator which is used to translate the output of the Cycle Counter to input format for the 7090 Computer. Since the flight of SA-2, a new cycle counter, the Beckman RCC-3, has been installed. This new system writes an IBM compatible tape, eliminating the trouble source of the tape translator, and promises to give more efficiency and accuracy in the reduction of frequency dependent telemetry measurements.

### Vibration Equipment

As of May 18, 1962, 296 plots of random vibration data have been produced. These plots cover the frequency range of 0 to 2500 cps. These analyses are of all the vibration measurements for SA-2. These data were reduced by utilizing the random wave analysis system manufactured by the Technical Products Company.

Concerning the low frequency data, an average of two plots per bending mode measurement was made. These plots cover the frequency range of 0 to 20 cps, and a  $\frac{1}{2}$  cycle bandwidth filter was used. The system employed for the reduction was the Panoramic Sub-Sonic Wave Analyzer.

Using the integrated vibration reduction, station 60 mean square vs. time plots have been produced, and all compressed composite data have been reduced.

Utilizing the Spectrometer System a total of 108  $\frac{1}{3}$  octave records have been reduced, and all  $\frac{1}{3}$  octave data have been finished for SA-2.

### Summary

In summation, it may be stated that the data reduction effort on SA-2 was much superior to that of SA-1. This may be attributed in part to the more reliable operation of the MicroSadic and the magnetic tape plotter. Reduction of telemetry data was virtually complete within 48 hours of receipt of the flight tapes though plotting required several more days. A total of 430 flight measurements were reduced in this time period. It is anticipated that acquisition of a second MicroSadic, a PCM ground station with plotting capabilities, an SC 4020 Digital Data Recorder with printing and plotting capabilities, and the completion of checkout and computer programming for the RCC-3 cycle counter will result in more timely data reduction for future Saturn flight and ground tests.

### F-2 UDOP DATA

The UDOP system provided position data from liftoff to destruction. The data were obtained exclusively from the close-in and uprange stations since failure to record timing rendered the downrange data unusable.

### Quality of Raw Data

A pronounced drop in receiver signal strength necessitated smoothing the cycle data from approximately 110 to 112 seconds. This area of noisy data closely corresponds to an interval of noise of less intensity on SA-1.

The pad receiver did not provide clean data during the period of vertical acceleration. Again, this data is similiar to the SA-1 data.

The remaining data, with the exception of short intervals of intermittent noise in the Blockhouse 34 data, were of good quality.

#### Evaluation of Reduced Data

Accuracy of position data from liftoff to 110 seconds is better than  $\pm 3$  meters in each position coordinate as indicated by comparisons with CZR from 0 - 19 seconds and with Azusa from 20 - 110 seconds. Computed estimates of error are well below 2 meters for the duration of flight. Even though the telemetered acceleration data were used as a basis for the smoothing between 110 and 112 seconds, the resulting degradation of position data at 162 seconds appears to be only about  $\pm 10$  meters.

#### Experimental Green Mountain UDOP Data

UDOP doppler data were recorded experimentally by Astrionics Division at the Green Mountain site. A reference frequency for the single UDOP station was furnished by an atomichron. Timing was provided by the Computation Division's Time station.

Good quality cycle data were obtained from 117.5 - 162.5 seconds even though the elevation angle ranged from -0.5 to only 2.0 degrees. Tabulated below are the average differences between cycle data computed from the UDOP trajectory and the Green Mountain data.

Time Interval	Av. Difference (CPS)
120 - 125	-2.4
125 - 130	-1.7
130 - 135	-0.7
135 - 140	-0.9
140 - 145	-0.1
145 - 150	0.7
150 - 155	0.3
155 - 160	1.5
160 - 162.5	1.1
<hr/>	<hr/>
120 - 162.5	-0.3

Lack of transmitter and reference oscillator coherence and the propagation path uncertainties are the reasonable sources of the differences above. Further evaluation is being performed in an attempt to separate the contributions from each source.

Time synchronization between Cape time and Computation Division time was determined from events recorded by telemetry at the Cape and on Green Mountain. The recorded Computation Division time was of very poor quality, apparently because of receiver saturation by a nearby data link transmitter. Consequently, to provide a clean time base for cycle counting purposes, a psuedo time was dubbed on the data tape. Correlation of the flight time and psuedo time was performed at two second intervals to compensate partially for tape speed variations.

#### F-3 METEOROLOGICAL DATA

The SA-2 Radiosonde Data were transmitted from Cape Canaveral to the Computation Division via card transceiver. Nine releases covering times from T-24 to T+5 hours were received. The card transceiver was in operation for approximately 5 hours. Three releases were of primary importance, the Patrick T-0 release, the Cape Canaveral T-0 release, and the T+2 hour release. These releases were processed by 7090 computer and were also compared against the Patrick Reference Atmosphere. The Rocketsonde T-0 Magnetic Tape was processed 8 days after the launch data. No difficulties were encountered in processing any of the meteorological data.

#### F-4 OPTICAL TRACKING DATA

Preliminary metric information on Project High Water concerning the growth rate of the ice cloud and the linear rate of the spiralling ends which appeared to "tail-off" were reduced from optical coverage of this experiment from Vero Beach. Additional reductions are planned which will yield final data concerning growth rates, density, and other pertinent data when other optical coverages are made available.

## APPENDIX G

## (U) FLIGHT SIMULATION OF CLUSTER PERFORMANCE

The vehicle specific impulse, thrust, and total weight loss rate were derived from the telemetered propulsion system measurements in a simulation of the tracked trajectory. Measured values or best estimates for the liftoff weight and propellant tanking weights are part of the inputs required in addition to the propulsion system measurements for the differential equations which represent the vehicle's powered flight motion.

Many combinations of specific impulse, thrust, and flow rates, which will satisfy the tracked trajectory within its accuracy limitations, can be derived if the liftoff weight and propellant tanking weights are allowed to vary.

Mean sea level vehicle specific impulse is shown versus liftoff weight in the upper portion of Figure G-1. All the values of specific impulse and liftoff weight which fall on the solid line will satisfy the tracked trajectory very closely. Any values which lie within the dashed lines will satisfy the tracked trajectory within its accuracy limitations.

Mean vehicle total weight loss rate is shown versus mean sea level vehicle thrust in the lower portion of Figure G-1. Variation of  $\pm \frac{1}{2}\%$  in liftoff weight is also shown in this figure.

The differences between the earth-fixed velocity and slant distance from the computed and tracked trajectories are shown versus range time in Figure G-2. The maximum difference between the velocity for the actual and simulated trajectories was less than 0.5 m/s.

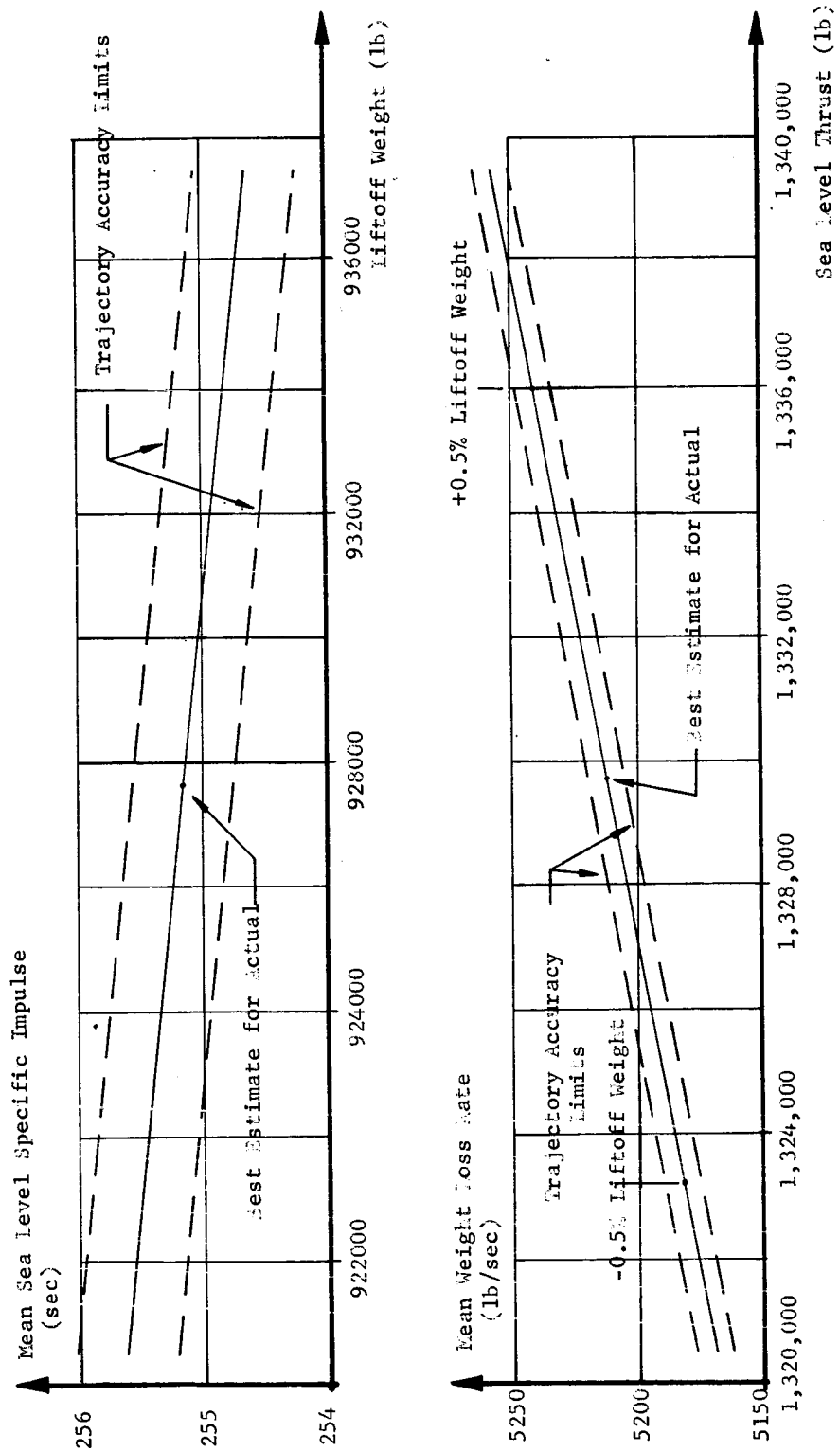


Fig. A-1 PROJECT SIMULATION RESULTS

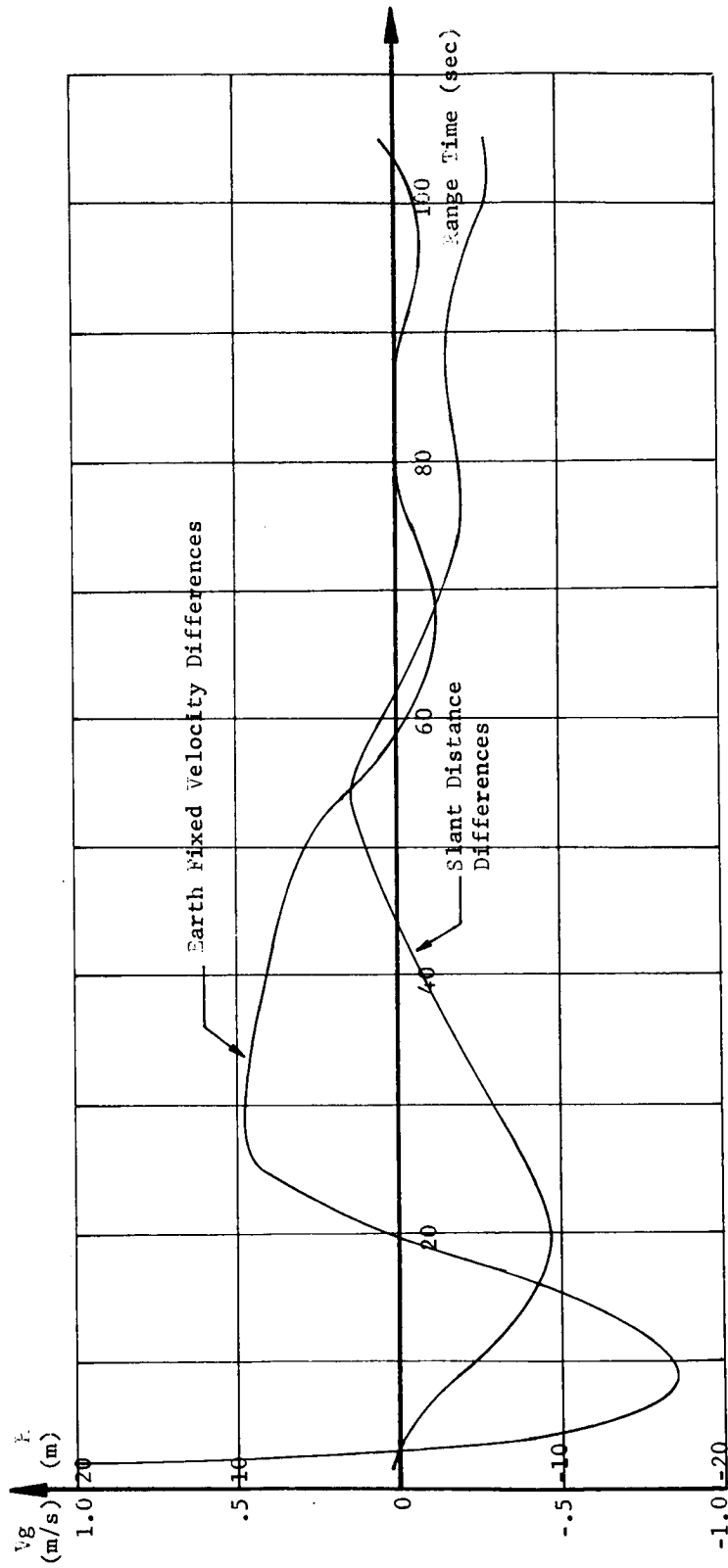


Fig. G-2 EARTH-FIXED VELOCITY AND SLANT DISTANCE (TRACKING-FIGURE SIMULATION)

## APPENDIX H

## (U) BIAS ADJUSTMENT OF FLIGHT MECHANICAL DATA

Flight data contains certain errors due to telemetering and data reduction processes, slight misalignments of sensors, and electronic noise. Since the flight mechanical measurements are fundamental to a large number of investigations an automatic method has been devised to take out the major portion of these errors. The total error in each measurement is thought to consist of two components; a constant bias component and a random component. The method of least squares is used to calculate the constant bias. The mathematical model utilizes the linearized form of the moment, normal force, control, and wind equations in the pitch and yaw planes.

First, the statistical properties of the random error in each measurement are calculated. Then these statistics are used to weight the least squares equations to compute the biases. The results of this bias calculation are used to adjust the data.

During the early portion of the flight the aerodynamic parameters of the vehicle may not be well defined and these inherent errors in coefficients will lead to improbable solutions in the bias equations. Hence, these calculations were carried out over the time span 25 to 90 seconds.

An indication of the possible biases in the measurements may be obtained by observing the measurements prior to ignition to see if they are shifted from the zero position. Table H-I shows the standard deviation of the random error in each measurement, the pre-ignition observed bias, the least squares calculated bias, and the standard deviation of this calculation.

The program used on SA-2 evaluation is an improved process over that used for SA-1. The latter case used a system of eight equations with the biases calculated being the average bias in the angle of attack measurements and the average bias in the actuator position measurements. Also, the statistics of the random error on each variable was an estimate based on the measuring range of its sensor. With SA-2, however, the system of equations has been expanded to sixteen, and the bias of each variable is an independent quantity. Furthermore, statistics of the observed random noise are actually calculated to give more realistic weighting to the equations. For comparative purposes the biases in SA-2 data were computed with both the old and new schemes and are shown in Table H-II. It should be noted that the maximum deviation in comparable values between the two methods is less than 0.1 degree.

The big advantage, however, is the determination of the individual biases in the local angles of attack and actuator positions.

The maximum calculated bias was  $-.62$  degrees for the platform pitch position minus program.

TABLE H-1

HYPERBOLICAL DATA BIAS CALCULATION SA-2

Telemetered Variable	Measurement Number	Standard Deviation of Random Error	Pre-ignition Observed Bias	Calculated Bias	S.D.* of Calculated Bias
Local Angle of Attack 1	116-30	.058 (deg)	-	.376(deg)	.032(deg)
Local Angle of Attack 2	117-30	.062 (deg)	-	-.180(deg)	.054(deg)
Local Angle of Attack 3	118-30	.049 (deg)	-	-.116(deg)	.032(deg)
Local Angle of Attack 4	119-30	.050 (deg)	-	-.100(deg)	.055(deg)
Pitch Actuator Position 1	11-1	.058 (deg)	.33 (deg)	.251(deg)	.018(deg)
Pitch Actuator Position 2	11-2	.086 (deg)	.08 (deg)	-.143(deg)	.022(deg)
Pitch Actuator Position 3	11-3	.080 (deg)	-.10 (deg)	-.016(deg)	.231(deg)
Pitch Actuator Position 4	11-4	.090 (deg)	.53 (deg)	.408(deg)	.232(deg)
Yaw Actuator Position 1	12-1	.052 (deg)	.13 (deg)	.225(deg)	.014(deg)
Yaw Actuator Position 2	12-2	.079 (deg)	.29 (deg)	.222(deg)	.018(deg)
Yaw Actuator Position 3	12-3	.042 (deg)	-.43 (deg)	-.490(deg)	.117(deg)
Yaw Actuator Position 4	12-4	.039 (deg)	-.31 (deg)	-.396(deg)	.117(deg)
Platform Pitch Position Minus Program	11-15	.040 (deg)	-.68 (deg)	-.019(deg)	.032(deg)
Yaw Attitude Error Angle	12-15	.060 (deg)	-.40 (deg)	-.373(deg)	.017(deg)
Pitch Normal Acceleration	116-11	.124 (m/sec <sup>2</sup> )	-.25 (m/sec <sup>2</sup> )	.015(m/sec <sup>2</sup> )	.005(m/sec <sup>2</sup> )
Yaw Normal Acceleration	111-11	.069 (m/sec <sup>2</sup> )	-.04 (m/sec <sup>2</sup> )	.040(m/sec <sup>2</sup> )	.003(m/sec <sup>2</sup> )

\* Standard deviation

TABLE H-II  
COMPARISON OF 8 AND 16 EQUATION  
BIAS DETERMINATION

Variable	Biases Calculated from 16 Equation Scheme	Biases Calculated from 8 Equation Scheme
Average Pitch Angle of Attack	-.140 (deg)	-.009 (deg)
Average Yaw Angle of Attack	.130 (deg)	.075 (deg)
Average Pitch Actuator Position	.125 (deg)	.203 (deg)
Average Yaw Actuator Position	-.112 (deg)	-.122 (deg)
Platform Pitch Position Minus Program	-.619 (deg)	-.523 (deg)
Yaw Attitude Error Angle	-.373 (deg)	-.376 (deg)
Normal Acceleration Pitch	.015 (m/sec <sup>2</sup> )	.024 (m/sec <sup>2</sup> )
Normal Acceleration Yaw	.042 (m/sec <sup>2</sup> )	.044 (m/sec <sup>2</sup> )

## APPENDIX I

## (U) PROJECT HIGHWATER

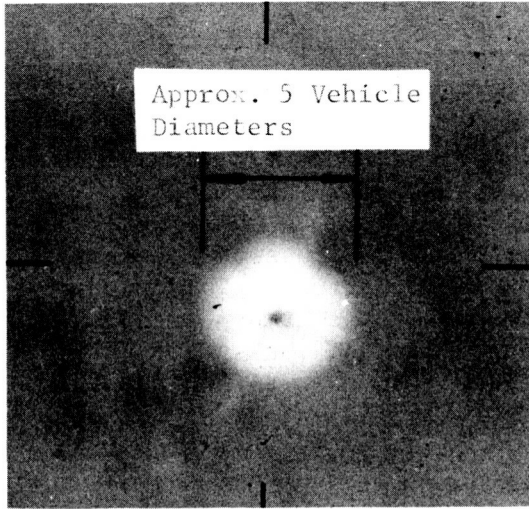
An on-board experiment was performed during the SA-2 flight. This experiment entailed the destruction of the SA-2 vehicle using the command destruct system to release approximately 86,000 kg of water into the atmosphere at an altitude of 105.3 km (162.56 sec). Release of the water was performed to introduce a perturbation in the concentrations of the naturally occurring constituents of the atmosphere of sufficient magnitude to permit a worthwhile study of the system as it returns to equilibrium. The following objectives were set-up for this experiment in an effort to obtain the most valuable information available during this man-made perturbation:

1. Measurements of rates of reactions involving  $H_2O$ ,  $OH$ ,  $O$ ,  $O_2$ ,  $O_3$  and  $H$  in the atmosphere in the region between 100 and 135 km.
2. Measurements of electron production process rates in and near the E region of the ionosphere.
3. Observations of the behavior of ice in the upper atmosphere.
4. Through observations of the gas bubble (vapor) measurements on the dynamic structure and behavior of the atmosphere at and around the point of release.

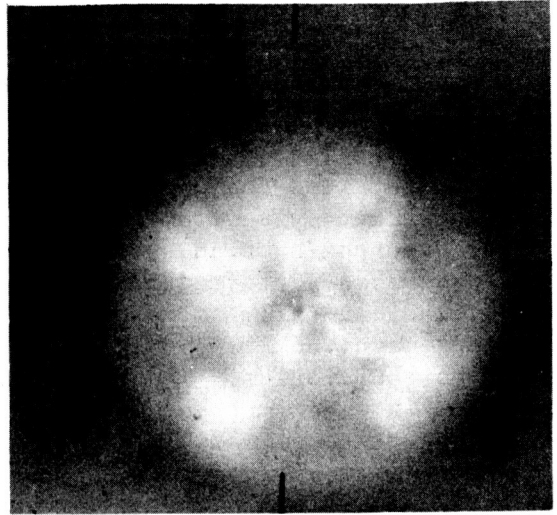
It was anticipated that immediately subsequent to the initial release of the water from Saturn SA-2, approximately 15,000 kg of water would be deposited in the atmosphere in the form of vapor in a region extending from approximately 100 km to 125 km altitude. The forward motion of this cloud stopped quite rapidly but remained visible for only approximately 10 seconds to the unaided eye. The remaining ballast in the form of ice continued along a trajectory similar to that which the vehicle would have followed if it had not been destroyed.

Considerable data was gathered, although optical data acquisition was hampered in the Cape area by juxtaposition of the sun and prevented at Jupiter and GBI tracking stations by clouds.

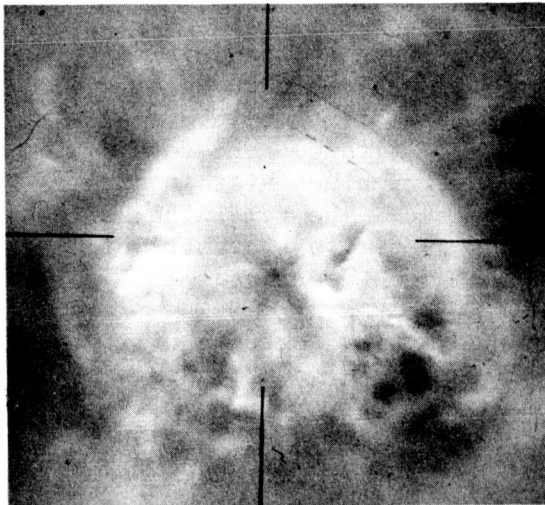
Figure I-1 presents a picture sequence of the Project Highwater experiment for the first 2 seconds.



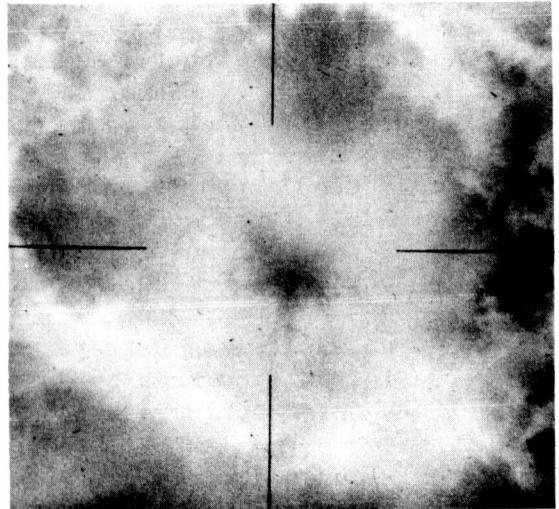
Burst +0.05 Seconds



Burst +0.20 Seconds



Burst +0.30 Seconds



Burst +2.0 Seconds

FIGURE I-1 PICTURE SEQUENCE OF PROJECT HIGHWATER  
EXPERIMENT

MPR-SAT-WF-62-5

(U) APPROVAL

SATURN SA-2 FLIGHT EVALUATION

Fridtjof Speer

Fridtjof A. Speer

Chairman, Saturn Flight Evaluation Working Group

Oswald H. Lange

Oswald H. Lange

Director, Saturn Systems Office

Wernher von Braun

Wernher von Braun

Director, Marshall Space Flight Center

## SA-2 FLIGHT EVALUATION REPORT

## (U) DISTRIBUTION

Dr. von Braun, M-DIR  
Dr. Rees, M-DEP-R&D  
Mr. Gorman, M-DEP-ADM

M-AERO

Dr. Geissler, M-AERO-DIR  
Mr. Jean, M-AERO-PS (4)  
Mr. Dahm, M-AERO-A (2)  
Mr. Vaughan, M-AERO-G (3)  
Mr. Ryan, M-AERO-D  
Mr. Holderer, M-AERO-E  
Dr. Speer, M-AERO-F (18)  
Dr. Hoelker, M-AERO-P

M-L&M

Mr. Hueter, M-L&M-DIR (2)

M-COMP

Dr. Hoelzer, M-COMP-DIR  
Mr. Fortenberry, M-COMP-A  
Mr. Moore, M-COMP-R  
Mr. Shaver, M-COMP-S

M-ME

Mr. Kuers, M-ME-DIR  
Mr. Groth, M-ME-TS (4)

M-FPO

Mr. Koelle, M-FPO-DIR (2)  
Mr. Weaver, M-FPO

M-ASTR

Dr. Haeussermann, M-ASTR-DIR  
Mr. Noel, M-ASTR-TSJ  
Mr. Wagon, M-ASTR-TSR  
Mr. Digesu, M-ASTR-A  
Mr. Taylor, M-ASTR-R  
Mr. Fichtner, M-ASTR-E  
Mr. Baggs - Mr. Stroud, M-ASTR-E  
Mr. Boehm, M-ASTR-M  
Mr. Hosenthien, M-ASTR-F  
Mr. Blackstone, M-ASTR-FF

Mr. Mandel, M-ASTR-G  
Mr. Hoberg, M-ASTR-I  
Mr. Bell, M-ASTR-IM  
Mr. Moore, M-ASTR-N  
Mr. McMahan, M-ASTR-NT (5)

M-LOD

Dr. Debus, M-LOD-DIR  
Dr. Knothe, M-LOD-TS  
Dr. Gruene, M-LOD-G (3)  
Mr. Sandler, M-LOD-E (4)  
Mr. Collins, M-LOD-EP  
Mr. Poppel, M-LOD-D  
Mr. Darby, M-LOD-DHE  
Mr. Body, M-LOD-DS  
Mr. Zeiler, M-LOD-M (3)  
Col. Bidgood, M-LOD-F  
Major Petrone, M-LOD-H (3)

Mr. Schulze, M-REL (3)

M-QUAL

Mr. Grau, M-QUAL-DIR  
Mr. Klauss, M-QUAL-TS  
Mr. Wittmann, M-QUAL-E  
Mr. Urbanski, M-QUAL-M  
Mr. Brooks, M-QUAL-P  
Mr. Peck, M-QUAL-PS  
Mr. Smith, M-QUAL-Q

M-RP

Dr. Stuhlinger, M-RP-DIR  
Mr. Miles, Jr., M-RP-R  
Dr. Shelton, M-RP-N  
Dr. Lundquist, M-RP-P  
Dr. Heller, M-RP-T  
Mr. Thompson, M-RP-I

M-SAT

Dr. Lange, M-SAT-DIR  
Dr. Kuettner, M-SAT-AP  
Mr. Vreuls, M-SAT (5)  
Mr. D.R. Bowden, M-SAT-SII (Downey)

M-P&VE

Mr. Mrazek, M-P&VE-DIR  
Mr. Wiedner, M-P&VE-DIR  
Mr. Burrows, M-P&VE-REL  
Mr. Palaora, M-P&VE-V  
Mr. Glover, M-P&VE-VA (2)  
Mr. Stein, M-P&VE-VE  
Mr. McCullough, M-P&VE-VG  
Mr. Barraza, M-P&VE-VK  
Mr. Seymour, M-P&VE-OH (2)  
Mr. Schulze, M-P&VE-E (2)  
Mr. Hurber, M-P&VE-EA  
Mr. Kistler, M-P&VE-EF  
Mr. Hoffman, M-P&VE-ES  
Mr. Shramm, M-P&VE-F  
Mr. Lucas, M-P&VE-M  
Mr. Fellows, M-P&VE-NP  
Mr. Paul, M-P&VE-P (2)  
Mr. Thompson, M-P&VE-PA  
Mr. Reed, M-P&VE-PL  
Mr. Furman, M-P&VE-PM  
Mr. Wood, M-P&VE-PT  
Mr. Connell, M-P&VE-PH  
Mr. Heusinger, M-P&VE-PP (3)  
Mr. Kroll, M-P&VE-S  
Mr. Verble, M-P&VE-SB  
Mr. Hunt, M-P&VE-SD (6)  
Mr. Sterett, M-P&VE-SS

M-TPC

Mr. Smith, M-TPC

M-TEST

Mr. Heimburg, M-TEST-DIR  
Mr. Auter, M-TEST-E  
Mr. Sieber, M-TEST-M  
Mr. Thornton, M-TEST-MC  
Mr. Driscoll, M-TEST-T  
Mr. Tessmann, M-TEST-C

M-MS

M-MS-IPL (8)  
M-MS-IP

M-PAT

Mr. Warden, M-PAT

M-H

## DISTRIBUTION (cont')

EXTERNAL

Headquarters, National Aeronautics & Space Administration  
Washington 25, D.C.

Assistant to the Administration: Franklyn W. Phillips  
Office of Plans & Program Evaluation: Abraham Hyatt  
Office of Scientific & Technical Information: Melvin S. Day  
Associate Administrator: Robert C. Seamans, Jr.  
Office of Programs  
Director of Reliability & Quality Assurance: Landis S. Gephart

Office of Manned Space Flight  
Director: D. Brainerd Holmes  
Deputy Director (Systems): Joseph F. Shea  
Director of Launch Vehicles & Propulsion: Milton W. Rosen

Office of Space Sciences  
Director: Homer E. Newell  
Launch Vehicles & Propulsion Programs  
Director: Donald H. Heaton  
Attn: Richard B. Canright (10)

Office of Advanced Research & Technology  
Director: Thomas F. Dixon  
Director of Propulsion and Power Generation: John L. Sloop

Office of Applications  
Director: Morton J. Stoller  
Morris Tepper

Goddard Space Flight Center  
4555 Overlook Avenue  
Washington 25, D.C.  
Attn: Herman LaGow

Director, Ames Research Center: Smith J. DeFrance  
National Aeronautics & Space Administration  
Moffett Field, California

Manned Spacecraft Center  
Houston 1, Texas - P.O. Box 1537  
Attn: Director: Robert R. Gilruth  
Robert Smith (5)

Director, Langley Research Center: Floyd L. Thompson  
National Aeronautics & Space Administration  
Langley Field, Virginia

Director, Lewis Research Center: Abe Silverstein  
National Aeronautics & Space Administration  
21000 Brookpark Road  
Cleveland 35, Ohio

Director, Western Operations Office: Robert W. Kamm  
National Aeronautics & Space Administration  
150 Pico Blvd., Santa Monica, California

Director, Flight Research Center: Paul F. Bikle  
National Aeronautics & Space Administration  
P.O. Box 273  
Edwards, California

Director, Wallops Station: R.L. Krieger  
National Aeronautics & Space Administration  
Wallops Island, Virginia

Jet Propulsion Lab  
4800 Oak Grove Drive  
Pasadena 2, California  
Attn: Irl Newlan, Reports Group

Jet Propulsion Laboratories, CCMTA  
Attn: H. Levy (4)

Office of the Asst. Sec. of Defense for Research & Engineering  
Room 3E1065  
The Pentagon  
Washington 25, D.C.  
Attn: Tech Library

Director of Guided Missiles  
Office of the Secretary of Defense  
Room 3E131  
The Pentagon  
Washington 25, D.C.

Commander, Armed Services Tech Info Agency (5)  
Arlington Hall Station  
Arlington 12, Va.  
Attn: TIPCR (Transmittal per Cognizant Act. Security Instruction)

U.S. Atomic Energy Commission, Sandia Corp.  
University of California Radiation Lab  
Tech Info Div  
P.O. Box 808  
Livermore, California  
Attn: Clovis Craig

U.S. Atomic Energy Commission, Sandia Corp.  
Livermore Br, P.O. Box 969  
Livermore, California  
Attn: James McMin, Document Control Sec.

Central Intelligence Agency (2)  
2430 E Street, N. W.  
Washington 25, D.C.  
Attn: Liaison Div, OCD

Director, National Security Agency  
Washington 25, D.C.  
Attn: CREF-22

Commanding General (3)  
White Sands Proving Ground  
New Mexico  
Attn: ORDBS-OMTIO-TL

Commander, AF Missile Test Center (3)  
Patrick AFB, Florida  
Attn: Tech Info & Intelligence Office, MTGRY

Chief of Staff, U.S. Air Force (2)  
The Pentagon  
Washington 25, D.C.  
1 Cpy marked for DCS/D AFDRD  
1 Cpy marked for DCS/D AFDRD-EX

Commander (5)  
Wright Air Development Center  
Wright-Patterson Air Force Base, Ohio  
Attn: WCOSI-3

Commander  
Air Force Flight Test Center  
Edwards AFB, California  
Attn: FTOTL

Commander  
Air Force Ballistic Missile Div  
Hdqrs, ARDC, Air Force Unit Post Office  
Los Angeles 45, California  
Attn: WDSOT

Commander-in-Chief  
Strategic Air Command  
Offutt AFB, Nebraska  
Attn: Dir of Opns, Missile Division

Commander (2)  
Arnold Engineering Development Center  
Arnold Air Force Station, Tennessee  
Attn: Tech. Library

Commander  
Air Force Missile Development Center  
Holloman Air Force Base  
New Mexico  
Attn: Tech Library (SRLT)

Commander  
U.S. Naval Air Missile Test Center  
Point Mugu, California

Chief, Bureau of Weapons (4)  
Dept. of Navy  
Washington 25, D.C.  
1 Cpy to RESI, 1 Cpy to SP, 1 Cpy to AD3  
1 Cpy to REW3

Chief of Naval Research  
Department of Navy  
Washington 25, D.C.  
Code 463

Director (2)  
U.S. Naval Research Lab  
Washington 25, D.C.  
Attn: Code 2027

Douglas Aircraft Company, Inc.  
Missile and Space Systems Engineering  
Santa Monica, California  
Attn: H.M. Thomas (1)  
A.J. German (5)

CCMD, Huntsville Industrial Center  
Attn: H. Bader, Jr. (2)

ORDAB-HT Technical Library, ABMA (5)  
ORDAB-C Control Office, ABMA

Aerospace Corporation  
2400 East El Segundo  
El Segundo, California  
Attn: D.C. Bakeman

Arinc Research Corporation  
1700 K Street, N.W.  
Washington 6, D.C.  
Attn: W. J. Willoughby

Boeing Corporation  
Saturn Booster Operations  
Seattle 24, Washington  
Attn: R.H. Nelson

North American Aviation  
Space & Information Division Systems  
12214 Lakewood Boulevard  
Downey, California  
Attn: A Shimizu (1)  
W.F. Parker (1)

Rocketdyne  
6633 Canogo Avenue  
Canogo Park, California  
Attn: O.I. Thorsen (3)

Chrysler Space Division  
Michoud Operations  
Attn: V.J. Vehko (1)  
B. Heinrich (5)

Headquarters  
6570th Aerospace Medical Division (AFSC)  
U.S. Air Force  
Wright Patterson Air Force Base, Ohio  
Attn: H.E. Vongierke

Radio Corporation of America  
Defense Electronic Products  
Data Systems Division  
8500 Balboa Blvd  
Van Nuys, California  
Attn: L.R. Hund, Librarian

Martin Company  
Space Systems Division  
Baltimore 3, Maryland  
Attn: W.P. Sommers